

# Directing stem cell fate using plant extracts and their bioactive compounds

**Edited by**

Hiroko Isoda, Francis G. Szele, Yun-Wen Zheng, DongZhu Xu, Kazunori Sasaki and Farhana Ferdousi

**Published in**

Frontiers in Cell and Developmental Biology  
Frontiers in Pharmacology



## FRONTIERS EBOOK COPYRIGHT STATEMENT

The copyright in the text of individual articles in this ebook is the property of their respective authors or their respective institutions or funders. The copyright in graphics and images within each article may be subject to copyright of other parties. In both cases this is subject to a license granted to Frontiers.

The compilation of articles constituting this ebook is the property of Frontiers.

Each article within this ebook, and the ebook itself, are published under the most recent version of the Creative Commons CC-BY licence. The version current at the date of publication of this ebook is CC-BY 4.0. If the CC-BY licence is updated, the licence granted by Frontiers is automatically updated to the new version.

When exercising any right under the CC-BY licence, Frontiers must be attributed as the original publisher of the article or ebook, as applicable.

Authors have the responsibility of ensuring that any graphics or other materials which are the property of others may be included in the CC-BY licence, but this should be checked before relying on the CC-BY licence to reproduce those materials. Any copyright notices relating to those materials must be complied with.

Copyright and source acknowledgement notices may not be removed and must be displayed in any copy, derivative work or partial copy which includes the elements in question.

All copyright, and all rights therein, are protected by national and international copyright laws. The above represents a summary only. For further information please read Frontiers' Conditions for Website Use and Copyright Statement, and the applicable CC-BY licence.

ISSN 1664-8714  
ISBN 978-2-83251-184-8  
DOI 10.3389/978-2-83251-184-8

## About Frontiers

Frontiers is more than just an open access publisher of scholarly articles: it is a pioneering approach to the world of academia, radically improving the way scholarly research is managed. The grand vision of Frontiers is a world where all people have an equal opportunity to seek, share and generate knowledge. Frontiers provides immediate and permanent online open access to all its publications, but this alone is not enough to realize our grand goals.

## Frontiers journal series

The Frontiers journal series is a multi-tier and interdisciplinary set of open-access, online journals, promising a paradigm shift from the current review, selection and dissemination processes in academic publishing. All Frontiers journals are driven by researchers for researchers; therefore, they constitute a service to the scholarly community. At the same time, the *Frontiers journal series* operates on a revolutionary invention, the tiered publishing system, initially addressing specific communities of scholars, and gradually climbing up to broader public understanding, thus serving the interests of the lay society, too.

## Dedication to quality

Each Frontiers article is a landmark of the highest quality, thanks to genuinely collaborative interactions between authors and review editors, who include some of the world's best academicians. Research must be certified by peers before entering a stream of knowledge that may eventually reach the public - and shape society; therefore, Frontiers only applies the most rigorous and unbiased reviews. Frontiers revolutionizes research publishing by freely delivering the most outstanding research, evaluated with no bias from both the academic and social point of view. By applying the most advanced information technologies, Frontiers is catapulting scholarly publishing into a new generation.

## What are Frontiers Research Topics?

Frontiers Research Topics are very popular trademarks of the *Frontiers journals series*: they are collections of at least ten articles, all centered on a particular subject. With their unique mix of varied contributions from Original Research to Review Articles, Frontiers Research Topics unify the most influential researchers, the latest key findings and historical advances in a hot research area.

Find out more on how to host your own Frontiers Research Topic or contribute to one as an author by contacting the Frontiers editorial office: [frontiersin.org/about/contact](https://frontiersin.org/about/contact)



# Directing stem cell fate using plant extracts and their bioactive compounds

## Topic editors

Hiroko Isoda — University of Tsukuba, Japan

Francis G. Szele — University of Oxford, United Kingdom

Yun-Wen Zheng — University of Tsukuba, Japan

DongZhu Xu — University of Tsukuba, Japan

Kazunori Sasaki — National Institute of Advanced Industrial Science and Technology (AIST), Japan

Farhana Ferdousi — University of Tsukuba, Japan

## Citation

Isoda, H., Szele, F. G., Zheng, Y.-W., Xu, D., Sasaki, K., Ferdousi, F., eds. (2023). *Directing stem cell fate using plant extracts and their bioactive compounds*. Lausanne: Frontiers Media SA. doi: 10.3389/978-2-83251-184-8

# Table of contents

- 05 **Editorial: Directing Stem Cell Fate Using Plant Extracts and Their Bioactive Compounds**  
Farhana Ferdousi, Kazunori Sasaki, Dongzhu Xu, Yun-Wen Zheng, Francis G Szele and Hiroko Isoda
- 09 **Recruitment of Mesenchymal Stem Cells to Damaged Sites by Plant-Derived Components**  
Akito Maeda
- 21 **Caffeine Compromises Proliferation of Human Hippocampal Progenitor Cells**  
Vikki Houghton, Andrea Du Preez, Sophie Lefèvre-Arbogast, Chiara de Lucia, Dorraïn Y. Low, Mireia Urpi-Sarda, Silvie R. Ruigrok, Barbara Altendorfer, Raúl González-Domínguez, Cristina Andres-Lacueva, Ludwig Aigner, Paul J. Lucassen, Aniko Korosi, Cécilia Samieri, Claudine Manach and Sandrine Thuret
- 33 **Effects of Isorhamnetin in Human Amniotic Epithelial Stem Cells *in vitro* and Its Cardioprotective Effects *in vivo***  
Kazuhiro Aonuma, Farhana Ferdousi, DongZhu Xu, Kenichi Tominaga and Hiroko Isoda
- 44 **Sugarcane (*Saccharum officinarum* L.) Top Extract Ameliorates Cognitive Decline in Senescence Model SAMP8 Mice: Modulation of Neural Development and Energy Metabolism**  
Kengo Iwata, Qingqing Wu, Farhana Ferdousi, Kazunori Sasaki, Kenichi Tominaga, Haruhisa Uchida, Yoshinobu Arai, Francis G. Szele and Hiroko Isoda
- 65 **Fisetin Promotes Hair Growth by Augmenting TERT Expression**  
Chisato Kubo, Mizuki Ogawa, Norihisa Uehara and Yoshinori Katakura
- 78 **Tectorigenin Alleviates Inflammation, Apoptosis, and Ossification in Rat Tendon-Derived Stem Cells via Modulating NF-Kappa B and MAPK Pathways**  
Safwat Adel Abdo Moqbel, Kai Xu, Zhonggai Chen, Langhai Xu, Yuezhe He, Zhipeng Wu, Chiyuan Ma, Jisheng Ran, Lidong Wu and Yan Xiong
- 95 **New Amphiphilic Squalene Derivative Improves Metabolism of Adipocytes Differentiated From Diabetic Adipose-Derived Stem Cells and Prevents Excessive Lipogenesis**  
Munkhzul Ganbold, Farhana Ferdousi, Takashi Arimura, Kenichi Tominaga and Hiroko Isoda
- 109 **Global Gene Expression Profiling Reveals Isorhamnetin Induces Hepatic-Lineage Specific Differentiation in Human Amniotic Epithelial Cells**  
Yoshiaki Uchida, Farhana Ferdousi, Yun-Wen Zheng, Tatsuya Oda and Hiroko Isoda

- 126 ***Alpinia oxyphylla* Miq. and Its Active Compound *P*-Coumaric Acid Promote Brain-Derived Neurotrophic Factor Signaling for Inducing Hippocampal Neurogenesis and Improving Post-cerebral Ischemic Spatial Cognitive Functions**  
Yacong He, Shuang Chen, Bun Tsoi, Shuhua Qi, Bing Gu, Zhenxing Wang, Cheng Peng and Jiangang Shen
- 147 **Microalgae *Aurantiochytrium* Sp. Increases Neurogenesis and Improves Spatial Learning and Memory in Senescence-Accelerated Mouse-Prone 8 Mice**  
Kazunori Sasaki, Noelia Geribaldi-Doldán, Qingqing Wu, Julie Davies, Francis G. Szele and Hiroko Isoda
- 161 **Fraxinellone Has Anticancer Activity by Inducing Osteosarcoma Cell Apoptosis via Promoting Excessive Autophagy Flux**  
Bin He, Wenkan Zhang and Jiaming He
- 172 **Luteolin Modulates Neural Stem Cells Fate Determination: *In vitro* Study on Human Neural Stem Cells, and *in vivo* Study on LPS-Induced Depression Mice Model**  
Mariem Achour, Farhana Ferdousi, Kazunori Sasaki and Hiroko Isoda



# Editorial: Directing Stem Cell Fate Using Plant Extracts and Their Bioactive Compounds

Farhana Ferdousi<sup>1,2</sup>, Kazunori Sasaki<sup>1,2</sup>, Dongzhu Xu<sup>1,3</sup>, Yun-Wen Zheng<sup>4</sup>, Francis G Szele<sup>5</sup> and Hiroko Isoda<sup>1,2,6\*</sup>

<sup>1</sup>AIST-University of Tsukuba Open Innovation Laboratory for Food and Medicinal Resource Engineering (FoodMed-OIL), AIST, University of Tsukuba, Tsukuba, Japan, <sup>2</sup>Alliance for Research on the Mediterranean and North Africa (ARENA), University of Tsukuba, Tsukuba, Japan, <sup>3</sup>Cardiovascular Division, Institute of Clinical Medicine, Faculty of Medicine, University of Tsukuba, Tsukuba, Japan, <sup>4</sup>Department of Gastrointestinal and Hepato-Biliary-Pancreatic Surgery, Faculty of Medicine, University of Tsukuba, Tsukuba, Japan, <sup>5</sup>Department of Physiology, Anatomy and Genetics, University of Oxford, Oxford, United Kingdom, <sup>6</sup>Faculty of Life and Environmental Sciences, University of Tsukuba, Tsukuba, Japan

**Keywords:** plant extract, bioactive compound, stem cell differentiation, neurogenesis, mesenchymal stem cell, human amniotic epithelial cells, hair growth, anticancer activity

## Editorial on the Research Topic

### Directing Stem Cell Fate Using Plant Extracts and their Bioactive Compounds

The rapidly evolving field of stem cell therapy has great potential for treating a broad array of diseases, including currently incurable diseases. However, the use of stem cell-based products as therapeutics is often limited by high rejection rate, insufficient availability, and expensive *in vitro* expansion methods (McNeish, 2004; Laustriat et al., 2010; Rubin and Haston, 2011). The external control of stem cells using plant-derived bioactive compounds, such as polyphenols, flavonoids, tannins, terpenoids, and fatty acids, may provide potential solutions to overcome many of these current limitations. Many naturally occurring bioactive compounds have been shown to promote stem cell proliferation and lineage-specific differentiation (Udallamaththa et al., 2016). This Research Topic aimed to cover promising and novel research findings on the effects of plant extracts and their bioactive compounds on regulating cell division and differentiation of pluripotent and adult stem cells and stem cells obtained from alternative sources. This article Research Topic includes ten original research articles, one brief research report, and one review article covering the potentials of bioactive compounds for neurodegenerative, cardiovascular, metabolic, cancer, musculoskeletal, and hair loss diseases through regulating stem cell proliferation and differentiation. Below we present the focus and key findings of each article.

Mesenchymal stem cells (MSCs) are multipotent progenitor cells that can be differentiated into skin cells, such as fibroblasts and keratinocytes. Apart from their differentiation capacity, MSCs exert unique paracrine actions to accelerate wound healing and maintain tissue homeostasis and, therefore, have been regarded as a potentially promising therapeutic option for tissue injury and diseases (Guillamat-Prats, 2021). Plant-derived components that can promote biological events, such as migration and homing of MSCs, may offer novel therapeutic options for regenerative medicine. The review by Maeda addresses the role of plant-derived components in promoting the migration and homing of MSCs to damaged sites, where they contribute to the healing process (Maeda).

The following group of five original research articles was dedicated to exploring the potential of plant components on neurodegenerative and neuropsychiatric conditions through regulating neural stem cells (NSCs) proliferation and differentiation *in vitro* and *in vivo* (Houghton et al.; Iwata et al.; Achour et al.; He Y. et al.; Sasaki et al.).

An interesting paper by Houghton et al. reported that exposure to supraphysiological caffeine condition could significantly reduce progenitor integrity and proliferation of human hippocampal

## OPEN ACCESS

### Edited and reviewed by:

Valerie Kouskoff,  
The University of Manchester,  
United Kingdom

### \*Correspondence:

Hiroko Isoda  
isoda.hiroko.ga@u.tsukuba.ac.jp

### Specialty section:

This article was submitted to  
Stem Cell Research,  
a section of the journal  
Frontiers in Cell and Developmental  
Biology

**Received:** 31 May 2022

**Accepted:** 08 June 2022

**Published:** 29 June 2022

### Citation:

Ferdousi F, Sasaki K, Xu D,  
Zheng Y-W, Szele FG and Isoda H  
(2022) Editorial: Directing Stem Cell  
Fate Using Plant Extracts and Their  
Bioactive Compounds.  
Front. Cell Dev. Biol. 10:957601.  
doi: 10.3389/fcell.2022.957601



progenitor cells, HPC0A07/03, compared to control conditions. This finding indicates that regular dietary components, such as caffeine, can affect cognitive outcomes by influencing NSC integrity and proliferation and highlights the potential of leveraging dietary interventions to promote cognitive health.

Iwata et al. evaluated the benefits of sugarcane (*Saccharum officinarum* L.) top as a putative dietary supplement to improve aging consequences using *in vitro* and *in vivo* strategies. They showed that the ethanolic extract of sugarcane top (STEE), rich in caffeoylquinic acid derivatives, could rescue age-associated decline in spatial learning and memory, increase the number of newborn neurons in the subgranular zone of hippocampus, and restore the levels of neurotransmitters in the cerebral cortex of senescence-accelerated mouse SAMP8. They also demonstrated that STEE enhanced cellular energy metabolism through upregulation of glycolytic reaction in human neuroblastoma cells, SH-SY5Y, and positively affected proliferation, induced neuronal differentiation and astrocyte morphogenesis in human NSCs (hNSCs).

He Y. et al. analyzed the effect of *Alpinia oxyphylla* Miq. extract (AOM) and its bioactive compound *p*-coumaric acid (*p*-CA) on post-stroke recovery in rats. They reported that both AOM and *p*-CA improved cognitive functions, reduced anxiety, and increased hippocampal neurogenesis in the post-middle cerebral artery occlusion ischemic rats *in vivo* through activating BDNF/TrkB/AKT signaling pathway.

The study by Sasaki et al. investigated the neurodevelopmental and neuroprotective effects of the microalgae *Aurantiochytrium* sp. in a number of experimental models. They reported that *Aurantiochytrium* inhibited amyloid- $\beta$ -induced cell death and increased ATP production in SH-SY5Y human neuroblastoma cells, increased proliferation of murine neurospheres, improved spatial learning and memory in the senescence-accelerated SAMP8 mice and enhanced neurogenesis in the mice hippocampal dentate gyrus.

The final article in this Research Topic by Achour et al. reported that natural flavone luteolin inhibited notch signaling and therefore inhibited the self-renewal of hNSCs, and directed the differentiation of hNSCs towards astrocytes likely via mediating WNT- $\beta$ -catenin-BMP2-STAT3 pathways. *In vivo*, luteolin improved neuroinflammation by decreasing proinflammatory cytokine levels in mice astrocytes and sera and increased neurotransmitter and neurotrophic factor levels in the hypothalamus in lipopolysaccharide (LPS)-induced neuroinflammatory model of depression in mice. They have also presented a comprehensive whole-genome transcriptome analysis, which provided a detailed view of the changes in biological functions in mice hippocampus and brain-derived NSCs by luteolin administration and highlighted the possible therapeutic benefits of luteolin in neuroinflammatory and neurodegenerative diseases.

All these five papers had a common parameter-neurogenesis in hippocampus. Discovering adult hippocampal neurogenesis (AHN) led to a paradigm shift in neuroscience. Adult-born hippocampal neurons are one of the key mediators of hippocampus-dependent functions, such as learning, memory encoding, mood regulation, and stress response. Recent scientific

evidence suggests that impairment of AHN underlies the pathophysiology of neurodegenerative and affective disorders (Mu and Gage, 2011; Baptista and Andrade, 2018; Toda et al., 2019; Gomes-Leal, 2021). Therefore, hippocampal neurogenesis-inspired therapies using plant-derived bioactive compounds offer a promising approach to reducing symptoms of neurodegenerative and mood disorders in humans (Zhang et al., 2014; Sasikumar et al., 2022).

In this article Research Topic, there are two interesting studies on perinatal stem cell human amniotic epithelial cells (hAECs/hAECs) (Aonuma et al.; Uchida et al.). The hAECs are obtained from discarded term placenta and therefore are readily available. hAECs possess both ESC-like pluripotent potential and adult stem cell-like immunomodulatory properties. In recent years, stem-cell-based approaches using ESCs and iPSC have received great attention as effective drug screening tools. However, invasive extraction and expensive cell reprogramming and maintenance procedures as well as ethical constraints, limit the use of these types of stem cells for drug screening (Chen et al., 2014). In this context, hAECs offer a suitable alternative to ESCs and iPSCs (Miki et al., 2005; Murphy et al., 2010; Miki, 2018). In their study, Aonuma et al. considered hAECs as a drug screening tool and investigated the cardiac antifibrotic potential of a plant flavonol isorhamnetin in hAECs through whole-genome transcriptome analysis and then validated the findings in angiotensin II (AngII)-induced mice model of cardiac fibrosis and hypertrophy. On the other hand, Uchida et al. reported that isorhamnetin regulated early biological events to induce hepatic-lineage-specific differentiation in hAECs in the absence of any growth factor or cytokine. The differentiated hAECs expressed a subset of hepatic differentiation-related genes, induced cytochromes P450 (CYPs) mRNA levels, and showed some key functional properties of hepatic cells, including indocyanine green (ICG) uptake and release, glycogen storage, and urea secretion. There are few other studies that explored directed differentiation potential of different natural bioactive compounds in hAECs (Ferdousi et al., 2019; Bejaoui et al., 2021), while other studies explored improved therapeutic potential of hAECs in combinations with natural compounds (Ferdousi et al., 2020; Xu et al., 2021). These study findings would encourage multidirectional research approaches through integrating natural bioactive compounds with the existing hAECs research platforms (Ferdousi and Isoda, 2022).

The study by Kubo et al. has drawn much attention due to its promising findings on the hair growth potential of several polyphenols. Hair thinning and alopecia is more than just cosmetic concern and has a significant negative impact on the quality of life. To date, only two compounds, finasteride and minoxidil, are commonly used to improve hair loss conditions, but they are not without side effects. Therefore, there has been growing interest in natural bioactive compounds with properties that promote hair growth or limit hair loss as a safe alternative to drug-based therapy (Park and Lee, 2021). However, although many medicinal plants have been used anecdotally from ancient times to prevent hair loss, the scientific evidence is lacking about whether and how these plant-derived products are effective for the treatment of hair thinning and alopecia. In their study, Kubo

et al. used an *in vitro* screening system in the human keratinocyte cell line, HaCaT, to identify polyphenols that can augment the expression of telomerase reverse transcriptase (TERT), a catalytic subunit of the enzyme telomerase, that activates the hair follicle bulge stem cells and triggers the initiation of new hair follicle growth phase and thereby promotes hair growth. They have identified the polyphenols-fisetin and resveratrol as potent hTERT-augmenting compounds that also enhanced  $\beta$ -catenin and hair growth cycle-related growth factors *in vitro* and *in vivo*.

Moqbel et al. investigated the anti-inflammatory effects of tectorigenin, an extracted component of *Belamcanda chinensis*, on TNF $\alpha$ -stimulated tendon-derived stem cells (TDSCs) and an animal model of tendinopathy. TDSCs are pluripotent stem cells that control tendon homeostasis and play a central role in tendon regeneration and healing and, therefore, are considered a potential cell-based therapy for tendon injuries (Wei and Lu, 2021). Moqbel et al. showed that tectorigenin inhibited TNF $\alpha$ -induced matrix-degradation, inflammation, apoptosis, senescence, and osteogenic differentiation of TDSCs in NF- $\kappa$ B/MAPK-dependent manner *in vitro*. Furthermore, tectorigenin ameliorated tendinopathy in a tendon transection rat model. This study highlights the potential of plant-derived compounds with strong anti-inflammatory effects in tendinopathy and other musculoskeletal disorders.

The study by Ganbold et al. explored the effect of a new amphiphilic squalene derivative (HH-Sq) in comparison to squalene (Sq) on the adipocyte differentiation of adipose-derived stem cells (ASCs) obtained from type 2 diabetic subject. ASCs are adult stem cells that can be differentiated into mesodermal cell lineages, including adipocytes, osteocytes, myocytes, and chondrocytes and have the potential to be used for cell therapy in the treatment of insulin resistance, obesity, and type 2 diabetes (Mazini et al., 2020). On the other hand, Sq is a polyunsaturated hydrocarbon found in deep-sea shark liver oil, numerous plant oils and algae (Spanova and Daum, 2011). Ganbold et al. demonstrated that the amphiphilic HH-Sq, synthesized by adding mono ethylene glycol moiety to Sq, showed improved metabolism of adipocytes, enhanced energy homeostasis and insulin sensitivity, and importantly, in contrast to Sq, HH-Sq prevented excessive lipogenesis in the presence of adipocyte differentiation. This finding emphasizes the enhanced therapeutic potentials of synthesized derivatives from a natural compound in cell-based therapies.

He B. et al. reported that fraxinellone (FRA), the bioactive component isolated from the *D. dasycarpus* plant, inhibited the proliferation and migration of human osteosarcoma cells HOS and MG63 in a dose-dependent manner. FRA simultaneously induced osteosarcoma cell apoptosis and increased autophagy flux *in vitro*. The authors further demonstrated the anticancer effects of FRA in the xenograft orthotopic mice model. They have proposed that the anticancer effects of FRA were achieved through autophagy flux. Targeting autophagy is recognized as a promising therapeutic strategy to overcome drug resistance and reduce metastasis in osteosarcoma (Liao et al., 2019). The study findings of He B. et al. would strengthen the idea of exploiting more plant natural compounds as potential novel antitumor therapeutics for osteosarcoma by targeting autophagy pathways.

Taken together, the current Research Topic provides multidirectional insights on plant-derived natural compounds-based research in stem cells.

## AUTHOR CONTRIBUTIONS

FF contributed to drafting the manuscript. All authors listed have made a substantial, direct, and intellectual contribution to the work and approved it for publication.

## FUNDING

HI was supported by the Japan Science and Technology Agency (JST); Science and Technology Research Partnership for Sustainable Development (SATREPS, Grant No. JPMJSA1506).

## ACKNOWLEDGMENTS

We would like to thank all the contributing authors for their outstanding work and all the reviewers for their valuable time, careful thoughts, and constructive suggestions to enrich these manuscripts. We also would like to sincerely thank the members of the editorial office of Frontiers in Cell and Developmental Biology for their support.

## REFERENCES

- Baptista, P., and Andrade, J. P. (2018). Adult Hippocampal Neurogenesis: Regulation and Possible Functional and Clinical Correlates. *Front. Neuroanat.* 12, 44. doi:10.3389/fnana.2018.00044
- Bejaoui, M., Ferdousi, F., Zheng, Y.-W., Oda, T., and Isoda, H. (2021). Regulating Cell Fate of Human Amnion Epithelial Cells Using Natural Compounds: an Example of Enhanced Neural and Pigment Differentiation by 3,4,5-Tri-O-Caffeoylquinic Acid. *Cell Commun. Signal* 19 (1), 26. doi:10.1186/s12964-020-00697-5
- Chen, K. G., Mallon, B. S., McKay, R. D. G., and Robey, P. G. (2014). Human Pluripotent Stem Cell Culture: Considerations for Maintenance, Expansion, and Therapeutics. *Cell stem Cell* 14 (1), 13–26. doi:10.1016/j.stem.2013.12.005
- Ferdousi, F., and Isoda, H. (2022). Regulating Early Biological Events in Human Amniotic Epithelial Stem Cells Using Natural Bioactive Compounds: Extendable Multidirectional Research Avenues. *Front. Cell Dev. Biol.* 10, 865810. doi:10.3389/fcell.2022.865810
- Ferdousi, F., Kondo, S., Sasaki, K., Uchida, Y., Ohkohchi, N., Zheng, Y.-W., et al. (2020). Microarray Analysis of Verbenalin-Treated Human Amniotic Epithelial Cells Reveals Therapeutic Potential for Alzheimer's Disease. *Aging* 12 (6), 5516–5538. doi:10.18632/aging.102985
- Ferdousi, F., Sasaki, K., Uchida, Y., Ohkohchi, N., Zheng, Y.-W., and Isoda, H. (2019). Exploring the Potential Role of Rosmarinic Acid in Neuronal Differentiation of Human Amnion Epithelial Cells by Microarray Gene Expression Profiling. *Front. Neurosci.* 13, 779. doi:10.3389/fnins.2019.00779

- Gomes-Leal, W. (2021). Adult Hippocampal Neurogenesis and Affective Disorders: New Neurons for Psychic Well-Being. *Front. Neurosci.* 15, 712. doi:10.3389/fnins.2021.594448
- Guillamat-Prats, R. (2021). The Role of MSC in Wound Healing, Scarring and Regeneration. *Cells* 10 (7), 1729. doi:10.3390/cells10071729
- Kubo, C., Ogawa, M., Uehara, N., and Katakura, Y. (2020). Fisetin Promotes Hair Growth by Augmenting TERT Expression. *Front. Cell Dev. Biol.* 8, 566617. doi:10.3389/fcell.2020.566617
- Laustriat, D., Gide, J., and Peschanski, M. (2010). Human Pluripotent Stem Cells in Drug Discovery and Predictive Toxicology. *Biochem. Soc. Trans.* 38(4), 1051–1057. doi:10.1042/BST0381051
- Liao, Y. X., Yu, H. Y., Lv, J. Y., Cai, Y. R., Liu, F., He, Z. M., et al. (2019). Targeting Autophagy Is a Promising Therapeutic Strategy to Overcome Chemoresistance and Reduce Metastasis in Osteosarcoma. *Int. J. Oncol.* 55 (6), 1213–1222. doi:10.3892/ijo.2019.4902
- Mazini, L., Rochette, L., Admou, B., Amal, S., and Malka, G. (2020). Hopes and Limits of Adipose-Derived Stem Cells (ADSCs) and Mesenchymal Stem Cells (MSCs) in Wound Healing. *Ijms* 21 (4), 1306. doi:10.3390/ijms21041306
- McNeish, J. (2004). Embryonic Stem Cells in Drug Discovery. *Nat. Rev. Drug Discov.* 3 (1), 70–80. doi:10.1038/nrd1281
- Miki, T., Lehmann, T., Cai, H., Stolz, D. B., and Strom, S. C. (2005). Stem Cell Characteristics of Amniotic Epithelial Cells. *Stem cells* 23 (10), 1549–1559. doi:10.1634/stemcells.2004-0357
- Miki, T. (2018). Stem Cell Characteristics and the Therapeutic Potential of Amniotic Epithelial Cells. *Am. J. Reprod. Immunol.* 80 (4), e13003. doi:10.1111/aji.13003
- Mu, Y., and Gage, F. H. (2011). Adult Hippocampal Neurogenesis and its Role in Alzheimer's Disease. *Mol. Neurodegener.* 6 (1), 85–89. doi:10.1186/1750-1326-6-85
- Murphy, S., Rosli, S., Acharya, R., Mathias, L., Lim, R., Wallace, E., et al. (2010). Amnion Epithelial Cell Isolation and Characterization for Clinical Use. *Curr. Protoc. Stem Cell Biol.* 13 (1), 1E 6 1–1E 6 25. doi:10.1002/9780470151808.sc01e06s13
- Park, S., and Lee, J. (2021). Modulation of Hair Growth Promoting Effect by Natural Products. *Pharmaceutics* 13 (12), 2163. doi:10.3390/pharmaceutics13122163
- Rubin, L. L., and Haston, K. M. (2011). Stem Cell Biology and Drug Discovery. *BMC Biol.* 9 (1), 42–11. doi:10.1186/1741-7007-9-42
- Sasikumar, P., Aswathy, M., Prem, P. T., Radhakrishnan, K. V., and Chakrapani, P. S. B. (2022). Plant Derived Bioactive Compounds and Their Potential to Enhance Adult Neurogenesis. *Phytomedicine Plus* 2 (1), 100191.
- Spanova, M., and Daum, G. (2011). Squalene - Biochemistry, Molecular Biology, Process Biotechnology, and Applications. *Eur. J. Lipid Sci. Technol.* 113 (11), 1299–1320. doi:10.1002/ejlt.201100203
- Toda, T., Parylak, S. L., Linker, S. B., and Gage, F. H. (2019). The Role of Adult Hippocampal Neurogenesis in Brain Health and Disease. *Mol. Psychiatry* 24 (1), 67–87. doi:10.1038/s41380-018-0036-2
- Udalamaththa, V. L., Jayasinghe, C. D., and Udagama, P. V. (2016). Potential Role of Herbal Remedies in Stem Cell Therapy: Proliferation and Differentiation of Human Mesenchymal Stromal Cells. *Stem Cell Res. Ther.* 7 (1), 110. doi:10.1186/s13287-016-0366-4
- Wei, B., and Lu, J. (2021). Characterization of Tendon-Derived Stem Cells and Rescue Tendon Injury. *Stem Cell Rev Rep* 17 (5), 1534–1551. doi:10.1007/s12015-021-10143-9
- Xu, Z., Liu, C., Wang, R., Gao, X., Hao, C., and Liu, C. (2021). A Combination of Lycopene and Human Amniotic Epithelial Cells Can Ameliorate Cognitive Deficits and Suppress Neuroinflammatory Signaling by Choroid Plexus in Alzheimer's Disease Rat. *J. Nutr. Biochem.* 88, 108558. doi:10.1016/j.jnutbio.2020.108558
- Zhang, E., Shen, J., and So, K. F. (2014). Chinese Traditional Medicine and Adult Neurogenesis in the hippocampus. *J. traditional complementary Med.* 4 (2), 77–81. doi:10.4103/2225-4110.130372

**Conflict of Interest:** The authors declare that the research was conducted in the absence of any commercial or financial relationships that could be construed as a potential conflict of interest.

**Publisher's Note:** All claims expressed in this article are solely those of the authors and do not necessarily represent those of their affiliated organizations, or those of the publisher, the editors and the reviewers. Any product that may be evaluated in this article, or claim that may be made by its manufacturer, is not guaranteed or endorsed by the publisher.

Copyright © 2022 Ferdousi, Sasaki, Xu, Zheng, Szele and Isoda. This is an open-access article distributed under the terms of the Creative Commons Attribution License (CC BY). The use, distribution or reproduction in other forums is permitted, provided the original author(s) and the copyright owner(s) are credited and that the original publication in this journal is cited, in accordance with accepted academic practice. No use, distribution or reproduction is permitted which does not comply with these terms.



# Recruitment of Mesenchymal Stem Cells to Damaged Sites by Plant-Derived Components

Akito Maeda\*

*Skin Regeneration, PIAS Collaborative Research, Graduate School of Pharmaceutical Science, Osaka University, Suita, Japan*

## OPEN ACCESS

### Edited by:

Hiroko Isoda,  
University of Tsukuba, Japan

### Reviewed by:

Philippe Bourin,  
Independent Researcher, Toulouse,  
France

Hojjat Naderi-Meshkin,  
Queen's University Belfast,  
United Kingdom

### \*Correspondence:

Akito Maeda  
maeda-aki@phs.osaka-u.ac.jp

### Specialty section:

This article was submitted to  
Stem Cell Research,  
a section of the journal  
*Frontiers in Cell and Developmental  
Biology*

**Received:** 27 March 2020

**Accepted:** 11 May 2020

**Published:** 09 June 2020

### Citation:

Maeda A (2020) Recruitment  
of Mesenchymal Stem Cells  
to Damaged Sites by Plant-Derived  
Components.  
*Front. Cell Dev. Biol.* 8:437.  
doi: 10.3389/fcell.2020.00437

Mesenchymal stem cells (MSCs) are capable of differentiating into a limited number of diverse cells and secrete regenerative factors that contribute to the repair of damaged tissue. In response to signals emitted by tissue damage, MSCs migrate from the bone marrow and area surrounding blood vessels within tissues into the circulating blood, and accumulate at the site of damage. Hence, MSC transplantation therapy is beginning to be applied to the treatment of various intractable human diseases. Recent medicinal plants studies have shown that plant-derived components can activate cell functions. For example, several plant-derived components activate cell signaling pathways, such as phosphatidylinositol 3-kinase and mitogen-activated protein kinase (MAPK), enhance expression of the CXCL12/CXCR4 axis, stimulate extracellular matrix remodeling, and consequently, promote cell migration of MSCs. Moreover, plant-derived components have been shown to promote recruitment of MSCs to damaged tissues and enhance healing in disease models, potentially advancing their therapeutic use. This article provides a comprehensive review of several plant-derived components that activate MSC migration and homing to damaged sites to promote tissue repair.

**Keywords:** mesenchymal stem cells, cell migration, plant-derived components, cell therapy, tissue repair

## INTRODUCTION

Mesenchymal stem cells (MSCs) are capable of differentiating into a limited yet diverse range of cells, and secrete regenerative factors that contribute to the repair of damaged tissues (Uccelli et al., 2008). MSCs in humans and animals have numerous characteristics, including the expression of specific cell surface markers, some of which are used as criteria for the detection of MSCs in tissues. The International Society for Cellular Therapy proposed that human MSCs should be identified according to positive expression for CD73, CD90, and CD105, and negative for CD11b or CD14, CD19 or CD79 $\alpha$ , CD34, CD45, and HLA-DR expression (Dominici et al., 2006). MSCs have been identified in several tissues, including the bone marrow, adipose tissue, cord blood, placenta, and pulp (Pittenger et al., 2019). MSCs have also been reported to migrate to wound sites during the healing process (Wu et al., 2010). Specifically, MSCs have been shown to move from the perivascular area of tissue into the blood circulation in response to signals emitted after tissue damage, and subsequently MSCs in the blood circulation may accumulate in damaged tissue (Rochefort et al., 2006; Iinuma et al., 2015). Thus, MSCs exhibit homing properties, which allows for their spontaneous accumulation at the site of injury.



It has been shown that methods capable of promoting the migration and homing of MSCs to damaged tissue enhance their effect in cell therapy (Park et al., 2015). These models have been reported to implement several approaches including the preconditioning of MSCs, recombinant MSCs, engineering of cell surface proteins of MSCs, and modification of target tissues (Becker and Riet, 2016). To assess MSC migration *in vitro*, either the Boyden chamber method or the Transwell method have been used, which examine movement between concentration gradients, created by separating active substances with a permeable membrane, or by the Scratch wound method using movement in two dimensions, respectively (Justus et al., 2014). Alternatively, for the detection of MSC migration *in vivo*, researchers have developed MSCs labeled with fluorescent dyes, magnetic substances, and radioactive substances, or genetically modified MSCs that express reporters, which are transplanted into a living organism (Krueger et al., 2018). Recently, several clinical trials using cell therapy to transfer exogenous MSCs into the body for treatment of various types of tissue damage and diseases, have demonstrated many advantages and are nearing completion [clinical trials databases: [www.clinicaltrials.gov](http://www.clinicaltrials.gov), 306 studies using MSCs with study completed status in February 2020]. The application of MSC therapy has been reported for a broad range of disorders, including various skin diseases, bone defects, cardiac disorders, and brain damage (Kim et al., 2017; Wang et al., 2018; Ward et al., 2018; Presen et al., 2019). In addition, advanced research has been conducted to develop MSCs as cell vectors for application in cancer treatment (Mohr and Zwacka, 2018). Therefore, new materials that enhance the recruitment of transplanted MSCs into damaged tissues, may further improve their therapeutic effect.

Cell migration is stimulated by chemokines, cytokines, growth factors, and other biomolecules, through a number of molecularly and pharmacologically defined signaling pathways (Marquez-Curtis and Janowska-Wieczorek, 2013). MSC migration has been shown to be activated by factors such as CXCL12 (SDF-1), MIP-1, HGF, VEGF, and PDGF. Moreover, specific signaling pathway molecules including CXCR4, phosphatidylinositol 3-kinase (PI3K), mitogen-activated protein kinase (MAPK), and small G proteins have been reported to be involved in the regulation of MSC migration. It has also been reported that hypoxic preconditioning stimulates the expression of genes involved in cell migration, thereby activating MSC migration (Rochefort et al., 2006; Meng et al., 2018). Upon reaching the target site, MSCs can degrade the intercellular matrix and use as a scaffold to migrate through tissue.

Medicinal plants have historically been used in folk medicine to relieve various symptoms and diseases. Studies of compounds derived from medicinal plants have shown that they can molecularly activate various functions in cells and tissues (Shedoeva et al., 2019). In fact, it has been reported that plant-derived components can activate signal transduction pathways related to cell motility (Cho et al., 2014). Although there are few reports concerning plant-related components involved in MSC migration, they represent a promising class of potential candidates to enhance the therapeutic effects of MSC therapy. Nevertheless, it has been reported that plant-derived components

activate MSC migration through specific signaling pathways, mobilize MSCs to injured organs, and have healing effects. Moreover, such information may be useful for identifying more effective chemical compounds in the future. Therefore, this article reviews plant-derived components that have been shown to activate MSC migration, and homing, to damaged sites in animal models, where they contribute to the healing process.

## ACTIVATION OF MSC MIGRATION BY PLANT-DERIVED COMPONENTS

Several studies have reported that plant-derived components promote MSC migration, which may contribute to healing of damaged tissue (Table 1). This effect is triggered by stimulating mechanisms involved in MSC migration (Figure 1 and Table 2). Below we discuss the implicated plant-derived components in detail.

### Protocatechuic Acid

The phenolic compound protocatechuic acid (PCA) has been isolated from a number of herbs and edible plants (Khan et al., 2015). PCA has been reported to have various pharmacological effects such as anti-oxidant, anti-inflammatory, anti-hyperglycemic, anti-apoptotic and antimicrobial activity. PCA has also been shown to inhibit the proliferation and migration of airway smooth muscle cells in tracheal inflammatory conditions (Liu Y. D. et al., 2019), while also suppressing the proliferation and migration of cardiac fibroblasts associated with p38 MAPK activation in a cardiac fibrosis model (Song and Ren, 2019).

Additionally, studies on MSC migration, using Transwell assays and gelatin-coated membranes, have shown that PCA isolated from the kernel of *Alpinia oxyphylla* (0.5 mM or more) enhanced adipose tissue-derived mesenchymal stem cell (AMSC) migration (Wang et al., 2008), which subsequently inhibited initiation of early apoptotic events. Furthermore, following PCA treatment, cell morphology and surface markers remained unchanged, and AMSCs retained their osteocyte, adipocyte, and cardiomyocyte-like cell differentiation potential properties. Although PCA has been shown to stimulate AMSC proliferation, while retaining their functional pluripotency (Wang et al., 2009), it has also been reported that PCA has a stimulatory effect on osteocyte differentiation and a suppressive effect on adipocyte differentiation in mouse embryo-derived MSC (Rivera-Piza et al., 2017).

The mechanism associated with PCA-stimulated MSC migration involves an increase in the expression of membrane-type matrix metalloproteinase-1 (MT1-MMP) and activation of matrix metalloproteinase-2 (MMP-2) in AMSCs. Since it has been reported that PCA activates three MAPKs (extracellular signal-regulated kinase1/2; Erk1/2, c-Jun N-terminal kinase; JNK and p38), which in turn activate the MMP signal in Schwann cell migration (Ju et al., 2015), PCA may serve to activate MAPKs involved in upstream signaling of MT1-MMP and MMP2 during AMSC migration. However, further studies are required to verify whether various doses of PCA activate MAPKs and promote

**TABLE 1** | Plant-derived components promote MSC migration and healing in animal models.

Component	MSC source	Assessment of MSC migration	Therapeutic model and Administration method	References
Protocatechuic acid (PCA)	AMSC	Transwell method	–	Wang et al., 2008
Cinnamtannin B-1	BMSC	Boyden chamber method, FACS analysis for MSC marker, Detection of luc-expressing MSC	Transdermal administration to the mouse model of skin wound healing	Fujita et al., 2015
Cannabinoids	AMSC, BMSC	Boyden chamber method, Immunofluorescent analysis of MSC	Implantation of the component-loaded microspheres in the rat model of bone-defect	Schmuhl et al., 2014; Kamali et al., 2019
Icariin (ICA)	BMSC	Transwell method, Scratch wound method, Detection of BrdU-labeled MSC	Preconditioning MSCs were injected intravenously into the rabbit model of cartilage-defect	Jiao et al., 2018; Zhu et al., 2018
Tanshinone IIA (Tan IIA)	BMSC	Transwell method, Detection of Dil-labeled MSC	Oral administration to the rat model of acute myocardial infarction	Tong et al., 2011
Astragaloside IV (AS IV)	BMSC	Transwell method, Detection of Dio-labeled MSC	Preconditioning MSCs were injected intravenously into the rat model of acute myocardial infarction	Xie et al., 2013
Tetramethylpyrazine (TMP)	BMSC	Transwell method, Detection of BrdU-labeled MSC	Preconditioning MSCs were injected intravenously into the rat model of cerebral ischemia, or Intraperitoneal administration to the model	Li et al., 2017a, 2019
Guanxin danshen formulation (GXDS) (Including Tanshinone IIA)	BMSC	Detection of GFP-expressing MSC	Oral administration to the rat model of acute myocardial infarction	Han et al., 2019

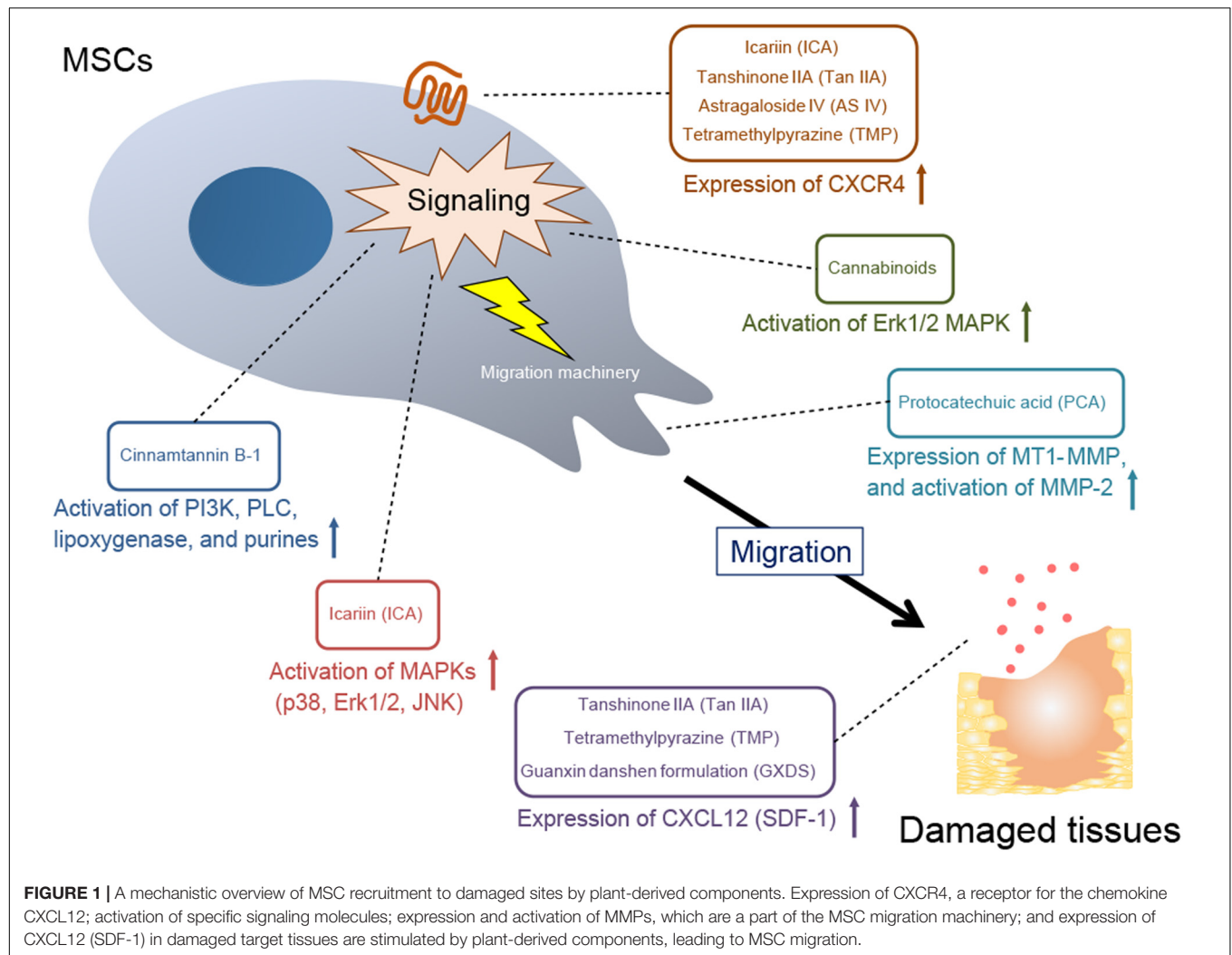


**TABLE 2 |** Plant-derived components stimulate signaling for MSC migration.

Component	MSC source	Effects on MSC migration	References
Protocatechuic acid (PCA)	AMSC	Expression of MT1-MMP, and activation of MMP-2	Wang et al., 2008
Cinnamtannin B-1	BMSC	Activation of PI3K, PLC, lipoxygenase, and purines	Fujita et al., 2015
Cannabinoids	AMSC	Activation of Erk1/2 MAPK	Schmuhl et al., 2014
Icariin (ICA)	BMSC	Activation of MAPKs (p38, Erk1/2, JNK), and Expression of CXCR4	Jiao et al., 2018; Zhu et al., 2018
Tanshinone IIA (Tan IIA)	BMSC	Expression of CXCL12 (SDF-1) in target tissue, and CXCR4 in MSCs	Tong et al., 2011
Astragaloside IV (AS IV)	BMSC	Expression of CXCR4	Xie et al., 2013
Tetramethylpyrazine (TMP)	BMSC	Expression of CXCL12 (SDF-1) in target tissue, and CXCR4 in MSCs	Li et al., 2017a, 2019
Guanxin danshen formulation (GXDS) (Including Tanshinone IIA)	BMSC	Expression of CXCL12 (SDF-1) in target tissue	Han et al., 2019

migration of MSCs. MMPs play a key role in AMSC entry and migration through extracellular matrix (ECM) barriers, such as the basement membrane (Nitzsche et al., 2017). In the process of cell migration across the ECM barrier, PCA-stimulated AMSCs may promote pericellular ECM degradation by MMPs, thereby partially promoting cell migration. These studies provide evidence for the mechanism by which PCA may facilitate MSC migration to organs in MSC therapy.

## Cinnamtannin B-1

Cinnamtannin B-1 is a proanthocyanidin found in specific plants such as *Cinnamomum zeylanicum* (Sánchez-Rubio et al., 2018). Cinnamtannin B-1 exhibits anti-inflammatory, anti-oxidant and anti-thrombotic properties (López et al., 2008), and also protects neurons from ischemia/reperfusion-induced dysfunction (Chi et al., 2013), while inhibiting survival of cancer cells (Carriere et al., 2018), and protecting pancreatic acinar cells during pancreatitis (Rivera-Barreno et al., 2010).

*Mallotus philippinensis* bark extract also contains cinnamtannin B-1 (Furumoto et al., 2014). The use of this extract has been shown to increase migration of bone marrow-derived mesenchymal stem cells (BMSCs) and enhance wound healing in a mouse model (Furumoto et al., 2014). In fact, the efficacy of the extract on BMSC migration has been shown to be higher in comparison to other skin cell types. Histopathological features observed upon treatment with the extract indicated tissue repair by enhancement of angiogenesis and granulation tissue. *Mallotus philippinensis* fruit glandular hair also promoted wound healing via anti-oxidant and anti-inflammatory activity in a rat model (Gangwar et al., 2015).

Cinnamtannin B-1 has also been shown to promote BMSC migration when administered within the range of 0.8–2 µg/ml, and enhanced wound healing in a mouse model following topical administration (1.2 and 2.4 µg/wound) (Fujita et al., 2015). Further, examination of BMSC recruitment in blood circulation via cell marker analysis showed that mobilization of endogenous MSCs into the blood increased following cinnamtannin B-1 treatment. Image analysis of an animal model implanted with luciferase-expressing BMSC indicated that cinnamtannin B-1 increased BMSC accumulation at the wound site and promoted wound healing. Furthermore, cinnamtannin B-1-induced BMSC migration was attenuated by inhibitors of PI3K, phospholipase C (PLC), lipoxygenase (LOX), and

purine, implicating the associated signaling pathways in BMSC migration. In addition, morelloflavone, a biflavonoid constituent from *Garcinia vilseniana* Pierre with structural similarities to cinnamtannin B-1, also enhanced BMSC migration with a similar pharmacological profile (Karanjgaokar et al., 1967). Therefore, structurally related compounds may also be effective in treating skin wounds by inducing mobilization of BMSCs.

## Cannabinoid

Cannabinoids are chemical components found in cannabis plants, with more than 100 varieties (Grof, 2018). The two primary types include cannabidiol (CBD) and tetrahydrocannabinol (THC), with the latter serving as the primary psychoactive component. CB1, CB2, TRPV1 and orphan G protein-coupled receptor GPR55, have been reported to exist as endogenous cannabinoid receptors (Hryhorowicz et al., 2018). Cannabinoids have a variety of effects, in addition to their analgesic properties (Kaur et al., 2016). Specifically, cannabinoids inhibit the growth and migration of gliomas (Vaccani et al., 2005), inhibit inflammation via neutrophil recruitment (Schicho et al., 2011), promote wound healing through cell adhesion as well as migration of fibroblasts and keratinocytes (Wang et al., 2016; Liu C. et al., 2019), and promote bone formation by osteoblast regulation (Idris and Ralston, 2012).

It has also been reported that CBD, administered within the range of 0.01–3 µM, increased AMSC migration in a dose-dependent manner (Schmuhl et al., 2014). However, CBD-induced AMSC migration was antagonized by inhibition of the Erk1/2 MAPK pathway via attenuated Erk1/2 phosphorylation in the presence of a CB2 receptor antagonist and GRP55 agonist. Conversely, Erk1/2-dependent migratory effects were observed following stimulating with CB2 receptor agonist and GPR55 antagonist. Thus, the basis for CBD-induced MSC migration involves activation of CB2 or inhibition of GPR55, which subsequently activates Erk1/2. Furthermore, long-term treatment with CBD has been shown to differentiate AMSCs into osteoblasts (Schmuhl et al., 2014). Hence, prolonged incubation of AMSC with CBD may enhance bone regeneration. In fact, recently, using a bone deficient rat model, it was reported that microspheres supplemented with CBD promoted the recruitment of MSCs and regeneration of bone defects (Kamali et al., 2019).

Similarly, the major psychoactive component,  $\Delta^9$ -tetrahydrocannabinol ( $\Delta^9$ -THC), also increased AMSC

migration (Lüder et al., 2017). In the case of THC, migration of AMSCs is facilitated by CB1 through Erk1/2 activation, although THC has been reported to respond to both CB1 and CB2 (Pertwee, 2008). However, since cannabinoids can respond to many functional proteins, further research is needed to obtain a complete understanding of their pharmacological effects (Hryhorowicz et al., 2018).

## Icariin

Icariin (ICA) is a flavonoid glycoside isolated from *Epimedium* and is a primary component of the Chinese herb *Herba Epimedii* (Li et al., 2015). It has been reported that ICA possesses broad therapeutic activities, such as anti-oxidant, tonic, aphrodisiac, neuro-protective, cardio-protective, anti-rheumatic, anti-cancer, and anti-osteoporotic effects (Li et al., 2015). ICA has also been reported to promote BMSC proliferation, bone formation, and chondrogenic differentiation (Wang et al., 2014; Qin et al., 2015). Furthermore, treatment of AMSCs with ICA in a rat model of diabetes-related erectile dysfunction, protected against oxidative stress via PI3K signaling and improved AMSC survival, leading to enhanced therapeutic potential (Wang X. et al., 2017). Furthermore, combining ICA and MSCs was shown to promote angiogenesis and neurogenesis, as a result of increased production of VEGF and brain-derived neurotrophic factor (BDNF) through activation of PI3K and Erk1/2 MAPK, in an ischemic stroke rat model (Liu D. et al., 2018). ICA may also improve wound and periodontal pathology by promoting keratinocyte proliferation and migration, as well as by promoting survival and migration of periodontal ligament fibroblasts (Liu H. J. et al., 2018; Mi et al., 2018).

ICA administered at 1  $\mu$ M was reported to significantly increase BMSC migration by stimulating actin stress fiber formation (Jiao et al., 2018). MAPK signals, such as p38, Erk1/2 and JNK, were activated during BMSC migration following ICA stimulation. In the presence of MAPK inhibitors, BMSC migration was also inhibited, and actin stress fiber formation was abolished. Thus, ICA may promote BMSC migration by increasing actin stress fiber formation through MAPK signaling. ICA also promotes CXCR4 expression, which is a signaling molecule upstream of MAPK, in BMSC migration through the activation of hypoxia inducible factor-1 (HIF-1) (Zhu et al., 2018). Moreover, transplantation of ICA-treated BMSCs in a cartilage-deficient rabbit model, accelerated the migration of BMSCs to the cartilage-deficient region in comparison to non-treated BMSCs (Jiao et al., 2018). These results suggest that ICA-treated BMSC may be effective in treating cartilage defects.

## Tanshinone IIA

Tanshinone IIA (Tan IIA) is a diterpene quinone and one of the major active compounds of *Salvia miltiorrhiza* (Lamiaceae) (Ren et al., 2019). *Salvia miltiorrhiza* has been widely used as a herbal medicine in the clinical treatment of cardiovascular diseases (Li et al., 2018a). Tan IIA has anti-oxidant and anti-inflammatory properties as well as multiple pharmacological benefits such as cardio-protection, neuroprotection, vascular protection, and anti-cancer effects (Li et al., 2018a; Ren et al., 2019). As for cell

migration, Tan IIA has been shown to inhibit vascular endothelial cell proliferation and migration by inhibiting VEGF expression and its signaling pathways (Xing et al., 2015; Fan et al., 2017; Lee et al., 2017).

Tan IIA has been reported to have an effect on MSC differentiation including promoting osteogenic differentiation in BMSCs (Qian et al., 2015), cord blood MSCs (Heo et al., 2017), Wharton's jelly MSCs (Cabrera-Pérez et al., 2019), and periodontal ligament stem cells (Liu X. et al., 2019). In addition, Tan IIA effectively induced the differentiation of cord blood MSCs into liver cells in a rat model of cirrhosis (Yang et al., 2015), BMSCs into neuronal cells in a rat spinal cord injury model (Zhang et al., 2018), and placental MSCs into cardiomyocytes *in vitro* (Li K. et al., 2018). Furthermore, it has been reported that Tan IIA combined with MSC treatment exhibited a neuronal protective effect via suppression of neuronal apoptosis in a vascular dementia rat model (Kong et al., 2017), as well as by suppressing amyloid-related protein production and inflammation in an A $\beta$ 25-35-induced AD rat model (Huang et al., 2019).

Additionally, administration of 1–4  $\mu$ M Tan IIA has been shown to significantly enhance BMSC migration (Tong et al., 2011). In a rat model of acute myocardial infarction, oral administration of Tan IIA at 30 mg/kg/d combined with BMSC transplantation increased BMSC recruitment to the damaged area following myocardial infarction, resulting in restored normal function of the left ventricle (LV) systolic and end-diastolic pressure, as well as enhanced VEGF expression in the infarcted region. Immunological detection of the occlusion site also suggests that Tan IIA may promote CXCL12 expression in the infarcted area, while increasing CXCL12 levels in peripheral blood. However, Tan IIA-induced BMSC migration was inhibited by a CXCR4 blocker. Furthermore, Tan IIA treatment was shown to enhance CXCR4 expression in BMSCs. These results suggest that Tan IIA increases CXCL12 expression at the site of injury, and increases BMSC migration by enhancing CXCR4 expression in BMSCs. Thus, Tan IIA may be effective in treating ischemic heart disease by MSC therapy.

## Astragaloside IV

Astragaloside IV (AS IV) is an active saponin and the major active ingredient of *Astragalus membranaceus*, used in traditional Chinese medicine (Li et al., 2017b). *Astragalus membranaceus*, commonly used with *S. miltiorrhiza* including Tan IIA, is commonly used to enhance cardiovascular disease protection (Wang D. et al., 2017). Moreover, AS IV has demonstrated pharmacological action for cerebral injury, cardiovascular disease, liver, diabetic nephropathy, and cancer (Li et al., 2017b). It has also been shown to reduce infarct size and arrhythmias, while improving ventricular function in ischemic heart disease (Xu et al., 2007). In cell migration, AS IV treatment enhances the proliferation and migration of a human osteoblast-like cell line, which may be facilitated by activation of the Hedgehog signaling pathway (Guo et al., 2019). AS IV also inhibits proliferation and migration of human dermal vascular smooth muscle cells, stimulated by PDGF-BB secreted during vascular injury, through inhibition of p38 MAPK signaling (Chen et al., 2014). It has also



been reported that AS IV and Tan IIA promote tubular structure formation of BMSC-derived endothelial cell cells, similar to that of blood vessels, via the expression of connexins and cell connection (Li et al., 2018b).

Lastly, BMSCs stimulated with AS IV, administered at 0.4 µg/ml, was reported to increase CXCR4 expression, indicating that BMSC migration to its ligand CXCL12 was enhanced (Xie et al., 2013). In addition, this enhanced migration was suppressed by CXCR4 inhibitors. Additionally, in a rat model of acute myocardial infarction, BMSCs stimulated with AS IV displayed increased homing to ischemic myocardial sites, suggesting that AS IV enhances BMSC recruitment via increased CXCR4 expression. Although the effect of AS IV on MSC migration was not as strong as that observed with Tan IIA, when the two components are administered together, a synergistic enhancement of BMSC migration was observed, hence this combinatorial strategy may increase the efficacy of MSC transplant therapy.

## Tetramethylpyrazine

Tetramethylpyrazine (TMP) is pyrazine and an alkaloid isolated from Rhizoma Chuanxiong (*Ligusticum wallichii*) (Zhao et al., 2016). TMP functions as a neuro-protective, anti-apoptotic, anti-cancer, vasodilator, and anti-inflammatory agent (Zhao et al., 2016). With respect to cell migration, TMP increases brain microvascular endothelial cell proliferation and migration by partially increasing VEGF secretion (Zhang et al., 2014), and promoting migration of the neural progenitor by inducing CXCL12 expression through activation of the PI3K pathway (Kong et al., 2016). Alternatively, TMP inhibits the migration of neutrophils activated by inflammation in a rat cerebral ischemia model, which was reported to involve Akt and Erk signaling (Chang et al., 2015).

TMP was also shown to enhance growth and neuronal differentiation of BMSCs. Further, it was suggested to have anti-aging effects on the nervous system (Song et al., 2019). A Chinese therapy, the Jiuxin pill, containing TMP and borneol, is known to promote exosome secretion from cardiac MSCs, which may have a positive therapeutic effect on heart disease (Ruan et al., 2018). In MSC migration, pretreatment with 10–200 µM TMP causes increased BMSC migration in a dose-dependent manner (Li et al., 2017a). TMP also promoted CXCR4 expression, which was inhibited by a CXCR4 blocker. Intravenous administration of TMP-pretreated BMSCs into a cerebral ischemic rat model demonstrated improved neurological function and enhanced recruitment of BMSCs to cerebral ischemic sites. In addition, angiogenesis and the expression of both CXCL12 and CXCR4 were promoted at the ischemia site. In a separate study, the combination of transplanted BMSCs and intraperitoneal administration of TMP (40 mg/kg/d) in a cerebral ischemia model not only promoted the CXCL12/CXCR4 axis, but also regenerated blood vessels and nerves via enhancement of VEGF and BDNF expression, leading to functional recovery (Li et al., 2019). Taken together, these results show that the combination of MSCs and TMP may contribute to CXCL12/CXCR4 axis augmentation and neuronal regeneration, suggesting that they may be effective in treating cerebral ischemic injury.

## Guanxin Danshen Formulation

Guanxin Danshen (GXDS), a Chinese herbal medicine, is an effective formulation for the treatment of ischemic heart diseases (Deng et al., 2017). The GXDS formulation is comprised of three materials: *Salvia miltiorrhiza* (Lamiaceae), *Panax notoginseng* (Lamiaceae), and *Dalbergia odorifera* (Fabaceae). It contains Tanshinone IIA, salvianolic acid B (Wang et al., 2013), ginsenoside Rb1, ginsenoside RG1, notoginsenoside R1 (Wan et al., 2007), and flavanols (Liu et al., 2005).

GXDS has also proven effective in MSC treatments. For instance, oral administration of GXDS (100 mg/kg/d) in combination with BMSC transplantation in a rat model of acute myocardial infarction improved cardiac function of the LV ejection fraction, LV fractional shortening, and LV end-systolic volume (Han et al., 2019). In addition, GXDS administration in combination with BMSC transplantation not only reduced cell apoptosis detected by TUNEL staining, but also enhanced peri- and infarcted angiogenesis, increased local CXCL12 expression and the number of BMSCs homing to the infarcted area, while also reducing the size of the myocardial infarction region. Therefore, it is suggested that GXDS increases the migration of MSCs by up-regulating the expression of CXCL12 at the site of infarction. However, since this formulation may contain Tan IIA, it is possible that this component could have contributed to the observed effects (Tong et al., 2011). Nevertheless, the combination of GXDS and MSC therapy has the potential to improve ischemic heart disease, including myocardial infarction.

Moreover, other Chinese herbal extracts have been shown to stimulate MSC migration. For example, oily extract from *Catharmus tinctorius* (1–50 µg/ml) promotes rat BMSC migration through Rho-associated protein kinase 2 (ROCK2) signaling *in vitro* (Liu X. et al., 2019). In addition, Bushen Huoxue decoction (100 µg/ml), a mixture comprised of eleven Chinese herbs, increase rat BMSC migration *in vitro* by regulating MiR-539-5p miRNA (Hu et al., 2019) and activating Wnt5a-related cell motility (Shen et al., 2018). Despite these observations, none of the individual compounds responsible have been identified from these extracts.

## DISCUSSION

This article focused on a comprehensive review of plant-derived components that increase MSC migration and promote recovery from tissue damage. Studies on the promotion of MSC migration by plant-derived components have exposed a variety of characteristics and advantages (Tables 1, 2). For example, although PCA was only found to be effective at high doses, its potential has been demonstrated and has been suggested to function by increasing the expression and activation of MMPs, which then degrade the ECM to enhance MSC invasion into tissues (Wang et al., 2008). Studies on cinnamtannin B-1 have shown that structurally related flavonoids also have MSC migration activity (Fujita et al., 2015). Thus, expanding upon this structural framework offers the potential to develop more active compounds through structure-based drug development. Since CBD, a non-psychoactive cannabinoid, can promote MSC

**TABLE 3 |** Therapeutic effects of plant-derived components and their effects on MSCs.

Component	Plant	Therapeutic effects of component	Effects of component on MSC	Therapeutic model by component and MSC transplantation
Protocatechuic acid (PCA)	<i>Alpinia oxyphylla</i> (Zingiberaceae) Khan et al., 2015	Anti-oxidant, Anti-inflammatory, Anti-hyperglycemic, Anti-apoptotic, Antimicrobial Khan et al., 2015, Inhibition of the proliferation and migration of airway smooth muscle cells in tracheal inflammatory conditions Liu Y. D. et al., 2019, Suppression of the proliferation and migration of cardiac fibroblasts in a cardiac fibrosis Song and Ren, 2019, Activation of the MMP signal in Schwann cell migration Ju et al., 2015	Migration Wang et al., 2008, Proliferation Wang et al., 2009, Stimulatory on osteocyte differentiation and suppressive on adipocyte differentiation Rivera-Piza et al., 2017	–
Cinnamtannin B-1	<i>Mallotus philippinensis</i> (Euphorbiaceae) Furumoto et al., 2014	Anti-oxidant, Anti-inflammatory, Anti-thrombotic López et al., 2008, Neuro-protective Chi et al., 2013, Pancreatic-protective Rivera-Barreno et al., 2010, Anti-cancer Carriere et al., 2018, Wound healing Gangwar et al., 2015	Migration Furumoto et al., 2014; Fujita et al., 2015	Wound healing Fujita et al., 2015
Cannabinoids	<i>Cannabis sativa</i> (Cannabaceae) Grof, 2018	Analgesic effects Kaur et al., 2016, Anti-inflammatory Schicho et al., 2011, Anti-gliomas Vaccani et al., 2005, Wound healing Wang et al., 2016; Liu C. et al., 2019, Bone formation Idris and Ralston, 2012	Migration Schmuhl et al., 2014; Lüder et al., 2017, Osteocyte differentiation Schmuhl et al., 2014	Bone-defect Kamali et al., 2019
Icariin (ICA)	<i>Epimedium</i> (Berberidaceae) Li et al., 2015	Anti-oxidant, Tonic, Aphrodisiac, Neuro-protective, Cardio-protective, Anti-rheumatic, Anti-cancer, Anti-osteoporotic Li et al., 2015, Wound healing by effects for keratinocyte proliferation and migration Mi et al., 2018, Improvement of periodontal pathology by effects for survival and migration of periodontal ligament fibroblasts Liu H. J. et al., 2018	Migration Jiao et al., 2018; Zhu et al., 2018, Proliferation, Osteocyte differentiation Qin et al., 2015, Chondrogenic differentiation Wang et al., 2014, Cell survival Wang X. et al., 2017, Neuronal regeneration in cooperation with MSCs Liu D. et al., 2018	Cartilage-defect Jiao et al., 2018, Diabetes-associated erectile dysfunction Wang X. et al., 2017, Cerebral ischemia Liu D. et al., 2018
Tanshinone IIA (Tan IIA)	<i>Salvia miltiorrhiza</i> (Lamiaceae) Ren et al., 2019	Anti-oxidant, Anti-inflammatory, Cardio-protective, Neuro-protective, Vascular-protective, Anti-cancer Li et al., 2018a; Ren et al., 2019 Inhibition of vascular endothelial cell proliferation and migration in angiogenesis-related pathologies Xing et al., 2015; Fan et al., 2017; Lee et al., 2017	Migration Tong et al., 2011, Osteogenic differentiation Qian et al., 2015; Heo et al., 2017; Cabrera-Pérez et al., 2019; Liu X. et al., 2019, Hepatocyte differentiation Yang et al., 2015, Neuronal differentiation Zhang et al., 2018, Cardiomyocyte differentiation Li K. et al., 2018, Neuro-protection in cooperation with MSCs Kong et al., 2017; Huang et al., 2019	Acute myocardial infarction Tong et al., 2011 Liver cirrhosis Yang et al., 2015, Spinal cord injury Zhang et al., 2018, Vascular dementia Kong et al., 2017, Aβ25-35-induced AD Huang et al., 2019
Astragaloside IV (AS IV)	<i>Astragalus membranaceus</i> (Leguminosae) Li et al., 2017b	Anti-oxidant, Anti-inflammatory, Cardio-protective, Neuro-protective, Hepato-protective, Nephro-protective, Anti-cancer Li et al., 2017b, Improvement of ventricular function in ischemic heart disease Xu et al., 2007, Enhancement of the proliferation and migration of a human osteoblast-like cell Guo et al., 2019, Inhibition of the abnormal proliferation and migration of human dermal vascular smooth muscle cells Chen et al., 2014	Migration Xie et al., 2013, Angiogenesis of MSC-derived endothelial cell-like cells by co-stimulation with Tan IIA Li et al., 2018b	Acute myocardial infarction Xie et al., 2013

(Continued)

TABLE 3 | Continued

Component	Plant	Therapeutic effects of component	Effects of component on MSC	Therapeutic model by component and MSC transplantation
Tetramethylpyrazine (TMP)	Rhizoma Chuanxiong (Ligusticum wallichii) Zhao et al., 2016	Anti-oxidant, Anti-inflammatory, Neuro-protective, Anti-apoptotic, Anti-cancer, Vasodilator Zhao et al., 2016, Increase of brain microvascular endothelial cell proliferation and migration Zhang et al., 2014, Promotion of migration of the neural progenitor Kong et al., 2016, Inhibition of the migration of neutrophils activated by inflammation Chang et al., 2015.	Migration Li et al., 2017a, 2019, Neuronal differentiation Song et al., 2019, Jiuxin pill containing TMP promotes exosome secretion from MSCs Ruan et al., 2018 Angiogenesis in cooperation with MSCs Li et al., 2017a, 2019 Neurogenesis in cooperation with MSCs Li et al., 2019	Cerebral ischemia Li et al., 2017a, 2019
Guanxin danshen formulation (GXDS) (Including Tanshinone IIA)	Salvia miltiorrhiza (Lamiaceae), Panax notoginseng (Lamiaceae), Dalbergia odorifera (Fabaceae) Deng et al., 2017	Cardio-protective Deng et al., 2017	Migration Han et al., 2019	Acute myocardial infarction Han et al., 2019

migration and bone differentiation, and is currently being therapeutically developed, for example in sustained-release drugs from the encapsulated microspheres of biodegradable polymers, it represents a potentially advanced option for bone repair (Schmuhl et al., 2014; Kamali et al., 2019). ICA, when used to pretreat MSCs, promote their migration to cartilage-defect sites (Jiao et al., 2018; Zhu et al., 2018), as well as their proliferation (Qin et al., 2015), bone differentiation (Li et al., 2015), and cartilage differentiation (Wang et al., 2014), and thus, may significantly improve healing related to skeletal defects. Tan IIA has been shown to increase CXCL12 expression at the site of injury as well as CXCR4 on transplanted MSCs, leading to enhanced MSC migration to the injured area, which may prove effective in the treatment of ischemic heart disease (Tong et al., 2011). Interestingly, AS IV and Tan IIA were found to synergistically enhance MSC migration, thus presenting potential for combined therapeutic approaches involving plant-derived components (Xie et al., 2013). The use of TMP in combination with MSCs, or as a pretreatment agent, not only promotes the migration of MSCs to the site of injury, but also enhances the effect of MSCs on the regeneration of nerves and blood vessels (Li et al., 2017a, 2019). Consequently, TMP has potential for the treatment of cerebral ischemia damage. Finally, GXDS, when administered orally, in combination with MSC transplantation, may improve acute myocardial infarction by reducing apoptosis at the site of injury, generating new blood vessels, and promoting MSC migration by increasing CXCL12 expression (Han et al., 2019).

The diverse array of mechanisms by which plant-derived components facilitate MSC migration include ECM remodeling, activation of intracellular signaling pathways, such as PI3K and MAPK, and enhanced expression of the CXCL12/CXCR4 axis (Figure 1 and Table 2). The plants from which these compounds have been isolated have been used in traditional medicine practices and as such, a significant amount of useful information is available with regard to their use in several indications. Many associated factors have already been analyzed in detail, including their identification, structural classification and therapeutic

efficacy. Since each plant-derived component exhibits therapeutic effects in specific conditions, the disease models are designed based on the indication of the components, expecting the synergistic effects in MSC therapy (Table 3). Consequently, these disease models have demonstrated the benefits of MSC treatment as well as the additional therapeutic effects of many plant-derived components. Furthermore, medicinal plants have many uses and often have the advantage of being administered orally. The methods of administering plant-derived components *in vivo* for MSC migration enhancement include MSC pretreatment, as well as transdermal, intravenous, intraperitoneal and oral approaches.

Mesenchymal stem cells are believed to play an important role in tissue regeneration after organ damage, and MSC-based therapeutic approaches have been implemented in a variety of disease models (Pittenger et al., 2019). Methods to control the kinetics of transplanted MSCs can be very useful in a variety of applications, including organ regeneration, protection from tissue damage, and treatment of refractory cancers (Park et al., 2015; Becker and Riet, 2016). Herein, we have provided a comprehensive review of plant-derived components that control the migration of MSCs, and may offer novel therapeutic options for regenerative medicine.

## Challenges and Future Prospects

Currently, a gap exists between cell-level migration and *in vivo* recruitment. Additionally, several issues have been described including, how to achieve specificity and effective dosing for MSC *in vivo*, how to confirm component toxicity, and how to address the limitations of MSC dynamic tracking technology *in vivo* for cell kinetic analysis of MSC transplant (Krueger et al., 2018). To solve these issues, tests for drug development must determine the tissue specificity and effective dose of each component *in vivo*, as well as analyze individual toxicity.

As a supplement to cell dynamic analysis, it is also necessary to accumulate omics information on the effects of plant-derived components on MSC mobilization in disease models. For example, with the progress of MSC research, analysis of

single cells using techniques such as RNA-Seq, will allow for examination of detailed cellular functions along with the MSC fates at the genetic level (Liu S. et al., 2019). Moreover, the effects and suitability of plant-derived components in various MSCs at the genetic level may be elucidated. Furthermore, it has been shown that exosomes secreted by MSCs have a healing effect, and contain a large number of biomolecules such as miRNAs, cytokines, growth factors and enzymes, thereby demonstrating that advances are being made in defining the molecular basis for the therapeutic action of MSCs (Yin et al., 2019).

## CONCLUSION

Plant-derived components, which promote MSC migration, accelerate the healing of tissue damage. Moreover, MSC migration by plant-derived components may be mediated by signaling molecules such as CXCL12/CXCR4, PI3K, MAPK, and MMPs. Ingredients derived from medicinal plants are useful as there already exists invaluable information on medicinal plants for traditional use. In addition, the structural characteristics of plant-derived components are important to understand their

effect on MSC migration activity, and may be potential seeds for drug discovery. Therefore, plant-derived components that enhance MSC recruitment to damaged sites may provide novel tools for improved treatment approaches.

## AUTHOR CONTRIBUTIONS

AM contributed to the design and implementation of the research and writing of the manuscript.

## FUNDING

This work was supported by Budget for Joint Research at the Osaka University (J170901076).

## ACKNOWLEDGMENTS

We would like to thank Editage (www.editage.com) for English language editing.

## REFERENCES

- Becker, A. D., and Riet, I. V. (2016). Homing and migration of mesenchymal stromal cells: how to improve the efficacy of cell therapy? *World J. Stem Cells* 8, 73–87. doi: 10.4252/wjsc.v8.i3.73
- Cabrera-Pérez, R., Monguió-Tortajada, M., Gámez-Valero, A., Rojas-Márquez, R., Borrás, F. E., Roura, S., et al. (2019). Osteogenic commitment of Wharton's jelly mesenchymal stromal cells: mechanisms and implications for bioprocess development and clinical application. *Stem Cell. Res. Ther.* 10:356. doi: 10.1186/s13287-019-1450-3
- Carriere, P. P., Kapur, N., Mir, H., Ward, A. B., and Singh, S. (2018). Cinnamtannin B-1 inhibits cell survival molecules and induces apoptosis in colon cancer. *Int. J. Oncol.* 53, 1442–1454. doi: 10.3892/ijo.2018.4489
- Chang, C. Y., Kao, T. K., Chen, W. Y., Ou, Y. C., Li, J. R., Liao, S. L., et al. (2015). Tetramethylpyrazine inhibits neutrophil activation following permanent cerebral ischemia in rats. *Biochem. Biophys. Res. Commun.* 463, 421–427. doi: 10.1016/j.bbrc.2015.05.088
- Chen, Z., Cai, Y., Zhang, W., Liu, X., and Liu, S. (2014). Astragaloside IV inhibits platelet-derived growth factor-BB-stimulated proliferation and migration of vascular smooth muscle cells via the inhibition of p38 MAPK signaling. *Exp. Ther. Med.* 8, 1253–1258. doi: 10.3892/etm.2014.1905
- Chi, Z., Ma, X., Cui, G., Li, M., and Li, F. (2013). Cinnamtannin B-1 regulates cell proliferation of spinal cord astrocytes and protects the cell from oxygen-glucose-serum deprivation/reoxygenation-induced apoptosis. *Int. J. Mol. Sci.* 14, 15827–15837. doi: 10.3390/ijms140815827
- Cho, M., Yoon, H., Park, M., Kim, Y. H., and Lim, Y. (2014). Flavonoids promoting HaCaT migration: I. Hologram quantitative structure-activity relationships. *Phytomedicine* 21, 560–569. doi: 10.1016/j.phymed.2013.10.006
- Deng, X., Xing, X., Sun, G., Xu, X., Wu, H., Li, G., et al. (2017). Guanxin Danshen formulation protects against myocardial ischemia reperfusion injury-induced left ventricular remodeling by upregulating estrogen receptor  $\beta$ . *Front. Pharmacol.* 8:777. doi: 10.3389/fphar.2017.00777
- Dominici, M., Le Blanc, K., Mueller, I., Slaper-Cortenbach, I., Marini, F., Krause, D., et al. (2006). Minimal criteria for defining multipotent mesenchymal stromal cells. the international society for cellular therapy position statement. *Cytotherapy* 8, 315–317. doi: 10.1080/14653240600855905
- Fan, K., Li, S., Liu, G., Yuan, H., Ma, L., and Lu, P. (2017). Tanshinone IIA inhibits high glucose-induced proliferation, migration and vascularization of human retinal endothelial cells. *Mol. Med. Rep.* 16, 9023–9028. doi: 10.3892/mmr.2017.7743
- Fujita, K., Kuge, K., Ozawa, N., Sahara, S., Zaiki, K., Nakaoji, K., et al. (2015). Cinnamtannin B-1 promotes migration of mesenchymal stem cells and accelerates wound healing in mice. *PLoS One* 10:e0144166. doi: 10.1371/journal.pone.0144166
- Furumoto, T., Ozawa, N., Inamia, Y., Toyoshima, M., Fujita, K., Zaiki, K., et al. (2014). *Mallotus philippinensis* bark extracts promote preferential migration of mesenchymal stem cells and improve wound healing in mice. *Phytomedicine* 21, 247–253. doi: 10.1016/j.phymed.2013.09.003
- Gangwar, M., Gautam, M. K., Ghildiyal, S., Nath, G., and Goel, R. K. (2015). *Mallotus philippinensis* Muell. Arg fruit glandular hairs extract promotes wound healing on different wound model in rats. *BMC Complement. Altern. Med.* 15:123. doi: 10.1186/s12906-015-0647-y
- Grof, C. P. L. (2018). *Cannabis*, from plant to pill. *Br. J. Clin. Pharmacol.* 84, 2463–2467. doi: 10.1111/bcp.13618
- Guo, L. H., Cao, Y., Zhuang, R. T., Han, Y., and Li, J. (2019). Astragaloside IV promotes the proliferation and migration of osteoblast-like cells through the hedgehog signaling pathway. *Int. J. Mol. Med.* 43, 830–838. doi: 10.3892/ijmm.2018.4013
- Han, X. J., Li, H., Liu, C. B., Luo, Z. R., Wang, Q. L., Mou, F. F., et al. (2019). Guanxin Danshen formulation improved the effect of mesenchymal stem cells transplantation for the treatment of myocardial infarction probably via enhancing the engraftment. *Life Sci.* 233:116740. doi: 10.1016/j.lfs.2019.116740
- Heo, J. S., Lee, S. G., and Kim, H. O. (2017). Distal-less homeobox 5 is a master regulator of the osteogenesis of human mesenchymal stem cells. *Int. J. Mol. Med.* 40, 1486–1494. doi: 10.3892/ijmm.2017.3142
- Hryhorowicz, S., Walczak, M., Zakerska-Banaszak, O., Slomski, R., and Skrzypczak-Zielinska, M. (2018). Pharmacogenetics of cannabinoids. *Eur. J. Drug Metab. Pharmacokinet.* 43:1. doi: 10.1007/s13318-017-0416-z
- Hu, L., Liu, Y., Wang, B., Wu, Z., Chen, Y., Yu, L., et al. (2019). MiR-539-5p negatively regulates migration of rMSCs induced by Bushen Huoxue decoction through targeting Wnt5a. *Int. J. Med. Sci.* 16, 998–1006. doi: 10.7150/ijms.33437
- Huang, N., Li, Y., Zhou, Y., Zhou, Y., Feng, F., Shi, S., et al. (2019). Neuroprotective effect of tanshinone IIA-incubated mesenchymal stem cells on A $\beta$ 25-35-induced neuroinflammation. *Behav. Brain Res.* 365, 48–55. doi: 10.1016/j.bbr.2019.03.001
- Idris, A. I., and Ralston, S. H. (2012). Role of cannabinoids in the regulation of bone remodeling. *Front. Endocrinol.* 3:136. doi: 10.3389/fendo.2012.00136
- Iinuma, S., Aikawa, E., Tamai, K., Fujita, R., Kikuchi, Y., Chino, T., et al. (2015). Transplanted bone marrow-derived circulating PDGFR $\alpha$  cells restore type



- VII collagen in recessive dystrophic epidermolysis bullosa mouse skin graft. *J. Immunol.* 194, 1996–2003. doi: 10.4049/jimmunol.1400914
- Jiao, F., Tang, W., Huang, H., Zhang, Z., Liu, D., Zhang, H., et al. (2018). Icariin promotes the migration of BMSCs in vitro and in vivo via the MAPK signaling pathway. *Stem Cells Int.* 2018:2562105. doi: 10.1155/2018/2562105
- Ju, D. T., Kuo, W. W., Ho, T. J., Paul, C. R., Kuo, C. H., Viswanatha, V. P., et al. (2015). Protocatechuic acid from *Alpinia oxyphylla* induces Schwann cell migration via ERK1/2, JNK and p38 activation. *Am. J. Chin. Med.* 43, 653–665. doi: 10.1142/s0192415x15500408
- Justus, C. R., Leffler, N., Echevarria, M. R., and Yang, L. V. (2014). In vitro cell migration and invasion assays. *J. Vis. Exp.* 88:e51046. doi: 10.3791/51046
- Kamali, A., Oryan, A., Hosseini, S., Ghanian, M. H., Alizadeh, M., Baghaban Eslaminejad, M., et al. (2019). Cannabidiol-loaded microspheres incorporated into osteoconductive scaffold enhance mesenchymal stem cell recruitment and regeneration of critical-sized bone defects. *Mater. Sci. Eng. C.* 101, 64–75. doi: 10.1016/j.msec.2019.03.070
- Karanjgaokar, C. G., Radhakrishnan, P. V., and Venkataraman, K. (1967). Morelloflavone, a 3-(8-) flavonylflavanone, from the heartwood of *Garcinia morella*. *Tetrahedron Lett.* 8, 3195–3198. doi: 10.1016/s0040-4039(01)89897-x
- Kaur, R., Ambwani, S. R., and Singh, S. (2016). Endocannabinoid system: a multi-facet therapeutic target. *Curr. Clin. Pharmacol.* 11, 110–117. doi: 10.2174/1574884711666160418105339
- Khan, A. K., Rashid, R., Fatima, N., Mahmood, S., Mir, S., Khan, S., et al. (2015). Pharmacological activities of protocatechuic acid. *Acta Pol. Pharm.* 72, 643–650.
- Kim, K. H., Blasco-Morente, G., Cuende, N., and Arias-Santiago, S. (2017). Mesenchymal stromal cells: properties and role in management of cutaneous diseases. *J. Eur. Acad. Dermatol. Venerol.* 31, 414–423. doi: 10.1111/jdv.13934
- Kong, D., Liu, Q., Xu, G., Huang, Z., Luo, N., Huang, Y., et al. (2017). Synergistic effect of tanshinone IIA and mesenchymal stem cells on preventing learning and memory deficits via anti-apoptosis, attenuating tau phosphorylation and enhancing the activity of central cholinergic system in vascular dementia. *Neurosci. Lett.* 637, 175–181. doi: 10.1016/j.neulet.2016.11.024
- Kong, X., Zhong, M., Su, X., Qin, Q., Su, H., Wan, H., et al. (2016). Tetramethylpyrazine promotes migration of neural precursor cells via activating the phosphatidylinositol 3-kinase pathway. *Mol. Neurobiol.* 53, 6526–6539. doi: 10.1007/s12035-015-9551-1
- Krueger, T. E. G., Thorek, D. L. J., Denmeade, S. R., Isaacs, J. T., and Brennen, W. N. (2018). Concise review: mesenchymal stem cell-based drug delivery: the good, the bad, the ugly, and the promise. *Stem Cells Transl. Med.* 7, 651–663. doi: 10.1002/sctm.18-0024
- Lee, H. P., Liu, Y. C., Chen, P. C., Tai, H. C., Li, T. M., and Fong, Y. C. (2017). Tanshinone IIA inhibits angiogenesis in human endothelial progenitor cells in vitro and in vivo. *Oncotarget* 8, 109217–109227. doi: 10.18632/oncotarget.22649
- Li, C., Li, Q., Mei, Q., and Lu, T. (2015). Pharmacological effects and pharmacokinetic properties of icariin, the major bioactive component in Herba Epimedii. *Life Sci.* 126, 57–68. doi: 10.1016/j.lfs.2015.01.006
- Li, K., Song, J., Zhao, Q., Wang, B., Zhang, Y., Wang, X., et al. (2018). Effective component of *Salvia miltiorrhiza* in promoting cardiomyogenic differentiation of human placenta-derived mesenchymal stem cells. *Int. J. Mol. Med.* 41, 962–968. doi: 10.3892/ijmm.2017.3293
- Li, L., Chu, L., Fang, Y., Yang, Y., Qu, T., Zhang, J., et al. (2017a). Preconditioning of bone marrow-derived mesenchymal stromal cells by tetramethylpyrazine enhances cell migration and improves functional recovery after focal cerebral ischemia in rats. *Stem Cell Res. Ther.* 8:112. doi: 10.1186/s13287-017-0565-7
- Li, L., Chu, L., Ren, C., Wang, J., Sun, S., Li, T., et al. (2019). Enhanced migration of bone marrow-derived mesenchymal stem cells with tetramethylpyrazine and its synergistic effect on angiogenesis and neurogenesis after cerebral ischemia in rats. *Stem Cells Dev.* 228, 871–881. doi: 10.1089/scd.2018.0254
- Li, L., Hou, X., Xu, R., Liu, C., and Tu, M. (2017b). Research review on the pharmacological effects of astragaloside IV. *Fundam. Clin. Pharmacol.* 31, 17–36. doi: 10.1111/fcp.12232
- Li, Z., Xu, S., and Liu, P. (2018a). *Salvia miltiorrhiza* Burge (Danshen): a golden herbal medicine in cardiovascular therapeutics. *Acta Pharmacol. Sin.* 39, 802–824. doi: 10.1038/aps.2017.193
- Li, Z., Zhang, S., Cao, L., Li, W., Ye, Y. C., Shi, Z. X., et al. (2018b). Tanshinone IIA and Astragaloside IV promote the angiogenesis of mesenchymal stem cell-derived endothelial cell-like cells via upregulation of Cx37, Cx40 and Cx43. *Exp. Ther. Med.* 15, 1847–1854. doi: 10.3892/etm.2018.6428
- Liu, C., Qi, X., Alhabeil, J., Lu, H., and Zhou, Z. (2019). Activation of cannabinoid receptors promote periodontal cell adhesion and migration. *J. Clin. Periodontol.* 46, 1264–1272. doi: 10.1111/jcpe.13190
- Liu, D., Ye, Y., Xu, L., Yuan, W., and Zhang, Q. (2018). Icariin and mesenchymal stem cells synergistically promote angiogenesis and neurogenesis after cerebral ischemia via PI3K and ERK1/2 pathways. *Biomed. Pharmacother.* 108, 663–669. doi: 10.1016/j.biopha.2018.09.071
- Liu, H. J., Liu, X. Y., and Jing, D. B. (2018). Icariin induces the growth, migration and osteoblastic differentiation of human periodontal ligament fibroblasts by inhibiting Toll-like receptor 4 and NF- $\kappa$ B p65 phosphorylation. *Mol. Med. Rep.* 18, 3325–3331. doi: 10.3892/mmr.2018.9302
- Liu, R.-X., Wang, Q., Guo, H. Z., Li, L., Bi, K. S., and Guo, D. A. (2005). Simultaneous determination of 10 major flavonoids in *Dalbergia odorifera* by high performance liquid chromatography. *J. Pharm. Biomed. Anal.* 39, 469–476. doi: 10.1016/j.jpba.2005.04.007
- Liu, S., Stroncek, D. F., Zhao, Y., Chen, V., Shi, R., Chen, J., et al. (2019). Single cell sequencing reveals gene expression signatures associated with bone marrow stromal cell subpopulations and time in culture. *J. Transl. Med.* 17:23. doi: 10.1186/s12967-018-1766-2
- Liu, X., Niu, Y., Xie, W., Wei, D., and Du, Q. (2019). Tanshinone IIA promotes osteogenic differentiation of human periodontal ligament stem cells via ERK1/2-dependent Runx2 induction. *Am. J. Transl. Res.* 11, 340–350.
- Liu, Y. D., Sun, X., Zhang, Y., Wu, H. J., Wang, H., and Yang, R. (2019). Protocatechuic acid inhibits TGF- $\beta$ 1-induced proliferation and migration of human airway smooth muscle cells. *J. Pharmacol. Sci.* 139, 9–14. doi: 10.1016/j.jpsh.2018.10.011
- Liu, Y. M., Li, W. Y., Xu, L. L., Yu, L. J., Luo, Y. W., Li, X. C., et al. (2019). *Catharmus tinctorius* volatile oil promote the migration of mesenchymal stem cells via ROCK2/Myosin light chain signaling. *Chin. J. Nat. Med.* 17, 506–516. doi: 10.1016/s1875-5364(19)30072-x
- López, J. J., Jardín, I., Salido, G. M., and Rosado, J. A. (2008). Cinnamtannin B-1 as an antioxidant and platelet aggregation inhibitor. *Life Sci.* 82, 977–982. doi: 10.1016/j.lfs.2008.03.009
- Lüder, E., Ramer, R., Peters, K., and Hinz, B. (2017). Decisive role of P42/44 mitogen-activated protein kinase in  $\Delta$ 9-tetrahydrocannabinol-induced migration of human mesenchymal stem cells. *Oncotarget* 8, 105984–105994. doi: 10.18632/oncotarget.22517
- Marquez-Curtis, L. A., and Janowska-Wieczorek, A. (2013). Enhancing the migration ability of mesenchymal stromal cells by targeting the SDF-1/CXCR4 axis. *Biomed. Res. Int.* 2013:561098. doi: 10.1155/2013/561098
- Meng, S. S., Xu, X. P., Chang, W., Lu, Z. H., Huang, L. L., Xu, J. Y., et al. (2018). LincRNA-p21 promotes mesenchymal stem cell migration capacity and survival through hypoxic preconditioning. *Stem Cell Res. Ther.* 9:280. doi: 10.1186/s13287-018-1031-x
- Mi, B., Liu, J., Liu, G., Zhou, W., Liu, Y., Hu, L., et al. (2018). Icariin promotes wound healing by enhancing the migration and proliferation of keratinocytes via the AKT and ERK signaling pathway. *Int. J. Mol. Med.* 42, 831–838. doi: 10.3892/ijmm.2018.3676
- Mohr, A., and Zwacka, R. (2018). The future of mesenchymal stem cell-based therapeutic approaches for cancer – from cells to ghosts. *Cancer Lett.* 414, 239–249. doi: 10.1016/j.canlet.2017.11.025
- Nitzsche, F., Müller, C., Lukomska, B., Jolkkonen, J., Deten, A., and Boltze, J. (2017). Concise review: MSC adhesion cascade-insights into homing and transendothelial migration. *Stem Cells* 35, 1446–1460. doi: 10.1002/stem.2614
- Park, J. S., Suryaprakash, S., Lao, Y. H., and Leong, K. W. (2015). Engineering mesenchymal stem cells for regenerative medicine and drug delivery. *Methods* 84, 3–16. doi: 10.1016/j.ymeth.2015.03.002
- Pertwee, R. G. (2008). The diverse CB1 and CB2 receptor pharmacology of three plant cannabinoids: delta9-tetrahydrocannabinol, cannabidiol and delta9-tetrahydrocannabivarin. *Br. J. Pharmacol.* 153, 199–215. doi: 10.1038/sj.bjp.0707442

- Pittenger, M. F., Discher, D. E., Péault, B. M., Phinney, D. G., Hare, J. M., and Caplan, A. I. (2019). Mesenchymal stem cell perspective: cell biology to clinical progress. *NPJ Regen. Med.* 4:22. doi: 10.1038/s41536-019-0083-6
- Presen, D. M., Traweger, A., Gimona, M., and Redl, H. (2019). Mesenchymal stromal cell-based bone regeneration therapies: from cell transplantation and tissue engineering to therapeutic secretomes and extracellular vesicles. *Front. Bioeng. Biotechnol.* 7:352. doi: 10.3389/fbioe.2019.00352
- Qian, K., Xu, H., Dai, T., and Shi, K. (2015). Effects of Tanshinone IIA on osteogenic differentiation of mouse bone marrow mesenchymal stem cells. *Naunyn-Schmiedeberg's Arch. Pharmacol.* 388, 1201–1209. doi: 10.1007/s00210-015-1154-x
- Qin, S., Zhou, W., Liu, S., Chen, P., and Wu, H. (2015). Icaritin stimulates the proliferation of rat bone mesenchymal stem cells via ERK and p38 MAPK signaling. *Int. J. Clin. Exp. Med.* 8, 7125–7133.
- Ren, J., Fu, L., Nile, S. H., Zhang, J., and Kai, G. (2019). *Salvia miltiorrhiza* in treating cardiovascular diseases: a review on its pharmacological and clinical applications. *Front. Pharmacol.* 10:753. doi: 10.3389/fphar.2019.00753
- Rivera-Barreno, R., del Castillo-Vaquero, A., Salido, G. M., and Gonzalez, A. (2010). Effect of cinnamtannin B-1 on cholecystokinin-8-evoked responses in mouse pancreatic acinar cells. *Clin. Exp. Pharmacol. Physiol.* 37, 980–988. doi: 10.1111/j.1440-1681.2010.05424.x
- Rivera-Piza, A., An, Y. J., Kim, D. K., Lee, S. H., Kim, J. B., Choi, J. S., et al. (2017). Protocatechuic acid enhances osteogenesis, but inhibits adipogenesis in C3H10T1/2 and 3T3-L1 cells. *J. Med. Food.* 20, 309–319. doi: 10.1089/jmf.2016.3833
- Rocheffort, G. Y., Delorme, B., Lopez, A., Herauld, O., Bonnet, P., Charbord, P., et al. (2006). Multipotential mesenchymal stem cells are mobilized into peripheral blood by hypoxia. *Stem Cells* 24, 2202–2208. doi: 10.1634/stemcells.2006-0164
- Ruan, X. F., Ju, C. W., Shen, Y., Liu, Y. T., Kim, I. M., Yu, H., et al. (2018). Suxiao Jiuxin pill promotes exosome secretion from mouse cardiac mesenchymal stem cells in vitro. *Acta Pharmacol. Sin.* 39, 569–578. doi: 10.1038/aps.2018.19
- Sánchez-Rubio, F., Fernández-Santos, M. R., Castro-Vázquez, L., García-Álvarez, O., Maroto-Morales, A., Soler, A. J., et al. (2018). Cinnamtannin B-1, a novel antioxidant for sperm in red deer. *Anim. Reprod. Sci.* 195, 44–52. doi: 10.1016/j.anireprosci.2018.05.004
- Schicho, R., Bashashati, M., Bawa, M., McHugh, D., Saur, D., Hu, H. M., et al. (2011). The atypical cannabinoid O-1602 protects against experimental colitis and inhibits neutrophil recruitment. *Inflamm. Bowel Dis.* 17, 1651–1664. doi: 10.1002/ibd.21538
- Schmuhl, E., Ramer, R., Salamon, A., Peters, K., and Hinz, B. (2014). Increase of mesenchymal stem cell migration by cannabidiol via activation of p42/44 MAPK. *Biochem. Pharmacol.* 87, 489–501. doi: 10.1016/j.bcp.2013.11.016
- Shedoeva, A., Leavesley, D., Upton, Z., and Fan, C. (2019). Wound healing and the use of medicinal plants. *Evid. Based Complement Alternat. Med.* 2019, 2684108. doi: 10.1155/2019/2684108
- Shen, W., Luo, H., Xu, L., Wu, Z., Chen, H., Liu, Y., et al. (2018). Wnt5a mediates the effects of Bushen Huoxue decoction on the migration of bone marrow mesenchymal stem cells in vitro. *Chin. Med.* 13:45. doi: 10.1186/s13020-018-0200-2
- Song, H., and Ren, J. (2019). Protocatechuic acid attenuates angiotensin II-induced cardiac fibrosis in cardiac fibroblasts through inhibiting the NOX4/ROS/p38 signaling pathway. *Phytother. Res.* 33, 2440–2447. doi: 10.1002/ptr.6435
- Song, X., Dai, J., Li, H., Li, Y., Hao, W., Zhang, Y., et al. (2019). Anti-aging effects exerted by tetramethylpyrazine enhances self-renewal and neuronal differentiation of rat bMSCs by suppressing NF- $\kappa$ B signaling. *Biosci. Rep.* 39:BSR20190761. doi: 10.1042/bsr20190761
- Tong, Y., Xu, W., Han, H., Chen, Y., Yang, J., Qiao, H., et al. (2011). Tanshinone IIA increases recruitment of bone marrow mesenchymal stem cells to infarct region via up-regulating stromal cell-derived factor-1/CXC chemokine receptor 4 axis in a myocardial ischemia model. *Phytomedicine* 18, 443–450. doi: 10.1016/j.phymed.2010.10.009
- Uccelli, A., Moretta, L., and Pistoia, V. (2008). Mesenchymal stem cells in health and disease. *Nat. Rev. Immunol.* 8, 726–736. doi: 10.1038/nri2395
- Vaccani, A., Massi, P., Colombo, A., Rubino, T., and Parolaro, D. (2005). Cannabidiol inhibits human glioma cell migration through a cannabinoid receptor-independent mechanism. *Br. J. Pharmacol.* 144, 1032–1036. doi: 10.1038/sj.bjp.0706134
- Wan, J. B., Li, S. P., Chen, J. M., and Wang, Y. T. (2007). Chemical characteristics of three medicinal plants of the *Panax* genus determined by HPLC-ELSD. *J. Sep. Sci.* 30, 825–832. doi: 10.1002/jssc.200600359
- Wang, D., Liu, Y., Zhong, G., Wang, Y., Zhang, T., Zhao, Z., et al. (2017). Compatibility of Tanshinone IIA and Astragaloside IV in attenuating hypoxia-induced cardiomyocytes injury. *J. Ethnopharmacol.* 204, 67–76. doi: 10.1016/j.jep.2017.03.053
- Wang, F., Tang, H., Zhu, J., and Zhang, J. H. (2018). Transplanting mesenchymal stem cells for treatment of ischemic stroke. *Cell Transplant.* 27, 1825–1834. doi: 10.1177/0963689718795424
- Wang, H., Liu, T. Q., Zhu, Y. X., Guan, S., Ma, X. H., and Cui, Z. F. (2009). Effect of protocatechuic acid from *Alpinia oxyphylla* on proliferation of human adipose tissue-derived stromal cells in vitro. *Mol. Cell Biochem.* 330, 47–53. doi: 10.1007/s11010-009-0099-0
- Wang, H., Liu, T.-Q., Guan, S., Zhu, Y.-X., and Cui, Z.-X. (2008). Protocatechuic acid from *Alpinia oxyphylla* promotes migration of human adipose tissue-derived stromal cells in vitro. *Eur. J. Pharmacol.* 599, 24–31. doi: 10.1016/j.ejphar.2008.09.030
- Wang, L. L., Zhao, R., Li, J. Y., Li, S. S., Liu, M., Wang, M., et al. (2016). Pharmacological activation of cannabinoid 2 receptor attenuates inflammation, fibrogenesis, and promotes re-epithelialization during skin wound healing. *Eur. J. Pharmacol.* 786, 128–136. doi: 10.1016/j.ejphar.2016.06.006
- Wang, X., Liu, C., Xu, Y., Chen, P., Shen, Y., Xu, Y., et al. (2017). Combination of mesenchymal stem cell injection with icaritin for the treatment of diabetes-associated erectile dysfunction. *PLoS One* 12:e0174145. doi: 10.1371/journal.pone.0174145
- Wang, Y., Peng, H., Shen, Y., Zhao, R., and Huang, L. (2013). The profiling of bioactive ingredients of differently aged *Salvia miltiorrhiza* roots. *Microsc. Res. Tech.* 76, 947–954. doi: 10.1002/jemt.22253
- Wang, Z. C., Sun, H. J., Li, K. H., Fu, C., and Liu, M. Z. (2014). Icaritin promotes directed chondrogenic differentiation of bone marrow mesenchymal stem cells but not hypertrophy in vitro. *Exp. Ther. Med.* 7, 543–550. doi: 10.1002/ctm.17-0210
- Ward, M. R., Abadeh, A., and Connelly, K. A. (2018). Concise review: rational use of mesenchymal stem cells in the treatment of ischemic heart disease. *Stem Cells Transl. Med.* 7, 543–550. doi: 10.1002/sctm.17-0210
- Wu, Y., Zhao, R. C., and Tredget, E. E. (2010). Concise review: bone marrow-derived stem/progenitor cells in cutaneous repair and regeneration. *Stem Cells* 28, 905–915. doi: 10.1002/stem.420
- Xie, J., Wang, H., Song, T., Wang, Z., Li, F., Ma, J., et al. (2013). Tanshinone IIA and astragaloside IV promote the migration of mesenchymal stem cells by up-regulation of CXCR4. *Protoplasma* 250, 521–530. doi: 10.1007/s00709-012-0435-1
- Xing, Y., Tu, J., Zheng, L., Guo, L., and Xi, T. (2015). Anti-angiogenic effect of tanshinone IIA involves inhibition of the VEGF/VEGFR2 pathway in vascular endothelial cells. *Oncol. Rep.* 33, 163–170. doi: 10.3892/or.2014.3592
- Xu, X. L., Ji, H., Gu, S. Y., Shao, Q., Huang, Q. J., and Cheng, Y. P. (2007). Modification of alterations in cardiac function and sarcoplasmic reticulum by astragaloside IV in myocardial injury in vivo. *Eur. J. Pharmacol.* 568, 203–212. doi: 10.1016/j.ejphar.2007.04.007
- Yang, L., Wang, Y., Wang, X., and Liu, Y. (2015). Effect of allogeneic umbilical cord mesenchymal stem cell transplantation in a rat model of hepatic cirrhosis. *J. Tradit. Chin. Med.* 35, 63–68. doi: 10.1016/s0254-6272(15)30010-8
- Yin, K., Wang, S., and Zhao, R. C. (2019). Exosomes from mesenchymal stem/stromal cells: a new therapeutic paradigm. *Biomark. Res.* 7, 8. doi: 10.1186/s40364-019-0159-x
- Zhang, M., Gao, F., Teng, F., and Zhang, C. (2014). Tetramethylpyrazine promotes the proliferation and migration of brain endothelial cells. *Mol. Med. Rep.* 10, 29–32. doi: 10.3892/mmr.2014.2169
- Zhang, X. M., Ma, J., Sun, Y., Yu, B. Q., Jiao, Z. M., Wang, D., et al. (2018). Tanshinone IIA promotes the differentiation of bone marrow mesenchymal

- stem cells into neuronal-like cells in a spinal cord injury model. *J. Transl. Med.* 16, 193. doi: 10.1186/s12967-018-1571-y
- Zhao, Y., Liu, Y., and Chen, K. (2016). Mechanisms and clinical application of tetramethylpyrazine (an interesting natural compound isolated from *Ligusticum Wallichii*): Current status and perspective. *Oxid. Med. Cell. Longev.* 2016, 2124638. doi: 10.1155/2016/2124638
- Zhu, H., Wang, X., Han, Y., Zhang, W., Xin, W., Zheng, X., et al. (2018). Icariin promotes the migration of bone marrow stromal cells via the SDF-1 $\alpha$ /HIF-1 $\alpha$ /CXCR4 pathway. *Drug Des. Devel. Ther.* 12, 4023–4031. doi: 10.2147/dddt.s179989

**Conflict of Interest:** The author declares that the research was conducted in the absence of any commercial or financial relationships that could be construed as a potential conflict of interest.

Copyright © 2020 Maeda. This is an open-access article distributed under the terms of the Creative Commons Attribution License (CC BY). The use, distribution or reproduction in other forums is permitted, provided the original author(s) and the copyright owner(s) are credited and that the original publication in this journal is cited, in accordance with accepted academic practice. No use, distribution or reproduction is permitted which does not comply with these terms.



# Caffeine Compromises Proliferation of Human Hippocampal Progenitor Cells

Vikki Houghton<sup>1†</sup>, Andrea Du Preez<sup>1†</sup>, Sophie Lefèvre-Arbogast<sup>2</sup>, Chiara de Lucia<sup>1</sup>, Dorrain Y. Low<sup>3</sup>, Mireia Urpi-Sarda<sup>4</sup>, Silvie R. Ruigrok<sup>5</sup>, Barbara Altendorfer<sup>6</sup>, Raúl González-Domínguez<sup>4</sup>, Cristina Andres-Lacueva<sup>4</sup>, Ludwig Aigner<sup>6</sup>, Paul J. Lucassen<sup>5</sup>, Aniko Korosi<sup>5</sup>, Cécilia Samieri<sup>2</sup>, Claudine Manach<sup>3</sup> and Sandrine Thuret<sup>1,7\*</sup>

<sup>1</sup> Department of Basic and Clinical Neuroscience, Maurice Wohl Clinical Neuroscience Institute, Institute of Psychiatry, Psychology and Neuroscience, King's College London, London, United Kingdom, <sup>2</sup> University of Bordeaux, INSERM, BPH, U1219, Bordeaux, France, <sup>3</sup> INRA, UMR 1019, Human Nutrition Unit, Université Clermont Auvergne, Clermont-Ferrand, France, <sup>4</sup> Nutrition, Food Science and Gastronomy Department, Faculty of Pharmacy and Food Science, CIBER Fragilidad y Envejecimiento Saludable, Instituto de Salud Carlos III, University of Barcelona, Barcelona, Spain, <sup>5</sup> Brain Plasticity Group, Swammerdam Institute for Life Sciences, Center for Neuroscience, University of Amsterdam, Amsterdam, Netherlands, <sup>6</sup> Institute of Molecular Regenerative Medicine, Spinal Cord Injury and Tissue Regeneration Center Salzburg, Paracelsus Medical University, Salzburg, Austria, <sup>7</sup> Department of Neurology, University Hospital Carl Gustav Carus, Technische Universität Dresden, Dresden, Germany

## OPEN ACCESS

### Edited by:

Kazunori Sasaki,  
National Institute of Advanced  
Industrial Science and Technology  
(AIST), Japan

### Reviewed by:

Johannes Boltze,  
University of Warwick,  
United Kingdom  
Lorena Varela-Nallar,  
Andres Bello University, Chile

### \*Correspondence:

Sandrine Thuret  
Sandrine.1.thuret@kcl.ac.uk

<sup>†</sup>These authors have contributed  
equally to this work

### Specialty section:

This article was submitted to  
Stem Cell Research,  
a section of the journal  
Frontiers in Cell and Developmental  
Biology

**Received:** 08 June 2020

**Accepted:** 31 July 2020

**Published:** 08 September 2020

### Citation:

Houghton V, Du Preez A,  
Lefèvre-Arbogast S, de Lucia C,  
Low DY, Urpi-Sarda M, Ruigrok SR,  
Altendorfer B,  
González-Domínguez R,  
Andres-Lacueva C, Aigner L,  
Lucassen PJ, Korosi A, Samieri C,  
Manach C and Thuret S (2020)  
Caffeine Compromises Proliferation  
of Human Hippocampal Progenitor  
Cells. *Front. Cell Dev. Biol.* 8:806.  
doi: 10.3389/fcell.2020.00806

The age-associated reduction in the proliferation of neural stem cells (NSCs) has been associated with cognitive decline. Numerous factors have been shown to modulate this process, including dietary components. Frequent consumption of caffeine has been correlated with an increased risk of cognitive decline, but further evidence of a negative effect on hippocampal progenitor proliferation is limited to animal models. Here, we used a human hippocampal progenitor cell line to investigate the effects of caffeine on hippocampal progenitor integrity and proliferation specifically. The effects of five caffeine concentrations (0 mM = control, 0.1 mM ~ 150 mg, 0.25 mM ~ 400 mg, 0.5 mM ~ 750 mg, and 1.0 mM ~ 1500 mg) were measured following acute (1 day) and repeated (3 days) exposure. Immunocytochemistry was used to quantify hippocampal progenitor integrity (i.e., SOX2- and Nestin-positive cells), proliferation (i.e., Ki67-positive cells), cell count (i.e., DAPI-positive cells), and apoptosis (i.e., CC3-positive cells). We found that progenitor integrity was significantly reduced in supraphysiological caffeine conditions (i.e., 1.0 mM ~ 1500 mg), but relative to the lowest caffeine condition (i.e., 0.1 mM ~ 150 mg) only. Moreover, repeated exposure to supraphysiological caffeine concentrations (i.e., 1.0 mM ~ 1500 mg) was found to affect proliferation, significantly reducing % Ki67-positive cells relative to control and lower caffeine dose conditions (i.e., 0.1 mM ~ 150 mg and 0.25 mM ~ 400 mg). Caffeine treatment did not influence apoptosis and there were no significant differences in any measure between lower doses of caffeine (i.e., 0.1 mM, 0.25 mM, 0.5 mM) – representative of daily human caffeine intake – and control conditions. Our study demonstrates that dietary components such as caffeine can influence NSC integrity and proliferation and may be indicative of a mechanism by which diet affects cognitive outcomes.

**Keywords:** adult hippocampal neurogenesis, diet, caffeine, hippocampal progenitor integrity, hippocampal progenitor proliferation



## INTRODUCTION

Adult hippocampal neurogenesis (AHN), the formation of new neurons from neural progenitor cells, has recently regained considerable attention, particularly in the human hippocampus (Kempermann et al., 2018; Lucassen et al., 2020). This highly vascularized “neurogenic niche” retains developmental signals and morphogens that influence cell proliferation, differentiation, and survival throughout life (Spalding et al., 2013; Gonçalves et al., 2016). The rates at which these processes occur have been associated with hippocampal-dependent learning and memory functions (Snyder et al., 2005; Clelland et al., 2009; Sahay et al., 2011) and this association is particularly interesting when considering aging and cognitive decline, during which hippocampal function typically deteriorates (Small et al., 2002). Moreover, neural progenitor proliferation declines in rodents as aging progresses (Heine et al., 2004; Rao et al., 2006) and this has been strongly correlated with impaired performance in spatial memory and learning tasks (Sahay et al., 2011; Villeda et al., 2011).

This association with cognitive decline presents AHN as a unique target for preventative interventions. Accordingly, rescuing later life neurogenesis has recently gained interest and a focus has been given to the factors that modulate neurogenesis (Baptista and Andrade, 2018). While neurogenesis is facilitated by the neurogenic niche, it is not only central nervous system-derived signals that influence AHN. Indeed, AHN is also modulated by both the external environment (Lledo et al., 2006) and the system milieu (Villeda et al., 2011; Yousef et al., 2019). For example, stress and sleep deprivation have been shown to reduce AHN (Gould et al., 1998; Hairston et al., 2005; Lucassen et al., 2010), while running increases neurogenesis (van Praag et al., 2005). Moreover, these environmental factors have been similarly correlated with spatial learning and memory (Nilsson et al., 1999; Oomen et al., 2010, 2014), highlighting the possibility of leveraging behavioral interventions to target the neurogenic process and, consequently, cognitive ability.

Diet is another environmental factor that has been shown to influence the neurogenic process (Stangl and Thuret, 2009; Miquel et al., 2018; Abbink et al., 2020). *Drosophila* research shows that nutritional factors can influence the exit of neural hippocampal progenitors from quiescence (Chell and Brand, 2010; Spéder and Brand, 2014), and other nutritional-based changes to the hippocampal progenitor pool have been likewise demonstrated across other species (Spéder et al., 2011; Sakayori et al., 2013; Cavallucci et al., 2016). For instance, in humans, the nutrient-sensing pathways: the mammalian target of rapamycin (mTOR), sirtuin, and insulin-like growth factor 1, have all been associated with hippocampal progenitor maintenance (de Lucia et al., 2020). However, the influence of nutrition and meal content on the hippocampal progenitor pool occurs in a complex manner, with the nature of change dependent on the food groups consumed. For instance, a high fat diet has been shown to decrease proliferation in rats (Lindqvist et al., 2006), while omega-3 fatty acids increase proliferation in lobsters (Beltz et al., 2007). Interestingly, these changes to proliferation directionally correspond with their associated

cognitive outcomes, as omega-3 has been shown to improve cognitive outcomes, while high fat diets impair cognitive performance (Winocur and Greenwood, 2005; Fotuhi et al., 2009; Witte et al., 2009; Yam et al., 2019). Thus, the variable nature of meal content and its influence on proliferation may provide a flexible and unique mechanism of regulating the neurogenic process within the human population. However, further defining the dietary components that affect the neurogenic process and their direction of influence is crucial before such dietary-based interventions can be developed.

Caffeine, the most widely consumed psychostimulant in the world (Ferré, 2016), has been widely implicated as a cognitive modulator (Rosso et al., 2008; Glade, 2010). Caffeine consumption has traditionally been argued to produce health benefits on a neurological basis, including protection against cognitive decline in women aged over 65 years (Ritchie et al., 2007; Arab et al., 2011). However, we recently demonstrated a negative effect of caffeine on cognition, identifying caffeine as one of 22 metabolites predictive of cognitive decline in an aging population, over a 13-year period (Low et al., 2019). Further evidence to support a negative effect of caffeine comes from animal models that focus on hippocampal neuronal proliferation. Specifically, when administered chronically, physiologically relevant doses of caffeine decreased neuronal precursor proliferation in rats (Wentz and Magavi, 2009), which was further correlated with impaired hippocampal-dependent learning and memory (Han et al., 2007). However, due to *in vivo* imaging constraints (Ho et al., 2013), the effect of caffeine on human hippocampal progenitor proliferation has not yet been explored. With the mixed clinical evidence on the impact of caffeine on cognitive decline and its large-scale consumption worldwide, further investigation is warranted. Determining the effects of caffeine on proliferation and the neurogenic process overall, and ultimately cognition, will contribute to our understanding of how diet affects these phenomena, which could assist in the development of appropriate interventions.

Therefore, this study investigated the effects of caffeine on human hippocampal progenitor proliferation, focusing on hippocampal proliferation, progenitor integrity (i.e., maintenance of the stem cell pool and proliferative/differentiative capacity), and progenitor apoptosis. We used a human hippocampal progenitor cell line, for the first time, to investigate, (i) the effects of five caffeine concentrations, and (ii) the effects of acute and repeated exposure to caffeine – all on hippocampal progenitor integrity, proliferation and apoptosis.

## MATERIALS AND METHODS

### Cell Line and Culture Conditions

The human fetal hippocampal multipotent progenitor cell line *HPC0A07/03* (HPC; ReNeuron Ltd., Surrey, United Kingdom) was used in all experiments as previously described (de Lucia et al., 2020; Smeeth et al., in press). Cells were acquired from 12-week old female fetal tissue in accordance with United States and United Kingdom ethical and legal guidelines, and transfected

with the c-mycERTAM gene construct creating an immortalized cell line that proliferates in the presence of the synthetic drug 4-hydroxy-tamoxifen (4-OHT) and spontaneously differentiates in its absence. For further details see **Supplementary Material**.

HPCs were cultured in reduced modified medium (RMM), namely Dulbecco's Modified Eagle's Media/F12 (DMEM:F12, Sigma), supplemented with 0.03% human albumin solution (Zenab), 100 µg/mL human apo-transferrin, 16.2 µg/mL human putrescine diHCl, 5 µg/mL human recombinant insulin, 60 ng/mL progesterone, 2 mM L-glutamine and 40 ng/mL sodium selenite. For proliferation, the medium also included 10 ng/mL human basic fibroblast growth factor (bFGF), 20 ng/mL human epidermal growth factor (EGF) and 100 nM 4-OHT. Cells were grown on tissue culture flasks (Nunc, Denmark), incubated at 37°C, 5% CO<sub>2</sub> and saturated humidity, and were routinely passaged at 80% confluency before being plated for experiments.

## Proliferation Assay

The HPC proliferation assay was carried out as previously described (de Lucia et al., 2020; Smeeth et al., in press). Briefly, HPCs were seeded into two 96-well plates (Nunc, Denmark) per experiment: one plate for acute (one-time) caffeine treatment, the other for repeated caffeine treatment. Plates were seeded at a density of  $1.2 \times 10^4$ , at P21 in caffeine-free proliferation media, with three technical replicates and three biological replicates. All cells, excluding the control conditions, received caffeine treatment 24 h after seeding. Cells undergoing acute treatment were left undisturbed for 48 h, while cells undergoing repeated exposure received another caffeine treatment 24 h after the initial treatment. Control conditions were incubated in caffeine-free proliferation media in all instances. Seventy-two hours after seeding, all plates were washed and fixed as previously described (de Lucia et al., 2020; Smeeth et al., in press). **Figure 1** depicts the assay timeline as per the two exposure conditions. For details on the proliferation assays and fixation methods see **Supplementary Material**.

## Caffeine Treatments

Caffeine (5 g) was obtained from Sigma (MO, United States) in powdered form, with a molecular weight of 194.19 g/mol. Caffeine conditions were as follows: control (no caffeine, media only); low (0.1 mM, ~150 mg, ~1 cup); moderate (0.25 mM, ~400 mg, ~2–3 cups); high (0.5 mM, ~750 mg, ~5 cups); and supraphysiological (1.0 mM, ~1500 mg, ~10 cups), reflecting human intake habits and previous animal models (Wentz and Magavi, 2009; Efsa Panel on Dietetic Products, Nutrition, and Allergies (NDA), 2015). Caffeine concentrations were calculated based on previous research stating that 150 mg of caffeine, the mean caffeine content of a Starbucks cappuccino (Ludwig et al., 2014), is approximately equivalent to 0.1 mM (Su et al., 2013a,b). For full details on the caffeine treatments see **Supplementary Material**.

## Immunocytochemistry

Cell count, progenitor cell integrity, progenitor proliferation, and cell death were visualized using 4',6-diamidino-2-phenylindole

(DAPI), Nestin and SRY-Box Transcription Factor 2 (SOX2), Ki67, and cleaved caspase-3 (CC3), respectively, using immunocytochemistry as previously described (de Lucia et al., 2020; Smeeth et al., in press). For protocol details, antibodies used, and representative images see **Supplementary Figure S1**.

## Image Analysis

Immunostainings were quantified using the semi-automated CellInsight NXT High Content Screening (HCS) platform (Thermo Fisher Scientific) and Studio Cell Analysis Software (Thermo Fisher Scientific), as previously described (de Lucia et al., 2020; Smeeth et al., in press). This platform relies on light intensity thresholds, which identify DAPI (wavelength 386) or secondary antibody fluorescence (wavelengths 488 and 555). These thresholds, combined with other parameters based on cell size and shape, identify cells stained by each antibody in an unbiased way and enable semi-automated quantification of immunocytochemical stains. Threshold settings were set by an author blinded to exposure/concentration and parameters were kept constant across experiments. For further details on the protocols and parameters used see **Supplementary Material**.

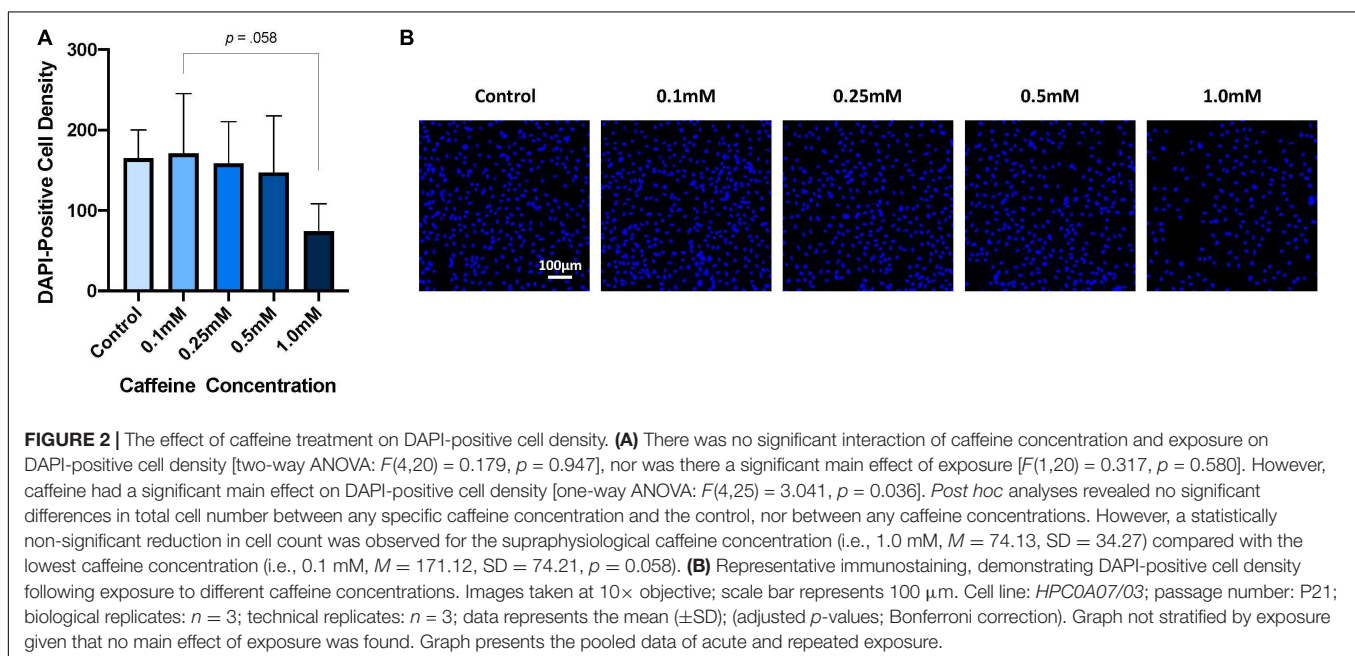
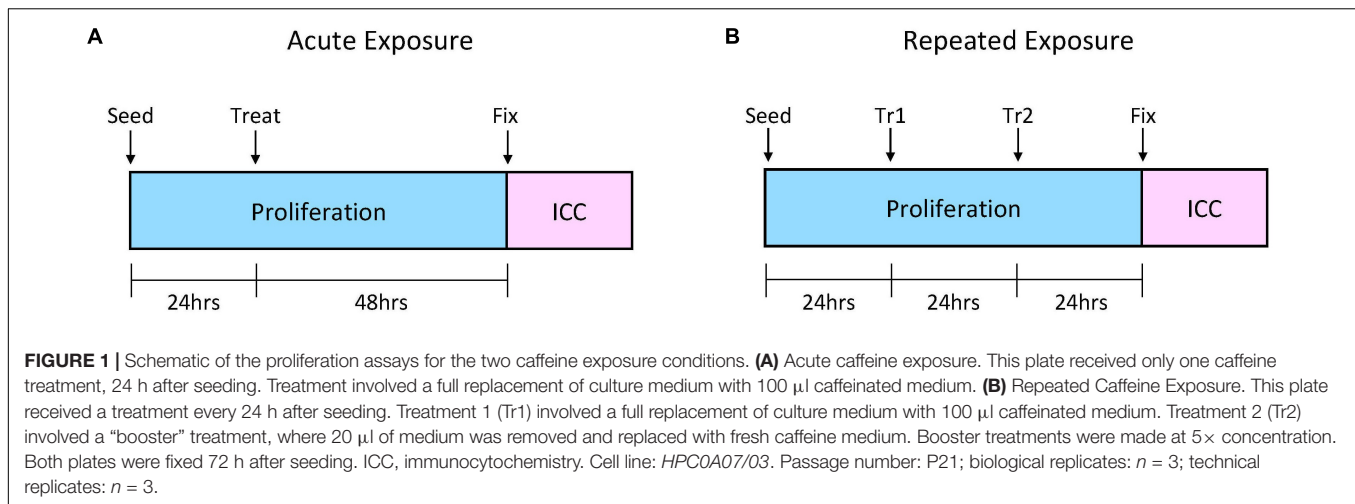
## Statistical Analyses

Data analyses were conducted using IBM SPSS Statistics 26 (IBM Ltd., Portsmouth, United Kingdom). All data were assessed for normality using probability-probability plots and the Kolmogorov-Smirnov test, and for homogeneity of variance using the Levene's test. For data that did not conform to normality and/or homoscedasticity non-parametric statistical tests were applied. To evaluate differences between DAPI, Ki67, C33, and Ki67/CC3, a two-way analysis of variance (ANOVA) with a Bonferroni *post hoc* correction was applied. To evaluate differences in SOX2, Nestin, and Nestin/SOX2 a series of Kruskal-Wallis tests with Dunn's *post hoc* corrections were applied. All tests carried out were two-sided and the alpha criterion used was  $p < 0.05$ . Data are represented as the mean (M) and standard deviation (SD), or the median (Mdn) and interquartile range (IQR).

## RESULTS

### Exposure to Caffeine Reduces Cell Number

There was no significant interaction of caffeine concentration and exposure type, i.e., repeated versus acute caffeine treatment, on cell number, as measured by DAPI-positive cell density ( $p = 0.947$ ), nor was there a significant main effect of exposure ( $p = 0.580$ ). However, as shown in **Figures 2A,B**, there was a main effect of caffeine concentration on DAPI-positive cell density ( $p = 0.036$ ), such that higher caffeine doses reduced cell number. However, due to issues of power, *post hoc* analyses revealed no specific differences between any of the caffeine conditions, but, although not statistically significant, an observed 58.6% reduction in cell count for the



supraphysiological dose (i.e., 1.0 mM  $\sim$  1500 mg) relative to the lowest caffeine dose (i.e., 0.1 mM  $\sim$  150 mg) was seen ( $p = 0.058$ ).

### Exposure to Supraphysiological Caffeine Concentrations Reduces Hippocampal Progenitor Integrity Compared With Lower Caffeine Doses Only

There was no significant main effect of exposure on hippocampal progenitor integrity, as measured by both % Nestin-positive ( $p = 0.901$ ) and % SOX2-positive ( $p = 0.917$ ) cells. However, as shown in **Figure 3**, there was a significant main effect of caffeine concentration on both % Nestin-positive ( $p = 0.034$ ) and % SOX2-positive cells ( $p = 0.016$ ), all while controlling for cell number.

*Post hoc* analyses revealed that the supraphysiological caffeine concentration (i.e., 1.0 mM  $\sim$  1500 mg) significantly reduced the % Nestin-positive cells by 1.5% relative to the lowest caffeine concentration (i.e., 0.1 mM  $\sim$  150 mg;  $p = 0.016$ ; **Figures 3A,D**). No significant differences in % Nestin-positive cells for any of the caffeine concentrations relative to control were observed (0.1 mM  $\sim$  150 mg:  $p > 0.99$ ; 0.25 mM  $\sim$  400 mg:  $p > 0.99$ ; 0.5 mM  $\sim$  750 mg:  $p > 0.99$ ; 1.0 mM  $\sim$  1500 mg:  $p = 0.388$ ). However, it should be noted that the supraphysiological caffeine dose was reduced relative to control conditions but did not survive multiple comparison correction (non-adjusted  $p = 0.039$ ).

Similar to Nestin data, *post hoc* analyses of % SOX2-positive cells revealed that the supraphysiological caffeine dose (i.e., 1.0 mM  $\sim$  1500 mg) significantly reduced % SOX2-positive cells by 2.3%, again, relative to the lowest caffeine



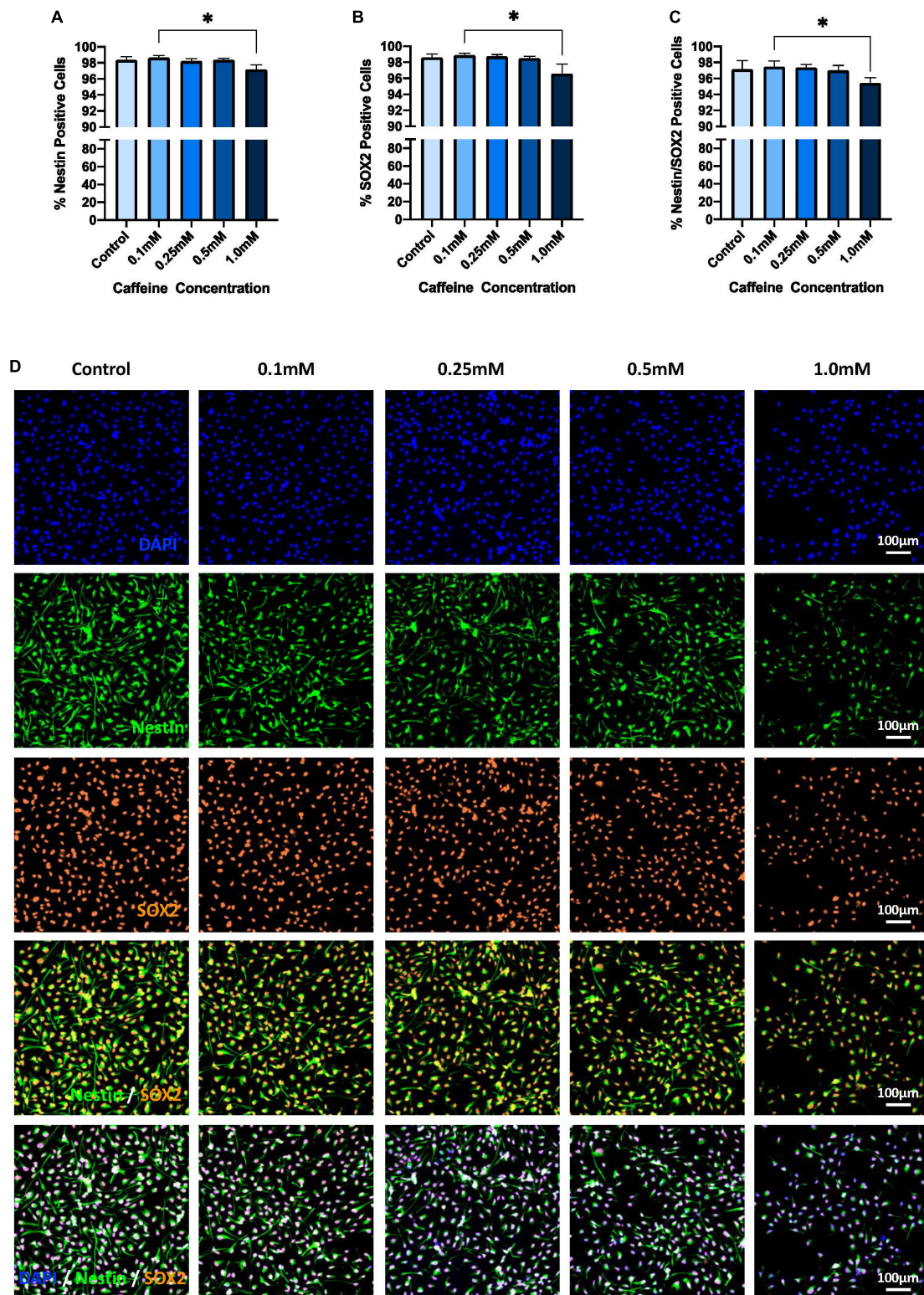


**FIGURE 3 |** The effect of caffeine treatment on % Nestin-, % SOX2-, and Nestin/SOX2-positive cells. **(A)** There was no significant main effect of exposure on % Nestin-positive cells (Kruskal–Wallis test,  $H = 0.02$ ,  $df = 1$ ,  $p = 0.901$ ) but there was a significant main effect of caffeine (Kruskal–Wallis test,  $H = 10.38$ ,  $df = 4$ ,  $p = 0.034$ ). Dunn's *post hoc* analyses revealed that the supraphysiological caffeine concentration (i.e., 1.0 mM; Mdn = 97.2, IQR = 1.99) had significantly reduced stem cell integrity compared with the lowest caffeine concentration (i.e., 0.1 mM, Mdn = 98.66, IQR = 0.72,  $p = 0.016$ ). **(B)** There was no significant main effect of (Continued)

**FIGURE 3 | Continued**

exposure on % SOX2-positive cells (Kruskal–Wallis test,  $H = 0.01$ ,  $df = 1$ ,  $p = 0.917$ ) but there was a significant main effect of caffeine (Kruskal–Wallis test,  $H = 12.17$ ,  $df = 4$ ,  $p = 0.016$ ). Dunn's *post hoc* analyses revealed that the supraphysiological caffeine concentration (i.e., 1.0 mM; Mdn = 96.59, IQR = 2.8) was significantly reduced compared with the lowest caffeine concentration (i.e., 0.1 mM, Mdn = 98.9, IQR = 0.81,  $p = 0.013$ ). **(C)** There was no significant main effect of exposure on % Nestin/SOX2-positive cells (Kruskal–Wallis test,  $H = 0.03$ ,  $df = 1$ ,  $p = 0.868$ ) but there was a significant main effect of caffeine (Kruskal–Wallis test,  $H = 11.61$ ,  $df = 4$ ,  $p = 0.021$ ). Dunn's *post hoc* analyses revealed the supraphysiological caffeine concentration (i.e., 1.0 mM; Mdn = 95.46, IQR = 3.98) was significantly reduced compared with the lowest caffeine concentration (i.e., 0.1 mM, Mdn = 97.48, IQR = 1.11,  $p = 0.016$ ). **(D)** Representative immunostaining, demonstrating, in order from the top panel, DAPI-positive cell density, % Nestin-, % SOX2-, and % Nestin/SOX2-positive cells following exposure to different caffeine concentrations. Images taken at 10× objective; scale bar represents 100  $\mu\text{m}$ . % Nestin-, % SOX2-, and % Nestin/SOX2-positive cells are controlled for by DAPI. Cell line: HPC0A07/03; passage number: P21; biological replicates:  $n = 3$ ; technical replicates:  $n = 3$ ; Data represents the median ( $\pm$ IQR); \* $p < 0.05$ ; (adjusted  $p$ -values; Dunn's correction). Graphs not stratified by exposure given that no main effect of exposure was found. Graphs present the pooled data of acute and repeated exposure.

concentration (0.1mM  $\sim$  150 mg,  $p = 0.013$ ; **Figures 3B,D**). Moreover, there was an observed reduction, albeit not statistically significant, in % SOX2-positive cells in the supraphysiological caffeine dose relative to the moderate caffeine concentration, i.e., 0.25 mM  $\sim$  400 mg ( $p = 0.059$ ). Again, no significant differences were observed relative to control conditions (0.1 mM  $\sim$  150 mg:  $p \geq 0.99$ ; 0.25 mM  $\sim$  400 mg:  $p > 0.99$ ; 0.5 mM  $\sim$  750 mg:  $p > 0.99$ ; 1.0 mM  $\sim$  1500 mg:  $p = 0.304$ ). However, as with the Nestin data, % SOX2-positive cells in the supraphysiological caffeine condition were reduced relative to control but did not survive multiple comparison correction (non-adjusted  $p = 0.03$ ).

Unsurprisingly, a similar results pattern was observed for % Nestin/SOX2-positive cells. Specifically, no significant main effect of exposure ( $p = 0.868$ ) was observed, but there was a significant main effect of caffeine on % Nestin/SOX2-positive cells ( $p = 0.021$ ), with the supraphysiological concentration reducing % Nestin/SOX2-positive cells by 2.1% relative to the lowest caffeine concentration only ( $p = 0.016$ ; **Figures 3C,D**). Moreover, the % Nestin/SOX2-positive cells for the supraphysiological dose was reduced compared with the control condition (non-adjusted  $p = 0.029$ ) and the moderate caffeine concentration, i.e., 0.25 mM  $\sim$  400 mg (non-adjusted  $p = 0.008$ ) but these did not survive multiple comparison correction.

### Repeated Exposure to Supraphysiological Caffeine Concentrations Reduces Hippocampal Progenitor Proliferation

There was no significant interaction effect of caffeine and exposure on proliferation, as measured by the percentage of Ki67-positive cells ( $p = 0.102$ ). However, as shown in **Figures 4A,D**, there was both a significant main effect of exposure ( $p = 0.009$ ) and caffeine concentration ( $p < 0.001$ ) on the % Ki67-positive cells, all while controlling for cell number. Specifically, repeated exposure to the supraphysiological caffeine concentration (i.e., 1.0 mM  $\sim$  1500 mg) significantly reduced proliferation by 37% relative to control conditions ( $p = 0.001$ ), by 39.5% relative to the lowest caffeine dose (i.e., 0.1 mM  $\sim$  150 mg;  $p < 0.001$ ), and by 37.7% relative to the moderate caffeine dose (i.e., 0.25 mM  $\sim$  400 mg;  $p = 0.001$ ). No significant differences were found between the control condition and the other caffeine concentrations, i.e., 0.1 mM ( $p > 0.99$ ), 0.25 mM ( $p > 0.99$ ), and 0.5 mM ( $p = 0.446$ ), nor were any significant

differences observed for acute exposure, that is, a single, one-time caffeine treatment.

### Exposure to Caffeine Does Not Affect Apoptosis

As depicted in **Figures 4B,D**, there was no significant interaction of caffeine concentration and exposure on apoptosis, as measured by % CC3-positive cells ( $p = 0.616$ ), nor was there a significant main effect of exposure ( $p = 0.571$ ) or caffeine concentration ( $p = 0.474$ ) – all while controlling for cell number. Furthermore, as shown in **Figures 4C,D**, there was no significant interaction of caffeine concentration and exposure on proliferative cell death, as measured by % Ki67/CC3-positive cells ( $p = 0.797$ ), nor was there a significant main effect of exposure ( $p = 0.759$ ) or caffeine concentration ( $p = 0.167$ ) – again, all while controlling for cell number.

## DISCUSSION

In this study we explore the effects of acute and repeated caffeine exposure at different concentrations on hippocampal progenitor proliferation, integrity, and apoptosis, using an *in vitro* hippocampal cellular model. We demonstrate that a repeated supraphysiological dose of caffeine, i.e., 1.0 mM  $\sim$  1500 mg or  $\sim$ 10 cups of coffee, significantly reduces progenitor proliferation, as measured by % Ki67-positive cells, relative to the control condition (no caffeine) and to both the lowest (i.e., 0.1 mM  $\sim$  150 mg or  $\sim$ 1 cup) and moderate (i.e., 0.25 mM  $\sim$  400 mg or 2–3 cups) caffeine concentrations. Moreover, the supraphysiological dose ( $\sim$ 10 cups of coffee), whether acutely or repeatedly administered, negatively influences progenitor integrity, as measured by both % Nestin- and % SOX2-positive cells, but only when compared with the lowest caffeine dose ( $\sim$ 1 cup of coffee). Finally, we show that caffeine, irrespective of the degree of exposure or concentration, does not affect overall, or proliferative, cell death, as measured by % CC3-positive cells and % Ki67/CC3-positive cells, respectively.

Our finding that repeated treatment with a supraphysiological caffeine concentration, that is, intake of  $\sim$ 10 cups of coffee, reduces hippocampal progenitor proliferation directly contrasts previous findings from Wentz and Magavi (2009), who used an animal model and observe that supraphysiological doses increase proliferation. However, this inconsistency could be attributed



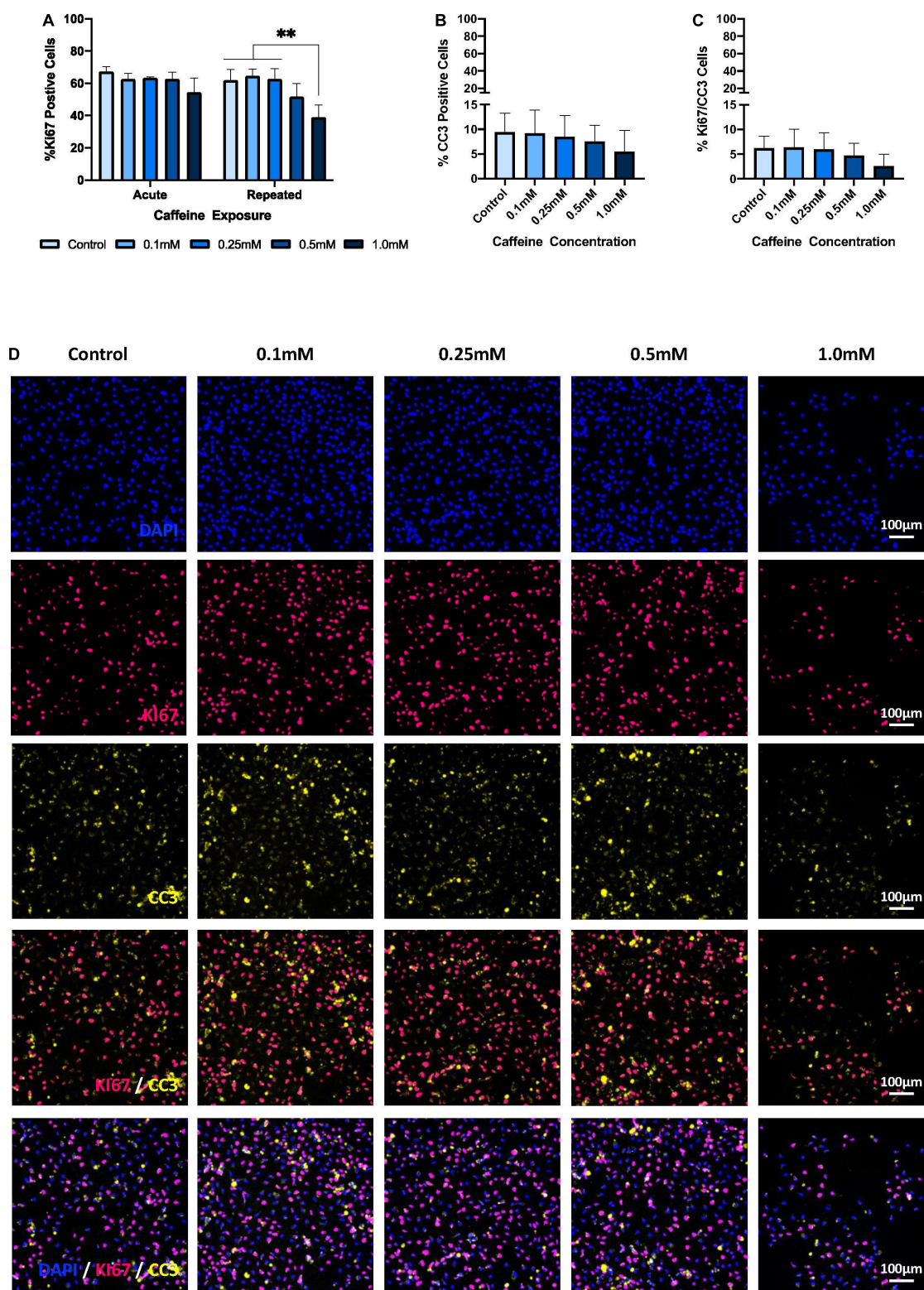


**FIGURE 4 |** The effect of caffeine treatment on % Ki67-, % CC3-, and % Ki67/CC3-positive cells. **(A)** There was no significant interaction effect of caffeine concentration and exposure on % Ki67-positive cells [two-way ANOVA:  $F(4,20) = 2.235$ ,  $p = 0.102$ ]. However, a significant main effect of both exposure [two-way ANOVA:  $F(1,20) = 8.292$ ,  $p = 0.009$ ], and caffeine concentration [two-way ANOVA:  $F(4,20) = 9.81$ ,  $p < 0.001$ ] was found on % Ki67-positive cells. Specifically, Bonferroni *post hoc* analyses revealed that repeated treatment with the supraphysiological concentration (i.e., 1.0 mM;  $M = 39.05$ ,  $SD = 7.5$ ) significantly reduced

(Continued)

**FIGURE 4 | Continued**

proliferation compared with the control ( $M = 61.94$ ,  $SD = 6.69$ ,  $p = 0.001$ ), the lowest caffeine dose (i.e., 0.1 mM;  $M = 64.580$ ,  $SD = 4.403$ ,  $p < 0.001$ ), and the moderate caffeine dose (i.e., 0.25 mM;  $M = 62.68$ ,  $SD = 6.35$ ,  $p = 0.001$ ). **(B)** There was no significant main effect of caffeine [one-way ANOVA:  $F(4,25) = 9.09$ ,  $p = 0.474$ ], exposure [two-way ANOVA:  $F(1,20) = 0.331$ ,  $p = 0.571$ ], nor an interaction effect [two-way ANOVA:  $F(4,20) = 0.677$ ,  $p = 0.616$ ] on apoptosis, that is % CC3-positive cells. **(C)** There was no significant main effect of caffeine [one-way ANOVA:  $F(4,25) = 1.767$ ,  $p = 0.167$ ], exposure [two-way ANOVA:  $F(1,20) = 0.097$ ,  $p = 0.759$ ], nor an interaction effect [two-way ANOVA:  $F(4,20) = 0.413$ ,  $p = 0.797$ ] on % CC3/Ki67-positive cells. **(D)** Representative immunostaining, demonstrating, in order from the top panel, DAPI-positive cell density, % Ki67-, % CC3-, and % Ki67/CC3-positive cells following exposure to different caffeine concentrations. Images taken at 10 $\times$  objective; scale bar represents 100  $\mu$ m. % Ki67-, % CC3-, and % Ki67/CC3-positive cells are controlled for by DAPI. Cell line: HPC0A07/03; passage number: P21; biological replicates:  $n = 3$ ; technical replicates:  $n = 3$ ; data represents the mean ( $\pm$ SD); \*\* $p < 0.01$  (adjusted  $p$ -values; Bonferroni correction). Graphs **(B,C)** are not stratified by exposure given that no main effect of exposure was found. Graphs **(B,C)** present the pooled data of acute and repeated exposure.

to differences in study design; all previous findings were from an animal model, and therefore are not entirely translatable to our own study design that uses a human *in vitro* cellular model. Furthermore, our study found no effect of lower caffeine doses on hippocampal proliferation, despite previous literature demonstrating a decrease in proliferation (Han et al., 2007; Wentz and Magavi, 2009). While the discrepancies between our findings and that of the previous literature could be a consequence of the different models used, it is more likely attributable to the different timescales investigated. While our study investigated repeated exposure over 72-h of proliferation, Wentz and Magavi (2009) and Han et al. (2007) investigated caffeine exposure over 7 days and 4 weeks, respectively. In the context of our work, while the supraphysiological caffeine concentration is strong enough to produce a detrimental effect over a short period of time, our 72-h paradigm may be insufficient to replicate the results seen from chronic exposure with lower, more physiologically relevant doses. Therefore, future work should seek to extend our paradigm to explore the longer-term effects of chronic, rather than repeated treatment, with physiologically relevant caffeine concentrations.

Previously unexplored within an *in vitro* model of HPCs, our findings relating to % Nestin- and % SOX2-positive cells may provide some insight into the mechanisms by which the supraphysiological caffeine dose influences proliferation. Used as markers for progenitor integrity in this study, Nestin and SOX2 represent the maintenance of the stem cell pool, with their knockout having been shown to lead to a reduction in total neural stem cell (NSC) quantity (Favaro et al., 2009; Park et al., 2010). In particular, SOX2 has been implicated as an important requirement for the maintenance of self-renewal and pluripotency in human embryonic hippocampal progenitors (Fong et al., 2008), and this has been further demonstrated in adult neural hippocampal progenitors. Ferri et al. (2004) found that knocking down SOX2 leads to reduced proliferation and a depletion of the neural hippocampal progenitor pool – a finding seemingly consistent with our own. Indeed, we report a reduction in both % Nestin-, % SOX- and % Nestin/SOX2-positive cells, and simultaneously find no change in either the total % CC3-positive cells or % CC3/Ki67-positive cells (i.e., specifically proliferative cell death), suggesting that the observed decrease in proliferation following repeated supraphysiological caffeine treatment could stem from a reduction in the hippocampal progenitor pool itself. However, given that Ki67 was not co-labeled with SOX2, this requires further substantiation. We do not know if the observed reduction in % Ki67-positive cells derive directly from

the observed decrease in % SOX2-positive cells. It is possible that the two may be independent; our findings for proliferation could pertain to a reduction in the proliferative capacity and/or speed of NSCs rather than as a knock-on effect of a reduced progenitor pool.

Interestingly, we find no statistically significant effect of supraphysiological caffeine doses on SOX2 relative to control conditions, however we believe that this could potentially be due to issues of power (Cremers et al., 2017), given that prior to *post hoc* adjustment, the supraphysiological concentration of  $\sim 10$  cups of coffee shows a reduction in both % Nestin-, % SOX2-, and % Nestin/Ki67-positive cells, all relative to control conditions. Furthermore, it is notable that hippocampal progenitor integrity was statistically assessed using non-parametric methods, which are typically less powerful than parametric equivalents (Siegel, 1957). Therefore, it would be highly profitable for future research to include a greater sample size to more fully elucidate the effect of supraphysiological caffeine concentrations on hippocampal progenitor integrity.

The precise mechanisms by which caffeine affects proliferation are widely unknown, but the observed changes to % SOX2-positive cells may provide some insight. Caffeine has commonly been associated with protein kinase B (PKB or Akt) signaling; specifically, it has been attributed to downregulating Akt signaling in a wide range of cell types, from HeLa to mouse epidermal cell lines (Nomura et al., 2005; Saiki et al., 2011). Pertinently, Akt signaling has been linked with SOX2, having been shown to promote the expression of SOX2 adult hippocampal neural progenitor cells (Peltier et al., 2010). Furthermore, Akt signaling itself decreases with age, akin to SOX2 expression and neurogenesis overall, but its reactivation has been shown to ameliorate age-related defects in neuronal development (Tang et al., 2019). It is therefore possible that our finding of reduced % SOX2-positive cells following supraphysiological caffeine treatment is a product of downregulated Akt signaling. To our knowledge, the effect of caffeine on Akt signaling within an HPC cell line has not yet been investigated, and therefore future research would be instrumental in validating a link between caffeine and SOX2 expression in HPCs and revealing whether this action could be mediated by Akt signaling.

While our work reveals a negative effect of supraphysiological caffeine on human hippocampal progenitor integrity and proliferation, there are some limitations in that our model may have influenced the extent to which caffeine affects this process. For example, caffeine is metabolized in the liver by

the enzyme CYP1A2, which accounts for approximately 90% of caffeine metabolism (Arnaud, 2011). Interestingly, a C/A polymorphism in intron 1 of the CYP1A2 gene appears to affect CYP1A2 enzymatic activity, and ultimately alter the rate of caffeine metabolism (Sachse et al., 2001). Indeed, Butler et al. (1992) defined CYP1A2 activity as being trimodally distributed, with slow, intermediate, and rapid metabolizers, as determined by caffeine urinary metabolite analyses. Essentially, the rates of caffeine clearance differ depend on an individual's genetic variant, and therefore the amount of time that caffeine is present in the systemic environment is subject to interindividual differences. These differences in caffeine metabolic rates have been associated with differences in the risk of some neurodegenerative diseases, with individuals possessing the C allele, i.e., slow metabolizers, having decreased caffeine-related risk of Parkinson's Disease (Popat et al., 2011; Chuang et al., 2016). Therefore, it is possible that this polymorphism may also mediate differences in the way caffeine affects proliferation, especially considering that caffeine reaches the brain via the systemic environment. Our study measures the direct effect of caffeine exposure on hippocampal progenitor cells, without accounting for differential metabolic rates in the liver caused by the CYP1A2 polymorphism.

Furthermore, while the caffeine concentrations used in our study reflect "intake," this is not representative of peak plasma levels obtained following caffeine metabolism. Indeed, around 99% of caffeine is metabolized into paraxanthine, theobromine, and theophylline (Arnaud, 1993; Nehlig, 2018) and, thus, only residual caffeine remains in the systemic environment. For instance, consumption of 160 mg of caffeine, in the form of a hot coffee, was shown to produce an average peak plasma level of 3.74  $\mu\text{g/mL}$ , or 19.26  $\mu\text{M}$ , in humans (White et al., 2016). The lowest caffeine concentration in our study, 0.1 mM, represents approximately 150 mg of caffeine (Su et al., 2013a,b), or one Starbucks cappuccino (Ludwig et al., 2014), whereas plasma caffeine levels typically reach between 20 and 50  $\mu\text{M}$  (Graham, 2001). Therefore, the levels of caffeine tested in this study reflect supranutritional doses, not the physiologically relevant concentrations that would reach the neurogenic niche *in vivo*. However, this study provides proof of concept that caffeine can modulate hippocampal progenitor proliferation, but it would be profitable for future research to investigate the effects of nutritional and supranutritional caffeine concentrations on this process over time. Understanding when in the trajectory of the neurogenic process these changes occur would be hugely beneficial for developing more targeted prevention strategies. Applying a growth curve analysis strategy to the proliferation and differentiation assays could be a viable solution.

An additional limitation to our work is that although CC3 is a commonly used marker for apoptosis, there are multiple modes of cell death, and even several pathways of apoptotic cell death (Galluzzi et al., 2018) that cannot be captured by a single marker, and particularly under stressful conditions *in vivo* (Riegelsberger et al., 2011). Thus, although we observe no change in apoptosis in the context of our work, additional markers (e.g., Annexin and TUNEL) would provide a more comprehensive overview of the apoptotic process.

Furthermore, although our aim was to explore the effect of caffeine on hippocampal progenitor cells, given that diet has been shown to specifically influence neural hippocampal progenitor behavior (Spéder et al., 2011; Sakayori et al., 2013), our work would hugely benefit from exploring the impact of caffeine on neural progenitor differentiation. By only investigating proliferation, we do not know what longer-term, knock-on effects might arise from caffeine treatment, with respect to differentiation and/or survival. Given that early changes to the hippocampal progenitor pool can reduce neurogenesis and result in morphological abnormalities of the resulting neurons (Cavallaro et al., 2008), future work should seek to extend our paradigm to also evaluate the impact of caffeine on differentiation and neuron morphology in order to more fully capture the impact of caffeine on the neurogenic process as a whole.

Finally, it is important to acknowledge that cell models are somewhat removed from an *in vivo* system making it challenging to account for any organism-wide changes. Furthermore, our model specifically is hindered by the lack of microglia, which play a key role in NSC regulation (Cunningham et al., 2013; Liu et al., 2013) and by the use of fetal NSCs to study proliferation during later life stages. Additionally, our findings should be interpreted with caution when generalizing to both male and females, given that this is a female cell line. Research shows sexual dimorphism in cognition (Ycaza Herrera et al., 2019), caffeine metabolism (Adan et al., 2008; Denden et al., 2016) and neurogenesis (Greiner et al., 2019).

However, despite these limitations to our work, this study is the first, to our knowledge, to investigate the direct effects of caffeine on hippocampal progenitor proliferation and integrity using a human *in vitro* cellular model. NSC proliferation is influenced by a range of systemic and environmental factors that are difficult to control for in an *in vivo* environment (Azari and Reynolds, 2016) – an issue that is mostly controlled for in *in vitro* models. Moreover, species and strain differences have long been a criticism of animal models (Martić-Kehl et al., 2012), and proliferation in particular has been shown to widely differ amongst mammalian species (Amrein et al., 2011). Therefore, our work investigates the direct effect of caffeine on human hippocampal stem cell proliferation and is thus likely to yield results with greater translational value.

Additionally, it is worth mentioning that our results have implications beyond the impact of metabolites or drugs on learning, aging, and cognitive decline. Indeed, recent research has highlighted the interaction of certain drugs with NSCs (Ikhsan et al., 2019), something with which our results are in strong accordance. Notably, there is a strong evidence base demonstrating a clear interaction of antidepressants with NSCs (Santarelli et al., 2003; Anacker et al., 2011), producing an increase in hippocampal progenitor proliferation. However, there is limited data available for substances beyond antidepressants (Ikhsan et al., 2019), especially concerning those of a non-pharmacological nature. Therefore, not only do our findings contribute to the growing discussion surrounding drug-NSC interactions, but they also provide evidence of such an interaction with a dietary-based substance, highlighting the possibility of utilizing diet as a non-pharmacological intervention to positively



influence hippocampal neurogenesis. However, further research is required to identify positive dietary components and fully elucidate their interaction with NSCs and their effect on hippocampal neurogenesis.

## CONCLUSION

In summary, our study demonstrates that dietary components such as caffeine can influence hippocampal progenitor proliferation and may be indicative of one mechanism by which diet affects cognitive outcomes. However, future research that (i) further explores the effects of human consumption-related caffeine doses on both neural progenitor proliferation and differentiation, and (ii) correlates this with cognitive outcomes, are now needed.

## DATA AVAILABILITY STATEMENT

All datasets presented in this study are included in the article/**Supplementary Material**.

## AUTHOR CONTRIBUTIONS

VH: design and conceptualization of the study, data collection, statistical analysis, data interpretation, and drafting and revising the manuscript for intellectual content. AD: design and conceptualization of the study, data collection, supervision, statistical analysis, data interpretation, and drafting and revising the manuscript for intellectual content. SL-A: statistical analysis, data interpretation, and revising the manuscript for intellectual

content. CL, DL, MU-S, SR, BA, RG-D, CA-L, LA, PL, AK, CS, and CM: data interpretation and revising the manuscript for intellectual content. ST: design and conceptualization of the study, statistical analysis, data interpretation, and drafting and revising the manuscript for intellectual content. All authors contributed to the article and approved the submitted version.

## FUNDING

This project was part of the EU consortium DCogPlast “Diet Cognition and Plasticity” funded by JPI-HDHL (Medical Research Council UK: MR/N030087/1; French National Research Agency ANR-15-HDHL-0002-05; PCIN-2015-229- MINECO; CiberFES- Cofund by FEDER Program from EU, 2017SGR1546 and ICREA 2018 Academia Award from the Generalitat de Catalunya), the BMFWF under BMFWF-10.420/0009-WF/V/3c/2015. PL was supported by the Urban Mental Health RPA from the University of Amsterdam.

## ACKNOWLEDGMENTS

This is a short text to acknowledge the contributions of specific colleagues, institutions, or agencies that aided the efforts of the authors.

## SUPPLEMENTARY MATERIAL

The Supplementary Material for this article can be found online at: <https://www.frontiersin.org/articles/10.3389/fcell.2020.00806/full#supplementary-material>

## REFERENCES

- Abbink, M. R., Schipper, L., Naninck, E. F., de Vos, C. M., Meier, R., van der Beek, E. M., et al. (2020). The effects of early life stress, postnatal diet modulation, and long-term western-style diet on later-life metabolic and cognitive outcomes. *Nutrients* 12:570. doi: 10.3390/nu12020570
- Adan, A., Prat, G., Fabbri, M., and Sánchez-Turet, M. (2008). Early effects of caffeinated and decaffeinated coffee on subjective state and gender differences. *Prog. Neuro Psychopharmacol. Biol. Psychiatry* 32, 1698–1703. doi: 10.1016/j.pnpbp.2008.07.005
- Amrein, I., Isler, K., and Lipp, H. P. (2011). Comparing adult hippocampal neurogenesis in mammalian species and orders: influence of chronological age and life history stage. *Eur. J. Neurosci.* 34, 978–987. doi: 10.1111/j.1460-9568.2011.07804.x
- Anacker, C., Zunsain, P. A., Cattaneo, A., Carvalho, L. A., Garabedian, M. J., Thuret, S., et al. (2011). Antidepressants increase human hippocampal neurogenesis by activating the glucocorticoid receptor. *Mol. Psychiatry* 16, 738–750. doi: 10.1038/mp.2011.26
- Arab, L., Biggs, M. L., O'Meara, E. S., Longstreth, W. T., Crane, P. K., and Fitzpatrick, A. L. (2011). Gender differences in tea, coffee, and cognitive decline in the elderly: the cardiovascular health study. *J. Alzheimers Dis.* 27, 553–566. doi: 10.3233/jad-2011-110431
- Arnaud, M. J. (1993). “Metabolism of caffeine and other components of coffee,” in *Caffeine, Coffee, and Health*, ed. S. Garattini (Pennsylvania, PA: Raven Press), 43–95.
- Arnaud, M. J. (2011). “Pharmacokinetics and metabolism of natural methylxanthines in animal and man,” in *Methylxanthines*, ed. B. B. Fredholm (Berlin: Springer), 33–91. doi: 10.1007/978-3-642-13443-2\_3
- Azari, H., and Reynolds, B. A. (2016). In vitro models for neurogenesis. *Cold Spring Harb. Perspect. Biol.* 8:a021279. doi: 10.1101/cshperspect.a021279
- Baptista, P., and Andrade, J. P. (2018). Adult hippocampal neurogenesis: regulation and possible functional and clinical correlates. *Front. Neuroanat.* 12:44. doi: 10.3389/fnana.2018.00044
- Beltz, B. S., Thlusty, M. F., Benton, J. L., and Sandeman, D. C. (2007). Omega-3 fatty acids upregulate adult neurogenesis. *Neurosci. Lett.* 415, 154–158. doi: 10.1016/j.neulet.2007.01.010
- Butler, M. A., Lang, N. P., Young, J. F., Caporaso, N. E., Vineis, P., Hayes, R. B., et al. (1992). Determination of CYP1A2 and NAT2 phenotypes in human populations by analysis of caffeine urinary metabolites. *Pharmacogenetics* 2, 116–127. doi: 10.1097/00008571-199206000-00003
- Cavallaro, M., Mariani, J., Lancini, C., Latorre, E., Caccia, R., Gullo, F., et al. (2008). Impaired generation of mature neurons by neural stem cells from hypomorphic Sox2 mutants. *Development* 135, 541–557. doi: 10.1242/dev.010801
- Cavallucci, V., Fidaleo, M., and Pani, G. (2016). Neural stem cells and nutrients: poised between quiescence and exhaustion. *Trends Endocrinol Metab.* 27, 756–769. doi: 10.1016/j.tem.2016.06.007
- Chell, J. M., and Brand, A. H. (2010). Nutrition-responsive glia control exit of neural stem cells from quiescence. *Cell* 143, 1161–1173. doi: 10.1016/j.cell.2010.12.007
- Chuang, Y. H., Lill, C. M., Lee, P. C., Hansen, J., Lassen, C. F., Bertram, L., et al. (2016). Gene-environment interaction in Parkinson's disease: coffee,

- ADORA2A, and CYP1A2. *Neuroepidemiology* 47, 192–200. doi: 10.1159/000450855
- Clelland, C. D., Choi, M., Romberg, C. C. G. J., Clemenson, G. D., Fragniere, A., Tyers, P., et al. (2009). A functional role for adult hippocampal neurogenesis in spatial pattern separation. *Science* 325, 210–213. doi: 10.1126/science.1173215
- Cremers, H. R., Wager, T. D., and Yarkoni, T. (2017). The relation between statistical power and inference in fMRI. *PLoS One* 12:e0184923. doi: 10.1371/journal.pone.0184923
- Cunningham, C. L., Martínez-Cerdeño, V., and Noctor, S. C. (2013). Microglia regulate the number of neural precursor cells in the developing cerebral cortex. *J. Neurosci.* 33, 4216–4233. doi: 10.1523/JNEUROSCI.3441-12.2013
- de Lucia, C., Murphy, T., Steves, C. J., Dobson, R. J., Proitsi, P., and Thuret, S. (2020). Lifestyle mediates the role of nutrient-sensing pathways in cognitive aging: cellular and epidemiological evidence. *Commun. Biol.* 3, 1–17. doi: 10.1038/s42003-020-0844-1
- Denden, S., Bouden, B., Haj Khelil, A., Ben Chibani, J., and Hamdaoui, M. H. (2016). Gender and ethnicity modify the association between the CYP1A2 rs762551 polymorphism and habitual coffee intake: evidence from a meta-analysis. *Genet. Mol. Res.* 15:487. doi: 10.4238/gmr.15027487
- Efsa Panel on Dietetic Products, Nutrition, and Allergies (NDA) (2015). Scientific Opinion on the safety of caffeine. *EFSA J.* 13:4102. doi: 10.2903/j.efsa.2015.4102
- Favaro, R., Valotta, M., Ferri, A. L., Latorre, E., Mariani, J., Giachino, C., et al. (2009). Hippocampal development and neural stem cell maintenance require Sox2-dependent regulation of Shh. *Nat. Neurosci.* 12, 1248–1256. doi: 10.1038/nn.2397
- Ferré, S. (2016). Mechanisms of the psychostimulant effects of caffeine: implications for substance use disorders. *Psychopharmacology* 233, 1963–1979. doi: 10.1007/s00213-016-4212-2
- Ferri, A. L., Cavallaro, M., Braidà, D., Di Cristofano, A., Canta, A., Vezzani, A., et al. (2004). Sox2 deficiency causes neurodegeneration and impaired neurogenesis in the adult mouse brain. *Development* 131, 3805–3819. doi: 10.1242/dev.01204
- Fong, H., Hohenstein, K. A., and Donovan, P. J. (2008). Regulation of self-renewal and pluripotency by Sox2 in human embryonic stem cells. *Stem Cells* 26, 1931–1938. doi: 10.1634/stemcells.2007-1002
- Fotuhi, M., Mohassel, P., and Yaffe, K. (2009). Fish consumption, long-chain omega-3 fatty acids and risk of cognitive decline or Alzheimer disease: a complex association. *Nat. Rev. Neurol.* 5, 140–152. doi: 10.1038/ncpneuro1044
- Galluzzi, L., Vitale, I., Aaronson, S. A., Abrams, J. M., Adam, D., Agostinis, P., et al. (2018). Molecular mechanisms of cell death: recommendations of the nomenclature committee on cell death 2018. *Cell Death Differ.* 25, 486–541. doi: 10.1038/s41418-017-0012-4
- Glade, M. J. (2010). Caffeine—not just a stimulant. *Nutrition* 26, 932–938. doi: 10.1016/j.nut.2010.08.004
- Gonçalves, J. T., Schafer, S. T., and Gage, F. H. (2016). Adult neurogenesis in the hippocampus: from stem cells to behavior. *Cell* 167, 897–914. doi: 10.1016/j.cell.2016.10.021
- Gould, E., Tanapat, P., McEwen, B. S., Flugge, G., and Fuchs, E. (1998). Proliferation of granule cell precursors in the dentate gyrus of adult monkeys is diminished by stress. *Proc. Natl. Acad. Sci. U.S.A.* 95, 3168–3171. doi: 10.1073/pnas.95.6.3168
- Graham, T. E. (2001). Caffeine and exercise. *Sports Med.* 31, 785–807. doi: 10.2165/00007256-200131110-00002
- Greiner, J. F. W., Merten, M., Kaltschmidt, C., and Kaltschmidt, B. (2019). Sexual dimorphisms in adult human neural, mesoderm-derived, and neural crest-derived stem cells. *FEBS Lett.* 593, 3338–3352. doi: 10.1002/1873-3468.13606
- Hairston, I. S., Little, M. T., Scanlon, M. D., Barakat, M. T., Palmer, T. D., Sapolsky, R. M., et al. (2005). Sleep restriction suppresses neurogenesis induced by hippocampus-dependent learning. *J. Neurophysiol.* 94, 4224–4233. doi: 10.1152/jn.00218.2005
- Han, M. E., Park, K. H., Baek, S. Y., Kim, B. S., Kim, J. B., Kim, H. J., et al. (2007). Inhibitory effects of caffeine on hippocampal neurogenesis and function. *Biochem. Biophys. Res. Commun.* 356, 976–980. doi: 10.1016/j.bbrc.2007.03.086
- Heine, V. M., Maslam, S., Joels, M., and Lucassen, P. J. (2004). Prominent decline of newborn cell proliferation, differentiation, and apoptosis in the aging dentate gyrus, in absence of an age-related hypothalamus-pituitary-adrenal axis activation. *Neurobiol. Aging* 25, 361–375. doi: 10.1016/s0197-4580(03)00090-3
- Ho, N. F., Hooker, J. M., Sahay, A., Holt, D. J., and Roffman, J. L. (2013). In vivo imaging of adult human hippocampal neurogenesis: progress, pitfalls and promise. *Mol. Psychiatr.* 18, 404–416. doi: 10.1038/mp.2013.8
- Ikhshan, M., Palumbo, A., Rose, D., Zille, M., and Boltze, J. (2019). Neuronal stem cell and drug interactions: a systematic review and meta-analysis: concise review. *Stem Cells Transl. Med.* 8, 1202–1211. doi: 10.1002/sctm.19-0020
- Kempermann, G., Gage, F. H., Aigner, L., Song, H., Curtis, M. A., Thuret, S., et al. (2018). Human adult neurogenesis: evidence and remaining questions. *Cell Stem Cell* 23, 25–30. doi: 10.1016/j.stem.2018.04.004
- Lindqvist, A., Mohapel, P., Bouter, B., Frielingsdorf, H., Pizzo, D., Brundin, P., et al. (2006). High-fat diet impairs hippocampal neurogenesis in male rats. *Eur. J. Neurol.* 13, 1385–1388. doi: 10.1111/j.1468-1331.2006.01500.x
- Liu, J., Hjorth, E., Zhu, M., Calzarossa, C., Samuelsson, E.-B., Schultzberg, M., et al. (2013). Interplay between human microglia and neural stem/progenitor cells in an allogeneic co-culture model. *J. Cell. Mol. Med.* 17, 1434–1443. doi: 10.1111/jcmm.12123
- Lledo, P. M., Alonso, M., and Grubb, M. S. (2006). Adult neurogenesis and functional plasticity in neuronal circuits. *Nat. Rev. Neurosci.* 7, 179–193. doi: 10.1038/nrn1867
- Low, D. Y., Lefèvre-Arbogast, S., González-Domínguez, R., Urpi-Sarda, M., Micheau, P., Petera, M., et al. (2019). Diet-related metabolites associated with cognitive decline revealed by untargeted metabolomics in a prospective cohort. *Mol. Nutr. Food Res.* 2019:1900177. doi: 10.1002/mnfr.201900177
- Lucassen, P. J., Fitzsimons, C. P., Salta, E., and Maletic-Savatic, M. (2020). Adult neurogenesis, human after all (again): classic, optimized, and future approaches. *Behav. Brain Res.* 2020, 112458. doi: 10.1016/j.bbr.2019.112458
- Lucassen, P. J., Meerlo, P., Naylor, A. S., Van Dam, A. M., Dayer, A. G., Fuchs, E., et al. (2010). Regulation of adult neurogenesis by stress, sleep disruption, exercise and inflammation: Implications for depression and antidepressant action. *Eur. Neuropsychopharm.* 20, 1–17. doi: 10.1016/j.euroneuro.2009.08.003
- Ludwig, I. A., Mena, P., Calani, L., Cid, C., Del Rio, D., Lean, M. E., et al. (2014). Variations in caffeine and chlorogenic acid contents of coffees: what are we drinking? *Food Funct.* 5, 1718–1726. doi: 10.1039/C4FO00290C
- Martić-Kehl, M. I., Schibli, R., and Schubiger, P. A. (2012). Can animal data predict human outcome? Problems and pitfalls of translational animal research. *Eur. J. Nucl. Med. Mol. Imaging* 9, 1492–1496. doi: 10.1007/s00259-012-2177-x
- Miquel, S., Champ, C., Day, J., Aarts, E., Bahr, B. A., Bakker, M., et al. (2018). Poor cognitive ageing: vulnerabilities, mechanisms and the impact of nutritional interventions. *Ageing Res. Rev.* 42, 40–55. doi: 10.1016/j.arr.2017.12.004
- Nehlig, A. (2018). Interindividual differences in caffeine metabolism and factors driving caffeine consumption. *Pharmacol. Rev.* 70, 384–411. doi: 10.1124/pr.117.014407
- Nilsson, M., Perfilieva, E., Johansson, U., Orwar, O., and Eriksson, P. S. (1999). Enriched environment increases neurogenesis in the adult rat dentate gyrus and improves spatial memory. *J. Neurobiol.* 39, 569–578. doi: 10.1002/(sici)1097-4695(19990615)39:4<569::aid-neu10>3.0.co;2-f
- Nomura, M., Ichimatsu, D., Moritani, S., Koyama, I., Dong, Z., Yokogawa, K., et al. (2005). Inhibition of epidermal growth factor-induced cell transformation and Akt activation by caffeine. *Mol. Carcinog.* 44, 67–76. doi: 10.1002/mc.20120
- Oomen, C. A., Bekinschtein, P., Kent, B. A., Saksida, L. M., and Bussey, T. J. (2014). Adult hippocampal neurogenesis and its role in cognition. *Wiley Interdiscip. Rev. Cogn. Sci.* 5, 573–587. doi: 10.1002/wcs.1304
- Oomen, C. A., Soeters, H., Audureau, N., Vermunt, L., Van Hasselt, F. N., Manders, E. M., et al. (2010). Severe early life stress hampers spatial learning and neurogenesis, but improves hippocampal synaptic plasticity and emotional learning under high-stress conditions in adulthood. *J. Neurosci.* 30, 6635–6645. doi: 10.1523/JNEUROSCI.0247-10.2010
- Park, D., Xiang, A. P., Mao, F. F., Zhang, L., Di, C. G., Liu, X. M., et al. (2010). Nestin is required for the proper self-renewal of neural stem cells. *Stem Cells* 28, 2162–2171. doi: 10.1002/stem.541
- Peltier, J., Conway, A., Keung, A. J., and Schaffer, D. V. (2010). Akt increases Sox2 expression in adult hippocampal neural progenitor cells, but increased Sox2 does not promote proliferation. *Stem Cells Dev.* 20, 1153–1161. doi: 10.1089/scd.2010.0130
- Popat, R. A., Van Den Eeden, S. K., Tanner, C. M., Kamel, F., Umbach, D. M., Marder, K., et al. (2011). Coffee, ADORA2A, and CYP1A2: the caffeine connection in Parkinson's disease. *Eur. J. Neurol.* 18, 756–765. doi: 10.1111/j.1468-1331.2011.03353.x
- Rao, M. S., Hattiangady, B., and Shetty, A. K. (2006). The window and mechanisms of major age-related decline in the production of new neurons within the

- dentate gyrus of the hippocampus. *Aging Cell* 5, 545–558. doi: 10.1111/j.1474-9726.2006.00243.x
- Riegelberger, U.-M., Deten, A., Pösel, C., Zille, M., Kranz, A., Boltze, J., et al. (2011). Intravenous human umbilical cord blood transplantation for stroke: impact on infarct volume and caspase-3-dependent cell death in spontaneously hypertensive rats. *Exp. Neurol.* 227, 218–223. doi: 10.1016/j.expneurol.2010.11.008
- Ritchie, K., Carrière, I., De Mendonça, A., Portet, F., Dartigues, J. F., Rouaud, O., et al. (2007). The neuroprotective effects of caffeine: a prospective population study (the Three City Study). *Neurology* 69, 536–545. doi: 10.1212/01.wnl.0000266670.35219.0c
- Rosso, A., Mossey, J., and Lippa, C. F. (2008). Caffeine: neuroprotective functions in cognition and Alzheimer's disease. *Am. J. Alzheimer Dis. Dement.* 23, 417–422. doi: 10.1177/1533317508320083
- Sachse, C., Brockmüller, J., Bauer, S., and Roots, I. (2001). Functional significance of a C→A polymorphism in intron 1 of the cytochrome P450 CYP1A2 gene tested with caffeine. *Br. J. Clin. Pharmacol.* 47, 445–449. doi: 10.1046/j.1365-2125.1999.00898.x
- Sahay, A., Scobie, K. N., Hill, A. S., O'Carroll, C. M., Kheirbek, M. A., Burghardt, N. S., et al. (2011). Increasing adult hippocampal neurogenesis is sufficient to improve pattern separation. *Nature* 472, 466–470. doi: 10.1038/nature09817
- Saiki, S., Sasazawa, Y., Imamichi, Y., Kawajiri, S., Fujimaki, T., Tanida, I., et al. (2011). Caffeine induces apoptosis by enhancement of autophagy via PI3K/Akt/mTOR/p70S6K inhibition. *Autophagy* 7, 176–187. doi: 10.4161/auto.7.2.14074
- Sakayori, N., Kimura, R., and Osumi, N. (2013). Impact of lipid nutrition on neural stem/progenitor cells. *Stem Cells Int.* 2013:973508. doi: 10.1155/2013/973508
- Santarelli, L., Saxe, M., Gross, C., Surget, A., Battaglia, F., Dulawa, S., et al. (2003). Requirement of hippocampal neurogenesis for the behavioral effects of antidepressants. *Science* 301, 805–809. doi: 10.1126/science.1083328
- Siegel, S. (1957). Nonparametric statistics. *Am. Stat.* 11, 13–19. doi: 10.1080/00031305.1957.10501091
- Small, S. A., Tsai, W. Y., De La Paz, R., Mayeux, R., and Stern, Y. (2002). Imaging hippocampal function across the human life span: is memory decline normal or not? *Ann. Neurol.* 51, 290–295. doi: 10.1002/ana.10105
- Smeeth, D. M., Kouroukidou, I., Duarte, R. R., Powell, T. R., and Thuret, S. (in press). Prolactin, estradiol and testosterone differentially impact human hippocampal neurogenesis in an *in vitro* model. *Neuroscience* doi: 10.1016/j.neuroscience.2019.12.021
- Snyder, J. S., Hong, N. S., McDonald, R. J., and Wojtowicz, J. M. (2005). A role for adult neurogenesis in spatial long-term memory. *Neuroscience* 130, 843–852. doi: 10.1016/j.neuroscience.2004.10.009
- Spalding, K. L., Bergmann, O., Alkass, K., Bernard, S., Salehpour, M., Huttner, H. B., et al. (2013). Dynamics of hippocampal neurogenesis in adult humans. *Cell* 153, 1219–1227. doi: 10.1016/j.cell.2013.05.002
- Spéder, P., and Brand, A. H. (2014). Gap junction proteins in the blood-brain barrier control nutrient-dependent reactivation of *Drosophila* neural stem cells. *Dev. Cell* 30, 309–321. doi: 10.1016/j.devcel.2014.05.021
- Spéder, P., Liu, J., and Brand, A. H. (2011). Nutrient control of neural stem cells. *Curr. Opin. Cell Biol.* 23, 724–729. doi: 10.1016/j.ceb.2011.08.004
- Stangl, D., and Thuret, S. (2009). Impact of diet on adult hippocampal neurogenesis. *Genes Nutr.* 4, 271–282. doi: 10.1007/s12263-009-0134-5
- Su, S. J., Chang, K. L., Su, S. H., Yeh, Y. T., Shyu, H. W., and Chen, K. M. (2013). Caffeine regulates osteogenic differentiation and mineralization of primary adipose-derived stem cells and a bone marrow stromal cell line. *Int. J. Food Sci. Nutr.* 64, 429–436. doi: 10.3109/09637486.2012.759184
- Su, S. H., Shyu, H. W., Yeh, Y. T., Chen, K. M., Yeh, H., and Su, S. J. (2013). Caffeine inhibits adipogenic differentiation of primary adipose-derived stem cells and bone marrow stromal cells. *Toxicol. Vitro* 27, 1830–1837. doi: 10.1016/j.tiv.2013.05.011
- Tang, C., Wang, M., Wang, P., Wang, L., Wu, Q., and Guo, W. (2019). Neural stem cells behave as a functional niche for the maturation of newborn neurons through the secretion of PTN. *Neuron* 101, 32–44. doi: 10.1016/j.neuron.2018.10.051
- van Praag, H., Shubert, T., Zhao, C., and Gage, F. H. (2005). Exercise enhances learning and hippocampal neurogenesis in aged mice. *J. Neurosci.* 25, 8680–8685. doi: 10.1523/JNEUROSCI.1731-05.2005
- Villeda, S. A., Luo, J., Mosher, K. I., Zou, B., Britschgi, M., Bieri, G., et al. (2011). The ageing systemic milieu negatively regulates neurogenesis and cognitive function. *Nature* 477, 90–94. doi: 10.1038/nature10357
- Wentz, C. T., and Magavi, S. S. (2009). Caffeine alters proliferation of neuronal precursors in the adult hippocampus. *Neuropharmacology* 56, 994–1000. doi: 10.1016/j.neuropharm.2009.02.002
- White, J. R. Jr., Padowski, J. M., Zhong, Y., Chen, G., Luo, S., Lazarus, P., et al. (2016). Pharmacokinetic analysis and comparison of caffeine administered rapidly or slowly in coffee chilled or hot versus chilled energy drink in healthy young adults. *Clin. Toxicol.* 54, 308–312. doi: 10.3109/15563650.2016.1146740
- Winocur, G., and Greenwood, C. E. (2005). Studies of the effects of high fat diets on cognitive function in a rat model. *Neurobiol. Aging* 26, 46–49. doi: 10.1016/j.neurobiolaging.2005.09.003
- Witte, A. V., Fobker, M., Gellner, R., Knecht, S., and Flöel, A. (2009). Caloric restriction improves memory in elderly humans. *Proc. Natl. Acad. Sci. U.S.A.* 106, 1255–1260. doi: 10.1073/pnas.0808587106
- Yam, K. Y., Schipper, L., Reemst, K., Ruigrok, S. R., Abbink, M. R., Hoeijmakers, L., et al. (2019). Increasing availability of  $\omega$ -3 fatty acid in the early-life diet prevents the early-life stress-induced cognitive impairments without affecting metabolic alterations. *FASEB J.* 33, 5729–5740. doi: 10.1096/fj.201802297R
- Ycaza Herrera, A., Wang, J., and Mather, M. (2019). The gist and details of sex differences in cognition and the brain: how parallels in sex differences across domains are shaped by the locus coeruleus and catecholamine systems. *Prog. Neurobiol.* 176, 120–133. doi: 10.1016/j.pneurobio.2018.05.005
- Yousef, H., Czupalla, C. J., Lee, D., Chen, M. B., Burke, A. N., Zera, K. A., et al. (2019). Aged blood impairs hippocampal neural precursor activity and activates microglia via brain endothelial cell VCAM1. *Nat. Med.* 25, 988–1000. doi: 10.1038/s41591-019-0440-4

**Conflict of Interest:** The authors declare that the research was conducted in the absence of any commercial or financial relationships that could be construed as a potential conflict of interest.

Copyright © 2020 Houghton, Du Preez, Lefèvre-Arbogast, de Lucia, Low, Urpi-Sarda, Ruigrok, Altendorfer, González-Domínguez, Andres-Lacueva, Aigner, Lucassen, Korosi, Samieri, Manach and Thuret. This is an open-access article distributed under the terms of the Creative Commons Attribution License (CC BY). The use, distribution or reproduction in other forums is permitted, provided the original author(s) and the copyright owner(s) are credited and that the original publication in this journal is cited, in accordance with accepted academic practice. No use, distribution or reproduction is permitted which does not comply with these terms.



# Effects of Isorhamnetin in Human Amniotic Epithelial Stem Cells *in vitro* and Its Cardioprotective Effects *in vivo*

Kazuhiro Aonuma<sup>1,2</sup>, Farhana Ferdousi<sup>2,3</sup>, DongZhu Xu<sup>2,4</sup>, Kenichi Tominaga<sup>2</sup> and Hiroko Isoda<sup>1,2,3,5\*</sup>

<sup>1</sup> School of Integrative and Global Majors (SIGMA), University of Tsukuba, Tsukuba, Japan, <sup>2</sup> AIST-University of Tsukuba Open Innovation Laboratory for Food and Medicinal Resource Engineering (FoodMed-OIL), AIST, University of Tsukuba, Tsukuba, Japan, <sup>3</sup> Alliance for Research on the Mediterranean and North Africa (ARENA), University of Tsukuba, Tsukuba, Japan, <sup>4</sup> Cardiovascular Division, Institute of Clinical Medicine, Faculty of Medicine, University of Tsukuba, Tsukuba, Japan, <sup>5</sup> Faculty of Life and Environmental Sciences, University of Tsukuba, Tsukuba, Japan

## OPEN ACCESS

### Edited by:

Sveva Bollini,  
University of Genoa, Italy

### Reviewed by:

Laura Iop,  
University of Padua, Italy  
Olga Pershina,  
Research Institute of Pharmacology  
and Regenerative Medicine Named  
ED Goldberg (RAS), Russia

### \*Correspondence:

Hiroko Isoda  
isoda.hiroko.ga@u.tsukuba.ac.jp

### Specialty section:

This article was submitted to  
Stem Cell Research,  
a section of the journal  
Frontiers in Cell and Developmental  
Biology

**Received:** 30 June 2020

**Accepted:** 31 August 2020

**Published:** 29 September 2020

### Citation:

Aonuma K, Ferdousi F, Xu D,  
Tominaga K and Isoda H (2020)  
Effects of Isorhamnetin in Human  
Amniotic Epithelial Stem Cells *in vitro*  
and Its Cardioprotective Effects  
*in vivo*.  
Front. Cell Dev. Biol. 8:578197.  
doi: 10.3389/fcell.2020.578197

Cardiac hypertrophy and fibrosis are major pathophysiologic disorders that lead to serious cardiovascular diseases (CVDs), such as heart failure and arrhythmia. It is well known that transforming growth factor  $\beta$  (TGF $\beta$ ) signaling pathways play a major role in the proliferation of cardiac hypertrophy and fibrosis, which is mainly stimulated by angiotensin II (AngII). This study aimed to investigate the cardioprotective potential of isorhamnetin (ISO) in human amniotic epithelial stem cells (hAECs) through global gene expression analysis and to confirm its beneficial effects on cardiac hypertrophy and fibrosis in the AngII-induced *in vivo* model. *In vitro*, biological processes including TGF $\beta$ , collagen-related functions, and inflammatory processes were significantly suppressed in ISO pretreated hAECs. *In vivo*, continuous AngII infusion using an osmotic pump induced significant pathological fibrosis and myocardial hypertrophy, which were remarkably suppressed by ISO pretreatment. ISO was found to reverse the enhanced TGF $\beta$  and Collagen type I alpha 1 mRNA expression induced by AngII exposure, which causes cardiovascular remodeling in ventricular tissue. These findings indicate that ISO could be a potential agent against cardiac hypertrophy and fibrosis.

**Keywords:** human amniotic epithelial stem cells, drug screening, isorhamnetin, cardiac fibrosis, angiotensin II, translational medicine

## INTRODUCTION

Pathological cardiac fibrosis is a fundamental process in the excessive accumulation of extracellular matrix (ECM) such as collagen (Travers et al., 2016), which plays a key role in the disruption of the myocardial architecture, myocardial disarray, and electrical and mechanical cardiomyocyte dysfunction (Izawa et al., 2005). In addition, the loss of normal ECM structure impairs the integrity of cell-to-cell contraction, further isolates myocardial fibers, impairs oxygen supply, and causes atrophy and necrosis (Kai et al., 2006). Thus, cardiac fibrosis leads to various heart diseases, including cardiac hypertrophy, arrhythmia, and heart failure (Weber et al., 2008; Yue et al., 2011) and is considered an independent risk factor for cardiac morbidity and mortality (Bang et al., 2017;



Jin et al., 2018). Controlling hypertrophic remodeling and fibrotic changes may therefore offer a promising therapeutic strategy for reducing the cardiovascular disease (CVD) burden.

In recent years, increasing numbers of small molecules derived from or based on bioactive compounds of medicinal plants have been synthesized and screened for their potential therapeutic and preventive effects in CVD. However, the discovery of drugs is greatly hampered by the gap between the validation of the compound and its successful clinical application (Pott et al., 2020). One of the primary reasons for this translational inefficiency is the unpredictability of the currently used *in vitro* cellular models and the complexity of the *in vivo* microenvironment. Even the most high-throughput screening assays utilize monolayer cell cultures, where the crucial elements of drug-biology interactions are lost (Li and Kilian, 2015). Therefore, physiologically more relevant *in vitro* human models for screening and validation of thousands of compounds are in high demand in both academic research and the pharmaceutical industry. In this context, stem-cell-based approaches using human pluripotent stem cells, including both human embryonic stem cell (ESC) and induced pluripotent stem cell (iPSC), have received great attention as effective tools for drug screening, not only for CVDs but also for other metabolic and neuronal diseases (Grskovic et al., 2011; Engle and Puppala, 2013). However, cell resources, ethical constraints, invasive extraction procedures, and expensive cell reprogramming and maintenance procedures make this type of stem cell less favorable as a practical source for drug screening (Chen et al., 2014).

In this context, human amniotic epithelial stem cells (hA ESCs) possess substantial advantages over other stem cells. hA ESCs are derived from term placenta after delivery and are discarded after birth. Therefore, they are readily available, do not require invasive harvesting procedures, and pose no ethical concerns. Most importantly, as hA ESCs are derived from pluripotent epiblasts, they maintain ESC-like multilineage differentiation potential. Studies have shown that upon appropriate differentiation protocol, hA ESCs can be differentiated into liver, pancreas and lung epithelium from endodermal origin, bone, and fat cells from mesodermal origin as well as neural cells from ectodermal origin (Miki et al., 2005, 2010; Toda et al., 2007; Parolini et al., 2008; Murphy et al., 2010; Zhou et al., 2013). Importantly, hA ESCs also have cardiogenic and angiogenic differentiation potential (Miki et al., 2005; Fang et al., 2012; Wu et al., 2017; Serra et al., 2018). Furthermore, hA ESCs have no tumorigenic, weak immunogenic, and strong immunomodulatory properties, and demonstrate mesenchymal stem cell (MSC)-like phenotypes as well (Miki, 2018; Yang et al., 2018; De Coppi and Atala, 2019). Thus, hA ESCs provide an excellent model system for drug discovery.

At the University of Tsukuba Hospital, the Tsukuba Human Tissue Biobank Center (THB) was established in November 2013 with the aim to reserve human biospecimens to facilitate medical research (Takeuchi et al., 2016). Among a variety of cellular samples, hA ESCs isolated from the donated full-term placenta are also preserved for research applications. In our previous studies, the stemness characteristics of hA ESCs

received from THB have been investigated (Ferdousi et al., 2019; Furuya et al., 2019). Although the primary amniotic epithelial cells were heterogenous, the hA ESCs isolated from the adherent subpopulations of passaged primary cells have widely expressed stemness markers. Besides, hA ESCs cultured in a 3D microenvironment as spheroids, have highly expressed the stemness-related genes compared to their 2D counterpart as well as compared to iPSCs and MSCs (Ferdousi et al., 2019). We have previously investigated the gene expression profiles of several natural compounds in hA ESCs (Ferdousi et al., 2019, 2020) in an effort to screen eligible natural compounds for further in-depth investigations. Among the compounds that we have screened in hA ESCs, isorhamnetin (ISO) exerts cardiac morphogenesis, and antifibrotic potential.

Isorhamnetin, also known as 3-Methylquercetin or 3'-Methoxyquercetin, is one of the most common and widely distributed plant flavonols. It has anti-inflammatory, antioxidant, antiadipogenic, and antitumor activities (Hu et al., 2015; Yang et al., 2016). We have previously reported the anti-oxidant, antiobesity, and antifibrotic effects of ISO in rodent models (Zar Kalai et al., 2013; Ganbold et al., 2019). Ganbold et al. (2019) reported that ISO could alleviate steatosis and fibrosis in a non-alcoholic steatohepatitis (NASH) mouse model by reducing the expression of liver injury marker transforming growth factor  $\beta$  (*Tgf $\beta$* ), and the fibrogenic marker Collagen type I alpha 1 (*Col1a1*). However, little is known about the possible protective effect of ISO against cardiac fibrosis or hypertrophy (Gao et al., 2017).

This study aimed to investigate the cardioprotective potential of ISO in hA ESCs through global gene expression analysis and to observe its effect on angiotensin II (AngII)-induced fibrosis and hypertrophy in the myocardium of mice.

## MATERIALS AND METHODS

### *In vitro* Study

#### hA ESCs Extraction and Culture

The procedure of cell isolation and cell culture have been explained elsewhere in detail (Ferdousi et al., 2019, 2020; Furuya et al., 2019). Briefly, hA ESCs were obtained from the term placenta donated by mothers who underwent cesarean delivery. The amnion was washed with 200 mL of Hank's Basic Salt Solution–Calcium and Magnesium Free (CMF-HBSS) after manual separation from the chorion and was cut into smaller pieces using a surgical scissor. The cells were maintained in placental epithelial cell basal medium (Promocell, # C-26140). The medium was changed every 2–4 days. To subculture hA ESCs, the plates were first washed twice with 10 mL of PBS. Then, 3 mL of pre-digestion buffer, pre-warmed to 37°C, was added to the plate. The cells were then incubated at 37°C for 5 min. Subsequently, 5 mL of 0.05% (w/v) trypsin-EDTA, pre-warmed to 37°C, was added to the plate and incubated at 37°C for 10 min. Finally, 5 mL of Dulbecco's modified Eagle's medium (DMEM) was added to stop the reaction. The cell suspension was then centrifuged twice at 200 rpm for 4 min at 4°C.



## hAESC 3D Spheroid Formation and Cell Treatment

Lipidure<sup>TM</sup> (NOF Corporation, Cat. # CMS206; 400  $\mu$ L) solution was placed into each well of the 3D culture plate (Elplasia<sup>TM</sup>, Kuraray Co., Ltd., Cat # RB 500 400 NA 24) at a concentration of 50 mg in 10 mL absolute ethanol. Lipidure solution was aspirated out after 2 min. Then, the plate was dried for 3 h, 400  $\mu$ L of PBS was placed in each well, and the plate was centrifuged at  $2,000 \times g$  for 15 min at room temperature. After discarding the PBS, the wells were washed twice with 400  $\mu$ L of PBS. The plates were then stored in a cell culture incubator until use. Spheroids were formed by seeding hA ESCs ( $8 \times 10^5$  cells) in placental basal epithelial cell medium in 24-well plates. The initial culture was maintained for 24 h, and the control samples for day 0 were collected before adding the treatment. After 24 h, the medium was changed with 20  $\mu$ M ISO (Sigma-Aldrich, Japan). The medium was changed every 48 h, and the cells were maintained for 10 days. Control samples were maintained in placental basal epithelial cell medium, which was also changed every 48 h.

## hAESC RNA Extraction and Quantification

Total RNA was extracted using 1 mL of ISOGEN (Nippon Gene, Japan) following the manufacturer's instructions. RNA quality and quantity were measured using a NanoDrop 2000 spectrophotometer (Thermo Fisher Scientific, Wilmington, DE, United States).

## Microarray Gene Expression Profiling

Affymetrix microarray gene expression profiling was performed using GeneChip<sup>®</sup> 3' Expression Arrays and 3' IVT PLUS Reagent Kit (Affymetrix Inc., Santa Clara, CA, United States). From 100 ng of total RNA, amplified and biotinylated complementary RNA (cRNA) was generated for each sample following the user's manual. For hybridization, 9.4  $\mu$ G cRNA was used. Human genome array strips (HG-U219) were hybridized for 16 h in a 45°C incubator, washed, and stained. Finally, imaging was performed in the GeneAtlas Fluidics and Imaging Station.

## Microarray Data Processing and Analysis

Microarray analysis was conducted for two biological replicates of day 0 (D0) control, and three biological replicates of day 10 (D10) control and D10 ISO treated hA ESCs. Microarray raw image data (.cel file) were processed and normalized following the robust multichip average (RMA) algorithm using Expression Console Software (Affymetrix, Japan). Subsequent analysis was carried out using the freely available software Transcriptome Analysis Console (TAC) version 4 (Affymetrix, Japan). Differentially expressed genes (DEGs) were characterized as fold change  $\geq 1.5$  (in linear space) and  $p < 0.05$  (one-way between-subject). Gene ontology (GO) analysis was carried out using the Molecular Signatures Database (MSigDB) of Gene Set Enrichment Analysis online tool<sup>1</sup> (Mootha et al., 2003; Subramanian et al., 2005) and DAVID (Database for Annotation, Visualization, and Integrated Discovery, version 6.8) (Huang et al., 2008; Sherman et al., 2008). Heat maps were generated using a web tool Heatmapper<sup>2</sup> (Babicki et al., 2016).

<sup>1</sup><https://software.broadinstitute.org/gsea/index.jsp>

<sup>2</sup><http://www.heatmapper.ca/>

## In vivo Study

### Animal Preparation

Animal preparation: Male C57Bl/6 mice were (8 weeks of age; Japan Charles River Kanagawa, Japan) randomly assigned into three groups: control, AgII-administered group (AgII), and AgII and ISO-treated group (AgII + ISO). Mice in the AgII and AgII + ISO groups were continuously administered AgII (1,000 ng/kg/hr) with a mini-osmotic pump model (Alzet, model 2002, Cupertino, United States) for 2 weeks. Mice in the control group were infused with 0.85% saline. One week before the implantation of the mini-osmotic pumps, mice in the AgII + ISO group were administered ISO (5 mg/kg) intraperitoneally every day for 3 weeks. ISO was suspended in 0.1% dimethyl sulfoxide and 1% polypropylene glycol. Suspensions were freshly prepared and administered at a constant volume of 0.3 mL. Mice in the control and AgII groups were given the same volume of the vehicle solution (0.1% dimethyl sulfoxide, 1% polypropylene glycol, and normal saline) by intraperitoneal injection. Hearts were isolated immediately after exsanguination. Part of the left ventricles was fixed in 4% paraformaldehyde and embedded in paraffin for histological analysis. The remaining left ventricles were kept in liquid nitrogen for further analysis.

### Echocardiography

Echocardiography was performed using a Doppler echocardiographic system (Vevo 2100; Visual Sonics, Toronto, Canada). The mice were anesthetized with 1% isoflurane. Then, parasternal short-axis and parasternal long-axis 2D-guided echocardiographic views of the left ventricle (LV) were obtained at the level of the papillary muscles. The M-mode measurements of LV posterior wall thickness (LVPWT) and interventricular septal thickness (IVST) were obtained at the end of diastole and systole. LV mass was calculated using the following formula (Marwick et al., 2015):

$$\text{LV mass} = 1.04 [(\text{LVEDd} + \text{LVPWT} + \text{IVST})^3 - \text{LVEDd}^3] \times 0.8 + 0.6$$

LVEDd = LV end-diastolic dimension

### Histological Examination

Left ventricle was fixed in 4% paraformaldehyde and embedded in paraffin. The epicardium of the mid-lateral wall was cut into 2  $\mu$ m thick sections. All specimens were stained with Masson trichrome (MT) and hematoxylin-eosin (H-E) stain and examined under a light microscope (BZX710; Keyence, Osaka, Japan). Transmural distribution of the percentage area of fibrosis was calculated as the total area of fibrosis (defined as the amount of collagen deposition stained with the aniline blue) divided by the sum of the total tissue area. Myocyte area was measured in  $\sim 50$  cells at the site of a visible nucleus in each slide stained with H-E. The cross-sectional area of each myocyte (an average of 50 cardiomyocytes for each animal) was measured across the region corresponding to the visible nucleus in H-E stained slides.

### Real-Time Polymerase Chain Reaction (RT-PCR)

Total RNA was extracted from ventricular tissue using an RNeasy Mini Kit (Qiagen, Valencia, CA, United States) according to the

supplier's protocol. Total RNA (1 µg) was reverse transcribed to cDNA using a High-Capacity cDNA Reverse Transcription Kit (Thermo Fisher Scientific, Inc., Waltham, MA, United States). Real-time quantitative PCR was performed with PrimeTime Gene Expression Master Mix (Integrated DNA Technologies) on the ABI Prism 7500 FAST sequence detection system (Applied Biosystems, Foster City, CA, United States). The following primers were used for the experiment: natriuretic peptide B (*Nppb*; Mm.PT.588584045.g), *Col1a1* (Mm.PT.587562513), *Tgfb1* (Mm.PT.5811254750), and *Tgfb2* (Mm.PT.5814105470). Gene expression levels were normalized to the housekeeping gene, 18S rRNA (4319413E, Thermo Fisher Scientific).

## Chemicals

ISO was synthesized from quercetin (Fujifilm Wako Pure Chemical Corp., Tokyo, Japan) following the protocol of the National Institute of Advanced Industrial Science and Technology (Kato et al., 2016) and was used for *in vitro* and *in vitro* experiments. AgII was purchased from Wako Pure Chemical Industries Ltd (Osaka, Japan).

## Statistical Analysis

Results are expressed as the mean  $\pm$  standard deviation. A one-way analysis of variance (ANOVA) followed by Tukey's *post hoc* test was performed to examine the differences between pairs of treatment groups. Differences were considered statistically significant at  $p < 0.05$ . All analyses were performed using IBM SPSS version 21.0 software (IBM Co., Armonk, NY, United States).

## Ethical Considerations

The protocol for the hAESC study was reviewed and approved by the Ethical Review Committee of the University of Tsukuba. Informed written consent was obtained from the mothers who donated the placenta after delivery.

After receiving approval from the Institutional Animal Experiment Committee of the University of Tsukuba, animal experiments were carried out in accordance with the Guide for the Care and Use of Laboratory Animals published by the US National Institutes of Health, the Regulation for Animal Experiments in the University of Tsukuba, and the Fundamental Guideline for Proper Conduct of Animal Experiments and Related Activities in Academic Research Institutions under the jurisdiction of the Ministry of Education, Culture, Sports, Science and Technology of Japan.

# RESULTS

## ISO Regulated Cardiac Development and Fibrosis-Associated GO and KEGG Pathways

A total of 1210 unique genes (after excluding duplicate probe IDs) were differentially expressed (fold change  $> 1.5$ ;  $p < 0.05$ ) in ISO-treated hAESCs compared to untreated controls at D10. Among them, 528 genes were significantly upregulated, whereas 682 genes were downregulated (Figure 1A). Compared to D0

control, a total of 3449 and 3884 genes were significantly (fold change  $> 2$ ;  $p < 0.05$ ) regulated in D10 control and D10 ISO-treated hAESCs, respectively (Supplementary Figure 1). Compared to undifferentiated hAESCs at D0, control hAESCs at D10 regulated epithelial-mesenchymal transition (EMT), cell cycle, cell division, autophagy, and apoptosis-associated GO (Supplementary Figure 1), whereas ISO-treated hAESCs regulated anti-inflammatory and TGF $\beta$ -related biological functions as well as EMT. The differentiation potential was toward myogenesis (Supplementary Figure 1). We have previously reported that the undifferentiated hAESCs expressed several stem cell markers, and the 3D hAESC spheroids showed significantly higher expression of stemness-related genes than their 2D counterparts.

In this article, we will mainly explain the GO enriched by DEGs between D10 ISO-treated and untreated control hAESCs. Significantly enriched biological processes included ECM organization, TGF $\beta$  and collagen-related processes, and anti-inflammatory functions. Both canonical and non-canonical Wnt signaling pathways and MAPK pathways were regulated. Cell adhesion, cell migration, wound healing, EMT, and apoptosis were also significantly regulated. Additionally, several cardiovascular development-associated pathways were also significantly regulated, which included but were not limited to heart development, angiogenesis, smooth muscle cell proliferation and migration, endothelial cell proliferation, artery morphogenesis, and blood vessel remodeling. Furthermore, ventricular cardiac muscle cell action potential, heart contraction, and myoblast differentiation-associated biological processes were significantly enriched (Figure 1B). Similarly, significantly enriched molecular functions included ECM structural constituents, elasticity, and binding as well as collagen binding, TGF $\beta$  binding, and fibronectin binding (Figure 1C). The most significant KEGG pathways were ECM-receptor interaction, focal adhesion, and PI3K-Akt, p53, TGF $\beta$ , MAPK, AMPK, and Jak-STAT pathways (Figure 1D). Heat map (Figure 1E) and boxplots (Figure 1F) show that fibrosis-associated genes had decreased expression profiles in ISO-treated hAESCs compared to untreated control cells. Finally, hierarchical cluster analysis of KEGG pathways and biological processes identified 33 clusters. The most significant cluster involved three KEGG pathways: ECM-receptor interaction, PI3K-Akt signaling pathway, and focal adhesion (enrichment score 4.89, Figure 1G). Genes involved in this cluster and their fold changes are listed in Supplementary Table 1.

## ISO Abrogated AgII-Induced Ventricular Hypertrophy *in vivo*

To investigate the protective effect of ISO on abnormal cardiac structure induced by AgII, two-dimensional echocardiography was performed (Figures 2A,B). The echocardiography results indicate that the interventricular septum (IVS) and left ventricular posterior wall (LVPW) thickness, at both systole and diastole, were significantly increased in AgII-induced mice ( $p < 0.01$  vs. control), while the increased IVS and LVPW thickness were significantly decreased by ISO treatment

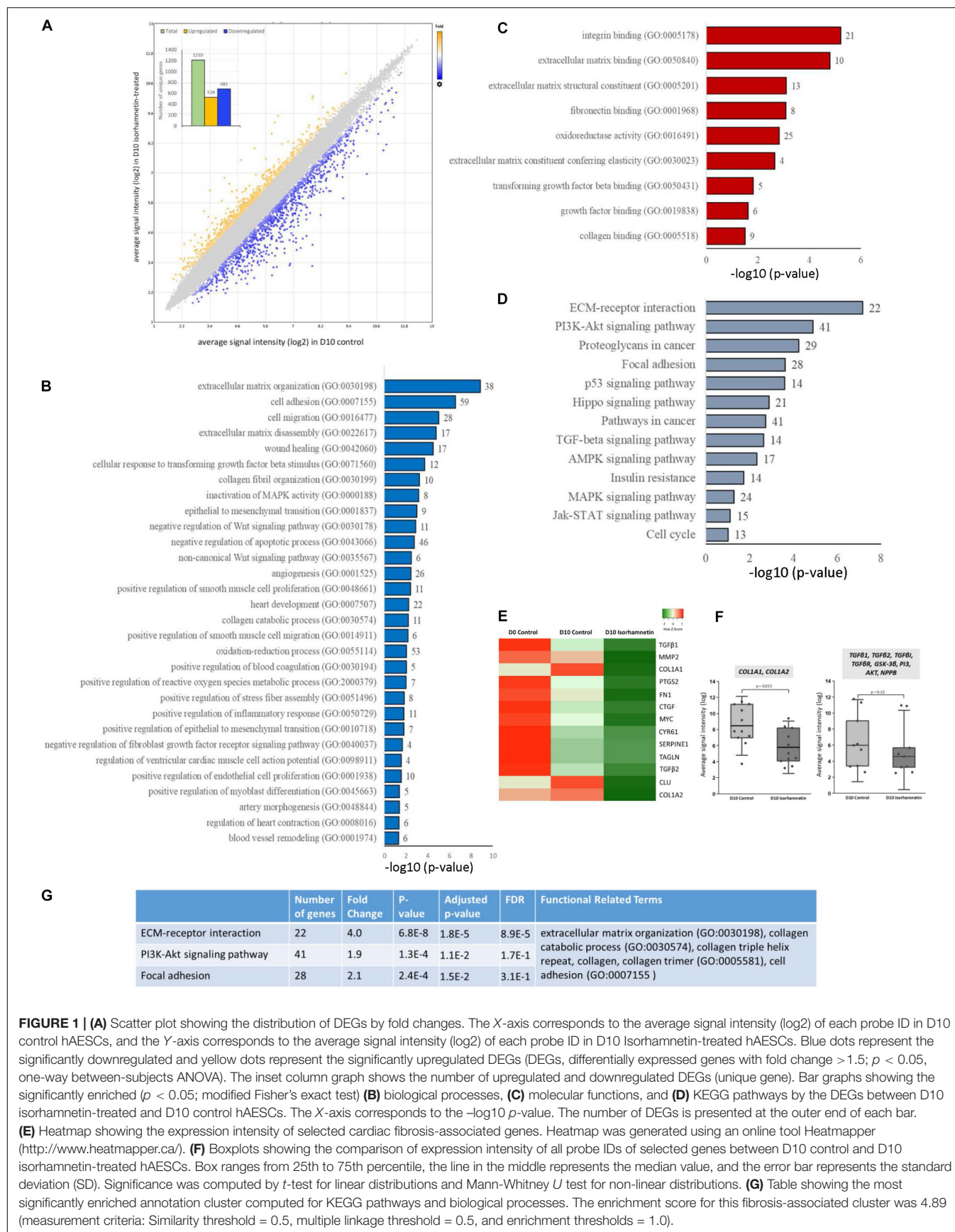
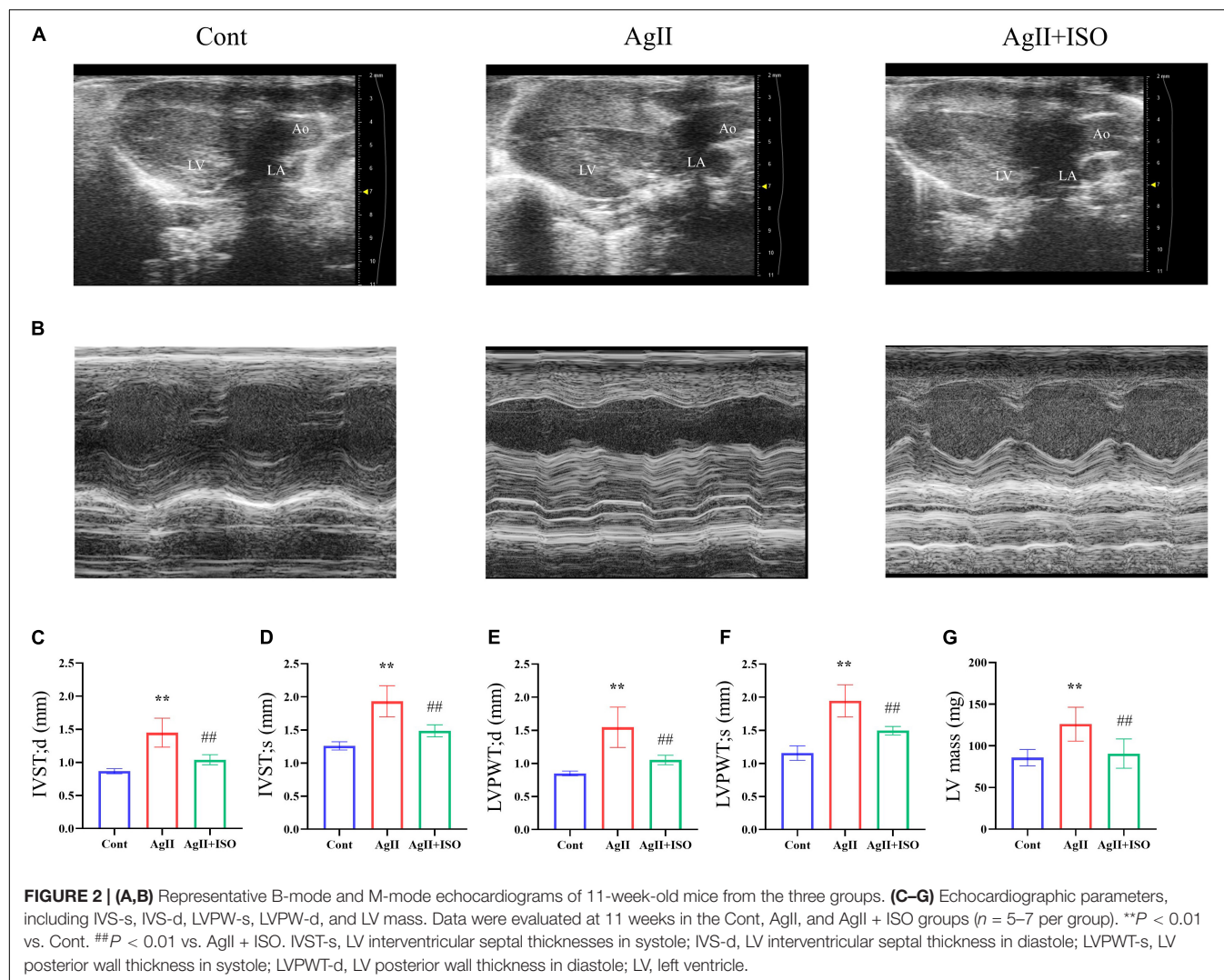


**FIGURE 1 | (A)** Scatter plot showing the distribution of DEGs by fold changes. The X-axis corresponds to the average signal intensity (log2) of each probe ID in D10 control hAECs, and the Y-axis corresponds to the average signal intensity (log2) of each probe ID in D10 Isorhamnetin-treated hAECs. Blue dots represent the significantly downregulated and yellow dots represent the significantly upregulated DEGs (DEGs, differentially expressed genes with fold change > 1.5;  $p < 0.05$ , one-way between-subjects ANOVA). The inset column graph shows the number of upregulated and downregulated DEGs (unique gene). Bar graphs showing the significantly enriched ( $p < 0.05$ ; modified Fisher's exact test) biological processes, molecular functions, and KEGG pathways by the DEGs between D10 isorhamnetin-treated and D10 control hAECs. The X-axis corresponds to the  $-\log_{10}$  p-value. The number of DEGs is presented at the outer end of each bar. **(B)** Bar graphs showing the significantly enriched ( $p < 0.05$ ; modified Fisher's exact test) biological processes, molecular functions, and KEGG pathways by the DEGs between D10 isorhamnetin-treated and D10 control hAECs. The X-axis corresponds to the  $-\log_{10}$  p-value. The number of DEGs is presented at the outer end of each bar. **(C)** Bar graphs showing the significantly enriched ( $p < 0.05$ ; modified Fisher's exact test) biological processes, molecular functions, and KEGG pathways by the DEGs between D10 isorhamnetin-treated and D10 control hAECs. The X-axis corresponds to the  $-\log_{10}$  p-value. The number of DEGs is presented at the outer end of each bar. **(D)** Bar graphs showing the significantly enriched ( $p < 0.05$ ; modified Fisher's exact test) biological processes, molecular functions, and KEGG pathways by the DEGs between D10 isorhamnetin-treated and D10 control hAECs. The X-axis corresponds to the  $-\log_{10}$  p-value. The number of DEGs is presented at the outer end of each bar. **(E)** Heatmap showing the expression intensity of selected cardiac fibrosis-associated genes. Heatmap was generated using an online tool Heatmapper (<http://www.heatmapper.ca/>). **(F)** Boxplots showing the comparison of expression intensity of all probe IDs of selected genes between D10 control and D10 isorhamnetin-treated hAECs. Box ranges from 25th to 75th percentile, the line in the middle represents the median value, and the error bar represents the standard deviation (SD). Significance was computed by t-test for linear distributions and Mann-Whitney  $U$  test for non-linear distributions. **(G)** Table showing the most significantly enriched annotation cluster computed for KEGG pathways and biological processes. The enrichment score for this fibrosis-associated cluster was 4.89 (measurement criteria: Similarity threshold = 0.5, multiple linkage threshold = 0.5, and enrichment thresholds = 1.0).





(Figures 2C–F). In addition, B-mode images indicated that the walls of LV were enlarged by AgII and were restored by ISO treatment. Moreover, LV mass was significantly increased in the AgII-induced group. ISO could abrogate the AgII-induced increase in LV mass (Figure 2G).

### ISO Reversed AgII-Induced Morphological Abnormalities in Cardiac Tissue *in vivo*

MT staining images showed that ISO significantly prevented the myocardial fibrotic responses induced by AgII (Figure 3A). Compared to the control group, H-E images showed severe disorganization of myofibrillar arrays, and cytoplasmic vacuolization and infiltration with neutrophil granulocytes in AgII-treated mice. ISO pretreatment remarkably reduced the pathological abnormalities (Figure 3B). The percentage of total fibrotic area was significantly increased in AgII-induced group, whereas ISO treatment could significantly reduce the percentage of fibrosed area (Figure 3C). Furthermore, ISO significantly

reduced the AgII-mediated increase in cardiomyocyte size (measured as cross-sectional area; CSA) (Figure 3D). The ratio of heart weight/body weight (HW/BW) was significantly increased by stimulation with AgII ( $p < 0.01$  vs. control), while ISO significantly reduced the increase in HW/BW (Figure 3E).

### ISO Prevented AgII-Induced Expression of Inflammatory and Fibrogenic Markers in Mouse Cardiac Tissue *in vivo*

To confirm the preventive effects of ISO on fibrogenic and hypertrophy markers observed in microarray analysis of hAECs, we conducted RT-PCR in ventricular tissue to quantify the expression of *Tgfb1*, *Tgfb2*, *Col1a1*, and *Nppb*.

*Tgfb1* plays an important role in the development of myocardial fibrosis by promoting the production and deposition of collagens (Lijnen et al., 2000). AgII administration has been reported to increase the expression of *Tgfb1* *in vivo*, leading to cardiac fibrosis. In addition, overexpression of *Tgfb1* induces the mRNA expression of collagen type I (*Col1A1*)

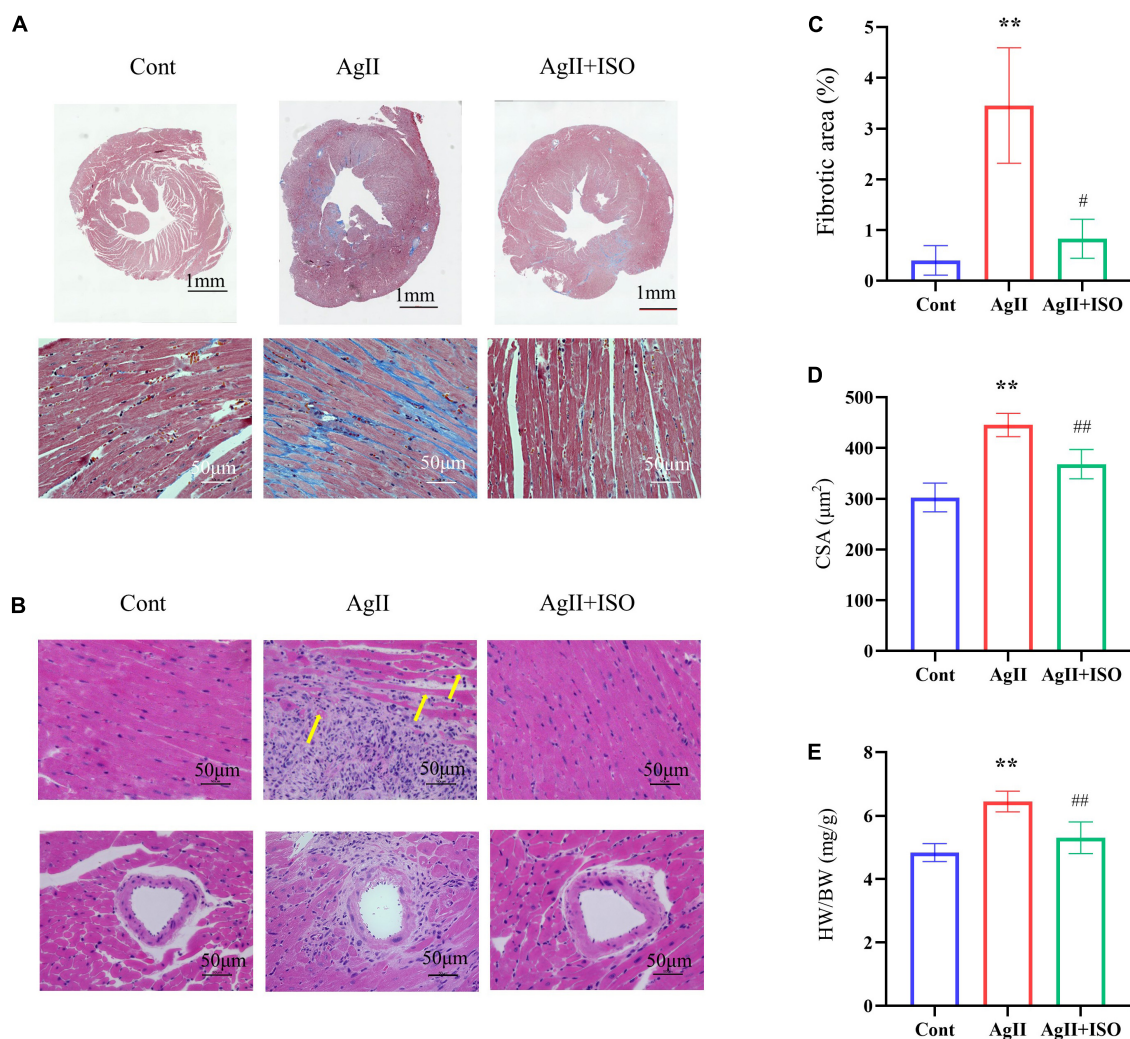


**FIGURE 3 |** Histological analyses of MT staining (A) and H-E staining (B) of each group of mice at 11 weeks. The yellow arrows indicate cytoplasmic vacuolization of cardiomyocytes. (C) The fibrotic area to the total area ( $n = 3$  per group). (D) The results of the quantitative analysis of the cross-sectional area (CSA). (E) The statistical results of HW/BW ( $n = 7$  per group). \* $P < 0.05$ , \*\* $P < 0.01$  vs. Cont. # $P < 0.05$ , ## $P < 0.01$  vs. AgII + ISO.

in rodent cardiac fibroblasts. We found that ISO significantly attenuated AgII-induced expression of *Tgfb1*, *Tgfb2*, and *Col1a1* (Figure 4).

Furthermore, pretreatment with ISO significantly decreased AgII-induced overexpression of *Nppb*. It encodes the brain natriuretic peptide (BNP) hormone, which is an important biomarker in clinical cardiology. In response to increased cardiac stress, fibrosis, and hypertrophy, BNP is strongly upregulated in the ventricular cardiac muscle.

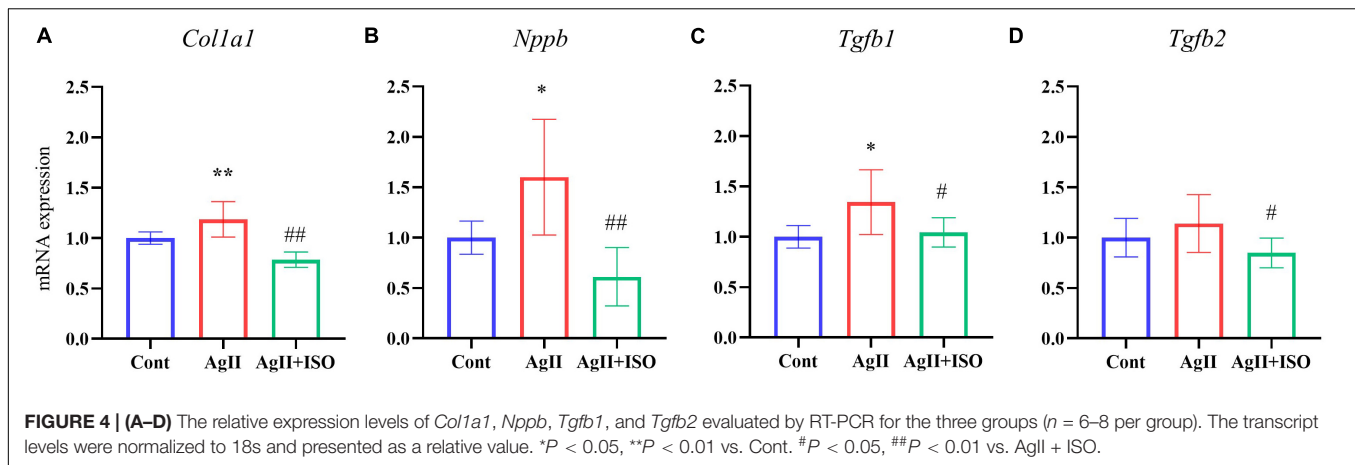
## DISCUSSION

In this study, we showed that ISO regulated cardiac fibrosis-related GO and KEGG pathways in hAESC. We then successfully translated the *in vitro* findings in the *in vivo* model. ISO suppressed myocardial hypertrophy and fibrosis induced by AgII

in mice ventricles. In short, the present study demonstrates that ISO could be a valuable pharmaceutical or dietary supplement.

Both pathological fibrosis and hypertrophy of the heart can induce heart failure and other serious cardiac diseases. These are also independent risk factors for cardiac morbidity and mortality. Conventional drugs, including angiotensin-converting enzyme inhibitors,  $\beta$ -blockers, statins, and aldosterone antagonists, are used for the inhibition of cardiac fibrosis and associated complications, however, their effects are secondary to the alleviation of cardiac dysfunction rather than directly targeting cardiac hypertrophy or fibrosis (Zannad et al., 2000; Bauersachs et al., 2001; Klapholz, 2009). Therefore, the discovery of novel compounds with profibrotic potential is urgently needed. Considering the inefficient translation of CVD drugs from hundreds of chemical libraries, a stemcell-based drug screening approach would be most appropriate. In this context, hAESC, a perinatal stem cell that possesses both ESC-like pluripotent





potential and adult stem cell-like immunomodulatory properties, has drawn great attention from researchers worldwide because of their considerable advantages over other stem cells. hAECs are readily available, have minimum ethical concerns, and are cost-effective. A number of studies have demonstrated the multilineage differentiation potential of hAECs (Miki et al., 2005, 2010; Toda et al., 2007; Parolini et al., 2008; Murphy et al., 2010; Zhou et al., 2013). Notably, hAECs have also been reported to differentiate into cardiomyocytes (Miki et al., 2005; Fang et al., 2012) and endothelial cells (Wu et al., 2017; Serra et al., 2018). Therefore, hAESC is a good alternative tool for screening potential drugs for CVD.

One of the major obstacles of translating hAECs into the clinic is the heterogeneity in primary amnion epithelial cell population and discrepancies in their cell surface profiling (Centurione et al., 2018) that can be primarily attributed to isolation protocols, gestational age, passage number, and epithelial to mesenchymal transition (Ghamari et al., 2020). However, hAECs isolated from the adherent subpopulations of passaged primary cells, and cultured in 3D environment may successfully overcome these limitations and may express a higher level of stemness properties (Ferdousi et al., 2019; Furuya et al., 2019). Additionally, protocol for immortalized human amniotic epithelial cells with high expressions of stem cell markers has been reported (Zhou et al., 2013).

In the present study, we have evaluated the cardioprotective potential of ISO in hAECs. Previously, we have reported that ISO, a flavonol, alleviates hepatic fibrosis in NASH model mice (Ganbold et al., 2019). Although several flavonols have been reported to improve cardiac dysfunction and fibrosis (Suzuki et al., 2007; Li et al., 2013; Geetha et al., 2014; Guo et al., 2015; Zhang et al., 2018), very little is known about the effect of ISO on cardiac hypertrophy and fibrosis. Microarray analysis of ISO-treated hAECs revealed that ISO has strong antifibrotic effects as well as anti-inflammatory and antioxidative functions. Additionally, ISO showed myogenic and angiogenic differentiation potential in hAECs. Interestingly, GO analysis showed that ISO targeted similar biological functions in hAECs that were reported to be regulated in the early stage of AgII-induced cardiac remodeling in a

mouse model (Dang et al., 2015). We also found that ISO significantly regulated both canonical and non-canonical Wnt pathways, TGF $\beta$ , and MAPK pathways, all of which are cross-regulated in the progression of profibrotic changes in the heart (Działo et al., 2018).

Next, we evaluated the effect of ISO on AgII-induced progression of myocardial fibrosis and hypertrophy *in vivo*. We found that ISO could effectively attenuate the expression levels of *Tgfb1* induced by AgII. TGF $\beta$ 1, a potent fibrogenic cytokine, plays an important role in the synthesis of collagen, fibronectin, or other intercellular substances, which leads to enhanced expression levels of collagen type I. Much evidence suggests that TGF $\beta$ 1 overexpression is a common pathway for various pathological factors that cause myocardial fibrosis. TGF $\beta$ 1 has also been shown to prevent or reverse organ fibrosis via the TGF $\beta$ /Smad signaling system.

Myocardial collagen consists mainly of type I and type III collagen. Type I collagen (Lu et al., 2018) attenuates the network for cardiac muscle cells and strengthens myocardial tissue. Although collagen initially has a structural role in preventing ventricular rupture, an increase in the ratio of type I to type III collagen has been reported in hearts with chronic congestive heart failure, which ultimately leads to myocardial death. The present study showed that the expression of *Col1a1* enhanced by AgII was significantly reduced by ISO treatment. We hypothesized that ISO could reverse the expression levels of collagen by attenuating TGF $\beta$ 1 pathways, thereby suppressing the development of fibrosis.

Furthermore, this study shows that ISO significantly suppressed *Nppb* gene expression. *Nppb* encodes BNP hormone, which is an important biomarker in clinical cardiology (Diamandis et al., 2014). In response to increased cardiac stress, fibrosis, and hypertrophy, BNP is strongly upregulated in the ventricular cardiac muscle (Kerkelä et al., 2015). BNP inhibits renin secretion, thereby inhibiting the renin-angiotensin-aldosterone system. Therefore, our findings indicate that ISO has the effects on cardiac hypertrophy and fibrosis.

It has been reported that ISO ameliorates cardiac hypertrophy and fibrosis induced by aortic banding (Gao et al., 2017), however, there has been no report on the effect of ISO on

AgII loading. Although the mechanism of angiotensin-induced cardiac disease has largely been clarified, researchers are still searching for effective drugs. A commonly used animal model is the subcutaneous infusion of AgII into mice. Osmotic pumps are designed to continuously deliver compounds to small animals at a constant rate. This technique is commonly used to induce AF, aortic aneurysm, and hypertension, leading to serious heart disease or sudden death (Wu et al., 2019). AgII 1,000 ng/kg/min is commonly used. Based on this background, we conducted this experiment with reference to this dose. AgII, a vasoactive peptide, is a key regulator of hypertension, inflammatory response, hypertrophy, and fibrosis through the regulation of multiple signaling pathways, such as NF- $\kappa$ B and TGF $\beta$ 1/Smad (Shang et al., 2008). Our results indicated that chronic AgII infusion remarkably induced left ventricular wall extension, dilation, pathological hypertrophy, fibrosis, and macrophage infiltration, and that ISO completely eliminated these abnormalities induced by AgII. ISO significantly suppressed fibrosis in the interstitial myocardium and around blood vessels showed in MT staining. Furthermore, ISO prevented the living cells surrounded by dead cells that eventually became oxygen-deficient, leading to heart failure and sudden death.

## CONCLUSION

Our evidence suggests that hAESC has important implications as an alternative tool for the screening and development of drugs and dietary supplements in future. Our results also demonstrate that ISO could effectively suppress hypertrophy and fibrosis induced by AgII in cardiac tissue by regulating TGF $\beta$  pathways. ISO could have beneficial effects on potential clinical consequences of CVDs by regulating the activity of the renin-angiotensin system.

## DATA AVAILABILITY STATEMENT

All data generated or analyzed during this study are included in this article and its **Supplementary Information**. Microarray data are deposited in the Gene Expression Omnibus (GEO) under accession number: GSE153149 (<https://www.ncbi.nlm.nih.gov/geo/query/acc.cgi?acc=GSE153149>).

## REFERENCES

- Babicki, S., Arndt, D., Marcu, A., Liang, Y., Grant, J. R., Maciejewski, A., et al. (2016). Heatmapper: web-enabled heat mapping for all. *Nucleic Acids Res.* 44, W147–W153.
- Bang, C. N., Soliman, E. Z., Simpson, L. M., Davis, B. R., Devereux, R. B., and Okin, P. M. (2017). Electrocardiographic left ventricular hypertrophy predicts cardiovascular morbidity and mortality in hypertensive patients: the ALLHAT Study. *Am. J. Hypertens.* 30, 914–922. doi: 10.1093/ajh/hpx067
- Bauersachs, J., Galuppo, P., Fraccarollo, D., Christ, M., and Ertl, G. (2001). Improvement of left ventricular remodeling and function by hydroxymethylglutaryl coenzyme A reductase inhibition with cerivastatin in rats with heart failure after myocardial infarction. *Circulation* 104, 982–985.

## ETHICS STATEMENT

The protocol for the hAESC study was reviewed and approved by the Ethical Review Committee of the University of Tsukuba. Informed written consent was obtained from the mothers who donated the placenta after delivery. After receiving approval from the Institutional Animal Experiment Committee of the University of Tsukuba, animal experiments were carried out in accordance with the Guide for the Care and Use of Laboratory Animals published by the US National Institutes of Health, the Regulation for Animal Experiments in the University of Tsukuba, and the Fundamental Guideline for Proper Conduct of Animal Experiments and Related Activities in Academic Research Institutions under the jurisdiction of the Ministry of Education, Culture, Sports, Science and Technology of Japan.

## AUTHOR CONTRIBUTIONS

KA: investigation. KA and FF: formal analysis, data curation, software, visualization, and writing-original draft. DX: methodology, validation, supervision, and resources. KT: investigation, validation, and resources. HI: conceptualization, methodology, resources, supervision, project administration, funding acquisition, and writing-review and editing. All authors made substantial contributions to this article and approved the final version of the article.

## FUNDING

This research was partially supported by the Japan Science and Technology Agency (JST), Science and Technology Research Partnership for Sustainable Development (SATREPS, Grant No. JPMJSA1506).

## SUPPLEMENTARY MATERIAL

The Supplementary Material for this article can be found online at: <https://www.frontiersin.org/articles/10.3389/fcell.2020.578197/full#supplementary-material>

- Centurione, L., Passaretta, F., Centurione, M. A., De Munari, S., Vertua, E., Silini, A., et al. (2018). Mapping of the human placenta: experimental evidence of amniotic epithelial cell heterogeneity. *Cell Transpl.* 27, 12–22.
- Chen, K. G., Mallon, B. S., McKay, R. D. G., and Robey, P. G. (2014). Human pluripotent stem cell culture: considerations for maintenance, expansion, and therapeutics. *Cell Stem Cell* 14, 13–26. doi: 10.1016/j.stem.2013.12.005
- Dang, M.-Q., Zhao, X.-C., Lai, S., Wang, X., Wang, L., Zhang, Y.-L., et al. (2015). Gene expression profile in the early stage of angiotensin II-induced cardiac remodeling: a time series microarray study in a mouse model. *Cell. Physiol. Biochem.* 35, 467–476.
- De Coppi, P., and Atala, A. (2019). “Stem cells from the amnion,” in *Principles of Regenerative Medicine*, 3rd Edn, eds A. Atala, R. Lanza, A. G. Mikos, and R. Nerem (Boston: Academic Press), 133–148.

- Diamandis, E. P., Maisel, A., Jaffe, A. S., and Clerico, A. (2014). Q & A: natriuretic peptides in heart failure. *Clin. Chem.* 60, 1040–1046.
- Działo, E., Tkacz, K., and Błyszczuk, P. (2018). Crosstalk between TGF- $\beta$  and WNT signalling pathways during cardiac fibrogenesis. *Acta Biochim. Polonica* 65, 341–349.
- Engle, S. J., and Puppala, D. (2013). Integrating human pluripotent stem cells into drug development. *Cell Stem Cell* 12, 669–677.
- Fang, C.-H., Jin, J., Joe, J.-H., Song, Y.-S., So, B.-I., Lim, S. M., et al. (2012). In vivo differentiation of human amniotic epithelial cells into cardiomyocyte-like cells and cell transplantation effect on myocardial infarction in rats: comparison with cord blood and adipose tissue-derived mesenchymal stem cells. *Cell Transpl.* 21, 1687–1696.
- Ferdousi, F., Kondo, S., Sasaki, K., Uchida, Y., Ohkohchi, N., Zheng, Y.-W., et al. (2020). Microarray analysis of verbenalin-treated human amniotic epithelial cells reveals therapeutic potential for Alzheimer's disease. *Aging* 12:5516.
- Ferdousi, F., Sasaki, K., Ohkohchi, N., Zheng, Y.-W., and Isoda, H. (2019). Exploring the potential role of rosmarinic acid in neuronal differentiation of human amnion epithelial cells by microarray gene expression profiling. *Front. Neurosci.* 13:779. doi: 10.3389/fnins.2019.00779
- Furuya, K., Zheng, Y.-W., Sako, D., Iwasaki, K., Zheng, D.-X., Ge, J.-Y., et al. (2019). Enhanced hepatic differentiation in the subpopulation of human amniotic stem cells under 3D multicellular microenvironment. *World J. Stem Cells* 11:705.
- Ganbold, M., Owada, Y., Ozawa, Y., Shimamoto, Y., Ferdousi, F., Tominaga, K., et al. (2019). Isorhamnetin alleviates steatosis and fibrosis in mice with nonalcoholic steatohepatitis. *Sci. Rep.* 9:16210. doi: 10.1038/s41598-019-52736-y
- Gao, L., Yao, R., Liu, Y., Wang, Z., Huang, Z., Du, B., et al. (2017). Isorhamnetin protects against cardiac hypertrophy through blocking PI3K-AKT pathway. *Mol. Cell. Biochem.* 429, 167–177.
- Geetha, R., Yogalakshmi, B., Sreeja, S., Bhavani, K., and Anuradha, C. V. (2014). Troxerutin suppresses lipid abnormalities in the heart of high-fat–high-fructose diet-fed mice. *Mol. Cell. Biochem.* 387, 123–134.
- Ghamari, S.-H., Abbasi-Kangevari, M., Tayebi, T., Bahrami, S., and Niknejad, H. (2020). The bottlenecks in translating placenta-derived amniotic epithelial and mesenchymal stromal cells into the clinic: current discrepancies in marker reports. *Front. Bioeng. Biotechnol.* 8:180. doi: 10.3389/fbioe.2020.00180
- Grskovic, M., Javaherian, A., Strulovici, B., and Daley, G. Q. (2011). Induced pluripotent stem cells—opportunities for disease modelling and drug discovery. *Nat. Rev. Drug Discov.* 10, 915–929.
- Guo, H., Zhang, X., Cui, Y., Zhou, H., Xu, D., Shan, T., et al. (2015). Taxifolin protects against cardiac hypertrophy and fibrosis during biomechanical stress of pressure overload. *Toxicol. Appl. Pharmacol.* 287, 168–177.
- Hu, S., Huang, L., Meng, L., Sun, H., Zhang, W., and Xu, Y. (2015). Isorhamnetin inhibits cell proliferation and induces apoptosis in breast cancer via Akt and mitogen-activated protein kinase signaling pathways. *Mol. Med. Rep.* 12, 6745–6751.
- Huang, D. W., Sherman, B. T., and Lempicki, R. A. (2008). Systematic and integrative analysis of large gene lists using DAVID bioinformatics resources. *Nat. Protoc.* 4:44. doi: 10.1038/nprot.2008.211
- Izawa, H., Murohara, T., Nagata, K., Isobe, S., Asano, H., Amano, T., et al. (2005). Mineralocorticoid receptor antagonism ameliorates left ventricular diastolic dysfunction and myocardial fibrosis in mildly symptomatic patients with idiopathic dilated cardiomyopathy: a pilot study. *Circulation* 112, 2940–2945. doi: 10.1161/CIRCULATIONAHA.105.571653
- Jin, L., Sun, S., Ryu, Y., Piao, Z. H., Liu, B., Choi, S. Y., et al. (2018). Gallic acid improves cardiac dysfunction and fibrosis in pressure overload-induced heart failure. *Sci. Rep.* 8, 1–11. doi: 10.1038/s41598-018-27599-4
- Kai, H., Mori, T., Tokuda, K., Takayama, N., Tahara, N., Takemiya, K., et al. (2006). Pressure overload-induced transient oxidative stress mediates perivascular inflammation and cardiac fibrosis through angiotensin II. *Hypertens. Res.* 29, 711–718. doi: 10.1291/hypres.29.711
- Kato, K., Ninomiya, M., Tanaka, K., and Koketsu, M. (2016). Effects of functional groups and sugar composition of quercetin derivatives on their radical scavenging properties. *J. Nat. Prod.* 79, 1808–1814. doi: 10.1021/acs.jnatprod.6b00274
- Kerkelä, R., Ulvila, J., and Magga, J. (2015). Natriuretic peptides in the regulation of cardiovascular physiology and metabolic events. *J. Am. Heart Assoc.* 4, 1–13. doi: 10.1161/JAHA.115.002423
- Klapholz, M. (2009).  *$\beta$ -Blocker Use for. (the) Stages of Heart Failure*. Amsterdam: Elsevier, 718–729. doi: 10.4065/84.8.718
- Li, M., Jiang, Y., Jing, W., Sun, B., Miao, C., and Ren, L. (2013). Quercetin provides greater cardioprotective effect than its glycoside derivative rutin on isoproterenol-induced cardiac fibrosis in the rat. *Can. J. Physiol. Pharmacol.* 91, 951–959. doi: 10.1139/cjpp-2012-0432
- Li, Y., and Kilian, K. A. (2015). Bridging the gap: from 2D cell culture to 3D microengineered extracellular matrices. *Adv. Healthc. Mater.* 4, 2780–2796. doi: 10.1002/adhm.201500427
- Lijnen, P. J., Petrov, V. V., and Fagard, R. H. (2000). Induction of cardiac fibrosis by transforming growth factor- $\beta$ 1. *Mol. Genet. Metab.* 71, 418–435. doi: 10.1006/mgme.2000.3032
- Lu, Y., Kamel-El Sayed, S. A., Wang, K., Tiede-Lewis, L. A. M., Grillo, M. A., Veno, P. A., et al. (2018). Live imaging of type I collagen assembly dynamics in osteoblasts stably expressing GFP and mCherry-tagged collagen constructs. *J. Bone Miner. Res.* 33, 1166–1182. doi: 10.1002/jbmr.3409
- Marwick, T. H., Gillebert, T. C., Aurigemma, G., Chirinos, J., Derumeaux, G., Galderisi, M., et al. (2015). Recommendations on the use of echocardiography in adult hypertension: a report from the European association of cardiovascular imaging (EACVI) and the American society of echocardiography (ASE). *J. Am. Soc. Echocardiogr.* 28, 727–754. doi: 10.1016/j.echo.2015.05.002
- Miki, T. (2018). Stem cell characteristics and the therapeutic potential of amniotic epithelial cells. *Am. J. Reprod. Immunol.* 80:e13003. doi: 10.1111/aji.13003
- Miki, T., Lehmann, T., Cai, H., Stolz, D. B., and Strom, S. C. (2005). Stem cell characteristics of amniotic epithelial cells. *Stem cells* 23, 1549–1559. doi: 10.1634/stemcells.2004-0357
- Miki, T., Marongiu, F., Dorko, K., Ellis, E. C., and Strom, S. C. (2010). Isolation of amniotic epithelial stem cells. *Curr. Protoc. Stem Cell Biol.* 12, 1E. 3.1–1E. 3.10. doi: 10.1002/9780470151808.sc01e03s12
- Mootha, V. K., Lindgren, C. M., Eriksson, K.-F., Subramanian, A., Sihag, S., Lehar, J., et al. (2003). PGC-1 $\alpha$ -responsive genes involved in oxidative phosphorylation are coordinately downregulated in human diabetes. *Nat. Genet.* 34:267. doi: 10.1038/ng1180
- Murphy, S., Rosli, S., Acharya, R., Mathias, L., Lim, R., Wallace, E., et al. (2010). Amnion epithelial cell isolation and characterization for clinical use. *Curr. Prot. Stem Cell Biol.* 13, 1E. 6.1–1E. 6.25. doi: 10.1002/9780470151808.sc01e06s13
- Parolini, O., Alviano, F., Bagnara, G. P., Bilic, G., Bühring, H. J., Evangelista, M., et al. (2008). Concise review: isolation and characterization of cells from human term placenta: outcome of the first international workshop on placenta derived stem cells. *Stem Cells* 26, 300–311. doi: 10.1634/stemcells.2007-0594
- Pott, A., Rottbauer, W., and Just, S. (2020). Streamlining drug discovery assays for cardiovascular disease using zebrafish. *Expert Opin. Drug Discov.* 15, 27–37. doi: 10.1080/17460441.2020.1671351
- Serra, M., Marongiu, M., Contini, A., Miki, T., Cadoni, E., Laconi, E., et al. (2018). Evidence of amniotic epithelial cell differentiation toward hepatic sinusoidal endothelial cells. *Cell Transpl.* 27, 23–30. doi: 10.1177/096368971727541
- Shang, L. L., Sanyal, S., Pfahnl, A. E., Jiao, Z., Allen, J., Liu, H., et al. (2008). NF- $\kappa$ B-dependent transcriptional regulation of the cardiac *scn5a* sodium channel by angiotensin II. *Am. J. Physiol. Cell Physiol.* 294, 372–379. doi: 10.1152/ajpcell.00186.2007
- Sherman, B. T., Huang, D. W., and Lempicki, R. A. (2008). Bioinformatics enrichment tools: paths toward the comprehensive functional analysis of large gene lists. *Nucleic Acids Res.* 37, 1–13. doi: 10.1093/nar/gkn923
- Subramanian, A., Tamayo, P., Mootha, V. K., Mukherjee, S., Ebert, B. L., Gillette, M. A., et al. (2005). Gene set enrichment analysis: a knowledge-based approach for interpreting genome-wide expression profiles. *Proc. Natl. Acad. Sci. U.S.A.* 102, 15545–15550. doi: 10.1073/pnas.0506580102
- Suzuki, J. I., Ogawa, M., Futamatsu, H., Kosuge, H., Sagesaka, Y. M., and Isobe, M. (2007). Tea catechins improve left ventricular dysfunction, suppress myocardial inflammation and fibrosis, and alter cytokine expression in rat autoimmune myocarditis. *Eur. J. Heart Fail.* 9, 152–159. doi: 10.1016/j.ejheart.2006.05.007
- Takeuchi, T., Noguchi, M., Kawakami, Y., and Ohkohchi, N. (2016). Use of human biospecimen resources for drug discovery: approach of tsukuba human tissue biobank center. *Regul. Sci. Med. Prod.* 6, 57–63. doi: 10.14982/rsmpp.6.57

- Toda, A., Okabe, M., Yoshida, T., and Nikaido, T. (2007). The potential of amniotic membrane/amnion-derived cells for regeneration of various tissues. *J. Pharmacol. Sci.* 105, 215–228.
- Travers, J. G., Kamal, F. A., Robbins, J., Yutzey, K. E., and Blaxall, B. C. (2016). Cardiac fibrosis: the fibroblast awakens. *Circ. Res.* 118, 1021–1040. doi: 10.1161/CIRCRESAHA.115.306565
- Weber, K. T., Sun, Y., and Diez, J. (2008). Fibrosis: a living tissue and the infarcted heart. *J. Am. Coll. Cardiol.* 52, 2029–2031. doi: 10.1016/j.jacc.2008.09.012
- Wu, Q., Fang, T., Lang, H., Chen, M., Shi, P., Pang, X., et al. (2017). Comparison of the proliferation, migration and angiogenic properties of human amniotic epithelial and mesenchymal stem cells and their effects on endothelial cells. *Int. J. Mol. Med.* 39, 918–926. doi: 10.3892/ijmm.2017.2897
- Wu, Y. X., Han, X., Chen, C., Zou, L. X., Dong, Z. C., Zhang, Y. L., et al. (2019). Time series gene expression profiling and temporal regulatory pathway analysis of angiotensin II induced atrial fibrillation in mice. *Front. Physiol.* 10, 1–10. doi: 10.3389/fphys.2019.00597
- Yang, J. H., Kim, S. C., Kim, K. M., Jang, C. H., Cho, S. S., Kim, S. J., et al. (2016). *Isorhamnetin attenuates liver fibrosis by inhibiting TGF- $\beta$ /Smad signaling and relieving oxidative stress.* *Eur. J. Pharmacol.* 783, 92–102. doi: 10.1016/j.ejphar.2016.04.042
- Yang, P.-J., Yuan, W.-X., Liu, J., Li, J.-Y., Tan, B., Qiu, C., et al. (2018). Biological characterization of human amniotic epithelial cells in a serum-free system and their safety evaluation. *Acta Pharmacol. Sin.* 39, 1305–1316. doi: 10.1038/aps.2018.22
- Yue, L., Xie, J., and Nattel, S. (2011). Molecular determinants of cardiac fibroblast electrical function and therapeutic implications for atrial fibrillation. *Cardiovasc. Res.* 89, 744–753. doi: 10.1093/cvr/cvq329
- Zannad, F., Alla, F., Dousset, B., Perez, A., and Pitt, B. (2000). Limitation of excessive extracellular matrix turnover may contribute to survival benefit of spironolactone therapy in patients with congestive heart failure: insights from the randomized aldactone evaluation study (RALES). *Circulation* 102, 2700–2706. doi: 10.1161/01.CIR.102.22.2700
- Zar Kalai, F., Han, J., Ksouri, R., El Omri, A., Abdely, C., and Isoda, H. (2013). Antiobesity effects of an edible halophyte *Nitraria retusa* Forssk in 3T3-L1 preadipocyte differentiation and in C57B6/J mice fed a high fat diet-induced obesity. *Evid. Based Complement. Altern. Med.* 2013:368658. doi: 10.1155/2013/368658
- Zhang, N., Wei, W.-Y., Li, L.-L., Hu, C., and Tang, Q.-Z. (2018). Therapeutic potential of polyphenols in cardiac fibrosis. *Front. Pharmacol.* 9:122. doi: 10.3389/fphar.2018.00122
- Zhou, K., Koike, C., Yoshida, T., Okabe, M., Fathy, M., Kyo, S., et al. (2013). Establishment and characterization of immortalized human amniotic epithelial cells. *Cell. Reprogram.* 15, 55–67. doi: 10.1089/cell.2012.0021

**Conflict of Interest:** The authors declare that the research was conducted in the absence of any commercial or financial relationships that could be construed as a potential conflict of interest.

Copyright © 2020 Aonuma, Ferdousi, Xu, Tominaga and Isoda. This is an open-access article distributed under the terms of the Creative Commons Attribution License (CC BY). The use, distribution or reproduction in other forums is permitted, provided the original author(s) and the copyright owner(s) are credited and that the original publication in this journal is cited, in accordance with accepted academic practice. No use, distribution or reproduction is permitted which does not comply with these terms.





# Sugarcane (*Saccharum officinarum* L.) Top Extract Ameliorates Cognitive Decline in Senescence Model SAMP8 Mice: Modulation of Neural Development and Energy Metabolism

## OPEN ACCESS

### Edited by:

Daniele Bottai,  
University of Milan, Italy

### Reviewed by:

Juan Manuel Encinas,  
Achucarro Basque Center  
for Neuroscience, Spain  
Keiko Unno,  
University of Shizuoka, Japan

### \*Correspondence:

Francis G. Szele  
francis.szele@dpag.ox.ac.uk  
Hiroko Isoda  
isoda.hiroko.ga@u.tsukuba.ac.jp

† These authors have contributed  
equally to this work

### Specialty section:

This article was submitted to  
Stem Cell Research,  
a section of the journal  
Frontiers in Cell and Developmental  
Biology

**Received:** 17 June 2020

**Accepted:** 03 September 2020

**Published:** 06 October 2020

### Citation:

Iwata K, Wu Q, Ferdousi F,  
Sasaki K, Tominaga K, Uchida H,  
Arai Y, Szele FG and Isoda H (2020)  
Sugarcane (*Saccharum officinarum*  
L.) Top Extract Ameliorates Cognitive  
Decline in Senescence Model SAMP8  
Mice: Modulation of Neural  
Development and Energy Metabolism.  
Front. Cell Dev. Biol. 8:573487.  
doi: 10.3389/fcell.2020.573487

Kengo Iwata<sup>1,2</sup>, Qingqing Wu<sup>3,4</sup>, Farhana Ferdousi<sup>3,5</sup>, Kazunori Sasaki<sup>3,5</sup>,  
Kenichi Tominaga<sup>5</sup>, Haruhisa Uchida<sup>2</sup>, Yoshinobu Arai<sup>2</sup>, Francis G. Szele<sup>4\*†</sup> and  
Hiroko Isoda<sup>1,3,5,6\*†</sup>

<sup>1</sup> School of Integrative and Global Majors, University of Tsukuba, Tsukuba, Japan, <sup>2</sup> Nippo Co., Ltd., Daito, Japan, <sup>3</sup> Alliance  
for Research on the Mediterranean and North Africa, University of Tsukuba, Tsukuba, Japan, <sup>4</sup> Department of Physiology,  
Anatomy and Genetics, University of Oxford, Oxford, United Kingdom, <sup>5</sup> AIST-University of Tsukuba Open Innovation  
Laboratory for Food and Medicinal Resource Engineering (FoodMed-OIL), AIST, University of Tsukuba, Tsukuba, Japan,  
<sup>6</sup> Faculty of Life and Environmental Sciences, University of Tsukuba, Tsukuba, Japan

Age-related biological alterations in brain function increase the risk of mild cognitive impairment and dementia, a global problem exacerbated by aging populations in developed nations. Limited pharmacological therapies have resulted in attention turning to the promising role of medicinal plants and dietary supplements in the treatment and prevention of dementia. Sugarcane (*Saccharum officinarum* L.) top, largely considered as a by-product because of its low sugar content, in fact contains the most abundant amounts of antioxidant polyphenols relative to the rest of the plant. Given the numerous epidemiological studies on the effects of polyphenols on cognitive function, in this study, we analyzed polyphenolic constituents of sugarcane top and examined the effect of sugarcane top ethanolic extract (STEE) on a range of central nervous system functions *in vitro* and *in vivo*. Orally administrated STEE rescued spatial learning and memory deficit in the senescence-accelerated mouse prone 8 (SAMP8) mice, a non-transgenic strain that spontaneously develops a multisystemic aging phenotype including pathological features of Alzheimer's disease. This could be correlated with an increased number of hippocampal newborn neurons and restoration of cortical monoamine levels in STEE-fed SAMP8 mice. Global genomic analysis by microarray in cerebral cortices showed multiple potential mechanisms for the cognitive improvement. Gene set enrichment analysis (GSEA) revealed biological processes such as neurogenesis, neuron differentiation, and neuron development were significantly enriched in STEE-fed mice brain compared to non-treated SAMP8 mice. Furthermore, STEE treatment significantly regulated genes involved in neurotrophin signaling, glucose metabolism, and neural development in mice brain. Our *in vitro* results suggest that

STEE treatment enhances the metabolic activity of neuronal cells promoting glucose metabolism with significant upregulation of genes, namely *PGK1*, *PGAM1*, *PKM*, and *PC*. STEE also stimulated proliferation of human neural stem cells (hNSCs), regulated bHLH factor expression and induced neuronal differentiation and astrocytic process lengthening. Altogether, our findings suggest the potential of STEE as a dietary intervention, with promising implications as a novel nutraceutical for cognitive health.

**Keywords:** cognitive function, sugarcane top, polyphenol, energy metabolism, neural development, SAMP8

## INTRODUCTION

Cognitive decline, such as memory loss and learning deficit, is highly associated with aging. This has been implicated to be mediated by oxidative stress, mitochondrial dysfunction, and defective apoptotic processes in the process of normal brain aging (Ginneken, 2017). In addition, other protein abnormalities such as increased amyloid- $\beta$  (A $\beta$ ) plaques, phosphorylated tau and neurofibrillary tangles, and Lewy bodies are the pathological hallmarks of severe brain disorders, including Alzheimer's disease (AD). Age-related brain disorders are generally accompanied by other pathologies, including cortical (particularly hippocampal) shrinkage, abnormal immune response and neurogenesis, and decreased neurotransmitter concentration, which could theoretically be pharmacological targets (Nelson and Tabet, 2015; Poulouse et al., 2017). With the rapid growth of the aging population and increasing awareness of the risk of dementia, prevention and treatment of age-related cognitive decline have become research priorities. Pharmacological therapies are currently limited, and recently attention has turned to the role of dietary interventions or nutraceuticals in this respect (Williams et al., 2011; Howes et al., 2020).

Sugarcane (*Saccharum officinarum* L.) is one of the most widely distributed plants in subtropical and tropical regions and is cultivated as an important source of sugar. From the industrial point of view, the most profitable part of the plant is the stem, which contains relatively high concentrations of sugar. In contrast, the top part of sugarcane including leaves (sugarcane top) are often treated as waste, although some of them are used in fermented silage. However, it has been reported that sugarcane top in fact contains a larger amount of polyphenol with antioxidant properties compared to its stem (Colombo et al., 2005, 2006; Sun et al., 2014).

Caffeoylquinic acid (CQA), also known as chlorogenic acid, is a naturally occurring antioxidant polyphenol found in various plants. CQA derivatives have been shown to have neuroprotective effects and to improve learning and memory via inhibition of A $\beta$  aggregation and enhancement of ATP production both *in vitro* and *in vivo* (Han et al., 2010; Miyamae et al., 2011b, 2012). Furthermore, past studies have shown that CQA-rich plant extracts can ameliorate aging-related cognitive deficit, depressive behavior, and amyloid pathologies *in vivo* (Sasaki et al., 2013; Wu et al., 2016; Lim et al., 2018; Ishida et al., 2020). Moreover, our recent study suggested that intracorporeal mono-CQAs, degraded from 3,4,5-tricaffeoylquinic acid, stimulate hippocampal neurogenesis (Sasaki et al., 2019a). CQA derivatives

have been reported as a major compound in the sugarcane top of the fraction possessing potent antioxidant properties (Maeda et al., 2010). Therefore, sugarcane top might be a promising bioresource containing neuroactive chemicals.

In the present study, the senescence-accelerated mouse strain SAMP8 was used as an *in vivo* model (Rhea and Banks, 2017) to evaluate the effect of sugarcane top extract on pathological aging. This non-transgenic strain shows similar neuropathological features of neurodegenerative diseases such as AD, and encompasses A $\beta$  alterations, increased oxidative stress, augmented tau phosphorylation, as well as learning and memory deficits (Butterfield and Poon, 2005; Pallas et al., 2008; Takeda, 2009; Morley et al., 2012). We used human-derived cells to characterize the effect and potential mechanisms of sugarcane top extract on neuronal energy metabolism and neural stem cell fate *in vitro*. Chemical analysis of the extract from sugarcane tops was performed to unveil its composition, and then several *in vivo* and *in vitro* biological assays were performed to examine the possible effect of the extract on cognitive health.

## MATERIALS AND METHODS

### Preparation of Sugarcane Top Ethanolic Extract (STEE)

Sugarcane (*Saccharum officinarum* L.) tops were collected from a plantation in Asakura, Fukuoka, Japan. Milled sugarcane tops were donated by the Nippo Co., Ltd. (Daito, Osaka, Japan). The milled plant was extracted by maceration with ethanol/water (70:30, v/v) for 2 weeks, with a ratio of plant powder/solvent of 10% (w/v). The extract was filtered through 0.22  $\mu$ m membranes (Merk Millipore, Billerica, MA, United States) and the dried extract was obtained through rotary evaporation and freeze-drying (yield was approximately 13–14%; 130–140 mg per g of the plant powder).

The extract was dissolved in ethanol/water (70:30, v/v) and stocked for all the *in vitro* experiments. For all the *in vivo* experiments, the extract was dissolved in Mill-Q water.

### Chemical Analysis

The chemical analysis was performed using the Prominence HPLC system (Shimadzu, Kyoto, Japan) equipped with a solvent delivery pump (LC-20AD), autosampler (SIL-20AC), and ELS detector (ELSD-LTII). For the analysis, samples were extracted from milled sugarcane tops using Speed Extractor E-916 (Buchi AG, Uster, Switzerland) with ethanol/water (80:20, v/v). The

extracts were evaporated, freeze-dried, and filtered before use. ZORBAX SB-C18 reversed-phase columns (250 × 4.6 mm, 3.5 μm, Agilent, Santa Clara, CA, United States) were used and the column thermostat was maintained at 40°C. The mobile phase consisted of: A. formic acid/water (10:90, v/v), B. acetonitrile/methanol (50:50, v/v) with a 0–100% gradient for 40 min. Chromatography was carried out in gradient mode, using a flow rate of 1.0 mL/min, with detection wavelength at 328 nm. Four concentrations of pure compounds were prepared: 0.2, 0.3, 0.4, and 0.5 μg/mL, as external standards. Each injection volume was 10 μL. Pure chemical compounds of 3-*O*-caffeoylquinic acid (3-CQA), 5-*O*-caffeoylquinic acid (5-CQA) and 3-*O*-feruloylquinic acid (3-FQA) were purchased from the Nagara Science (Gifu, Japan). Isoorientin (ISO, chemically defined as luteolin-6-*C*-glucoside) was purchased from Sigma-Aldrich (St. Louis, MO, United States). Presented chemical structures were drawn in MarvinSketch (ChemAxon, Budapest, Hungary) software.

## In vitro Experiments

### Cells and Cell Culture

In this study, the human neuroblastoma cell line SH-SY5Y and human fetal neural stem cells (hNSCs) were cultured and used for subsequent experiments *in vitro*. SH-SY5Y cells were purchased from the ATCC (Manassas, VA, United States) and hNSCs (StemPro Neural Stem Cells, A15654) were from the Gibco-Thermo Fisher (Grand Island, NY, United States). SH-SY5Y cells were cultured in Dulbecco's modified Eagle's medium (DMEM)/F12 (1:1, v/v) (Gibco) supplemented with 15% fetal bovine serum (FBS, Gibco), 1% non-essential amino acids solution (NEAA, Wako-Fujifilm, Osaka, Japan), and 1% anti-bacterial penicillin/streptomycin. hNSCs were cultured in knockout DMEM/F12 (1:1, v/v) supplemented with 2% StemPro Neural Supplement, 20 ng/mL basic fibroblast growth factor (bFGF), 20 ng/mL epidermal growth factor (EGF), 2 mM Glutamax Supplement (all above reagents were from Gibco), 6 units/mL heparin, and 200 μM ascorbic acid (proliferation medium). The cells were maintained at 37°C in a 95% air/5% CO<sub>2</sub> humidified incubator.

SH-SY5Y cells expanded as adherent monolayer cultures and were passaged when the culture was confluent (every 3–4 days, up to 8 passages) using cell detachment reagent TrypLE Express (Gibco). hNSCs expanded as free-floating aggregates (Neurospheres) and were passaged when a sphere diameter was ≤150 μm at the maximum (every 9–11 days, up to 3 passages until cells started unexpected differentiation) by dissociation with StemPro Accutase reagent (Gibco). However, the majority of neurospheres were smaller than 150 μm and the cultures had good viability upon passaging.

### 3-(4,5-Dimethylthiazol-2-yl)-2,5-Diphenyltetrazolium Bromide (MTT) Assay

The MTT assay was used to determine the metabolic activity and cellular viability of SH-SY5Y cells. Briefly, the mitochondrial oxidoreductase activity was assessed using a colorimetric reaction of MTT, and the activity of the enzyme could be converted into

cellular viability. The cells ( $2 \times 10^5$  cells/mL) were cultured in 96-well plates/a 96-well plate for 24 h (DMEM/F12 with 15% FBS, 1% NEAA, and 1% penicillin/streptomycin). Then the cells were treated with different concentrations of STEE mixed with serum-reduced Opti-MEM (Gibco) for 72 h. After the treatment, the culture medium was replaced by MTT solution and the cells were incubated for another 6 h to crystallize. Crystallized MTT was dissolved in 10% SDS and the optical density (OD) was measured at 570 nm with a microplate reader Varioskan LUX (Thermo Fisher Scientific, Rockford, IL, United States).

### Flow Cytometry

Total viable cell numbers were determined using flow cytometry. SH-SY5Y cells were plated in a 6-well plate ( $2 \times 10^5$  cells/mL) and stabilized for 24 h. The cells were then treated with 50 μg/mL of STEE for different time durations: 0, 12, 24, 48, and 72 h. After the treatment, the cells were detached with TrypLE Express and placed in flow cytometry tubes. Cell suspension was diluted in Guava ViaCount Reagent (Luminex, Austin, TX, United States) to immunolabel viable cells. Finally, the total viable cell numbers were determined using ViaCount assay with flow cytometer Guava easyCyte 8HT (Luminex).

### Measurement of Intracellular ATP Production

Intracellular ATP levels were measured by using a bioluminescence assay kit (Toyo Ink, Tokyo, Japan). The cells were seeded in a 96-well plate at a density of  $2 \times 10^5$  cells/mL and were incubated for 24 h. Then the cells were treated with 50 μg/mL of STEE for different time durations: 12, 24, and 48 h. After the treatment, the cells were dissolved in luciferin–luciferase solution and the suspensions were transferred to a white bottom 96-well plate. ATP levels were measured as luminescence with a Varioskan LUX multimode multiplate reader.

### Thymidine Analog Incorporation *in vitro*

The cells were labeled with the synthetic nucleoside 5-Bromo-2'-deoxyuridine (BrdU, Tokyo Chemical Industry, Tokyo, Japan) to identify the proliferation rates of hNSC. The neurospheres were cultured with different concentrations (10, 25, and 50 μg/mL) of STEE for 24 h, and subsequently, 10 μM of BrdU was added to the medium. The cells were incubated for another 24 h; after that, the neurospheres were dissociated with Accutase reagent and plated on Geltrex matrix solution (Gibco) pre-coated culture vessels with knockout DMEM/F12 (1:1, v/v) containing 2% StemPro Neural Supplement, 2 mM Glutamax Supplement, 6 units/mL heparin, and 200 μM ascorbic acid (differentiation medium). After the incubation in the medium containing different concentrations of STEE for 12 h, the cells were processed for immunostaining or RNA extraction.

### hNSC Differentiation

The cells were cultured as an adherent to let the hNSC differentiate into neural lineages (Schmuck et al., 2017). The neurospheres were pre-treated with different concentrations (10, 25, and 50 μg/mL) of STEE for 24 h and then were dissociated with Accutase reagent. After dissociation, the cells were plated

on the Nunc Lab-Tek Chamber Slide System (Thermo Fisher Scientific) pre-coated with Geltrex solution and cultured in differentiation medium containing different concentrations of STEE for 7 days. After the differentiation experiments, each culture was used for subsequent immunocytochemical analysis.

### Immunocytochemistry

The cells were washed once briefly with PBS, fixed with 4% ice-cold paraformaldehyde (PFA) for 30 min, and then permeabilized with 0.2% Triton-X for 5 min. For BrdU detection, the following DNA denaturation procedure was done—cells were incubated with 2 N HCl for 30 min and 0.1 M borate buffer (0.1 M Na<sub>2</sub>B<sub>4</sub>O<sub>7</sub>, pH = 8.5) for another 15 min. After three washes with PBS, cells were incubated with 5% normal goat serum for 1 h at room temperature to block non-specific binding, and subsequently incubated with the following primary antibodies diluted in blocking solution (1% normal goat serum in PBS) for overnight at 4°C: rabbit monoclonal anti-HuC + HuD (HuC/D, 1:500, Abcam, Cambridge, United Kingdom) and mouse monoclonal anti-BrdU (1:200, Invitrogen, Carlsbad, CA, United States) to detect neural progenitors or thymidine analog; rabbit polyclonal anti-GFAP (1:1000, Novus Biologicals, Centennial, CO, United States) and mouse monoclonal anti-beta III tubulin (Tuj1, 1:1000, Abcam) to detect differentiated astrocytes or neurons. After the incubation and PBS washes, cells were incubated with secondary antibodies diluted in PBS for 1 h at room temperature in the dark. Secondary antibodies conjugated to Alexa Fluor 488 or 594 (1:500, Abcam) were used. After the incubation and PBS washes, coverslips were mounted onto glass slides with drops of ProLong Diamond (Invitrogen), including DAPI to stain nuclei. Fluorescent imaging was observed with a confocal microscope TCS SP8 (Leica, Germany).

ImageJ software (National Institutes of Health, Bethesda, MD, United States) was used for counting marker-positive cells, and the length of astrocytic processes were measured using the NeuronJ plugin for ImageJ. Three independent experiments were performed and 8–10 randomly captured sections per well were analyzed.

## In vivo Experiments

### Animals

We used 16-weeks-old male SAMP8 mice (Japan SLC, Shizuoka, Japan) for in vivo experiments. The SAMP8 mice have spatial learning impairments from 12 weeks of age and spatial memory loss commencing from 16 weeks of age (Ikegami et al., 1992; Flood and Morley, 1997; Cheng et al., 2008; Rhea and Banks, 2017). Also, senescence-accelerated mouse resistant 1 (SAMR1) mice, which have a SAM-related genotype and show resistance to accelerated senescence, were used as controls for SAMP8 as described before (Takeda, 2009). The mice were housed individually under controlled temperature (21–23°C) and photoperiod (12-h light/dark) and provided food and water *ad libitum*. All animal procedures were performed according to the guidelines of the Council of Physiological Society, Japan. Experimental protocols were approved by the Ethics Animal Care and Use Committee (18-356), University of Tsukuba, Japan.

### STEE Administration and Thymidine Analog Incorporation *in vivo*

After 1 week of acclimatization, SAMP8 mice were randomly divided into two groups: SAMP8 water-administered group ( $n = 10$ ) and STEE-administered group ( $n = 10$ ). SAMR1 water-administered group ( $n = 10$ ) were housed as normal aging controls. STEE was dissolved in Mill-Q water and orally administered to SAMP8 mice at 20 mg/kg for 30 days. This concentration was determined following our previous study (Sasaki et al., 2013). SAMP8 controls and SAMR1 mice were administered the equal volume of Mill-Q water to that of the extract. After completion of the 30 days administration, the mice were tested in the behavioral test for 8 days, and the administration was continued during this period also.

BrdU was administered to the mice via the drinking water (Tough and Sprent, 1996; Sasaki et al., 2019a). Briefly, BrdU diluted in drinking water at 1 mg/mL was given to the mice for nine consecutive days starting from the 14th day of STEE administration.

### Morris Water Maze (MWM)

The MWM test was performed to evaluate the learning and memory ability of mice, according to our previous studies (Sasaki et al., 2013, 2019a). The MWM consisted of a circular pool (120 cm in diameter and 45 cm in height) filled with water (30 cm in depth) kept at  $23 \pm 2^\circ\text{C}$ . Provisional four quadrants were set in the pool, and an invisible escape platform (10 cm in diameter) was installed and submerged 1 cm below the surface of the water at the midpoint of one quadrant. In the trials, the mice were allowed to swim to escape from the water (to land on the platform) within 60 s. The mice were given four tests each day for 7 days.

On the final day, the escape platform was removed, and the mice were allowed to swim freely for 60 s (the probe test). The number of crossings over the position where the platform was located, and the time spent in the target quadrant were recorded.

### Immunohistochemistry

After 24 h of the MWM probe trial, the mice were sacrificed by cervical dislocation. The brains were extracted from mice for immunohistochemical analysis, fixed in 4% PFA for 14 days at 4°C, then equilibrated in 30% sucrose/PBS (w/v) for 48 h at 4°C. Coronal brain sections (30  $\mu\text{m}$ ) were obtained using the SM2010R sliding microtome (Leica). Sections were stored at  $-20^\circ\text{C}$  in cryoprotectant solution (ethylene glycol, glycerol, 0.1 M phosphate buffer, pH 7.4, 1:1:1:2 by volume) until usage. For immunolabeling, every sixth tissue sections were mounted on SuperFrost Ultra Plus Adhesion slides (Thermo Fisher Scientific) and allowed to dry for at least 30 min at room temperature. Slides were washed in PBS to remove excess cryoprotectant solution. Antigen retrieval was performed for immunolabeling with anti-BrdU antibody by heating slides incubated in 2N HCl solution for 20 min at 42°C. Slides were rinsed in PBS three times before permeabilization for 15 min in PBS containing 0.03% Triton X-100 (PBS-T). Sections were blocked in 10% donkey serum in PBS-T for 1 h at room temperature. Primary antibodies were diluted, as



specified below, in blocking buffer and incubated overnight. Sections were washed then incubated with fluorochrome-conjugated specific secondary antibodies for 2 h at room temperature. Slides were coverslipped using FluorSave reagent (Merck Millipore).

For evaluation of results, images were obtained using a Nikon Ti-Eclipse microscope (Nikon, Japan). For quantification, confocal images were obtained with a Zeiss LSM 710 laser scanning confocal microscope (Leica) with 1  $\mu$ M Z-stacks for stereological quantification. Primary antibodies used were: rat monoclonal anti-BrdU (1:200, Abcam), rabbit polyclonal anti-DCX (1:200, CST, Danvers, MA, United States), and chicken polyclonal anti-GFAP (1:200, Abcam). Every eighth tissue section was sampled for quantification. Using tiled images, the whole dentate gyrus was quantified using ImageJ software in a blinded fashion. At least three sections were counted per animal.

## ELISA

The cerebral cortex was isolated from the extracted brain and homogenized with ultrasonication in RIPA Lysis Buffer (Santa Cruz, Dallas, TX, United States), including protease inhibitors, on ice. The homogenates were centrifuged at 16,000 *g* for 20 min, and the resulting supernatant was used for the measurement of neurotransmitters by ELISA.

The monoamine levels (dopamine; DA, norepinephrine; NE, and serotonin; 5-HT) in the tissue were determined with a sandwich ELISA (ImmuSmol, Talence, France). Acetylcholine (ACh) levels were measured by the ELISA kit (BioVison, Milpitas, CA, United States) according to the manufacturer's instructions. A 2D Quant kit (GE Healthcare, Piscataway, NJ, United States) was used to normalize each neurotransmitter level to total protein concentration.

## Transcriptome Analysis

### RNA Isolation

Total RNA was isolated from SH-SY5Y cells or neurospheres treated with STEE for 24 h, adherent hNSCs dissociated from STEE pre-treated neurospheres, and cerebral cortices of the mice. ISOGEN kit (Nippon Gene, Toyama, Japan) was used to extract total RNA from cells according to a protocol as previously described (Han et al., 2010).

### Reverse Transcription and qRT-PCR

Isolated RNAs were reverse transcribed with SuperScript IV VILO Master Mix (Applied Biosystems, Foster City, CA, United States) according to the manufacturer's protocol.

Quantitative real-time polymerase chain reaction (qRT-PCR) was performed on Applied Biosystems 7500 RT-PCR System as follows: 2 min at 50°C, 10 min at 95°C and then 45 cycles of PCR (15 s at 95°C; 1 min at 60°C). The primers (Applied Biosystems) used for RT-PCR were: *ACTB* (Hs01060665\_g1), *GAPDH* (Hs02786624\_g1), *PGK1* (Hs00943178\_g1), *PGAM1* (Hs01652468\_g1), *PKM* (Hs00761782\_s1), *PC* (Hs01085875\_g1), *TUBB3* (Hs00801390\_s1), *GFAP* (Hs00909233\_m1), *PDGFRA* (Hs00998018\_m1), *NES* (Hs04187831\_g1), *ASCL1* (Hs00269932\_m1), and *HES1* (Hs00172878\_m1). Amplification was performed with TaqMan Gene Expression Master Mix

(Applied Biosystems). *ACTB* or *GAPDH* levels were used for internal controls, and the relative expression levels of each transcript were determined in triplicate from three independent experiments.

### Microarray Gene Expression Profiling

RNA samples extracted from cerebral cortices were amplified and biotinylated with Affymetrix 3' IVT PLUS Reagent Kit (Affymetrix, Santa Clara, CA, United States), according to the manufacturer's instructions. Biotinylated complementary RNA (cRNA) was hybridized onto Affymetrix Mouse Genome 430 PM array strips (Affymetrix) for 16 h at 45°C in the hybridization station. The hybridized arrays were washed, stained, and scanned with GeneAtlas Fluidics and Imaging Station. Then the gene-level information (CHP files) was obtained from the probe intensity files (CEL files) using robust multichip analysis (RMA) summarization algorithm in Expression Console software (Affymetrix<sup>1</sup>). Subsequent analysis of the obtained data was carried out in Transcriptome Analysis Console (TAC) ver.4 software (Thermo Fisher Scientific). Microarray was conducted for two mRNA biological samples of each group. Differentially expressed genes (DEGs) with *p*-Value < 0.05 (one-way between-subjects ANOVA) were included for gene ontology (GO) analysis. The Molecular Signatures Database (MSigDB) of Gene Set Enrichment Analysis (GSEA) web tool was used to determine whether the gene sets show statistically significant and concordant differences between two biological states<sup>2</sup> (Subramanian et al., 2005; Liberzon, 2014). Graphical presentations were generated in Microsoft Excel 2016 (Microsoft, Redmond, WA, United States). Heatmaps were generated using Morpheus software<sup>3</sup>. Venn-diagram was generated using an open source tool<sup>4</sup>. Microarray dataset are deposited in the Gene Expression Omnibus (GEO) under Accession Number: GSE151727<sup>5</sup>.

### Statistical Analysis

Data are presented as means  $\pm$  standard error of means (SEM) unless otherwise indicated. Normal distribution was tested by the Shapiro–Wilk normality test. Student's *t*-tests (unpaired) were performed to determine significant difference between two groups. A one-way analysis of variance (ANOVA) followed by Dunnett's *post hoc* test was applied to compare each of the treatment conditions with a single control group. Differences in viable cell numbers between the treatment groups at various time points were assessed using two-way ANOVA followed by Sidak's *post hoc* test. For *in vivo* experiments, differences in escape latency among the treatment groups at different time points were assessed using two-way repeated-measures ANOVA with Fisher's LSD test. Other behavioral tests were compared using either one- or two-way (for repeated measures) ANOVA with Fisher's LSD test for normally

<sup>1</sup><http://www.affymetrix.com>

<sup>2</sup><https://www.gsea-msigdb.org/gsea/index.jsp>

<sup>3</sup><http://software.broadinstitute.org/Morpheus>

<sup>4</sup><http://bioinformatics.psb.ugent.be/webtools/Venn/>

<sup>5</sup><https://www.ncbi.nlm.nih.gov/geo/info/linking.html>

distributed data. In the case of non-normally distributed data, the Kruskal–Wallis test followed by Dunn's *post hoc* test was performed. The level of significance was set at  $\alpha < 0.05$ . All the statistical analyses and graphical representations were performed using GraphPad Prism 8 (GraphPad, San Diego, CA, United States).

## RESULTS

Firstly, we evaluated the effect of STEE on age-associated decline in spatial learning and memory in SAMP8 mice using the MWM test. Secondly, we determined the effects of STEE on hippocampal neurogenesis and cortical monoamine levels in SAMP8 mice brains by immunohistochemical and biochemical analysis, respectively. Next, we performed a comprehensive transcriptome analysis of the cortex by microarray to reveal beneficial biological events regulated by STEE, which were further validated in a variety of experiments in human fetal brain-derived neurospheres and in human SH-SY5Y cells.

### HPLC Revealed Major Polyphenolic Constituents in the Sugarcane Top

In the chromatogram generated by HPLC, we observed four major peaks (Figure 1A). Peaks were identified as derived from 3-CQA, 5-CQA, 3-FQA, and ISO, respectively (Figure 1B). The concentrations of 3-CQA, 5-CQA, 3-FQA and ISO in the extract were determined as approximately  $3.52 \pm 0.15$ ,  $4.91 \pm 0.06$ ,  $6.24 \pm 0.51$ , and  $4.27 \pm 0.01$  mg, respectively (per g of the extract).

### STEE Ameliorated Spatial Learning and Memory Deficit in SAMP8 Mice

SAMP8 mice were administered STEE extract (20 mg/kg, p.o.) or water for 30 days, then the mice were tested in the MWM to evaluate their memory (experimental timeline is shown in Figure 2A). In the MWM test, the animals were trained to find the hidden platform for 7 days, with 4 trials per day. The time the mice spent to find the platform was analyzed and termed as escape latency. In the training sessions, the escape latency of the STEE-fed mice was significantly reduced in comparison with the SAMP8 controls from the 5th to the 7th day of the test (Figure 2B). Also, escape latency in the STEE-fed mice significantly decreased on days 5, 6, and 7 of the trial compared to day 1 (before the trial). There was no significant difference in escape latency before and after the trial sessions in the SAMP8 controls (Figure 2C). However, the SAMR1+water and SAMP8+STEE groups both showed significantly reduced escape latency between day 1 and day 7.

The time spent in the target quadrant tended to increase in the STEE-fed mice ( $p = 0.054$ ) compared to the SAMP8 controls (Figure 2D). In the probe test (on the 8th day), there was a significant difference in the crossing time across the virtual platform between the STEE-fed mice and the SAMP8 controls (Figure 2E). No difference was observed in the behavioral tests between SAMP8+STEE and SAMR1 control.

Taken together, these data demonstrate the effect of STEE on the recovery of cognitive functions in SAMP8 mice.

### STEE Tended to Induce Adult Hippocampal Neurogenesis (AHN) of SAMP8 Mice

We examined the subgranular zone (SGZ) because the MWM is a hippocampal-dependent task, while spatial memory is strongly associated with SGZ neurogenesis (Anacker and Hen, 2017). All animals were given BrdU in their drinking water to label dividing cells during treatment and BrdU labeling in the SGZ was quantified. Immunolabeling for BrdU revealed no significant changes between groups [ $F(2, 6) = 1.798$ ,  $p = 0.244$ ] (Figures 3A,B), indicating no statistically significant difference in neural proliferation in the SGZ between SAMR1 mice and SAMP8 controls given water, as well as between SAMP8 controls given water and SAMP8 mice given STEE. We then investigated whether neurogenesis might be affected. We, therefore, quantified the proportion of newborn neurons (BrdU<sup>+</sup>DCX<sup>+</sup>) (Figure 3C) or progenitors and cycling astrocytic stem cells (BrdU<sup>+</sup>GFAP<sup>+</sup>) (Figure 3D). As a result, no significant difference was found between groups, although STEE showed a non-significant trend of elevated BrdU<sup>+</sup>DCX<sup>+</sup> newborn neurons (approximately 1.6-fold increase).

These results indicate that the cognitive decline of SAMP8 was independent of AHN, but that the rescue effect of STEE might be correlated with the increased AHN and further neurodevelopment.

### STEE Restored Levels of Neurotransmitters in SAMP8 Brains

The cerebral cortex, which plays a critical role in cognition and memory, was separated and collected from the extracted brains of mice. Neurotransmitter levels in the cortical tissue homogenates were measured by ELISA. DA, NE, and ACh levels in the cerebral cortices were significantly reduced in SAMP8 controls compared to SAMR1 mice, whereas oral administration of STEE restored neurotransmitter levels in the cortices of SAMP8 mice (Figures 4A,B,D). There was a slight decrease in 5-HT levels ( $p = 0.078$ ) in the cortices of SAMP8 compared to SAMR1 mice. This tendency was partially reversed by STEE administration ( $p = 0.262$ ) (Figure 4C).

The above findings indicate that increased neurotransmitter levels in the cerebral cortex might be correlated with the rescue of age-related memory loss in SAMP8 mice.

### STEE Regulated a Wide Range of Biological Processes in the Cerebral Cortex of SAMP8 Mice

Microarray analysis was performed on cerebral cortex of the mice to investigate the mechanism underlying the effects of STEE. Volcano plots in Figures 5A,B show the significantly regulated genes (SAMP8 control vs. SAMR1 mice and STEE-fed SAMP8 vs. SAMP8 control, respectively). After data processing, we identified 1594 unique DEGs (921 upregulated, 673 downregulated) in SAMP8 controls compared to SAMR1 mice, and 689 unique DEGs (339 upregulated, 350 downregulated) in

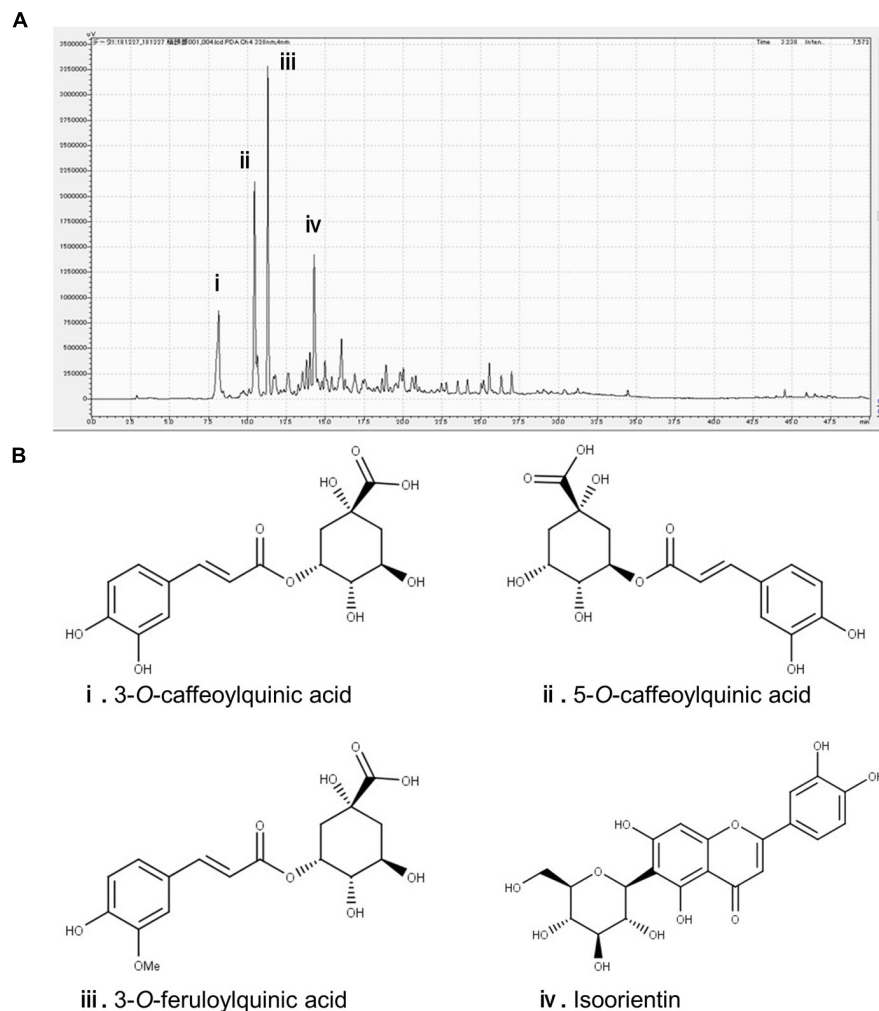


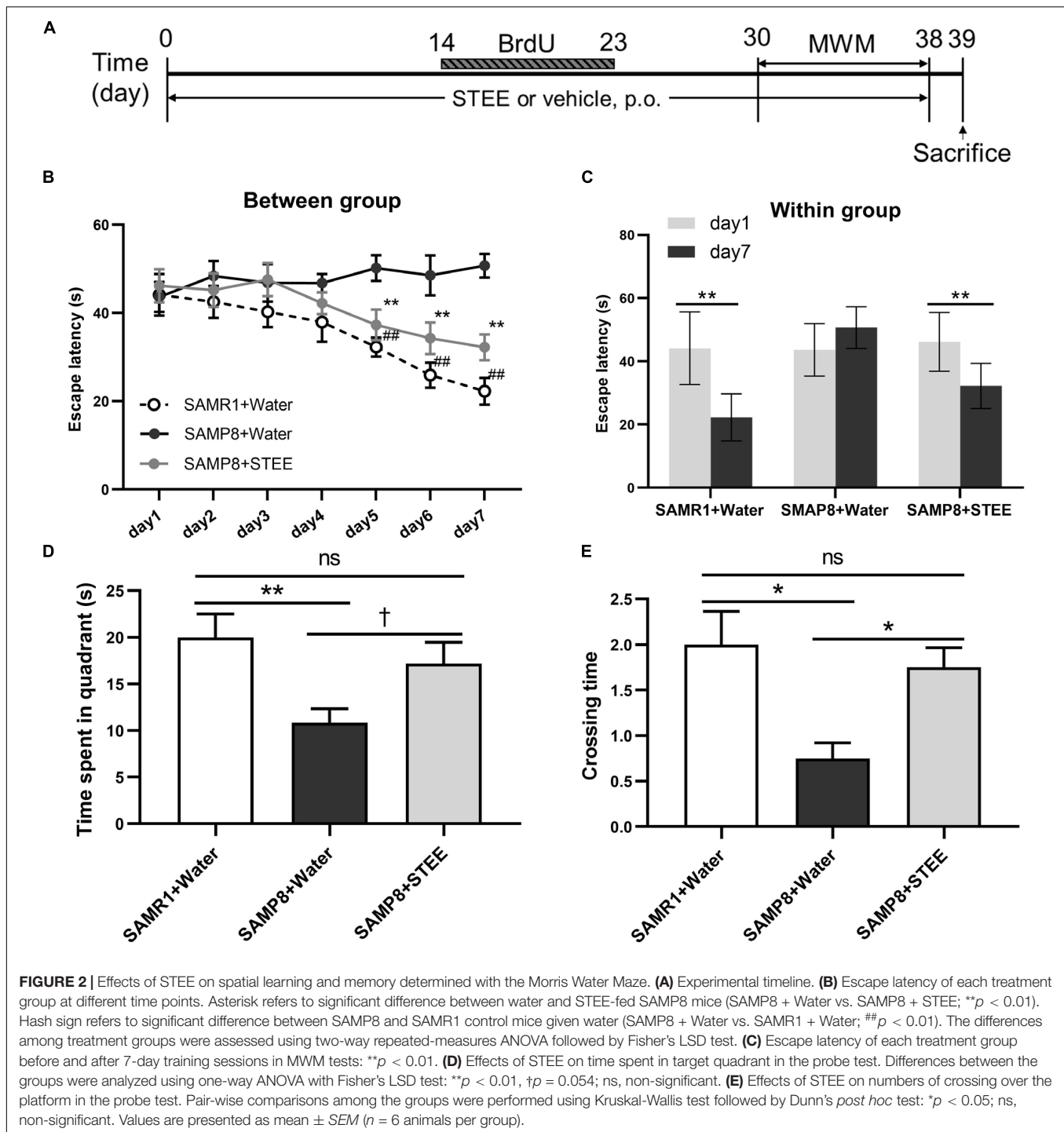
**FIGURE 1 |** Identification of the major polyphenolic constituents of sugarcane top extract through HPLC. The gradient profile was 0–100%, 40 min and the detection wavelength was at 328 nm. **(A)** Representative HPLC chromatogram of the extract. **(B)** Major peaks were identified as 3-O-caffeoylquinic acid **(i)**, 5-O-caffeoylquinic acid **(ii)**, 3-O-feruloylquinic acid **(iii)**, and isoorientin **(iv)**. The concentrations of the phenolic compounds in the extract were measured at the peaks as **(i)**  $3.52 \pm 0.15$ , **(ii)**  $4.91 \pm 0.06$ , **(iii)**  $6.24 \pm 0.51$ , and **(iv)**  $4.27 \pm 0.01$  mg/g.

STEE-fed SAMP8 compared to SAMP8 controls. Distribution of fold changes of DEGs is shown in **Supplementary Figure 1**.

Venn diagrams show common and unique sets of DEGs between the groups (**Figures 5C,D**). Sixty-three genes were downregulated in SAMP8 control (vs. SAMR1) but were upregulated in STEE-fed SAMP8 (vs. SAMP8 control). And, 56 genes were upregulated in SAMP8 control (vs. SAMR1) but downregulated in STEE-fed SAMP8 (vs. SAMP8 control). Among these 119 genes which were regulated in the same direction both in STEE-fed SAMP8 and SAMR1 (compared to SAMP8 control), four genes are associated with transforming growth factor (TGF) beta signaling (systemic name: M5896); nine genes are associated with protein kinase activity (GO:0004672); eight genes are associated with presynapse (GO:0098793); 13 genes are associated with neuron projection (GO:0043005).

GSEA revealed significantly enriched gene sets by the DEGs between SAMP8 control and SAMR1 mice, and between

STEE-fed SAMP8 and SAMP8 control. Top significantly enriched biological processes include, but not limited to, regulation of cell differentiation (GO:0045595), neurogenesis (GO:0022008), neuron differentiation (GO:0030182), regulation of cell death (GO:0010941), neuron development (GO:0048666), regulation of response to stress (GO:0080134), cytoskeleton organization (GO:0007010), central nervous system development (GO:0007417), and cell morphogenesis involved in differentiation (GO:0000904). Also, Hallmark gene sets TGF beta signaling, glycolysis (systemic name: M5937), and phosphoinositide 3-kinase (PI3K)/protein kinase B (Akt)/mammalian target of rapamycin (mTOR) signaling (systemic name: M5923) were enriched by the DEGs. Hallmark gene sets summarize and represent specific well-defined biological states or processes and display coherent expression (**Figure 5E**). Biological processes are arranged in the bar chart according to *p*-Value (hypergeometric *p*-Value).



## STEE Regulated Expression of Genes Associated With Neurotrophin Signaling, Glucose Metabolism, and Neural Development in Cerebral Cortex of SAMP8 Mice

Figure 6A shows the top 10 significantly enriched Kyoto Encyclopedia of Genes and Genomes (KEGG) pathways by

the DEGs between the groups according to false discovery rate (FDR)  $q$ -Value. DEGs between SAMP8 control and SAMR1 mice significantly enriched endocytosis, cancer, ubiquitin-mediated proteolysis, and mitogen-activated protein kinase (MAPK) signaling pathways as well as axon guidance and pyruvate metabolism pathways. On the other hand, axon guidance and regulation of cytoskeleton are the top-ranked KEGG pathways enriched by the DEGs



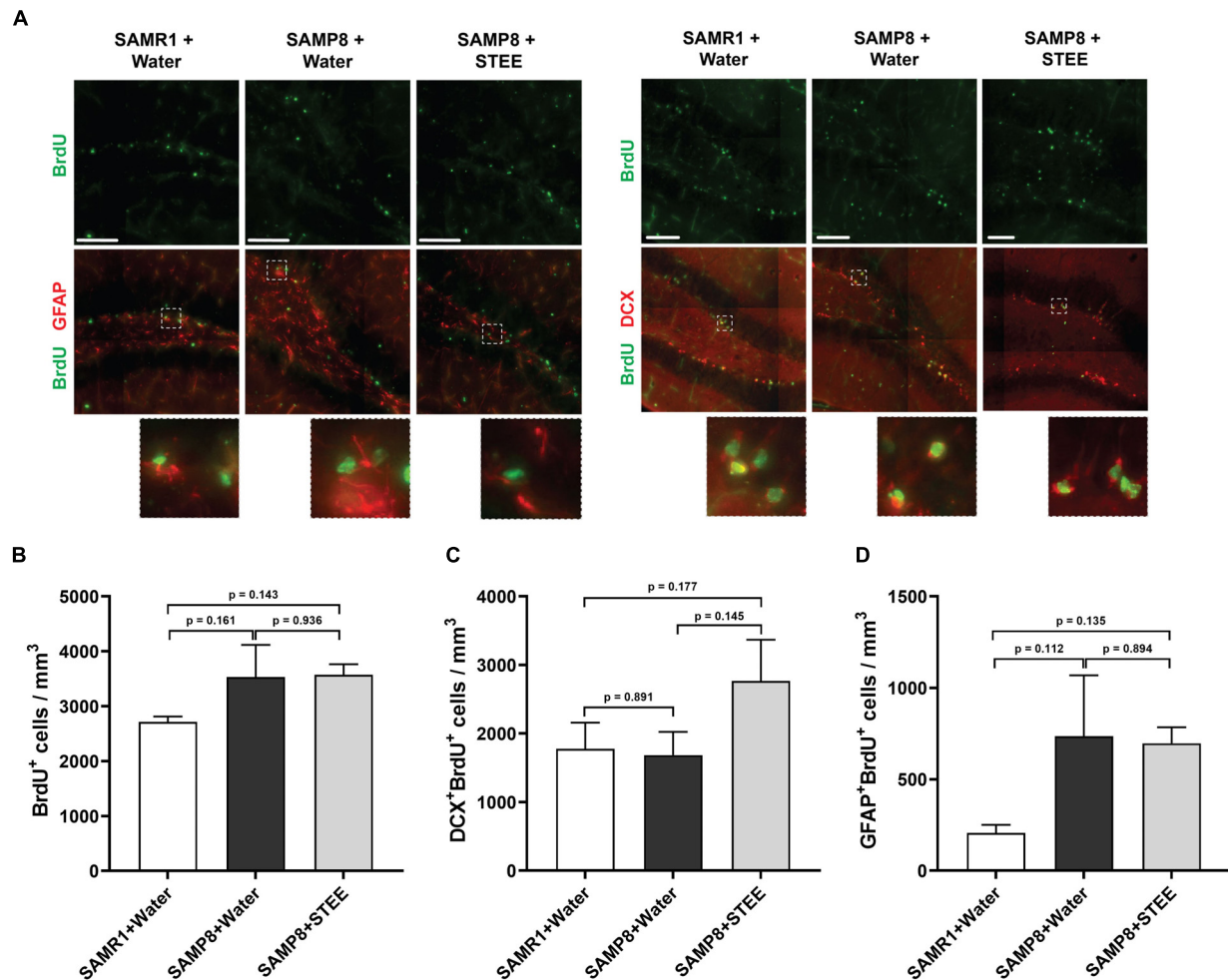
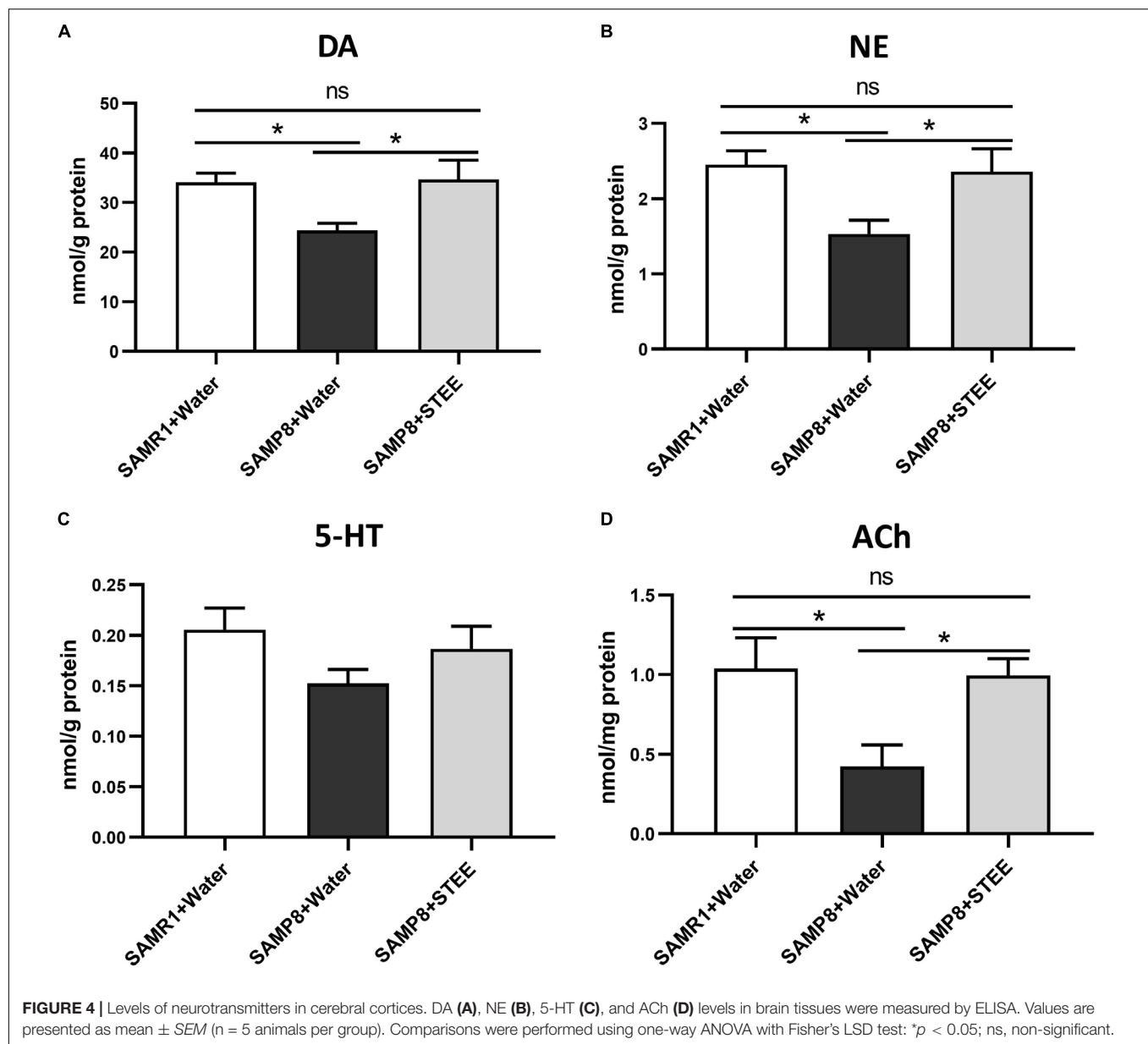


**FIGURE 3 |** Levels of proliferation and differentiation markers in the hippocampal SGZ. **(A)** Representative images of immunolabeling for BrdU, DCX, and GFAP in SAMR1 mice given water, SAMP8 mice given water and SAMP8 mice given STEE. Scale bar: 100  $\mu$ m. **(B)** Total number of BrdU positive proliferating cells in the SGZ of animals. **(C)** Number of DCX/BrdU double-positive newborn immature neurons. **(D)** Number of GFAP/BrdU double-positive cycling astrocytic stem cells and progenitors. The error bar represents the  $\pm$  SEM ( $n = 3$  animals per group). Comparisons were performed through one-way ANOVA with Fisher's LSD test.

between STEE-fed SAMP8 and SAMP8 control. Neurotrophin signaling, phosphatidylinositol signaling system, and cell adhesion molecules (CAMs) are also included among the top 10 enriched pathways between STEE-fed SAMP8 and SAMP8 control.

The heatmaps show the relative intensity of the genes which were regulated in the same direction (**Figure 6B**) both in STEE-fed SAMP8 and SAMR1 compared to SAMP8 control, or which were regulated specifically in STEE-treated SAMP8 (**Figure 6C**). The relative intensity is shown as average of duplicates for each. Presented genes are mainly involved in neurotrophin signaling, glucose metabolism, and neural development. Heatmap in **Figure 6B** shows the average expression intensities of Teneurin transmembrane protein 4 (*Tenm4*), TNF receptor-associated factor (Traf) 6 (*Traf6*), Netrin 5 (*Ntn5*), Protein kinase D1 (*Prkd1*), Glycoprotein m6b (*Gpm6b*), Solute carrier family 16 (monocarboxylic acid transporters), member 4 (*Slc16a4*), TRAF2 and NCK

interacting kinase (*Tnik*), SMAD family member 6 (*Smad6*), Syndecan 4 (*Sdc4*), Myelin basic protein (*Mbp*), Inositol 1,4,5-trisphosphate receptor type 2 (*Itpr2*), Synaptotagmin I (*Syt1*), Pyruvate dehydrogenase kinase, isoenzyme 1 (*Pdk1*), Teneurin transmembrane protein 2 (*Tenm2*), LIM-domain containing, protein kinase (*Limk1*), Basic helix-loop-helix family, member e22 (*Bhlhe22*), Tumor necrosis factor receptor superfamily, member 25 (*Tnfrsf25*), Mitogen-activated protein kinase kinase 3 (*Map2k3*), V-crk sarcoma virus CT10 oncogene homolog (avian)-like (*Crkl*), Growth arrest and DNA-damage-inducible 45 beta (*Gadd45b*), Leucine rich repeat containing G protein coupled receptor 5 (*Lgr5*), Glial fibrillary acidic protein (*Gfap*), SRY-box containing gene 4 (*Sox4*), Platelet derived growth factor, B polypeptide (*Pdgfb*), SMAD family member 1 (*Smad1*), Sonic hedgehog (*Shh*), and Activin A receptor, type 1 (*Acvr1*). Heatmap in **Figure 6C** shows the average expression intensities of Rho family GTPase 1 (*Rnd1*), ELAV (embryonic lethal, abnormal vision, Drosophila)-like

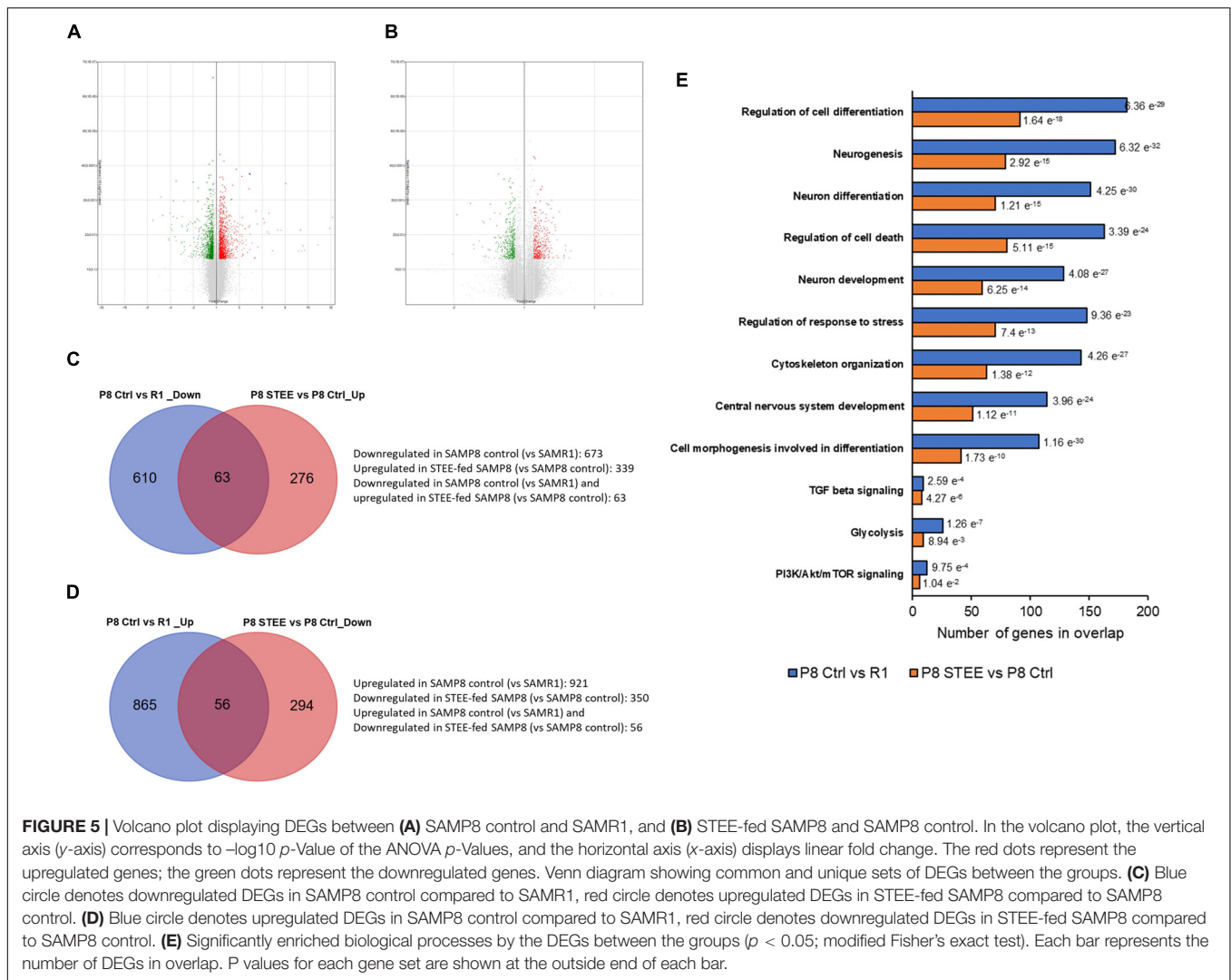


4 (Hu antigen D) (*Elavl4*), Dicer 1, ribonuclease type III (*Dicer1*), CD34 antigen (*Cd34*), C-mer proto-oncogene tyrosine kinase (*Mertk*), Sema domain, immunoglobulin domain (Ig), short basic domain, secreted, (semaphorin) 3A (*Sema3a*), Neurotrophic tyrosine kinase, receptor, type 2 (*Ntrk2*), Pyruvate dehydrogenase kinase, isoenzyme 3 (*Pdk3*), Mitogen-activated protein kinase 11 (*Mapk11*), Phosphatidylinositol 3-kinase, regulatory subunit, polypeptide 1 (p85 alpha) (*Pik3r1*), Vascular cell adhesion molecule 1 (*Vcam1*), Matrix metalloproteinase 9 (*Mmp9*), Nodal (*Nodal*), Chemokine (C-C motif) receptor 5 (*Ccr5*), Musashi RNA-binding protein 2 (*Msi2*), Patched homolog 1 (*Ptch1*), B cell leukemia/lymphoma 2 (*Bcl2*), and Jagged 1 (*Jag1*). Characteristics of each gene presented in the heatmaps are shown in the **Supplementary Tables 1, 2**. A schematic diagram has been presented showing the possible

mechanism of action and future research scope of STEE (**Supplementary Figure 2**).

### STEE Enhanced Cellular Energy Metabolism Through Upregulation of Glycolytic Reaction in SH-SY5Y Cells

The MTT assay was conducted in SH-SY5Y cells treated with different doses of STEE to evaluate its effect on metabolic activity and cellular viability. STEE treatment increased SH-SY5Y cell MTT activity (129% at the maximum) at a dose of 10  $\mu$ g/mL and above. On the other hand, no significant difference was observed after STEE treatment in the numbers of total viable cells between groups at all time points (12, 24, 48, and 72 h). These data indicate that STEE does not affect neuronal cell viability or



proliferation but may affect cell metabolic activity. The data is shown in **Supplementary Figure 3**.

To further verify whether enhanced cellular energy metabolism contributed to the above results, intracellular ATP levels were evaluated. ATP is one of the important indicators of cellular energy production. As shown in **Figure 7A**, 50  $\mu\text{g/mL}$  of STEE increased intracellular ATP levels (121% at the maximum) at all time points (12, 24, and 48 h). These data support that STEE enhanced energy metabolism in neuronal cells.

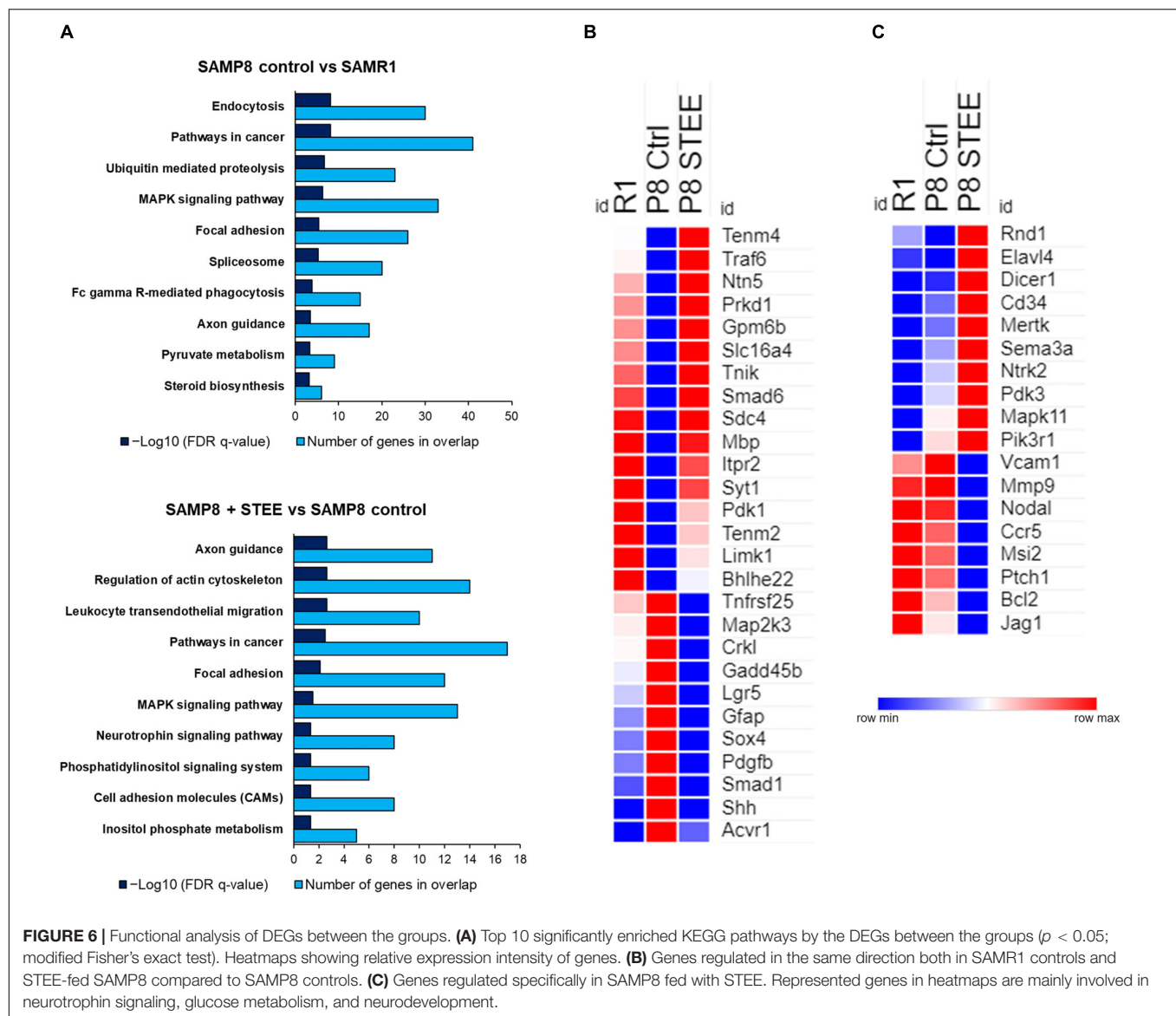
To corroborate the interaction between promoted ATP levels and energy metabolism, the expressions of several genes involved in glycolytic reactions were evaluated by qRT-PCR. STEE-treated cultures (24 h) exhibited significant increases in Phosphoglycerate kinase 1 (*PGK1*), Phosphoglycerate mutase 1 (*PGAM1*), Pyruvate kinase (*PKM*), and Pyruvate carboxylase (*PC*) transcript levels (Fold change 2.63, 2.55, 1.31, and 1.74, respectively, **Figure 7B**).

Given the relationship between intracellular ATP production and the glycolytic pathway, these results indicate that STEE

stimulated glycolysis and anaplerosis, followed by an increase in cellular energy metabolism.

## STEE Regulated the Expression of Neural Development-Related Genes in Neurospheres

Given the *in vivo* effects of STEE on SGZ, we hypothesized that STEE might enhance neural differentiation. The transcript levels of several neurodevelopmental factors were evaluated in neurospheres to investigate whether STEE affects neural stem cell development. Tubulin beta 3 (*TUBB3*), Glial fibrillary acidic protein (*GFAP*), Platelet-derived growth factor receptor alpha (*PDGFRA*), and Nestin (*NES*) were selected as neuronal, astrocytic, oligodendrocytic, and stem cell markers, respectively. As shown in **Figure 7C**, 24 h STEE treatment increased the expression of *TUBB3* and *GFAP* in a dose-dependent manner (Fold change 1.89 and 1.80 at the maximum, respectively), whereas the expressions of *PDGFRA* and *NES* were decreased (Fold change  $-1.71$  and  $-1.47$



at the maximum, respectively). These findings suggest that STEE may induce the cells to lose their stem cell features, transform into the transitional type, and differentiate into neurons or astrocytes.

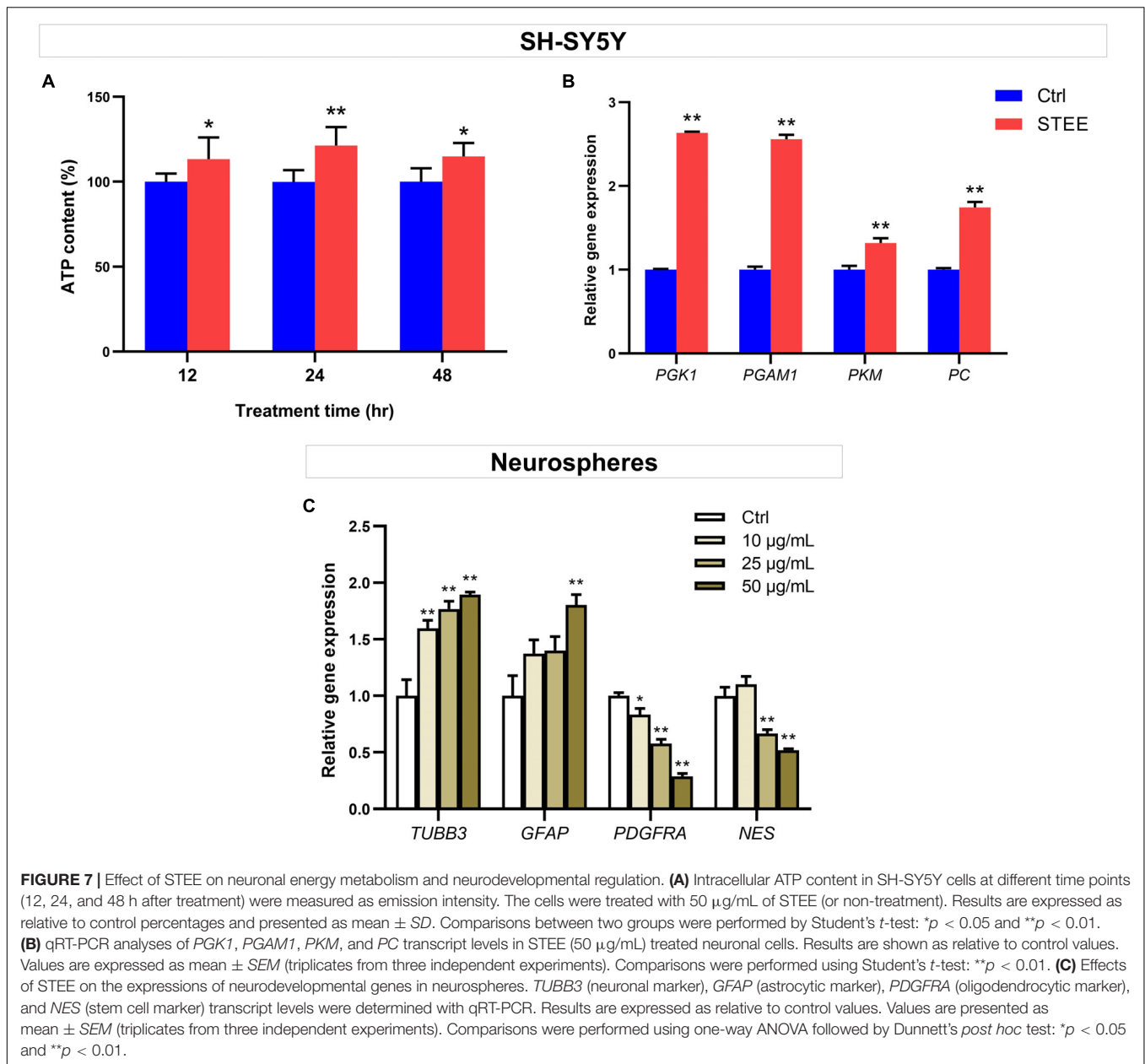
## STEE Affected Proliferation and the Early Phase of Differentiation in hNSCs

Human fetal brain derived-neurospheres were exposed to BrdU to assess the effect of STEE on hNSCs proliferation. Cells that went through the S phase of the cell cycle incorporated BrdU, which was detected with immunocytochemistry and co-stained with neural progenitor markers. While several neural progenitor markers have been established, Hu proteins (HuB, HuC, and HuD) are reportedly expressed at very early stages of neuronal development, and continue to be expressed in immature neurons (Akamatsu et al., 1999, 2005). Here, as

well as BrdU, HuC/D protein expression was evaluated in the cultures at an early differentiation stage (12 h after plating) to assess the pro-neurogenic effects of STEE (**Figure 8A**). As shown in **Figure 8B**, STEE treatment significantly increased the percentage of BrdU<sup>+</sup> cells (120% at 25  $\mu$ g/mL STEE-treated group and 122% at 50  $\mu$ g/mL STEE-treated group) compared to controls. Cultures in the presence of STEE exhibited no changes in the percentages of HuC/D<sup>+</sup> cells; however, a significant increase was observed in the proportion of HuC/D<sup>+</sup>BrdU<sup>+</sup> cells (275% at 25  $\mu$ g/mL STEE-treated group and 276% at 50  $\mu$ g/mL STEE-treated group) in the cultures treated with STEE compared to untreated control (**Figures 8C,D**). These results indicate that STEE induces the proliferation of hNSC and activates newly divided cells to differentiate into neuronal cells *in vitro* cultures.

On the basis of these results showing the pro-neurogenic effect of STEE, qRT-PCR analysis was carried out to corroborate



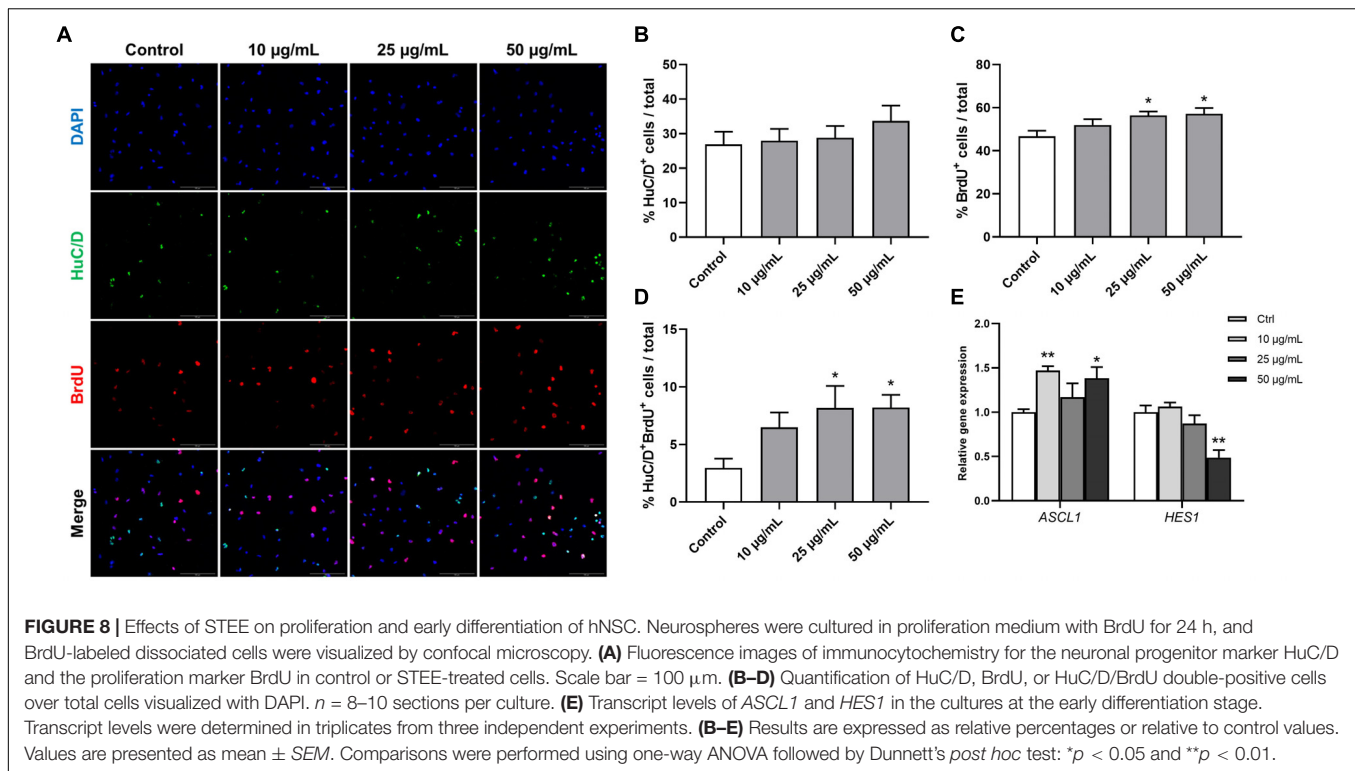


the involvement of transcription factors. RNA was extracted from cells cultured under the same conditions as above, and the expression of Achaete-scute homolog 1 (*ASCL1*) and Hairy and enhancer of split 1 (*HES1*) were evaluated. *Ascl1* and *Hes1* are basic-helix-loop-helix (bHLH) transcription factors. Gene expression dynamics of these factors regulate the quiescence versus activation of neural stem cells in the early developmental phase (Sueda et al., 2019). As expected, *ASCL1* expression showed a significant increase (1.47-fold with 10  $\mu$ g/mL and 1.38-fold with 50  $\mu$ g/mL) and *HES1* expression showed a significant decrease (−1.51-fold with 50  $\mu$ g/mL) in the STEE-treated cultures compared to control (Figure 8E). These findings reflect the stimulation of *Ascl1* and *Hes1* expression dynamics toward an activation of stem cells.

These results suggest that STEE promoted hNSC proliferation and differentiation at early culture stages due to the dynamic regulation of transcription factors.

## STEE Induced Neural Differentiation and Expansion in hNSCs

To further investigate the possible effect of STEE on hNSC differentiation, changes in the proportion of cell populations were analyzed in 7-day cultures (Figure 9A). As shown in Figure 9C, STEE exposure increased the percentage of Tuj1<sup>+</sup> neuronal cells (139% at the maximum). No significant change was observed in the proportion of GFAP<sup>+</sup> astrocytic cells (Figure 9B); however, their processes were observed to be expanded in STEE-treated



cultures (**Figures 9A,D**). Interestingly, the tracing analysis using ImageJ showed an extended total length of astrocytic processes (approximately 1.6-fold increase at the maximum) (**Figure 9E**), indicating STEE did not induce differentiation into astrocytes but affected to morphological expansion.

Altogether, these findings suggest that STEE could contribute to neuronal differentiation and astrocyte morphogenesis in *in vitro* cultures.

## DISCUSSION

The present study revealed the polyphenolic constituents of STEE, and demonstrated that they could enhance neuronal energy metabolism and induce neural stem cell development. Moreover, STEE reversed spatial memory deficits in SAMP8 mice.

Several animal models that mimic the symptoms of age-related neurodegenerative diseases, such as AD, have been established. SAMP8 mice precociously and progressively develop a multisystemic aging phenotype, including learning and memory deficits, as well as pathological features similar to those of AD (Butterfield and Poon, 2005; Pallas et al., 2008; Takeda, 2009; Morley et al., 2012). Therefore, SAMP8 mice are considered advantageous compared to transgenic strains for sporadic AD research (Pallas et al., 2008; Ito, 2013). In the present study, we found that treatment of SAMP8 mice with STEE for 30 days significantly improved performance in the MWM behavioral test, indicating that STEE may rescue cognitive decline in SAMP8

mice, possibly via the amelioration of biochemical pathologies as supported by our *in vitro* results.

The process of neurogenesis occurs mainly in two neurogenic niches: the dentate gyrus (DG) of the hippocampus and the subventricular zone (SVZ) of the lateral ventricles (Spalding et al., 2013; Aimone et al., 2014). These niches have neural stem/progenitor cell pools within which cells divide and generate neurons (and glia), and decades of studies have established that new neurons are continually produced in these two locations in the mammalian brain throughout adulthood. Although a recent study suggested persistent adult hippocampal neurogenesis in human (Boldrini et al., 2018), not all studies have found evidence for human hippocampal neurogenesis in adults (Sorrells et al., 2018), likely caused by differences in immunohistochemical parameters such as post-mortem handling of tissue (Flor-García et al., 2020). Neurogenic capacity declines with age, exacerbated in neurodegenerative diseases such as AD (Lazarov and Marr, 2010; Lee et al., 2012; Winner and Winkler, 2015; Trinchero et al., 2017; Moreno-Jiménez et al., 2019). Approaches to improve neurogenic defects have been studied as a therapeutic target, and the effect of dietary polyphenols on promoting neurogenesis has been suggested as a potential therapeutic candidate (Phillips, 2017). In this study, given the association between AHN and spatial memory, we performed BrdU labeling to examine AHN. The total number of BrdU<sup>+</sup> cells was unchanged among all three groups: SAMR1 and SAMP8 controls, as well as STEE-fed SAMP8 mice. We, therefore, examined changes in newborn neurons (BrdU<sup>+</sup>DCX<sup>+</sup>) or astrocytic precursor cells (BrdU<sup>+</sup>GFAP<sup>+</sup>) in the SGZ of SAMP8 mice. Our findings suggest that even the subtle increase of the newborn neuron

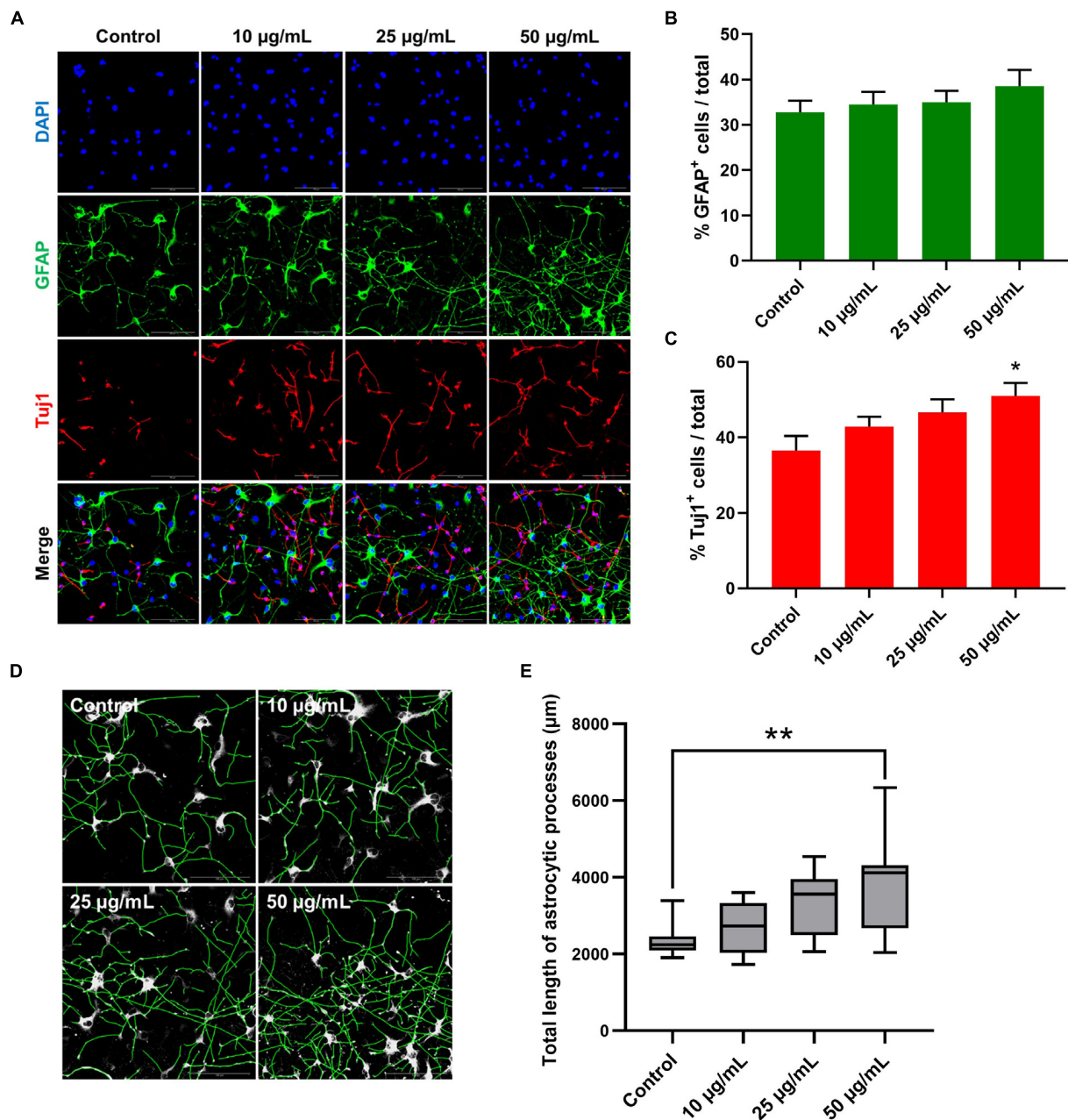


**FIGURE 9 |** Effects of STEE on hNSC differentiation. hNSCs were cultured as a monolayer for 7 days in differentiation medium only (control cells) or in differentiation medium with different concentrations of STEE (treatment cells). Immunostained cells were visualized by confocal microscopy. **(A)** Fluorescence images of immunocytochemistry for astrocytic marker GFAP and neuronal marker Tuj1 in the control and STEE-treated cells. Scale bar = 100 µm. **(B,C)** Quantification of GFAP or Tuj1 positive cells over total cells visualized with DAPI. Results are expressed as relative percentages. Comparisons were performed using one-way ANOVA followed by Dunnett's *post hoc* test: \**p* < 0.05. Error bars represent the ± SEM (*n* = 8–10 sections per culture). **(D)** Effects of STEE on the length of astrocytic processes. Representative images of outlined GFAP positive processes, and **(E)** quantification of total length of the processes. Results are shown as box plots. Each box ranges from 25th to 75th percentile, the line in the middle represents the median value, the error bar represents the ± SEM (*n* = 8–10 sections per culture). Asterisks refer to statistical significance by Kruskal–Wallis test followed by Dunn's *post hoc* test: \*\**p* < 0.01.

population by about 60% may potentially be biologically relevant as STEE treatment could restore behavioral loss of SAMP8 mice in the MWM task. Plausibly, this increase in new immature neurons might be more pronounced if, for instance, STEE was given over a longer period or at higher doses.

Further studies should address optimal dosing for memory and neurogenic enhancement.

The potential of STEE to induce neurogenesis is more strongly supported by our *in vitro* studies with hNSC. Indeed, the myriad effects of STEE *in vitro*, as well as *in vivo*,

suggest a number of candidate cellular mechanisms by which it could rescue age-related cognitive decline. Neural stem cell fate and development are regulated by several factors, among which bHLH transcription factors play an important role in proliferation and differentiation. *Ascl1* (also known as *Mash1*) is one of the bHLH factors, and is expressed in transit-amplifying cells, which proliferate and soon generate neuroblasts (Kim et al., 2011; Andersen et al., 2014; Sueda et al., 2019). On the other hand, repressor-type bHLH factors, such as *Hes1*, lead to suppression of *Ascl1* and contribute to maintaining the quiescence of the cells. In this context, downregulated *HES1* expression in the cultures with STEE at the early differentiation stage corresponds to increased *ASCL1* expression and subsequent decrease of stem cell quiescence in hNSC. This can also be correlated with the downregulation of nestin expression in neurospheres cultured with STEE. These findings provoke interest in potential modulation of signaling pathways such as Notch by bHLH (Mizutani et al., 2007; Imayoshi et al., 2010; Andersen et al., 2014). Downregulation of *Jag1*, one of the cell surface ligands of Notch receptors, in STEE-fed mouse brain also raises interest. Moreover, the increased percentage of *Tuj1*<sup>+</sup> neuronal cells in the hNSC adherent culture corresponds well with the results of qRT-PCR analysis in neurospheres and immunocytochemical analysis at early culture stages. The significant upregulation of *HuD*-encoding *Elavl4* and *Dicer*-encoding *Dicer1* and the significant downregulation of *Musashi-2*-encoding *Msi2* in the cerebral cortex of STEE-fed mice indicate evoked differentiation of cortical NSCs by STEE (Sakakibara et al., 2001; Akamatsu et al., 2005; Kawase-Koga et al., 2010; Saurat et al., 2013). Moreover, the modulated genes such as *Tenm2*, *Sox4*, and *Shh* in STEE-fed SAMP8 mouse brain suggest the possible effect of the extract as a neurodevelopmental modulator *in vivo* (Kenzelmann et al., 2007; Dave et al., 2011; Kamachi and Kondoh, 2013). Similar expressions of *Tenm2*, *Sox4*, and *Shh* were also observed in SAMR1 mouse brain.

While our findings from the SAMP8 mouse model are seemingly in conflict with our *in vitro* results, it should be noted that our investigations are specific to the SAMP8 mouse and therefore do not rule out potential effects on other mouse models of dementia or with different doses of STEE. Critically, neurogenic deficits in the SAMP8 mouse model have been largely characterized in aged mice. Gang et al., for example, only saw a significant decrease in *BrdU*<sup>+</sup> and *DCX*<sup>+</sup> cells in 10-month old SAMP8 mice compared to age-matched SAMR1 controls (Gang et al., 2011). A separate study by Díaz-Moreno et al. reported reduced neurogenesis in 14-month old SAMP8 mice (Díaz-Moreno et al., 2013). Our study showed that STEE could reverse the memory deficits in SAMP8 mice in the MWM task at 4 months of age. Because the MWM task is hippocampal-dependent, we tested for the potential involvement of AHN in the rescue of spatial memory deficits in the STEE-fed mice. Our findings corroborated prior studies that showed neurogenic changes do not occur between SAMR1 mice and SAMP8 controls at this age. Although we cannot discard the relevance between the slightly increased AHN and the improved spatial learning and memory, further studies are warranted to examine potential positive effects of STEE in aged SAMP8 mice with more overt

cognitive and neurogenic deficits. We found several effects of STEE *in vitro*; thus, it is plausible that STEE might influence a range of subtle cellular changes that cumulatively reverse the memory decline in SAMP8 mice. Notably, we found that STEE promoting spatial memory recovery is correlated with the restoration of cortical DA, NE, and ACh levels.

Regulation of monoamine levels in the brain is critical for maintaining cognitive function, and an imbalance of monoamine transmitters such as DA, NE, and 5-HT plays a major role in the onset and progression of cognitive disorders (Naoi et al., 2018). As well as catecholaminergic neurons, cholinergic neurons are widely distributed in the CNS. The cholinergic system is involved in critical physiological processes such as attention, learning and memory, and wakefulness (Ferreira-Vieira et al., 2016). Therefore, modulation of neurotransmitter levels has been suggested as a therapeutic target, as evidenced by the use of serotonin reuptake inhibitors (SSRIs) and acetylcholinesterase inhibitors (AChEIs) for the treatment of cognitive impairment (Recanatini and Valenti, 2004). Degeneration of catecholaminergic neurons (including dopaminergic and noradrenergic) seriously worsens in SAMP8 mice from 8 months on (Karasawa et al., 1997), and significant decrease of ACh level has been observed in 3-month old SAMP8 mice hippocampi and cortices (Zhang et al., 2017). Enhanced synaptic plasticity in the cerebral cortex of STEE-fed mice could be explained by the significant upregulation of *Mbp*, a major myelin protein and essential for saltatory nerve conduction, and of *Syt1*, an important regulator of synaptic vesicle transport (Fields, 2015; Schupp et al., 2016). *Mbp* and *Syt1* were also upregulated in SAMR1 mice compared to SAMP8 controls. Additionally, the upregulation of phagocytic receptor *Mertk* and somatic  $Ca^{2+}$  mediator *Itpr2* may suggest developmental synapse pruning and remodeling by astrocytes in the brain of STEE-fed mice (Chung et al., 2013; Yang et al., 2016). Restored cortical neurotransmission in SAMP8 mice by STEE administration might contribute to the behavioral improvement of mice in the MWM task; however, the MWM task has an aspect that depends on hippocampal brain function. In this context, there is room for investigation on changes in hippocampal neurotransmitter levels, which is also important to neurogenesis (Lazarov and Marr, 2010; Winner and Winkler, 2015; Naoi et al., 2018).

In addition to our *in vivo* work, SH-SY5Y cells were used for *in vitro* assays. This cell line is known to have catecholaminergic neuron characteristics including expression of cholinergic (and dopaminergic) neuronal markers (Kume et al., 2008; Kovalevich and Langford, 2013). Our experimental results obtained from SH-SY5Y cultures showed that STEE stimulated neuronal cell metabolic activity through upregulation of glycolysis evidenced by increased transcript levels of *PGK1*, *PGAM1*, *PKM* and *PC* in the cells. Mitochondrial dysfunction is characterized as one of the biological processes accompanying aging and its associated cognitive decline, and is linked to decreased antioxidant defenses due to high energy demands (Grimm and Eckert, 2017). As an approach to enhance mitochondrial activity and reduce cognitive decline, the antioxidant properties of phytochemicals have received significant attention. For example, anthocyanin, which is a naturally occurring potent antioxidant, has been



reported to improve spatial memory and restore brain ATP levels *in vivo* (Andres-Lacueva et al., 2005; Gutierrez et al., 2012). Recent studies have shown that increasing glycolysis by PGK1 activation slows neurodegeneration in Parkinson's disease (Cai et al., 2019). PGAM1, in turn, is reported to be protective against neuronal damage from oxidative stress or ischemia (Kim et al., 2020). Another protein we studied, PKM is one of the rate-limiting enzymes in the glycolytic reaction, and finally, PC connects glycolysis and the tricarboxylic acid (TCA) cycle through its catalytic action. The rapid increase of oxidative stress in SAMP8 mice is evidenced as elevated levels of oxidative stress markers such as lipid peroxide in the cerebral cortex of 4–8 weeks old young SAMP8 mice compared to SAMR1 controls (Sato et al., 1996). The present study suggests that STEE can promote glucose metabolism in neuronal cells, which in turn can counter age-related neuronal oxidative damage and reduced neurotransmission. Also, neurons prioritize lactate-uptake over glucose to sustain their oxidative demands; therefore, supply of lactate mediated through astrocytic glycolysis is thought to be critically important for maintaining neuronal activity and memory formation (Suzuki et al., 2011; Alberini et al., 2018). Indeed, the upregulation of pyruvate dehydrogenase kinases (PDKs), *Pdk1* and *Pdk3*, and a monocarboxylate transporter-encoding *Slc16a4* *in vivo* may indicate active production and transport of lactate in STEE-fed mice. (Tadi et al., 2015). *Pdk1* and *Slc16a4* were also upregulated in SAMR1 mice compared to SAMP8 controls. Although the present study with hNSCs suggests that STEE might contribute to astrocytic process lengthening, the association between cellular energy metabolism and morphogenesis is uncertain. However, the findings would encourage the investigation of the effects of STEE on astrocyte function, including their glucose metabolism.

Microarray analysis showed the increased expression of *Ntrk2*, specifically in STEE-fed mice brain when compared to SAMP8 control. *Ntrk2* encodes tropomyosin receptor kinase B (TrkB), which is a receptor for neurotrophins such as brain-derived neurotrophic factor (BDNF). TrkB has several isoforms, among them, TrkB-FL is a full-length receptor, and TrkB-T1 is a truncated subtype. TrkB-FL signaling contributes to BDNF signal transduction as well as to nervous system development, including myelination and cell survival, through several classical pathways such as the PI3K/Akt pathway (Cosgaya et al., 2002; Gupta et al., 2013; Tejeda and Diaz-Guerra, 2017). TrkB-T1 transduces the Rho signaling pathway and regulates cellular morphogenesis or  $\text{Ca}^{2+}$  influx (Rose et al., 2003; Ohira et al., 2007). We also found that STEE treatment upregulated *Pik3r1* and *Limk1* expressions. *Pik3r1* is the predominant regulatory isoform of PI3K and encodes p85 $\alpha$  subunit of PI3K. LIMK1 is activated downstream of Rho signaling and plays an essential role in synaptic transmission, plasticity, and memory formation. Therefore, it may be anticipated that the observed neurodevelopmental effects of STEE in this study were mediated by the activation of TrkB and Rho signaling evident by the upregulation of their downstream effectors *Pik3r1* and *Limk1*, respectively (Gupta et al., 2013; Tejeda and Diaz-Guerra, 2017; Ravindran et al., 2019). Particularly, recently explored role of astrocytic TrkB-T1 signaling in astrocyte morphogenesis (Holt et al., 2019) warrants

further research on the effect of STEE and its active compounds on TrkB activation.

Chemical analysis revealed CQA derivatives as the major polyphenols in the sugarcane top. CQA and its derivatives are broadly distributed phytochemicals in plants and their health benefits are widely investigated. Previous studies have reported that CQA and its derivatives have antibacterial, anticancer, antihyperglycemic, and neuroprotective properties (Kimura et al., 1985; Yoshimoto et al., 2002; Matsui et al., 2004; Miyamae et al., 2011a). Our previous studies have reported that CQA derivatives could activate mitochondrial ATP production mediated through energy metabolism promotion characterized by the upregulation of glycolytic enzymes (Han et al., 2010; Miyamae et al., 2011a). Also, Ferulic acid, one of the cinnamic acid derivatives, has shown antidepressant-like effects modulated by the increased expression of glycolytic genes, including *PKM* and *PC* and by increased monoamine levels in the mouse brain limbic system (Sasaki et al., 2019b). Moreover, our recent study has suggested that CQA derivative increases G0/G1 cell cycle arrest in hNSC and leads to its differentiation (Sasaki et al., 2019a). Considering the facts mentioned above, we can postulate that the CQAs in the sugarcane top extract may act as the glycolysis up-regulators and neural stem cell fate regulators observed in the present study. An ultra-high-performance liquid chromatography tandem mass spectrometry study by Su et al. has demonstrated that several mono-CQA and di-CQA isomers can pass through the blood-brain barrier (BBB) (Su et al., 2014). Although in our study, we have not explicitly investigated the effect of STEE on endothelial cells of the BBB, we found that STEE induced astrocytic process lengthening in hNSCs, and decreased expression of *Tnfrsf25*, *Vcam1*, and *Mmp9* in mice cortex, suggesting that STEE may improve age-associated degeneration of BBB properties (Wosik et al., 2007). ISO, a natural flavonoid, is a luteolin glycoside as shown in its chemical identification name- luteolin-6-C-glucoside. ISO exists in several plants such as rooibos (*Aspalathus Linearis*) (Breiter et al., 2011), and has been reported to exhibit a variety of bioactivities, including antioxidant, anti-inflammatory, and anticancer effects (Tunali et al., 2007; Yuan et al., 2013, 2016). Furthermore, a previous study has reported that ISO acts as an ATP non-competitive glycogen synthase kinase-3 $\beta$  (GSK3 $\beta$ ) inhibitor and alleviates tau phosphorylation and A $\beta$  toxicity (Liang et al., 2016). Therefore, this luteolin glycoside may also contribute to oxidative stress reduction and mitochondrial activation by enhancing cellular oxidative metabolism (Theeuwes et al., 2017; Yang et al., 2017). Also, GSK3 $\beta$  inhibition can induce neural stem cell proliferation and neurogenesis (Morales-Garcia et al., 2012), suggesting potential effects of ISO on neurogenesis. Daily intake of coffee or rooibos has not been reported to cause any serious damage to health. Additionally, several plant extracts, such as *Ilex guayusa*, rich in mono- and di-CQA derivatives have been approved by the FDA as GRAS (generally regarded as safe; GRAS Notice No. GRN 000869). Also, Amano et al. have reported that minor gastrointestinal side effects can be observed only in very high dose of 5-CQA (>100  $\mu\text{M}$ ), whereas 1 g of STEE has approximately 13.86  $\mu\text{M}$  of 5-CQA (Amano et al., 2019). Therefore, daily intake of these polyphenols is unlikely to cause

any serious side effects. In addition to the major peaks, several other peaks were also observed in the chromatogram. Analysis of those minor peaks may lead to identification of further interesting phytochemicals in the extract. However, previous studies on the bioactivities of the compounds identified as the major constituents of STEE in the present study suggest that the extract from this freely available and plentiful biological resource is a promising nutrient source having a unique phytochemical make-up and showing physiological activity on several aspects of brain function.

Our previous study has shown that caffeoylquinic acid-rich plant extract ameliorated cognitive decline in SAMP8 mice but did not affect behavioral activities in SAMR1 mice (Sasaki et al., 2013). Therefore, in the present study, we did not include the STEE-fed SAMR1 group. This is supported by the literature, whereby SAMP8 investigations typically include the SAMP8 and SAMR1 controls without SAMR1 + treatment group (Yang et al., 2020).

## CONCLUSION

In conclusion, our data is the first to demonstrate that STEE ameliorates age-related cognitive function likely through modulation of neuronal energy metabolism and neural differentiation from neural stem/progenitor cells. In the present study, we used a single concentration of STEE for the *in vivo* experiments; therefore, further careful studies with multiple sample concentrations are required to reveal optimal dosage for the induction of neural activity *in vivo*. One of the advantages of STEE is that they contain multiple bioactive compounds that can target multiple pathologies simultaneously, and therefore, can be more efficacious than traditional drugs for age-related impairment of brain functions. The findings of this study suggest the potential of STEE as a novel nutritional intervention or nutraceutical for cognitive health.

## DATA AVAILABILITY STATEMENT

All datasets generated for this study are included in this article/**Supplementary Material**. Microarray data are deposited in the NCBI Gene Expression Omnibus (GEO) under accession number: GSE151727 (<https://www.ncbi.nlm.nih.gov/geo/query/acc.cgi?acc=GSE151727>).

## REFERENCES

- Aimone, J. B., Li, Y., Lee, S. W., Clemenson, G. D., Deng, W., and Gage, F. H. (2014). Regulation and function of adult neurogenesis: from genes to cognition. *Physiol. Rev.* 94, 991–1026. doi: 10.1152/physrev.00004.2014
- Akamatsu, W., Fujihara, H., Mitsuhashi, T., Yano, M., Shibata, S., Hayakawa, Y., et al. (2005). The RNA-binding protein HuD regulates neuronal cell identity and maturation. *Proc. Natl. Acad. Sci. U.S.A.* 102, 4625–4630. doi: 10.1073/pnas.0407523102
- Akamatsu, W., Okano, H. J., Osumi, N., Inoue, T., Nakamura, S., Sakakibara, S., et al. (1999). Mammalian ELAV-like neuronal RNA-binding proteins HuB and

## ETHICS STATEMENT

All animal procedures were performed according to the guidelines of the Council of Physiological Society, Japan. Experimental protocols were approved by the Ethics Animal Care and Use Committee of University of Tsukuba, Japan.

## AUTHOR CONTRIBUTIONS

KI and QW investigated the data, performed the methodology, carried out the formal analysis and data curation, wrote the original draft of the manuscript, and visualized the data. FF performed the software, carried out the formal analysis, and wrote, reviewed, and edited the manuscript. KS and KT investigated the data, performed the methodology, and validated the data. YA and HU contributed to conceptualization and resources. FS and HI contributed to conceptualization, resources, wrote, reviewed, and edited the manuscript, supervised the data, and carried out the project administration and funding acquisition. All the authors made substantial contributions to this article and approved the final article.

## FUNDING

This research was partially supported by the Nippo Co., Ltd., Japan Science and Technology Agency (JST), Science and Technology Research Partnership for Sustainable Development (SATREPS, Grant No. JPMJSA1506).

## ACKNOWLEDGMENTS

The authors would like to thank Dr. Yasuhiro Shimamoto and Ms. Shoko Ebisuya from AIST for their valuable assistance in HPLC. They also grateful to Shigeaki Amano, a representative director of the Amanoshouten Co., Ltd. (Asakura, Fukuoka, Japan), for the preparation of milled sugarcane top.

## SUPPLEMENTARY MATERIAL

The Supplementary Material for this article can be found online at: <https://www.frontiersin.org/articles/10.3389/fcell.2020.573487/full#supplementary-material>

- HuC promote neuronal development in both the central and the peripheral nervous systems. *Proc. Natl. Acad. Sci. U.S.A.* 96, 9885–9890. doi: 10.1073/pnas.96.17.9885
- Alberini, C. M., Cruz, E., Descalzi, G., Bessières, B., and Gao, V. (2018). Astrocyte glycogen and lactate: new insights into learning and memory mechanisms. *Glia* 66, 1244–1262. doi: 10.1002/glia.23250
- Amano, Y., Honda, H., Nukada, Y., Ikeda, N., Yamane, M., Nakano, K., et al. (2019). Safety pharmacological evaluation of the coffee component, caffeoylquinic acid, and its metabolites, using *ex vivo* and *in vitro* profiling assays. *Pharmaceuticals* 12:110. doi: 10.3390/ph12030110

- Anacker, C., and Hen, R. (2017). Adult hippocampal neurogenesis and cognitive flexibility - linking memory and mood. *Nat. Rev. Neurosci.* 18, 335–346. doi: 10.1038/nrn.2017.45
- Andersen, J., Urban, N., Achimastou, A., Ito, A., Simic, M., Ullom, K., et al. (2014). A transcriptional mechanism integrating inputs from extracellular signals to activate hippocampal stem cells. *Neuron* 83, 1085–1097. doi: 10.1016/j.neuron.2014.08.004
- Andres-Lacueva, C., Shukitt-Hale, B., Galli, R. L., Jauregui, O., Lamuela-Raventos, R. M., and Joseph, J. A. (2005). Anthocyanins in aged blueberry-fed rats are found centrally and may enhance memory. *Nutr. Neurosci.* 8, 111–120. doi: 10.1080/10284150500078117
- Boldrini, M., Fulmore, C. A., Tartt, A. N., Simeon, L. R., Pavlova, I., Poposka, V., et al. (2018). Human hippocampal neurogenesis persists throughout aging. *Cell Stem Cell* 22, 589–599.e5. doi: 10.1016/j.stem.2018.03.015
- Breiter, T., Laue, C., Kressel, G., Groll, S., Engelhardt, U. H., and Hahn, A. (2011). Bioavailability and antioxidant potential of rooibos flavonoids in humans following the consumption of different rooibos formulations. *Food Chem.* 128, 338–347. doi: 10.1016/j.foodchem.2011.03.029
- Butterfield, D. A., and Poon, H. F. (2005). The senescence-accelerated prone mouse (SAMP8): a model of age-related cognitive decline with relevance to alterations of the gene expression and protein abnormalities in Alzheimer's disease. *Exp. Gerontol.* 40, 774–783. doi: 10.1016/j.exger.2005.05.007
- Cai, R., Zhang, Y., Simmering, J. E., Schultz, J. L., Li, Y., Fernandez-Carasa, I., et al. (2019). Enhancing glycolysis attenuates Parkinson's disease progression in models and clinical databases. *J. Clin. Invest.* 129, 4539–4549. doi: 10.1172/JCI129987
- Cheng, H., Yu, J., Jiang, Z., Zhang, X., Liu, C., Peng, Y., et al. (2008). Acupuncture improves cognitive deficits and regulates the brain cell proliferation of SAMP8 mice. *Neurosci. Lett.* 432, 111–116. doi: 10.1016/j.neulet.2007.12.009
- Chung, W. S., Clarke, L. E., Wang, G. X., Stafford, B. K., Sher, A., Chakraborty, C., et al. (2013). Astrocytes mediate synapse elimination through MEGF10 and MERTK pathways. *Nature* 504, 394–400. doi: 10.1038/nature12776
- Colombo, R., Lencas, F. M., and Yariwake, J. H. (2006). Determination of flavonoids in cultivated sugarcane leaves, bagasse, juice and in transgenic sugarcane by liquid chromatography-UV detection. *J. Chromatogr. A* 1103, 118–124. doi: 10.1016/j.chroma.2005.11.007
- Colombo, R., Yariwake, J. H., Queiroz, E. F., Ndjoko, K., and Hostettmann, K. (2005). On-line identification of sugarcane (*Saccharum officinarum* L.) methoxyflavones by liquid chromatography-UV detection using post-column derivatization and liquid chromatography-mass spectrometry. *J. Chromatogr. A* 1082, 51–59. doi: 10.1016/j.chroma.2005.01.083
- Cosgaya, J. M., Chan, J. R., and Shooter, E. M. (2002). The neurotrophin receptor p75(NTR) as a positive modulator of myelination. *Science* 298, 1245–1248. doi: 10.1126/science.1076595
- Dave, R. K., Ellis, T., Toumpas, M. C., Robson, J. P., Julian, E., Adolphe, C., et al. (2011). Sonic hedgehog and notch signaling can cooperate to regulate neurogenic divisions of neocortical progenitors. *PLoS One* 6:e14680. doi: 10.1371/journal.pone.0014680
- Diaz-Moreno, M., Hortiguera, R., Goncalves, A., Garcia-Carpio, I., Manich, G., Garcia-Bermudez, E., et al. (2013). Abeta increases neural stem cell activity in senescence-accelerated SAMP8 mice. *Neurobiol. Aging* 34, 2623–2638. doi: 10.1016/j.neurobiolaging.2013.05.011
- Ferreira-Vieira, T. H., Guimaraes, I. M., Silva, F. R., and Ribeiro, F. M. (2016). Alzheimer's disease: targeting the cholinergic system. *Curr. Neuropharmacol.* 14, 101–115. doi: 10.2174/1570159x13666150716165726
- Fields, R. D. (2015). A new mechanism of nervous system plasticity: activity-dependent myelination. *Nat. Rev. Neurosci.* 16, 756–767. doi: 10.1038/nrn4023
- Flood, J. F., and Morley, J. E. (1997). Learning and memory in the SAMP8 mouse. *Neurosci. Biobehav. Rev.* 22, 1–20. doi: 10.1016/S0149-7634(96)00063-2
- Flor-García, M., Terreros-Roncal, J., Moreno-Jiménez, E. P., Ávila, J., Rábano, A., and Llorens-Martin, M. (2020). Unraveling human adult hippocampal neurogenesis. *Nat. Protoc.* 15, 668–693. doi: 10.1038/s41596-019-0267-y
- Gang, B., Yue, C., Han, N., Xue, H., Li, B., Sun, L., et al. (2011). Limited hippocampal neurogenesis in SAMP8 mouse model of Alzheimer's disease. *Brain Res.* 1389, 183–193. doi: 10.1016/j.brainres.2011.03.039
- Ginneken, V. V. (2017). Are there any Biomarkers of Aging? Biomarkers of the Brain. *Biomed. J. Sci. Tech. Res.* 1, 193–207. doi: 10.26717/bjstr.2017.01.000151
- Grimm, A., and Eckert, A. (2017). Brain aging and neurodegeneration: from a mitochondrial point of view. *J. Neurochem.* 143, 418–431. doi: 10.1111/jnc.14037
- Gupta, V. K., You, Y., Gupta, V. B., Klistorner, A., and Graham, S. L. (2013). TrkB receptor signalling: implications in neurodegenerative, psychiatric and proliferative disorders. *Int. J. Mol. Sci.* 14, 10122–10142. doi: 10.3390/ijms140510122
- Gutierrez, J. M., Carvalho, F. B., Schetinger, M. R., Rodrigues, M. V., Schmatz, R., Pimentel, V. C., et al. (2012). Protective effects of anthocyanins on the ectonucleotidase activity in the impairment of memory induced by scopolamine in adult rats. *Life Sci.* 91, 1221–1228. doi: 10.1016/j.lfs.2012.09.013
- Han, J., Miyamae, Y., Shigemori, H., and Isoda, H. (2010). Neuroprotective effect of 3,5-di-O-caffeoylquinic acid on SH-SY5Y cells and senescence-accelerated-prone mice 8 through the up-regulation of phosphoglycerate kinase-1. *Neuroscience* 169, 1039–1045. doi: 10.1016/j.neuroscience.2010.05.049
- Holt, L. M., Hernandez, R. D., Pacheco, N. L., Torres Ceja, B., Hossain, M., and Olsen, M. L. (2019). Astrocyte morphogenesis is dependent on BDNF signaling via astrocytic TrkB.T1. *eLife* 8:e44667. doi: 10.7554/eLife.44667
- Howes, M. R., Perry, N. S. L., Vasquez-Londono, C., and Perry, E. K. (2020). Role of phytochemicals as nutraceuticals for cognitive functions affected in ageing. *Br. J. Pharmacol.* 177, 1294–1315. doi: 10.1111/bph.14898
- Ikegami, S., Shumiya, S., and Kawamura, H. (1992). Age-related changes in radial-arm maze learning and basal forebrain cholinergic systems in senescence accelerated mice (SAM). *Behav. Brain Res.* 51, 15–22. doi: 10.1016/S0166-4328(05)80307-9
- Imayoshi, I., Sakamoto, M., Yamaguchi, M., Mori, K., and Kageyama, R. (2010). Essential roles of Notch signaling in maintenance of neural stem cells in developing and adult brains. *J. Neurosci.* 30, 3489–3498. doi: 10.1523/JNEUROSCI.4987-09.2010
- Ishida, K., Yamamoto, M., Misawa, K., Nishimura, H., Misawa, K., Ota, N., et al. (2020). Coffee polyphenols prevent cognitive dysfunction and suppress amyloid beta plaques in APP/PS2 transgenic mouse. *Neurosci. Res.* 154, 35–44. doi: 10.1016/j.neures.2019.05.001
- Ito, K. (2013). Frontiers of model animals for neuroscience: two prosperous aging model animals for promoting neuroscience research. *Exp. Anim.* 62, 275–280. doi: 10.1538/expanim.62.275
- Kamachi, Y., and Kondoh, H. (2013). Sox proteins: regulators of cell fate specification and differentiation. *Development* 140, 4129–4144. doi: 10.1242/dev.091793
- Karasawa, N., Nagatsu, I., Sakai, K., Nagatsu, T., Watanabe, K., and Onozuka, M. (1997). Immunocytochemical study of catecholaminergic neurons in the senescence-accelerated mouse (SAM-P8) brain. *J. Neural Transm.* 104, 1267–1275. doi: 10.1007/BF01294727
- Kawase-Koga, Y., Low, R., Otaegi, G., Pollock, A., Deng, H., Eisenhaber, F., et al. (2010). RNAase-III enzyme Dicer maintains signaling pathways for differentiation and survival in mouse cortical neural stem cells. *J. Cell Sci.* 123(Pt 4), 586–594. doi: 10.1242/jcs.059659
- Kenzelmann, D., Chiquet-Ehrismann, R., and Tucker, R. P. (2007). Teneurins, a transmembrane protein family involved in cell communication during neuronal development. *Cell. Mol. Life Sci.* 64, 1452–1456. doi: 10.1007/s00018-007-7108-9
- Kim, E. J., Ables, J. L., Dickel, L. K., Eisch, A. J., and Johnson, J. E. (2011). Ascl1 (Mash1) defines cells with long-term neurogenic potential in subgranular and subventricular zones in adult mouse brain. *PLoS One* 6:e18472. doi: 10.1371/journal.pone.0018472
- Kim, W., Kwon, H. J., Jung, H. Y., Yoo, D. Y., Kim, D. W., and Hwang, I. K. (2020). Phosphoglycerate mutase 1 reduces neuronal damage in the hippocampus following ischemia/reperfusion through the facilitation of energy utilization. *Neurochem. Int.* 133:104631. doi: 10.1016/j.neuint.2019.104631
- Kimura, Y., Okuda, H., Okuda, T., Hatano, T., Agata, I., and Arichi, S. (1985). Studies on the activities of tannins and related compounds from medicinal plants and drugs. VI. Inhibitory effects of caffeoylquinic acids on histamine release from rat peritoneal mast cells. *Chem. Pharm. Bull.* 33, 690–696. doi: 10.1248/cpb.33.690
- Kovalevich, J., and Langford, D. (2013). Considerations for the use of SH-SY5Y neuroblastoma cells in neurobiology. *Methods Mol. Biol.* 1078, 9–21. doi: 10.1007/978-1-62703-640-5\_2



- Kume, T., Kawato, Y., Osakada, F., Izumi, Y., Katsuki, H., Nakagawa, T., et al. (2008). Dibutylryl cyclic AMP induces differentiation of human neuroblastoma SH-SY5Y cells into a noradrenergic phenotype. *Neurosci. Lett.* 443, 199–203. doi: 10.1016/j.neulet.2008.07.079
- Lazarov, O., and Marr, R. A. (2010). Neurogenesis and Alzheimer's disease: at the crossroads. *Exp. Neurol.* 223, 267–281. doi: 10.1016/j.expneurol.2009.08.009
- Lee, S. W., Clemenson, G. D., and Gage, F. H. (2012). New neurons in an aged brain. *Behav. Brain Res.* 227, 497–507. doi: 10.1016/j.bbr.2011.10.009
- Liang, Z., Zhang, B., Su, W. W., Williams, P. G., and Li, Q. X. (2016). C-Glycosylflavones Alleviate Tau Phosphorylation and Amyloid Neurotoxicity through GSK3 $\beta$  Inhibition. *ACS Chem. Neurosci.* 7, 912–923. doi: 10.1021/acschemneuro.6b00059
- Liberzon, A. (2014). A description of the Molecular Signatures Database (MSigDB) Web site. *Methods Mol. Biol.* 1150, 153–160. doi: 10.1007/978-1-4939-0512-6\_9
- Lim, D. W., Han, T., Jung, J., Song, Y., Um, M. Y., Yoon, M., et al. (2018). Chlorogenic Acid from Hawthorn Berry (*Crataegus pinnatifida* Fruit) Prevents Stress Hormone-Induced Depressive Behavior, through Monoamine Oxidase B-Reactive Oxygen Species Signaling in Hippocampal Astrocytes of Mice. *Mol. Nutr. Food Res.* e1800029. doi: 10.1002/mnfr.201800029 [Epub ahead of print].
- Maeda, G., Hirose, N., and Tsushida, T. (2010). Antioxidant activity of sugarcane top and determination of active compounds. *Bulle. Okinawa Prefect. Agric. Res. Cent.* 4, 52–57.
- Matsui, T., Ebuchi, S., Fujise, T., Abesundara, K. J., Doi, S., Yamada, H., et al. (2004). Strong antihyperglycemic effects of water-soluble fraction of Brazilian propolis and its bioactive constituent, 3,4,5-tri-O-caffeoylquinic acid. *Biol. Pharm. Bull.* 27, 1797–1803. doi: 10.1248/bpb.27.1797
- Miyamae, Y., Han, J., Sasaki, K., Terakawa, M., Isoda, H., and Shigemori, H. (2011a). 3,4,5-tri-O-caffeoylquinic acid inhibits amyloid  $\beta$ -mediated cellular toxicity on SH-SY5Y cells through the upregulation of PGAM1 and G3PDH. *Cytotechnology* 63, 191–200. doi: 10.1007/s10616-011-9341-1
- Miyamae, Y., Kurisu, M., Han, J., Isoda, H., and Shigemori, H. (2011b). Structure-activity relationship of caffeoylquinic acids on the accelerating activity on ATP production. *Chem. Pharm. Bull.* 59, 502–507. doi: 10.1248/cpb.59.502
- Miyamae, Y., Kurisu, M., Murakami, K., Han, J., Isoda, H., Irie, K., et al. (2012). Protective effects of caffeoylquinic acids on the aggregation and neurotoxicity of the 42-residue amyloid  $\beta$ -protein. *Bioorg. Med. Chem.* 20, 5844–5849. doi: 10.1016/j.bmc.2012.08.001
- Mizutani, K., Yoon, K., Dang, L., Tokunaga, A., and Gaiano, N. (2007). Differential Notch signalling distinguishes neural stem cells from intermediate progenitors. *Nature* 449, 351–355. doi: 10.1038/nature06090
- Morales-Garcia, J. A., Luna-Medina, R., Alonso-Gil, S., Sanz-Sancristobal, M., Palomo, V., Gil, C., et al. (2012). Glycogen synthase kinase 3 inhibition promotes adult hippocampal neurogenesis *in vitro* and *in vivo*. *ACS Chem. Neurosci.* 3, 963–971. doi: 10.1021/cn300110c
- Moreno-Jiménez, E. P., Flor-García, M., Terreros-Roncal, J., Rábano, A., Cafini, F., Pallas-Bazarra, N., et al. (2019). Adult hippocampal neurogenesis is abundant in neurologically healthy subjects and drops sharply in patients with Alzheimer's disease. *Nat. Med.* 25, 554–560. doi: 10.1038/s41591-019-0375-9
- Morley, J. E., Armbricht, H. J., Farr, S. A., and Kumar, V. B. (2012). The senescence accelerated mouse (SAMP8) as a model for oxidative stress and Alzheimer's disease. *Biochim. Biophys. Acta* 1822, 650–656. doi: 10.1016/j.bbdis.2011.11.015
- Naio, M., Maruyama, W., and Shamoto-Nagai, M. (2018). Type A monoamine oxidase and serotonin are coordinately involved in depressive disorders: from neurotransmitter imbalance to impaired neurogenesis. *J. Neural Transm.* 125, 53–66. doi: 10.1007/s00702-017-1709-8
- Nelson, L., and Tabet, N. (2015). Slowing the progression of Alzheimer's disease; what works? *Ageing Res. Rev.* 23(Pt B), 193–209. doi: 10.1016/j.arr.2015.07.002
- Ohira, K., Funatsu, N., Homma, K. J., Sahara, Y., Hayashi, M., Kaneko, T., et al. (2007). Truncated TrkB-T1 regulates the morphology of neocortical layer I astrocytes in adult rat brain slices. *Eur. J. Neurosci.* 25, 406–416. doi: 10.1111/j.1460-9568.2007.05282.x
- Pallas, M., Camins, A., Smith, M. A., Perry, G., Lee, H. G., and Casadesus, G. (2008). From aging to Alzheimer's disease: unveiling "the switch" with the senescence-accelerated mouse model (SAMP8). *J. Alzheimers Dis.* 15, 615–624. doi: 10.3233/jad-2008-15408
- Phillips, C. (2017). Lifestyle Modulators of Neuroplasticity: How Physical Activity, Mental Engagement, and Diet Promote Cognitive Health during Aging. *Neural Plast.* 2017:3589271. doi: 10.1155/2017/3589271
- Poulose, S. M., Miller, M. G., Scott, T., and Shukitt-Hale, B. (2017). Nutritional factors affecting adult neurogenesis and cognitive function. *Adv. Nutr.* 8, 804–811. doi: 10.3945/an.117.016261
- Ravindran, S., Nalavadi, V. C., and Muddashetty, R. S. (2019). BDNF induced translation of limk1 in developing neurons regulates dendrite growth by fine-tuning cofilin1 activity. *Front. Mol. Neurosci.* 12:64. doi: 10.3389/fnmol.2019.00064
- Recanatini, M., and Valenti, P. (2004). Acetylcholinesterase inhibitors as a starting point towards improved Alzheimer's disease therapeutics. *Curr. Pharm. Des.* 10, 3157–3166. doi: 10.2174/1381612043383313
- Rhea, E. M., and Banks, W. A. (2017). The SAMP8 mouse for investigating memory and the role of insulin in the brain. *Exp. Gerontol.* 94, 64–68. doi: 10.1016/j.exger.2016.12.009
- Rose, C. R., Blum, R., Pichler, B., Lepier, A., Kafitz, K. W., and Konnerth, A. (2003). Truncated TrkB-T1 mediates neurotrophin-evoked calcium signalling in glia cells. *Nature* 426, 74–78. doi: 10.1038/nature01983
- Sakakibara, S., Nakamura, Y., Satoh, H., and Okano, H. (2001). RNA-binding protein Musashi2: developmentally regulated expression in neural precursor cells and subpopulations of neurons in mammalian CNS. *J. Neurosci.* 21, 8091–8107. doi: 10.1523/jneurosci.21-20-08091.2001
- Sasaki, K., Davies, J., Doldan, N. G., Arao, S., Ferdousi, F., Szele, F. G., et al. (2019a). 3,4,5-Tricafeoylquinic acid induces adult neurogenesis and improves deficit of learning and memory in aging model senescence-accelerated prone 8 mice. *Aging* 11, 401–422. doi: 10.18632/aging.101748
- Sasaki, K., Han, J., Shimozone, H., Villareal, M. O., and Isoda, H. (2013). Caffeoylquinic acid-rich purple sweet potato extract, with or without anthocyanin, imparts neuroprotection and contributes to the improvement of spatial learning and memory of SAMP8 mouse. *J. Agric. Food Chem.* 61, 5037–5045. doi: 10.1021/jf3041484
- Sasaki, K., Iwata, N., Ferdousi, F., and Isoda, H. (2019b). Antidepressant-like effect of ferulic acid via promotion of energy metabolism activity. *Mol. Nutr. Food Res.* 63:e1900327. doi: 10.1002/mnfr.201900327
- Sato, E., Oda, N., Ozaki, N., Hashimoto, S., Kurokawa, T., and Ishibashi, S. (1996). Early and transient increase in oxidative stress in the cerebral cortex of senescence-accelerated mouse. *Mech. Ageing Dev.* 86, 105–114. doi: 10.1016/0047-6374(95)01681-3
- Saurat, N., Andersson, T., Vasistha, N. A., Molnár, Z., and Livesey, F. J. (2013). Dicer is required for neural stem cell multipotency and lineage progression during cerebral cortex development. *Neural Dev.* 8:14. doi: 10.1186/1749-8104-8-14
- Schmuck, M. R., Temme, T., Dach, K., de Boer, D., Barenys, M., Bendt, F., et al. (2017). Omnisphero: a high-content image analysis (HCA) approach for phenotypic developmental neurotoxicity (DNT) screenings of organoid neurosphere cultures *in vitro*. *Arch. Toxicol.* 91, 2017–2028. doi: 10.1007/s00204-016-1852-2
- Schupp, M., Malsam, J., Ruiter, M., Scheutzw, A., Wierda, K. D., Söllner, T. H., et al. (2016). Interactions between SNAP-25 and synaptotagmin-1 are involved in vesicle priming, clamping spontaneous and stimulating evoked neurotransmission. *J. Neurosci.* 36, 11865–11880. doi: 10.1523/jneurosci.1011-16.2016
- Sorrells, S. F., Paredes, M. F., Cebrian-Silla, A., Sandoval, K., Qi, D., Kelley, K. W., et al. (2018). Human hippocampal neurogenesis drops sharply in children to undetectable levels in adults. *Nature* 555, 377–381. doi: 10.1038/nature25975
- Spalding, K. L., Bergmann, O., Alkass, K., Bernard, S., Salehpour, M., Huttner, H. B., et al. (2013). Dynamics of hippocampal neurogenesis in adult humans. *Cell* 153, 1219–1227. doi: 10.1016/j.cell.2013.05.002
- Su, D., Huang, J., Song, Y., and Feng, Y. (2014). Comparative pharmacokinetics and tissue distribution study of mono-, and di-caffeoylquinic acids isomers of *Ainsliae fragrans* Champ by a fast UHPLC-MS/MS method. *Fitoterapia* 99, 139–152. doi: 10.1016/j.fitote.2014.09.011
- Subramanian, A., Tamayo, P., Mootha, V. K., Mukherjee, S., Ebert, B. L., Gillette, M. A., et al. (2005). Gene set enrichment analysis: a knowledge-based approach for interpreting genome-wide expression profiles. *Proc. Natl. Acad. Sci. U.S.A.* 102, 15545–15550. doi: 10.1073/pnas.0506580102



- Sueda, R., Imayoshi, I., Harima, Y., and Kageyama, R. (2019). High Hes1 expression and resultant Ascl1 suppression regulate quiescent vs. active neural stem cells in the adult mouse brain. *Genes Dev.* 33, 511–523. doi: 10.1101/gad.323196.118
- Sun, J., He, X. M., Zhao, M. M., Li, L., Li, C. B., and Dong, Y. (2014). Antioxidant and nitrite-scavenging capacities of phenolic compounds from sugarcane (*Saccharum officinarum* L.) tops. *Molecules* 19, 13147–13160. doi: 10.3390/molecules190913147
- Suzuki, A., Stern, S. A., Bozdagi, O., Huntley, G. W., Walker, R. H., Magistretti, P. J., et al. (2011). Astrocyte-neuron lactate transport is required for long-term memory formation. *Cell* 144, 810–823. doi: 10.1016/j.cell.2011.02.018
- Tadi, M., Allaman, I., Lengacher, S., Grenningloh, G., and Magistretti, P. J. (2015). Learning-induced gene expression in the hippocampus reveals a role of neuron-astrocyte metabolic coupling in long term memory. *PLoS One* 10:e0141568. doi: 10.1371/journal.pone.0141568
- Takeda, T. (2009). Senescence-accelerated mouse (SAM) with special references to neurodegeneration models, SAMP8 and SAMP10 mice. *Neurochem. Res.* 34, 639–659. doi: 10.1007/s11064-009-9922-y
- Tejeda, G. S., and Diaz-Guerra, M. (2017). Integral characterization of defective BDNF/TrkB signalling in neurological and psychiatric disorders leads the way to new therapies. *Int. J. Mol. Sci.* 18:268. doi: 10.3390/ijms18020268
- Theeuwes, W. F., Gosker, H. R., Langen, R. C. J., Verhees, K. J. P., Pansters, N. A. M., Schols, A. M. W. J., et al. (2017). Inactivation of glycogen synthase kinase-3 $\beta$  (GSK-3 $\beta$ ) enhances skeletal muscle oxidative metabolism. *Biochim. Biophys. Acta* 1863, 3075–3086. doi: 10.1016/j.bbdis.2017.09.018
- Tough, F. D., and Sprent, J. (1996). Turnover of Naive- and Memory-phenotype T Cells. *J. Exp. Med.* 179, 1127–1135.
- Trinchero, M. F., Buttner, K. A., Sulkes Cuevas, J. N., Temprana, S. G., Fontanet, P. A., Monzon-Salinas, M. C., et al. (2017). High plasticity of new granule cells in the aging hippocampus. *Cell Rep.* 21, 1129–1139. doi: 10.1016/j.celrep.2017.09.064
- Tunali, Z., Kosar, M., Kupeli, E., Calis, I., and Baser, K. H. (2007). Antioxidant, anti-inflammatory, anti-nociceptive activities and composition of *Lythrum salicaria* L. extracts. *J. Ethnopharmacol.* 110, 539–547. doi: 10.1016/j.jep.2006.10.024
- Williams, P., Sorribas, A., and Howes, M. J. (2011). Natural products as a source of Alzheimer's drug leads. *Nat. Prod. Rep.* 28, 48–77. doi: 10.1039/c0np00027b
- Winner, B., and Winkler, J. (2015). Adult neurogenesis in neurodegenerative diseases. *Cold Spring Harb. Perspect. Biol.* 7:a021287. doi: 10.1101/cshperspect.a021287
- Wosik, K., Biernacki, K., Khouzam, M. P., and Prat, A. (2007). Death receptor expression and function at the human blood brain barrier. *J. Neurol. Sci.* 259, 53–60. doi: 10.1016/j.jns.2006.08.018
- Wu, J., Chen, H., Li, H., Tang, Y., Yang, L., Cao, S., et al. (2016). Antidepressant potential of chlorogenic acid-enriched extract from *eucommia ulmoides* oliver bark with neuron protection and promotion of serotonin release through enhancing synapsin I expression. *Molecules* 21:260. doi: 10.3390/molecules21030260
- Yang, J., Yang, H., Liu, Y., Li, X., Qin, L., Lou, H., et al. (2016). Astrocytes contribute to synapse elimination via type 2 inositol 1,4,5-trisphosphate receptor-dependent release of ATP. *eLife* 5:e15043. doi: 10.7554/eLife.15043
- Yang, K., Chen, Z., Gao, J., Shi, W., Li, L., Jiang, S., et al. (2017). The Key roles of GSK-3 $\beta$  in regulating mitochondrial activity. *Cell. Physiol. Biochem.* 44, 1445–1459. doi: 10.1159/000485580
- Yang, Y., Li, S., Huang, H., Lv, J., Chen, S., Dias, B. C. P., et al. (2020). Comparison of the protective effects of ginsenosides Rb1 and Rg1 on improving cognitive deficits in SAMP8 mice based on anti-neuroinflammation mechanism. *Front. Pharmacol.* 11:834. doi: 10.3389/fphar.2020.00834
- Yoshimoto, M., Yahara, S., Okuno, S., Islam, M. S., Ishiguro, K., and Yamakawa, O. (2002). Antimutagenicity of mono-, di-, and tricaffeoylquinic acid derivatives isolated from sweetpotato (*Ipomoea batatas* L.) leaf. *Biosci. Biotechnol. Biochem.* 66, 2336–2341. doi: 10.1271/bbb.66.2336
- Yuan, L., Han, X., Li, W., Ren, D., and Yang, X. (2016). Isoorientin Prevents hyperlipidemia and liver injury by regulating lipid metabolism, antioxidant capability, and inflammatory cytokine release in high-fructose-fed mice. *J. Agric. Food Chem.* 64, 2682–2689. doi: 10.1021/acs.jafc.6b00290
- Yuan, L., Wang, J., Xiao, H., Wu, W., Wang, Y., and Liu, X. (2013). MAPK signaling pathways regulate mitochondrial-mediated apoptosis induced by isoorientin in human hepatoblastoma cancer cells. *Food Chem. Toxicol.* 53, 62–68. doi: 10.1016/j.fct.2012.11.048
- Zhang, S. J., Xu, T. T., Li, L., Xu, Y. M., Qu, Z. L., Wang, X. C., et al. (2017). Bushen-Yizhi formula ameliorates cognitive dysfunction through SIRT1/ER stress pathway in SAMP8 mice. *Oncotarget* 8, 49338–49350. doi: 10.18632/oncotarget.17638

**Conflict of Interest:** KI, HU, and YA are employed by the Nippo Co., Ltd.

The remaining authors declare that the research was conducted in the absence of any commercial or financial relationships that could be construed as a potential conflict of interest.

Copyright © 2020 Iwata, Wu, Ferdousi, Sasaki, Tominaga, Uchida, Arai, Szele and Isoda. This is an open-access article distributed under the terms of the Creative Commons Attribution License (CC BY). The use, distribution or reproduction in other forums is permitted, provided the original author(s) and the copyright owner(s) are credited and that the original publication in this journal is cited, in accordance with accepted academic practice. No use, distribution or reproduction is permitted which does not comply with these terms.



# Fisetin Promotes Hair Growth by Augmenting TERT Expression

Chisato Kubo<sup>1</sup>, Mizuki Ogawa<sup>1</sup>, Norihisa Uehara<sup>2</sup> and Yoshinori Katakura<sup>1,3\*</sup>

<sup>1</sup> Laboratory of Cellular Regulation Technology, Department of Bioscience and Biotechnology, Graduate School of Bioresources and Bioenvironmental Sciences, Kyushu University, Fukuoka, Japan, <sup>2</sup> Department of Molecular Cell Biology and Oral Anatomy, Faculty of Dental Science, Kyushu University, Fukuoka, Japan, <sup>3</sup> Laboratory of Cellular Regulation Technology, Department of Bioscience and Biotechnology, Faculty of Agriculture, Kyushu University, Fukuoka, Japan

## OPEN ACCESS

### Edited by:

Hiroko Isoda,  
University of Tsukuba, Japan

### Reviewed by:

Xiaohua Lei,  
Chinese Academy of Sciences (CAS),  
China  
Weiming Qiu,  
General Hospital of Central Theater  
Command, China

### \*Correspondence:

Yoshinori Katakura  
katakura@grt.kyushu-u.ac.jp

### Specialty section:

This article was submitted to  
Stem Cell Research,  
a section of the journal  
Frontiers in Cell and Developmental  
Biology

**Received:** 28 May 2020

**Accepted:** 24 September 2020

**Published:** 15 October 2020

### Citation:

Kubo C, Ogawa M, Uehara N and  
Katakura Y (2020) Fisetin Promotes  
Hair Growth by Augmenting TERT  
Expression.  
Front. Cell Dev. Biol. 8:566617.  
doi: 10.3389/fcell.2020.566617

Although thinning hair and alopecia are not recognized as severe diseases, hair loss has implications for mental health and quality of life; therefore, a large number of studies have been carried out to develop novel hair growth agents. In the present study, we aimed to examine the potential of telomerase reverse transcriptase (TERT), because *TERT* overexpression in skin activates resting hair follicle bulge stem cells, which triggers initiation of a new hair follicle growth phase and promotes hair synthesis. To this end, we screened polyphenols that activate *TERT* expression in keratinocytes, and identified resveratrol and fisetin as strong *hTERT*-augmenting compounds. These polyphenols also regulated the gene expression of cytokines such as *IGF-1* and *KGF*, which activate the  $\beta$ -catenin pathway, and *TGF- $\beta$ 1*, which plays an important role in maintaining the niche of hair follicle stem cells, thus are thought to play roles in promoting hair growth. We additionally showed that these polyphenols, especially fisetin, promoted hair growth from the shaved dorsal skin of mice, which suggests that these polyphenols activate the transition from telogen to anagen phase. Histological studies indicated that the dorsal skin of mice treated with these polyphenols contained numerous hair follicles and was thickened compared with that in control mice. Furthermore, on the dorsal skin of mice treated with resveratrol and fisetin, a number of proliferating cells (Ki67<sup>+</sup> cells) were observed around the hair papilla. These results suggest that resveratrol and fisetin induce a shift from telogen to anagen in the hair follicle by inducing proliferation of hair follicle bulge stem cells, thus promoting hair growth.

**Keywords:** TERT, hair-growth, polyphenol, fisetin, resveratrol, HaCaT, C57BL/6

## INTRODUCTION

Various methods for the treatment of hair thinning and alopecia have been developed. Among them, the use of medicinal compounds has been shown to drastically improve hair growth. Two well-known compounds, finasteride and minoxidil, are used to improve thin hair and alopecia. Finasteride, a synthetic 5- $\alpha$ -reductase inhibitor, is used to treat alopecia by suppressing male hormones, but is reported to cause sexual dysfunction (Shen et al., 2018). Minoxidil was originally used as an antihypertensive medication, but is now used as a topical formulation for promoting hair growth. Despite its widespread use, the precise mechanisms of action of minoxidil are not fully understood (Suchonwanit et al., 2019). As a result, in this study, we focused on telomerase reverse transcriptase (TERT) as a novel target for the induction of hair growth.

*TERT*, the protein component of telomerase, maintains telomere length, and is activated in stem cells, progenitor cells, and cancer cells. Sarin et al. (2005) reported that conditional transgenic induction of *TERT* in the mouse skin epithelium caused a rapid transition from telogen (the resting phase of the hair follicle cycle) to anagen (the active phase), thereby promoting robust hair growth. *TERT* overexpression induced the proliferation of stem cells in the hair follicle bulge region, resulting in histological changes around the hair follicle and subsequent hair growth. Choi et al. (2008) also showed that *TERT* in skin keratinocytes facilitated the activation of resting hair follicle stem cells, which triggers the initiation of a new hair follicle growth phase and promoting hair synthesis. These reports indicated that augmentation of *TERT* in skin keratinocytes can be a novel target for hair growth promotion, suggesting that original hair growth promoting compounds with a distinct point of action from finasteride and minoxidil can be found. In the present study, we used a novel screening system for compounds that activate the human *TERT* (*hTERT*) promoter in keratinocytes in order to identify candidates that promote hair growth.

To date, we have developed several screening systems based on the same concept. The CMV promoter region of the *EGFP* expression vector was replaced with the promoter of the gene of interest and introduced into tissue-derived cell lines. These recombinant cells were treated with food components, polyphenols, and compounds, and changes in *EGFP* fluorescence were monitored using an imaging cytometer (IN Cell Analyzer 1000) (Harada et al., 2016; Zhao et al., 2016; Chong et al., 2019). We successfully identified promoter-activating polyphenols and lactic acid bacteria. In the present study, we used a similar system, in which the *EGFP* reporter vector under the control of the *hTERT* promoter was introduced into the human keratinocyte cell line, HaCaT, and successfully identified several polyphenols that augmented *hTERT* expression. We sought to investigate whether these *hTERT*-augmenting polyphenols promote hair growth, and to clarify the molecular mechanisms underlying their hair-growth-promoting effects.

## MATERIALS AND METHODS

### Cell Line

The HaCaT human keratinocyte cell line (Riken Bioresource Center, Tsukuba, Japan) was cultured in Dulbecco's Modified Eagle's Medium (DMEM; Nissui, Tokyo, Japan) supplemented with 10% fetal bovine serum (FBS; Life Technologies, Gaithersburg, MD, United States) at 37°C in a 5% CO<sub>2</sub> atmosphere.

### Screening System for Polyphenols That Activate the *hTERT* Promoter

The human *hTERT* promoter (−298 to −25) was cloned into pEGFP-C3 (TaKaRa, Shiga, Japan), whose CMV promoter was removed by *AseI* and *NheI* digestion (Fujiki et al., 2007). The resulting plasmid (*hTERTp-EGFP*) was transduced into HaCaT cells [HaCaT (*hTERTp-EGFP*)]. Changes in the *EGFP* fluorescence derived from *hTERTp-EGFP* were monitored using

an IN Cell Analyzer 1000 (GE Healthcare, Amersham Place, United Kingdom) (Zhao et al., 2016; Chong et al., 2019).

### Quantitative Reverse Transcription-Polymerase Chain Reaction

RNA was prepared from cells using the High Pure RNA Isolation kit (Roche Diagnostics GmbH, Mannheim, Germany) and from skin samples using the RNeasy Fibrous Tissue Mini Kit (Qiagen, Hilden, Germany) as described in the manufacturers' protocols. cDNA was prepared using the SuperScript IV Reverse Transcriptase (Thermo Fisher Scientific KK, Tokyo, Japan), as described previously (Sugihara et al., 2019). Quantitative reverse transcription-polymerase chain reaction (qRT-PCR) was performed using the Thunderbird SYBR qPCR mix (Toyobo, Osaka, Japan) and Thermal Cycler Dice Real Time System TP-800 (Takara). Samples were analyzed in triplicate, and gene expression levels were normalized to the corresponding  $\beta$ -actin level. The PCR primer sequences used were as follows: human  $\beta$ -actin forward primer 5'-TGGCAGCCAGCACAATGAA-3' and reverse primer 5'-CTAAGTCATAGTCCGCCTAGAAGCA-3'; human *AXIN2* forward primer 5'-TGGTGCCCTACCATGACACA-3' and reverse primer 5'-TGGTCAACCTCAAGACCTTTAAGA-3'; *hTERT* forward primer 5'-CGTACAGTTTCACGCATGTG-3' and reverse primer 5'-ATGACGCGCAGGAAAAATG-3'; *IGF-1* forward primer 5'-TCACCTTCACCAGCTCTGCC-3' and reverse primer 5'-AAGCCCCTGTCTCCACACAC-3'; *KGF* forward primer 5'-GGACACACAACGGAGGGGAA-3' and reverse primer 5'-TGCCATAGGAAGAAGTGGGCT-3'; *TGF- $\beta$ 1* forward primer 5'-AACCGGCCTTCTCTGCTTCT-3' and reverse primer 5'-ACGCAGCAGTTCTTCTCCGT-3'; mouse  $\beta$ -actin forward primer 5'-GAGGTCTTTACGGATGTCAAC-3' and reverse primer 5'-GGCCAGGTCATCACTATTG-3'; *mTERT* forward primer 5'-CAGCCATACATGGGCCAGTTC-3' and reverse primer 5'-ACAGGCTGCTGCTGCTCTCA-3'; mouse  $\beta$ -catenin forward primer 5'-GCTGCTGTCTATTCCGAATGTC-3' and reverse primer 5'-GGCACCAATGTCCAGTCCAA-3'.

### Luciferase Assay

A reporter containing TCF/LEF elements (M50 Super 8 × TOPFlash) (Veeman et al., 2003) (Addgene, Cambridge, MA, United States) was used as the reporter vector (Harada et al., 2016). The luciferase assay was performed using the Dual-Luciferase Reporter Assay System (Promega, Madison, WI, United States), as described previously (Yamashita et al., 2014).

### Western Blot

Cell lysates were prepared using NP-40 lysis buffer (0.5% Nonidet P-40, 5 mM EDTA, 2 mM Na<sub>3</sub>VO<sub>4</sub>, 10 mM Tris-HCl (pH 7.6), 150 mM NaCl, 5 mg/mL aprotinin, 1 mM PMSF). Protein concentration was determined using the Protein Assay Dye (Bio-Rad Laboratories, Hercules, CA, United States). Proteins (20  $\mu$ g) were separated using 12% SDS-PAGE and transferred to a PVDF membrane (GE Healthcare). The membrane was probed with anti- $\beta$ -catenin antibody (#8480; Cell Signaling, Danvers,

MA, United States) or anti- $\beta$ -actin antibody (013-24553; Fujifilm Wako Pure Chemicals, Osaka, Japan). Horseradish peroxidase-labeled anti-rabbit IgG antibody (GE Healthcare) and anti-mouse IgG antibody (GE Healthcare) were used as the secondary antibodies. The proteins were detected using an ImmunoStar LD chemiluminescence detection kit (Fujifilm Wako Pure Chemicals) and visualized with a LAS-1000 Lumino Image analyzer (Fujifilm, Tokyo, Japan).

## Immunocytochemistry

Cells were fixed with 4% paraformaldehyde and blocked with blocking buffer (1  $\times$  PBS/5% goat serum/0.3% Triton X-100). Cells were labeled with anti-active- $\beta$ -catenin (8E7, Merck Millipore, Billerica, MA, United States) at 4°C overnight. After washing the cells, cells were incubated with secondary antibodies (Alexa Fluor 555 anti-mouse IgG, Thermo Fisher Scientific)

at room temperature for 1 hr. After washing the cells, active- $\beta$ -catenin was observed under the fluorescence microscope (EVOS Cell Imaging System, Thermo Fisher Scientific).

## Cell Growth

HaCaT cells ( $1.0 \times 10^4$  cells) were seeded onto a 96-well plate (Becton Dickinson, Franklin Lakes, NJ). After 6 h, polyphenols (10  $\mu$ M) were added to the wells. HaCaT cells were treated everyday with 10  $\mu$ M of polyphenols, and cell proliferation was monitored using a Cell Counting Kit-8 (Dojindo, Kumamoto, Japan).

## Gene Knockdown Using shRNA

The oligonucleotides (sh-hTERT1 top: 5'-GATCCCCGCTCGTGGAGACCATCTTTCTTTCGAAGAGAGAAGATGGTCTCCACGA-3', sh-hTERT1 bottom: 5'-AGCTTAAAAAGCTCGTGGAGACCATCTTTCTCTCTTCGAA

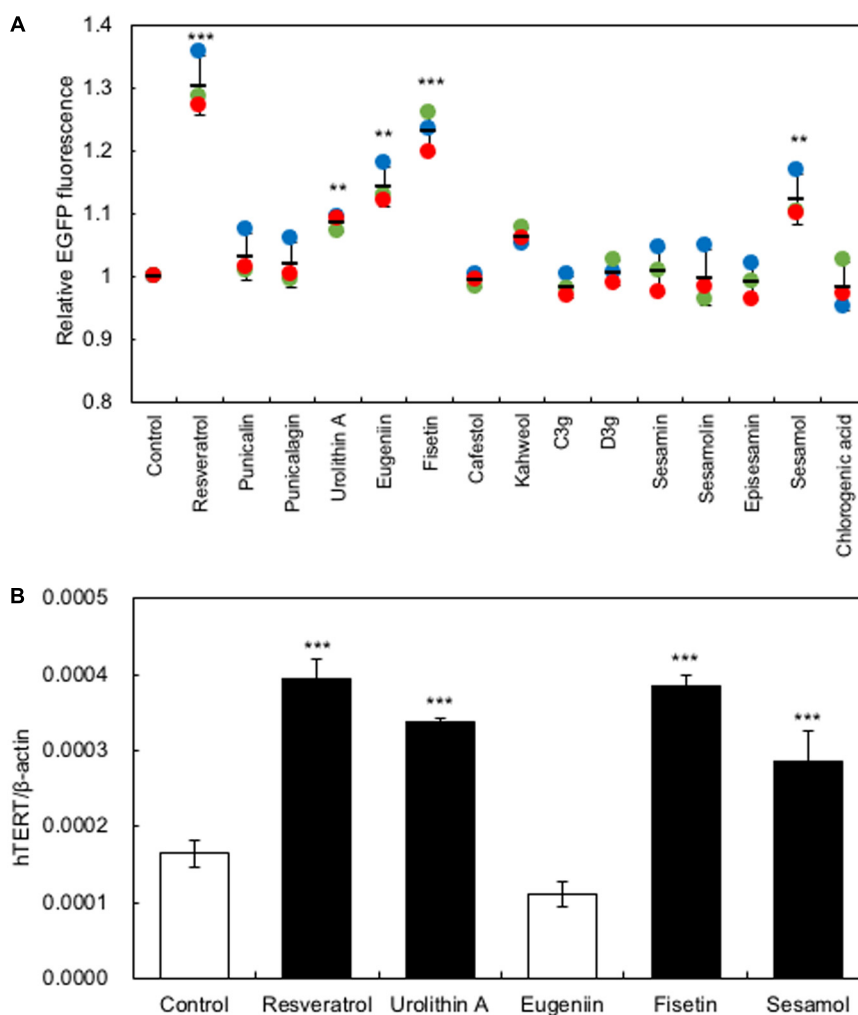


**FIGURE 1 |** Screening for polyphenols that activate *hTERT* transcription in HaCaT cells. **(A)** Screening for polyphenols that activate *hTERT* transcription. Polyphenols (10  $\mu$ M) were added to the HaCaT(hTERTp-EGFP) cells and cultured for 48 h; then, changes in EGFP fluorescence were monitored using an IN Cell Analyzer 1000. **(B)** The effect of polyphenols on the expression of endogenous *hTERT* in HaCaT cells was evaluated by qRT-PCR. Statistical significance was determined using a two-sided Student's *t*-test. Statistical significance was defined as  $P < 0.05$  (\*\* $P < 0.01$ ; \*\*\* $P < 0.001$ ).



AGAAAGATGGTCTCCA-3'; sh-hTERT2 top: 5'-GATCCCCGGAAGAGTGTCTGGAGCAAGTTTCGAAGAGAC TTGCTCCAGACACTCTT-3', sh-hTERT2 bottom: 5'-AGCTTAAAAAGGAAGAGTGTCTGGAGCAAGTCTCTTCGAA ACTTGCTCCAGACACT-3') containing siRNA-expressing sequences targeting *hTERT* were cloned into the pSUPER.retro vector, as described previously (Harada et al., 2014, 2016). Viral supernatants were produced after transfection of 293T cells with pGag-pol, pVSV-G, and individual expression vectors (pSUPER.retro-sh-hTERT1, pSUPER.retro-sh-hTERT2, or pSUPER.retro-scramble shRNA) using the HilyMax reagent (Dojindo), as previously described (Yamashita et al., 2014). The target cells were infected with this viral supernatant for 24 h at 37°C. After infection, the cells were selected with 3 µg/mL puromycin (Enzo Life Sciences, Farmingdale, NY, United States) for 3 days.

## Investigation of Hair Growth in Experimental Animals

Six-week-old male C57BL/6 mice were obtained from Clea Japan (Tokyo, Japan) and allowed to adapt for a week, with food and water provided *ad libitum*. The dorsal skin of the mice was shaved

with an electrical shaver at seven weeks of age; at this stage of growth, all of the hair follicles were synchronized in the telogen stage (Kim et al., 2014). Then, 0.05 mL of a 0.1% solution of polyphenol in 50% ethanol was applied and made fit in by spatula topically every day, for 35 days, and hair growth was evaluated. All mouse experiments and protocols were in accordance with the Guide for the Care and Use of Laboratory Animals, and were approved by the Ethics Committees on Animal Experimentation (Kyushu University; approval number: A28-077-0).

## Immunohistological Analysis

Skin tissue samples were fixed in 10% formalin buffer. Then, the fixative was removed using running water for 1 h. Skin pieces were dehydrated in ethanol, immersed in xylene, infiltrated with paraffin, and embedded in paraffin blocks. Paraffin-embedded hair follicles were sectioned into 5-µm-thick sections, which were stained with hematoxylin and eosin. For immunohistochemical analysis, tissue sections were deparaffinized, rehydrated, and soaked in 1 × HistoVT One (Nacalai Tesque, Kyoto, Japan). The sections were then heated at 90°C for 20 min to activate antigens. After washing with 0.1% Tween 20/TBS, tissues were blocked with Blocking One Histo (Nacalai Tesque) for 1 h at room

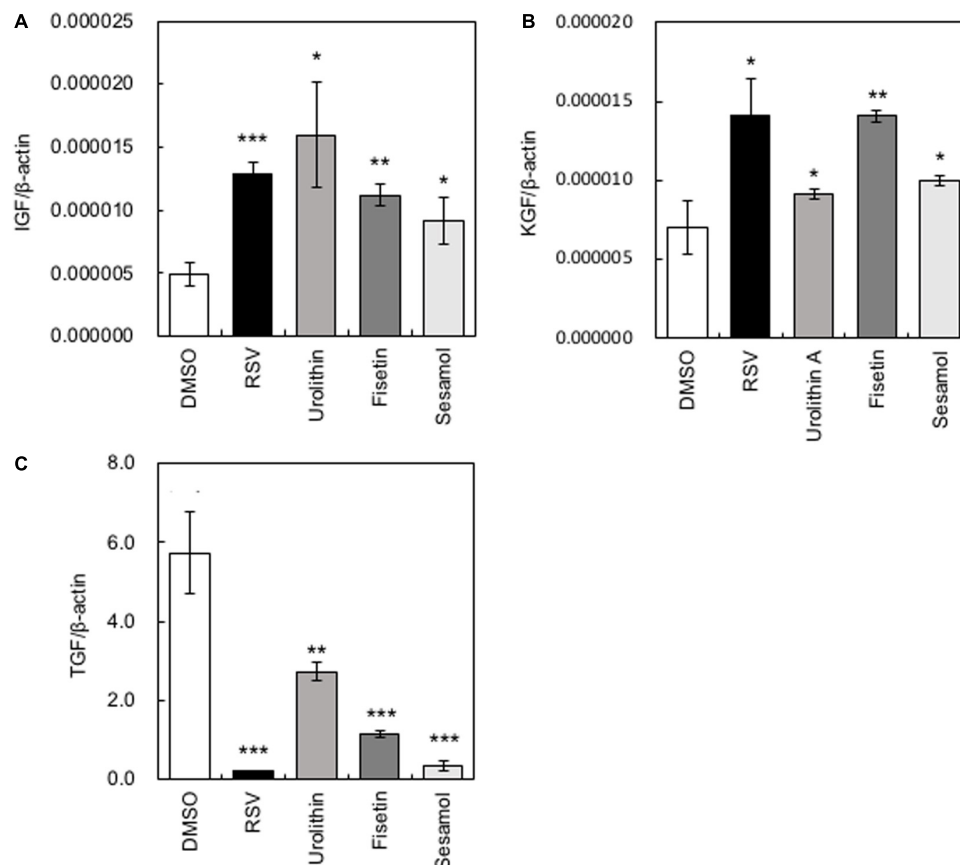


**FIGURE 2 |** Effects of polyphenols on the expression of cytokine-encoding genes in HaCaT cells. After HaCaT cells were treated with polyphenols, the gene expression levels of *IGF-1* (A), *KGF* (B), and *TGF-β1* (C) were measured by qRT-PCR. Statistical significance was determined using a two-sided Student's *t*-test. Statistical significance was defined as  $P < 0.05$  (\* $P < 0.05$ ; \*\* $P < 0.01$ ; \*\*\* $P < 0.001$ ).

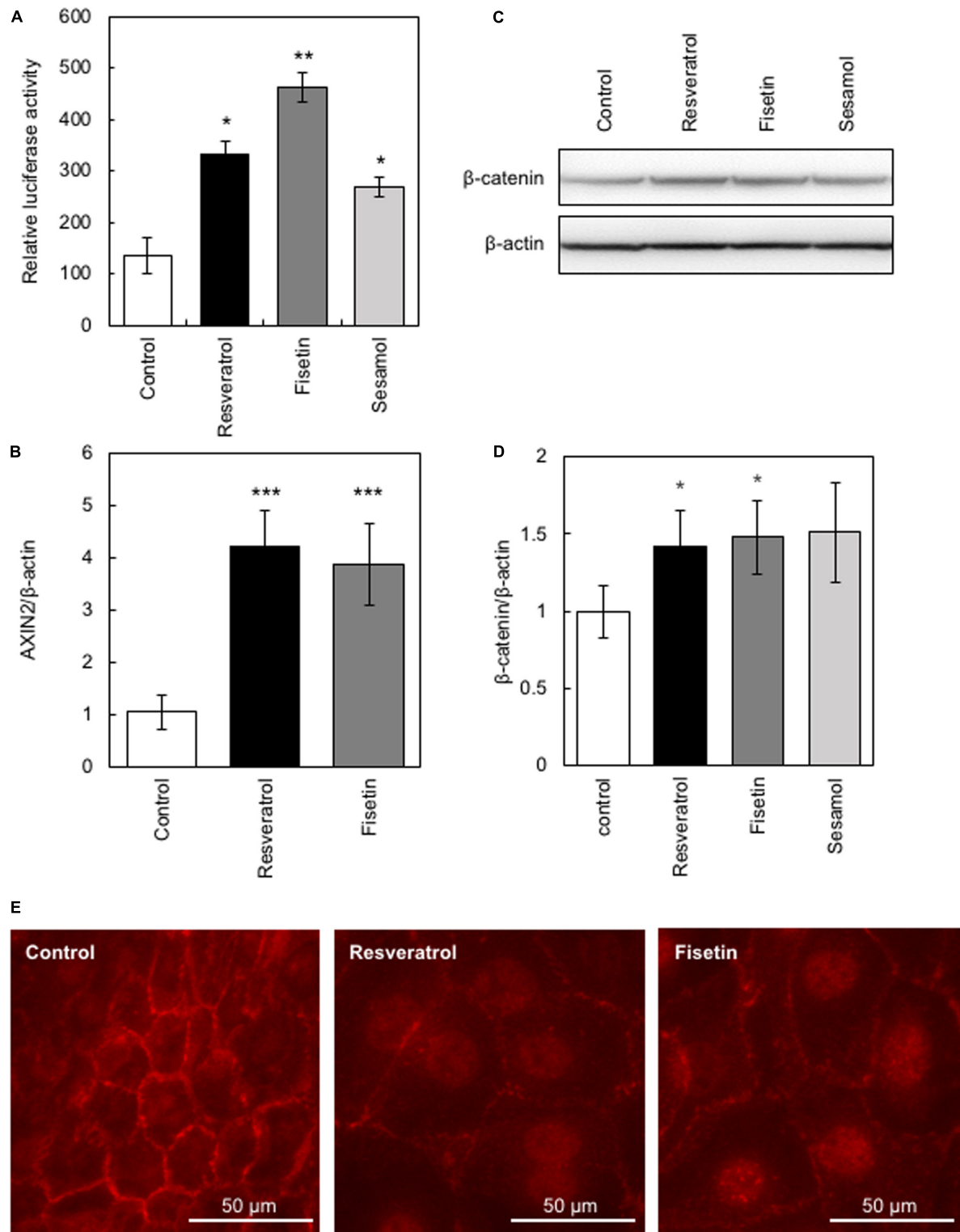


**FIGURE 3 |** Effects of polyphenols on  $\beta$ -catenin activity. The effect of these polyphenols on the activity of  $\beta$ -catenin was evaluated. **(A)** The TOP-Flash reporter assay was performed to evaluate  $\beta$ -catenin activity in HaCaT cells treated with polyphenols. **(B)** The effect of polyphenols on AXIN2 expression was evaluated by qRT-PCR. **(C,D)** The effect of polyphenols on protein expression of  $\beta$ -catenin was evaluated by western blotting using anti- $\beta$ -catenin antibody. Band intensities were quantitatively determined using ImageJ software. **(E)** The effect of polyphenols on activity of  $\beta$ -catenin was evaluated by immunofluorescence study using anti-active  $\beta$ -catenin antibody. Statistical significance was determined using a two-sided Student's *t*-test. Statistical significance was defined as  $P < 0.05$  (\* $P < 0.05$ ; \*\* $P < 0.01$ ; \*\*\* $P < 0.001$ ).

temperature. Tissues were first stained with primary antibodies (anti-Ki-67, #12202, Cell Signaling Technology; anti-TERT, NB100-317, Novus Biologicals, Co., United States; anti-active- $\beta$ -catenin, Merck Millipore, and anti-CD34, ab81289, Abcam, Cambridge, United Kingdom), and subsequently with secondary antibodies (Alexa Fluor 555 anti-rabbit IgG, Alexa Fluor 555 anti-mouse IgG or Alexa Fluor 488 anti-mouse, Thermo Fisher Scientific). After staining with Vectashield mounting medium (Vector Laboratories, Burlingame, CA, United States), tissue samples were observed under a confocal laser-scanning microscope (FV1000, Olympus, Tokyo, Japan).

## Statistical Analysis

All experiments were performed at least 3 times, and the corresponding data are shown. The results are presented as mean  $\pm$  standard deviation. Statistical significance was determined using a two-sided Student's *t*-test. Statistical significance was defined as  $P < 0.05$  (\* $P < 0.05$ ; \*\* $P < 0.01$ ; \*\*\* $P < 0.001$ ).

## RESULTS

### Screening for Polyphenols That Activate *hTERT* Transcription in HaCaT Cells

In the present study, we used a system to screen polyphenols that activate *hTERT* expression in recombinant HaCaT cells expressing the *EGFP* gene under the control of the *hTERT* promoter [HaCaT (*hTERTp*-EGFP)]. Firstly, we investigated the optimal concentration of polyphenols to augment *hTERT* expression by *in vitro* study, then used 10  $\mu$ M of polyphenols for further experiments. Polyphenols (10  $\mu$ M) were added to the HaCaT(*hTERTp*-EGFP) cells and cultured for 48 h; then, changes in EGFP fluorescence were monitored using an IN Cell Analyzer 1000 to identify polyphenols that enhance *hTERT* transcription.

As **Figure 1A** shows, treatment with several polyphenols, including resveratrol, urolithin A, eugenin, sesamol, and fisetin, resulted in significantly increased levels of EGFP fluorescence, indicating that these polyphenols activated the *hTERT* promoter (**Figure 1A**). Next, we performed qRT-PCR to test for the effect of these polyphenols on the expression of endogenous *hTERT* in HaCaT cells. We found that the polyphenols, except eugenin, augmented the expression of *hTERT* in HaCaT cells (**Figure 1B**).

### Effects of Polyphenols on the Expression of Cytokine-Encoding Genes in HaCaT Cells

Several growth factors have been reported to be related to the hair growth cycle (Rho et al., 2005). We measured the gene expression levels of *Insulin-like growth factor (IGF-1)*, *Keratinocyte growth factor (KGF)*, and *Transforming growth factor $\beta$ 1 (TGF- $\beta$ 1)*. When HaCaT cells were treated with polyphenols, the gene expression levels of *IGF-1* and *KGF* increased significantly, while those of *TGF- $\beta$ 1* decreased significantly (**Figure 2**). Among the polyphenols, urolithin A showed relatively low effects on the expression of *KGF* and *TGF- $\beta$ 1*; therefore, we omitted urolithin A from subsequent experiments.

### Effects of Polyphenols on $\beta$ -Catenin Activity

The  $\beta$ -catenin signaling pathway has been reported to be involved in the transcriptional regulation of *hTERT* and hair growth regulation (Shin et al., 2014); therefore, we evaluated the effects of the present polyphenols on the activity of  $\beta$ -catenin using the TOP-Flash reporter assay. Results clearly showed that polyphenols significantly augmented  $\beta$ -catenin activity (**Figure 3A**). Next, we evaluated the effects of these polyphenols on the protein expression and activity of  $\beta$ -catenin by western blotting and immunofluorescence study, respectively. Results showed that resveratrol and fisetin significantly increased the

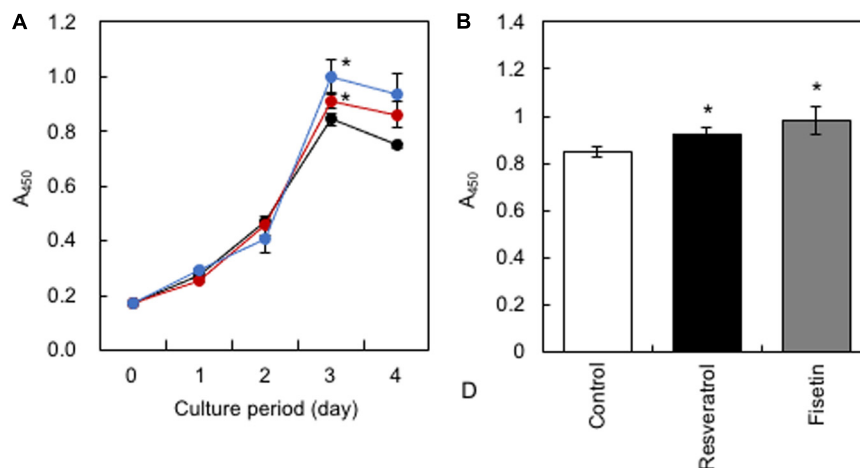


**FIGURE 4 |** Effect of polyphenols on the growth of HaCaT cells. **(A)** After HaCaT cells were treated with 10  $\mu$ M of polyphenols, cell proliferation was monitored using the Cell Counting Kit-8. **(B)** The proliferation index on the 3rd day was determined. Statistical significance was determined using a two-sided Student's *t*-test. Statistical significance was defined as  $P < 0.05$  (\* $P < 0.05$ ).

$\beta$ -catenin expression (Figures 3C,D), and activated  $\beta$ -catenin through inducing nuclear transport (Figure 3E). Furthermore, these polyphenols augmented the expression of *AXIN2*,

downstream target of  $\beta$ -catenin (Figure 3B). These findings collectively demonstrate that resveratrol and fisetin activate the  $\beta$ -catenin pathway.

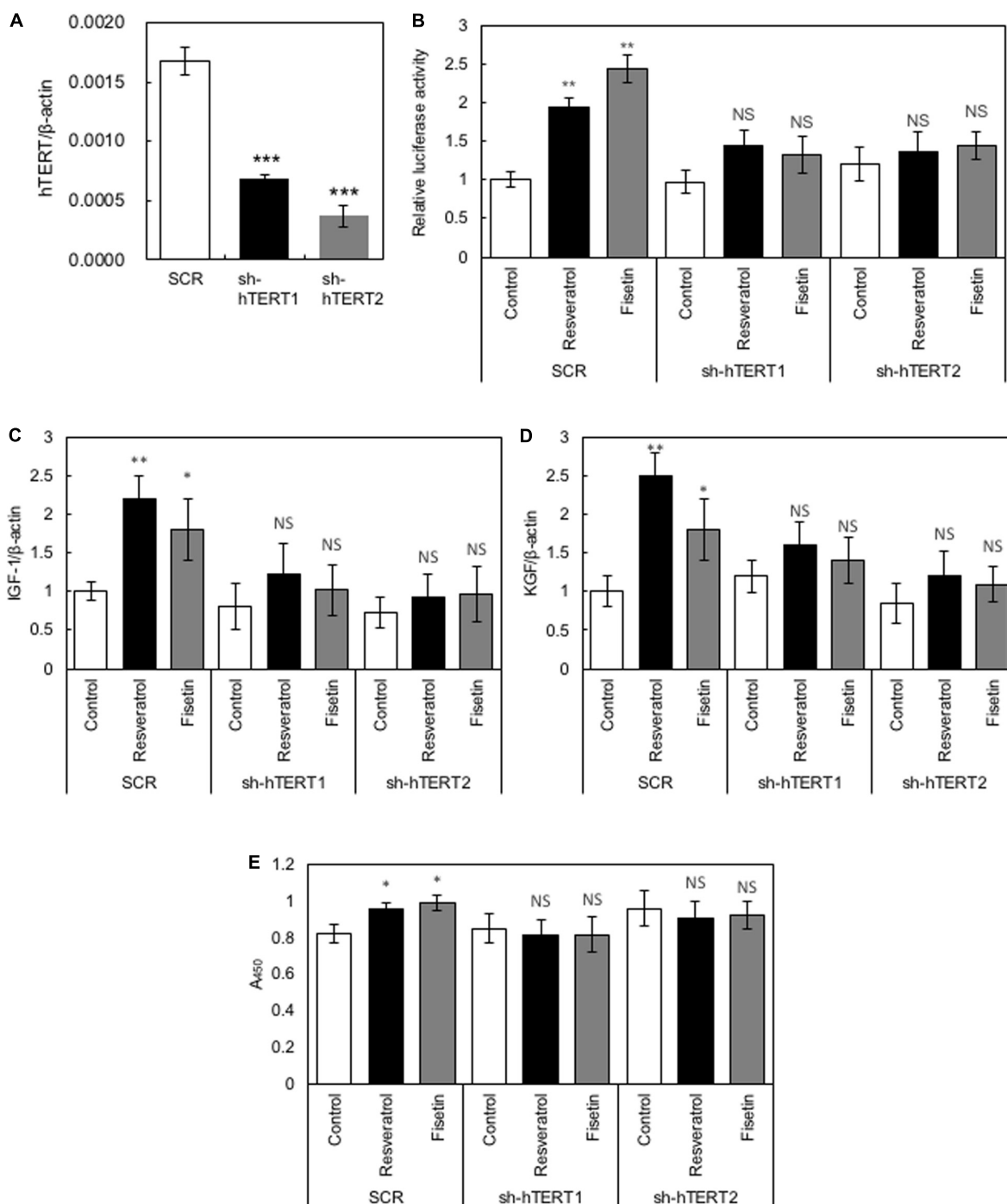


**FIGURE 5 |** Role of *hTERT* in the polyphenol-induced effects on HaCaT cells. **(A)** Relative expression levels of *hTERT* in HaCaT cells transduced with retroviruses expressing shRNA targeting *hTERT* (sh-hTERT1 and 2) and scramble shRNA (SCR) were evaluated by qRT-PCR. HaCaT cells whose *hTERT* expression was reduced by shRNA (sh-hTERT-1 and 2) were treated with polyphenols, and relative  $\beta$ -catenin activity **(B)**, cytokine gene expression **(C,D)**, and cell proliferation **(E)** was determined. Statistical significance was determined using a two-sided Student's *t*-test. Statistical significance was defined as  $P < 0.05$  (\* $P < 0.05$ ; \*\* $P < 0.01$ ; \*\*\* $P < 0.001$ ).



## Effects of Polyphenols on the Growth of HaCaT Cells

HaCaT cells were treated daily with 10  $\mu$ M of polyphenols, and cell proliferation was monitored using the Cell Counting Kit-8. Results showed that resveratrol and fisetin significantly increased the growth of HaCaT cells (Figures 4A,B).

## Role of hTERT in the Polyphenol-Induced Effects on HaCaT Cells

To elucidate whether hTERT plays a role in the polyphenol-induced effects on HaCaT cells, we generated recombinant

HaCaT cells in which the expression of *hTERT* was downregulated using shRNA (sh-hTERT-1 and sh-hTERT2). As shown in Figure 5A, these recombinant HaCaT cell lines showed significantly reduced expression of *hTERT* compared with that in control HaCaT cells transduced with scramble shRNA (SCR). Then, we tested the effects of polyphenols, including resveratrol and fisetin, on the  $\beta$ -catenin activity, cytokine gene expression and cell growth by using these recombinant cell lines. The results clearly showed that polyphenol-induced activation of  $\beta$ -catenin activity (Figure 5B), enhancement of cytokine gene expression (Figures 5C,D) and growth enhancement in HaCaT cells (Figure 5E) were abrogated by the knockdown of

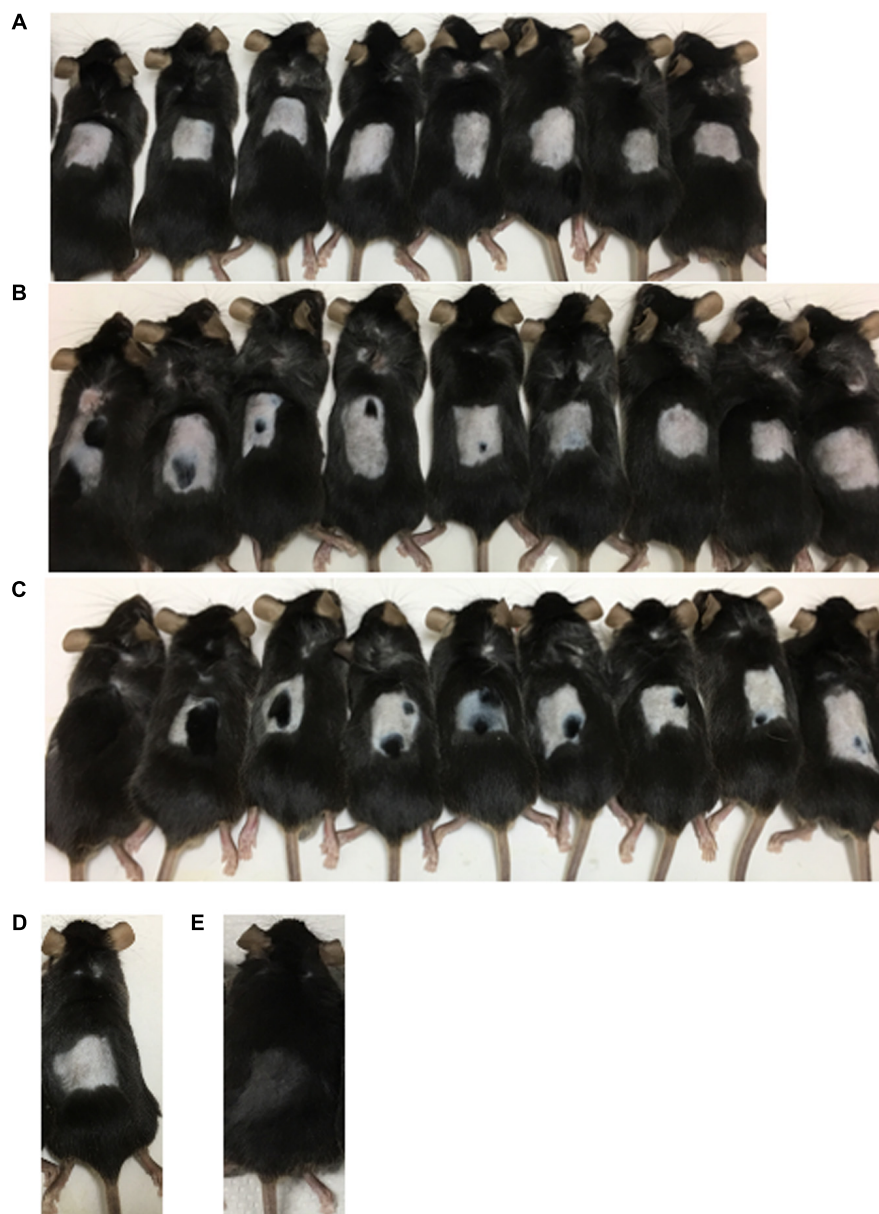


**FIGURE 6 |** Promotion of hair growth by polyphenol treatment in mice. After the application of polyphenols on the dorsal skin of C57BL/6 mice for 35 days, the effect on hair growth was evaluated (A, Control; B, Resveratrol; C, Fisetin; D, Telogen phase; E, Anagen phase).

*hTERT*. These findings indicate that *hTERT* is involved in the polyphenol-induced effects on HaCaT cells.

## Promotion of Hair Growth by Polyphenols in Mice

The C57BL/6 mice were divided into three groups (control, resveratrol, and fisetin). Experiments to evaluate enhancement of hair growth were performed as described in the Materials and Methods. After treatment for 35 days, the effects of polyphenols on hair growth were evaluated (Figure 6). First, mice treated with a solvent control did not show enhanced hair growth, indicating that the telogen phase was maintained for 35 days in the mice even after they were shaved. The results showed that the polyphenols enhanced hair growth in the mice (Figures 6B,C). In particular, fisetin strongly activated hair growth. All nine mice showed enhanced hair growth upon treatment with fisetin (Figure 6C); in comparison, only five of the nine mice in the resveratrol treatment group showed enhanced hair growth (Figure 6B). The difference in the hair

growth rate in the experimental group might be caused by the variation in application of polyphenols. These results suggest that polyphenols, in particular fisetin, activated the transition from telogen to anagen phase, and therefore promoted hair growth.

## Effects of Polyphenols on the Skin Tissue of Mice

We examined mouse *TERT* (*mTERT*) and  $\beta$ -catenin gene expression in the dorsal skin cells of mice treated with polyphenols. Results showed that the *mTERT* (Figures 7A,B) and  $\beta$ -catenin (Figures 7C,D) gene expressions in these cells were significantly augmented in mice treated with resveratrol and fisetin compared with that in mice treated with the control. Therefore, the present polyphenols augment *mTERT* and  $\beta$ -catenin gene expressions in the dorsal skin cells of mice as well as in the human keratinocyte cell line, HaCaT. Histological analysis at 35 days revealed that hair follicles from control mice had remained in the telogen phase, whereas those from mice treated with resveratrol and fisetin had entered anagen (Figures 8A–C).

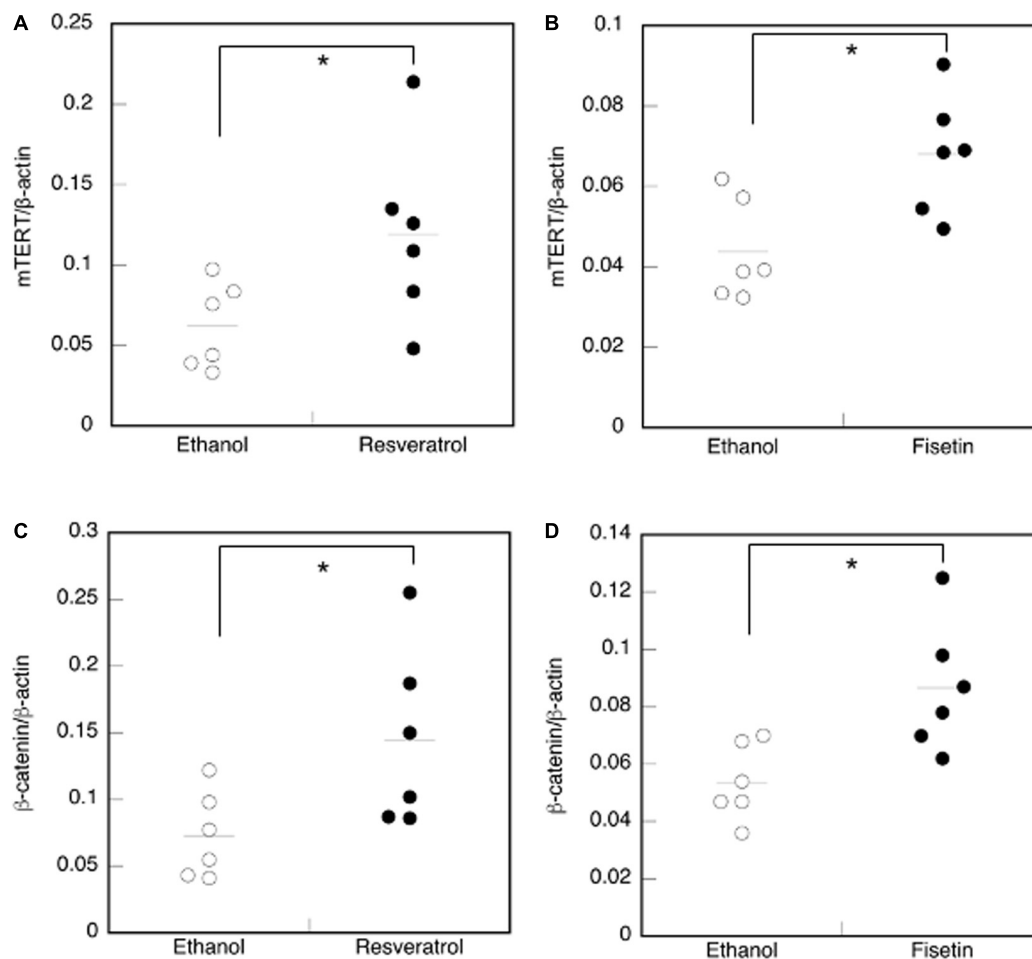


**FIGURE 7 |** Effect of polyphenols on the expression of *mTERT* and  $\beta$ -catenin in the dorsal skin cells of mice. The expression of the *mTERT* (A,B) and  $\beta$ -catenin genes (C,D) in the dorsal skin cells of mice treated with polyphenols was investigated by qRT-PCR. Statistical significance was determined using a two-sided Student's *t*-test. Statistical significance was defined as  $P < 0.05$  (\* $P < 0.05$ ).

In addition, the hair follicles in dorsal skin of mice treated with resveratrol and fisetin were found to be significantly grown (**Figure 8D**). Results suggest that resveratrol and fisetin induce a shift from telogen to anagen in the hair follicle.

Next, we attempted to determine whether *TERT* induction in epidermis enhances the formation of hair follicle; to this end, we measured the proliferation of cells in skin sections containing hair follicles. On the dorsal skin of mice treated with resveratrol (**Figure 9B**) and fisetin (**Figure 9C**), and non-treated mice (**Figure 9A**), a number of proliferating cells (Ki67<sup>+</sup> cells, arrow head) were observed around hair matrix and around outer/inner root sheath (ORS/IRS). These results indicate that *hTERT* induction in the epidermis triggers the proliferation of cells such as hair follicle dermal papilla, hair matrix cells and ORS/IRS, which results in the formation of hair follicle and promotion of hair growth in mice treated with *hTERT*-augmenting polyphenols.

Finally, we tested the expression of marker proteins (Tert,  $\beta$ -catenin and CD34) in the skin section treated with fisetin during the process of hair growth. Early anagen was detected 2–3 weeks after the treatment with fisetin, and active anagen was formed about another week after its emergence. The expression of marker proteins in non-treated skin sections were also shown in **Figure 9D**. Tert was strongly expressed in skin epithelium (EP),

hair bulge (HB) and dermal papilla (DP) at early anagen, and showed a pan-epithelial expression at active anagen.  $\beta$ -catenin was consistently detected in ORS, IRS, hair shaft and DP during the course of hair growth, but its expression in DP clearly increased at active anagen. CD34, a cell membrane marker of hair follicle stem cells, was highly detected in the cells surrounding HB at early and active anagen (**Figure 9D**). CD34<sup>+</sup>/Ki67<sup>+</sup> cells were found around HB region, suggesting that hair follicle stem cells were vigorously proliferating. Although CD34<sup>+</sup> cells can be detected in the skin section of control mice, the number of CD34<sup>+</sup> cells increased in the skin section of fisetin-treated mice.

## DISCUSSION

### Identification of Polyphenols That Augment *hTERT* Transcription

In the present study, we used a reporter HaCaT cell line that expressed *EGFP* under the control of the *hTERT* promoter in order to identify polyphenols that activate *hTERT* transcription. We identified two polyphenols, namely resveratrol and fisetin that promoted hair growth in experimental mice. Although many researchers have identified polyphenols that regulate *hTERT* transcription (Chen et al., 2017), many of these have been

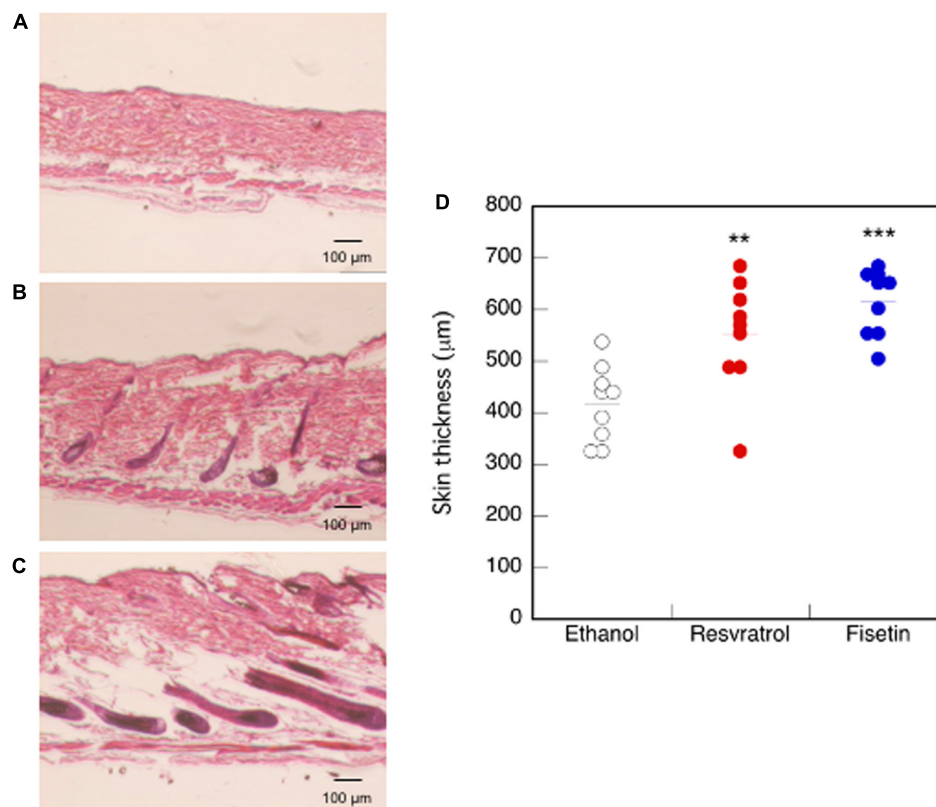


**FIGURE 8 |** Effect of polyphenols on the dorsal skin of mice. After 35 days of treatment, histological analysis of dorsal skin was performed after H&E staining (**A**, Control; **B**, Resveratrol; **C**, Fisetin). (**D**) The length between epidermis and subcutaneous layer at the dorsal skin was quantitatively determined using ImageJ. Statistical significance was determined using a two-sided Student's *t*-test. Statistical significance was defined as  $P < 0.05$  (\*\* $P < 0.01$ ; \*\*\* $P < 0.001$ ).



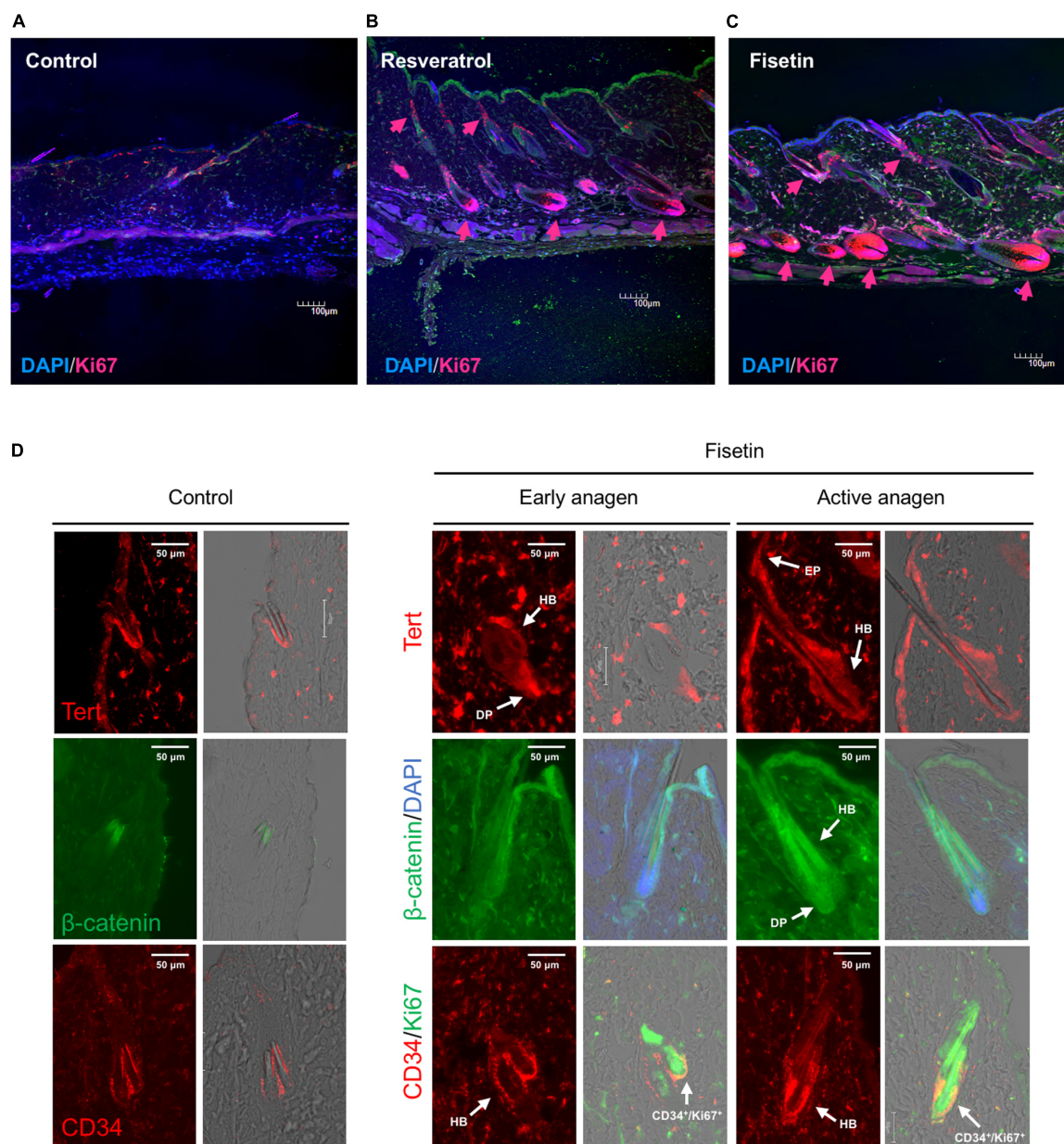


**FIGURE 9 |** Effect of treatment with polyphenols on the proliferation of cells and expression of marker proteins in the skin sections with hair follicles. After 35 days of treatment, immunohistological analysis of skin sections was performed using anti-Ki-67 antibody and DAPI staining (**A**, Control; **B**, Resveratrol; **C**, Fisetin; arrow head; Ki67<sup>+</sup> cells). (**D**) Immunohistological analysis of skin sections treated with fisetin at early anagen and active anagen were performed using anti-Tert antibody, anti-active-β-catenin antibody and anti-CD34 antibody (DP, dermal papilla; Mx, matrix; EP, epithelium). Immunohistological analysis of non-treated skin sections were also shown (Control).

studied in the context of downregulation of *hTERT* transcription in cancer cells. We have previously reported that resveratrol activates *hTERT* transcription in normal human umbilical cord fibroblast cells (Yamashita et al., 2012). These results suggest that *hTERT* transcription is regulated by polyphenols in a manner that is dependent upon cell type and context.

In this study, resveratrol and fisetin showed strong hair-growth-promoting activity. Resveratrol and fisetin are natural polyphenolic compounds and have many pharmacological and

physiological activities (Bai et al., 2018). Recent studies have shown that both polyphenols are known to be a potent activator of sirtuin, a longevity gene, and calorie-restriction mimetics, suggesting that these polyphenols can alleviate aging-related functional decline in organisms (Villalba and Alcáin, 2012). The hair-growth-promoting activities of resveratrol and fisetin are recognized as novel anti-aging effects of these polyphenols. In a future study, we will seek to elucidate the structure-function relationships of these polyphenols and



identify the structural features of polyphenol that activate *hTERT* transcription.

## Involvement of Cytokines in Polyphenol-Induced Hair Growth Promotion

Various cytokines, including IGF-1, KGF, and TGF- $\beta$ 1, play essential roles in hair growth. IGF-1 plays a critical role in regulating cellular proliferation and migration during hair follicle development, while KGF stimulates hair follicle proliferation. In contrast, TGF- $\beta$ 1 is involved in the regulation of hair follicle regression by inducing apoptosis and inhibiting keratinocyte proliferation and in the maintenance of niche of hair follicle stem cells (Mesa et al., 2015). Several plant extracts promote hair growth by regulating the expression of hair-growth-related cytokines (Kim et al., 2014; Shin et al., 2016). In the present study, resveratrol and fisetin increased the expression of IGF-1 and KGF, and decreased that of TGF- $\beta$ 1, in HaCaT cells, thereby promoting hair growth. In future studies, we aim to clarify the mechanisms underlying polyphenol-induced regulation of cytokine expression.

## Involvement of $\beta$ -Catenin in Polyphenol-Induced Hair Growth Promotion

Numerous reports have described the interaction between Wnt/ $\beta$ -catenin and *hTERT*. Zhang and Hoffmeyer et al. have shown that *hTERT* is a novel target of the Wnt/ $\beta$ -catenin pathway (Hoffmeyer et al., 2012; Zhang et al., 2012). In contrast, Park et al. (2009) reported that *hTERT* functions as a transcriptional modulator of the Wnt/ $\beta$ -catenin signaling pathway. These results suggest a close link between the Wnt/ $\beta$ -catenin signaling pathway and *hTERT*. The present results clearly demonstrate that the *hTERT*-augmenting polyphenols, namely resveratrol and fisetin, activated  $\beta$ -catenin expression, and that polyphenols activated  $\beta$ -catenin in a manner dependently upon *hTERT*. Considering together with that  $\beta$ -catenin is involved in various stages of hair morphogenesis, induction of hair follicles and hair growth promotion (Gat et al., 1998; Närhi et al., 2008; Bejaoui et al., 2020), this polyphenol-induced activation of  $\beta$ -catenin via *hTERT* augmentation might be a key event for hair growth promotion.

## Molecular Basis for Hair-Growth-Promotion

Various plant extracts and chemicals with hair-growth-stimulating effects have been reported. Although precise underlying mechanisms remain unknown, these extracts and chemicals are considered to elicit these effects by accelerating blood flow, inducing a shift from telogen to anagen, mediating activation of the dermal papilla, inhibiting dihydrotestosterone, and exerting anti-inflammatory effects (Junlatat and Sripanidkulchai, 2014; Kim et al., 2014; Park et al., 2017; Shen et al., 2018; Zhang et al., 2019; Zhou et al., 2020). The hair follicle contains several different types of cells; among these, the dermal papilla cells are major components of hair that play a critical role in inducing anagen phase and maintaining

hair growth. Several growth factors, including IGF-1, KGF, and TGF- $\beta$ , are known to modulate the proliferation of the follicular epithelium, and control follicle development and cytokine expression in hair cells. In addition, The Wnt/ $\beta$ -catenin pathway is known to be important for the initiation, development, and growth of hair follicles as well as for the induction of anagen (Gat et al., 1998; Park et al., 2012). Several molecules, cells and signaling pathways are known to be involved in hair growth promotion,  $\beta$ -catenin was conceivable as a key molecule of *TERT*-augmenting polyphenol to promote hair growth. In our study, fisetin induced *Tert* in epidermis, which resulted in the proliferation of ORS/IRS and Mx, activation of hair follicle stem cells (CD34<sup>+</sup> cells) and  $\beta$ -catenin, which might resulted in the formation of hair follicle and promotion of hair growth. In future studies, we aim to clarify the whole picture of molecular mechanisms of *TERT*-augmenting polyphenol to promote hair growth.

## DATA AVAILABILITY STATEMENT

The raw data supporting the conclusions of this article will be made available by the authors, without undue reservation, to any qualified researcher.

## ETHICS STATEMENT

The animal study was reviewed and approved by the Ethics Committees on Animal Experimentation (Kyushu University).

## AUTHOR CONTRIBUTIONS

CK, MO, and NU performed the experiments and collected the data. YK developed the study design and wrote the manuscript. All authors contributed to the article and approved the submitted version.

## FUNDING

This study was partially supported by the Japan Science and Technology Agency (JST) and the Japan International Cooperation Agency's (JICA) Science and Technology Research Partnership for Sustainable Development (SATREPS, Grant No. JPMJSA1506).

## ACKNOWLEDGMENTS

We would like to thank N. Oshima (GE Healthcare) for providing expert assistance with the IN Cell Analyzer 1000. We would like to thank Editage (<http://www.editage.com>) for English language editing.

## REFERENCES

- Bai, X., Yao, L., Ma, X., and Xu, X. (2018). Small molecules as SIRT modulators. *Mini Rev. Med. Chem.* 18, 1151–1157. doi: 10.2174/1389557516666160620095103
- Bejaoui, M., Villareal, M. O., and Isoda, H. (2020). 3,4,5-tri-O-caffeoylquinic acid promoted hair pigmentation through  $\beta$ -catenin and its target genes. *Front. Cell Dev. Biol.* 8:175. doi: 10.3389/fcell.2020.00175
- Chen, R.-J., Wu, P.-H., Ho, C.-T., Way, T.-D., Pan, M.-H., Chen, H.-M., et al. (2017). P53-dependent downregulation of hTERT protein expression and telomerase activity induces senescence in lung cancer cells as a result of pterostilbene treatment. *Cell Death Dis.* 8:e2985. doi: 10.1038/cddis.2017.333
- Choi, J., Southworth, L. K., Sarin, K. Y., Venteicher, A. S., Ma, W., Chang, W., et al. (2008). TERT promotes epithelial proliferation through transcriptional control of a Myc- and Wnt-related developmental program. *PLoS Genet.* 4:e10. doi: 10.1371/journal.pgen.0040010
- Chong, Z., Matsuo, H., Onoue, S., Yamamoto, H., Ito, H., and Katakura, Y. (2019). Identification of polyphenols that repair the ultraviolet-B-induced DNA damage via SIRT1-dependent XPC/XPA activation. *J. Funct. Foods* 54, 119–127. doi: 10.1016/j.jff.2019.01.017
- Fujiki, T., Miura, T., Maura, M., Shiraishi, H., Nishimura, S., Imada, Y., et al. (2007). TAK1 represses transcription of the human telomerase reverse transcriptase gene. *Oncogene* 26, 5258–5266. doi: 10.1038/sj.onc.1210331
- Gat, U., DasGupta, R., Degenstein, L., and Fuchs, E. (1998). De novo hair follicle morphogenesis and hair tumors in mice expressing a truncated beta-catenin in skin. *Cell* 95, 605–614. doi: 10.1016/s0092-8674(00)81631-1
- Harada, G., Neng, Q., Fujiki, T., and Katakura, Y. (2014). Molecular mechanisms for the p38-induced cellular senescence in normal human fibroblast. *J. Biochem.* 156, 283–290. doi: 10.1093/jb/mvu040
- Harada, G., Pattarawat, P., Ito, K., Matsumoto, T., Hasegawa, T., and Katakura, Y. (2016). *Lactobacillus brevis* T2102 suppresses the growth of colorectal cancer cells by activating SIRT1. *J. Funct. Foods* 23, 444–452. doi: 10.1016/j.jff.2016.01.016
- Hoffmeyer, K., Raggioli, A., Rudloff, S., Anton, R., Hierholzer, A., Del Valle, I., et al. (2012). Wnt/ $\beta$ -catenin signaling regulates telomerase in stem cells and cancer cells. *Science* 336, 1549–1554. doi: 10.1126/science.1218370
- Junlatat, J., and Sripanidkulchai, B. (2014). Hair growth-promoting effect of *Carthamus tinctorius* floret extract. *Phytother. Res.* 28, 1030–1036. doi: 10.1002/ptr.5100
- Kim, E. J., Choi, J. Y., Park, B. C., and Lee, B.-H. (2014). Platycarya strobilacea S. et Z. extract has a high antioxidant capacity and exhibits hair growth-promoting effects in male C57BL/6 mice. *Prev. Nutr. Food Sci.* 19, 136–144. doi: 10.3746/pnf.2014.19.3.136
- Mesa, K. R., Rompolas, P., Zito, G., Myung, P., Sun, T. Y., Brown, S., et al. (2015). Niche-induced cell death and epithelial phagocytosis regulate hair follicle stem cell pool. *Nature* 522, 94–97. doi: 10.1038/nature14306
- Närhi, K., Järvinen, E., Birchmeier, W., Taketo, M. M., Mikkola, M. L., and Thesleff, I. (2008). Sustained epithelial beta-catenin activity induces precocious hair development but disrupts hair follicle down-growth and hair shaft formation. *Development* 135, 1019–1028. doi: 10.1242/dev.016550
- Park, B.-M., Bak, S.-S., Shin, K.-O., Kim, M., Kim, D., Jung, S.-H., et al. (2017). Promotion of hair growth by newly synthesized ceramide mimetic compound. *Biochem. Biophys. Res. Commun.* 491, 173–177. doi: 10.1016/j.bbrc.2017.07.069
- Park, J.-I., Venteicher, A. S., Hong, J. Y., Choi, J., Jun, S., Shkreli, M., et al. (2009). Telomerase modulates Wnt signalling by association with target gene chromatin. *Nature* 460, 66–72. doi: 10.1038/nature08137
- Park, P.-J., Moon, B.-S., Lee, S.-H., Kim, S.-N., Kim, A.-R., Kim, H.-J., et al. (2012). Hair growth-promoting effect of *Aconiti Ciliare Tuber* extract mediated by the activation of Wnt/ $\beta$ -catenin signaling. *Life Sci.* 91, 935–943. doi: 10.1016/j.lfs.2012.09.008
- Rho, S.-S., Park, S.-J., Hwang, S.-L., Lee, M.-H., Kim, C. D., Lee, I.-H., et al. (2005). The hair growth promoting effect of *Asiasari radix* extract and its molecular regulation. *J. Dermatol. Sci.* 38, 89–97. doi: 10.1016/j.jdermsci.2004.12.025
- Sarin, K. Y., Cheung, P., Gilson, D., Lee, E., Tennen, R. I., Wang, E., et al. (2005). Conditional telomerase induction causes proliferation of hair follicle stem cells. *Nature* 436, 1048–1052. doi: 10.1038/nature03836
- Shen, Y.-L., Li, X.-Q., Pan, R.-R., Yue, W., Zhang, L.-J., and Zhang, H. (2018). Medicinal plants for the treatment of hair loss and the suggested mechanisms. *Curr. Pharm. Des.* 24, 3090–3100. doi: 10.2174/1381612824666180911114810
- Shin, H., Cho, A.-R., Kim, D. Y., Munkhbayer, S., Choi, S.-J., Jang, S., et al. (2016). Enhancement of human hair growth using *Ecklonia cava* polyphenols. *Ann. Dermatol.* 28, 15–21. doi: 10.5021/ad.2016.28.1.15
- Shin, H.-S., Park, S.-Y., Hwang, E.-S., Lee, D.-G., Song, H.-G., Mavlonov, G. T., et al. (2014). The inductive effect of ginsenoside F2 on hair growth by altering the WNT signal pathway in telogen mouse skin. *Eur. J. Pharmacol.* 730, 82–89. doi: 10.1016/j.ejphar.2014.02.024
- Suchonwanit, P., Thammarucha, S., and Leerunyakul, K. (2019). Minoxidil and its use in hair disorders: a review. *Drug Des. Devel. Ther.* 13, 2777–2786. doi: 10.2147/DDDT.S214907
- Sugihara, Y., Onoue, S., Tashiro, K., Sato, M., Hasegawa, T., and Katakura, Y. (2019). Carnosine induces intestinal cells to secrete exosomes that activate neuronal cells. *PLoS One* 14:e0217394. doi: 10.1371/journal.pone.0217394
- Veeman, M. T., Slusarski, D. C., Kaykas, A., Louie, S. H., and Moon, R. T. (2003). Zebrafish prickles, a modulator of noncanonical Wnt/Fz signaling, regulates gastrulation movements. *Curr. Biol.* 13, 680–685.
- Villalba, J. M., and Alcáin, F. J. (2012). Sirtuin activators and inhibitors. *Biofactors* 38, 349–359. doi: 10.1002/biof.1032
- Yamashita, S., Ogawa, K., Ikei, T., Fujiki, T., and Katakura, Y. (2014). FOXO3a potentiates hTERT gene expression by activating c-MYC and extends the replicative life-span of human fibroblast. *PLoS One* 9:e101864. doi: 10.1371/journal.pone.0101864
- Yamashita, S., Ogawa, K., Ikei, T., Udono, M., Fujiki, T., and Katakura, Y. (2012). SIRT1 prevents replicative senescence of normal human umbilical cord fibroblast through potentiating the transcription of human telomerase reverse transcriptase gene. *Biochem. Biophys. Res. Commun.* 417, 630–634. doi: 10.1016/j.bbrc.2011.12.021
- Zhang, Y., Chen, S., Qu, F., Su, G., and Zhao, Y. (2019). In vivo and in vitro evaluation of hair growth potential of *Cacumen Platycladi*, and GC-MS analysis of the active constituents of volatile oil. *J. Ethnopharmacol.* 238:111835. doi: 10.1016/j.jep.2019.111835
- Zhang, Y., Toh, L., Lau, P., and Wang, X. (2012). Human telomerase reverse transcriptase (hTERT) is a novel target of the Wnt/ $\beta$ -catenin pathway in human cancer. *J. Biol. Chem.* 287, 32494–32511. doi: 10.1074/jbc.M112.368282
- Zhao, C., Sakaguchi, T., Fujita, K., Ito, H., Nishida, N., Nagatomo, A., et al. (2016). Pomegranate-derived polyphenols reduce reactive oxygen species production via SIRT3-mediated SOD2 activation. *Oxid. Med. Cell. Longev.* 2016:2927131. doi: 10.1155/2016/2927131
- Zhou, Y., Tang, G., Li, X., Sun, W., Liang, Y., Gan, D., et al. (2020). Study on the chemical constituents of nuts oil from *Prunus mira* Koehne and the mechanism of promoting hair growth. *J. Ethnopharmacol.* 258:112831. doi: 10.1016/j.jep.2020.112831

**Conflict of Interest:** The authors declare that the research was conducted in the absence of any commercial or financial relationships that could be construed as a potential conflict of interest.

Copyright © 2020 Kubo, Ogawa, Uehara and Katakura. This is an open-access article distributed under the terms of the Creative Commons Attribution License (CC BY). The use, distribution or reproduction in other forums is permitted, provided the original author(s) and the copyright owner(s) are credited and that the original publication in this journal is cited, in accordance with accepted academic practice. No use, distribution or reproduction is permitted which does not comply with these terms.



# Tectorigenin Alleviates Inflammation, Apoptosis, and Ossification in Rat Tendon-Derived Stem Cells via Modulating NF-Kappa B and MAPK Pathways

Safwat Adel Abdo Moqbel<sup>1†</sup>, Kai Xu<sup>1†</sup>, Zhonggai Chen<sup>2†</sup>, Langhai Xu<sup>1</sup>, Yuezhe He<sup>1</sup>, Zhipeng Wu<sup>3</sup>, Chiyuan Ma<sup>1</sup>, Jisheng Ran<sup>1</sup>, Lidong Wu<sup>1\*</sup> and Yan Xiong<sup>1\*</sup>

<sup>1</sup> Department of Orthopedic Surgery, The Second Affiliated Hospital, School of Medicine, Zhejiang University, Hangzhou, China, <sup>2</sup> Department of Orthopaedic Surgery, The Second Affiliated Hospital and Yuying Children's Hospital of Wenzhou Medical University, Wenzhou, China, <sup>3</sup> Department of Orthopaedics, The First Affiliated Hospital of Zhejiang Chinese Medical University, Hangzhou, China

## OPEN ACCESS

### Edited by:

Hiroko Isoda,  
University of Tsukuba, Japan

### Reviewed by:

Johannes F. W. Greiner,  
Bielefeld University, Germany  
Sina Naserian,  
INSERM UMR-S-MD 1197, Hôpital  
Paul-Brousse AP-HP, France

### \*Correspondence:

Lidong Wu  
wulidong@zju.edu.cn  
Yan Xiong  
xiongyanbear@zju.edu.cn

<sup>†</sup> These authors have contributed  
equally to this work

### Specialty section:

This article was submitted to  
Stem Cell Research,  
a section of the journal  
Frontiers in Cell and Developmental  
Biology

**Received:** 02 June 2020

**Accepted:** 24 September 2020

**Published:** 22 October 2020

### Citation:

Moqbel SAA, Xu K, Chen Z, Xu L,  
He Y, Wu Z, Ma C, Ran J, Wu L and  
Xiong Y (2020) Tectorigenin Alleviates  
Inflammation, Apoptosis,  
and Ossification in Rat  
Tendon-Derived Stem Cells via  
Modulating NF-Kappa B and MAPK  
Pathways.  
Front. Cell Dev. Biol. 8:568894.  
doi: 10.3389/fcell.2020.568894

Tendinopathy is a common musculoskeletal disorder that mainly affects athletes and people of older age. Tumor necrosis factor- $\alpha$  (TNF- $\alpha$ ) plays an important role in initiating tendinopathy. Tectorigenin, an extract component of *Belam-canda Chinesis*, possesses anti-inflammatory and anti-apoptosis activity. The present study was established to investigate the role of tectorigenin against the pathogenetic effects of TNF- $\alpha$  on tendon-derived stem cells (TDSCs) *in vivo* and *in vitro*. The findings indicated that TNF- $\alpha$  is able to induce TDSC inflammation, apoptosis, and ossification, as well as activate nuclear factor-kappa B and mitogen-activated protein kinase (MAPK). Furthermore, the results confirmed that tectorigenin is able to inhibit the TNF- $\alpha$ -induced inflammation, apoptosis, and ossification. Tectorigenin treatment decreases activation of NF-kappa B and MAPK signaling in TDSCs. Tectorigenin ameliorates tendinopathy in the *in vivo* rat model. Thus, these data reveal that tectorigenin can serve as a potential treatment for tendinopathy.

**Keywords:** TDSCs, tectorigenin, TNF- $\alpha$ , inflammation, apoptosis, ossification, MAPK, nuclear factor-kappa B pathway

## INTRODUCTION

Tendinopathy is a chronic disorder characterized by swelling, pain, ossification, and dysfunction of the tendon. Previous studies have shown that several factors can contribute to tendinopathy, such as tendon overload, injury, aging, and genetic conditions (Almekinders and Temple, 1998). Tendon-derived stem cells (TDSCs), which are extracted from tendon tissues, possess self-renewal and tendon-like tissue regeneration capabilities (Bi et al., 2007). TDSCs play a central role in tendon regeneration and healing as well as controlling tendon homeostasis (Ni et al., 2012). A change in their microenvironment leads to the dysfunction of TDSCs, resulting in degradation of tendon matrix and ultimately tendinopathy (Shi et al., 2019).

TNF- $\alpha$  is a cytokine associated with tendon inflammation, degeneration, and apoptosis, and it contributes to the suppression of proliferation of TDSCs (Hosaka et al., 2005; Han et al., 2017). TNF- $\alpha$  is able to induce the production of matrix degradation enzymes (Machner et al., 2003), which are associated with the inhibition of ECM synthesis (John et al., 2010). TNF- $\alpha$  is released

from tendon tissue during injury and malfunction (Millar et al., 2009; Morita et al., 2017). TNF- $\alpha$  was found to play an important role in tendon degeneration and was expressed in inflamed and scarred tendon (Schulze-Tanzil et al., 2011). TNF- $\alpha$  is well-known to play a role in initiating various signaling pathways, such as mitogen-activated protein kinase (MAPK) and nuclear factor kappa B (NF- $\kappa$ B pathways) (Akiyama et al., 2004). In addition, MAPK and NF- $\kappa$ B are known to govern several processes, such as inflammation, MMP secretion, apoptosis, and ossification in tendinopathy. The inhibition of TNF- $\alpha$  and targeting of MAPK and NF- $\kappa$ B offers potential in the treatment of tendinopathy. Previous studies have suggested and recognized Achilles tendon injury or Achilles tenotomy as a reproducible trauma-induced tendinopathy and heterotopic ossification model (Kaleağasioğlu et al., 2017; Lin et al., 2018). Therefore, in our study we established the rat tendinopathy model using tenotomy.

Tectorigenin (C16H12O6, Service number: 548-77-6; molecular weight, 300.26) a component of *Belamcanda chinensis*, has been used in several fields for its modulating effect against inflammation, oxidation, and osteoclastogenesis (Wang et al., 2013; Ma et al., 2018). Furthermore, tectorigenin is able to inhibit the MAPK and NF- $\kappa$ B signaling pathways (Lim et al., 2018; Ma et al., 2018). In the present study, we examined the role of tectorigenin on the inflammation, apoptosis, and ossification of TDSCs through the targeting of MAPK and NF- $\kappa$ B *in vitro*, in addition to its effect in tendinopathy in the rat model.

## MATERIALS AND METHODS

### Materials

Tectorigenin of purity higher than 98% was purchased from Biotech (Shanghai, China). Fetal bovine serum (FBS), minimum essential medium with alpha modification ( $\alpha$ -MEM), streptomycin, and penicillin were purchased from Gibco, United States. TNF- $\alpha$  was obtained from R&D Systems, United Kingdom. DMSO, bovine serum albumin (BSA), and collagenase I were all obtained from Sigma-Aldrich, St. Louis, MO, United States. Radioimmunoprecipitation assay (RIPA) buffer and bicinchoninic acid assay were obtained from Beyotime, Shanghai, China.

### Isolation and Culture of TDSCs

Tendon-derived stem cells were isolated and cultured as previously described (Xu et al., 2020). In brief, S-D rats (male, 3-week old,  $140 \pm 20$  g) were used to isolate the Achilles tendons. For isolation of TDSCs from tendinopathic rats, five rats received full Achilles tendon transection. After 7 days, the rats were killed to isolate the tendinopathic cells. Under sterile conditions, the tendons were cut into  $1.1 \text{ mm}^3$  particles, and the tissues were incubated with 0.1% collagenase type I at  $37^\circ\text{C}$  for 2–3 h on a horizontal shaker. The cells were collected as P0 and incubated with  $\alpha$ -MEM (with 10% FBS and 100 units/ml streptomycin + 100 units/ml penicillin) at  $37^\circ\text{C}$  with 5%  $\text{CO}_2$ , and the culture medium was replaced every 2–3 days. TDSCs from tendinopathic rats were seeded and divided into two tendinopathy and tectorigenin treatment groups. The medium

was replaced every 2 days; cells in the tectorigenin treatment group received a medium containing an equal amount of  $100 \mu\text{M}$  of tectorigenin. After the density of cells in the culture flask reached more than 80%, the cells were harvested for a further study. Normal TDSCs at P3 were used in this experiment.

### Identification of TDSC and Multipotency Assay

Tendon-derived stem cells were stained with fluorescent primary antibody in PBS for 40 min, and then washed three times. Flow cytometry was used to detect the surface markers. The following antibodies were used: FITC antirat (CD29 and CD44) and PE antirat (CD59 and CD90) BioLegend. To analyze the multipotency of TDSCs, cells were cultured and incubated with specific media. Osteogenic induction medium (Cyagen Biosciences) was used for 14 days, followed by Alizarin Red staining to visualize the differentiation of TDSCs into osteoblasts. Chondrogenesis was induced with chondrogenic differentiation medium (Cyagen Biosciences) for 21 days, after which Safranin O staining was used to visualize chondrogenic differentiation. Similarly, after incubation with adipogenic induction and maintenance media (Cyagen Biosciences) for 14 days, Oil Red staining was used to visualize the adipogenic differentiation of TDSCs. qRT-PCR was conducted to evaluate the markers of tenogenesis in TDSCs and other mesenchymal stem cells. The mRNA levels of collagen type I, scleraxis, tenomodulin, and mohawk were evaluated.

### TDSC Viability Assay

To measure the toxicity of tectorigenin and TNF- $\alpha$  on TDSC, CCK-8 assay (Dojindo Molecular, Tech., Japan) was used in accordance with the manufacturer's instructions. The cells were seeded into 96-well plates ( $5 \times 10^3$ /well), and then treated with various concentrations of tectorigenin or TNF- $\alpha$  for 24 h. The cells were then incubated with fresh media (containing 10% CCK-8 solution) for 3 h at  $37^\circ\text{C}$ ; thereafter, the optical density was read. This experiment was repeated three times.

### Apoptosis Assay

Annexin-V-FITC/Propidium Iodide (PI) Apoptosis Detection Kit (Keygen Biotech) was used to detect the apoptotic cells. A mount of  $10^6$  TDSCs was double stained using the apoptosis detection kit and analyzed using flow cytometry.

### RNA Extraction and qRT-PCR

Six-well plates were used to seed a tertiary culture (passage 3) of TDSCs in  $\alpha$ -MEM. When the growth density of the cells was greater than or equal to 75%, tectorigenin at 50 and  $100 \mu\text{M}$  was used to treat the cells for 1 h in the absence and presence of TNF- $\alpha$  for 24 h individually. After the media was removed and the cells were washed with PBS, TRIzol reagent (Invitrogen, Carlsbad, CA, United States) was used to extract total RNA on ice. Using DeNovix at 260 nm (A260)/A280 absorbance ratio total RNA was quantified. PrimeScript RT Master Mix (Takara) was used to synthesize cDNA. cDNA was synthesized at  $37^\circ\text{C}$  for 15 min and then at  $85^\circ\text{C}$  for 5 min. According to protocol, SYBR



Green qPCR (Applied Biosystems) and StepO-nePlus Real-Time PCR systems were used to conduct qRT-PCR. The primers are listed in **Table 1**. 18S was used as the control. Expression levels were quantified using the  $2^{-\Delta\Delta CT}$  method.

## Protein Isolation and Western Blot

Tendon-derived stem cells were cultured in four 25 cm<sup>2</sup> flasks and treated with tectorigenin. After collecting the cells, 100  $\mu$ l RIPA buffer (containing 1% phenylmethylsulfonyl fluoride + 0.1% phosphorylated proteinase inhibitor) was used to extract total protein for 50 min. BCA assay was used to quantify the proteins which were then denatured at 95–100°C for 5 min. The adjusted proteins were set in SDS-PAGE with a 10 or 15% gel and then transferred to a membrane. The membrane was blocked with BSA (5–10%) for 1–2 h and then washed three times for 10 min. After, the membranes were incubated with primary antibodies for 12 h at 4°C. Subsequently, the membranes were washed and incubated with secondary antibodies for 1 h. After removing and washing the secondary antibodies, the membranes were read using an ECL kit (Immobilon; cat. no. WBKLS005; KGaA). Bio-Rad ChemiDoc system was used to quantify the protein bands.

## Radiological Assessment

Calcifications of Achilles tendons of the rats were evaluated using X-ray machine. Lateral X-ray images of the legs of the rats were generated at 60 kV with a radiation intensity of 500 mAs (200 Ma).

## ALP Staining

Tendon-derived stem cells were seeded into 12-well plates with osteogenic induction medium with or without tectorigenin for 7 days. After washing with PBS, 4% paraformaldehyde was used to fix the cells for 30 min. ALP Color Development Kit (Beyotime Biotechnology, Shanghai, China) was used according to the protocol and then viewed under a microscope.

## Alizarin Red Staining

The cells were incubated in osteogenic differentiation media for 14 days and were washed with PBS. The cells were fixed with 4% paraformaldehyde for 20 min, and subsequently stained with 0.1% solution of Alizarin Red (Cyagen Biosciences) for 15 min, to identify mineral depositions and calcium-containing osteocytes.

## Senescence Assessment

Cells were cultured in 12-well plates with  $\alpha$ -MEM medium and then treated with tectorigenin for 1 h followed by TNF- $\alpha$  for 24 h. According to the manufacture's protocol, the  $\beta$ -galactosidase Activity Assay (Beyotime) was used to stain the cells for 24 h and the images were captured with microscope.

## Immunofluorescence

The TDSCs were prepared and then treated with tectorigenin for 1 h. The cells were then incubated with 10 ng/ml followed by TNF- $\alpha$  for 30 min. Subsequently, the cells were washed with PBS and then fixed with methanol for 20 min; 0.5% (v/v) Triton X-100 was used to permeabilize the cells and then blocked with

5% BSA for 1 h. The cells were then incubated with primary antibody against P65 at 4°C for more than 12 h, followed by incubation with fluorescein isothiocyanate-conjugated secondary antibody for 2 h. After washing with PBS, the nucleuses were stained with DAPI for 7 min, and then analyzed using fluorescence microscopy.

## Animal Experiment

Eighteen Sprague-Dawley rats (male; 200  $\pm$  10 g; 6 weeks old) were used in this experiment. The rats were divided into normal, tectorigenin-treated, and tendinopathy model groups. The tectorigenin-treated and tendinopathy model rats underwent Achilles tenotomy (Jiang et al., 2018). After anesthesia, the skin was shaved and sterilized. Subsequently, the skin and the paratenon were incised, and the fascicles of the Achilles tendon received full transection (5 mm proximal to the calcaneal insertion) perpendicular to the collagen fibers. After 1 week, the rats in the tectorigenin-treated group each received 100  $\mu$ M tectorigenin once a week at the area between the Achilles tendon and skin for 8 weeks **Supplementary Figure 2**, and the limbs of the rats were harvested thereafter. All animal experiment studies were controlled and approved by the Ethics Committee of the Second Affiliated Hospital, School of Medicine, Zhejiang University, Hangzhou, China.

## Histological Analysis and Immunohistochemical Staining

The tendon samples were cut into 4  $\mu$ M sections and then stained with HE, terminal deoxynucleotidyl transferase dUTP nick end labeling (TUNEL), and modified Masson staining according to their protocol. Immunohistochemical staining was conducted to evaluate tendinopathy in the tendon sections. The tendon sections were prepared and then subjected to antibodies against MMP-3 and MMP-13.

## Statistical Analysis

All data were represented as mean  $\pm$  SD, and one-way ANOVA with a subsequent *post hoc* Tukey method was performed for multiple comparisons. A *P*-value of less than 0.05 was considered significant.

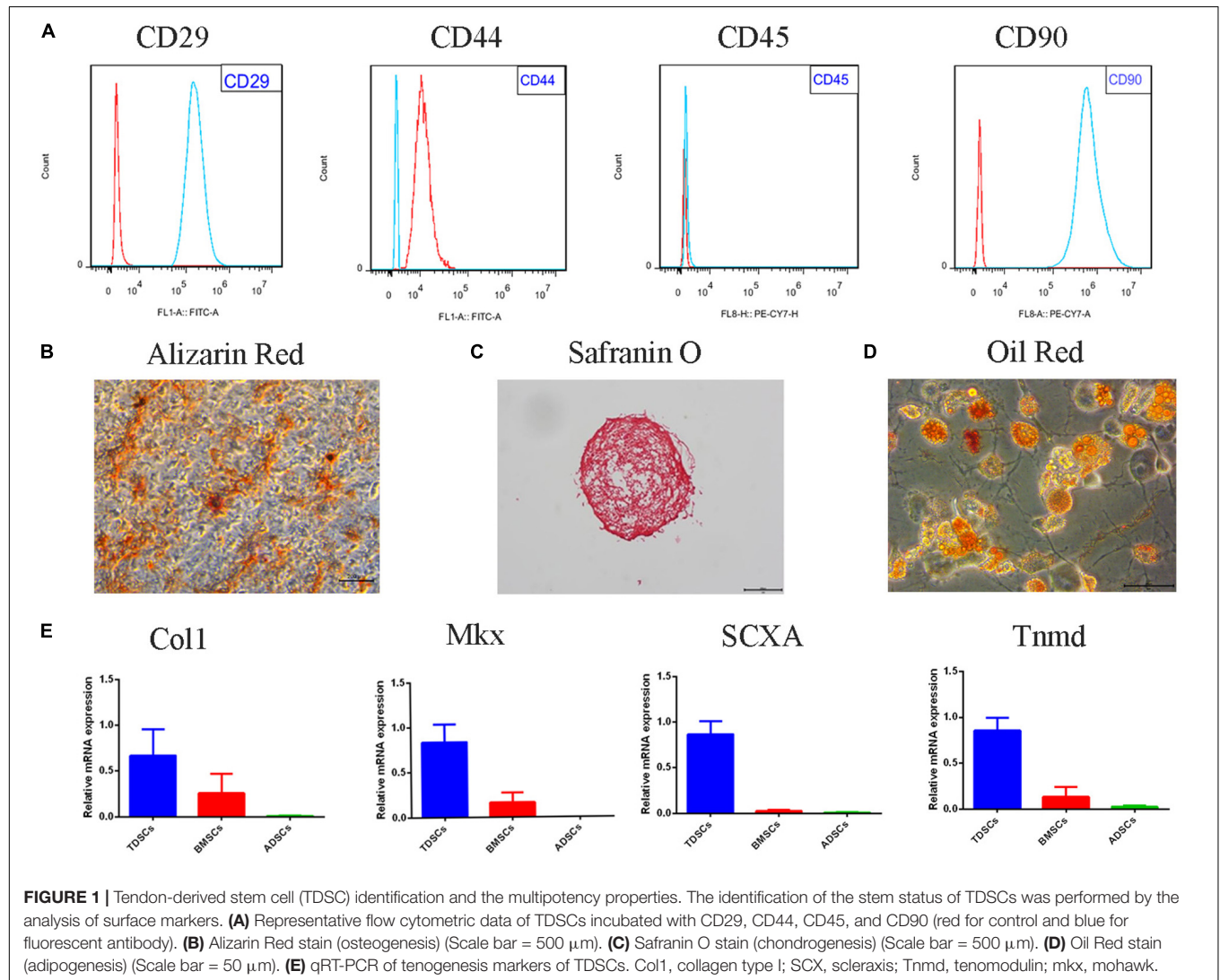
## RESULTS

### Identification of TDSCs

The TDSC surface marker analysis was conducted to identify the stem status of the cells. The findings confirmed that clonogenic cells express high levels of stem cell markers CD29, CD90, and CD44. The leukocyte marker CD45 showed undetectable levels (**Figure 1A**). In order to verify characteristics of the stem cells, multipotency of the clonogenic cells was analyzed. Alizarin Red staining showed calcium deposition in the cells layer (**Figure 1B**). Safranin O staining was used to identify of chondrogenic pellet exhibited positive potential toward chondrogenic phenotype (**Figure 1C**). Newly differentiated adipocytes were shown through Oil Red staining of adipogenic cultures (**Figure 1D**).

**TABLE 1** | Primer sequences used in this study.

Gene	Forward	Reverse
MMP-3	CAGGCATTGGCACAAGGTG	GTGGGTCACTTTCCCTGCAT
MMP-9	GCAAACCCTGCGTATTTCAT	GATAACCATCCGAGCGACCTTT
MMP-13	GCAAACCCTGCGTATTTCAT	GATAACCATCCGAGCGACCTTT
COX-2	GAGAGATGTATCCTCCACAGTCA	GACCAGGCACCAGACCAAG
iNOS	CCTACGAGGCGAAGAAGGACAG	CAGTTTGAGAGAGGAGGCTCCG
Col1	GAGAGCATGACCGATGGATT	CCTTCTTGAGGTTGCCACTC
Runx-2	ACTTCTGTGCTCGGTGCT	GACGGTTATGGTCAAGGTGAA
Scx	AACACGGCCTTCACTGCGCTG	CAGTAGCACGTTGCCAGGTG
Mkx	TTTACAAGCACCGTGACAACCC	ACAGTGTCTTCAGCCGTCGTG
Tnmd	TGGGGGAGCAAACACTTCTG	TCTTCTTCTGCCATTGCTGT
IL-6	AGCGATGATGCACTGTGAGA	GGAAGTCCAGAAGACCAGAGC
IL-10	TTCCATCCGGGTGACAATAA	TTCTGGGCCATGGTTCTCTGC
18S	CCTGAGAAACGGCTACCACA	ACCAGACTTGCCCTCCAATG



The mRNA levels of collagen type I, scleraxis, tenomodulin, and mohawk were higher in TDSCs compared with BMSCs and adipose tissue-derived stem cells (ADSCs) (Figure 1E).

## Effects of Tectorigenin on Rat TDSC Viability and Gene Expression *in vitro*

As shown in Figure 2, the CCK-8 assay was used to evaluate the cytotoxicity of tectorigenin. Tectorigenin at concentrations of 0, 10, 25, 50, 100, and 200  $\mu$ M were tested for 24 h, and the results showed that tectorigenin has no significant inhibition on TDSCs at concentrations  $\leq 100$   $\mu$ M (Figure 2A). Thus, in this work, concentrations at 50 and 100  $\mu$ M were used. Furthermore, tectorigenin did not have a significant impact on MMP-3, MMP-9, MMP-13, inducible nitric synthase (iNOS), cyclooxygenase-2 (COX-2), or collagen I in TDSCs at the protein and mRNA levels (Figures 2C,E,F).

## TNF- $\alpha$ Affects the Viability of TDSCs and Upregulates the Expression of MMPs and Inflammatory Genes *in vitro*

Similarly, CCK-8 was used to detect the influence of TNF- $\alpha$  on TDSCs. As shown in Figure 2B, TNF- $\alpha$  at concentration of 10 ng/ml showed notable suppression in TDSCs. Thus, in this experiment, 10 ng/ml was chosen. Furthermore, the effect of TNF- $\alpha$  at the 10-ng/ml concentration on MMP-3, MMP-9, MMP-13, iNOS, COX-2, and collagen I was examined at the mRNA and protein levels. The results showed that TNF- $\alpha$  is able to induce the expression of MMP-3, MMP-9, MMP-13, COX-2, and iNOS, as well as decreasing the expression of collagen I (Figures 2C,E,F).

## Tectorigenin Inhibits TNF- $\alpha$ -Induced TDSC Matrix-Degradation and Inflammatory Markers in Rat TDSCs and Alleviates Tendinopathic TDSCs

The effect of tectorigenin on TNF- $\alpha$ -induced TDSC matrix-degrading enzyme inflammation enzyme expression in rat TDSCs and in tendinopathic cells was evaluated. For normal rat TDSCs, the cells were treated with tectorigenin at concentrations 50 and 100  $\mu$ M for 1 h, and then incubated with TNF- $\alpha$  (10 ng/ml) for 24 h. The mRNA expressions of MMP-3, MMP-9, MMP-13, iNOS, COX-2, IL-6, IL-10, and collagen I were quantified using q-RT PCR. As shown in Figure 3A, the mRNA levels of MMP-3, MMP-9, MMP-13, iNOS, COX-2, IL-6, IL-10, and collagen I were alleviated by tectorigenin treatment. For protein assessment, TDSCs were cultured and treated with tectorigenin for 1 h, and then incubated with TNF- $\alpha$  (10 ng/ml) for 24 h. The cells were harvested and western blot was conducted to evaluate the protein levels of MMP-3, MMP-9, MMP-13, COX-2, iNOS, IL-6, IL-10, and collagen I. As shown in Figures 3B,C, tectorigenin at concentrations of 50 and 100  $\mu$ M is able to inhibit the TNF- $\alpha$ -induced high expression of MMP-3, MMP-9, MMP-13, COX-2, iNOS, and IL-6 and increase the expression of collagen I and IL-10. In addition, TDSCs were stimulated with TNF- $\alpha$  for 12 h to stimulate the inflammation, and then incubated with tectorigenin for 24 h. The mRNA and protein

levels were measured to detect the changes of MMP-3, MMP-9, MMP-13, COX-2, iNOS, IL-6, IL-10, and collagen I. Interestingly, the results showed the ability of tectorigenin to reduce the activation of those markers (Figures 3D–F). For the cells which were harvested from tendinopathic rats, they were divided to tendinopathy and tectorigenin treatment groups. The markers which have been described above were also evaluated at the mRNA and protein levels (Figure 4).

## Tectorigenin Inhibits TNF- $\alpha$ -Induced TDSC Apoptosis

The flow cytometry showed that tectorigenin is able to decrease TNF- $\alpha$ -induced apoptosis (Figure 5A). CCK-8 assay was performed to verify whether tectorigenin can protect TDSCs against TNF- $\alpha$ . As shown in Figure 5C, tectorigenin is able to suppress TNF- $\alpha$ -induced apoptosis in rat TDSCs. Western blotting analysis was used to evaluate the effect of tectorigenin against TNF- $\alpha$ -induced apoptosis, thus the protein levels of cleaved caspase-3, cleaved caspase-9, BAX, and Bcl<sub>2</sub> were examined in this experiment. The findings reveal that tectorigenin has the ability to decrease the TNF- $\alpha$ -induced apoptosis in TDSCs (Figures 5D,E).

## Tectorigenin Alleviates TNF- $\alpha$ -Induced TDSC Senescence

The protein level expressions of P53 and P16 were evaluated by western blotting. The data showed that cells incubated with TNF- $\alpha$  reflected high expression levels of P53 and P16, while tectorigenin decreased them (Figures 5F,G). Furthermore, the cells treated with TNF- $\alpha$  expressed a high level of SA- $\beta$ -Gal-positive TDSCs compared with the negative control group, and likewise tectorigenin was able to ameliorate this (Figure 5H).

## Tectorigenin Attenuates the Ossification in TDSCs

The mRNA and protein levels of RUNX-2 were evaluated using qRT-PCR and western blotting (Figures 6A–C). ALP staining and Alizarin Red staining were performed, and the results showed that TNF- $\alpha$  aggravated osteogenic differentiation in TDSCs. Treatment with tectorigenin showed alleviation of the ossification in TDSCs. As shown in Figure 6, RUNX-2 expression was higher in the TNF- $\alpha$ -treated group compared with the sham group and was reduced with treatment of tectorigenin. ALP staining and Alizarin Red staining showed that TNF- $\alpha$  induced osteogenic differentiation of TDSCs, while tectorigenin decreased these changes (Figures 6D–G). In this study, we stimulated the cells with TNF- $\alpha$  and then followed by tectorigenin treatment to measure the ability of tectorigenin to attenuate the ossification of TDSCs. The results showed that tectorigenin is able to alleviate TNF- $\alpha$ -induced ossification of TDSCs (Figures 6H–N).

## Tectorigenin Reduces TNF- $\alpha$ -Induced Activation of NF- $\kappa$ B and MAPK Signaling Pathway *in vitro*

Tendon-derived stem cells were pretreated with tectorigenin at concentrations of 0, 50, and 100  $\mu$ M for 1 h, and then

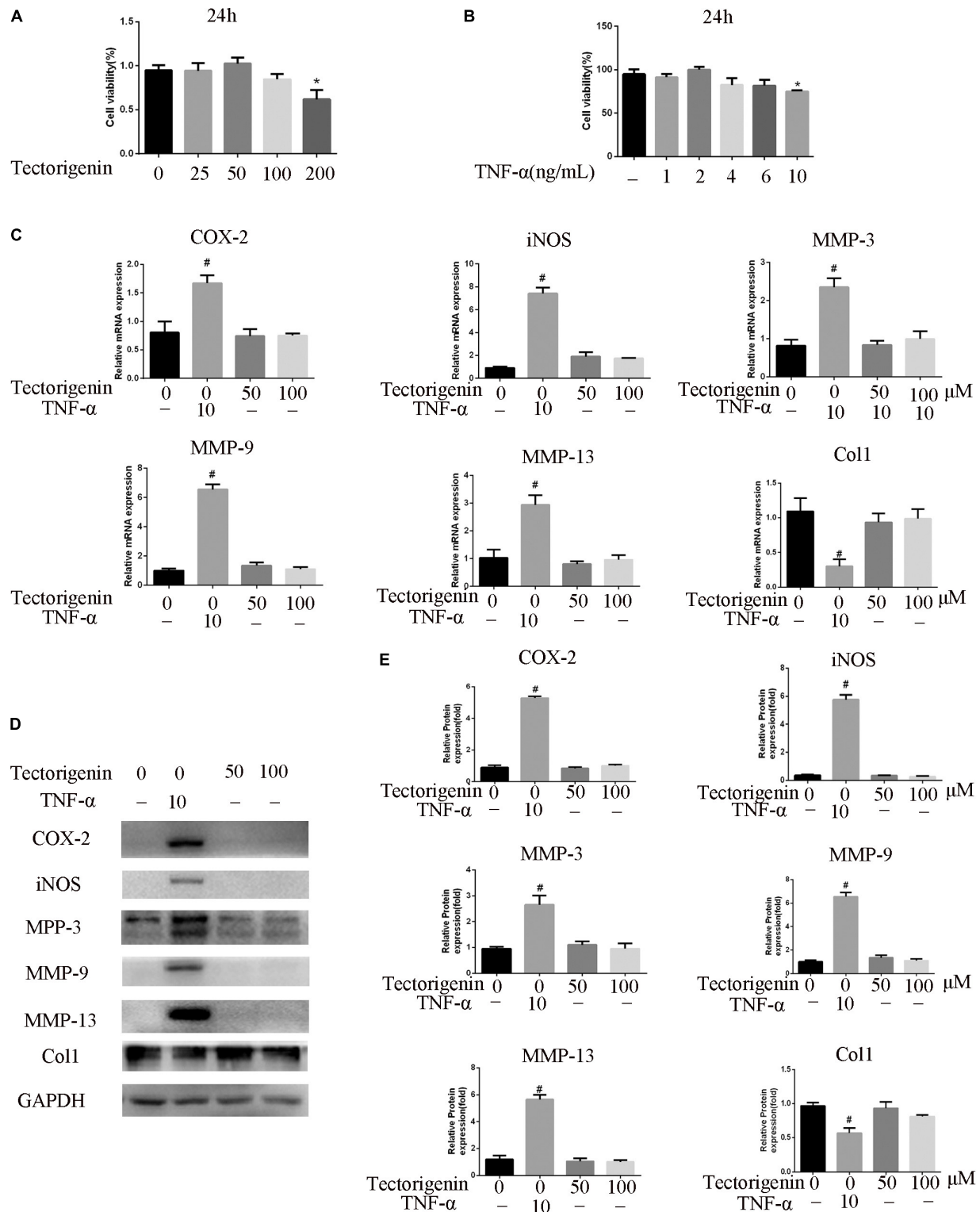


**FIGURE 2 |** The effect of tectorigenin and TNF-α on TDSCs viability. **(A)** TDSCs were incubated with various concentrations of tectorigenin for 24 h, and CCK-8 was set to measure the role of tectorigenin on TDSC viability. **(B)** Several concentrations of TNF-α were added to TDSCs for 24 h, and CCK-8 was conducted to evaluate the effect of TNF-α on TDSC viability. **(C)** TDSCs were treated with tectorigenin (50 and 100 μM) for 1 h and then incubated with TNF-α (10 ng/ml) for 24 h. **(D,E)** The expression of inflammatory markers, MMPs, and Col1 in TDSCs treated with 0, 50, and 100 μM tectorigenin in the presence and the absence of TNF-α using qRT-PCR and western blotting. The mean ± standard deviation was used to express the data,  $N = 3$ . # $P < 0.05$  vs. control group and \* $P < 0.05$  vs. TNF-α group. MMPs, matrix metalloproteinase; COX-2, cyclooxygenase-2; iNOS, inducible nitric synthase; TNF-α, tumor necrosis factor-α; Col1, collagen I.



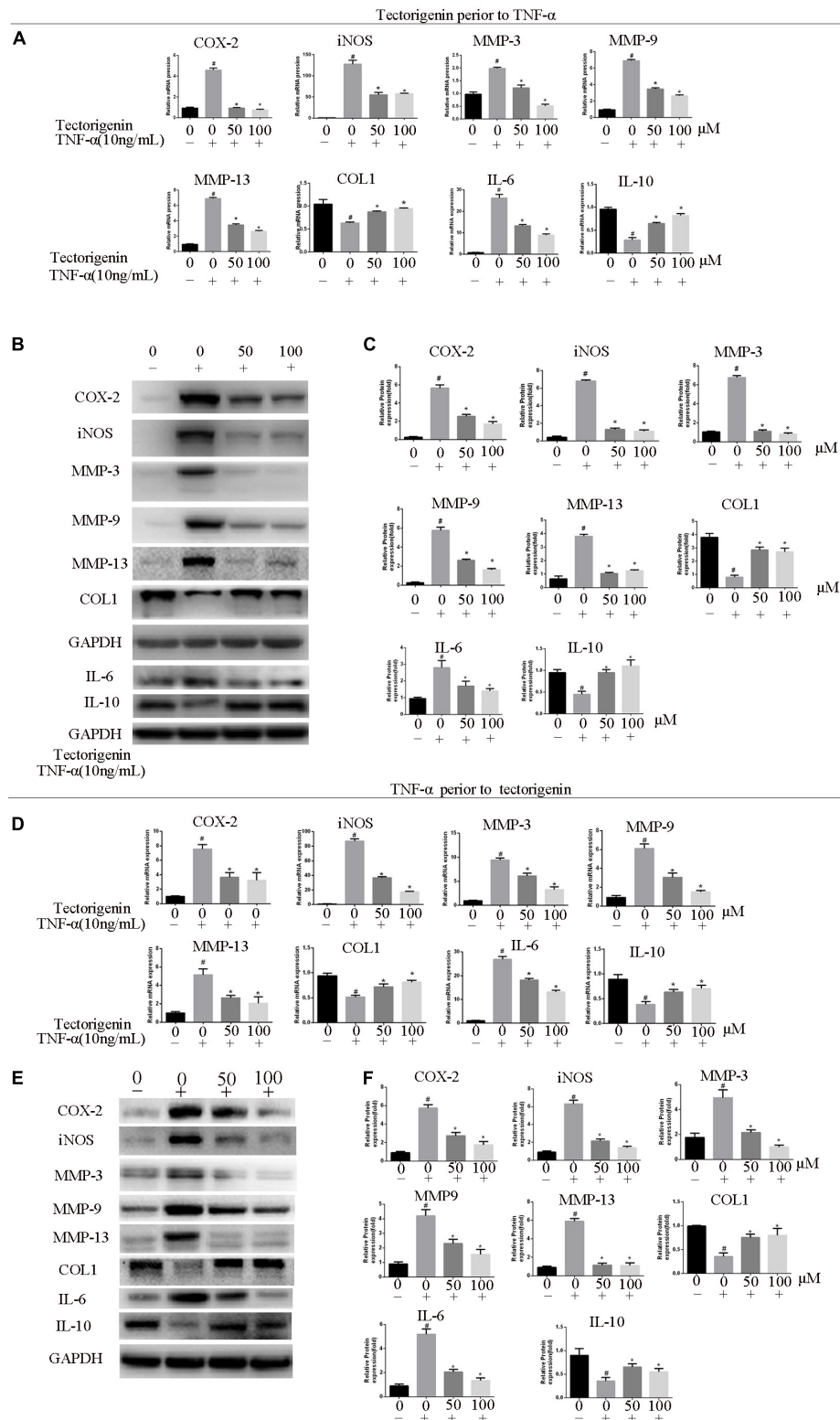


**FIGURE 3 |** Tectorigenin inhibits high expression levels of COX-2, iNOS, IL-6, and MMPs and upregulates collagen type I and IL-10 in TNF- $\alpha$ -induced tendinopathy in TDSs. TDSs were pretreated with tectorigenin and then incubated with TNF- $\alpha$  (10 ng/ml) for 24 h. **(A)** The expression of inflammatory markers, MMPs, IL-10, and collagen I were evaluated at mRNA level using qRT-PCR. **(B,C)** Western blot was used to evaluate the expression of inflammatory markers, MMPs, IL-10, and collagen I at the protein level. TDSs were stimulated with TNF- $\alpha$  to stimulate the inflammation for 12 h, and then incubated with tectorigenin for 24 h. **(D-F)** The mRNA and protein levels of the changes of MMP-3, MMP-9, MMP-13, COX-2, iNOS, IL-6, IL-10, and collagen I. The mean  $\pm$  standard deviation was used to express the data,  $N = 3$ .  $^{\#}P < 0.05$  vs. control group and  $^{*}P < 0.05$  vs. TNF- $\alpha$  group. MMPs, matrix metalloproteinase; COX-2, cyclooxygenase-2; iNOS, inducible nitric synthase; TNF- $\alpha$ , tumor necrosis factor- $\alpha$ ; Col1, collagen I.

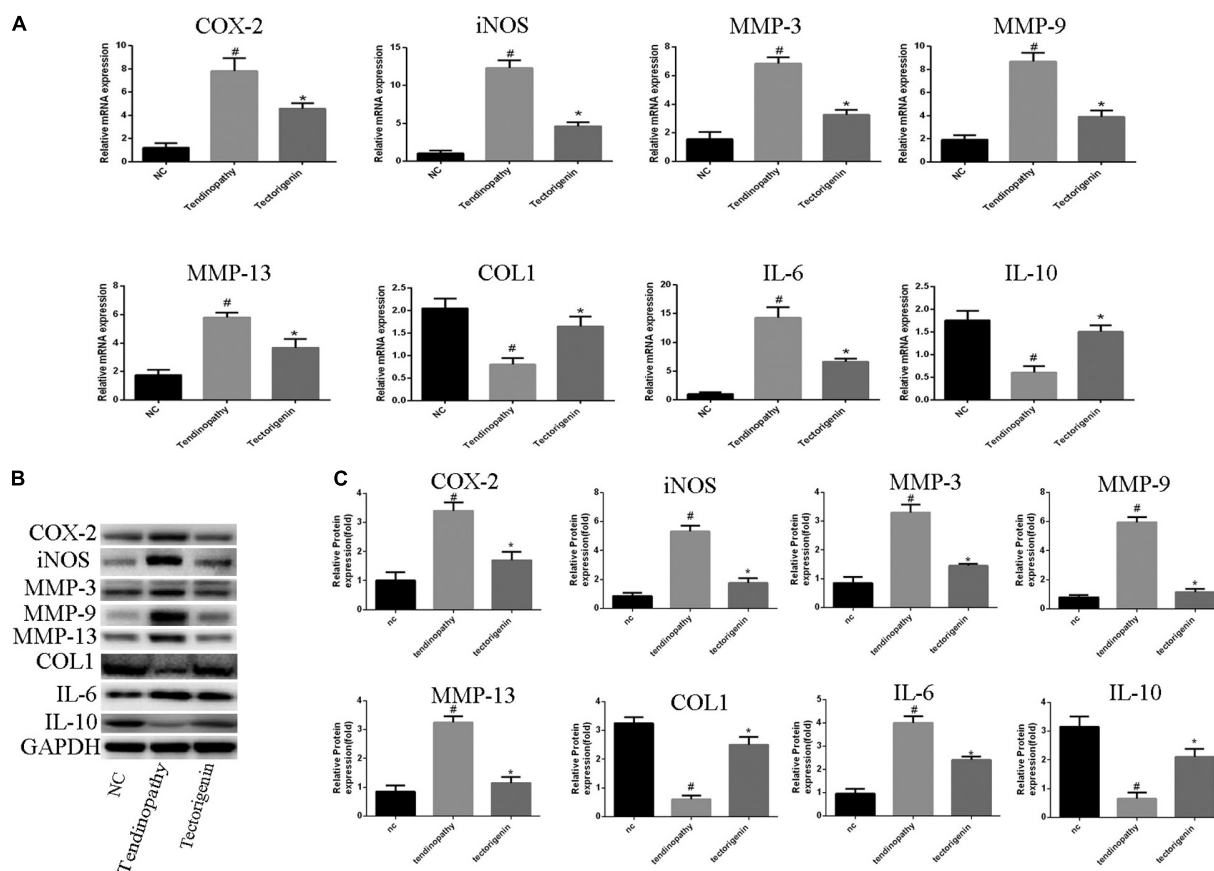


**FIGURE 4 |** The role of tectorigenin in tendinopathic rat TDSCs. The rats were received full Achilles tendon transection, and then the cells were isolated and seeded. The medium was substituted every 2 days with or without 100  $\mu$ M tectorigenin. **(A)** The expression of inflammatory markers, MMPs, IL-10, and collagen I were evaluated at mRNA level using qRT-PCR. **(B)** Western blot was used to evaluate the expression of inflammatory markers, MMPs, IL-10, and collagen I at the protein level. The mean  $\pm$  standard deviation was used to express the data,  $N = 3$ .  $^{\#}P < 0.05$  vs. control group and  $^*P < 0.05$  vs. tendinopathic cell group. MMPs, matrix metalloproteinase; COX-2, cyclooxygenase-2; iNOS, inducible nitric synthase; Col1, collagen I; IL-6, interleukin 6; IL-10, interleukin 10.

stimulated with TNF- $\alpha$  at 10 ng/ml for 30 min. Western blot assay was used to measure the protein levels of NF- $\kappa$ B (p65 and I $\kappa$ B $\alpha$ ) and MAPK (p38, Erk, and Jnk). As shown in **Figures 7, 8**, TNF- $\alpha$  activated NF- $\kappa$ B and MAPK pathways and upregulated the phosphorylation levels of p65, I $\kappa$ B $\alpha$ , P38, Erk, and Jnk. With tectorigenin treatment, all the TNF- $\alpha$  activations were inhibited. Furthermore, immunofluorescence showed that TNF- $\alpha$ -induced P65 translocation into nucleuses of TDSCs was blocked by treatment with 100  $\mu$ M tectorigenin (**Figure 7G**). In addition, TDSCs were stimulated with TNF- $\alpha$  for 30 min, and then incubated with tectorigenin for 1 h. Western blotting was conducted to detect the changes of NF- $\kappa$ B and MAPK signaling pathways. Interestingly, the results showed the ability of tectorigenin to reduce the activation of NF- $\kappa$ B (**Figures 7D–F**) and MAPK (**Figures 8E–I**). These results indicate that tectorigenin is able to inhibit the TNF- $\alpha$ -induced activation of NF- $\kappa$ B and MAPK pathways in TDSCs. Furthermore, tectorigenin is able to reduce IL-1 $\beta$ -induced activation of NF- $\kappa$ B and MAPK signaling pathways. The cells were incubated with tectorigenin for 1 h and stimulated with IL-1 $\beta$  at 10 ng/ml for 30 min. The results showed that tectorigenin

is able to inhibit IL-1 $\beta$ -induced activation of NF- $\kappa$ B and MAPK signaling pathways (**Figure 5**).

## Tectorigenin Alleviates Tendinopathy *in vivo* in Rat Model

To develop the tendinopathy model, a total of 12 rats received full Achilles tendon transection and were divided into tendinopathy model and tectorigenin-treated groups. Sham surgery was used for the six rats in the normal group. After 7 days of tendon transection, tectorigenin solution was injected weekly into the area between the Achilles tendon and skin in the tectorigenin-treated group for 8 weeks (**Figure 9A**). The effect of tectorigenin on rat tendinopathy *in vivo* was evaluated by HE staining and modified Masson staining. The arrangement of collagen fibers and fibroblasts was disrupted in the tendinopathy group compared with the sham group, and tectorigenin was able to reverse this (**Figures 9B,C**). Furthermore, as shown on X-ray image, tectorigenin was able to reverse calcification in Achilles tendons (**Figure 9D**). Additionally, immunohistochemistry staining confirmed that the tectorigenin-treated group had a

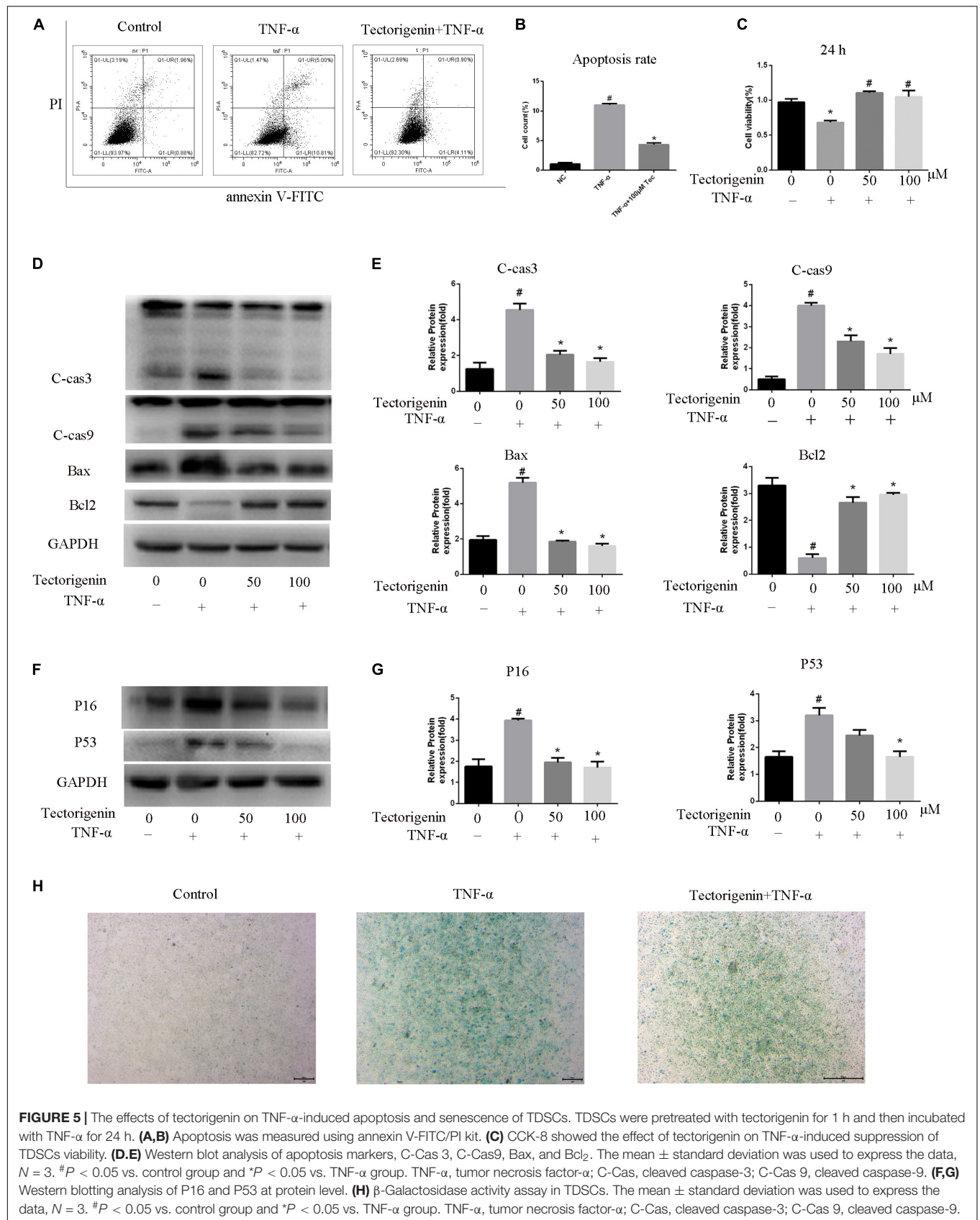


**FIGURE 5 |** The effects of tectorigenin on TNF- $\alpha$ -induced apoptosis and senescence of TDSCs. TDSCs were pretreated with tectorigenin for 1 h and then incubated with TNF- $\alpha$  for 24 h. **(A,B)** Apoptosis was measured using annexin V-FITC/PI kit. **(C)** CCK-8 showed the effect of tectorigenin on TNF- $\alpha$ -induced suppression of TDSCs viability. **(D,E)** Western blot analysis of apoptosis markers, C-Cas 3, C-Cas9, Bax, and Bcl2. The mean  $\pm$  standard deviation was used to express the data,  $N = 3$ .  $\#P < 0.05$  vs. control group and  $*P < 0.05$  vs. TNF- $\alpha$  group. TNF- $\alpha$ , tumor necrosis factor- $\alpha$ ; C-Cas, cleaved caspase-3; C-Cas 9, cleaved caspase-9. **(F,G)** Western blotting analysis of P16 and P53 at protein level. **(H)**  $\beta$ -Galactosidase activity assay in TDSCs. The mean  $\pm$  standard deviation was used to express the data,  $N = 3$ .  $\#P < 0.05$  vs. control group and  $*P < 0.05$  vs. TNF- $\alpha$  group. TNF- $\alpha$ , tumor necrosis factor- $\alpha$ ; C-Cas, cleaved caspase-3; C-Cas 9, cleaved caspase-9.

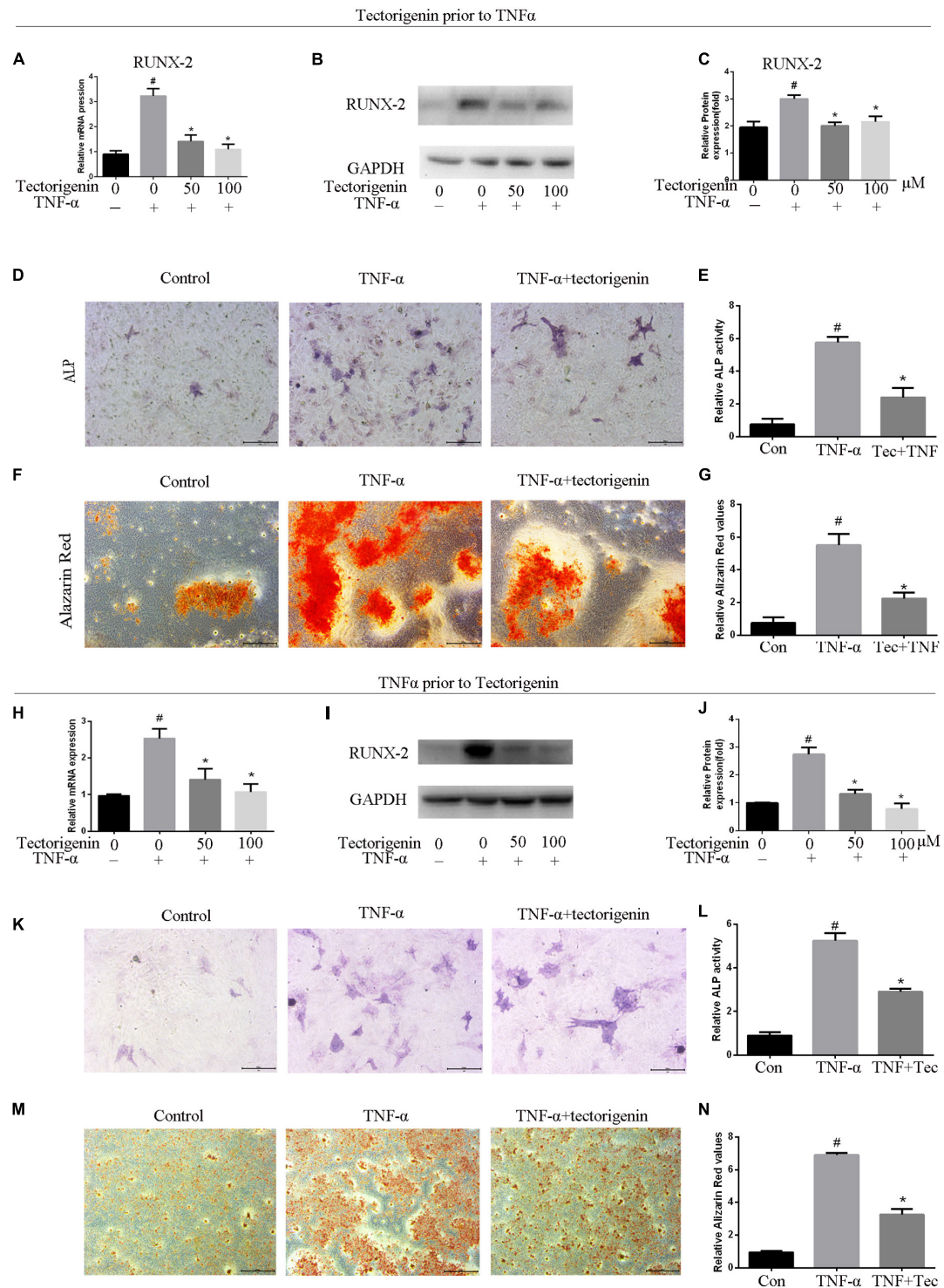


**FIGURE 6 |** Tectorigenin alleviates ossification in TDSs. The cells were cultured in osteogenic induction medium in companion with tectorigenin or TNF- $\alpha$  for 7 and 14 days. **(A)** mRNA level of RUNX-2 analyzed using qRT-PCR. **(B,C)** Protein level of RUNX-2 analyzed using western blot analysis. **(D,E)** ALP staining was set for 7 days and quantitative analysis, Scale bar = 200  $\mu$ M. **(F,G)** Alizarin Red staining was conducted in TDSs cultured for 14 days and quantitative analysis, Scale bar = 500  $\mu$ m. The second part of this figure (TNF- $\alpha$  prior to tectorigenin), the cells were stimulated with TNF- $\alpha$  followed by tectorigenin treatment. **(H)** mRNA level of RUNX-2 analyzed using qRT-PCR. **(I,J)** Protein level of RUNX-2 analyzed using western blot analysis. **(K,L)** ALP staining was set for 7 days and quantitative analysis, Scale bar = 200  $\mu$ M. **(M,N)** Alizarin Red staining was conducted in TDSs cultured for 14 days and quantitative analysis, Scale bar = 500  $\mu$ m. The mean  $\pm$  standard deviation was used to express the data,  $N = 3$ . <sup>#</sup> $P < 0.05$  vs. control group and <sup>\*</sup> $P < 0.05$  vs. TNF- $\alpha$  group. TNF- $\alpha$ , tumor necrosis factor- $\alpha$ ; ALP, alkaline phosphatase staining.



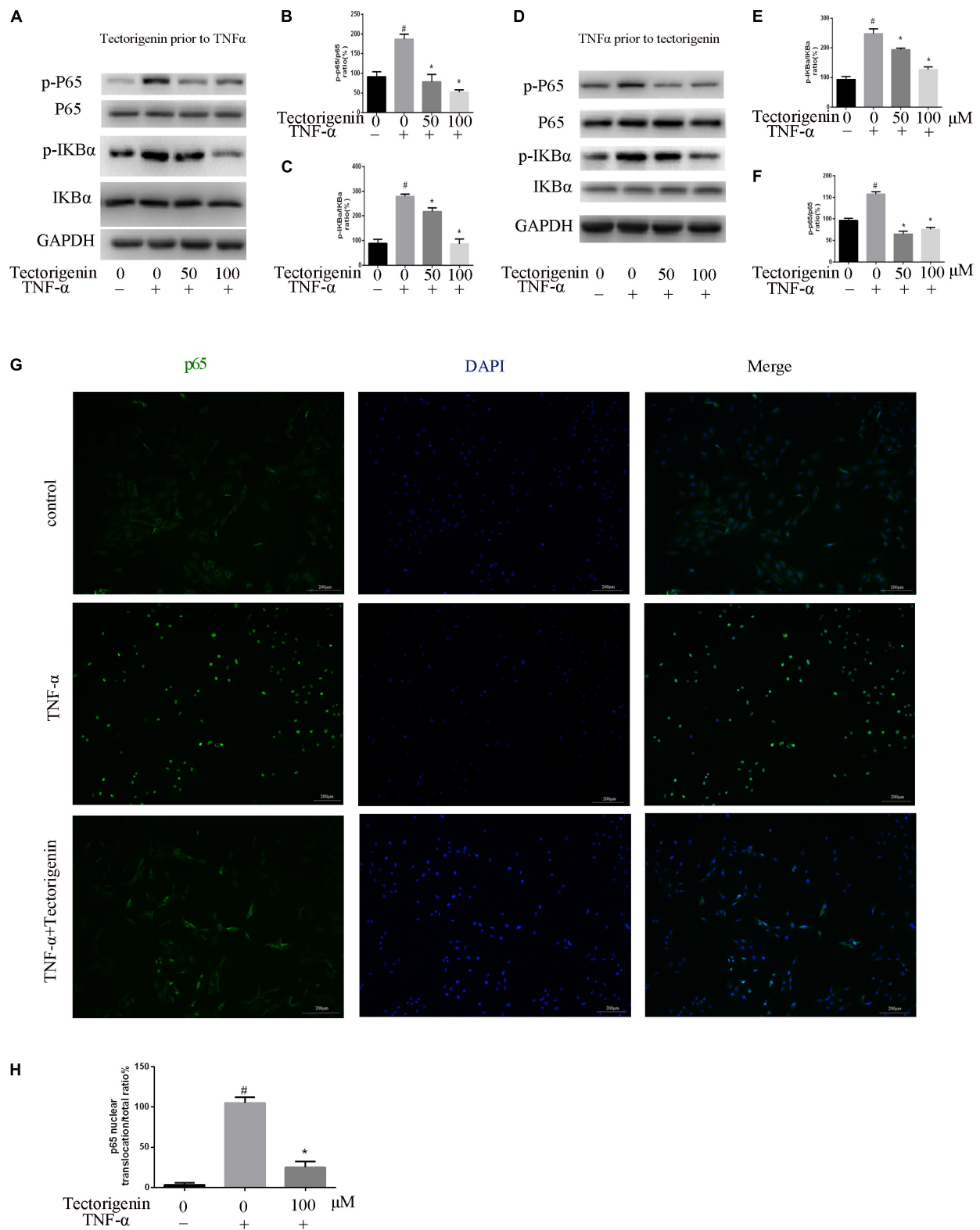
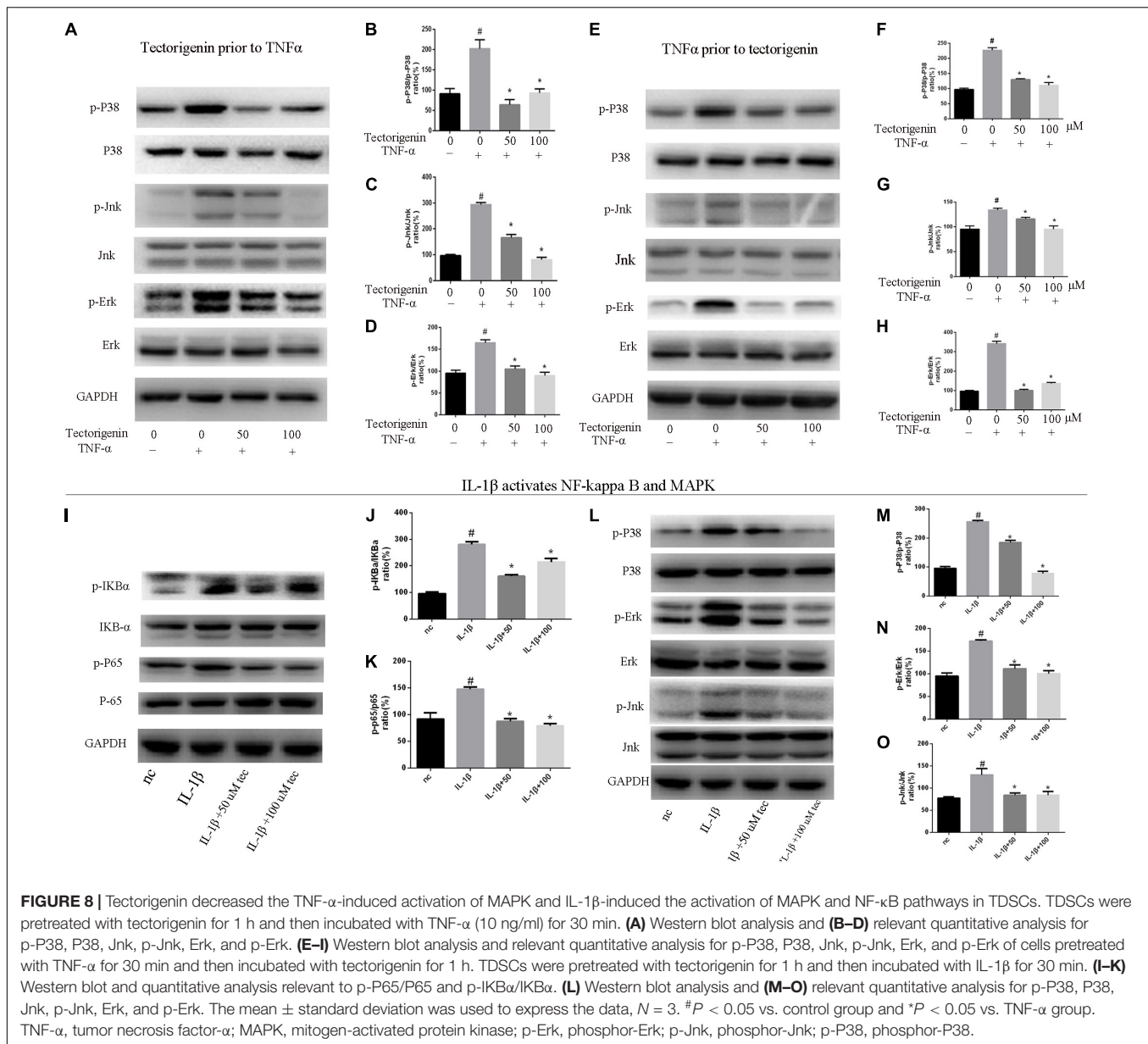


**FIGURE 7 |** Tectorigenin decreased the TNF- $\alpha$ -induced activation of nuclear factor-kappa B in TDSCs. TDSCs were pretreated with tectorigenin for 1 h and then incubated with TNF- $\alpha$  for 30 min. **(A–C)** Western blot and quantitative analysis relevant to p-P65/P65 and p-IKB $\alpha$ /IKB $\alpha$ . **(D–F)** Western blotting and the quantitative analysis relevant to p-P65/P65 and p-IKB $\alpha$ /IKB $\alpha$  of cells pretreated with TNF- $\alpha$  for 30 min and then incubated with tectorigenin for 1 h. **(G,H)** The nuclear translocation of P65 was detected by immunofluorescence microscopy. Green, p65; blue, DAPI. Scale bar = 100  $\mu$ m. The mean  $\pm$  standard deviation was used to express the data,  $N = 3$ . # $P < 0.05$  vs. control group and \* $P < 0.05$  vs. TNF- $\alpha$  group. TNF- $\alpha$ , tumor necrosis factor- $\alpha$ ; IKB $\alpha$ , nuclear factor-kappa B inhibitor  $\alpha$ .



lower expression of MMP-3 and MMP-13 compared with the positive control groups (Figures 10A,B,D,E). TUNEL staining was set to assess the apoptosis of tendon fibroblasts and showed that administration of tectorigenin can protect cells against apoptosis (Figures 10C,F). Collectively, these findings indicate that tectorigenin is able to alleviate tendinopathy in the *in vivo* rat model.

## DISCUSSION

Tendon-derived stem cells are able to differentiate into osteoblasts, tenocytes, adipocytes, chondrocytes, and fibroblasts (Lui, 2015). Among these cells, TDSCs tend to differentiate toward tenocytes (Bi et al., 2007). TDSCs serve a vital role in the

healing process of tendon after injury; however, the failure to heal may lead to tendon ossification (Yee Lui et al., 2011; Chaudhury, 2012). Thus, in this study, we investigate the effect of tectorigenin on tendinopathy in TDSCs *in vitro*.

TNF-α is well-known to inhibit the proliferation of TDSCs (Frasca et al., 2012) and induce apoptosis of TDSCs (Han et al., 2017). TNF-α can upregulate proinflammatory markers such as MMPs and IL-1 (Feldmann and Maini, 2001). Previous studies have demonstrated the association between chronic tendinopathy and the upregulation of TNF-α (Rath and Aggarwal, 1999).

In the present study, we confirmed that TNF-α induces TDSC inflammation and apoptosis as well as activates NF-κB and MAPK pathways in TDSCs. Furthermore, we verified that tectorigenin is able to reverse the TNF-α-induced dysfunction of TDSCs by regulating the NF-κB and MAPK pathways.

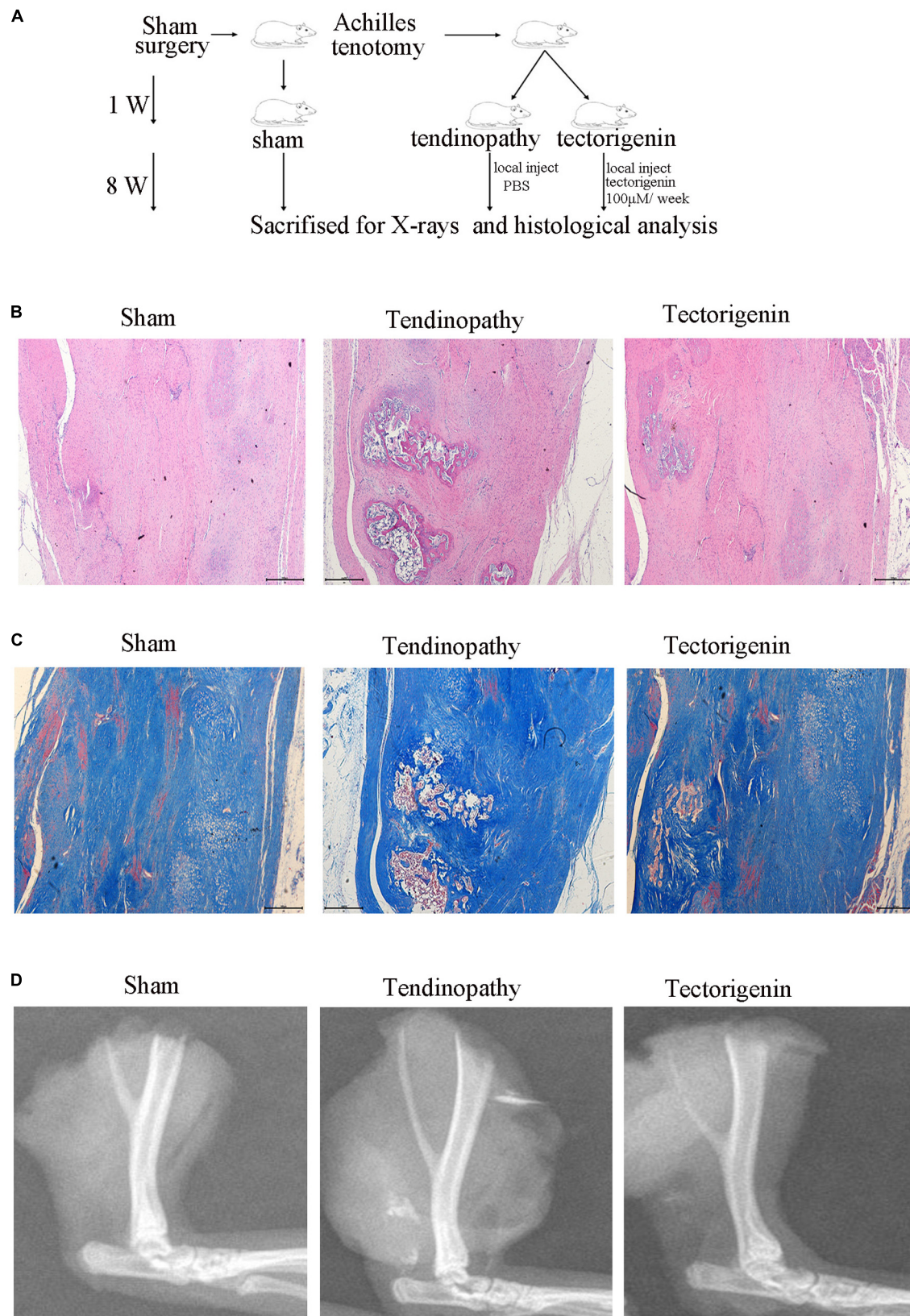


**FIGURE 9 |** Tectorigenin alleviates calcification of tendon. **(A)** A schematic representation for the *in vivo* study. **(B)** HE staining of Achilles's tendon for three groups, Scale bar = 500 µM. **(C)** Modified Masson staining of Achilles's tendon for three groups, Scale bar = 500 µM. **(D)** X-ray images of Achilles's tendon for three groups.



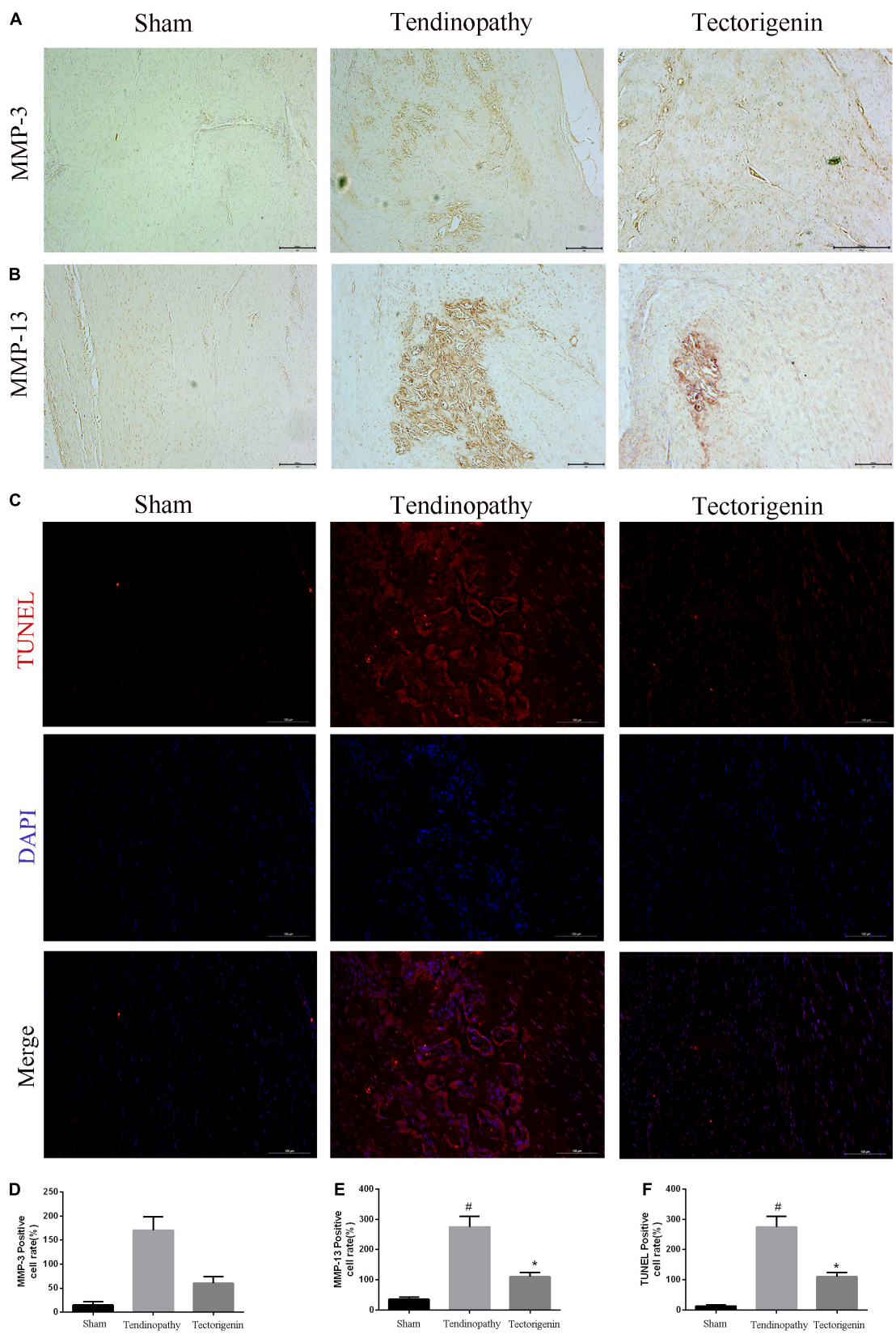


**FIGURE 10 |** The protective effect of tectorigenin in a rat tendinopathy model. **(A,B,D,E)** Immunohistochemistry for antibodies against MMP-3 and MMP-13 and quantitative analysis. **(C,F)** TUNEL staining of Achilles's tendon for three groups, Scale bar = 200 μM. #*P* < 0.05 vs. control group and \**P* < 0.05 vs. Tendinopathy group.



After the isolation of TDSCs and detection of stem cell markers, cell viability was evaluated. CCK-8 assay was used to analyze the effect of TNF- $\alpha$  and tectorigenin on TDSC viability. The results suggest that TNF- $\alpha$  suppresses TDSC viability at concentration of 10 ng/ml and tectorigenin at concentration of 200  $\mu$ M. Thus, we conducted our study using 10 ng/ml TNF- $\alpha$  and 50 and 100  $\mu$ M tectorigenin. Furthermore, we evaluated the role in tectorigenin in the absence of TNF- $\alpha$  on MMPs, collagen I, and inflammatory markers at both mRNA and protein levels. The results showed that tectorigenin has no obvious effects on the MMPs, collagen I, or inflammatory markers compared with the sham group.

It is widely accepted that the degenerative process of inflammation may lead to tendinopathy. Several inflammatory mediators, such as MMPs and COX-2 serve a role on the development of tendinopathy (Rees et al., 2014). MMPs are responsible for ECM remodeling and synthesis during tendon healing (Riley et al., 2002). COX-2 and iNOS have been known to participate in the progression of inflammatory diseases, and the suppression of iNOS and COX-2 has shown potential outcomes (Moita et al., 2013). Interleukin 6 (IL-6) was reported to inhibit the tenogenic markers of Achilles TDSC, such as collagen type I, scleraxis, and tenomodulin (Chen et al., 2018). In the present study, we found that TNF- $\alpha$  increased the expression of MMPs (MMP-3, MMP-9, and MMP-13), COX-2, IL-6, and iNOS, which were decreased in the tectorigenin treatment groups at both mRNA and protein levels. Previous studies showed that the increasing production of collagen I can enhance tendon healing (Chen et al., 2014). Interleukin (IL-10) is an anti-inflammatory cytokine that can block NF- $\kappa$ B pathway, and regulating of IL-10 family is promising for the treatment of human diseases (Wang et al., 2019b). Thus, we evaluated type I collagen and IL-10 at both mRNA and protein levels. The results showed that TNF- $\alpha$  decreased the level of collagen I and IL-10, while tectorigenin increased them.

Apoptosis is programmed cell death, which serves a vital role in tissue homeostasis. Apoptosis initiates several human diseases, such as autoimmune diseases and degenerative skeletomuscular diseases (Elmore, 2007). Generally, caspases, such as caspase-3, are tightly associated with apoptosis and are executioners of apoptosis. The regulatory proteins of apoptosis determine the fate of a cell; for example, Bax accelerates apoptosis, while Bcl-2 inhibits apoptosis (Oltvai et al., 1993). In the current study, TNF- $\alpha$  suppressed TDSC viability, upregulated apoptosis proteins (C-Cas3, C-cas9, Bax), and decreased the expression of Bcl-2, while it was alleviated by tectorigenin. Furthermore, TUNEL assay demonstrated that tendon ossification scars had a huge number of apoptotic cells in the tendinopathy group, which was alleviated by tectorigenin treatment. These outcomes suggest that tectorigenin exerts anti-apoptotic effects.

Additionally, the results showed that TNF- $\alpha$  can induce the senescence of TDSCs as well as increase the expression of P53 and P16. Senescence is an unrepairable limiting of cell growth and declination of self-renewal ability in stem cells. It is described by the increasing activity of SA- $\beta$ -gal and high expression of P53 and P16 (Helman et al., 2016; Huang et al., 2017). Our results showed that tectorigenin is able to reduce the TNF- $\alpha$ -induced high

expression of P53 and P16. Furthermore, tectorigenin decreased SA- $\beta$ -gal-positive TDSCs.

Heterotopic ossification in tendons leads to joint mobility restriction and pain. The pathogenetic process of heterotopic ossification is associated with osteoprogenitor stem cells (TDSCs) in tendon tissues. The heterotopic ossification can be a result of osteoid formation, which can be initiated by the abnormal ossification of TDSC (Jiang et al., 2018). In this study, the outcomes showed that tectorigenin reduced the TNF- $\alpha$ -induced expression of RUNX-2 and decreased the osteogenic differentiation of TDSCs, made observable by ALP staining and Alizarin Red staining. *In vivo*, HE, and modified Masson staining showed that tectorigenin alleviated the ossification of tendon tissues.

A number of evidences have shown that MAPK and NF- $\kappa$ B pathways are involved in inflammation, apoptosis, and ossification; for example, ERK regulates apoptosis, while P38 mediates apoptosis and inflammation (Zhou et al., 2015). The activation of MAPK/Jnk pathway can enhance mineralization and increase ALP activity (Wang et al., 2014). The activation of NF- $\kappa$ B has been shown to induce the activation of MAPK pathway (Wang et al., 2019a). Our results showed that TNF- $\alpha$  initiated the activation of MAPK and NF- $\kappa$ B pathways. Tectorigenin blocked the phosphorylation of p65 and reduced the translocation of phospho-p65 from cytoplasm to nucleus. Furthermore, tectorigenin reduced the phosphorylation of NF- $\kappa$ B inhibitor  $\alpha$ . At the same level, tectorigenin reduced the phosphorylation of p38, Jnk, and Erk. In this study, TDSCs were stimulated with another inflammatory markers (IL-1 $\beta$ ) to evaluate that tectorigenin usage has interfered with MAPK and NF- $\kappa$ B pathways not directly interacting with TNF- $\alpha$  itself. The results showed the ability of tectorigenin to inhibit the activation of MAPK and NF- $\kappa$ B pathways.

## CONCLUSION

Our study showed that TNF- $\alpha$  insults TDSCs and contributes to the development of tendinopathy *via* increasing the activation of MAPK and NF- $\kappa$ B pathways. Treatment with tectorigenin reduced the activation of MAPK and NF- $\kappa$ B pathways in TNF- $\alpha$ -treated TDSCs, and thus played anti-inflammatory, anti-apoptotic, anti-senescence, and anti-ossification roles. Collectively, our outcomes have revealed a new agent for the treatment of tendinopathy.

## DATA AVAILABILITY STATEMENT

The raw data supporting the conclusions of this article will be made available by the authors, without undue reservation.

## ETHICS STATEMENT

The animal study was reviewed and approved by all the animal experiment study was controlled and approved by the protocol

Ethics Committee of the Second Affiliated Hospital, School of Medicine, Zhejiang University, Hangzhou, China.

## AUTHOR CONTRIBUTIONS

LW, YX, and SM took part in the designing of the experiments, contributed reagents, materials, and analysis tools. SM, KX, and ZW ran the experiments. SM, YH, LX, JR, and CM wrote the manuscript. SM and ZC participated in the analyzing of the data. All authors read and approved the final manuscript and listed have made substantial contributions to the study.

## REFERENCES

- Akiyama, M., Yamada, O., Hideshima, T., Yanagisawa, T., Yokoi, K., Fujisawa, K., et al. (2004). TNF $\alpha$  induces rapid activation and nuclear translocation of telomerase in human lymphocytes. *Biochem Biophys Res Commun* 316, 528–532. doi: 10.1016/j.bbrc.2004.02.080
- Almekinders, L. C., and Temple, J. D. (1998). Etiology, diagnosis, and treatment of tendonitis: an analysis of the literature. *Med Sci Sports Exerc* 30, 1183–1190. doi: 10.1097/00005768-199808000-00001
- Bi, Y., Ehrichtou, D., Kilts, T. M., Inkson, C. A., Embree, M. C., Sonoyama, W., et al. (2007). Identification of tendon stem/progenitor cells and the role of the extracellular matrix in their niche. *Nat Med* 13, 1219–1227. doi: 10.1038/nm1630
- Chaudhury, S. (2012). Mesenchymal stem cell applications to tendon healing. *Muscles Ligaments Tendons J* 2, 222–229.
- Chen, L., Liu, J. P., Tang, K. L., Wang, Q., Wang, G. D., Cai, X. H., et al. (2014). Tendon derived stem cells promote platelet-rich plasma healing in collagenase-induced rat achilles tendinopathy. *Cell Physiol Biochem* 34, 2153–2168. doi: 10.1159/000369659
- Chen, S., Deng, G., Li, K., Zheng, H., Wang, G., Yu, B., et al. (2018). Interleukin-6 promotes proliferation but inhibits tenogenic differentiation via the Janus kinase/signal transducers and activators of transcription 3 (JAK/STAT3) pathway in tendon-derived stem cells. *Medical science monitor: international medical journal of experimental and clinical research* 24, 1567. doi: 10.12659/msm.908802
- Elmore, S. (2007). Apoptosis: a review of programmed cell death. *Toxicol Pathol* 35, 495–516.
- Feldmann, M., and Maini, R. N. (2001). Anti-TNF alpha therapy of rheumatoid arthritis: what have we learned? *Annu Rev Immunol* 19, 163–196.
- Frasca, D., Romero, M., Diaz, A., Alter-Wolf, S., Ratliff, M., Landin, A. M., et al. (2012). A molecular mechanism for TNF- $\alpha$ -mediated downregulation of B cell responses. *J Immunol* 188, 279–286. doi: 10.4049/jimmunol.1003964
- Han, P., Cui, Q., Yang, S., Wang, H., Gao, P., and Li, Z. (2017). Tumor necrosis factor- $\alpha$  and transforming growth factor- $\beta$ 1 facilitate differentiation and proliferation of tendon-derived stem cells in vitro. *Biotechnol Lett* 39, 711–719. doi: 10.1007/s10529-017-2296-3
- Helman, A., Klochendler, A., Azazmeh, N., Gabai, Y., Horwitz, E., Anzi, S., et al. (2016). p16(Ink4a)-induced senescence of pancreatic beta cells enhances insulin secretion. *Nat Med* 22, 412–420.
- Hosaka, Y., Kirisawa, R., Ueda, H., Yamaguchi, M., and Takehana, K. (2005). Differences in tumor necrosis factor (TNF) $\alpha$  and TNF receptor-1-mediated intracellular signaling factors in normal, inflamed and scar-formed horse tendons. *J Vet Med Sci* 67, 985–991. doi: 10.1292/jvms.67.985
- Huang, W., Ao, P., Li, J., Wu, T., Xu, L., Deng, Z., et al. (2017). Autophagy Protects Advanced Glycation End Product-Induced Apoptosis and Expression of MMP-3 and MMP-13 in Rat Chondrocytes. *Biomed Res Int* 2017, 634 1919.
- Jiang, H., Chen, Y., Chen, G., Tian, X., Tang, J., Luo, L., et al. (2018). Leptin accelerates the pathogenesis of heterotopic ossification in rat tendon tissues via mTORC1 signaling. *J Cell Physiol* 233, 1017–1028. doi: 10.1002/jcp.25955

## FUNDING

This work was supported by the National Science Foundation of Zhejiang Province (LD19H060001) and the National Natural Science Foundation of China (Hangzhou, China; grant nos. 81871793 and 82001458).

## SUPPLEMENTARY MATERIAL

The Supplementary Material for this article can be found online at: <https://www.frontiersin.org/articles/10.3389/fcell.2020.568894/full#supplementary-material>

- John, T., Lodka, D., Kohl, B., Ertel, W., Jammrath, J., Conrad, C., et al. (2010). Effect of pro-inflammatory and immunoregulatory cytokines on human tenocytes. *J Orthop Res* 28, 1071–1077.
- Kaleağasioglu, F., Olcay, E., and Olgaç, V. J. K. S. (2017). Sports Traumatology, Arthroscopy, Statin-induced calcific Achilles tendinopathy in rats: comparison of biomechanical and histopathological effects of simvastatin, atorvastatin and rosuvastatin\*. 25, 1884–1891. doi: 10.1007/s00167-015-3728-z
- Lim, H. S., Kim, Y. J., Kim, B. Y., Park, G., and Jeong, S. J. (2018). The Anti-neuroinflammatory Activity of Tectorigenin Pretreatment via Downregulated NF- $\kappa$ B and ERK/JNK Pathways in BV-2 Microglial and Microglia Inactivation in Mice With Lipopolysaccharide. *Front Pharmacol* 9:462. doi: 10.3389/fphar.2018.00462
- Lin, X., Huang, M., Yin, G., Zhang, J., Zhang, Z., Lai, P., et al. (2018). Characterization of a Novel Calcific Achilles Tendinopathy Model in Mice: Contralateral Tendinopathy Induced by Unilateral Tenotomy. *Calcif Tissue Int* 103, 698–707. doi: 10.1007/s00223-018-0465-6
- Lui, P. P. (2015). A practical guide for the isolation and maintenance of stem cells from tendon. *Methods Mol Biol* 1212, 127–140. doi: 10.1007/7651\_2014\_92
- Ma, C., Xu, K., Meng, J., Ran, J., Adel Abdo Moqbel, S., Liu, A., et al. (2018). Tectorigenin inhibits RANKL-induced osteoclastogenesis via suppression of NF- $\kappa$ B signalling and decreases bone loss in ovariectomized C57BL/6. *J Cell Mol Med* 22, 5121–5131. doi: 10.1111/jcmm.13801
- Machner, A., Baier, A., Wille, A., Drynda, S., Pap, G., Drynda, A., et al. (2003). Higher susceptibility to Fas ligand induced apoptosis and altered modulation of cell death by tumor necrosis factor-alpha in periarthritic tenocytes from patients with knee joint osteoarthritis. *Arthritis Res Ther* 5, R253–R261. doi: 10.1084/jem.187.5.711
- Millar, N., Wei, A. Q., Molloy, T. J., Bonar, F., and Murrell, G. A. (2009). Cytokines and apoptosis in supraspinatus tendinopathy. *J Bone Joint Surg Br* 91, 417–424. doi: 10.1302/0301-620x.91b3.21652
- Moita, E., Gil-Izquierdo, A., Sousa, C., Ferreres, F., Silva, L. R., Valentão, P., et al. (2013). Integrated analysis of COX-2 and iNOS derived inflammatory mediators in LPS-stimulated RAW macrophages pre-exposed to Echinium plantagineum L. bee pollen extract. *PLoS One* 8:e59131. doi: 10.1371/journal.pone.0059131
- Morita, W., Dakin, S. G., Snelling, S. J. B., and Carr, A. J. (2017). Cytokines in tendon disease: A Systematic Review. *Bone Joint Res* 6, 656–664. doi: 10.1302/2046-3758.612.bjr-2017-0112.r1
- Ni, M., Lui, P. P., Rui, Y. F., Lee, Y. W., Lee, Y. W., Tan, Q., et al. (2012). Tendon-derived stem cells (TDSCs) promote tendon repair in a rat patellar tendon window defect model. *J Orthop Res* 30, 613–619. doi: 10.1002/jor.21559
- Oltvai, Z. N., Millman, C. L., and Korsmeyer, S. J. (1993). Bcl-2 heterodimerizes in vivo with a conserved homolog, Bax, that accelerates programmed cell death. *Cell* 74, 609–619. doi: 10.1016/0092-8674(93)90509-o
- Rath, P. C., and Aggarwal, B. B. (1999). TNF-induced signaling in apoptosis. *J Clin Immunol* 19, 350–364.
- Rees, J. D., Stride, M., and Scott, A. (2014). Tendons—time to revisit inflammation. *Br J Sports Med* 48, 1553–1557. doi: 10.1136/bjsports-2012-091957
- Riley, G. P., Curry, V., DeGroot, J., van El, B., Verzijl, N., Hazleman, B. L., et al. (2002). Matrix metalloproteinase activities and their relationship with collagen

- remodelling in tendon pathology. *Matrix Biol* 21, 185–195. doi: 10.1016/s0945-053x(01)00196-2
- Schulze-Tanzil, G., Al-Sadi, O., Wiegand, E., Ertel, W., Busch, C., Kohl, B., et al. (2011). The role of pro-inflammatory and immunoregulatory cytokines in tendon healing and rupture: new insights. *Scand J Med Sci Sports* 21, 337–351. doi: 10.1111/j.1600-0838.2010.01265.x
- Shi, L., Li, Y., Dai, G., Lin, Y. C., Li, G., Wang, C., et al. (2019). Impaired function of tendon-derived stem cells in experimental diabetes mellitus rat tendons: implications for cellular mechanism of diabetic tendon disorder. *Stem Cell Res Ther* 10, 27.
- Wang, L., Lee, W., Cui, Y. R., Ahn, G., and Jeon, Y. J. (2019a). Protective effect of green tea catechin against urban fine dust particle-induced skin aging by regulation of NF- $\kappa$ B, AP-1, and MAPKs signaling pathways. *Environ Pollut* 252(Pt B), 1318–1324. doi: 10.1016/j.envpol.2019.06.029
- Wang, Q., Cheng, X.-L., Zhang, D.-Y., Gao, X.-J., Zhou, L., Qin, X.-Y., et al. (2013). Tectorigenin Attenuates Palmitate-Induced Endothelial Insulin Resistance via Targeting ROS-Associated Inflammation and IRS-1 Pathway. *PLoS One* 8:e66417. doi: 10.1371/journal.pone.0066417
- Wang, X., Wong, K., Ouyang, W., and Rutz, S. (2019b). Targeting IL-10 family cytokines for the treatment of human diseases. *Cold Spring Harbor perspectives in biology* 11, a028548. doi: 10.1101/cshperspect.a028548
- Wang, Y., Li, J., Song, W., and Yu, J. (2014). Mineral trioxide aggregate upregulates odonto/osteogenic capacity of bone marrow stromal cells from craniofacial bones via JNK and ERK MAPK signalling pathways. *Cell Prolif* 47, 241–248. doi: 10.1111/cpr.12099
- Xu, L., Xu, K., Wu, Z., Chen, Z., He, Y., Ma, C., et al. (2020). Pioglitazone attenuates advanced glycation end products-induced apoptosis and calcification by modulating autophagy in tendon-derived stem cells. *J Cell Mol Med* 24, 2240–2251. doi: 10.1111/jcmm.14901
- Yee Lui, P. P., Wong, Y. M., Rui, Y. F., Lee, Y. W., Chan, L. S., and Chan, K. M. (2011). Expression of chondro-osteogenic BMPs in ossified failed tendon healing model of tendinopathy. *J Orthop Res* 29, 816–821. doi: 10.1002/jor.21313
- Zhou, J., Du, T., Li, B., Rong, Y., Verkhatsky, A., Peng, L., et al. (2015). Crosstalk Between MAPK/ERK and PI3K/AKT Signal Pathways During Brain Ischemia/Reperfusion. *ASN Neuro* 7, 1759091415602463.

**Conflict of Interest:** The authors declare that the research was conducted in the absence of any commercial or financial relationships that could be construed as a potential conflict of interest.

Copyright © 2020 Moqbel, Xu, Chen, Xu, He, Wu, Ma, Ran, Wu and Xiong. This is an open-access article distributed under the terms of the Creative Commons Attribution License (CC BY). The use, distribution or reproduction in other forums is permitted, provided the original author(s) and the copyright owner(s) are credited and that the original publication in this journal is cited, in accordance with accepted academic practice. No use, distribution or reproduction is permitted which does not comply with these terms.



# New Amphiphilic Squalene Derivative Improves Metabolism of Adipocytes Differentiated From Diabetic Adipose-Derived Stem Cells and Prevents Excessive Lipogenesis

Munkhzul Ganbold<sup>1</sup>, Farhana Ferdousi<sup>1,2</sup>, Takashi Arimura<sup>1</sup>, Kenichi Tominaga<sup>1</sup> and Hiroko Isoda<sup>1,2,3\*</sup>

<sup>1</sup> National Institute of Advanced Industrial Science and Technology (AIST)-University of Tsukuba Open Innovation Laboratory for Food and Medicinal Resource Engineering (FoodMed-OIL), Tsukuba, Ibaraki, Japan, <sup>2</sup> Alliance for Research on the Mediterranean and North Africa (ARENA), University of Tsukuba, Tsukuba, Ibaraki, Japan, <sup>3</sup> Faculty of Life and Environmental Sciences, University of Tsukuba, Tsukuba, Ibaraki, Japan

## OPEN ACCESS

### Edited by:

Dariusz Widera,  
University of Reading,  
United Kingdom

### Reviewed by:

Joseph Isaac Shapiro,  
Marshall University, United States  
Gianpaolo Papaccio,  
Second University of Naples, Italy

### \*Correspondence:

Hiroko Isoda  
isoda.hiroko.ga@u.tsukuba.ac.jp

### Specialty section:

This article was submitted to  
Stem Cell Research,  
a section of the journal  
*Frontiers in Cell and Developmental  
Biology*

**Received:** 29 June 2020

**Accepted:** 14 October 2020

**Published:** 04 November 2020

### Citation:

Ganbold M, Ferdousi F, Arimura T,  
Tominaga K and Isoda H (2020) New  
Amphiphilic Squalene Derivative  
Improves Metabolism of Adipocytes  
Differentiated From Diabetic  
Adipose-Derived Stem Cells  
and Prevents Excessive Lipogenesis.  
*Front. Cell Dev. Biol.* 8:577259.  
doi: 10.3389/fcell.2020.577259

Squalene (Sq) is a natural compound, found in various plant oils, algae, and larger quantity in deep-sea shark liver. It is also known as an intermediate of cholesterol synthesis in plants and animals including humans. Although evidences demonstrated its antioxidant, anticancer, hypolipidemic, and hepatoprotective and cardioprotective effects, its biological effects in cellular function might have been underestimated because of the water-insoluble property. To overcome this hydrophobicity, we synthesized new amphiphilic Sq derivative (HH-Sq). On the other hand, adipose-derived stem cells (ASCs) are a valuable source in regenerative medicine for its ease of accessibility and multilineage differentiation potential. Nevertheless, impaired cellular functions of ASCs derived from diabetic donor have still been debated controversially. In this study, we explored the effect of the HH-Sq in comparison to Sq on the adipocyte differentiation of ASCs obtained from subjects with type 2 diabetes. Gene expression profile by microarray analysis at 14 days of adipogenic differentiation revealed that HH-Sq induced more genes involved in intracellular signaling processes, whereas Sq activated more transmembrane receptor pathway-related genes. In addition, more important number of down-regulated and up-regulated genes by Sq and HH-Sq were not overlapped, suggesting the compounds might not only have difference in their chemical property but also potentially exert different biological effects. Both Sq and HH-Sq improved metabolism of adipocytes by enhancing genes associated with energy homeostasis and insulin sensitivity, *SIRT1*, *PRKAA2*, and *IRS1*. Interestingly, Sq increased significantly early adipogenic markers and lipogenic gene expression such as *PPARG*, *SREBF1*, and *CEBPA*, but not HH-Sq. As a consequence, smaller and fewer lipid droplet formation was observed in HH-Sq-treated adipocytes. Based on our



findings, we report that both Sq and HH-Sq improved adipocyte metabolism, but only HH-Sq prevented excessive lipogenesis without abrogating adipocyte differentiation. The beneficial effect of HH-Sq provides an importance of synthesized derivatives from a natural compound with therapeutic potentials in the application of cell therapies.

**Keywords:** squalene, derivative, ASC, diabetes, adipose-derived stem cell differentiation, adipocyte metabolism, adipocyte differentiation

## INTRODUCTION

Human adipose-derived stem cells (ASCs) are adult stem cells obtainable by liposuction procedure. By definition, ASCs present high capacity to proliferate after isolation without losing their stemness, at the same time potential to differentiate into mesodermal cell lineages, including adipocytes, chondrocytes, osteocytes, and myocytes under appropriate inducing condition.

The therapeutic and regenerative effect of ASCs on insulin resistance, obesity, and type 2 diabetes (T2D)-associated complications has been investigated for a variety of purposes (Mazini et al., 2020). For example, multiple infusion of ASCs in diabetes-induced rats reversed diabetes-related complications and protected tissue damages by alleviating inflammation (Yu et al., 2019). A recent study revealed that subcutaneous transplantation of ASC sheet prepared from non-diabetic mice into diabetic mice improved glucose intolerance (Ishida et al., 2020). Subcutaneous injection and local administration of human adipose-derived stromal vascular fraction cells showed a beneficial effect on microcirculation in ischemic diabetic feet and wound healing (Nie et al., 2011; Moon et al., 2019). Moreover, its application in tissue engineering and fat grafting in reconstructive surgery is being extensively explored (Naderi et al., 2014, 2017).

However, previous studies raised questions about the effectiveness of ASCs isolated from a diabetic and obese donor on the clinical use of stem cells because of the predisposition of impaired biological functions and altered transcriptomes due to its microenvironment, thus diminishing its therapeutic value and further cellular function in the recipient. Proliferation, viability, and migration capacity of ASCs from the obese environment are reduced, and its transcriptome is altered and inflamed (Vyas et al., 2019).

Squalene (Sq), a polyunsaturated hydrocarbon, is found ubiquitously in numerous plant oils (Owen et al., 2000; He et al., 2002; Shimizu et al., 2019) and algae (Kaya et al., 2011) and also larger quantity in deep-sea shark liver (Hernández-Pérez et al., 1997). Sq is also synthesized in plants and animals including humans as an intermediate of sterol synthesis such as cholesterol. Knockout murine in which upstream enzyme of Sq synthesis was disrupted presented lipid dystrophy, hepatic steatosis, and severe diabetic abnormalities, showing its indispensable physiological function in the organism (Yeh et al., 2018). Numerous evidences demonstrated its antioxidant, anticancer, hypolipidemic, and hepatoprotective and cardioprotective effects. Dietary Sq supplement (1%) prevented colon carcinogenesis in rats (Rao et al., 1998); rabbits fed with Sq (3%) for 7 weeks unexpectedly showed no more atheroma

than the controls (Kritchevsky et al., 1953); moreover, in Sq feeding (900 mg/d) in human studies, serum triglyceride and cholesterol contents were unchanged (Strandberg et al., 1990). Interestingly, contrary to the expected, in the same studies, Sq feeding did not increase serum cholesterol level, whereas serum Sq level was augmented 17 times in humans after 30 days. These findings altogether suggest that Sq might be accumulated in the serum because of the lack of efficient absorption, even though its biological effect is beneficial.

Naturally, Sq is characterized as a hydrophobic lipid, and its biological properties in cellular function might have been underestimated because of the low solubility. Thus, to overcome this water-insoluble property, a recent study proposed a lysosome-embedded Sq structure and showed its preferential cytotoxic effect on LAN5 cancer cells in their preliminary study (Costa et al., 2018).

We have recently synthesized Sq derivative (HH-Sq) (Sasaki et al., 2020), which gained amphiphilic property compared to Sq. In this *in vitro* study, we explored the effect of HH-Sq compared to Sq on adipocyte differentiation of ASCs derived from diabetic donors to determine whether the gained hydrophilicity of the derivative can promote Sq's biological effects and eventually be used in therapeutic application.

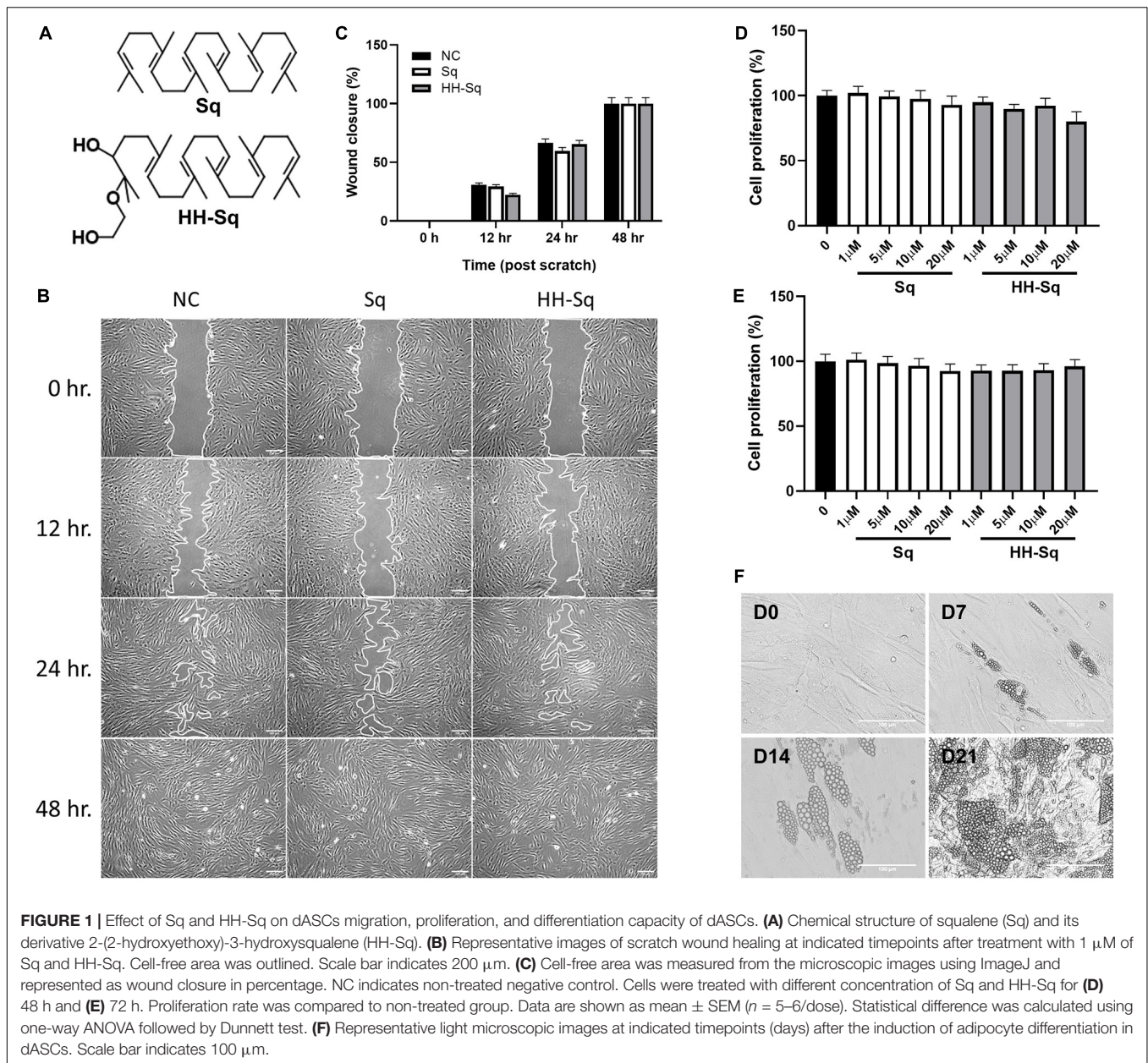
## MATERIALS AND METHODS

### Chemicals

Squalene was purchased from Fujifilm Wako (Tokyo, Japan). Sq mono ethylene glycol derivative, (2-(2-hydroxyethoxy)-3-hydroxysqualene) (HH-Sq), was synthesized as reported previously (Sasaki et al., 2020) and identified by spectral data (Figure 1A).

### Adipose-Derived Stem Cells Culture

Diabetic ASCs (dASCs) (T2D; 74-year-old Caucasian woman, body mass index = 25 kg/m<sup>2</sup>) was purchased from Lonza (Walkersville, MD, United States; Material number: PT-5008, tissue acquisition number: 29752). These cells were isolated from donated human tissue after obtaining permission for their use in research only by informed consent or legal authorization. Cells were cultured in ASC growth medium (ADSC-GM BulletKit<sup>TM</sup>) obtained from Lonza containing ASC basal medium supplemented with 10% fetal bovine serum, 1% L-glutamine, and gentamicin-amphotericin B (GA-1000) according to the manufacturer's instruction at 37°C in 5% CO<sub>2</sub> humidified incubator. Cells are subcultured 5,000 cells per cm<sup>2</sup> as recommended by the provider.



## Adipogenic Differentiation of dASCs

Cells were seeded at a density of  $3 \times 10^4$  cells per  $\text{cm}^2$  in the preadipocyte growth medium (PGM-2<sup>TM</sup> BulletKit; Lonza, Walkersville, MD, United States). Once cells reach confluence greater than 80%, adipogenesis is induced by changing medium to adipogenic differentiation medium (ADM). According to the manufacturer's instruction, ADM was prepared by adding rhInsulin, dexamethasone, IBMX, and indomethacin into PGM. The medium was changed every 10 to 12 days.

## Cell Proliferation Assay

Cell proliferation was determined using the CellTiter 96<sup>®</sup> AQueous One Solution Cell Proliferation Assay (Promega, Madison, WI, United States). Briefly, cells were seeded at

a density of  $1 \times 10^4$  cells per well in 96-well plate for overnight and then treated with increasing concentration of Sq and HH-Sq. After 24 and 48 h of incubation, 20  $\mu$ L per well of CellTiter 96<sup>®</sup> AQueous One Solution Reagent was added and incubated for 3 h. Soluble formazan produced was measured by absorbance at 490 nm using a microplate reader (Varioskan LUX).

## Cell Migration/Scratch Assay

Cells were grown in ADSC-GM until confluence in 6-well plate and then washed with phosphate-buffered saline (PBS) two times, scratched using a sterile 10  $\mu$ L micropipette tip, and incubated in ADSC-GM with treatment; the microscopic photo was taken at several timepoints; the cell-free area was measured using ImageJ.

## Lipid Droplets Staining

Cells were seeded on a chamber slide, and adipogenesis differentiation was induced in the presence or absence of Sq and HH-Sq as described above. Lipid droplets (LDs) formed after differentiation were stained by fluorescent neutral lipid dye 4,4-difluoro-1,3,5,7,8-pentamethyl-4-bora-3a,4a-diaza-s-indacene (BODIPY 493/503; Invitrogen, Eugene, OR, United States), mounted with ProLong™ Diamond Antifade Mountant with DAPI (Invitrogen, Eugene, OR, United States) for staining nucleus, and fluorescence images were obtained by using Leica TCS SP8 confocal microscope. For quantification of LD accumulation, cells were seeded in a 96-well plate and induced adipogenesis differentiation. After washing with PBS, 5  $\mu$ L of AdipoRed™ Assay Reagent (Lonza) was added in each well containing 200  $\mu$ L PBS and incubated for 10 min at room temperature. Fluorescence with excitation at 485 nm and emission at 572 nm was measured by using a microplate reader (Varioskan LUX).

## Microarray Analysis

Total RNA was extracted as above, and 250 ng of RNA was subjected to strand synthesis using GeneChip 3' IVT PLUS Reagent Kit (Affymetrix Inc., Santa Clara, CA, United States) and Affymetrix® 3' IVT Array Strips for GeneAtlas® System (GeneChip® HG-U219) following the manufacturer's protocol. Probe cell intensity values were obtained by GeneAtlas™ Imaging Station; CEL files from probe sets were generated by the Expression Console (Affymetrix) and then analyzed by Transcriptome Analysis Console v4.0 (Affymetrix, Japan) as described previously (Ganbold et al., 2019). We have used three technical replicates of each sample (IN, Sq, and HH-Sq) that represent the same hybridization mixture applied to three independent arrays. Gene expression values refer to Tukey bi-weight average of gene level intensity of all the replicates in a condition. A threshold value of fold change  $\geq \pm 1.2$  (in linear space) and  $p < 0.05$  [one-way between-subject analysis of variance (ANOVA)] employed by the manufacturer's analysis package was set to identify differentially expressed genes (DEGs). Downstream analyses were conducted using the functional annotation clustering of DAVID Informatics Resources 6.8<sup>1</sup> (Huang et al., 2009), and GSEA's Molecular Signatures Database v7.1<sup>2</sup> (Subramanian et al., 2005) for gene ontology (GO) and biological process (BP) clustering. GOs with  $p < 0.05$  in DAVID (modified Fisher exact test with default EASE score threshold 0.1) were considered as significantly enriched. The microarray dataset was deposited in the NCBI Gene Expression Omnibus (GEO) and is accessible with the accession number GSE153391<sup>3</sup>.

## ATP Assay

ATP production was determined by the "cell" ATP assay luminescent reagent version 2 (CA2-50, Toyo Benet, Japan). Cells were seeded in white clear-bottom 96-well plate, and induced

adipogenesis. After 14 days, according to the manufacturer's protocol, the luminescent reagent (100  $\mu$ L/well) was added and followed by 1 min on shaker and 10 min for incubation in dark at room temperature. Luminescence amount (RLU) was measured by microplate reader (Varioskan LUX) and normalized to cell number using Cell Count Normalization kit (Dojindo, Japan).

## Mitochondrial Staining by Rhodamine 123

Mitochondrial biogenesis was evaluated by rhodamine 123 assay. Cells were seeded in black clear-bottom 96-well plate and induced adipogenesis. At day 14 (D14), the supernatant was replaced by 50  $\mu$ M rhodamine 123 (Wako, Japan) dissolved in Hanks balanced salt solution (Gibco) containing 20 mM HEPES (100  $\mu$ L/well) and incubated at 37°C for 30 min. The supernatant was discarded and rinsed with the buffer two times before measuring rhodamine 123 fluorescence intensity [relative fluorescence unit (RFU)] using the excitation/emission at 485/525 nm by microplate reader (Varioskan LUX). RFU was normalized to cell number using Cell Count Normalization kit (Dojindo, Japan). After staining with rhodamine 123, cell nuclei were counterstained with 0.5  $\mu$ g/mL Hoechst 33342 (Molecular Probes, United States) dissolved in PBS (100  $\mu$ L/well) for 10 min at room temperature for fluorescent imaging using automated inverted microscope (IX83, Olympus).

## Glucose Uptake Assay

Glucose uptake was determined by Glucose CII test kit (Wako, Japan). Cells were seeded in 24-well plate and induced adipogenesis for 14 days. Differentiated adipocytes were starved in serum free medium for overnight. Next day, the medium was replaced with Krebs-Ringer-phosphate-HEPES (KRPH) buffer for glucose starvation. After 2 h of incubation, the buffer was replaced by KRPH containing 11 mM glucose with or without 1 nM insulin for 24 h. Glucose level in the supernatant was quantified by colorimetric assay according to the manufacturer's instruction.

## Real-Time Reverse Transcription-Polymerase Chain Reaction Analysis

Cells were seeded and induced adipogenesis in a 6-well plate. Total RNA was extracted by using ISOGEN reagent (Nippon Gene, Toyama, Japan) following the manufacturer's instruction. Complementary DNA was synthesized by reverse transcription from 1  $\mu$ g of RNA using SuperScript™ IV VILO™ Master Mix (Invitrogen, Carlsbad, CA, United States). The resultant cDNA (100 ng) was then amplified by the predesigned TaqMan® Gene Expression Assay and TaqMan® Gene Expression Master Mix (Applied Biosystems, Carlsbad, CA, United States) on the 7500 Fast Real-Time PCR System. All predesigned primers were purchased from the Applied Biosystems. Gene expression was normalized to *GAPDH* as an endogenous housekeeping gene, and the relative expression level was calculated using the  $2^{-\Delta \Delta C_t}$  method ( $n = 3$ ).

<sup>1</sup><https://david.ncifcrf.gov/>

<sup>2</sup><https://www.gsea-msigdb.org>

<sup>3</sup>[www.ncbi.nlm.nih.gov/geo](http://www.ncbi.nlm.nih.gov/geo)



## Capillary Immunoassay

Protein level was evaluated using ProteinSimple capillary immunoassay (Wes<sup>TM</sup>, ProteinSimple). dASCs induced adipogenesis in 6-well plate. Total protein was extracted at D14 using radioimmunoprecipitation assay buffer (Sigma-Aldrich, St. Louis, MO, United States) containing protease inhibitor cocktail (P8340, Sigma-Aldrich), and the protein concentration was quantified using 2-D Quant kit (GE Healthcare, Chicago, IL, United States). An equal amount (0.75  $\mu\text{g}/\mu\text{L}$ ) of protein diluted in sampling buffer (ProteinSimple) were loaded in 12- to 230-kDa, 25-lane plate (ProteinSimple) and run in WES WS3390 instrument following the manufacturer's instruction. Primary antibodies were purchased from Abcam. Anti-rabbit and anti-mouse secondary antibodies of Detection module for chemiluminescence (ProteinSimple) were used. Imaging and peak area were obtained from Compass for SW software (ProteinSimple). Peak areas were normalized to GAPDH as loading control, and relative ratio was calculated compared to IN.

## Statistics

All data are shown as the mean  $\pm$  SEM unless otherwise mentioned. Statistical analyses were conducted using GraphPad Prism 8.0. All data were assessed for normality (Shapiro–Wilk test) and kurtosis and skewness (D'Agostino–Pearson omnibus test). A one-way ANOVA followed by Dunnett *post hoc* test was performed to compare the treatment groups to the control group, whereas Tukey *post hoc* test was performed to compare among all three groups. Paired *t* test was used for within-group comparison at two different timepoints. A  $p < 0.05$  was considered significant.

## RESULTS

### Sq and HH-Sq Did Not Alter the Proliferative and Migratory Capacity of dASCs

Adipose-derived stem cells derived from T2D donor may have reduced or lost proliferation and migration potential leading to incapacity to differentiate (Pérez et al., 2015; Barbagallo et al., 2017; Vyas et al., 2019). Thus, we checked first if dASCs were maintaining its functions to proliferate and migrate as a sign of multipotent cells. After full confluence, cells in growth medium were subjected to a scratch/wound and then continued with the treatment of 1  $\mu\text{M}$  Sq and HH-Sq for up to 48 h (Figure 1B). Non-treated (NC) cells were observed to migrate toward the cell-free area 12 h after the initiation of the wound and covered greater than 50% after 24 h and completely closed by 48 h. The wound closure rate in each treatment group reached 100% versus NC at the 48-hour time point (Figure 1C). Treatment with Sq and HH-Sq did not interfere with the migratory capacity of dASCs.

Moreover, expansion potential in culture is an important criterion for further use of stem cell source to differentiate into numerous cell lineages. Therefore, the cell proliferation rate of dASCs was evaluated in the presence of different dose of Sq and HH-Sq (Figures 1D,E), and both compounds did not show any inhibitory effect on the dASC proliferation rate until 20  $\mu\text{M}$  of

dose up to 72 h (48 h,  $p = 0.179$ ; 72 h,  $p = 0.895$ ). These results suggest that dASCs still preserve their proliferative and migratory ability, on which the treatment with Sq and HH-Sq did not show any inhibitory effect.

### Adipocyte Differentiated From dASCs After Induction

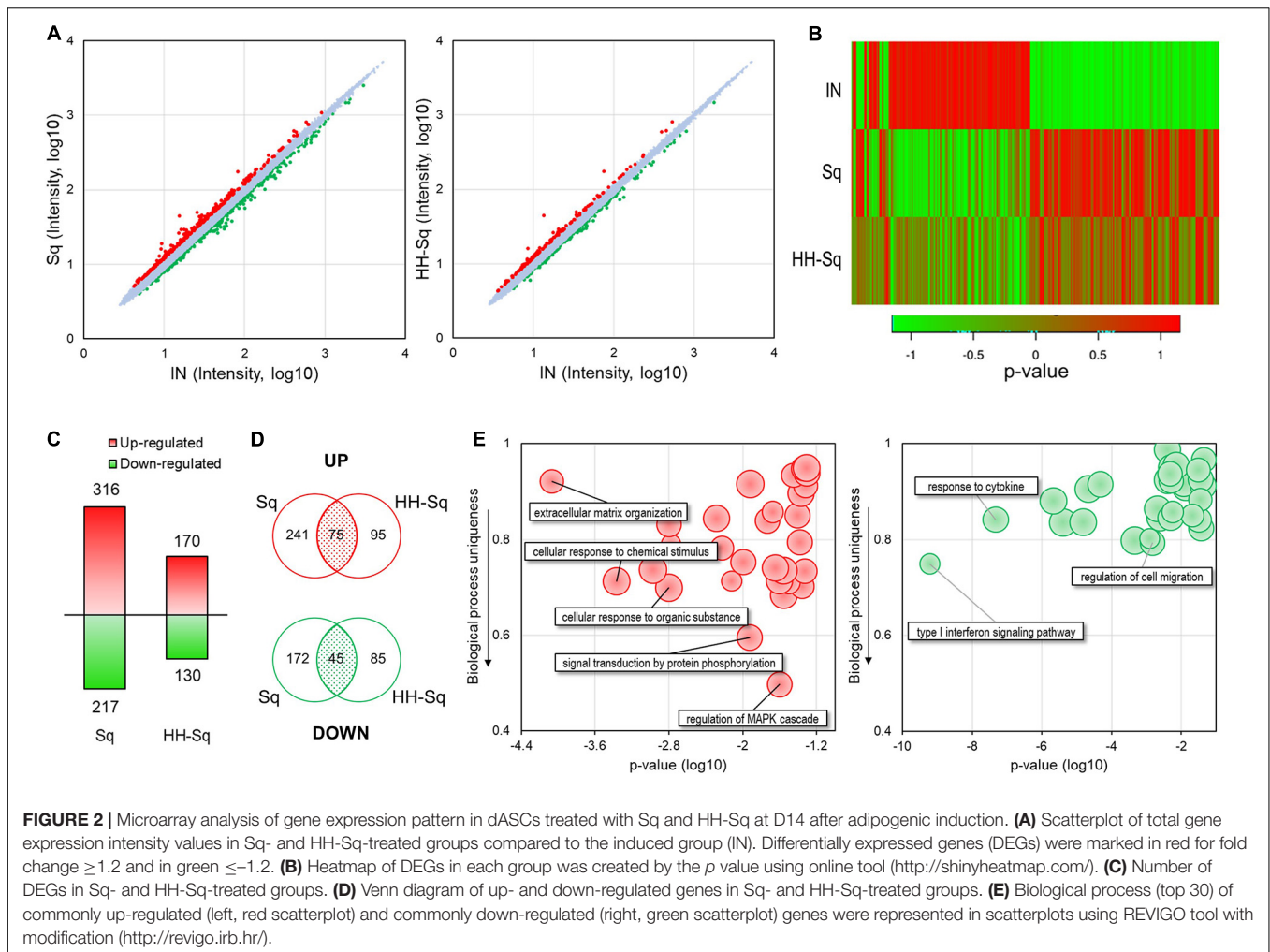
The primary role of stem cells from adipose tissue is to sustain adipocyte turnover by pooling newly differentiated adipocytes. However, evidences showing the capacity of dASCs to differentiate into adipocyte are still controversial (Pérez et al., 2015; Barbagallo et al., 2017). Thus, adipogenesis was induced in dASCs, and the appearance of LDs was observed 7, 14, and 21 days post-induction to explore the differentiation capacity and timing *in vitro* (Figure 1F). Only some of the cells began to show small LD formation at D7. Subsequently, by D14, the number of cells containing LDs occurred increasing along with the enlarged LD size leading the majority of cells engorged with LDs at D21. For further evaluation of the expression of genes, we chose dASCs differentiated on D14 as our model.

### Adipocyte-Induced dASCs Gene Expression Pattern Treated With Sq and HH-Sq

Next, we performed microarray analysis using dASCs of D14 after adipocyte differentiation treated with 1  $\mu\text{M}$  Sq and HH-Sq and explored the gene expression profile. Intensity value of total gene probe set after treatment with 1  $\mu\text{M}$  of Sq and HH-Sq compared to the non-treated adipocyte-induced control (IN) is shown (Figure 2A). Probes with a threshold of fold change  $\geq 1.2$  and  $p \leq 0.05$  were considered as DEGs and represented in the heatmap (Figure 2B). In the Sq-treated group, 532 genes were differentially expressed, of which 316 DEGs were up-regulated and 217 DEGs down-regulated, whereas in the HH-Sq-treated group, of 300 DEGs, 170 were up-regulated and 130 were down-regulated (Figure 2C). Subsequently, we analyzed if the respective up- and down-regulated genes in Sq and HH-Sq-treated groups were common or not using Venn diagram (Figure 2D). Interestingly, less than half of the up-regulated genes of HH-Sq (44%) and about one-fourth of Sq (23%) were overlapped, suggesting greater than the majority of genes were up-regulated in a compound-specific way. Similarly, genes overlapping in down-regulation in each group were lower than half of the total number.

Next, we identified main BPs involved in the commonly overexpressed (left, red) and underexpressed (right, green) genes applying GO analysis of DAVID and scattered the most relevant 30 processes according to their  $p$  value and uniqueness ratio differing from other BPs (Figure 2E). The most specific BP associated with GO terms mitogen-activated protein kinase (MAPK) cascade regulation (GO:0043408), signal transduction by protein phosphorylation (GO:0023014), and cellular response to chemical stimulus (GO:0070887) were up-regulated by both compounds. Applying the criteria of  $p > 0.05$  and containing more than two genes, none of the GO terms among the top 30 BPs involving the common down-regulated genes was specific





to adipogenesis (uniqueness ratio  $> 0.5$ ), signifying both Sq and HH-Sq do not have any particular common inhibitory effect on the adipogenesis process of dASCs.

## BPs Affected by Sq and HH-Sq Treatment in Adipogenesis of dASCs

Next, to investigate the BP specifically affected by the compound, we identified all BP-qualifying  $p$  value greater than 0.05 and containing more than two genes specifically enriched in GO BP FAT terms in Sq and HH-Sq-treated groups and then classified into transcription, signal transduction, metabolism, proliferation and cell death, and extracellular matrix-, immune- and movement-related processes according to their relevance (**Figures 3A,B**). Conversely, large general terms such as regulation of metabolic process (GO:0009893) and regulation of signaling (GO:0023051) were excluded, and terms that are repetitive or similar were merged. Globally, transcriptional activity increased in both treatment groups, as shown by the increased number of genes associated with transcription of polymerase II promoter (GO:0006357) and positive regulation of DNA-templated transcription

(GO:0045893); however, the number of genes enriched was two times higher in Sq group.

Among signal transducing events, MAPK pathway, extracellular signal-regulated protein kinase 1/2 cascade, and serine-threonine kinase activity-related gene expression were increased in Sq followed by cell proliferation regulatory and response to wounding processes activation. These results suggest that the overall MAPK cascade was activated to regulate cell cycle and proliferation during adipogenic differentiation. Hence, metabolic responses, including fatty acid metabolic process (GO:0006631), response to insulin (GO:0032868), and regulation of glucose import (GO:0046324), and cell cycle and growth process were down-regulated.

HH-Sq-treated cells have been found to not only up-regulate similar pathways such as MAPK cascade and serine-threonine kinase activity but also to directly over activates intracellular signal transduction (GO:1902531) and signal transduction by phosphorylation (GO:0023014) compared to Sq-treated cells. In addition, the HH-Sq treatment enhanced positive regulation of metabolic process (GO:0009893) and intracellular transport (GO:0046907). Interestingly, cytokine-mediated pathway (GO:0019221) and cytokine production (GO:0001816) were

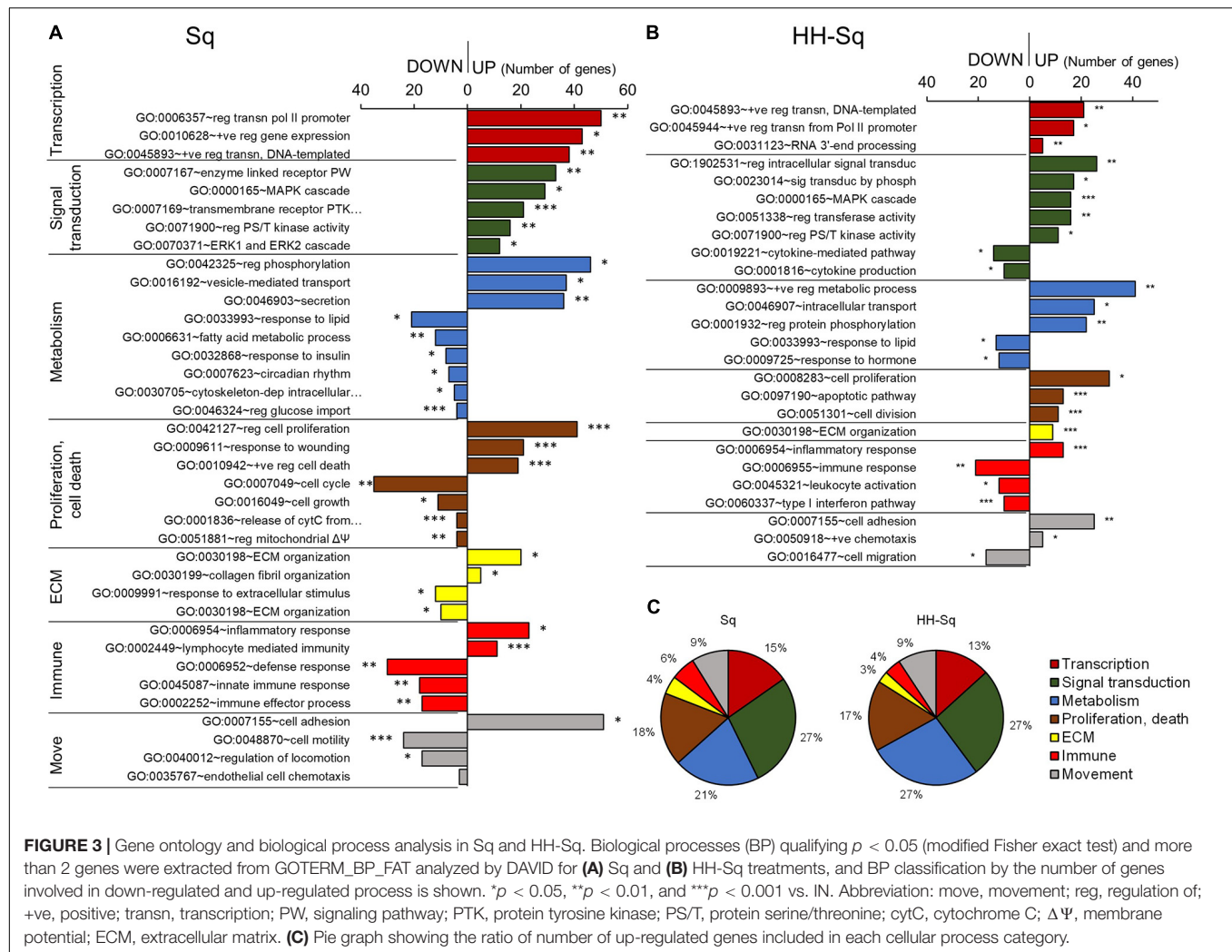


**FIGURE 3 |** Gene ontology and biological process analysis in Sq and HH-Sq. Biological processes (BP) qualifying  $p < 0.05$  (modified Fisher exact test) and more than 2 genes were extracted from GOTERM\_BP\_FAT analyzed by DAVID for (A) Sq and (B) HH-Sq treatments, and BP classification by the number of genes involved in down-regulated and up-regulated process is shown. \* $p < 0.05$ , \*\* $p < 0.01$ , and \*\*\* $p < 0.001$  vs. IN. Abbreviation: move, movement; reg, regulation of; +ve, positive; transn, transcription; PW, signaling pathway; PTK, protein tyrosine kinase; PS/T, protein serine/threonine; cytC, cytochrome C;  $\Delta\Psi$ , membrane potential; ECM, extracellular matrix. (C) Pie graph showing the ratio of number of up-regulated genes included in each cellular process category.

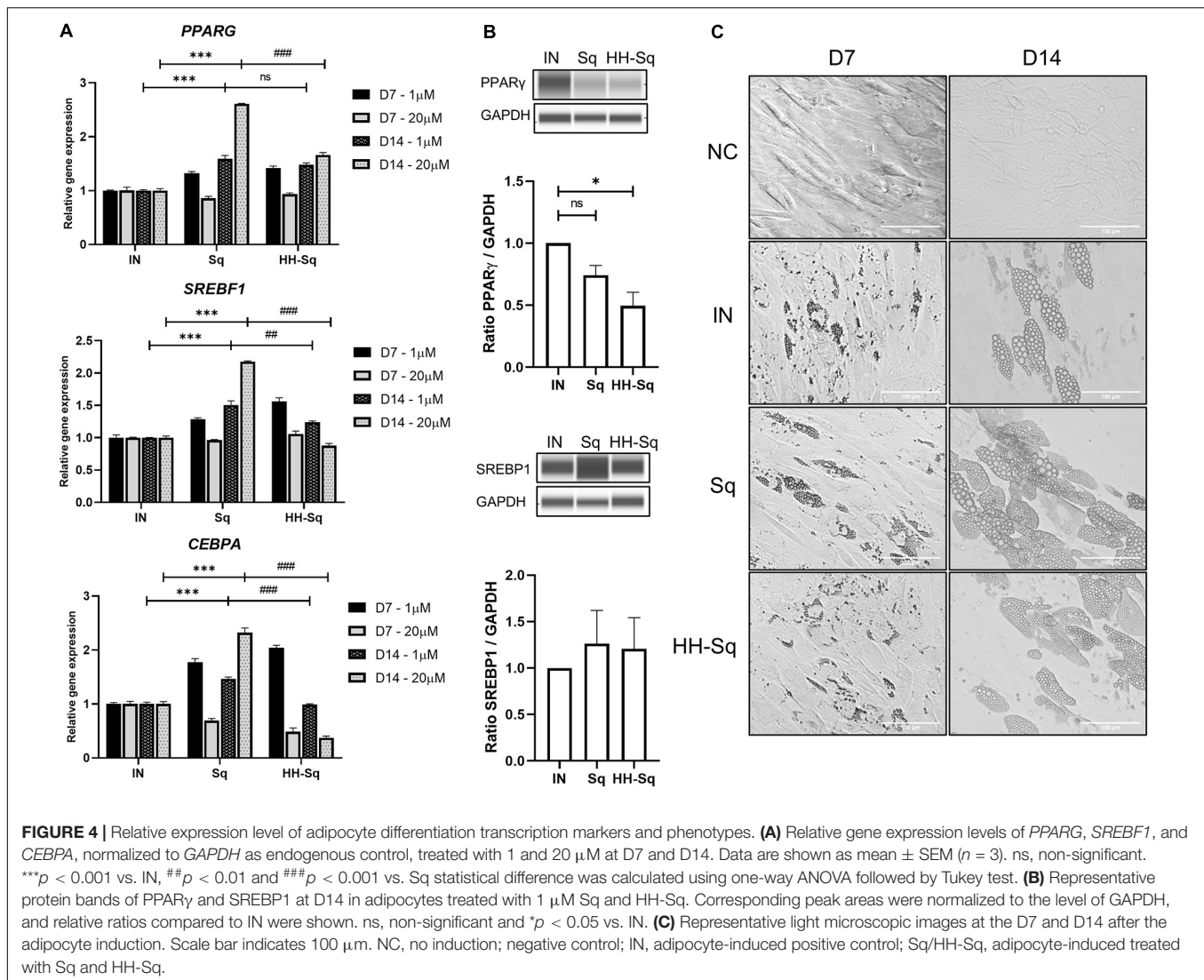
down-regulated, providing another HH-Sq-specific regulation. Inflammatory cytokines secreted by adipocytes in obese and diabetic environment are thought to be increased and promote systemic level of circulating proinflammatory cytokines, thereby contributing to insulin resistance development (Makki et al., 2013; Odegaard and Chawla, 2013). Collectively, the resulting changes show HH-Sq's more favorable effect in alleviating disease-related molecular impairment.

All up-regulated DEGs classified into the cellular processes in Sq and HH-Sq by the number of genes showed a similar ratio suggesting the derivative HH-Sq exerts biological effect, which is comparable to its mother molecule (Figure 3C).

## Sq and HH-Sq Promoted Preadipocyte Differentiation Transcription Regulators

Obesity- and diabetes-induced cellular dysfunctions affect adipose tissue-derived stem cell proliferation and differentiation capacity causing reduced turnover in adipocytes, ectopic fat accumulation, and reduced number of preadipocytes (Bost et al., 2005; Van Tienen et al., 2011; Oñate et al., 2012). Thus, we measured gene expression of transcription factors that

control adipogenesis in order to, first, validate the preadipocyte commitment of dASCs, and second, the effect of Sq and HH-Sq on those proadipogenic markers, which direct the differentiation. SREBP1c, peroxisome proliferator-activated receptor  $\gamma$  (PPAR $\gamma$ ), and C/EBP $\alpha$  are early adipogenic markers acting synergistically on the downstream gene expression (Cawthorn et al., 2012). Knockdown of *SREBF1* inhibited adipogenesis and blocked the expression of the other two early markers (Ayala-Sumano et al., 2011). Consequently, it was found that Sq treatments augmented gene expression of *PPARG*, *SREBF1*, and *CEBPA* compared to non-treated adipocyte-induced control (IN) (Figure 4A). However, the level of these gene expressions in HH-Sq-treated cells except *PPARG* remained inferior to that of Sq treatment, and it decreased in a time- and dose-dependent manner. Protein level of these transcription factors also remained lower in HH-Sq-treated adipocytes (Figure 4B). Of note, the effect of HH-Sq at D7 was comparable to that of Sq at D14 for *PPARG* and *SREBF1* and even higher in *CEBPA*, suggesting there is a temporal shift in the exertion of biological effect between these compounds. General aspect of adipocytes in differentiation at D7 and D14 is shown in Figure 4C. Smaller LDs were found in HH-Sq, whereas



Sq-treated cells showed larger, comparable to IN, droplets that were most likely due to up-regulation of early adipogenic factors.

### HH-Sq Induced Adipocytes With Fewer Lipid Droplets

Committed preadipocytes undergo maturation by accumulating LDs as one of their primary roles and expressing subsequent late marker genes of lipogenesis and lipolysis. First, we checked downstream adipocyte-specific gene expression after D7 and D14 (Figure 5A). The fatty acid-binding protein 4 (*FABP4*), also known as adipocyte protein 2, is believed to be expressed in preadipocytes and mature adipocytes and thus required for the maturation of differentiation (Shan et al., 2013). Treatment with Sq and HH-Sq overexpressed *FABP4* compared to IN, showing a similar pattern as early transcription markers; however, increased level in HH-Sq was significantly lower than that in Sq. Next, we measured gene expression of enzymes required for the formation of LDs. Fatty acid synthase (*FASN*) and diacylglycerol acyltransferase (*DGAT1*) are key lipogenic enzymes necessary for

triacylglycerol synthesis and LD formation (Schmid et al., 2005; Harris et al., 2011). Interestingly, both gene expressions were increased after D14 in Sq treatment, whereas only lesser extent for *FASN* not for *DGAT1* by HH-Sq treatment. Corresponding protein levels at D14 showed the similar tendency, however, the difference did not reach statistical significance (Figure 5B). Higher dose seemed to potentiate the effect of compounds, showing more increased expression of these genes by Sq and decreased by HH-Sq.

To extend this result, we observed the effect of treatments on the formation of LD; thus, cells were stained with a dye BODIPY at D14 and D21 after differentiation to visualize intracellular neutral lipids. A large number of newly formed LP appeared in the IN after D14, and its intensity and droplet size became more important by D21 (Figure 5C). Formed LD in Sq-treated cells seemed inferior after D14 of induction, but at D21, cells were engorged with lipids as much as observed in IN, and some cells showed slightly larger LD than IN. By contrast, LD density and size remained evidently fewer and smaller within the



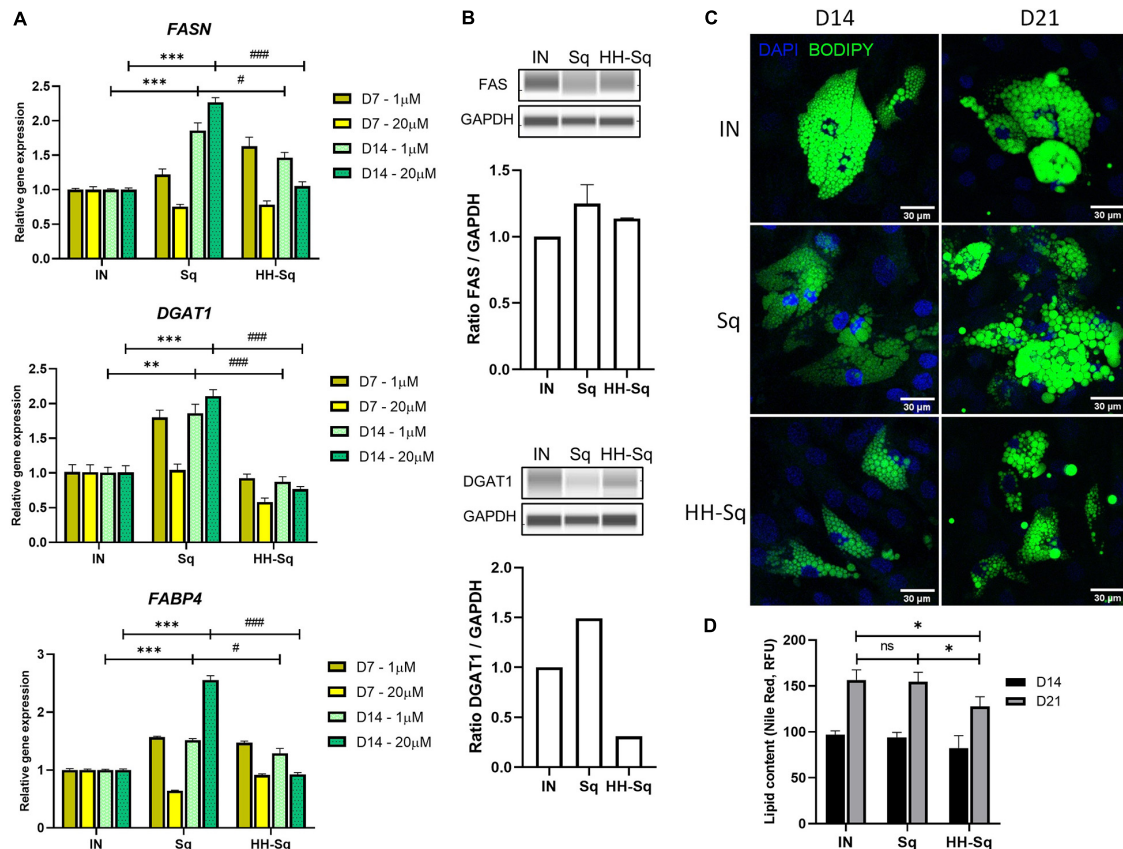


**FIGURE 5 |** Expression of adipogenic markers and lipid droplet (LD) accumulation after adipocyte induction in dASCs. **(A)** Relative gene expression levels of *FASN*, *DGAT1*, and *FABP4*, normalized to *GAPDH* as endogenous control, treated with 1 and 20  $\mu\text{M}$  at D7 and D14.  $**p < 0.01$ ,  $***p < 0.001$  vs. IN, and  $\#p < 0.05$  and  $###p < 0.001$  vs. Sq statistical difference was calculated using one-way ANOVA followed by Tukey test. **(B)** Representative protein bands of FAS and DGAT1. Corresponding peak areas were normalized to GAPDH, and relative ratios compared to IN were shown. **(C)** Representative fluorescence images of adipogenesis-induced dASCs treated with 1  $\mu\text{M}$  of Sq and HH-Sq. At D14 and D21 after adipogenesis induction, LDs were stained with BODIPY 493/503 (green) and nucleus counterstained with DAPI (blue). Scale bar indicates 30  $\mu\text{m}$ . **(D)** Lipid content was quantified by relative fluorescence unit (RFU) of Nile red staining ( $n = 4-5$ ). IN-adipocyte-induced, non-treated control. Data are shown as mean  $\pm$  SEM ( $n = 3$ ). ns, non-significant.  $*p < 0.05$  statistical difference was calculated using one-way ANOVA followed by Tukey test.

HH-Sq-treated cells. We also assessed the fluorescence intensity of lipids stained with Nile red dye. As observed in microscopic images, lipid content was significantly lower in HH-Sq-treated cells, whereas the lipid intensity was not different in Sq compared to IN up to D21 (**Figure 5D**). This suggests that the reduced presence of LD in HH-Sq-treated cells is in part due to inhibition of transcription factors but also due to partial inhibition of lipogenic enzymes.

## HH-Sq and Sq Increased Expression of Genes Involved in Metabolism

NAD-dependent deacetylase (*SIRT1*), a member of SIRTuins, has been suggested to be down-regulated in insulin-resistant tissue, and its activation improved insulin sensitivity (Sun et al., 2007). In addition, stearoyl-CoA desaturase 1 (*SCD1*), catalyzer in monosaturated fatty acid synthesis, is a key enzyme in *de novo* lipogenesis. Although gene expression of *SIRT1* and *SCD1* showed up-regulation in differentiated adipocytes exposed to 1  $\mu\text{M}$  Sq and HH-Sq, higher concentration (20  $\mu\text{M}$ ) of HH-Sq

stimulated the up-regulation of *SIRT1* and down-regulation of *SCD1* by D14, whereas Sq treatment showed the opposite effect (**Figure 6A**).

AMPK regulates a wide range of metabolic activities and activates *SIRT1* expression and its impairment involved in metabolic syndrome associated pathways (Ruderman et al., 2013). Thus, we measured the expression level of AMP-activated protein kinase (AMPK, gene *PRKAA2*) and insulin receptor substrate 1 (*IRS1*) as important markers of insulin sensitivity. Consistently, *PRKAA2* and *IRS1* genes were found to be overexpressed to the same extent in both treated cells at 1  $\mu\text{M}$ , and this change was highly significant at 20  $\mu\text{M}$  of HH-Sq (**Figure 6A**). Corresponding protein levels in cells treated at 1  $\mu\text{M}$  were not significant (**Figure 6B**). After 14 days of adipogenic differentiation, we measured the glucose uptake rate in presence of insulin. The glucose concentration present in the supernatant of HH-Sq was slightly lower than Sq and IN (**Figure 6C**), suggesting improved glucose uptake. These observations indicate that HH-Sq prevented more effectively



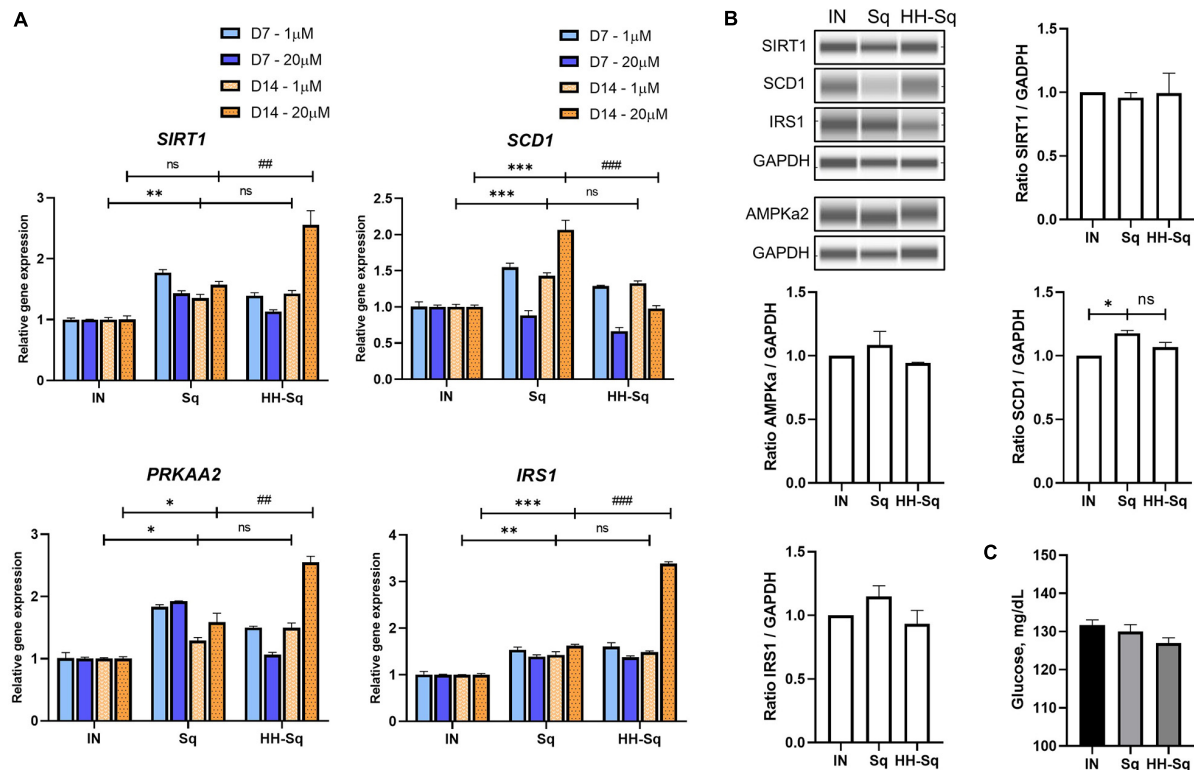


**FIGURE 6 |** Metabolism related gene expression and protein levels in differentiated dASCs. **(A)** Relative gene expression of *SIRT1*, *SCD1*, *PRKAA2*, and *IRS1*, normalized to *GAPDH* as endogenous control, treated with 1 and 20  $\mu$ M at D7 and D14. ns, non-significant. \* $p < 0.05$ , \*\* $p < 0.01$ , \*\*\* $p < 0.001$  vs. IN, and ## $p < 0.01$  and ### $p < 0.001$  vs. Sq statistical difference was calculated using one-way ANOVA followed by Tukey test. **(B)** Representative protein bands of *SIRT1*, *SCD1*, *IRS1*, and *AMPKa2*. Corresponding peak areas were normalized to *GAPDH*, and relative ratios compared to IN were shown. IN, adipogenesis-induced non-treated control. Data are shown as mean  $\pm$  SEM ( $n = 3$ ). ns, non-significant. \* $p < 0.05$  statistical difference was calculated using one-way ANOVA followed by Tukey test. **(C)** Glucose level measured in supernatant of differentiated dASCs at D14 in the presence of 11 mM (198 mg/dL) glucose and 1 nM human recombinant insulin.

overactivation of lipogenesis, and in turn, more metabolic gene expressions were enhanced.

## Mitochondrial Biogenesis Improved by Sq and HH-Sq Treatment

Mitochondria play an important role in energy homeostasis, apoptosis, and inflammation. In adipose tissue, mitochondrial metabolism and function are correlated to adipocyte differentiation, lipid metabolism, and insulin sensitivity (De Pauw et al., 2009). Therefore, mitochondrial dysfunction is widely reported to be implicated in metabolic diseases, obesity, and T2D (McBride et al., 2006; Green et al., 2011). Adipogenic transcription factors contribute in mitochondrial biogenesis during adipogenesis (Spiegelman et al., 2000). Thus, we evaluated mitochondrial biogenesis and ATP production in differentiated adipocytes at D7 and D14. As shown in **Figure 7A**, mitochondrial content increases throughout the adipogenesis from D7 to D14 in all groups. In Sq- and HH-Sq-treated cells, mitochondria remained nevertheless slightly augmented compared to IN. Mitochondrial proliferation in HH-Sq was accompanied by increased ATP production at D14 (**Figure 7B**), suggesting the process of adipogenesis and energy metabolism

were concomitantly stimulated. This finding of mitochondrial content in Sq was not correlated to the level of ATP content, which increased to a lesser extent from D7 to D14.

Mitochondrial biogenesis alteration and its dysfunction are in part attributed to inflammatory or pathologic condition, which further leads to development of metabolic diseases and insulin resistance (Kim et al., 2008). Thus, we sought to analyze the changes in inflammatory cytokines in correlation with the treatment of Sq and HH-Sq during adipogenesis. Cytokine gene expression pattern of microarray data revealed a clear correlation of HH-Sq treatment and the number of down regulated inflammatory cytokines, although both Sq and HH-Sq prevented overexpression of a large number of cytokines (**Figure 8A**; list of genes in **Supplementary Material**). Gene expression levels by quantitative polymerase chain reaction showed slightly ameliorated tendency in HH-Sq-treated cells; however, none of *IL6*, *IL1B*, and *CCL2* reached a statistical significance (**Figure 8B**).

## DISCUSSION

Pathogenic fat cells turn against their initial role in organism contributing to metabolic disorders such as obesity, T2D, and

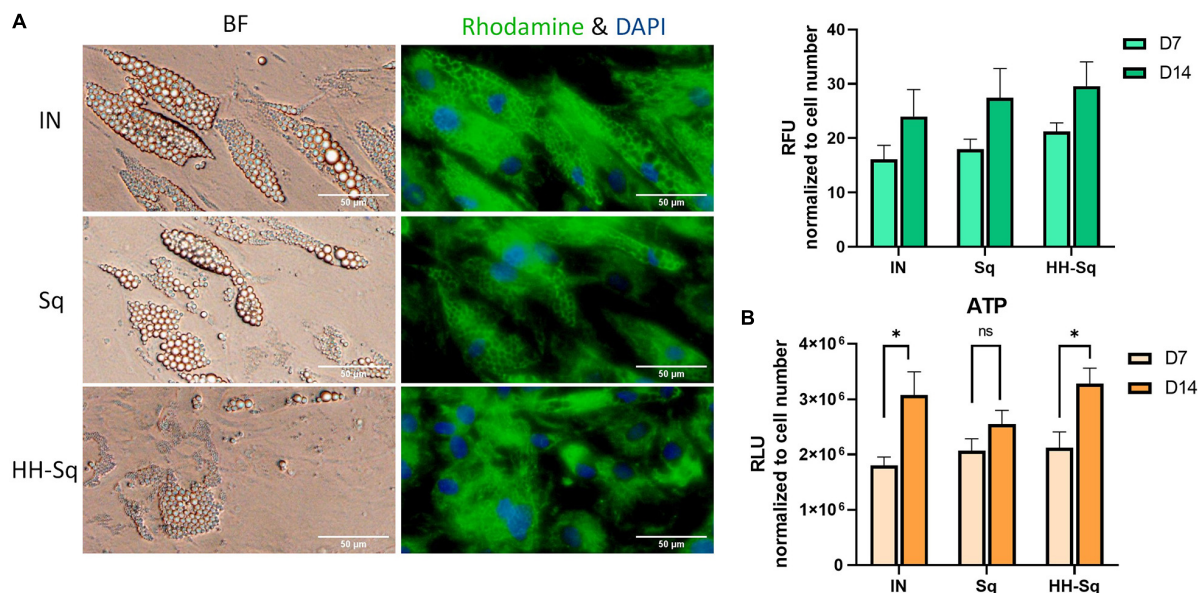


**FIGURE 7 |** Mitochondrial biogenesis and ATP production in dASCs after D14 adipocyte differentiation. **(A)** Representative images captured in bright field (BF) and fluorescence microscope showing mitochondrial biogenesis at D14 stained with rhodamine 123 (green) and nucleus counterstained with DAPI (blue). Scale bar indicates 50  $\mu$ m. Relative fluorescence unit (RFU) of rhodamine 123 was measured in 1  $\mu$ M Sq and HH-Sq treatments. **(B)** ATP production was measured in dASCs after adipocyte differentiation. ns, non-significant. \* $p < 0.05$  statistical difference was calculated using paired  $t$  test within group comparison at two different timepoints.

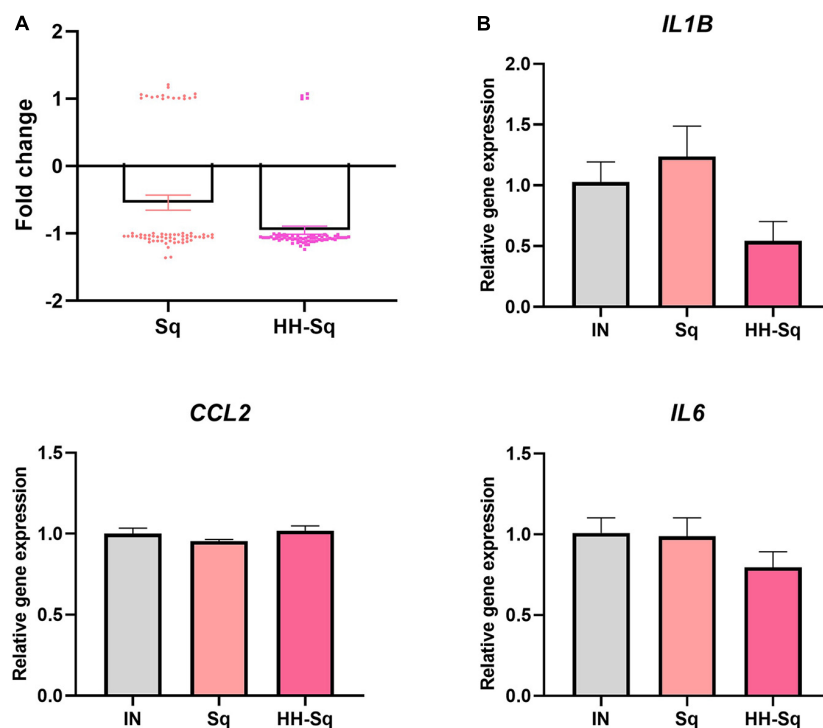


**FIGURE 8 |** Inflammatory cytokine gene expression in dASCs after D14 adipocyte differentiation. **(A)** Cytokines ( $n = 66$  genes) gene expression pattern with median averaging selected from microarray data. **(B)** Relative gene expression of *IL6*, *IL1B*, and *CCL2*, normalized to *GAPDH* as endogenous control, treated with 1  $\mu$ M Sq and HH-Sq until D14.

cardiovascular diseases through insulin resistance, an increase of free fatty acids, and impaired adipokines secretion (Van Gaal et al., 2006; Skurk et al., 2007). To compete with old hypertrophied pathogenic adipose tissue (Skurk et al., 2007) emitting undesired biological effects, researchers have been seeking more functional and responsive compounds that can promote new adipocyte differentiation, while not depleting the number of stem cells in reserve (McLaughlin et al., 2007; Ghaben and Scherer, 2019).

Adipose-derived stem cells have the properties of self-renewal and migration (Mazini et al., 2020). ASCs derived from subjects with diabetes showed the similar migratory and proliferative capacity in the absence and presence of Sq and HH-Sq, suggesting that the dASCs maintained the stem cell features, and both compounds exhibited neither depletion of stem cells nor interference on proliferation and migration.

Observations from global microarray data such as up- and down-regulated genes following the treatment with Sq and HH-Sq showed, respectively, different patterns in the number of genes and the process compared to that of commonly regulated genes. Despite this, MAPK cascade and protein serine-threonine kinase activity were commonly up-regulated. MAPK cascade is an important effector activated by extracellular stimuli to induce a long-term cellular response by triggering transcription of genes in the nucleus.

After adipocyte differentiation at D14, various genes involved in transcriptional regulation of adipogenesis differentiation were induced by Sq and HH-Sq treatment. For example, early markers, *PPARG*, *SREBF1*, and *CEBPA*, were overexpressed by Sq and lesser extent by HH-Sq. This ratio was preserved in the downstream lipogenic gene expression. Sq overactivated *FABP4*, *DGAT1*, and *FASN*, whereas their increased level of expression by HH-Sq was significantly lower compared to Sq. Furthermore, the observed effect of HH-Sq was more important at a higher dose. The resulting changes could be observed in LD size and intensity. In HH-Sq-treated adipocytes, the lipogenic genes were down-regulated with the formation of less and smaller LD up to D21 after differentiation.

The role of SCD1 is still controversial. SCD1 deficiency reduced lipogenesis and improved insulin sensitivity in adipose tissue (Flowers and Ntambi, 2008; Ralston and Mutch, 2015); however, SCD1-deficient mice have altered fatty acid re-esterification and glyceroneogenesis in white adipose tissue (Dragos et al., 2017). In Sq- and HH-Sq-treated cells, *SCD1* gene expression was increased but did not show any aberrant lipid accumulation in adipocytes. Hui et al. (2017) reported that mice with adipose tissue specific ablation of *SIRT1* are more susceptible to insulin resistance and argued adipocyte SIRT1 plays an important role in glucose homeostasis through modulation of macrophages. We observed a significant increase of *SIRT1* in Sq- and HH-Sq-treated adipocytes, which suggests improved glucose homeostasis.

Moreover, studies reported that AMPK is an important sensor of metabolic changes, and its level is highly reduced in insulin-resistant and morbidly obese subjects (Xu et al., 2012; Desjardins and Steinberg, 2018) and is activated in

response to energy metabolism through AMPK-SIRT1-PCG-1 $\alpha$  pathway to enhance mitochondrial oxidative function in adipocytes (Chau et al., 2010). In addition, IRS1 is known as a major insulin receptor substrate in mediating insulin action, and Rondinone et al. (1997) found that the level of IRS1 was significantly reduced in adipocytes of subjects with non-insulin-dependent T2D. Despite increased mitochondrial content both in Sq and HH-Sq indicates the induction of adipogenesis, ATP production level in Sq remained lower by D14. It might be inferred that more ATP was consumed for lipogenesis compared to HH-Sq, which is consistent with the results of overexpressed lipogenic genes followed by Sq treatment. Increased mitochondrial biogenesis and ATP production in HH-Sq-treated cells and the amelioration of glucose uptake in correlation with increased expression of *IRS1* can provide all collectively the benefic effect of HH-Sq in regulation of energy metabolism in adipocytes and its differentiation.

Local inflammatory status in adipose tissue systematically attracts macrophages and leukocytes as well as transforms resident macrophages into an activated form, which collectively aggravates insulin resistance and system inflammation (Chawla et al., 2011; Russo and Lumeng, 2018). Down-regulation of genes related to cytokine production and cytokine-mediated pathway by HH-Sq treatment also suggests that HH-Sq may have an anti-inflammatory effect because low-grade inflammation has been reported being increased in adipocytes of obese subjects due to the proinflammatory cytokines (Lasselin et al., 2014), which affect the pathogenicity of adipocytes (Ghaben and Scherer, 2019). Selected cytokine gene expression data from microarray ( $n = 66$  genes) including individual gene expression levels (*IL6*, *IL1B*, and *CCL2*) tended to be ameliorated by HH-Sq treatment, whereas Sq-treated cells were not different than non-treated cells. However, the direct effect on adipocytes was not statistically significant; several protective effects might be stimulated. HH-Sq may improve inflammatory status in systemic level as adipose tissue macrophages are also inflammatory and contribute to adipocyte inflammation. This is supported by Sasaki et al. (2020) findings showing the anti-inflammatory effect of HH-Sq in murine macrophage model.

HH-Sq was synthesized from Sq by adding monoethylene glycol moiety with the aim of improving its hydrophilicity; however, the compounds actually exhibited difference at gene expression level in adipocyte differentiation. In particular, transmembrane receptor protein tyrosine kinase pathway and enzyme-linked receptor pathway genes were enriched by Sq treatment, whereas intracellular signal transduction and transduction by phosphorylation activities were specifically activated by HH-Sq as found by microarray analysis. Furthermore, the effect of HH-Sq on early adipogenic markers seems to precede that of Sq, showing comparable effect at D7 to Sq at D14. This suggests that HH-Sq might have penetrated cell membrane more actively than Sq and exerted its effect faster, which may, in part, explain the increased intracellular signaling genes in HH-Sq-treated cells. Intracellular signaling is necessary for long-term effect at the nucleus level by initiating gene expression, rather than short-term effect in cytoplasmic level.

In contrast, processes related to glucose transport and insulin signaling such as cytoskeleton-dependent intracellular transport (GO:0030705), response to insulin (GO:0032868), regulation of glucose import (GO:0046324), and response to growth factor (GO:0070848) were down-regulated in Sq-treated cells, suggesting Sq does not only weakly reach intracellular environment but also affect insulin signaling effector molecules at probably cell membrane level.

According to the current findings, it could be assumed that both Sq and HH-Sq exert an adipogenic effect on dASCs, and HH-Sq specifically enhances energy metabolism and insulin signaling without aberrantly activating lipogenesis during adipocyte differentiation. Effect of HH-Sq on ASCs derived from altered microenvironment can contribute to the resolution of insulin resistance and obesity-associated metabolic disorders, and the further development of an alternative class of therapeutics derived from a natural compound, and application in tissue engineering of fat. Nevertheless, future research should explore the molecular mechanism by which HH-Sq triggers intracellular signaling.

## DATA AVAILABILITY STATEMENT

The datasets presented in this study can be found in online repositories. The names of the repository/repositories and

accession number(s) can be found below: <https://www.ncbi.nlm.nih.gov/>, GSE153391.

## AUTHOR CONTRIBUTIONS

MG: conceptualization, methodology, investigation, visualization, validation, and original draft writing. MG and FF: formal analysis and data curation. FF: performed microarray experiment. TA and KT: synthesized HH-Sq. FF, HI, and TA: writing review & editing. KT and HI: supervision and funding acquisition. All authors reviewed the manuscript.

## FUNDING

This study was supported by the Japan Science and Technology Agency (JST); Science and Technology Research Partnership for Sustainable Development (SATREPS, Grant No. JPMJSA1506).

## SUPPLEMENTARY MATERIAL

The Supplementary Material for this article can be found online at: <https://www.frontiersin.org/articles/10.3389/fcell.2020.577259/full#supplementary-material>

## REFERENCES

- Ayala-Summano, J. T., Velez-Delvalle, C., Beltrán-Langarica, A., Marsch-Moreno, M., Cerbón-Solorzano, J., and Kuri-Harcuch, W. (2011). Srebf1a is a key regulator of transcriptional control for adipogenesis. *Sci. Rep.* 1, 1–8. doi: 10.1038/srep00178
- Barbagallo, I., Li Volti, G., Galvano, F., Tettamanti, G., Pluchinotta, F. R., Bergante, S., et al. (2017). Diabetic human adipose tissue-derived mesenchymal stem cells fail to differentiate in functional adipocytes. *Exp. Biol. Med.* 242, 1079–1085. doi: 10.1177/1535370216681552
- Bost, F., Aouadi, M., Caron, L., and Binétruy, B. (2005). The role of MAPKs in adipocyte differentiation and obesity. *Biochimie* 87, 51–56. doi: 10.1016/j.biochi.2004.10.018
- Cawthorn, W. P., Scheller, E. L., and MacDougald, O. A. (2012). Adipose tissue stem cells meet preadipocyte commitment: going back to the future. *J. Lipid Res.* 53, 227–246. doi: 10.1194/jlr.R021089
- Chau, M. D. L., Gao, J., Yang, Q., Wu, Z., and Gromada, J. (2010). Fibroblast growth factor 21 regulates energy metabolism by activating the AMPK-SIRT1-PGC-1 $\alpha$  pathway. *Proc. Natl. Acad. Sci. U.S.A.* 107, 12553–12558. doi: 10.1073/pnas.1006962107
- Chawla, A., Nguyen, K. D., and Goh, S. Y. P. (2011). Macrophage-mediated inflammation in metabolic disease. *Nat. Rev. Immunol.* 11, 738–749. doi: 10.1038/nri3071
- Costa, M. A., Mangione, M. R., Santonocito, R., Passantino, R., Giacomazza, D., and Librizzi, F. (2018). Biophysical characterization of asolectin-squalene liposomes. *Colloids Surfaces B Biointerfaces* 170, 479–487. doi: 10.1016/j.colsurfb.2018.06.032
- De Pauw, A., Tejerina, S., Raes, M., Keijer, J., and Arnould, T. (2009). Mitochondrial (dys)function in adipocyte (de)differentiation and systemic metabolic alterations. *Am. J. Pathol.* 175, 927–939. doi: 10.2353/ajpath.2009.081155
- Desjardins, E. M., and Steinberg, G. R. (2018). Emerging role of AMPK in brown and beige adipose tissue (BAT): implications for obesity, insulin resistance, and Type 2 Diabetes. *Curr. Diab. Rep.* 18:80. doi: 10.1007/s11892-018-1049-6
- Dragos, S. M., Bergeron, K. F., Desmarais, F., Sutor, K., Wright, D. C., and Mounier, C. (2017). Reduced SCD1 activity alters markers of fatty acid reesterification, glyceroneogenesis, and lipolysis in murine white adipose tissue and 3T3-L1 adipocytes. *Am. J. Physiol. Cell Physiol.* 313, C295–C304. doi: 10.1152/ajpcell.00097.2017
- Flowers, M. T., and Ntambi, J. M. (2008). Role of stearoyl-coenzyme A desaturase in regulating lipid metabolism. *Curr. Opin. Lipidol.* 19, 248–256. doi: 10.1097/MOL.0b013e3282f9b54d.Role
- Ganbold, M., Owada, Y., Ozawa, Y., Shimamoto, Y., Ferdousi, F., and Tominaga, K. (2019). Isorhamnetin alleviates steatosis and fibrosis in mice with nonalcoholic steatohepatitis. *Sci. Rep.* 9:16210. doi: 10.1038/s41598-019-52736-y
- Ghaben, A. L., and Scherer, P. E. (2019). Adipogenesis and metabolic health. *Nat. Rev. Mol. Cell Biol.* 20, 242–258. doi: 10.1038/s41580-018-0093-z
- Green, D. R., Galluzzi, L., and Kroemer, G. (2011). Mitochondria and the autophagy-inflammation-cell death axis in organismal aging. *Science* 333, 1109–1112. doi: 10.1126/science.1201940
- Harris, C. A., Haas, J. T., Streeper, R. S., Stone, S. J., Kumari, M., and Yang, K. (2011). DGAT enzymes are required for triacylglycerol synthesis and lipid droplets in adipocytes. *J. Lipid Res.* 52, 657–667. doi: 10.1194/jlr.M013003
- He, H. P., Cai, Y., Sun, M., and Corke, H. (2002). Extraction and purification of squalene from *Amaranthus* grain. *J. Agric. Food Chem.* 50, 368–372. doi: 10.1021/jf010918p
- Hernández-Pérez, M., Gallego, R. M. R., Alayón, P. J. P., and Hernández, A. B. (1997). Squalene content in livers from deep-sea sharks caught in Canary Island waters Margarita. *Mar. Fresh Water Res.* 48, 573–576. doi: 10.1071/MF97004
- Huang, D. W., Sherman, B. T., and Lempicki, R. A. (2009). Systematic and integrative analysis of large gene lists using DAVID bioinformatics resources. *Nat. Protoc.* 4, 44–57. doi: 10.1038/nprot.2008.211
- Hui, X., Zhang, M., Gu, P., Li, K., Gao, Y., Wu, D., et al. (2017). Adipocyte SIRT1 controls systemic insulin sensitivity by modulating macrophages in adipose tissue. *EMBO Rep.* 18, 645–657. doi: 10.15252/embr.201643184
- Ishida, M., Tatsumi, K., Okumoto, K., and Kaji, H. (2020). Adipose tissue-derived stem cell sheet improves glucose metabolism in obese mice. *Stem Cells Dev.* 29, 488–497. doi: 10.1089/scd.2019.0250



- Kaya, K., Nakazawa, A., Matsuura, H., Honda, D., Inouye, I., and Watanabe, M. M. (2011). Thraustochytrid *aurantiochytrium* sp. 18w-13a accumulates high amounts of squalene. *Biosci. Biotechnol. Biochem.* 75, 2246–2248. doi: 10.1271/bbb.110430
- Kim, J. A., Wei, Y., and Sowers, J. R. (2008). Role of mitochondrial dysfunction in insulin resistance. *Circ. Res.* 102, 401–414. doi: 10.1161/CIRCRESAHA.107.165472
- Kritchevsky, D., Moyer, A. W., and Tesar, W. C. (1953). Squalene feeding in experimental atherosclerosis. *Arch. Biochem. Biophys.* 44, 241–243. doi: 10.1016/0003-9861(53)90029-0
- Lasselin, J., Magne, E., Beau, C., Ledaguenel, P., Dexpert, S., Aubert, A., et al. (2014). Adipose inflammation in obesity: relationship with circulating levels of inflammatory markers and association with surgery-induced weight loss. *J. Clin. Endocrinol. Metab.* 99, 53–61. doi: 10.1210/jc.2013.2673
- Makki, K., Froguel, P., and Wolowczuk, I. (2013). Adipose tissue in obesity-related inflammation and insulin resistance: cells, cytokines, and chemokines. *ISRN Inflamm.* 2013, 1–12. doi: 10.1155/2013/139239
- Mazini, L., Rochette, L., Admou, B., Amal, S., and Malka, G. (2020). Hopes and limits of adipose-derived stem cells (ADSCs) and mesenchymal stem cells (MSCs) in wound healing. *Int. J. Mol. Sci.* 21:1306. doi: 10.3390/ijms21041306
- McBride, H. M., Neuspiel, M., and Wasiaik, S. (2006). Mitochondria: more than just a powerhouse. *Curr. Biol.* 16, 551–560. doi: 10.1016/j.cub.2006.06.054
- McLaughlin, T., Sherman, A., Tsao, P., Gonzalez, O., Yee, G., Lamendola, C., et al. (2007). Enhanced proportion of small adipose cells in insulin-resistant vs insulin-sensitive obese individuals implicates impaired adipogenesis. *Diabetologia* 50, 1707–1715. doi: 10.1007/s00125-007-0708-y
- Moon, K. C., Chung, H. Y., Han, S. K., Jeong, S. H., and Dhong, E. S. (2019). Possibility of injecting adipose-derived stromal vascular fraction cells to accelerate microcirculation in ischemic diabetic feet: a pilot study. *Int. J. Stem Cells* 12, 107–113. doi: 10.15283/ijsc18101
- Naderi, N., Combelleck, E. J., Griffin, M., Sedaghati, T., Javed, M., Findlay, M. W., et al. (2017). The regenerative role of adipose-derived stem cells (ADSC) in plastic and reconstructive surgery. *Int. Wound J.* 14, 112–124. doi: 10.1111/iwj.12569
- Naderi, N., Wilde, C., Haque, T., Francis, W., Seifalian, A. M., Thornton, C. A., et al. (2014). Adipogenic differentiation of adiposederived stem cells in 3-dimensional spheroid cultures (microtissue): implications for the reconstructive surgeon. *J. Plast. Reconstr. Aesthetic Surg.* 67, 1726–1734. doi: 10.1016/j.bjps.2014.08.013
- Nie, C., Yang, D., Xu, J., Si, Z., Jin, X., and Zhang, J. (2011). Locally administered Adipose-derived stem cells accelerate wound healing through differentiation and vasculogenesis. *Cell Transplant.* 20, 205–216. doi: 10.3727/096368910X520065
- Odegaard, J. I., and Chawla, A. (2013). Pleiotropic actions of insulin resistance and inflammation in metabolic homeostasis. *Science* 339, 172–177. doi: 10.1126/science.1230721
- Oñate, B., Vilahur, G., Ferrer-Lorente, R., Ybarra, J., Díez-Caballero, A., Ballesta-López, C., et al. (2012). The subcutaneous adipose tissue reservoir of functionally active stem cells is reduced in obese patients. *FASEB J.* 26, 4327–4336. doi: 10.1096/fj.12-207217
- Owen, R. W., Mier, W., Giacosa, A., Hull, W. E., Spiegelhalter, B., and Bartsch, H. (2000). Phenolic compounds and squalene in olive oils: the concentration and antioxidant potential of total phenols, simple phenols, secoiridoids, lignans and squalene. *Food Chem. Toxicol.* 38, 647–659. doi: 10.1016/S0278-6915(00)00061-2
- Pérez, L. M., Bernal, A., De Lucas, B., Martín, N. S., Mastrangelo, A., García, A., et al. (2015). Altered metabolic and stemness capacity of adipose tissue-derived stem cells from obese mouse and human. *PLoS One* 10:e0123397. doi: 10.1371/journal.pone.0123397
- Ralston, J. C., and Mutch, D. M. (2015). SCD1 inhibition during 3T3-L1 adipocyte differentiation remodels triacylglycerol, diacylglycerol and phospholipid fatty acid composition. *Prostaglandins Leukot. Essent. Fat. Acids* 98, 29–37. doi: 10.1016/j.plefa.2015.04.008
- Rao, C. V., Newmark, H. L., and Reddy, B. S. (1998). Chemopreventive effect of squalene on colon cancer. *Carcinogenesis* 19, 287–290. doi: 10.1093/carcin/19.2.287
- Rondinone, C. M., Wang, L. M., Lonnroth, P., Wesslau, C., Pierce, J. H., and Smith, U. (1997). Insulin receptor substrate (IRS) 1 is reduced and IRS-2 is the main docking protein for phosphatidylinositol 3-kinase in adipocytes from subjects with non-insulin-dependent diabetes mellitus. *Proc. Natl. Acad. Sci. U.S.A.* 94, 4171–4175. doi: 10.1073/pnas.94.8.4171
- Ruderman, N. B., Carling, D., Prentki, M., and Cacicedo, J. M. (2013). AMPK, insulin resistance, and the metabolic syndrome. *J. Clin. Invest.* 123, 2764–2772. doi: 10.1172/JCI67227.2764
- Russo, L., and Lumeng, C. N. (2018). Properties and functions of adipose tissue macrophages in obesity. *Immunology* 155, 407–417. doi: 10.1111/imm.13002
- Sasaki, K., Inami, Y., Tominaga, K., Kigoshi, H., Arimura, T., and Isoda, H. (2020). Synthesis of 2-(2-Hydroxyethoxy)-3-hydroxysqualene and characterization of its anti-inflammatory effects. *Biomed Res. Int.* 2020, 1–9. doi: 10.1155/2020/9584567
- Schmid, B., Rippmann, J. F., Tadayyon, M., and Hamilton, B. S. (2005). Inhibition of fatty acid synthase prevents preadipocyte differentiation. *Biochem. Biophys. Res. Commun.* 328, 1073–1082. doi: 10.1016/j.bbrc.2005.01.067
- Shan, T., Liu, W., and Kuang, S. (2013). Fatty acid binding protein 4 expression marks a population of adipocyte progenitors in white and brown adipose tissues. *FASEB J.* 27, 277–287. doi: 10.1096/fj.12-211516
- Shimizu, N., Ito, J., Kato, S., Eitsuka, T., Miyazawa, T., and Nakagawa, K. (2019). Significance of squalene in rice bran oil and perspectives on squalene oxidation. *J. Nutr. Sci. Vitaminol.* 65, S62–S66. doi: 10.3177/jnsv.65.S62
- Skurk, T., Alberti-Huber, C., Herder, C., and Hauner, H. (2007). Relationship between adipocyte size and adipokine expression and secretion. *J. Clin. Endocrinol. Metab.* 92, 1023–1033. doi: 10.1210/jc.2006-1055
- Spiegelman, B., Puigserver, P., and Wu, Z. (2000). Regulation of adipogenesis and energy balance. *Int. J. Obes.* 24, 8–10.
- Strandberg, T. E., Tilvis, R. S., and Miettinen, T. A. (1990). Metabolic variables of cholesterol during squalene feeding in humans: comparison with cholestyramine treatment. *J. Lipid Res.* 31, 1637–1643.
- Subramanian, A., Tamayo, P., Mootha, V. K., Mukherjee, S., Ebert, B. L., Gillette, M. A., et al. (2005). Gene set enrichment analysis: a knowledge-based approach for interpreting genome-wide expression profiles. *Proc. Natl. Acad. Sci. U.S.A.* 102, 15545–15550. doi: 10.1073/pnas.0506580102
- Sun, C., Zhang, F., Ge, X., Yan, T., Chen, X., Shi, X., et al. (2007). SIRT1 improves insulin sensitivity under insulin-resistant conditions by repressing PTP1B. *Cell Metab.* 6, 307–319. doi: 10.1016/j.cmet.2007.08.014
- Van Gaal, L. F., Mertens, I. L., and De Block, C. E. (2006). Mechanisms linking obesity with cardiovascular disease. *Nature* 444, 875–880. doi: 10.1038/nature05487
- Van Tienen, F. H. J., Van Der Kallen, C. J. H., Lindsey, P. J., Wanders, R. J., Van Greevenbroek, M. M., and Smeets, H. J. M. (2011). Preadipocytes of type 2 diabetes subjects display an intrinsic gene expression profile of decreased differentiation capacity. *Int. J. Obes.* 35, 1154–1164. doi: 10.1038/ijo.2010.275
- Vyas, K. S., Bole, M., Vasconez, H. C., Banuelos, J. M., Martinez-Jorge, J., Tran, N., et al. (2019). Profile of adipose-derived stem cells in obese and lean environments. *Aesthetic Plast. Surg.* 43, 1635–1645. doi: 10.1007/s00266-019-01397-3
- Xu, X. J., Gauthier, M. S., Hess, D. T., Apovian, C. M., Cacicedo, J. M., Gokce, N., et al. (2012). Insulin sensitive and resistant obesity in humans: AMPK activity, oxidative stress, and depot-specific changes in gene expression in adipose tissue. *J. Lipid Res.* 53, 792–801. doi: 10.1194/jlr.P022905
- Yeh, Y. S., Jheng, H. F., Iwase, M., Kim, M., Mohri, S., Kwon, J., et al. (2018). The mevalonate pathway is indispensable for adipocyte survival. *iScience* 9, 175–191. doi: 10.1016/j.isci.2018.10.019
- Yu, S., Cheng, Y., Zhang, L., Yin, Y., Xue, J., Li, B., et al. (2019). Treatment with adipose tissue-derived mesenchymal stem cells exerts anti-diabetic effects, improves long-term complications, and attenuates inflammation in type 2 diabetic rats. *Stem Cell Res. Ther.* 10, 1–18. doi: 10.1186/s13287-019-1474-8

**Conflict of Interest:** The authors declare that the research was conducted in the absence of any commercial or financial relationships that could be construed as a potential conflict of interest.

Copyright © 2020 Ganbold, Ferdousi, Arimura, Tominaga and Isoda. This is an open-access article distributed under the terms of the Creative Commons Attribution License (CC BY). The use, distribution or reproduction in other forums is permitted, provided the original author(s) and the copyright owner(s) are credited and that the original publication in this journal is cited, in accordance with accepted academic practice. No use, distribution or reproduction is permitted which does not comply with these terms.



# Global Gene Expression Profiling Reveals Isorhamnetin Induces Hepatic-Lineage Specific Differentiation in Human Amniotic Epithelial Cells

Yoshiaki Uchida<sup>1†</sup>, Farhana Ferdousi<sup>2,3†</sup>, Yun-Wen Zheng<sup>4</sup>, Tatsuya Oda<sup>3,4</sup> and Hiroko Isoda<sup>1,2,3,5\*</sup>

## OPEN ACCESS

### Edited by:

Karthikeyan Narayanan,  
University of Illinois at Chicago,  
United States

### Reviewed by:

Shailaja Rao,  
Stanford University, United States  
Kazuo Takayama,  
Kyoto University, Japan  
Roberto Gramignoli,  
Karolinska Institutet (KI), Sweden

### \*Correspondence:

Hiroko Isoda  
isoda.hiroko.ga@u.tsukuba.ac.jp

<sup>†</sup>These authors have contributed  
equally to this work

### Specialty section:

This article was submitted to  
Stem Cell Research,  
a section of the journal  
*Frontiers in Cell and Developmental  
Biology*

**Received:** 30 June 2020

**Accepted:** 13 October 2020

**Published:** 05 November 2020

### Citation:

Uchida Y, Ferdousi F, Zheng Y-W,  
Oda T and Isoda H (2020) Global  
Gene Expression Profiling Reveals  
Isorhamnetin Induces  
Hepatic-Lineage Specific  
Differentiation in Human Amniotic  
Epithelial Cells.  
*Front. Cell Dev. Biol.* 8:578036.  
doi: 10.3389/fcell.2020.578036

<sup>1</sup> School of Integrative and Global Majors (SIGMA), University of Tsukuba, Tsukuba, Japan, <sup>2</sup> Alliance for Research on the Mediterranean and North Africa (ARENA), University of Tsukuba, Tsukuba, Japan, <sup>3</sup> AIST-University of Tsukuba Open Innovation Laboratory for Food and Medicinal Resource Engineering (FoodMed-OIL), AIST, University of Tsukuba, Tsukuba, Japan, <sup>4</sup> Department of Gastrointestinal and Hepato-Biliary-Pancreatic Surgery, Faculty of Medicine, University of Tsukuba, Tsukuba, Japan, <sup>5</sup> Faculty of Life and Environmental Sciences, University of Tsukuba, Tsukuba, Japan

Human amnion epithelial cells (hAECs), derived from discarded term placenta, is anticipated as a new stem cell resource because of their advantages over embryonic stem cells (ESCs) and induced pluripotent stem cells (iPSCs), such as no risk of tumorigenicity and minimal ethical issue. hAECs have been reported to differentiate into hepatic-like cells (HLCs) with variable functionalities suitable for cell-based therapy of end-stage liver diseases, drug screening, and drug toxicity tests. On the other hand, a new research stream has been evolving to use natural compounds as stimulants of stem cell differentiation because of their high availability and minimum side effects. Isorhamnetin is a naturally occurring flavonoid commonly found in fruits and vegetables and has been reported to improve hepatic fibrosis and steatosis. In this present study, we have screened the differentiation potential of isorhamnetin in hAECs. The cells were grown on 3D cell culture and were treated with 20  $\mu$ M of synthesized isorhamnetin for 10 days without adding any additional growth factors. DNA microarray global gene expression analysis was conducted for differentially expressed genes between isorhamnetin-treated and untreated control cells, gene expression validation was carried out using RT-qPCR method, and finally, several hepatic functions were assessed. Microarray analysis showed that isorhamnetin could activate essential biological processes, molecular functions, and signaling pathways for hepatic differentiation. Hepatic progenitor markers, *EPCAM* and *DLK1*, were upregulated in the isorhamnetin-treated hAECs. *AFP* was downregulated, while *ALB* was upregulated on Day 10. Furthermore, isorhamnetin-treated cells could show increased CYP enzyme mRNA levels, ICG uptake and release, glycogen storage activity, and urea secretion. Additionally, isorhamnetin-treated cells did not show any trace of transdifferentiation

evident by significant downregulation of several colon- and cholangiocyte-specific markers. However, longer treatment with isorhamnetin did not promote hepatic maturation. Altogether, our findings indicate that isorhamnetin has a promising effect on directing the hepatic-lineage specific differentiation in hAECs.

**Keywords:** human amnion epithelial cell, isorhamnetin, hepatic-lineage-specific differentiation, microarray and bioinformatics, natural compound

## INTRODUCTION

Human amniotic epithelial cells (hAECs) are obtained from discarded term placenta, which is a medical waste product. hAECs are originated from the epiblast, thus retain pluripotent stem cell characteristics and give rise to all kinds of cells of three germ layers (Tamagawa et al., 2004; Miki et al., 2005; García-Castro et al., 2015). Besides, hAECs possess immune-privileged characteristics as they express all classical human leukocyte antigen (HLA) class I molecules as well as HLA-G (Adinolfi et al., 1982; Hammer et al., 1997), but do not express HLA class II molecules (Banas et al., 2008; Murphy et al., 2010). Moreover, hAECs do not possess telomerase and have no or low possibility of tumorigenicity (Miki et al., 2005; Bilic et al., 2008). hAECs have several other advantages over embryonic stem cells (ESCs) and induced pluripotent stem cells (iPSCs) such as easy isolation, reduced or no risk of rejection, and minimal ethical issues. Therefore, hAEC is anticipated as a new candidate for stem cell resource (Hori et al., 2006; Miki and Strom, 2006; Miki, 2011).

To date, several studies have shown that upon appropriate differentiation protocol, hAECs can be differentiated into cardiomyocytes, pancreas and lung epithelium, bone and fat cells as well as neural cells (Miki et al., 2005, 2010; Toda et al., 2007; Parolini et al., 2008; Murphy et al., 2010; Fang et al., 2012). Furthermore, studies have reported hepatic differentiation potentials of hAECs using multistep proliferation and differentiation protocols involving several combinations of growth factors and cytokines (Marongiu et al., 2011; Lin et al., 2015; Liu et al., 2018; Maymó et al., 2018). In our previous study, we have reported that the hAECs isolated from the adherent subpopulations of passaged primary cells have widely expressed stemness markers (Furuya et al., 2019). We have also shown that hAECs cultured in a 3D microenvironment as spheroids have highly expressed the stemness-related genes compared to their 2D counterpart (Ferdousi et al., 2019). In 3D culture of hAECs, we could generate functional hepatic organoids using several growth factors (Furuya et al., 2019).

**Abbreviations:** AFP, Alpha-fetoprotein; ALB, Albumin; BMP, Bone morphogenetic protein; COL1A1, Collagen type 1 alpha 1; CYP3A4, Cytochrome P450 3A4; CYP3A7, Cytochrome P450 3A7; DAVID, Database for Annotation, Visualization, and Integrated Discovery; DLK-1, Delta-like-1; EGF, Epidermal growth factor; EGFR, Epidermal growth factor receptor; EPCAM, Epithelial Cell Adhesion Molecule; ESC, Embryonic stem cell; FGF, Fibroblast growth factor; hAEC, Human amniotic epithelial cell; HHEX, Hematopoietically expressed homeobox; HLC, Hepatocyte-like cells; HNF4a, Hepatocyte nuclear factor 4 alpha; ICG, Indocyanine Green; iPSC, Induced pluripotent stem cell; Klf4, Kruppel Like Factor; LGR5, Leucine-rich-repeat-containing G-protein-coupled receptor 5; NANOG, Homeobox protein NANOG; OCT4, Octamer-binding transcription factor 4; PAS, Periodic Acid Schiff; TGF- $\beta$ , Transforming growth factor- $\beta$ .

In this context, a new research stream has been evolving to use medicinal plant extracts as stimulants of stem cells because of their high availability, low toxicity, and minimum side effects (Udalamaththa et al., 2016; Kornicka et al., 2017; Udagama and Udalamaththa, 2018; Saud et al., 2019). However, despite the fact that hAECs were discovered decades ago, few researches have been done on using natural compounds to optimize the microenvironment or to regulate the early biological events for controlled differentiation of hAECs. In our previous studies, we have reported that a natural compound rosmarinic acid could induce neuronal differentiation in hAEC (Ferdousi et al., 2019), whereas verbenalin-treated hAECs showed therapeutic potential for Alzheimer's disease (Ferdousi et al., 2020). Another recent study has reported that vitamin C, a natural antioxidant, could promote the proliferation, migration, and self-renewal of hAECs *in vitro* and elevate the therapeutic potential of hAECs in premature ovarian insufficiency model mice (Hou et al., 2020). However, no study to date reports a natural bioactive compound manipulates the molecular fate and directs hepatic lineage-specific differentiation in hAEC.

Isorhamnetin (3-Methylquercetin or 3'-Methoxyquercetin) is a flavonoid naturally occurring in several fruits and plant-derived foods. Several studies have reported its preventive effects against metabolic disorders, specifically against liver diseases (Lee et al., 2010; Yang et al., 2016; Zhang et al., 2016; Ganbold et al., 2019; Liu et al., 2019). Isorhamnetin exerts its bioactivities through regulating Wntless-related integration site (Wnt)/ $\beta$  catenin and transforming growth factor-beta (TGF $\beta$ ) signaling pathways. These pathways are implicated in almost every facet of liver biology- from liver cell fate decision to liver organogenesis and to liver pathologies (Clotman et al., 2005; Clotman and Lemaigre, 2006; Nejak-Bowen and Monga, 2008; Touboul et al., 2016; Russell and Monga, 2018).

In this perspective, we have hypothesized that isorhamnetin may have the potential to induce directed differentiation of hAECs toward hepatic lineage. In the present study, we have investigated the early biological events regulated by isorhamnetin to induce hepatic-lineage-specific differentiation of hAECs maintained in 3D culture conditions through gene expression profiling and further validated several hepatic function tests.

## MATERIALS AND METHODS

### Extraction of Amnion Epithelial Cells

In our previous studies, a detailed methodology of hAEC extraction, culture, and 3D spheroid formation have been documented (Ferdousi et al., 2019; Furuya et al., 2019). Briefly,

hAECs were extracted from the term placenta. The amnion was aseptically separated from the chorion and washed with Hank's Basic Salt Solution (CMF-HBSS). Pre-digestion buffer (CMF-HBSS, 0.5 mM EGTA) was added and then incubated at 37°C for 10 min. The pre-digestion buffer was discarded and 0.05% trypsin-EDTA was added and incubated for 40 min at 37°C. Two volume of DMEM was added and centrifuged at  $200 \times g$  for 10 min at 4°C. The supernatant was discarded, and the pellet was resuspended in DMEM.

## Cell Culture Maintenance

The cells were cultured in the Placental Epithelial Cell Basal Medium that contains no growth factor (Promo Cell, Cat. #C-26140). The medium was changed every 2 days. In order to subculture, cells were firstly washed with PBS and then the pre-digestion buffer was added. Cells were then incubated at 37°C for 5 min. Pre-digestion buffer was discarded and 0.05% trypsin-EDTA was added and incubated for 10 min at 37°C. Two volume of DMEM was added and centrifuged at  $200 \times g$  for 10 min at 4°C. After centrifugation, the supernatant was discarded, and the cell concentration was adjusted with a new medium.

## Preparation of 3D Cell Plate

To prepare a 3D cell culture plate, 400  $\mu$ l of Lipidure solution was placed into each well of the 3D culture plate (Elplasia, Kuraray Co., Ltd.) and was sit for 2 min. And then, the Lipidure solution was aspirated out, to dry the plate. After drying, PBS was placed in each well, and the plate was centrifuged at  $2000 \times g$  for 15 min at room temperature. The PBS was then discarded, and the wells were washed twice with PBS. The plate was in an incubator until use.

## Spheroid Formation and Compound Treatment on 3D Cell Culture

The cells were cultured in a 3D plate and maintained in the Placental Epithelial Cell Basal Medium (Promo Cell, Cat. #C-26140). Spheroid was formed by seeding  $8 \times 10^5$  cells. After 24 h, the medium was changed with isorhamnetin (20  $\mu$ M). The medium was changed every 2 days, and the cells were maintained for 10–20 days.

## RNA Extraction

Total RNA was extracted using 1 ml of ISOGEN (Nippon Gene, Japan). Chloroform (Wako, Japan) was added to obtain the supernatant aqueous phase. Then isopropanol (Sigma) was added at 0.8 volume, incubated for 5 min at 26°C (room temperature). The supernatant was discarded, and 1 ml of 70% EtOH was added and centrifuged (4°C,  $12,000 \times g$ , 5 min). The supernatant was discarded, and the RNA was dried at 26°C (room temperature) until no bubble was visible. Finally, the RNA solution was dissolved with Tris-EDTA buffer solution pH 8.0 (Sigma) and was quantified by using a NanoDrop 2000 spectrophotometer (Thermo Fisher Scientific, United States).

## Real-Time PCR

Complementary DNA synthesis was performed by using the Thermo Scientific Revert Aid First Strand cDNA Synthesis

Kit (Cat. #K1691) following the manufacturer's instructions. RT-qPCR was performed with the Superscript III reverse transcriptase kit (Invitrogen, United States) and 2720 Thermal cycler (Applied Biosystems, United States). For the quantification of amounts of transcripts, the TaqMan real-time RT-PCR amplification reactions were performed with a 7500 Fast Real-Time PCR system. TaqMan Universal PCR mix was used for the thermal cycling, and the run method was 95°C for 10 min, followed by 60 cycles of PCR (95°C for 15 s and 60°C for 1 min).

## Mitochondrial-Dependent Reduction of 3-(4,5-Dimethylthiazol-2-yl)-2,5-Diphenyltetrazolium Bromide (MTT) Assay

The cell viability was analyzed by using MTT assay to check the effects isorhamnetin on cytotoxicity. hAECs were seeded at  $2 \times 10^5$  cells/mL and incubated for 24 h. Cells were then treated with several concentrations of isorhamnetin for 72 h. After the treatment, MTT was added and incubated for 6 h at 37°C in the dark. After incubation, 10% sodium dodecyl sulfate (SDS) was added (100  $\mu$ l) and incubated for over-night at 37°C. The optical density (OD) was measured at 570 nm with a microplate reader Varioskan LUX (Thermo Scientific, Rockford, IL, United States).

## Affymetrix Microarray Gene Expression

We conducted Affymetrix microarray gene expression profiling using GeneChip 3' Expression Arrays and 3' IVT PLUS Reagent Kit (Affymetrix Inc., Santa Clara, CA, United States). We used 250 ng of total RNA from each sample to generate amplified and biotinylated cRNA from poly (A) RNA in a total RNA sample following the users' manual. For hybridization, 9.4  $\mu$ G of cRNA samples were used. Human Genome U219 array strips (HG-U219) were hybridized for 16 h in a 45°C incubator, washed and stained. Imaging was conducted in the GeneAtlas Fluidics and Imaging Station. Each HG-U219 array strip is comprised of more than 530,000 probes, which cover approximately 36,000 transcripts and variants and represent more than 20,000 unique genes. The microarray was performed on two biological replicates of D0 control cells, three biological replicates of D10 control and D10 isorhamnetin-treated hAECs each, and two biological replicates of D20 control and D20 isorhamnetin-treated hAECs each. All data are deposited in a public functional genomics data repository, Gene Expression Omnibus (GEO) (Barrett et al., 2012), under the accession number GSE148777<sup>1</sup>.

## Microarray Data Processing and Analysis

Expression Console Software (provided by the Affymetrix) was used to normalize the raw data following the robust multichip average (RMA) algorithm<sup>2</sup>. Subsequent analysis of the gene expression data was carried out in the freely available Transcriptome Analysis Console (TAC) version 4 (Affymetrix, Japan). Differentially expressed genes (DEGs) were defined as

<sup>1</sup><https://www.ncbi.nlm.nih.gov/geo/query/acc.cgi?acc=GSE148777>

<sup>2</sup><http://www.affymetrix.com>



the genes that satisfy both  $p$ -value  $< 0.05$  (one-way between-subjects ANOVA) and fold-change (in linear space)  $\geq 2$  criteria simultaneously. The Molecular Signatures Database (MSigDB, v7.1) of Gene Set Enrichment Analysis (GSEA) software was used to determine significantly enriched Hallmark gene sets and gene ontologies (GO)<sup>3</sup>. MSigDB is a collection of annotated gene sets and one of the most widely used databases for performing gene set enrichment analysis (Subramanian et al., 2005; Liberzon et al., 2011, 2015). For gene functional annotation and pathway analysis, we also used an online data mining tool Database for Annotation, Visualization and Integrated Discovery (DAVID) v6.8. For any given gene list, DAVID tools are able to identify enriched biological GO terms (biological process, molecular function, and cellular component) and can discover enriched functional-related gene groups (Huang et al., 2008; Sherman et al., 2008). Heat maps were generated using a visualization software Morpheus<sup>4</sup>. Venn diagram was created using an online tool<sup>5</sup>. All data generated or analyzed during this study are included in this published article and its **Supplementary Material**.

### Indocyanine Green (ICG) Uptake and Clearance

Indocyanine green (Tokyo Chemical Industry Co., Ltd.) was dissolved to 5 mg/ml in DMSO as the stock solution and was diluted in culture medium to 1 mg/ml as the working solution. After 10 days of treatment on the 3D cell plate, cells were transplanted in a tube, and ICG was added. Then the cells were incubated for 30 min at 37°C. After that, cells were washed three times with PBS and added culture medium. At this time, ICG uptake was detected by light microscopy. ICG clearance was detected after 6 h following previous protocols (Lin et al., 2015; Furuya et al., 2019).

### Periodic Acid-Schiff (PAS) Staining

Periodic acid-schiff stains the stored glycogen in cells. At first, cells were washed with water. And then formalin was added for 2 min. Cells were washed with water, and 0.5% periodic acid was added for 7 min, after this, incubated in Schiff's reagent for 10 min.

### Urea Assay

The concentration of urea in culture media was measured using the colorimetric assay according to the manufacturer's instructions (640-1, Sigma, Japan). To obtain the final absorbance value for determining urea concentrations from the standard curve, the absorbance of the basal medium was subtracted from the absorbance of each test sample.

### Statistical Analysis

Comparisons between treatment groups were conducted using one-way ANOVA followed by Tukey's *post hoc* test. Data were

presented as means  $\pm$  standard deviation (SD); unless otherwise mentioned.  $P < 0.05$  was considered as significant. All analyses were performed using GraphPad Prism 8 software (GraphPad Software Inc., San Diego, CA, United States).

### Ethics Statement

The Ethical Review Committee of the University of Tsukuba Hospital approved the protocol. Informed written consent was received from the mothers who donated the placenta after delivery.

## RESULTS

### 3D Cell Culture Enhanced the Pluripotency and Was Optimal Cell Culture for hAEC Differentiation

Recently, 3D cell culture has been widely used, especially in stem cell research, as it can closely mimic the microenvironment of our body and improve the differentiation. It was reported that cell culturing leads hAECs to lose their pluripotency (Ferdousi et al., 2019; Furuya et al., 2019). Thus, we first evaluated the effect of cell culture (2D or 3D) conditions on hAEC pluripotency. We found that several pluripotency markers, namely, Nanog Homeobox (*NANOG*), Octamer-binding transcription factor 4 (*OCT4*) and Sry-related HMG box gene 2 (*SOX2*), were significantly upregulated in 3D cell culture compared to 2D culture after 10 days (**Supplementary Figure 1A**). Thus, 3D cell culture was considered optimal for the hAEC differentiation in our research.

### 20 $\mu$ M of Isorhamnetin Was Determined as the Optimal Concentration for hAEC Differentiation

Next, the MTT assay was performed to decide the optimal concentration of isorhamnetin suitable for hAECs differentiation. From MTT assay, we found that up to the concentration of 10  $\mu$ M, the number of viable cells was slightly increased (**Supplementary Figure 1A**). At the concentration of 20  $\mu$ M, viable cell numbers on MTT significantly decreased. Therefore, firstly we evaluated gene expression changes in hAECs through microarray and RT-qPCR treated with 5, 10, and 20  $\mu$ M of isorhamnetin. However, no significant changes in gene expression levels of hepatic progenitor markers were observed in lower doses (data not shown). Treatment with 20  $\mu$ M isorhamnetin was found to be optimal to induce differentiation in hAECs.

### Isorhamnetin Regulated Gene Expression in hAECs on Day 10 (D10) Culture

**Figures 1A,B** show the DEGs in D10 isorhamnetin-treated hAECs compared to D0 and D10 control hAECs, respectively. A total of 1614 genes were differentially expressed in D10 isorhamnetin-treated hAECs compared to D0 control cells,

<sup>3</sup><https://software.broadinstitute.org/gsea/index.jsp>

<sup>4</sup><https://software.broadinstitute.org/morpheus>

<sup>5</sup><http://bioinformatics.psb.ugent.be/webtools/Venn/>

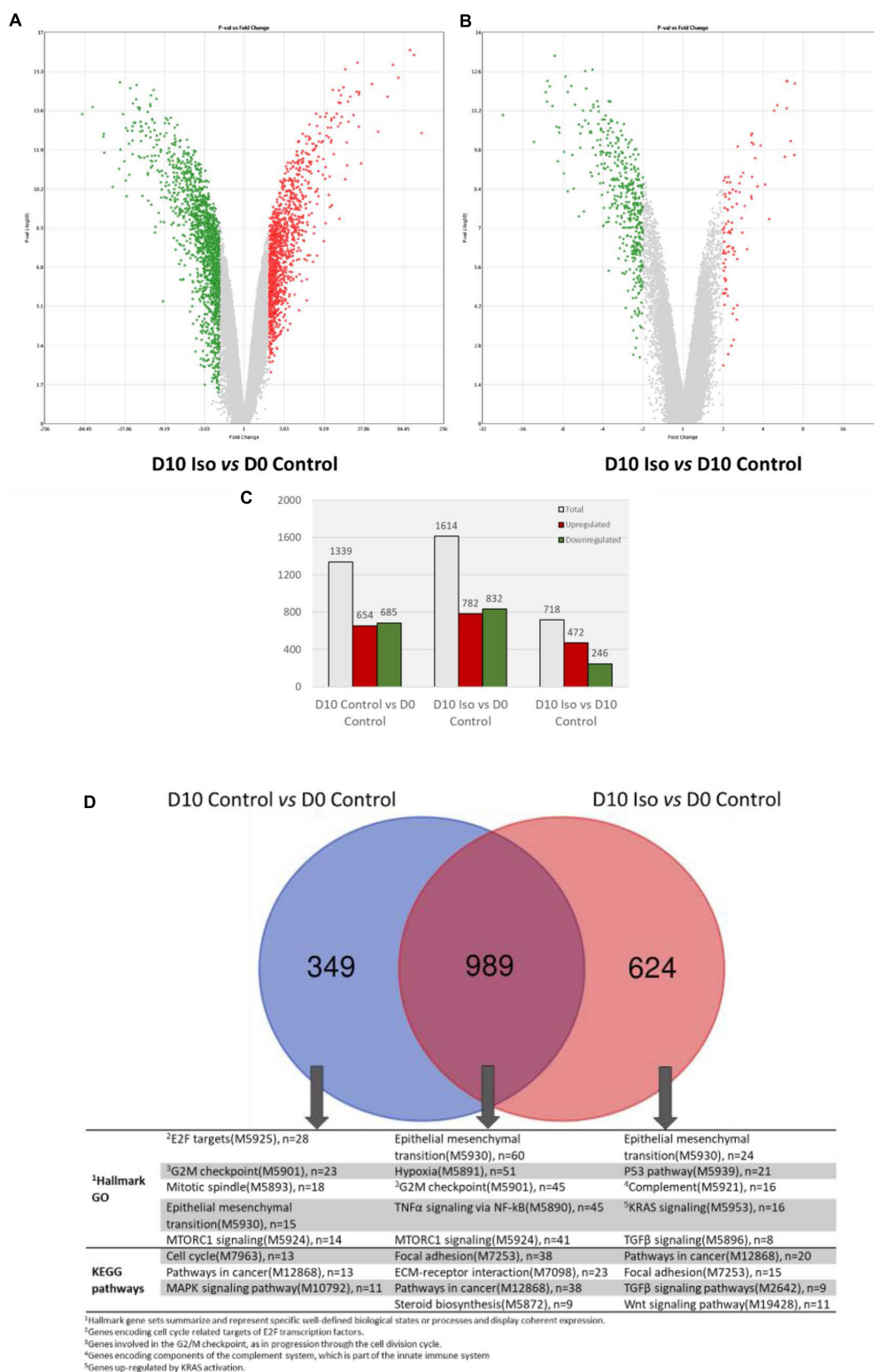


**FIGURE 1 |** Volcano plots showing DEGs (fold change > 2,  $p$  value < 0.05) between **(A)** D10 isorhamnetin-treated and D0 control hAECs, and **(B)** D10 isorhamnetin-treated and D10 control hAECs. The Y-axis corresponds to  $-\log_{10} p$ -value, and the X-axis displays linear fold change. The red dots represent the upregulated genes; the green dots represent the downregulated genes. **(C)** Bar graph showing number of DEGs in each treatment pair. **(D)** Venn diagram showing common and unique sets of DEGs between each exposure. Blue circle denotes DEGs between D10 and D0 controls; red circle denotes DEGs between D10 isorhamnetin-treated and D0 control hAECs. Iso, Isorhamnetin.

among which 782 DEGs were upregulated, and 832 DEGs were downregulated (**Figure 1C**). When compared to D10 control hAECs, total 718 genes were differentially expressed in D10 isorhamnetin-treated cells, of which 472 were upregulated and 246 were downregulated. However, longer treatment with isorhamnetin for 20 days did not show much effect on the gene expressions (**Supplementary Figures 2A–E**). Therefore, we evaluated the effect of isorhamnetin on hAECs on D10 culture.

**Figure 1D** shows the common and unique genes between D10 control and isorhamnetin-treated cells. Although cells were maintained in Placental Basal Medium, the control cells showed changes in gene expressions related to cell cycle and epithelial-mesenchymal transition (EMT). As reported earlier, hAECs are primarily committed to ectodermal lineage-derived cells (Pan et al., 2006) and can actually express neuronal markers without any induction. Among the DEGs, 989 were commonly regulated in both control and treatment cells. Common functions include EMT, cell division, cell adhesion, and as well as tumor necrosis factor alpha (TNF $\alpha$ ) signaling and steroid biosynthesis. On the other hand, 624 DEGs were uniquely regulated in isorhamnetin-treated cells, which particularly enriched transforming growth factor beta (TGF $\beta$ ) and Wnt/ $\beta$  catenin pathways. Top 20 up and downregulated DEGs between D10 treated and control hAECs and their functions are listed in **Supplementary Tables 1, 2**.

### Isorhamnetin Regulated Biological Processes (BP) in D10 hAECs Compared to Undifferentiated Control (D0)

Gene ontology analysis using DAVID's functional analysis tool shows that several BPs related to cell cycle, extracellular matrix (ECM) organization and mature liver functions were regulated in D10 treatment and control cells (**Figure 2**). While cell division and cell cycle associated GOs were highly enriched in D10 control cells, cell adhesion, cell-cell junction, EMT, ECM organization, Wnt, and TGF $\beta$  signaling GOs were highly enriched in D10 isorhamnetin-treated hAECs. Furthermore, several injury stimulus-related BPs, such as platelet degranulation, angiogenesis, wound healing, were highly enriched in isorhamnetin-treated cells. The fold enrichment is calculated as the ratio of the two proportions: the proportion of genes associated with the GO category in a list of DEGs of a study and the proportion of genes associated with that GO in the human genome (DAVID online tool).

Next, we identified top enriched molecular functions (MFs) in isorhamnetin-treated cells compared to D0 control cells, which include stearoyl-CoA 9-desaturase activity (GO:0004768), ECM constituent conferring elasticity (GO:0030023), type II TGF $\beta$  receptor binding (GO:0005114), connexin binding (GO:0071253), histone methyltransferase activity (GO:0042799), and insulin-like growth factor binding (GO:0005520) (**Figure 3A**).

We performed gene functional classification clusters of DEGs using "Gene Functional Classification Tool" of DAVID software (**Table 1**). Enrichment criteria was set as: medium classification stringency; Kappa Similarity Term Overlap = 4; Kappa Similarity

Threshold = 0.35; and Multiple Linkage Threshold = 0.5. Total 51 clusters were enriched by the DEGs between D10 isorhamnetin-treated hAECs and D0 control hAECs. Top enriched clusters included cell cycle, cell division, cell-adhesion, and cell junction-related GOs. DEGs between D10 isorhamnetin-treated hAECs and D10 control hAECs enriched 8 clusters, which included ECM migration, EMT, TGF $\beta$  signaling, and Wnt pathway-related GOs.

### Isorhamnetin Regulated Hepatic Differentiation Specific KEGG Pathways and Gene Functional Categories in D10 hAECs Compared to D10 Control

As GO analysis shows that both D10 control and D10 isorhamnetin-treated hAECs enriched similar BPs and MFs, we evaluated enriched functional categories of DEGs between D10 isorhamnetin-treated and D10 control cells (**Figure 3B**). Top enriched functional categories (according to fold enrichment) of the DEGs were catecholamine biosynthesis, heparan sulfate, growth factor binding, aminotransferase, proteoglycan, ECM, laminin EGF-like domain, and collagen.

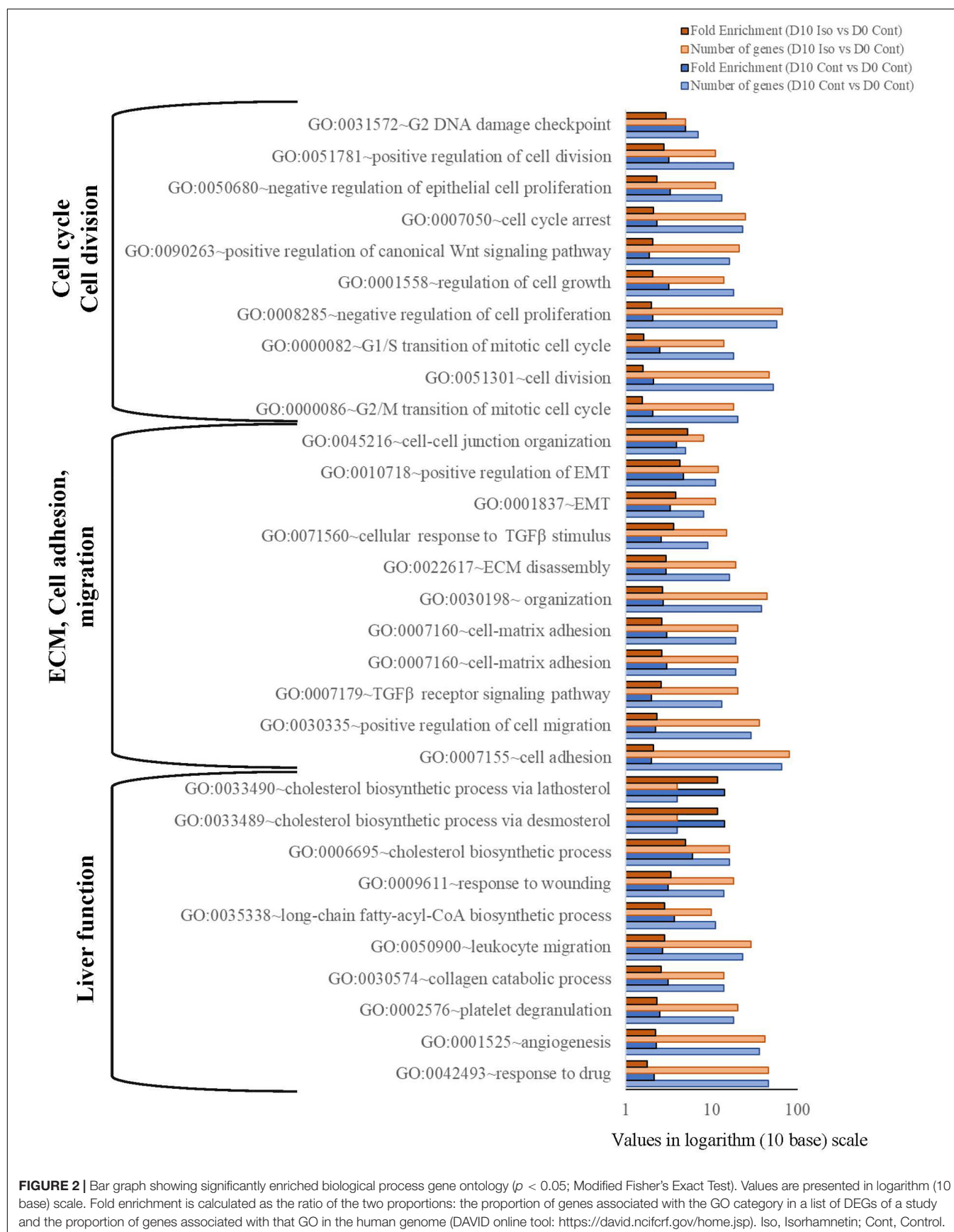
Next, we identified significantly enriched (Modified Fisher Exact *p*-values with EASE threshold 0.1) KEGG pathways by the DEGs between D10 isorhamnetin-treated and D10 control cells (**Figure 3C**). Top pathways include, but not limited to, FoxO, Hippo, AMPK, Wnt, PI3K-Akt, TGF $\beta$ , mTOR, insulin, Hedgehog, Sphingolipid, and Prolactin signaling pathways, all of which are essential signaling pathways for hepatocyte differentiation.

### Isorhamnetin Did Not Regulate the mRNA Levels of Definitive Endoderm (DE) Markers

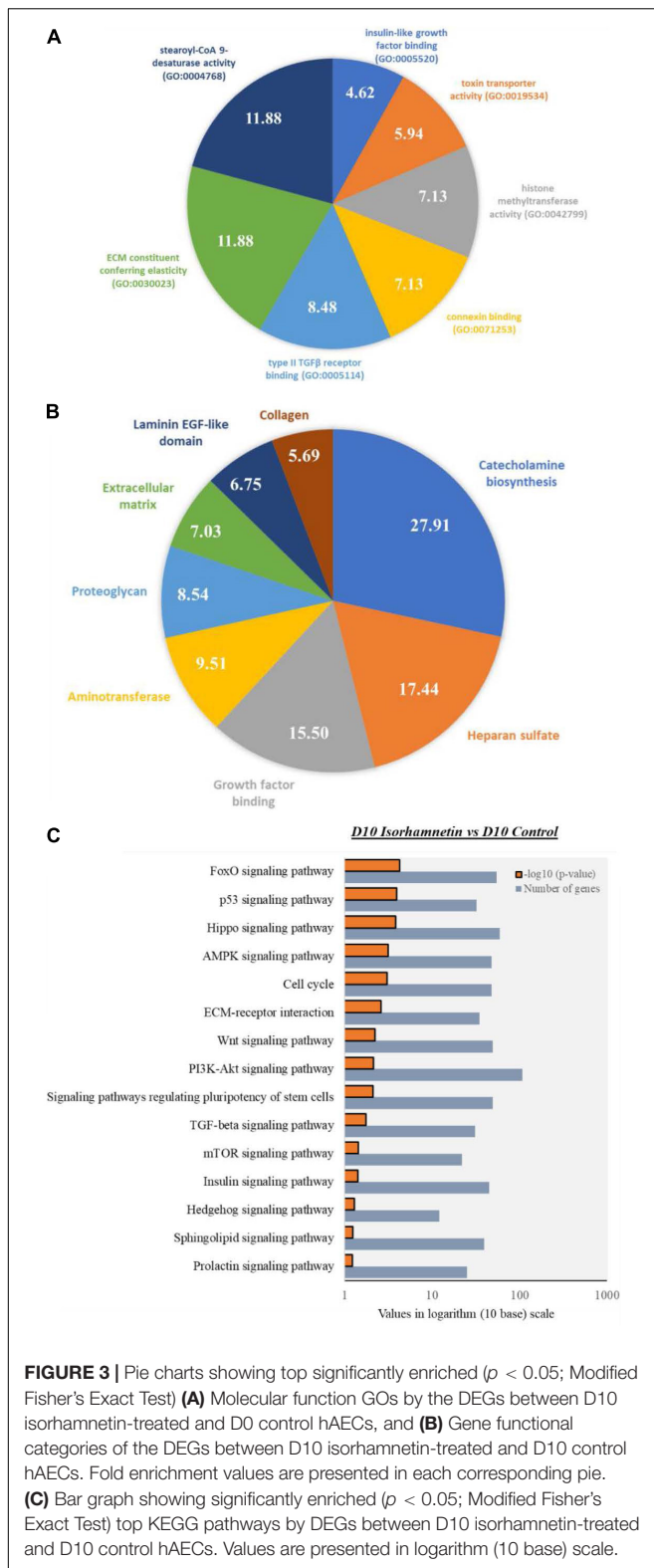
As the microarray results showed evidence of hepatic differentiation induction in isorhamnetin-treated hAECs, we further evaluated the expression of several DE markers in RT-qPCR on day 4 (D4) and D10 hAECs. However, DE markers *GATA4*, *FOXA2*, and *HNF4 $\alpha$*  could not be detected neither in control nor in treatment cells on D4 and D10 (data not shown). Only *SOX17* was downregulated in D4 treatment and control cells compared to undifferentiated D0 cells (**Supplementary Figure 3A**).

### Isorhamnetin Regulated the Gene Expression of the Hepatic Progenitor (HP) Markers

Next, we evaluated the expression of several HP markers in RT-qPCR. After 10 days of treatment with isorhamnetin, delta like non-canonical notch ligand 1 (*DLK-1*) and epithelial cell adhesion molecule (EPCAM) were significantly upregulated compared to both D0 and D10 controls (**Figure 4A**). Also, an endoderm marker SRY-Box transcription factor 17 (*SOX17*) was significantly downregulated in isorhamnetin-treated hAECs compared to both controls. Additionally, alpha fetoprotein (*AFP*) was significantly







downregulated and albumin (*ALB*) was significantly upregulated in hAECs after 10 days of isorhamnetin treatment (Figure 4A).

Furthermore, in microarray analysis, we found that the expression of genes related to undefined placenta (Figure 4B), and pluripotency (Figure 4C) were downregulated, while several hepatoblast (Figure 4D), and hepatocyte (Figure 4E) marker genes were upregulated in D10 isorhamnetin-treated hAECs.

## Isorhamnetin-Treated hAECs Did Not Retain Any Molecular Traces for Transdifferentiation and Dedifferentiation

We evaluated whether isorhamnetin regulated the gene expressions of other cell lineages or its effect was directed exclusively to hepatocytes. In microarray, we found that several GOs related to neurogenesis, endodermal and osteoblast differentiation as well as heart and muscle structure development were significantly downregulated (Figure 5A). Heatmaps shows that the signal intensities of immune cell marker *SIGLEC5*, lung fibrocyte marker *CD248*, stem cell marker *ABCG2*, erythroid differentiation marker *GYPE* as well as markers of myeloid/osteogenic (*BST5*), chondrogenic (*CD151*), adipocyte (*CD36*), and pancreatic (*CD55*) differentiation were significantly low in isorhamnetin-treated hAECs (Figure 5B). In addition, several cholangiocyte (Figure 5C) and colon (Figure 5D)-specific markers were downregulated in isorhamnetin-treated cells.

Next, we performed the RT-qPCR to validate the microarray findings. Isorhamnetin significantly downregulated the expression of colon progenitor marker *EPHB2*, adult intestinal stem cell marker *LGR5*, cholangiocyte marker *CK7*, and fibrocyte/osteoblast lineage marker *COL1A1* (Figure 5E).

## Isorhamnetin-Treated hAECs Showed Weak CYP Enzyme Activity

We further investigated whether the differentiated cells in isorhamnetin have attained the characteristics of mature hepatocytes. We evaluated endogenous metabolic markers of hepatic cytochrome P450 (CYP). In microarray analysis, several CYP enzymes, namely *CYP20A1*, *CYP4V2*, *CYP3A5*, *CYP2C8*, *CYP11A1*, showed higher expression in isorhamnetin-treated hAECs compared to undifferentiated and D10 control hAECs; however, the expressions were not consistent in all experimental replicates of treatment cells (Figure 6A). Even longer treatment with isorhamnetin did not improve CYP expressions (Supplementary Figure 3B). In RT-qPCR, *CYP3A7* was undetectable on D0 and significantly upregulated in D10 isorhamnetin group compared to both controls (D0 and D10) (Figure 6B). We also checked the *CYP4V2* expression, which was also significantly upregulated by isorhamnetin treatment. However, *CYP3A4* mRNA level was undetected in all samples (D10 and D20). Similarly, no inducible CYP enzyme activity of *CYP3A4* could be observed in isorhamnetin-treated hAECs (D10 and D20).

Next, we evaluated mRNA levels of lipid metabolism-related genes. Same as CYP enzymes, *APO* expressions were not consistent in all three replicates of isorhamnetin-treated hAECs (microarray results), although they showed relatively higher expressions compared to D0 and D10 controls

**TABLE 1 |** Gene functional classification clusters of DEGs between D10 isorhamnetin-treated and D0 control hAECs and D10 isorhamnetin-treated and D10 control hAECs.

Clusters and top enriched GO in cluster	Enrichment score	Genes in cluster
<b>D10 isorhamnetin treated vs. D0 control</b>		
<b>Cluster 1</b> cilium assembly (GO:0060271), microtubule cytoskeleton organization (GO:0000226), mitotic cell cycle (GO:0000278), cell division (GO:0051301), protein binding (GO:0005515), microtubule binding (GO:0008017)	13.63	<i>SPICE1, C1orf116, CEP95, BBOF1, SPATA18, CEP162, CEP55, CEP126, MAP7D3, KIAA0753, FILIP1L, CCDC113, MISR, MTUS2, MZT2A, NREP, RAB3IP, CEP68, CAMSAP2, ZNF365</i>
<b>Cluster 2</b> cell division (GO:0051301), mitotic cell cycle (GO:0000278), cell population proliferation (GO:0008283), regulation of mitotic spindle organization (GO:0060236), metaphase plate congression (GO:0051310), microtubule binding (GO:0008017), protein kinase binding (GO:0019901), protein binding (GO:0005515)	9.37	<i>TPX2, TACC3, SPICE1, CDCA3, PRC1, MISR, MAPRE2, FAM83D, CCNG2, MAP7D3</i>
<b>Cluster 3</b> cell-cell adhesion (GO:0098609), cell differentiation (GO:0030154), cell junction assembly (GO:0034329), transforming growth factor beta receptor signaling pathway (GO:0007179), zinc ion binding (GO:0008270), cadherin binding involved in cell-cell adhesion (GO:0098641)	9.17	<i>FBLIM1, TGFB111, PDLIM5, ZYX, PDLIM2, AJUBA, CRIP1, ZNF185, LIMS2, C11orf54, FHL2, FHL1, LMO7, LIMA1, LMCD1, CSRP2, CSRP1, PDLIM1, TES, PRICKLE2, PXN, PDLIM7</i>
<b>Cluster 4</b> apical constriction (GO:0003383), regulation of cell shape (GO:0008360), integrin-mediated signaling pathway (GO:0007229), transforming growth factor beta receptor signaling pathway (GO:0007179), protein binding (GO:0005515), structural constituent of cytoskeleton (GO:0005200)	7.54	<i>FERMT1, RAPH1, FRMD6, FERMT2</i>
<b>Cluster 5</b> protein ubiquitination (GO:0016567), transcription, DNA-templated (GO:0006351)	7.51	<i>FILIP1L, IRF2BP2, CRBN, PRR1</i>
<b>D10 isorhamnetin treated vs. D10 control</b>		
<b>Cluster 1</b> sequestering of TGFβ in ECM (GO:0035583), positive regulation of cell substrate adhesion (GO:0010811), cell-matrix adhesion (GO:0007160), extracellular matrix organization (GO:0030198), calcium ion binding (GO:0005509), extracellular matrix structural constituent (GO:0005201)	7.70	<i>THBS3, SUSU1, EFEMP2, FBN2, FBLN2, NPNT, LTBP2, LTBP1, DNER</i>
<b>Cluster 2</b> O-glycan processing (GO:0016266), G protein-coupled receptor signaling pathway (GO:0007186), cell surface receptor signaling pathway (GO:0007166), cell migration (GO:0016477), cell adhesion (GO:0007155), G protein-coupled receptor activity (GO:0004930)	7.42	<i>LGR5, UPK3BL, TMEM40, ALPK2, LY6G6C, GPR85, MYRFL, CLEC7A, TNFRSF25, KLK5, B3GNT3, GPR1, IGFBP7, VTCN1, PSG5, MFAP3L, KERA, BAMBI, TMPRSS11A, MMP23B, SLC39A4, APCDD1, MEST, SLC1A6, CADM1, LRRC32, C1QTNF6, KCNE4, SMC03, ADGRF5, TRBC1, ADGRF4, SEMA6D, SCARA3, SIGLEC5, B3GNT2, NTM, PAQR5, OPN3, IER3, TSPAN1, GPR155, CD248, RARRES1, IGFBPL1, ADGRF1, GALNT2, ABCG2, DNER, GALNT5, PRRG4, CSF2RB, FAM198B, AMIGO2, GPR37, SUSU1, TMPRSS11B, TMPRSS11E, ACKR3, CXADR, PTPRM, S1PR1</i>
<b>Cluster 3</b> cell-matrix adhesion (GO:0007160), anatomical structure morphogenesis (GO:0009653), protein binding (GO:0005515), co-receptor activity involved in Wnt signaling pathway, planar cell polarity pathway (GO:1904929)	7.25	<i>NTM, LYPD5, GPC4, CPM, MSLN, LY6G6C</i>
<b>Cluster 4</b> extracellular matrix organization (GO:0030198), collagen catabolic process (GO:0030574), extracellular matrix structural constituent (GO:0005201)	4.80	<i>EMILIN1, COL1A2, COL1A1, COL4A6</i>
<b>Cluster 5</b> positive regulation of tyrosine phosphorylation of STAT protein (GO:0042531), positive regulation of peptidyl-tyrosine phosphorylation (GO:0050731), cytokine-mediated signaling pathway (GO:0019221), cytokine receptor activity (GO:0004896)	4.09	<i>CSF2RB, GHR, IL6R, IL4R</i>

samples (**Figure 6C**). In RT-qPCR, neither *APOA1* nor *APOA2* showed significant difference from D10 control ( $p > 0.05$ ) (**Figure 6D**). *APOB* expression was significantly downregulated by isorhamnetin.

## Isorhamnetin-Treated hAECs Showed ICG Uptake, Glycogen Storage, and Urea Production

Finally, we assessed the ability of isorhamnetin-treated differentiated hAECs for mature hepatocyte functions. ICG is a cyanine dye that can be uptaken and subsequently cleared by hepatocytes. The ICG uptake and clearance test is used for a rapid assessment of liver function in clinical settings. We found that isorhamnetin-treated hAECs showed ICG uptake and clearance after 6 h; conversely, untreated D10 control cells did show very marginal/undetectable ICG uptake and clearance (**Figure 7A**).

Moreover, the liver has the ability to store glycogen. PAS can stain glycogen. Isorhamnetin-treated hAECs showed PAS stained cells, which indicated hAECs could store glycogen (**Figure 7B**). In a previously published article, it was shown that untreated hAECs could also exhibit PAS staining (Furuya et al., 2019). Similarly, in our study we found that untreated control group also had PAS stained cells.

Additionally, we measured urea and albumin secretion activities in isorhamnetin-treated hAECs. Treated hAECs secreted significantly higher urea compared to untreated control cells (**Figure 7C**). However, ALB secretion could not be detected in isorhamnetin-treated cells on the protein level on D10 and D20.

## DISCUSSION

In the present study, we have reported for the first time the potential role of a naturally occurring compound isorhamnetin in inducing hepatic-lineage-specific differentiation in hAECs maintained in 3D culture conditions in the absence of any other growth factor. We used whole-genome transcript analysis to study early biological events that regulated controlled differentiation in isorhamnetin-treated hAECs. After 10 days of treatment with isorhamnetin, the hAECs expressed a subset of hepatic differentiation-related genes, induced CYP mRNA levels, showed ICG uptake and release, stored glycogen, and secreted urea. However, the differentiated cells could not exert some key features of hepatic maturation, such as ALB secretion and CYP enzyme activity.

In the present study, we used hAECs that were isolated from the full-term placenta. The cells were preserved at the Tsukuba Human Tissue Biobank Center (THB) established at the University of Tsukuba Hospital (Takeuchi et al., 2016). The primary amnion epithelial cells were heterogeneous; however, hAECs isolated from the adherent subpopulations of passaged primary cells and cultured in 3D environment showed homogeneous characteristics (Furuya et al., 2019).

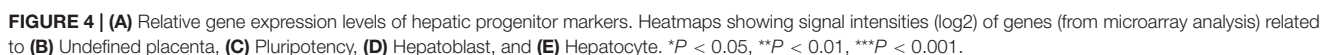
Isorhamnetin is an *O*-methylated flavonol occurring naturally in plants but is also a methylated metabolite of quercetin (Magar and Sohng, 2020). Studies have reported that isorhamnetin exerts

an anti-inflammatory effect in murine RAW264.7 cells (Boesch-Saadatmandi et al., 2011), inhibits the proliferation of breast cancer cells (Hu et al., 2015), protects HepG2 cells against oxidative stress (Yang et al., 2014), attenuates inflammatory bowel disease (Dou et al., 2014), and represses adipogenesis in 3T3-L1 cells (Lee et al., 2009). We have previously shown that isorhamnetin has antioxidant, antiobesity, and antifibrotic effects in rodent models (Zar Kalai et al., 2013; Ganbold et al., 2019). Isorhamnetin exerts its bioactivities through regulating Wnt upstream to  $\beta$  catenin in colorectal cancer cells (Park and Choi, 2010; Amado et al., 2011). Besides the effect on tumor cells, isorhamnetin may also function as a modulator of the Wnt pathway in other cell types. Also, isorhamnetin attenuates liver fibrosis by inhibiting TGF $\beta$  signaling pathways in hepatic stellate cells (Yang et al., 2016). Both Wnt/ $\beta$  catenin and TGF $\beta$  pathways are implicated in almost every facet of liver biology—from liver cell fate decision to liver organogenesis and to liver pathologies (Clotman et al., 2005; Clotman and Lemaigre, 2006; Nejak-Bowen and Monga, 2008; Touboul et al., 2016; Russell and Monga, 2018). We found that Wnt/ $\beta$  catenin and TGF $\beta$  pathways were highly enriched in isorhamnetin-treated hAECs, which may induce directed differentiation in hAECs.

Additionally, several other hepatic differentiation-related KEGG pathways were also enriched. Hedgehog Signaling is implicated in the proliferation of a liver stem cell subgroup named small hepatocyte-like progenitor cells as well as in end-stage liver diseases through orchestrating the wound healing process (Wang et al., 2016; Machado and Diehl, 2018). The Hippo signaling pathway controls liver cell fate and influences liver regeneration (Yimlamai et al., 2014; Manmadhan and Ehmer, 2019). FoxO signaling is considered as the metabolic regulator of the liver because of its involvement in hepatic gluconeogenesis and lipid metabolism (Shin et al., 2012; Tikhanovich et al., 2013). This pathway is reciprocally regulated by insulin through PI3K/Akt pathway. Among other enriched pathways, the mTOR pathway is involved in liver regeneration and autophagy functions (Fouraschen et al., 2013), and Sphingosine 1-Phosphate Signaling pathway in liver fibrosis through regulating pleiotropic cell responses to inflammation, such as cell survival, migration, and vascular permeability (González-Fernández et al., 2017). In addition, Prolactin signaling not only regulates postnatal liver growth in rodents (Moreno-Carranza et al., 2018) but also regulates liver regeneration by stimulating hepatocyte proliferation, promoting angiogenesis, downregulating IL-6, and upregulating SOCS3 (Moreno-Carranza et al., 2013).

Gene ontology analysis showed that 10 days treatment with isorhamnetin could significantly activate both early and late phase BPs involved in the induction of hepatic differentiation, including cell division, cell migration, cell adhesion, tight junction, EMT, ECM organization as well as cholesterol and fatty acid biosynthesis, angiogenesis, and wound healing.

Top enriched MFs showed isorhamnetin had histone methylation activity, which has been reported to enhance hepatic regeneration (Zlotorynski, 2019). Stearoyl-CoA desaturase activity has also been reported to modulate hepatocyte differentiation from human iPSCs (Rahimi et al., 2015). Also, connexin-mediated gap junctional intercellular communication





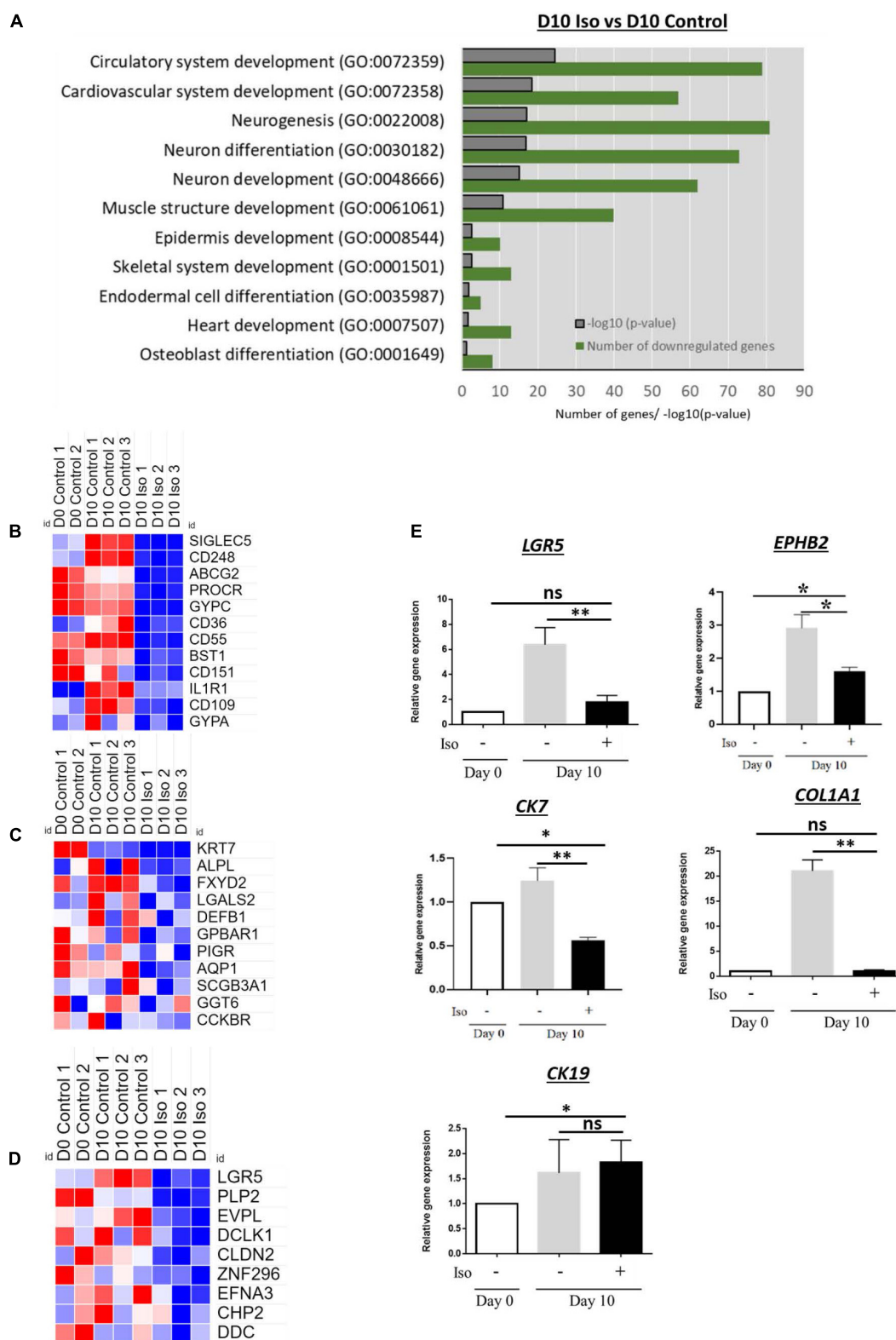


**FIGURE 5 | (A)** Bar graph showing significantly downregulated GO in D10 isorhamnetin-treated hAECs compared to D10 control. Heatmaps showing signal intensities (log2) of genes (from microarray analysis) related to **(B)** Transdifferentiation, **(C)** Cholangiocyte, and **(D)** Colon. **(E)** Relative expression levels of genes to trace transdifferentiation. \* $P < 0.05$ , \*\* $P < 0.01$ , ns: not significant.

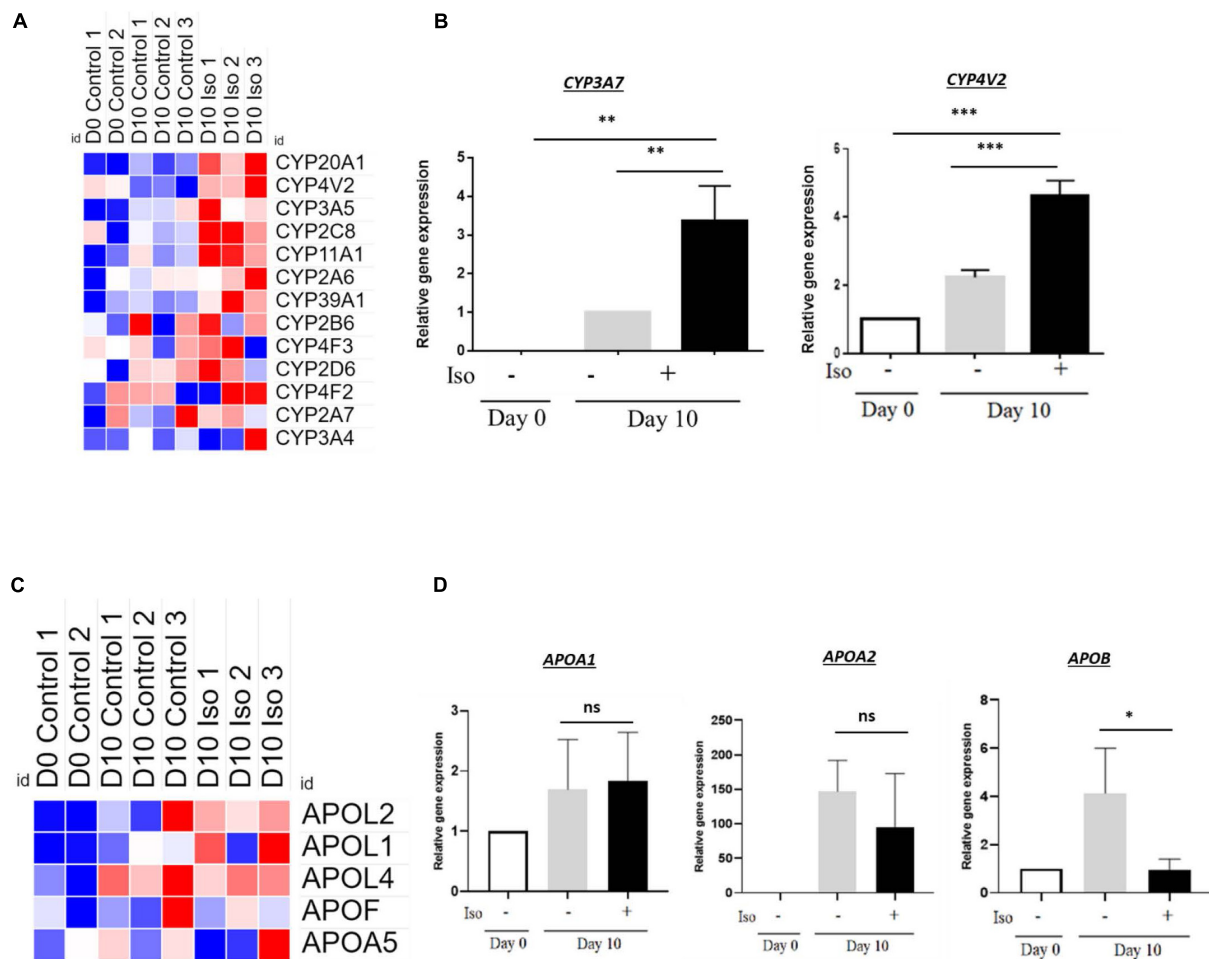


**FIGURE 6 | (A)** Heatmap showing signal intensities (log2) of CYP enzymes (from microarray analysis), **(B)** Relative gene expression of CYP enzymes. **(C)** Heatmap showing signal intensities (log2) of APO genes (from microarray analysis), **(D)** Relative expression levels of APO genes. \* $P < 0.05$ , \*\* $P < 0.01$ , \*\*\* $P < 0.001$ , ns: not significant.

is reported to modulate stepwise hepatic lineage restriction and maturation from ESCs (Qin et al., 2016).

Functional categories of downregulated DEGs included aminotransferase and collagen. Aminotransferases are the most common liver injury markers (McGill, 2016), whereas collagen induces liver fibrosis (McGill, 2016). Laminins, basement membrane protein family, have been implicated in the maintenance of hepatic differentiation (Kikkawa et al., 2011). Heparan sulfate proteoglycans are essential cofactors in receptor-growth factor interactions, as well as in cell-matrix adhesion and have been implicated in both normal and diseased liver conditions (Roskams et al., 1995; Tátrai et al., 2010).

Hepatic differentiation from stem cells is widely studied to apply for regenerative therapy and drug screening tests. It is already elucidated that the differentiation process for hepatocyte follows DE, progenitor, and then, hepatocyte. And during a certain stage, some genes are strongly and specifically expressed. In our study, we found that isorhamnetin downregulated the expression of DE marker *SOX17*; however, other DE

markers, *GATA4*, *FOXA2*, and HP marker *HNF4α* were not regulated. Previously, Marongiu et al. (2011) reported that hAECs pretreated with Activin A for 4 days for inducing endodermal commitment did not express *FOXA2* and *SOX17*, whereas Liu et al. (2018) reported that hAECs cultured in endodermal induction medium in the presence of EGF and bFGF for 2 days expressed both *Sox17* and *FOXA2*. However, neither of the studies reported *HNF4α* expression status. mRNA levels of other HP markers, *DLK-1* and *EPCAM* were significantly upregulated by isorhamnetin treatment. As shown before, the expression level of *AFP* was decreased, while *ALB* was increased in our study. It has been reported that *AFP* is strongly expressed in the progenitor phase, and then, *AFP* should be gently downregulated with the progression of hepatic differentiation. Oppositely, *ALB* expression increases with the progression of differentiation (Chaudhari et al., 2016). However, *ALB* secretion could not be detected on protein level on D10 and D20 isorhamnetin treatment despite significantly higher mRNA expression level on D10 isorhamnetin-treated

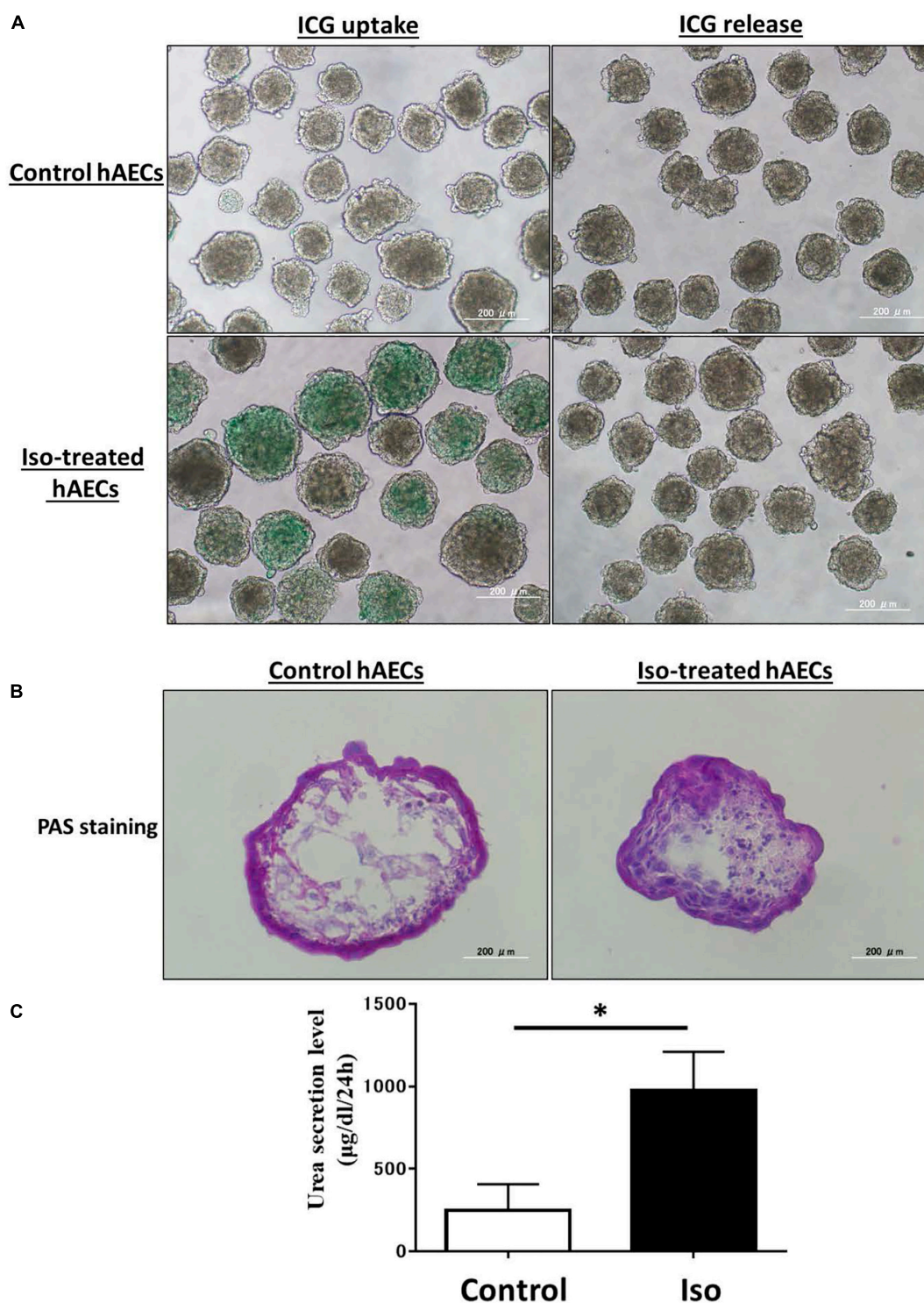


**FIGURE 7 | (A)** ICG uptake and release, **(B)** PAS staining, **(C)** Urea secretion assay. \* $P < 0.05$ .

hAECs. Previous study reported that ALB protein level was only detected after culturing hAECs in hepatic maturation medium containing EGF, Oncostatin M, HGF, dexamethasone, etc. (Liu et al., 2018).

We further evaluated several hepatic functions in the isorhamnetin-treated hAECs. CYP is a superfamily enzyme that catalyzes many exogenous compounds and endogenous oxidations. And some CYP enzymes, including CYP1A2 and

CYP3A4, catalyze drugs in the human liver (Rodríguez-Antona et al., 2001). CYP3A7 is produced in fetal liver; conversely, 3A4 is in the adult liver (Lacroix et al., 1997). Thus, the expression of these markers is essential for the functional hepatocytes and can be used to trace cell fate. We found that isorhamnetin significantly upregulated CYP3A7; however, CYP3A4 could not be detected. Even more prolonged treatment with isorhamnetin (day 20) neither expressed CYP3A4 nor showed its inducible enzyme activity. Previously, it was reported that hAECs cultured in a hepatogenic induction medium containing EGF, bFGF, HGF, and dexamethasone had low expression of mature hepatocyte marker CYP3A4 (Liu et al., 2018). Lin et al. (2015) also showed that hepatic differentiated AECs following a four-step hepatic differentiation protocol did not show any significant change in CYP3A4 mRNA levels. Additionally, hepatic lipid metabolism genes, APOA1 and APOA2, were also not regulated by isorhamnetin treatment on D10. Isorhamnetin-treated hAECs showed ICG uptake and release, glycogen storage, and urea secretion activities.

Altogether, our findings suggest that isorhamnetin could induce hepatic-lineage specific targeted differentiation in hAEC. Although the differentiated cells showed some functional characteristics of hepatocytes, they failed to achieve some key features such as ALB secretion and CYP enzyme activities.

Natural compounds with proven bioactivities can control cellular behavior and early biological and molecular events to direct the targeted differentiation of stem cells in a lineage-specific manner. Only a handful of studies were conducted to evaluate the effects of naturally occurring compounds on hAECs (Ferdousi et al., 2019, 2020; Hou et al., 2020). Furthermore, while current researches focus on the safety and efficacy of translating hAEC therapy into clinical practices (Murphy et al., 2010; Strom et al., 2013; Lim et al., 2017, 2018; Srinivasan et al., 2020), priming approaches using natural bioactive compounds to improve its effectiveness has not been explored. In the present study, as we could demonstrate that isorhamnetin, a methylated flavonol, induced hepatic-lineage specific differentiation in hAECs, other flavonols with similar chemical structure and functionality may show similar or better differentiation-inducing effects on hAECs.

In conclusion, our study is the first to report that a naturally occurring compound isorhamnetin could induce hepatic-lineage-specific differentiation in hAECs without any additional growth factor or cytokine. However, hepatic cell maturation could not be obtained even after treatment with isorhamnetin for a longer duration. Therefore, further research is warranted to explore potential bioactive compounds, and optimal culture condition and microenvironment to attain functional

hepatocytes from hAECs and finally to evaluate the differentiated cells in acute liver disease *in vivo* models.

## DATA AVAILABILITY STATEMENT

The datasets presented in this study can be found in online repositories. The names of the repository/repositories and accession number(s) can be found in the article/**Supplementary Material**. Microarray data are deposited in the Gene Expression Omnibus (GEO) under accession number GSE148777 (<https://www.ncbi.nlm.nih.gov/geo/query/acc.cgi?acc=GSE148777>).

## ETHICS STATEMENT

The Ethical Review Committee of the University of Tsukuba Hospital approved the protocol. Informed written consent was received from the mothers who donated the placenta after delivery.

## AUTHOR CONTRIBUTIONS

YU: investigation, data curation, formal analysis, visualization, and writing – original draft. FF: conceptualization, methodology, formal analysis, visualization, and writing – original draft. Y-WZ: conceptualization, methodology, funding acquisition, project administration, and supervision. TO: conceptualization, resources, and funding acquisition. HI: conceptualization, methodology, funding acquisition, project administration, resources, supervision, and writing – review and editing. All authors made substantial contributions to this article and approved the final article.

## FUNDING

This research was supported by the Japan Science and Technology Agency (JST); Science and Technology Research Partnership for Sustainable Development (SATREPS, Grant No. JPMJSA1506).

## SUPPLEMENTARY MATERIAL

The Supplementary Material for this article can be found online at: <https://www.frontiersin.org/articles/10.3389/fcell.2020.578036/full#supplementary-material>

## REFERENCES

- Adinolfi, M., Akle, C., McColl, I., Fensom, A., Tansley, L., Connolly, P., et al. (1982). Expression of HLA antigens,  $\beta$  2-microglobulin and enzymes by human amniotic epithelial cells. *Nature* 295, 325–327. doi: 10.1038/295325a0
- Amado, N. G., Fonseca, B. F., Cerqueira, D. M., Neto, V. M., and Abreu, J. G. (2011). Flavonoids: potential Wnt/ $\beta$ -catenin signaling modulators in cancer. *Life Sci.* 89, 545–554. doi: 10.1016/j.lfs.2011.05.003
- Banas, R. A., Trumppower, C., Bentlejewski, C., Marshall, V., Sing, G., and Zeevi, A. (2008). Immunogenicity and immunomodulatory effects of amnion-derived multipotent progenitor cells. *Hum. Immunol.* 69, 321–328. doi: 10.1016/j.humimm.2008.04.007
- Barrett, T., Wilhite, S. E., Ledoux, P., Evangelista, C., Kim, I. F., Tomashevsky, M., et al. (2012). NCBI GEO: archive for functional genomics data sets—update. *Nucleic Acids Res.* 41, D991–D995.



- Bilic, G., Zeisberger, S. M., Mallik, A. S., Zimmermann, R., and Zisch, A. H. (2008). Comparative characterization of cultured human term amnion epithelial and mesenchymal stromal cells for application in cell therapy. *Cell Transplant.* 17, 955–968. doi: 10.3727/096368908786576507
- Boesch-Saadatmandi, C., Loboda, A., Wagner, A. E., Stachurska, A., Jozkowicz, A., Dulak, J., et al. (2011). Effect of quercetin and its metabolites isorhamnetin and quercetin-3-glucuronide on inflammatory gene expression: role of miR-155. *J. Nutr. Biochem.* 22, 293–299. doi: 10.1016/j.jnutbio.2010.02.008
- Chaudhari, P., Tian, L., Deshmukh, A., and Jang, Y.-Y. (2016). Expression kinetics of hepatic progenitor markers in cellular models of human liver development recapitulating hepatocyte and biliary cell fate commitment. *Exp. Biol. Med.* 241, 1653–1662. doi: 10.1177/1535370216657901
- Clotman, F., Jacquemin, P., Plumb-Rudewicz, N., Pierreux, C. E., Van der Smissen, P., Dietz, H. C., et al. (2005). Control of liver cell fate decision by a gradient of TGF $\beta$  signaling modulated by Onecut transcription factors. *Genes Dev.* 19, 1849–1854. doi: 10.1101/gad.340305
- Clotman, F., and Lemaigre, F. P. (2006). Control of hepatic differentiation by activin/TGF $\beta$  signaling. *Cell Cycle* 5, 168–171. doi: 10.4161/cc.5.2.2341
- Dou, W., Zhang, J., Li, H., Kortagere, S., Sun, K., Ding, L., et al. (2014). Plant flavonol isorhamnetin attenuates chemically induced inflammatory bowel disease via a PXR-dependent pathway. *J. Nutr. Biochem.* 25, 923–933. doi: 10.1016/j.jnutbio.2014.04.006
- Fang, C.-H., Jin, J., Joe, J.-H., Song, Y.-S., So, B.-I., Lim, S. M., et al. (2012). In vivo differentiation of human amniotic epithelial cells into cardiomyocyte-like cells and cell transplantation effect on myocardial infarction in rats: comparison with cord blood and adipose tissue-derived mesenchymal stem cells. *Cell Transplant.* 21, 1687–1696. doi: 10.3727/096368912x653039
- Ferdousi, F., Kondo, S., Sasaki, K., Uchida, Y., Ohkohchi, N., Zheng, Y.-W., et al. (2020). Microarray analysis of verbenalin-treated human amniotic epithelial cells reveals therapeutic potential for Alzheimer's disease. *Aging* 12, 5516–5538. doi: 10.18632/aging.102985
- Ferdousi, F., Sasaki, K., Ohkohchi, N., Zheng, Y.-W., and Isoda, H. (2019). Exploring the potential role of rosmarinic acid in neuronal differentiation of human amnion epithelial cells by microarray gene expression profiling. *Front. Neurosci.* 13:779. doi: 10.3389/fnins.2019.00779
- Fouraschen, S. M., de Ruiter, P. E., Kwekkeboom, J., de Bruin, R. W., Kazemier, G., Metselaar, H. J., et al. (2013). mTOR signaling in liver regeneration: rapamycin combined with growth factor treatment. *World J. Transplant.* 3, 36–47. doi: 10.5500/wjtv.v3.i3.36
- Furuya, K., Zheng, Y.-W., Sako, D., Iwasaki, K., Zheng, D.-X., Ge, J.-Y., et al. (2019). Enhanced hepatic differentiation in the subpopulation of human amniotic stem cells under 3D multicellular microenvironment. *World J. Stem Cells* 11, 705–721. doi: 10.4252/wjsc.v11.i9.705
- Ganbold, M., Owada, Y., Ozawa, Y., Shimamoto, Y., Ferdousi, F., Tominaga, K., et al. (2019). Isorhamnetin alleviates steatosis and fibrosis in mice with nonalcoholic steatohepatitis. *Sci. Rep.* 9:16210.
- García-Castro, I. L., García-López, G., Ávila-González, D., Flores-Herrera, H., Molina-Hernández, A., Portillo, W., et al. (2015). Markers of pluripotency in human amniotic epithelial cells and their differentiation to progenitor of cortical neurons. *PLoS One* 10:e0146082. doi: 10.1371/journal.pone.0146082
- González-Fernández, B., Sánchez, D. I., González-Gallego, J., and Tuñón, M. J. (2017). Sphingosine 1-phosphate signaling as a target in hepatic fibrosis therapy. *Front. Pharmacol.* 8:579. doi: 10.3389/fphar.2017.00579
- Hammer, A., Hutter, H., Blaschitz, A., Mahner, W., Hartmann, M., Uchanska-Ziegler, B., et al. (1997). Amnion epithelial cells, in contrast to trophoblast cells, express all classical HLA class I molecules together with HLA-G. *Am. J. Reprod. Immunol.* 37, 161–171. doi: 10.1111/j.1600-0897.1997.tb00208.x
- Hori, J., Wang, M., Kamiya, K., Takahashi, H., and Sakuragawa, N. (2006). Immunological characteristics of amniotic epithelium. *Cornea* 25, S53–S58.
- Hou, S., Ding, C., Shen, H., Qian, C., Zou, Q., Lu, J., et al. (2020). Vitamin C improves the therapeutic potential of human amniotic epithelial cells in premature ovarian insufficiency disease. *Stem Cell Res. Ther.* 11:159.
- Hu, S., Huang, L., Meng, L., Sun, H., Zhang, W., and Xu, Y. (2015). Isorhamnetin inhibits cell proliferation and induces apoptosis in breast cancer via Akt and mitogen-activated protein kinase signaling pathways. *Mol. Med. Rep.* 12, 6745–6751. doi: 10.3892/mmr.2015.4269
- Huang, D. W., Sherman, B. T., and Lempicki, R. A. (2008). Systematic and integrative analysis of large gene lists using DAVID bioinformatics resources. *Nat. Protoc.* 4, 44–57. doi: 10.1038/nprot.2008.211
- Kikkawa, Y., Kataoka, A., Matsuda, Y., Takahashi, N., Miwa, T., Katagiri, F., et al. (2011). Maintenance of hepatic differentiation by hepatocyte attachment peptides derived from laminin chains. *J. Biomed. Mater. Res. A* 99, 203–210. doi: 10.1002/jbm.a.33176
- Kornicka, K., Kocherova, I., and Marycz, K. (2017). The effects of chosen plant extracts and compounds on mesenchymal stem cells—a bridge between molecular nutrition and regenerative medicine—concise review. *Phytother. Res.* 31, 947–958. doi: 10.1002/ptr.5812
- Lacroix, D., Sonnier, M., Moncion, A., Cheron, G., and Cresteil, T. (1997). Expression of CYP3A in the human liver—evidence that the shift between CYP3A7 and CYP3A4 occurs immediately after birth. *Eur. J. Biochem.* 247, 625–634. doi: 10.1111/j.1432-1033.1997.00625.x
- Lee, J., Jung, E., Lee, J., Kim, S., Huh, S., Kim, Y., et al. (2009). Isorhamnetin represses adipogenesis in 3T3-L1 cells. *Obesity* 17, 226–232. doi: 10.1038/oby.2008.472
- Lee, J., Lee, J., Jung, E., Hwang, W., Kim, Y.-S., and Park, D. (2010). Isorhamnetin-induced anti-adipogenesis is mediated by stabilization of  $\beta$ -catenin protein. *Life Sci.* 86, 416–423. doi: 10.1016/j.lfs.2010.01.012
- Liberzon, A., Birger, C., Thorvaldsdóttir, H., Ghandi, M., Mesirov, J. P., and Tamayo, P. (2015). The molecular signatures database hallmark gene set collection. *Cell Syst.* 1, 417–425. doi: 10.1016/j.cels.2015.12.004
- Liberzon, A., Subramanian, A., Pinchback, R., Thorvaldsdóttir, H., Tamayo, P., and Mesirov, J. P. (2011). Molecular signatures database (MSigDB) 3.0. *Bioinformatics* 27, 1739–1740. doi: 10.1093/bioinformatics/btr260
- Lim, R., Hodge, A., Moore, G., Wallace, E. M., and Sievert, W. (2017). A pilot study evaluating the safety of intravenously administered human amnion epithelial cells for the treatment of hepatic fibrosis. *Front. Pharmacol.* 8:549. doi: 10.3389/fphar.2017.00549
- Lim, R., Malhotra, A., Tan, J., Chan, S. T., Lau, S., Zhu, D., et al. (2018). First-in-human administration of allogeneic amnion cells in premature infants with bronchopulmonary dysplasia: a safety study. *Stem Cells Transl. Med.* 7, 628–635. doi: 10.1002/sctm.18-0079
- Lin, J. S., Zhou, L., Sagayaraj, A., Jumar, N. H. B., Choolani, M., Chan, J. K. Y., et al. (2015). Hepatic differentiation of human amniotic epithelial cells and in vivo therapeutic effect on animal model of cirrhosis. *J. Gastroenterol. Hepatol.* 30, 1673–1682. doi: 10.1111/jgh.12991
- Liu, N., Feng, J., Lu, X., Yao, Z., Liu, Q., Lv, Y., et al. (2019). Isorhamnetin inhibits liver fibrosis by reducing autophagy and inhibiting extracellular matrix formation via the TGF- $\beta$ 1/Smad3 and TGF- $\beta$ 1/p38 MAPK pathways. *Mediators Inflamm.* 2019:6175091.
- Liu, Q.-W., Liu, Q.-Y., Li, J.-Y., Wei, L., Ren, K.-K., Zhang, X.-C., et al. (2018). Therapeutic efficiency of human amniotic epithelial stem cell-derived functional hepatocyte-like cells in mice with acute hepatic failure. *Stem Cell Res. Ther.* 9:321.
- Machado, M. V., and Diehl, A. M. (2018). Hedgehog signalling in liver pathophysiology. *J. Hepatol.* 68, 550–562. doi: 10.1016/j.jhep.2017.10.017
- Magar, R. T., and Sohng, J. K. (2020). A review on structure, modifications and structure-activity relation of quercetin and its derivatives. *J. Microbiol. Biotechnol.* 30, 11–20. doi: 10.4014/jmb.1907.07003
- Manmadhan, S., and Ehmer, U. (2019). Hippo signaling in the liver—a long and ever-expanding story. *Front. Cell Dev. Biol.* 7:33. doi: 10.3389/fcell.2019.00033
- Marongiu, F., Gramignoli, R., Dorko, K., Miki, T., Ranade, A. R., Paola Serra, M., et al. (2011). Hepatic differentiation of amniotic epithelial cells. *Hepatology* 53, 1719–1729.
- Maymó, J. L., Riedel, R., Pérez-Pérez, A., Magatti, M., Maskin, B., Dueñas, J. L., et al. (2018). Proliferation and survival of human amniotic epithelial cells during their hepatic differentiation. *PLoS One* 13:e0191489. doi: 10.1371/journal.pone.0191489
- McGill, M. R. (2016). The past and present of serum aminotransferases and the future of liver injury biomarkers. *EXCLI J.* 15, 817–828.
- Miki, T. (2011). Amnion-derived stem cells: in quest of clinical applications. *Stem Cell Res. Ther.* 2:25. doi: 10.1186/scrt66
- Miki, T., Lehmann, T., Cai, H., Stolz, D. B., and Strom, S. C. (2005). Stem cell characteristics of amniotic epithelial cells. *Stem Cells* 23, 1549–1559. doi: 10.1634/stemcells.2004-0357

- Miki, T., Marongiu, F., Dorko, K., Ellis, E. C., and Strom, S. C. (2010). Isolation of amniotic epithelial stem cells. *Curr. Protoc. Stem Cell Biol.* 12, 1E.3.1–1E.3.9.
- Miki, T., and Strom, S. C. (2006). Amnion-derived pluripotent/multipotent stem cells. *Stem Cell Rev.* 2, 133–141. doi: 10.1007/s12015-006-0020-0
- Moreno-Carranza, B., Bravo-Manríquez, M., Baez, A., Ledesma-Colunga, M. G., Ruiz-Herrera, X., Reyes-Ortega, P., et al. (2018). Prolactin regulates liver growth during postnatal development in mice. *Am. J. Physiol. Regul. Integr. Comp. Physiol.* 314, R902–R908.
- Moreno-Carranza, B., Goya-Arce, M., Vega, C., Adán, N., Triebel, J., López-Barrera, F., et al. (2013). Prolactin promotes normal liver growth, survival, and regeneration in rodents: effects on hepatic IL-6, suppressor of cytokine signaling-3, and angiogenesis. *Am. J. Physiol. Regul. Integr. Comp. Physiol.* 305, R720–R726.
- Murphy, S., Rosli, S., Acharya, R., Mathias, L., Lim, R., Wallace, E., et al. (2010). Amnion epithelial cell isolation and characterization for clinical use. *Curr. Protoc. Stem Cell Biol.* 13, 1E.6.1–1E.6.25.
- Nejak-Bowen, K., and Monga, S. P. (2008). Wnt/ $\beta$ -catenin signaling in hepatic organogenesis. *Organogenesis* 4, 92–99. doi: 10.1016/org.4.2.5855
- Pan, L., Shu, J., and Cai, Z. (2006). The morphologic study of the characteristics of neurobiology of the amniotic membrane. *Chin. J. Rehabil. Med.* 21, 46–49.
- Park, S., and Choi, J. (2010). Inhibition of  $\beta$ -catenin/Tcf signaling by flavonoids. *J. Cell. Biochem.* 110, 1376–1385. doi: 10.1002/jcb.22654
- Parolini, O., Alviano, F., Bagnara, G. P., Bilic, G., Bühring, H. J., Evangelista, M., et al. (2008). Concise review: isolation and characterization of cells from human term placenta: outcome of the first international workshop on placenta derived stem cells. *Stem Cells* 26, 300–311. doi: 10.1634/stemcells.2007-0594
- Qin, J., Chang, M., Wang, S., Liu, Z., Zhu, W., Wang, Y., et al. (2016). Connexin 32-mediated cell-cell communication is essential for hepatic differentiation from human embryonic stem cells. *Sci. Rep.* 6:37388.
- Rahimi, Y., Mehdizadeh, A., Nozad Charoudeh, H., Nouri, M., Valaei, K., Fayezi, S., et al. (2015). Hepatocyte differentiation of human induced pluripotent stem cells is modulated by stearyl-CoA desaturase 1 activity. *Dev. Growth Differ.* 57, 667–674. doi: 10.1111/dgd.12255
- Rodríguez-Antona, C., Donato, M. T., Pareja, E., Gómez-Lechón, M.-J., and Castell, J. V. (2001). Cytochrome P-450 mRNA expression in human liver and its relationship with enzyme activity. *Arch. Biochem. Biophys.* 393, 308–315. doi: 10.1006/abbi.2001.2499
- Roskams, T., Moshage, H., De Vos, R., Guido, D., Yap, P., and Desmet, V. (1995). Heparan sulfate proteoglycan expression in normal human liver. *Hepatology* 21, 950–958. doi: 10.1002/hep.1840210410
- Russell, J. O., and Monga, S. P. (2018). Wnt/ $\beta$ -catenin signaling in liver development, homeostasis, and pathobiology. *Annu. Rev. Pathol. Mech. Dis.* 13, 351–378. doi: 10.1146/annurev-pathol-020117-044010
- Saud, B., Malla, R., and Shrestha, K. (2019). A review on the effect of plant extract on mesenchymal stem cell proliferation and differentiation. *Stem Cells Int.* 2019:7513404.
- Sherman, B. T., Huang, D. W., and Lempicki, R. A. (2008). Bioinformatics enrichment tools: paths toward the comprehensive functional analysis of large gene lists. *Nucleic Acids Res.* 37, 1–13. doi: 10.1093/nar/gkn923
- Shin, D.-J., Joshi, P., Hong, S.-H., Mosure, K., Shin, D.-G., and Osborne, T. F. (2012). Genome-wide analysis of FoxO1 binding in hepatic chromatin: potential involvement of FoxO1 in linking retinoid signaling to hepatic gluconeogenesis. *Nucleic Acids Res.* 40, 11499–11509. doi: 10.1093/nar/gks932
- Srinivasan, R. C., Strom, S. C., and Gramignoli, R. (2020). Effects of cryogenic storage on human amnion epithelial cells. *Cells* 9:1696. doi: 10.3390/cells9071696
- Strom, S. C., Skvorak, K., Gramignoli, R., Marongiu, F., and Miki, T. (2013). Translation of amnion stem cells to the clinic. *Stem Cells Dev.* 22, 96–102. doi: 10.1089/scd.2013.0391
- Subramanian, A., Tamayo, P., Mootha, V. K., Mukherjee, S., Ebert, B. L., Gillette, M. A., et al. (2005). Gene set enrichment analysis: a knowledge-based approach for interpreting genome-wide expression profiles. *Proc. Natl. Acad. Sci. U.S.A.* 102, 15545–15550. doi: 10.1073/pnas.0506580102
- Takeuchi, T., Noguchi, M., Kawakami, Y., and Ohkohchi, N. (2016). Use of human biospecimen resources for drug discovery—approach of tsukuba human tissue biobank center—. *Regul. Sci. Med. Prod.* 6, 57–63.
- Tamagawa, T., Ishiwata, I., and Saito, S. (2004). Establishment and characterization of a pluripotent stem cell line derived from human amniotic membranes and initiation of germ layers in vitro. *Hum. Cell* 17, 125–130. doi: 10.1111/j.1749-0774.2004.tb00028.x
- Tátrai, P., Egedi, K., Somorácz, Á., Van Kuppevelt, T. H., Dam, G. T., Lyon, M., et al. (2010). Quantitative and qualitative alterations of heparan sulfate in fibrogenic liver diseases and hepatocellular cancer. *J. Histochem. Cytochem.* 58, 429–441. doi: 10.1369/jhc.2010.955161
- Tikhonovich, I., Cox, J., and Weinman, S. A. (2013). Forkhead box class O transcription factors in liver function and disease. *J. Gastroenterol. Hepatol.* 28(Suppl. 1), 125–131. doi: 10.1111/jgh.12021
- Toda, A., Okabe, M., Yoshida, T., and Nikaido, T. (2007). The potential of amniotic membrane/amnion-derived cells for regeneration of various tissues. *J. Pharmacol. Sci.* 105, 215–228. doi: 10.1254/jphs.cr0070034
- Touboul, T., Chen, S., To, C. C., Mora-Castilla, S., Sabatini, K., Tukey, R. H., et al. (2016). Stage-specific regulation of the WNT/ $\beta$ -catenin pathway enhances differentiation of hESCs into hepatocytes. *J. Hepatol.* 64, 1315–1326. doi: 10.1016/j.jhep.2016.02.028
- Udagama, P. V., and Udalamaththa, V. (2018). “Application of herbal medicine as proliferation and differentiation effectors of human stem cells,” in *Herbal Medicine*, eds A. Vickers and C. Zollman (London: IntechOpen).
- Udalamaththa, V. L., Jayasinghe, C. D., and Udagama, P. V. (2016). Potential role of herbal remedies in stem cell therapy: proliferation and differentiation of human mesenchymal stromal cells. *Stem Cell Res. Ther.* 7:110.
- Wang, Z., Li, W., Li, C., Yang, Y., Li, W., Zhang, L., et al. (2016). Small hepatocyte-like progenitor cells may be a Hedgehog signaling pathway-controlled subgroup of liver stem cells. *Exp. Ther. Med.* 12, 2423–2430. doi: 10.3892/etm.2016.3675
- Yang, J. H., Kim, S. C., Kim, K. M., Jang, C. H., Cho, S. S., Kim, S. J., et al. (2016). Isorhamnetin attenuates liver fibrosis by inhibiting TGF- $\beta$ /Smad signaling and relieving oxidative stress. *Eur. J. Pharmacol.* 783, 92–102. doi: 10.1016/j.ejphar.2016.04.042
- Yang, J. H., Shin, B. Y., Han, J. Y., Kim, M. G., Wi, J. E., Kim, Y. W., et al. (2014). Isorhamnetin protects against oxidative stress by activating Nrf2 and inducing the expression of its target genes. *Toxicol. Appl. Pharmacol.* 274, 293–301. doi: 10.1016/j.taap.2013.10.026
- Yimlamai, D., Christodoulou, C., Galli, G. G., Yanger, K., Pepe-Mooney, B., Gurung, B., et al. (2014). Hippo pathway activity influences liver cell fate. *Cell* 157, 1324–1338. doi: 10.1016/j.cell.2014.03.060
- Zar Kalai, F., Han, J., Ksouri, R., El Omri, A., Abdelly, C., and Isoda, H. (2013). Antiobesity effects of an edible halophyte *Nitraria retusa* Forssk in 3T3-L1 preadipocyte differentiation and in C57B6/J mice fed a high fat diet-induced obesity. *Evid. Based Complement. Alternat. Med.* 2013:368658.
- Zhang, Y., Gu, M., Cai, W., Yu, L., Feng, L., Zhang, L., et al. (2016). Dietary component isorhamnetin is a PPAR $\gamma$  antagonist and ameliorates metabolic disorders induced by diet or leptin deficiency. *Sci. Rep.* 6:19288.
- Zlotorynski, E. (2019). Histone methylation boosts liver regeneration. *Nat. Rev. Mol. Cell Biol.* 20, 454–455. doi: 10.1038/s41580-019-0157-8

**Conflict of Interest:** The authors declare that the research was conducted in the absence of any commercial or financial relationships that could be construed as a potential conflict of interest.

Copyright © 2020 Uchida, Ferdousi, Zheng, Oda and Isoda. This is an open-access article distributed under the terms of the Creative Commons Attribution License (CC BY). The use, distribution or reproduction in other forums is permitted, provided the original author(s) and the copyright owner(s) are credited and that the original publication in this journal is cited, in accordance with accepted academic practice. No use, distribution or reproduction is permitted which does not comply with these terms.



# ***Alpinia oxyphylla* Miq. and Its Active Compound *P*-Coumaric Acid Promote Brain-Derived Neurotrophic Factor Signaling for Inducing Hippocampal Neurogenesis and Improving Post-cerebral Ischemic Spatial Cognitive Functions**

Yacong He<sup>1</sup>, Shuang Chen<sup>1</sup>, Bun Tsoi<sup>1</sup>, Shuhua Qi<sup>2</sup>, Bing Gu<sup>2</sup>, Zhenxing Wang<sup>3</sup>, Cheng Peng<sup>4</sup> and Jiangang Shen<sup>1,2\*</sup>

## OPEN ACCESS

### Edited by:

Kazunori Sasaki,  
National Institute of Advanced  
Industrial Science and Technology  
(AIST), Japan

### Reviewed by:

Carmen Castro,  
University of Cádiz, Spain  
Francis G. Szele,  
University of Oxford, United Kingdom

### \*Correspondence:

Jiangang Shen  
shenjg@hku.hk;  
shenjg@hkucc.hku.hk

### Specialty section:

This article was submitted to  
Stem Cell Research,  
a section of the journal  
Frontiers in Cell and Developmental  
Biology

**Received:** 29 June 2020

**Accepted:** 07 December 2020

**Published:** 18 January 2021

### Citation:

He Y, Chen S, Tsoi B, Qi S, Gu B,  
Wang Z, Peng C and Shen J (2021)  
*Alpinia oxyphylla* Miq. and Its Active  
Compound *P*-Coumaric Acid  
Promote Brain-Derived Neurotrophic  
Factor Signaling for Inducing  
Hippocampal Neurogenesis  
and Improving Post-cerebral Ischemic  
Spatial Cognitive Functions.  
Front. Cell Dev. Biol. 8:577790.  
doi: 10.3389/fcell.2020.577790

<sup>1</sup> School of Chinese Medicine, Li Ka Shing Faculty of Medicine, The University of Hong Kong, Hong Kong, China, <sup>2</sup> Medical Technology School, Xuzhou Key Laboratory of Laboratory Diagnostics, Xuzhou Medical University, Xuzhou, China, <sup>3</sup> Chengdu University of Traditional Chinese Medicine, Chengdu, China, <sup>4</sup> Key Laboratory of Standardization of Chinese Herbal Medicines of Ministry of Education, Pharmacy College, Chengdu University of Traditional Chinese Medicine, Chengdu, China

*Alpinia oxyphylla* Miq. (AOM) is a medicinal herb for improving cognitive functions in traditional Chinese medicine for poststroke treatment, but its efficacies and underlying mechanisms remain unknown. In the present study, we tested the hypothesis that AOM could induce adult hippocampal neurogenesis and improve poststroke cognitive impairment via inducing brain-derived neurotrophic factor (BDNF) signaling pathway. In order to test the hypothesis, we performed both *in vivo* rat experiments using transient middle cerebral artery occlusion (MCAO) model and *in vitro* neural stem cell (NSC) experiments using oxygen–glucose deprivation plus reoxygenation. First, AOM treatment significantly up-regulated the expression of BDNF, tropomyosin receptor kinase B (TrkB), and phosphorylated AKT (p-AKT) in the hippocampus, enhanced adult hippocampal neurogenesis, and improved the spatial learning/memory and cognitive functions in the post-MCAO ischemic rats *in vivo*. Next, *in vitro* studies confirmed *p*-coumaric acid (P-CA) to be the most effective compound identified from AOM extract with the properties of activating BDNF/TrkB/AKT signaling pathway and promoting NSC proliferation. Cotreatment of BDNF/TrkB-specific inhibitor ANA12 abolished the effects of P-CA on inducing BDNF/TrkB/AKT activation and the NSC proliferation. Finally, animal experiments showed that P-CA treatment enhanced the neuronal proliferation and differentiation in the hippocampus, improved spatial learning and memory functions, and reduced anxiety in the transient MCAO ischemic rats. In conclusion, P-CA is a representative compound from AOM for its bioactivities of activating BDNF/TrkB/AKT signaling pathway, promoting hippocampal neurogenesis, improving cognitive functions, and reducing anxiety in post-ischemic stroke rats.

**Keywords:** *Alpinia oxyphylla* Miq., *p*-coumaric acid, brain-derived neurotrophic factor, hippocampal neurogenesis, ischemic stroke

## BACKGROUND

Stroke is a major disease burden with high mortality and disability caused by impeded blood flow to the brain (Johnston et al., 2018). Stroke victims suffer from motor dysfunctions, paralysis, cognitive impairment (Mijajlović et al., 2017), and even sudden death (Donnan et al., 2008). Current therapeutic strategies including thrombolysis with tissue plasminogen activator and mechanical thrombectomy are effective for the recanalization of blood flow to the ischemic brain but have restrictive therapeutic windows within 4.5 and 6 h, respectively. The delayed thrombolytic treatment beyond the golden therapeutic windows carries the risks of the complications of intracranial hemorrhagic transformation and increases the mortality of stroke patients (Gravanis and Tsirka, 2008). To date, there is no medication for neuroprotection and neurogenesis in stroke treatment.

Adult neurogenesis brings new hope for seeking therapeutic targets to repairing a damaged brain and improving functional recovery in poststroke patients (Wang et al., 2012; Sun et al., 2013). The subventricular zone (SVZ), lining the lateral ventricle, and the subgranular zone in the dentate gyrus (DG) are the central regions of adult neurogenesis in the brain (Lois and Alvarez-Buylla, 1994; Eriksson et al., 1998). The newborn neurons in DG contribute to adult hippocampal neurogenesis for improving learning and memory functions (Deng et al., 2010). Adult hippocampal neurogenesis includes a series of sequential events to generate new excitatory granule cells in the DG. The newborn neurons go through several consecutive generation stages before integrating into the hippocampal circuit. First, radial glia-like precursor cells (type 1 cells) with astrocytic properties express the biomarkers of neural stem cells (NSCs). The cells give rise to intermediate progenitor cells with first glial (type 2a) and then neuronal (type 2b) phenotype. After developing into a migratory neuroblast-like stage (type 3), these newborn lineage-committed cells enter a maturation stage and extend their dendrites into the molecular layer and their axon to CA3, eventually forming granule cells (Markakis and Gage, 1999). By labeling various biomarkers, we can track the procedures of hippocampal neurogenesis at different stages. For example, doublecortin (DCX) shows a complete overlap in expression with the polysialylated neuronal cell adhesion molecule in the hippocampus, which are used as surrogate markers for adult neurogenesis (Kempermann et al., 2015). DCX is expressed at the stages of proliferation to postmitotic maturation and commonly used as a neurogenic biomarker (Encinas and Enikolopov, 2008; Kempermann et al., 2015; Chen et al., 2020). DCX and neuronal nuclei (NeuN) are commonly used as neurogenic biomarkers and costained with exogenous cell tracer 5'-bromo-2'-deoxyuridine (BrdU) to identify newly formed neurons and indicate adult neurogenesis in the central nervous system. BrdU, a thymidine analog, can be transferred into dividing cells by DNA synthesis (Lehner et al., 2011). After integrating into the new DNA, BrdU will be passed to daughter cells (Kee et al., 2002). The proliferation and differentiation of NSCs and/or neural progenitor cells (NPCs) can be marked by costaining BrdU and DCX and/or NeuN to

identify immature or mature neurons, respectively (Wojtowicz and Kee, 2006; Gao et al., 2018). Thus, these biomarkers facilitate the studies on exploring the underlying mechanisms of adult neurogenesis and seeking drug candidates for functional recovery in poststroke treatment.

Many extrinsic and intrinsic factors, which are generated from NSCs/NPCs, neurogenic niche and microenvironment form complex network regulations for adult neurogenesis in postischemic brain. Notch signaling, Wnt/ $\beta$ -catenin signaling pathway, sonic Hedgehog pathway, bone morphogenetic proteins, growth factors, neurotrophic factors, and neurotransmitters are well recognized as cellular signaling cascades contributing to poststroke neurogenesis (Bond et al., 2012; Faigle and Song, 2013; Liu et al., 2018; Wagenaar et al., 2018; Ho et al., 2020; Xu et al., 2020). Among them, brain-derived neurotrophic factor (BDNF) is a critical neurotrophic factor participating in the regulations of proliferation, differentiation, survival, and maturation of NSCs for neurogenesis. BDNF is formed by the combination of signal peptide, prodomain, and mature BDNF precursor form. The prodomain of BDNF is removed by cell proteases to promote the secretion of mature BDNF. By binding to tropomyosin receptor kinase B (TrkB) receptor, BDNF phosphorylation activates downstream pathways, including MAP kinase/CREB, PI-3 kinase/Akt, and Ras/Raf/MEK/Erk signaling pathways (Mohammadi et al., 2018). BDNF and its receptor TrkB are highly expressed in hippocampal region for memory formation (Egan et al., 2003). BDNF promotes neurological functional recovery in neonatal hypoxic-ischemic brain injury (Im et al., 2010). Endothelial-derived BDNF formation promotes the vasculature-mediated migration of neuronal precursors in the ischemic striatum (Grade et al., 2013). Overexpression of BDNF increases the survival rates of the transplanted NSCs and promotes neurological functional recovery in experimental ischemic stroke animal models (Lee et al., 2010; Chang et al., 2013; Rosenblum et al., 2015). Adenoviral transduction of BDNF gene in human bone marrow-derived mesenchymal stem cells (MSCs) efficiently promotes its survival after transplantation, enhances the proliferation of endogenous NSCs, and promotes functional recovery in a middle cerebral artery occlusion (MCAO) rat model (Jeong et al., 2014). BDNF increases the survival and differentiation of dental pulp stem cells (DPSCs) and promotes the recovery of neurological functions in a cerebral ischemia animal model with DPSC transplantation (Zhang X. et al., 2018). In addition, plasma BDNF level is used as a biomarker to reflect cell viability and functional recovery in the transplantation of MSCs (Nakamura et al., 2019). On the contrary, antisense oligonucleotides of BDNF inhibit proliferation and differentiation of NSCs in the ischemic brains (Li et al., 2017). Suppressing adult hippocampal neurogenesis worsens cognitive performance and decreases preexisting dentate neurons. Combined mimic exercise and elevating BDNF levels to enhance adult neurogenesis improve cognitive function and protect against subsequent neuronal cell death in an Alzheimer disease (AD) mouse model (Choi et al., 2018). Therefore, BDNF is an important therapeutic target for adult neurogenesis and functional recovery in poststroke treatment.



Traditional Chinese medicine (TCM) has been used for stroke treatment for centuries in China and East Asia. The direct experiences from human subjects provide fast-track sources for drug discovery. *Alpinia oxyphylla* Miq. (AOM) is a commonly used medicinal plant for improving cognitive functions in TCM formulas, but its efficacies and scientific basis remain unclear. In recent studies, AOM treatment has revealed to attenuate neuronal cell death, improve  $\beta$ -amyloid-induced cognitive impairment, reduce neuronal abnormalities in the cortex and hippocampus, and enhance memory in mice (Shi et al., 2014, 2015). AOM exerts antidepressant-like effects by targeting TrkB receptor-mediated pERK/pCREB/BDNF signal systems (Yan et al., 2016). However, whether AOM has neurogenesis-promoting effects for the functional recovery of learning and memory in ischemic stroke remains unknown. Herein, we report that AOM could promote hippocampal neurogenesis and enhance the functional recovery of learning and memory by inducing BDNF signaling pathway in transient ischemic stroke treatment. Furthermore, we have identified *p*-coumaric acid (P-CA) as the representative compound from AOM with the properties of promoting BDNF signaling for inducing hippocampal neurogenesis and improving functional recovery in post-ischemic stroke rat model.

## MATERIALS AND METHODS

### Herbal Materials and Reagents

*Alpinia oxyphylla* Miq. was purchased from Hong Kong Huaxin Pharmaceutical Inc. Ltd. (serial no. 170807), which was originally from Hainan province, China. Mouse multipotent neural progenitor or stem-like cells C17.2 [07062902, European Collection of Authenticated Cell Cultures (ECACC)] were purchased from Sigma-Aldrich (St. Louis, MO, United States). Thymidine analog BrdU (ab142567) and antibodies for BrdU (ab6326), SOX2 (ab97959), and BDNF (3B2) were purchased from Abcam (Cambridge, United Kingdom). Other antibodies for Ki67 (D3B5), NeuN (D4G4O), DCX (A8L1U), phospho-AKT (Ser473), AKT (C67E7),  $\beta$ -actin (8H10D10), and GAPDH (5174) were obtained from Cell Signaling Technology (Danvers, MA, United States). TrkB (sc-12) was ordered from Santa Cruz (Dallas, TX, United States). ANA12 was provided from Cayman Chemical (Ann Arbor, MI, United States). Solvents for high-performance liquid chromatography (HPLC) and liquid chromatography-mass spectrometry (LC-MS) analysis were at HPLC-grade. Compounds for quality control analysis including kaempferol, 5-hydroxymethylfurfural, chrysin, P-CA, nootkatone, (–)-epicatechol, catechin, protocatechuic acid, protocatechuic aldehyde, and tectochrysin with purity of greater than 98% were purchased from Chengdu Push Bio-technology Co., Ltd., China.

### AOM Extraction and Drug Solution

Dry raw materials of AOM (2 kg) were grinded into scraps and soaked in 20 L of 70% ethanol overnight. The mixture was sonicated three times (40 min per time). The solution was concentrated by rotary evaporator at 60°C. After ethanol

was evaporated, the solution was freeze-dried to obtain AOM extraction. For qualitative and quantitative analyses, we dissolved AOM extraction in ethanol (10 mg/mL) by ultrasonic for 30 min and performed HPLC analysis and LC-MS analysis.

In the LC-MS analysis, by comparing the ESI-MS data from QDa positive/negative scanning of AOM extract (Supplementary Figure 1) and the reported ESI-MS data of the potential neuronal bioactive components in AOM (Zhang Q. et al., 2018), we speculated 14 compounds in the AOM extracts, and we collected those compounds (>98% purity) for further verifications of the compounds in the AOM extract. Stock solution of each compound was made by dissolving 0.2 mg in 2 mL of ethanol under ultrasonic for 30 min. 100  $\mu$ L of stock solution was taken to obtain mixed standard solution. With HPLC and LC-MS experiments, 10 compounds were identified in the AOM extract, including 5-hydroxymethylfurfural, protocatechuic acid, catechin, protocatechuic aldehyde, (–)-epicatechol, P-CA, kaempferol, chrysin, nootkatone, and tectochrysin. After P-CA was identified to be the most effective compound, we then prepared the test solution by dissolving 50 mg of P-CA into 50 mL of 0.1% phosphoric acid–water and methanol (70:30) under ultrasonic for 30 min.

### Quality Control Analysis

We performed quality control study on AOM extract and characterized the chemical profiles of the AOM solution by using HPLC. Chromatographic separations were operated on an Agilent 1100 Series HPLC system with Shimadzu C18 column (4.6  $\times$  250 mm, 5  $\mu$ m). The following chromatographic parameters were used in the study: mobile phase A (acetonitrile) and mobile phase B (0.1% trifluoroacetate–water), flow rate at 1 mL/min, column temperature at 30°C, and detection wavelength at 220 nm. The gradient profiles were from 0 to 60 min, and the percentage of mobile phase A gradient was increased from 5 to 100%. LC-MS was operated by using Waters LC/MS ACQUITY QDA with CORTECS C18 column (4.6  $\times$  50 mm, 2.7  $\mu$ m). LC-MS was measured under the condition of ionization method-ESI (+/–), with a scanning range from 100 to 1,000. The following chromatographic parameters were used: mobile phase A (0.1% formic acid water) and mobile phase B (0.1% formic acid acetonitrile), flow rate at 0.5 mL/min, column temperature at 30°C, and detection wavelength at 220 and 254 nm. The gradient profile was that mobile phase B was increased from 5 to 95% for 6 min and held 95% for 3 min.

### Quantitative Analysis

We selected P-CA as a marker compound for quantitative control of the AOM extraction. P-CA was determined at the wavelength of 309 nm by using Shimadzu LC-2030c HPLC system and Waters symmetry C18 (4.6  $\times$  150 mm, 5  $\mu$ m). The chromatographic analysis was operated at the parameters: flow rate at 1 mL/min, 10- $\mu$ L sample injection volume, column temperature at 35°C, detection wavelength at 309 nm, mobile phase A (0.1% phosphoric acid–water), and mobile phase B (Methanol), constantly running 60 min. In quantitative experiments, linearity, precision, accuracy, sensitivity, repetitive, and stability were detected. The limits of detection (LODs) and

limits of quantitation (LOQs) under the present conditions were determined at a signal-to-noise ratio of approximately 3 and 10, respectively.

To obtain calibration curves, 10 concentrations of P-CA were analyzed in HPLC. The test solutions were made into six replicates in parallel manner for the precision of the measurement results. One test solution was injected for six times constantly to examine the repetition of the HPLC system. The accuracy was evaluated by the recovery rate test. In the verification study, equal amount of mixed sample solution and reference substance spiked solution was mixed and allocated into six solutions for recovery rate test. The actual value was compared with the theoretical value to calculate the recovery rates. The stability of test solution and reference solution during storage was measured by testing the changes of the main peak area after the test solution and the reference solution were placed at room temperature for 0, 2, 4, 6, 8, 12, and 18 h, respectively.

## Animals and Experimental Groups for AOM Extraction and P-CA Study

Male Sprague–Dawley (S.D.) rats (12 weeks old, weighing 260–290 g) were obtained from Laboratory Animal Unit, The University of Hong Kong. All animals were kept with tap water and standard food pellets, within a stable environment (temperature  $25^{\circ}\text{C} \pm 2^{\circ}\text{C}$ , humidity 40%, 12/12-h dark/night cycle) in an animal room. All animal experimental procedures and care were approved by the University Committee on the Use of Live Animals in Teaching and Research (CULATR no. 4664-18). The rats were randomly divided into three groups before surgery: sham-operated group, MCAO model group, and MCAO plus AOM treatment group. For P-CA study, three concentrations of P-CA were designed (low 50 mg/kg, middle 100 mg/kg, high 200 mg/kg treatment groups).

## Surgical Protocol

Sprague–Dawley rats were subjected to MCAO to induce cerebral ischemia animal model. The rats were anesthetized with 4% isoflurane and maintained at 2% isoflurane. The rats were then placed on a warm pat to maintain body temperature. Neck hair was shaved out with shaving cream, and the neck skin was disinfected three times with iodine and 70% ethanol. Under a

surgical microscope, a neck midline incision was made, and the superficial fascia was incised. Under the superficial fascia, a careful blunt dissection was performed to expose the common carotid artery (CCA), external carotid artery (ECA), and internal carotid artery (ICA) without damaging the vagus nerve. A 6-0 nylon suture was used to tighten the CCA and ECA. The ECA was cut and stumped with a needle. A 0.36-mm nylon suture covered with silicone was carefully inserted and pushed into the ICA until reached to the left middle cerebral artery in the place with the feeling of slight resistance. The ICA and ECA were carefully tightened with 6-0 nylon suture. The incision was closed with 3-0 nylon sutures. The muscle layer was sutured with a 6-0 polyglactin suture, and the incision layer was sutured with a 3-0 nylon suture. After 2 h of MCAO ischemia, the intraluminal suture was removed to induce reperfusion. The rats were kept warm until recovery from anesthesia. After that, we monitored the well-being of the rats, which were presumably free to access water and food.

## Drug Preparation and Administration

The *in vivo* animal experiment protocol is shown in **Figure 1**. The AOM extraction was dissolved in a water solution with 5% ethanol plus 5% polyethylene glycol 400 (PEG 400). In the AOM treatment group, at the onset of reperfusion, the AOM extraction was orally administered into the rats at the dosage of 6.3 g/kg, equivalent to the daily dose of raw herbal material in human subject. The AOM extraction was given to the rats for 13 consecutive days. In the P-CA treatment group, different dosages of P-CA (dissolved in saline at 50, 100, and 200 mg/kg) were intragastrically administered into the rats for 13 consecutive days. Sham-operated group and MCAO model group were intragastrically administered with 1 mL of vehicle solution. Body weight was daily recorded after surgery. The brain samples were collected at day 14 after cerebral ischemia for immunofluorescence staining study and Western blot.

## *In vivo* BrdU Incorporation

BrdU was intraperitoneally injected into the rats for 7 consecutive days at the dosage of 50 mg/kg according to that previously described (Wojtowicz and Kee, 2006).

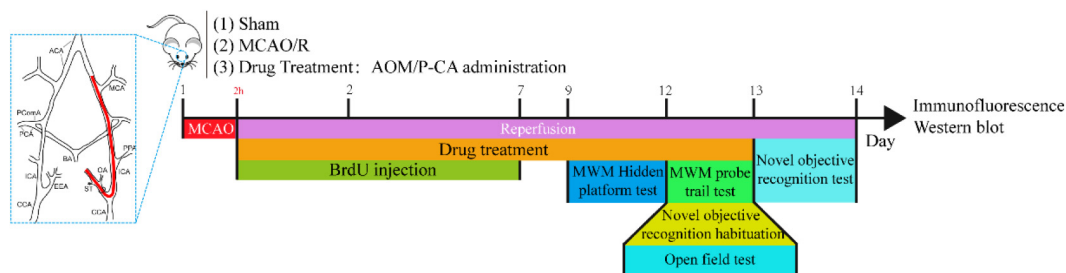


**FIGURE 1 |** Schematic illustration of experiment protocol for MCAO cerebral ischemia–reperfusion. Male Sprague–Dawley (S.D.) rats were subjected to 2 h of MCAO cerebral ischemia plus 14 days of reperfusion. AOM extract (6.3 g/kg, dissolved in 5% ethanol and 5% PEG 400), P-CA (50, 100, 200 mg/kg, dissolved in saline), and vehicle solution were orally given to the rats at onset of reperfusion after 2 h of MCAO cerebral ischemia and daily administered to the rats until day 13 of reperfusion. BrdU (50 mg/kg) was intraperitoneally injected to all animals for 7 consecutive days. Behavioral tests were conducted from day 9 to day 14.

## Behavioral Test for Neurological Severity Score Assessment

Neurological deficit was examined by using the modified neurological severity score (mNSS). The mNSS score reflects the neurological functions related to motor (muscle status, abnormal movement), sensory systems (visual, tactile, and proprioceptive), and the reflex and balance capabilities. The criteria of the mNSS scores ranging from 0 to 18 (0 for accessible/normal, 18 for functional maximum lesion) were adopted according to previous report (Chen et al., 2001).

## Morris Water Maze Test

Morris water maze test was performed to assess the cognitive functions in the sham control group, MCAO vehicle group, MCAO plus AOM treatment group, and MCAO plus P-CA treatment groups. The hidden platform training was carried out on the ninth day after surgery. In 4 days of training, each rat was allowed 60 s to find the platform in water tank twice per day. The probe trial was carried out on the 13th day in the whole treatment period. The test was recorded with a time limit of 70 s (Su et al., 2017). Latency time of reaching the platform, the distance, and the swimming time in the target region of the probe tail test were recorded for testing spatial learning and memory functions.

## Open-Field Test

The open-field test was performed at the 13th day by using an 80 × 80 × 50-cm acrylic black box. The square was divided into the center and outer edge. At the starting point, the rats were placed into the center square of the open field. Each 10-min trial was videotaped by an overhead camera. Distance, time, entries time in center, and total distance in the whole field were recorded by an overhead video and analyzed by using Smart 3.0 system (RWD, Delaware, United States).

## Novel Object Recognition Test

Novel objective recognition habituation was performed at the 13th day after surgical operation. Rats were placed into an 80 × 80 × 50-cm acrylic black box for 10 min. In the test, rats were first placed in the open box at the sample stage, allowed to explore two identical objects, and then returned to their cages. With a delay of 60 min, at the testing phase, the rats were returned to the box where they were exposed to two different objects: one was the same as the previously encountered objects, and the other was a novel object for the rats. The total time of exploration to those objects was 20 s (Lueptow, 2017). The exploration time on the novel object in the test phase was examined.

## Cell Culture

Mouse multipotent neural progenitor or cerebellum stem-like C17.2 cells were originally from ECACC. The cells were maintained in 75-cm<sup>2</sup> vented culture flasks using high-glucose Dulbecco modified eagle medium (DMEM, Gibco) with 10% heat-inactivated fetal bovine serum (Gibco), 1% penicillin/streptomycin (Gibco), and 1% 2 mM L-glutamine (Gibco). The C17.2 cells were cultured in a 37°C humidified incubator with a 5% CO<sub>2</sub>/95% air atmosphere.

## Oxygen–Glucose Deprivation Plus Reoxygenation Model and Drug Treatment

To mimic ischemic/reperfusion condition *in vitro*, C17.2 cells were exposed to the oxygen–glucose deprivation plus reoxygenation (OGD/R) condition. To induce OGD, these cells were cultured with glucose-free DMEM (Gibco) and incubated in a 37°C CO<sub>2</sub> incubator (Eppendorf New Brunswick Galaxy 48R) with oxygen control as 0.1% O<sub>2</sub> and 5% CO<sub>2</sub>/94.9% N<sub>2</sub>. The real-time condition was monitored by incubator reading. The C17.2 cells were exposed to the OGD for a 4-h period and following 20 h of reoxygenation by the replacement of DMEM with high glucose and returned to a 37°C humidified incubator with a 5% CO<sub>2</sub>/95% air atmosphere. The C17.2 cells were treated and incubated with corresponding compounds for 20 h after OGD.

To identify the bioactive compounds contributing to the neurogenic effects of AOM extract, we examined the effects of 10 identified compounds on inducing BDNF/TrkB/AKT expression and promoting proliferation in the C17.2 cells under OGD and reoxygenation conditions. These compounds, including 5-hydroxymethylfurfural, protocatechuic acid, catechin, protocatechuic aldehyde, (–)-epicatechol, P-CA, kaempferol, chrysin, nootkatone, and tectochrysin, were dissolved in dimethyl sulfoxide to obtain 100 mM stock solutions, which were added into the cells with final concentrations of 1, 10, and 100 μM. The cells were seeded in the 24- well plates with poly-D-lysine-coated (Trevigen, Gaithersburg, MD, United States) cover slips and normal 96-well plates, 6-well plates at a density of 2.5 × 10<sup>4</sup> cells/mL. The cells were allocated into the groups of control, OGD, and the OGD plus the selected compounds with three dosages.

## In vitro BrdU Labeling

BrdU stock solution (10 mM) was prepared and diluted into 10 μM BrdU labeling solution with cell culture medium. The BrdU labeling solution was filtered through a 0.2-μm filter under sterile condition. After 20 h of reoxygenation, the treatment medium in 96-well plates was replaced with the BrdU labeling solution for 1 h in 37°C and 5% CO<sub>2</sub> incubator. After that, the BrdU labeling solution was removed, and the cells were washed twice in phosphate-buffered saline (PBS).

## Immunofluorescence

For *in vivo* animal experiments, postfixed brain tissues were immersed in 30% sucrose solution at 4°C for complete dehydration, embedded in O.C.T., and cut into 30-μm sections. The frozen slices were retrieved with sodium citrate buffer. For *in vitro* cell experiments, after labeling with BrdU for 1 h, the cells were fixed with 4% paraformaldehyde for 15 min. The retrieved sections and the cells were incubated with 2 M HCl under room temperature for 1 h and then washed with 1% PBST (PBS + 1% Triton) three times for 15 min. Afterward, cells were blocked with 5% goat serum (GS) in 3% PBST (PBS + 3% triton) for 1 h. Sections were stained with primary antibodies including BrdU (rat, 1:400), Ki67 (rabbit, 1:400), DCX (rabbit, 1:400), and NeuN (rabbit, 1:400) overnight. The C17.2 cells were costained with



primary antibodies BrdU (rat, 1:400), Ki67 (rabbit, 1:400), and SOX2 (rabbit, 1:400). After incubation with primary antibodies at 4°C overnight, the samples were washed with 3% PBST three times for 15 min. All slices were stained with anti-rat 488 (1:800) and anti-rabbit 568 (1:800) for 2 h and counterstained the nucleus with DAPI (4',6'-diamidino-2-phenylindole) for 15 min in room temperature. Brain sections and cell samples were mounted with fluorescence mounting medium (Dako Agilent, Santa Clara, CA, United States), whereas the cells for high content screening (HCS) experiments were kept in PBS. Immunofluorescent images were captured by Carl Zeiss LSM 800 Confocal Laser Scanning Microscope and analyzed by ZEN offline. HCS experiment was performed by using GE Healthcare Life Sciences IN Cell Analyzer 6500HS and analyzed by IN Carta offline.

## Western Blot Analysis

Proteins were extracted by radioimmunoprecipitation assay buffer with 1% protease and phosphatase inhibitor cocktails (CST). The protein concentration was detected by BCA Protein Assay Kit (Thermo Fisher Scientific, United States). Protein lysates were separated by electrophoresis with 11% sodium dodecyl sulfate polyacrylamide (sodium dodecyl sulfate–polyacrylamide gel electrophoresis) gel, transferred to polyvinylidene fluoride membrane, and immunoblotted with primary antibodies including BDNF (Abcam, mouse, 1:1,000), TrkB (Santa Cruz, mouse, 1:100), AKT (CST, rabbit, 1:1,000), p-AKT (CST, rabbit, 1:1,000),  $\beta$ -actin (CST, mouse, 1:5,000), and GAPDH (CST, rabbit, 1:5,000) separately. Followed by horseradish peroxidase-conjugated secondary antibodies (1:2,000) incubation. Signals were detected by chemiluminescent ECL Select Kit (GE Healthcare, Chicago, IL, United States), captured by the Gel-Doc system (Bio-Rad, Hercules, CA, United States), and analyzed by Image Lab software (Bio-Rad, Hercules, CA, United States).

## Statistical Analysis

Data analysis was performed by using Prism 8 (GraphPad Software, United States). All data were expressed as mean  $\pm$  SEM. Student *t*-tests were used for two groups of designed experiments, and two-way analysis of variance was used to analyze multiple groups of comparisons followed by Tukey multiple-comparisons test to determine the difference between two groups where appropriate. Statistical significance was defined as  $p < 0.05$ .

## RESULTS

### Quality Control Study of AOM Extraction

We first conducted quality control study to identify the chemical ingredients of AOM extract using HPLC. We optimized the chromatographic conditions and obtained a well-separated chromatogram (Figure 2). We compared the retention time of AOM extract and mixed standards. The structures and retention time of those compounds are summarized in Table 1. By combining the results in LC-MS (Figure 3 and Supplementary Table 1), we confirmed 10 compounds in AOM extract, including 5-hydroxymethylfurfural, protocatechuic

acid, catechin, protocatechuic aldehyde, (–)-epicatechol, P-CA, kaempferol, chrysin, nootkatone, and tectochrysin. These identified compounds can be catalog as five flavonoids, three phenolic acid, one eremophilane, and one other compound.

We then established an HPLC method to quantitatively analyze P-CA as a marker compound in AOM extract. We examined the linearity, repetition, precision, accuracy, and stability of the HPLC method for P-CA detection. The standard curve was  $y = 7.5275 \times 10^7 x - 1.5917 \times 10^4$  with correlation coefficients (*r*) of 0.9998. The LODs and LOQs were 0.003163 and 0.01265  $\mu\text{g/mL}$ , respectively. The relative standard deviation (RSD) of the test solution was 3.41% for the repetitive and 1.75% for the precision results. The accuracy was assessed by overall recovery rate, which was 90% to 108%, and the RSD was 0.39%. The RSD of the stability assay for the test solution within 18 h was 4.15%, and the RSD rates of the interday precision and intraday precision were 2.48% and 2.06%, respectively. These results indicate that the HPLC method was highly sensitive and reliable, and the concentration of P-CA was identified to be 4.6  $\mu\text{g/g}$  in AOM extract.

### AOM Treatment Increases Body Weight and Promotes Spatial Learning and Memory in Post-MCAO Ischemic Rats

We investigated the effects of AOM on body weight, neurological deficit, spatial learning, and memory in transient cerebral ischemic rat model. The rats were subjected to 2 h of MCAO cerebral ischemia plus 14 days of reperfusion. AOM (6.3 g/kg per day) was orally administered to the rats for 13 days after surgical operation. As shown in Figure 4A, the body weight was time-dependently decreased in the MCAO vehicle group after surgical operation. AOM treatment group had significantly increased body weight than the MCAO vehicle group. Meanwhile, we evaluated the neurological dysfunction scores. The MCAO vehicle group had remarkably higher neurological deficit scores than sham control group. AOM treatment group showed a trend to reduce the neurological severity scores but had no statistically difference from the MCAO vehicle group (Figure 4B). We further evaluated spatial learning and long-term and short-term memory functions with Morris water maze and novel objective test. In the Morris water maze test, after 4 days of training, we tested the spatial learning and long-term memory functions by recording the time to reach the platform, the distance in target quadrant, and latency time to reach the platform. The AOM treatment group spent less time to reach the hidden platform than the MCAO vehicle group at day 4 (Figure 4C). In the probe trial, the AOM treatment group had remarkably longer swimming routes in target region than the MCAO vehicle treatment group (Figure 4D). Statistical analysis revealed that the AOM-treated rats had significantly improved parameters in the distance in target quadrant, latency time to reach the platform, and total distance in habituation. The AOM-treated rats had more distance and time in target region and spent less time to reaching platform region (Figure 4E). We also used open-field test to measure anxiety (Figures 4F,G) and novel objective recognition to detect short-term memory (Figure 4H). In the open-field test, the AOM



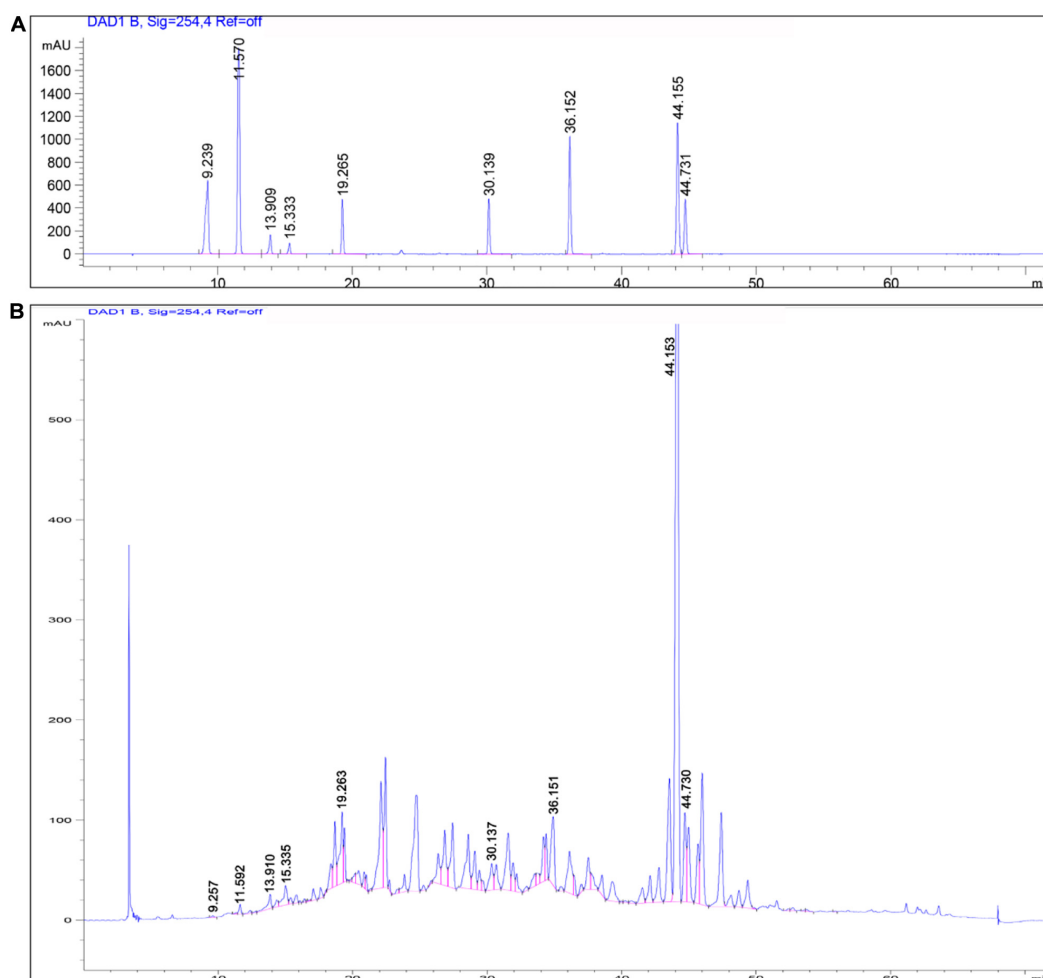


**FIGURE 2 |** HPLC chromatograms of mixed chemical standards **(A)** and AOM extract **(B)**. Parameters for HPLC detection: Shimadzu C18 column (4.6 × 250 mm, 5  $\mu$ m); mobile phase: gradient profile with acetonitrile (ACN)—0.1% trifluoroacetate—water from 5 to 100% in 60 min. Column temperature: 30°C; flow rate: 1.0 mL/min; UV detection: 220 nm.

treatment increased the distance and the time in the center region and the entry times to the center, suggesting the antianxiety effects. However, there was no significant difference in locomotor activity among the groups showing similar total distances in the whole regions. In the novel objective recognition test, the AOM treatment group showed better memory to the familiar objects and had more interest in exploring new objects than the MCAO vehicle group. Those results suggest that AOM could improve the quality of life, promote spatial learning/memory and recognition capacity, and reduce anxiety in the post-ischemic stroke rats.

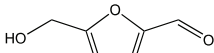
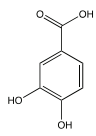
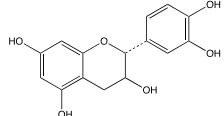
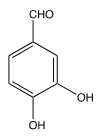
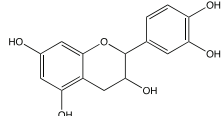
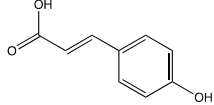
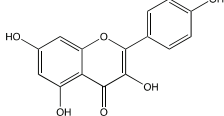
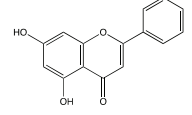
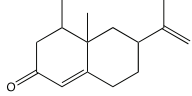
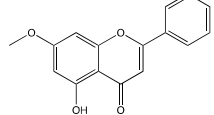
### AOM Promotes Adult Hippocampal Neurogenesis in Post-MCAO Ischemic Rats *via* Inducing BDNF Pathway

We then investigated the neurogenic effects of AOM on inducing proliferation and differentiation in the hippocampus of the post-MCAO ischemic rats by using immunofluorescence and Western blot analysis. Ki67 is a biomarker for indexing

the cells at proliferation stage, while BrdU is an analog of thymidine for marking newly generated cells. The dual-immunofluorescent staining of BrdU/Ki67 was used for detecting newly generated cells that were at proliferating stage and DAPI for nuclei identification. In addition, we performed the immunofluorescent experiments to identify newborn immature neurons and newborn mature neurons by using DCX NeuN, respectively. Dual-immunostaining imaging of BrdU/DCX and BrdU/NeuN in the postischemic brain regions was investigated. The results showed that AOM extract significantly increased the dual-positive staining populations of BrdU/Ki67, BrdU/DCX, and BrdU/NeuN in the DG and SVZ of the MCAO rats. Those results indicate that AOM could promote neurogenesis in hippocampus, SVZ, and striatum of post-MCAO ischemic rats (**Supplementary Figures 2–5**).

Neurotrophic factor BDNF is a crucial cellular signaling regulator in the process of hippocampal neurogenesis for improving learning and memory functions (Egan et al., 2003). Functional TrkB signaling is a crucial player in the proliferation

**TABLE 1 |** Representative compounds identified in AOM extract.

Peak no.	Retention time (min)	Formula	Molecular weight	Identification	Classification	Structure
1	9.257	C <sub>6</sub> H <sub>6</sub> O <sub>3</sub>	126.11	5-Hydroxymethylfurfural	Others	
2	11.592	C <sub>7</sub> H <sub>6</sub> O <sub>4</sub>	154.12	Protocatechuic acid	Phenolic acid	
3	13.910	C <sub>15</sub> H <sub>14</sub> O <sub>6</sub>	290.27	Catechin	Flavonoids	
4	13.910	C <sub>7</sub> H <sub>6</sub> O <sub>3</sub>	138.12	Protocatechuic aldehyde	Phenolic acid	
5	15.335	C <sub>15</sub> H <sub>14</sub> O <sub>6</sub>	290.26	(-)-Epicatechol	Flavonoids	
6	19.263	C <sub>9</sub> H <sub>8</sub> O <sub>3</sub>	164.16	<i>p</i> -Coumaric acid	Phenolic acid	
7	30.137	C <sub>15</sub> H <sub>10</sub> O <sub>6</sub>	286.23	Kaempferol	Flavonoid	
8	36.151	C <sub>15</sub> H <sub>10</sub> O <sub>4</sub>	254.24	Chrysin	Flavonoid	
9	44.153	C <sub>15</sub> H <sub>22</sub> O	218.34	Nootkatone	Eremophilane	
10	44.730	C <sub>16</sub> H <sub>12</sub> O <sub>4</sub>	268.26	Tectochrysin	Flavonoid	

of NSCs and the survival and functional integration of newborn neurons in adult hippocampus (Bergami et al., 2008; Li et al., 2008). Thus, we detected whether AOM could regulate BDNF/TrkB/AKT signaling for improving neurogenesis in the hippocampus regions (**Figure 5**). There was no statistical difference in the expression of BDNF and p-AKT in the hippocampus regions between the sham control group and the MCAO vehicle group. The AOM treatment group had significantly higher expression levels of BDNF, TrkB, and p-AKT in the hippocampus regions than the MCAO vehicle group. Those results suggest that AOM could activate BDNF/TrkB/AKT

signaling pathway and promote adult hippocampal neurogenesis in post-MCAO ischemic rats.

### ***p*-Coumaric Acid Serves as a BDNF Inducer for Promoting Neurogenesis in NSCs**

We then screened the active compounds from AOM with the properties of inducing BDNF signaling and promoting neurogenesis in the cultured C17.2 cells exposed to 4-h OGD plus 20-h reoxygenation. **Table 1** shows 10 compounds identified

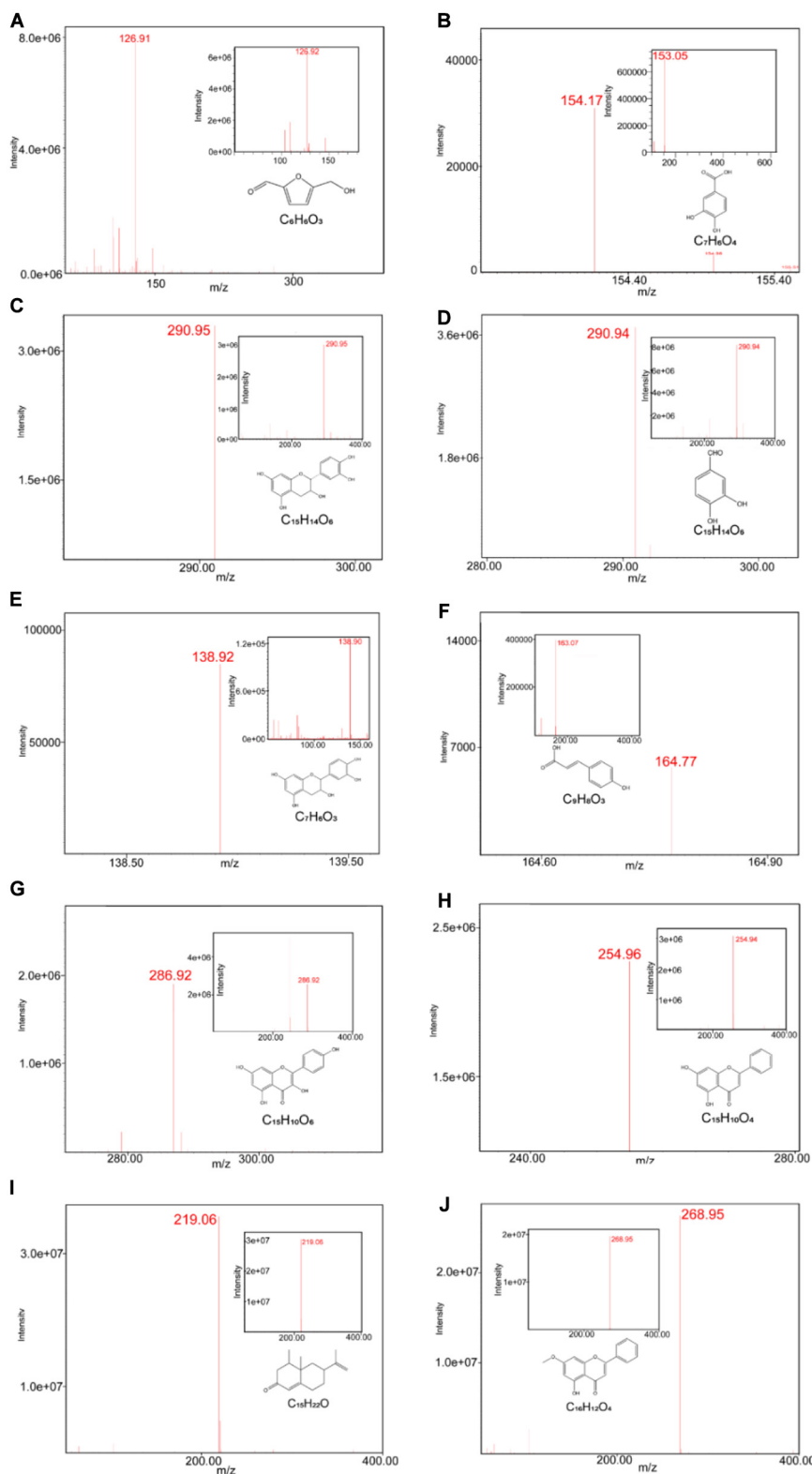


**FIGURE 3** | ESI-MS chromatograms of AOM extract. LC-MS was operated on Waters LC/MS ACQUITY QDA with CORTECS C18 column (2.7  $\mu$ m 4.6  $\times$  50 mm), measured under condition of ionization method-ESI (+/-) and scanned range from 100 to 1,000. ESI-MS chromatograms of 5-hydroxymethylfurfural (**A**), protocatechuic acid (**B**), catechin (**C**), (-)-epicatechol (**D**), protocatechuic aldehyde (**E**), *p*-coumaric acid (**F**), kaempferol (**G**), chrysin (**H**), nootkatone (**I**), tectochrysin (**J**), and their standards.

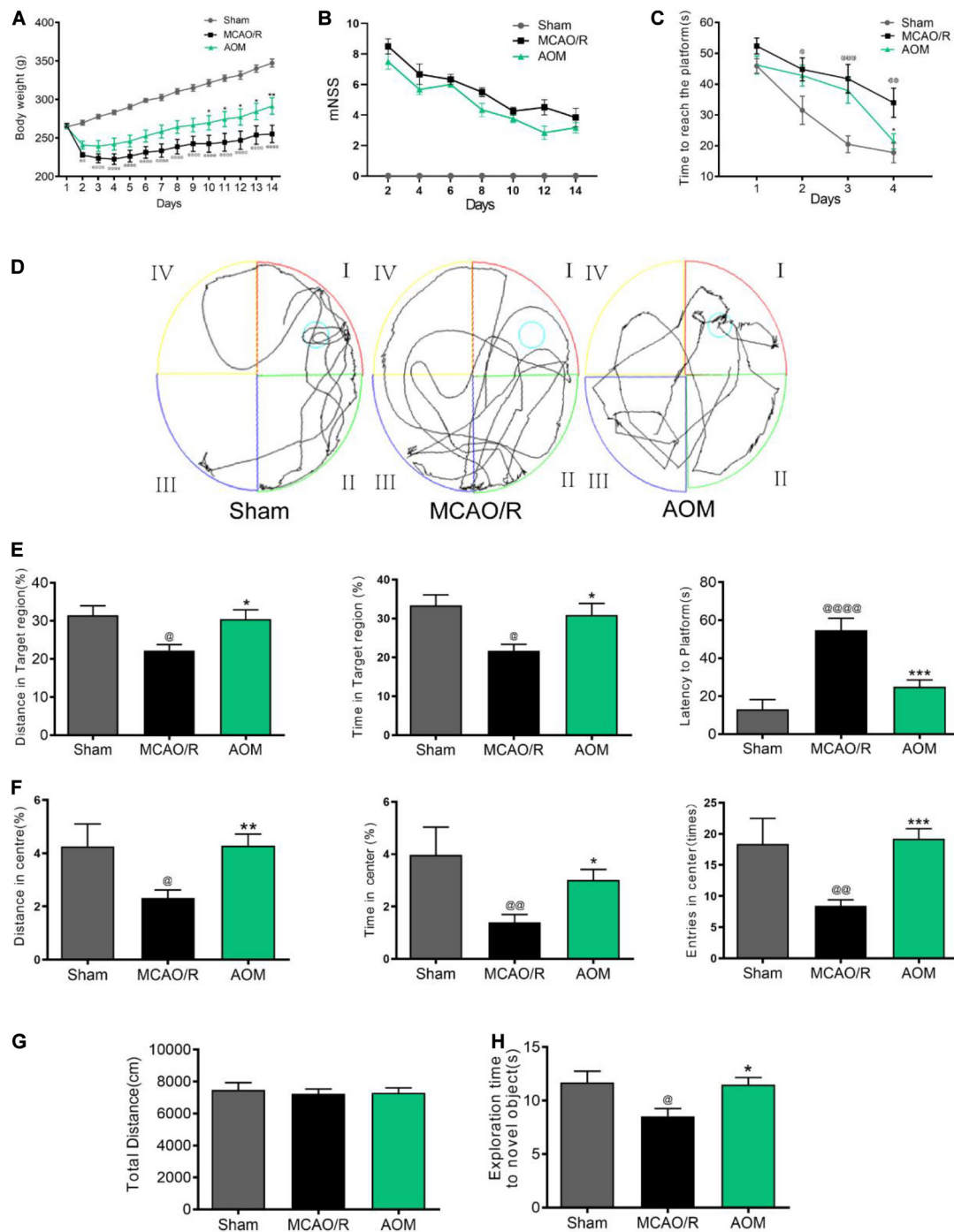


**FIGURE 4 |** AOM increased body weight and improved spatial learning and memory capacity in transient MCAO rats. S.D. rats were divided into sham control group (Sham), MCAO cerebral ischemia–reperfusion vehicle group (MCAO/R), and MCAO/R plus AOM treatment group (AOM). The rats were subjected to 2 h of MCAO cerebral ischemia plus 14 days of reperfusion. AOM extract (6.3 g/kg, dissolved in 5% ethanol and 5% PEG400) and vehicle solution were orally given to the rats at onset of reperfusion after 2 h of MCAO cerebral ischemia and daily administered for 13 days of reperfusion. **(A)** Body weight changes in sham control, MCAO/R, and AOM groups; **(B)** mNSS in sham control, MCAO/R, and AOM groups. The mNSS was assessed every 2 days. **(C–E)** Morris water maze test for evaluating spatial learning and long-term memory in transient MCAO rats: **(C)** Escape latency in 4 days of hidden platform test. **(D)** Swimming routes in the probe trial test. **(E)** Distance and time in the target quadrant of the probe trial and latency time before reaching platform region. **(F,G)** Open-field test was used to measure anxiety in transient MCAO rats. Distance, time, and entries in center region were recorded in the sham control, MCAO/R, and AOM treatment groups. AOM treatment reduced the anxiety **(F)** but had no effect on total distance moved during habituation **(G)**. **(H)** Novel objective recognition test for short-term memory: AOM increased exploration time on novel object in test phase of the MCAO rats. Data were presented as mean  $\pm$  SEM ( $n = 12$ –14); vs. sham,  $^{\circ}p < 0.05$ ,  $^{\circ\circ}p < 0.01$ ,  $^{\circ\circ\circ}p < 0.001$ ,  $^{\circ\circ\circ\circ}p < 0.0001$ ; vs. MCAO/R,  $^*p < 0.05$ ,  $^{**}p < 0.01$ ,  $^{***}p < 0.001$ .



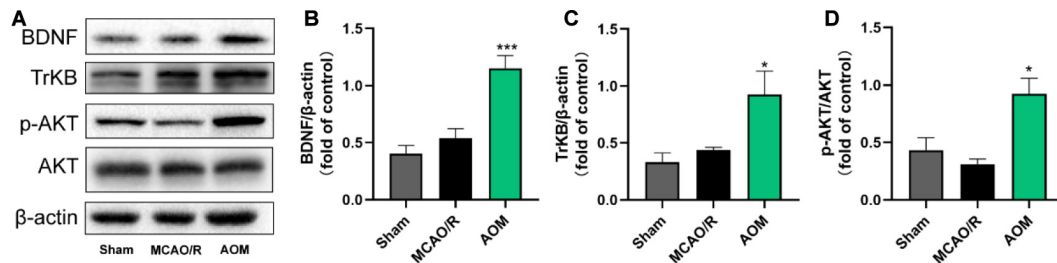


**FIGURE 5 |** *Alpinia oxyphylla* Miq. up-regulated expression of BDNF, TrkB, and phosphorylated AKT in the hippocampus of transient MCAO cerebral ischemic rats. S.D. rats were divided into groups of sham, MCAO/R, and AOM. The rats were subjected to 2 h of MCAO cerebral ischemia plus 14 days of reperfusion. AOM extract (6.3 g/kg, dissolved in 5% ethanol and 5% PEG400) and vehicle solution were orally given to the rats at onset of reperfusion after 2 h of MCAO cerebral ischemia and daily administered for 13 days of reperfusion. **(A)** Representative immunoblot results for expression of BDNF, TrkB, and phosphorylated AKT. **(B)** Statistical analysis of relative expression level of BDNF in sham, MCAO/R, and AOM groups. **(C)** Statistical analysis of relative expression level of TrkB in sham, MCAO/R, and AOM groups. **(D)** Statistical analysis of relative expression level of phosphorylated AKT in sham, MCAO/R, and AOM groups. Data were presented as mean  $\pm$  SEM ( $n = 6-8$ ); vs. MCAO/R, \* $p < 0.05$ , \*\*\* $p < 0.001$ .

from AOM. The cells were treated with these compounds at the concentrations of 1, 10, and 100  $\mu$ M. BrdU and Ki67 are commonly used biomarkers to analyze the proliferative activity of NSCs (Tanaka et al., 2011). By using HCS technology, we examined the rates of dual-positive staining of BrdU/Ki67 in the cells for identifying the proliferation-promoting effects. The compound 6, P-CA, was found to be the most effective ingredient to increase the BrdU/Ki67 dual-positive cells (**Figure 6A**). Meanwhile, P-CA treatment significantly up-regulated the expression of BDNF, TrkB, and p-AKT in the cells (**Figure 6B**). Cotreatment of ANA12 (20  $\mu$ M, a BDNF/TrkB specific inhibitor) abolished the effects of P-CA (100  $\mu$ M) on the induction of the expression of BDNF and TrkB (**Figure 6C**) and the increased rates of BrdU/Ki67 dual-positive staining in the C17.2 cells (**Figure 6D**). Furthermore, we performed immunofluorescent studies on the costaining of BrdU/SOX2, in which SOX2 is a critical marker for embryonic stem cells. P-CA treatment significantly increased the rates of BrdU/SOX2 positive cells whose effect was also abolished the cotreatment of ANA12 (**Figures 6E,F**). Those results suggest that P-CA could increase the survival of NSCs and stimulate the proliferation of NSCs *via* inducing BDNF/TrkB/AKT signaling pathway.

### P-CA Treatment Increases Body Weight, Improves Neurological Deficit Score, Promotes Spatial Learning and Memory, and Reduces Anxiety in Post-MCAO Ischemic Rats

We next investigated the effects of P-CA on body weight, mNSS, spatial learning, and memory in post-MCAO ischemic rats. In the P-CA treatment group, P-CA 50, 100, and 200 mg/kg were intragastrically administered into the rats at the onset of reperfusion after MCAO ischemia and used daily for 13 consecutive days. Vehicle solution was used in sham-operated group and MCAO vehicle group. The P-CA treatment increased body weight but had no effect on the neurological severity scores statistically (**Figures 7A,B**). We also performed the Morris water maze to evaluate the spatial learning and long-term memory

functions (**Figures 8A-E**), the open-field test to measure anxiety (**Figures 8F-I**), and the novel objective recognition to detect short-term memory (**Figure 8J**). In the Morris water maze test, the P-CA treatment significantly increased the distance and time in the target quadrant of the probe trial and decreased the latency time to reach the platform, suggesting the improvement of spatial learning and long-term memory functions. In the open-field test, the P-CA treatment increased the distance and time in center and the entry times in center region, suggesting the effects of reducing anxiety. In the novel objective recognition test, P-CA treatment increased the exploration time on novel object in test phase, indicating the improvement of short memory. These results suggest that P-CA could promote spatial learning, increase short and long-term memory abilities, and reduce anxiety in post-ischemic stroke rats.

### P-CA Treatment Promotes Adult Hippocampal Neurogenesis in Post-MCAO Ischemic Rat Brains *via* Inducing BDNF Signaling Pathway

We then investigated the effects of P-CA on promoting hippocampal neurogenesis in the post-MCAO ischemic rats. We detected dual-positive staining of BrdU/Ki67 for cell proliferation in hippocampal DG, SVZ, and striatum regions where DAPI was used for nuclei identification (**Figures 9A-D**). The P-CA treatment remarkably increased the rates of the BrdU/Ki67-positive cells in the hippocampal DG, SVZ, and striatum regions of the postischemic brain regions. Furthermore, we identified newborn immature neurons and newborn mature neurons as detected with BrdU/DCX (**Figures 10A-D**) and BrdU/NeuN (**Figures 11A-D**), respectively. As expected, P-CA treatment promoted the production of newborn immature and mature neurons in the hippocampus and striatum of the postischemic brains. We also performed the imaging analysis at XYZ planes with the dual staining of BrdU/Ki67, BrdU/DCX, and BrdU/NeuN in the DG and SVZ. P-CA treatment increased the dual-positive staining of BrdU/Ki67, BrdU/DCX, and BrdU/NeuN in the DG and

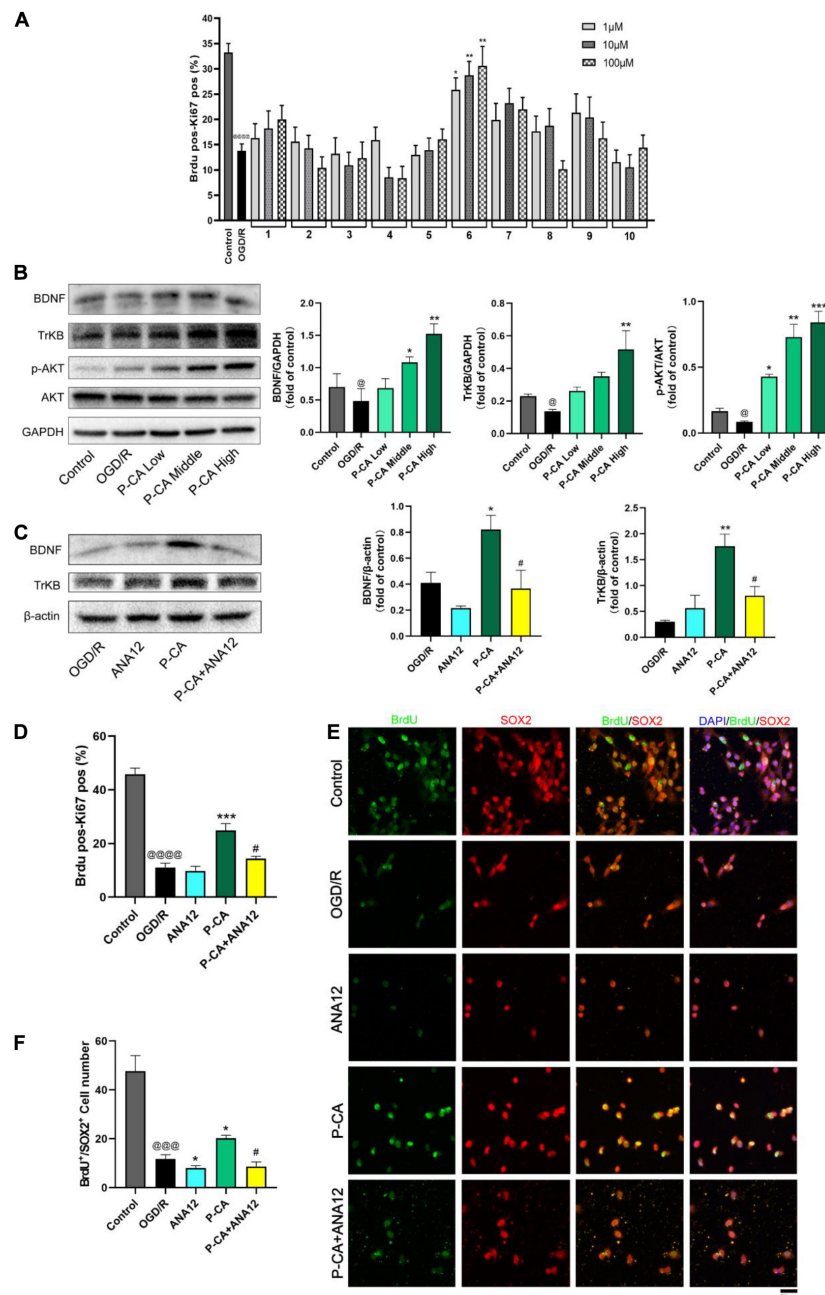
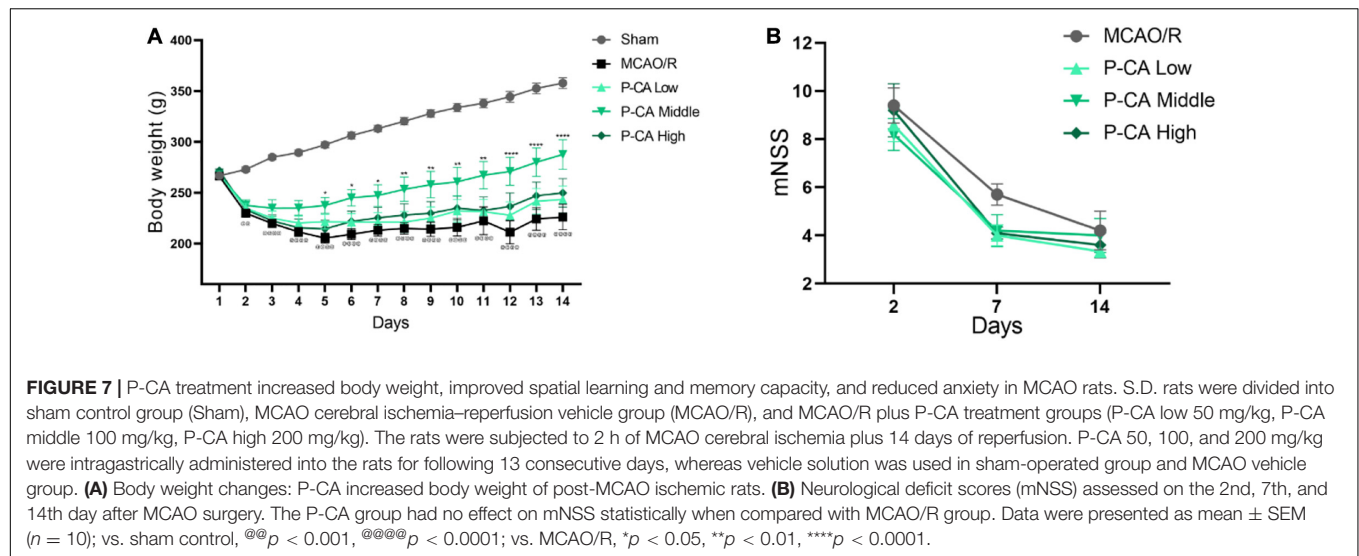


**FIGURE 6 |** Identification of P-CA as an active compound from AOM with property of inducing BDNF/TrkB/AKT signaling and promoting NSC proliferation in cultured mouse cerebellum stem like C17.2 cells *in vitro*. To mimic cerebral ischemia-reperfusion injury *in vitro*, the C17.2 cells were subjected to 4 h of oxygen glucose deprivation plus 20 h of reoxygenation (OGD/R). By using high content screening (HCS) technology, we examined the effects of 10 active compounds from AOM (1, 10, and 100 μM) on the rates of BrdU/Ki67 dual-positive-staining cells and BDNF/TrkB/AKT signaling in the C17.2 cells under OGD/R exposure. **(A)** The effects of 10 compounds (1, 10 and 100 μM) on rates (%) of the BrdU and Ki67 dual positive staining cells detected by HCS technology. Ten compounds: 1. 5-Hydroxymethylfurfural; 2. Protocatechuic acid; 3. Catechin; 4. (-)-Epicatechol; 5. Protocatechuic aldehyde; 6. P-Coumaric acid; 7. Kaempferol; 8. Chrysin; 9. Nootkatone; 10. Tectochrysin. Effects of these compounds (1, 10, and 100 μM) on the rates of BrdU/Ki67 dual-positive-staining cells counted by HCS technology (right). Dual-positive staining of BrdU and Ki67 indicates the NSC proliferation-promoting activity. P-CA was found to be the most effective compound to induce proliferation of NSCs. **(B)** Western blot analysis indicating the effects of P-CA (1, 10, and 100 μM) on the expression of BDNF, TrkB, and p-Akt. P-CA dose-dependently up-regulated the expression of BDNF, TrkB, and p-Akt. **(C)** TrkB inhibitor ANA12 (20 μM) abolished the effects of P-CA (100 μM) on the expression of BDNF and TrkB. **(D)** The effects of P-CA (100 μM) on rates (%) of the BrdU and Ki67 dual-positive-staining cells detected by HCS technology. ANA12 (20 μM) abolished the effects of P-CA (100 μM) on the BrdU/Ki67 dual-positive-staining cells. **(E)** Representative immunofluorescent staining of BrdU (green) and SOX2 (red) with nucleus (blue). **(F)** Representative immunofluorescent imaging for BrdU (green) and SOX2 (red) positive-staining cells colocalized with nucleus (blue) in C17.2. ANA12 (20 μM) abolished the effects of P-CA (100 μM) on the BrdU/SOX2 dual-positive-staining cells. Data were presented as mean ± SD (*n* = 3); vs. control @*p* < 0.05, @@@*p* < 0.001, @@@@*p* < 0.0001; vs. OGD/R \**p* < 0.05, \*\**p* < 0.01, \*\*\**p* < 0.001; vs. P-CA #*p* < 0.05.



SVZ (**Supplementary Figure 6**). These results indicate that P-CA could improve NSC differentiation for neurogenesis in poststroke treatment.

We further investigated the effects of P-CA on the expression of BDNF/TrkB/AKT signaling for improving neurogenesis in the hippocampus regions (**Figure 12**). There was no significant difference in the expression of BDNF, TrkB, and p-AKT in the hippocampus regions between sham control group and MCAO vehicle group. However, P-CA treatment significantly up-regulated the expression of BDNF, TrkB, and p-AKT in the hippocampus regions. Those results suggest that P-CA could activate BDNF/TrkB/AKT signaling pathway and promote adult hippocampal neurogenesis in post-MCAO ischemic rats.

## DISCUSSION

*Alpinia oxyphylla* Miq. is a medicinal herb used for improving cognitive functions in TCM practice, but the scientific evidence of its use is lacking. In the present study, we demonstrate that AOM enhances adult hippocampal neurogenesis and improves cognitive impairment *via* inducing BDNF/TrkB/AKT signaling pathway in post-ischemic stroke treatment. Furthermore, we identify that P-CA is a representative active compound from AOM to activate BDNF/TrkB/AKT signaling pathway and induce adult hippocampal neurogenesis for enhancing cognitive functions. To our knowledge, this is the first report to demonstrate that AOM and its active compound P-CA could promote adult hippocampal neurogenesis and improve cognitive impairment *via* inducing BDNF/TrkB/AKT signaling pathway in postischemic brains.

Previous studies have reported the bioactivities of AOM in improving cognitive functions and antidepressant (Koo et al., 2004; Shi et al., 2014; Yan et al., 2016). AOM improves cognitive functions in mouse cortex and hippocampus in amyloid  $\beta$ -induced AD mouse model (Shi et al., 2014). AOM exerts antidepressant-like effects through activating TrkB-mediated

BDNF signal pathway (Yan et al., 2016). AOM enhances learning disability and protects CA1 hippocampal neurons in a mouse model with CCA occlusion (Koo et al., 2004; Wang et al., 2018). Herein, we tested the hypothesis that AOM could induce adult hippocampal neurogenesis and improve poststroke cognitive impairment *via* inducing BDNF/TrkB/AKT signaling pathway. AOM treatment significantly increased body weight, indicating the recovery from surgical injury and good quality of life in poststroke care. However, there was no statistical difference in the mNSS between the MCAO vehicle group and AOM treatment group. Importantly, Morris water maze and novel objective recognition test revealed that the AOM treatment significantly improved spatial learning/memory and enhanced cognitive functions in the post-MCAO ischemic rats with the impaired learning and memory functions. Meanwhile, AOM treatment enhanced cell proliferation and neuronal differentiation as marked by dual-immunofluorescent staining of BrdU/Ki67, BrdU/DCX, and BrdU/NeuN in hippocampal DG, SVZ, and striatum. Those results suggest that AOM could promote adult hippocampal neurogenesis, improve the spatial learning/memory impairment, and enhance cognitive functions in post-MCAO ischemic rats.

Brain-derived neurotrophic factor is a crucial neurotrophic factor to mediate hippocampal neurogenesis for improving learning and memory functions (Egan et al., 2003). BDNF not only promotes neurogenesis but also plays crucial roles in the survival and maintenance of neuronal cells (Wei et al., 2015). BDNF exerts its essential roles in promoting the hippocampal neurogenesis and rescuing cognitive and motor dysfunctions in a transgenic model of dementia (Goldberg et al., 2015). TrkB signaling is a crucial player in the proliferation of NSCs and the survival and functional integration of newborn neurons in adult hippocampus (Bergami et al., 2008; Li et al., 2008). In the present study, we found that AOM treatment significantly up-regulated the expression of BDNF, TrkB, and p-AKT in the hippocampus, indicating the induction of BDNF signaling pathway for neurogenesis in post-MCAO ischemic rats.

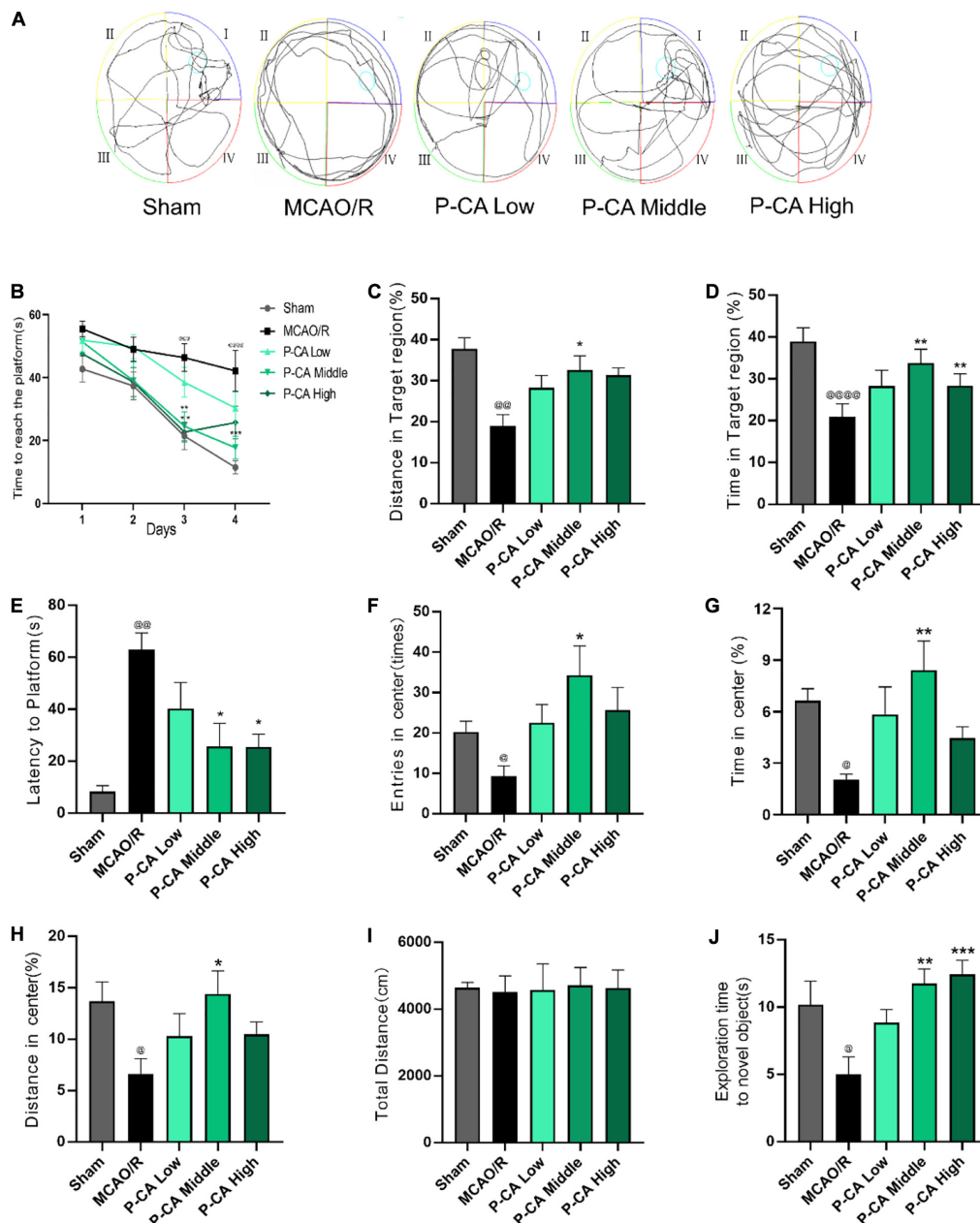


**FIGURE 8 |** P-CA treatment increased body weight, improved spatial learning and memory capacity, and reduced anxiety in MCAO rats. S.D. rats were divided into sham control group (Sham), MCAO cerebral ischemia–reperfusion vehicle group (MCAO/R), and MCAO/R plus P-CA treatment groups (P-CA low 50 mg/kg, P-CA middle 100 mg/kg, P-CA high 200 mg/kg). The rats were subjected to 2 h of MCAO cerebral ischemia plus 14 days of reperfusion. P-CA 50, 100, and 200 mg/kg were intragastrically administered into the rats for following 13 consecutive days, whereas vehicle solution was used in sham-operated group and MCAO vehicle group. **(A–E)** Morris water maze tests for spatial learning and long-term memory in the sham control, MCAO/R, and P-CA treatment groups: P-CA treatment revealed to improve spatial learning and long-term memory. **(B)** Escape latency in 4 days of hidden platform tests. **(A)** Swimming routes in the probe trial. **(C)** Distance and **(D)** time in the target quadrant of the probe tail test, and **(E)** latency time before reaching platform region. **(F–H)** Open-field test for anxiety in the sham control, MCAO/R, and P-CA treatment groups: Distance, time and entries in center region were recorded. P-CA treatment reduced the anxiety but had no effect on total distance moved during habituation **(I)**. **(J)** Novel objective recognition test for short-term memory: P-CA increased exploration time on novel object in test phase of the MCAO rats. Data were presented as mean  $\pm$  SEM ( $n = 10$ ); vs. sham control,  $^{\circ}p < 0.01$ ,  $^{\circ\circ}p < 0.001$ ,  $^{\circ\circ\circ}p < 0.001$ ,  $^{\circ\circ\circ\circ}p < 0.0001$ ; vs. MCAO/R,  $^*p < 0.05$ ,  $^{**}p < 0.01$ ,  $^{***}p < 0.001$ .

HCS technology is a sophisticated and efficient analytical method for drug discovery with application potentials for stem cell biology and genome studies (Fraietta and Gasparri, 2016).

Combined HPLC and HCS technologies provide an effective platform for identifying the bioactive ingredients from medicinal herbal productions. With HCS technology, we examined the



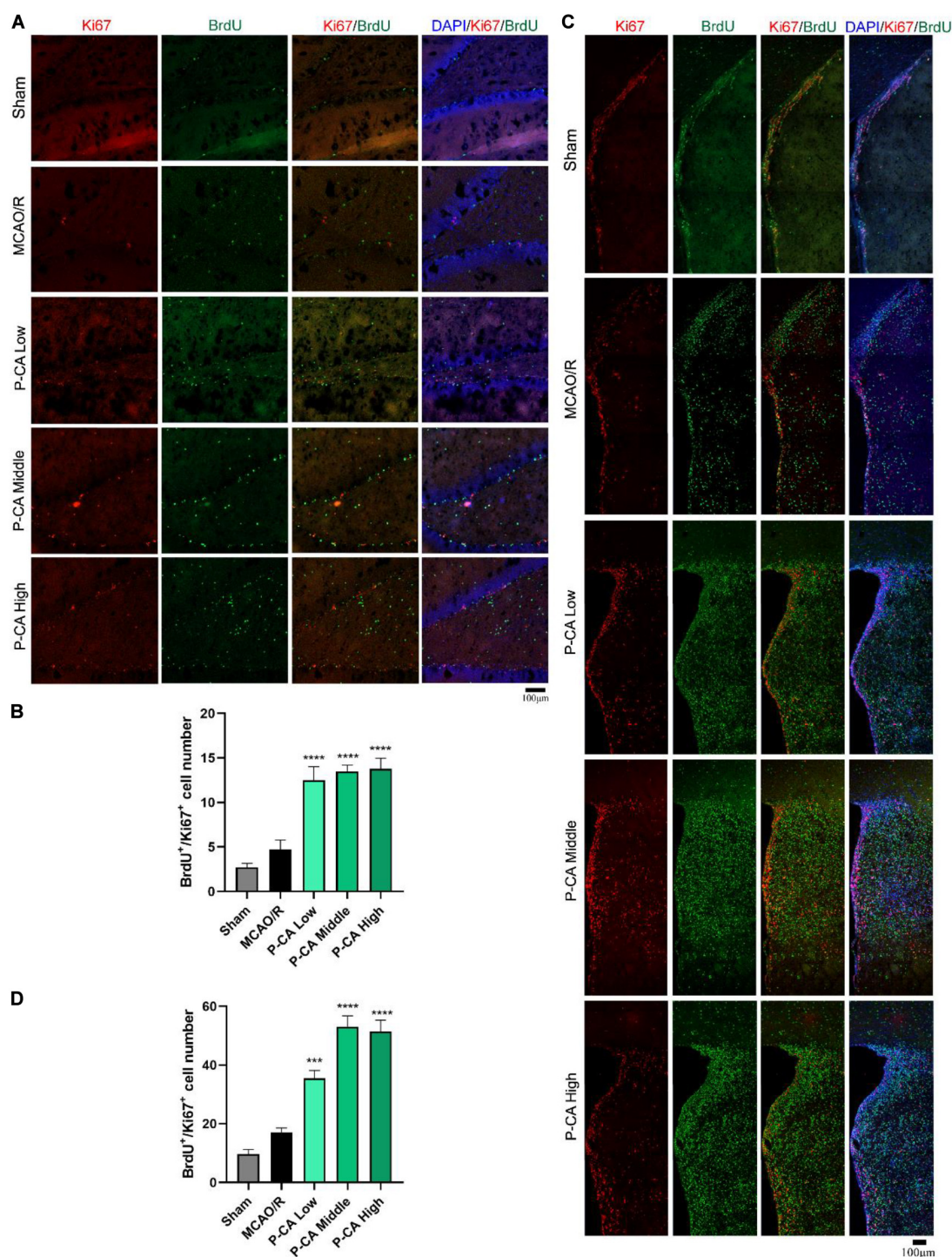


**FIGURE 9 |** P-CA promoted proliferation in hippocampus, SVZ, and striatum of transient MCAO ischemic rats. S.D. rats were divided into sham, MCAO/R and MCAO/R plus P-CA treatment groups (P-CA low 50 mg/kg, P-CA middle 100 mg/kg, P-CA high 200 mg/kg). The rats were subjected to 2 h of MCAO cerebral ischemia plus 14 days of reperfusion. P-CA 50, 100, and 200 mg/kg were intragastrically administered into the rats for following 13 consecutive days, whereas vehicle solution was used in sham-operated group and MCAO vehicle group. **(A)** Representative immunofluorescent imaging for BrdU (green) and Ki67 (red) positive-staining cells colocalized with nucleus (blue) in hippocampal DG. Dual-positive staining of BrdU/Ki67 refers to the newly generated cells which are still in proliferating. **(B)** Statistical analysis of BrdU<sup>+</sup>/Ki67<sup>+</sup> cell number in hippocampus in sham, MCAO/R, and P-CA groups. **(C)** Representative immunofluorescent imaging for BrdU (green) and Ki67 (red) positive-staining cells colocalized with nucleus (blue) in subventricular zone and striatum. **(D)** Statistical analysis of BrdU<sup>+</sup>/Ki67<sup>+</sup> cell number in striatum and SVZ in sham, MCAO/R, and P-CA groups. Data were presented as mean  $\pm$  SEM ( $n = 3$ –5 rats per group, 3 tissue sections per brain region used for imaging analysis); vs. MCAO/R, \*\*\* $p < 0.001$ , \*\*\*\* $p < 0.0001$ .

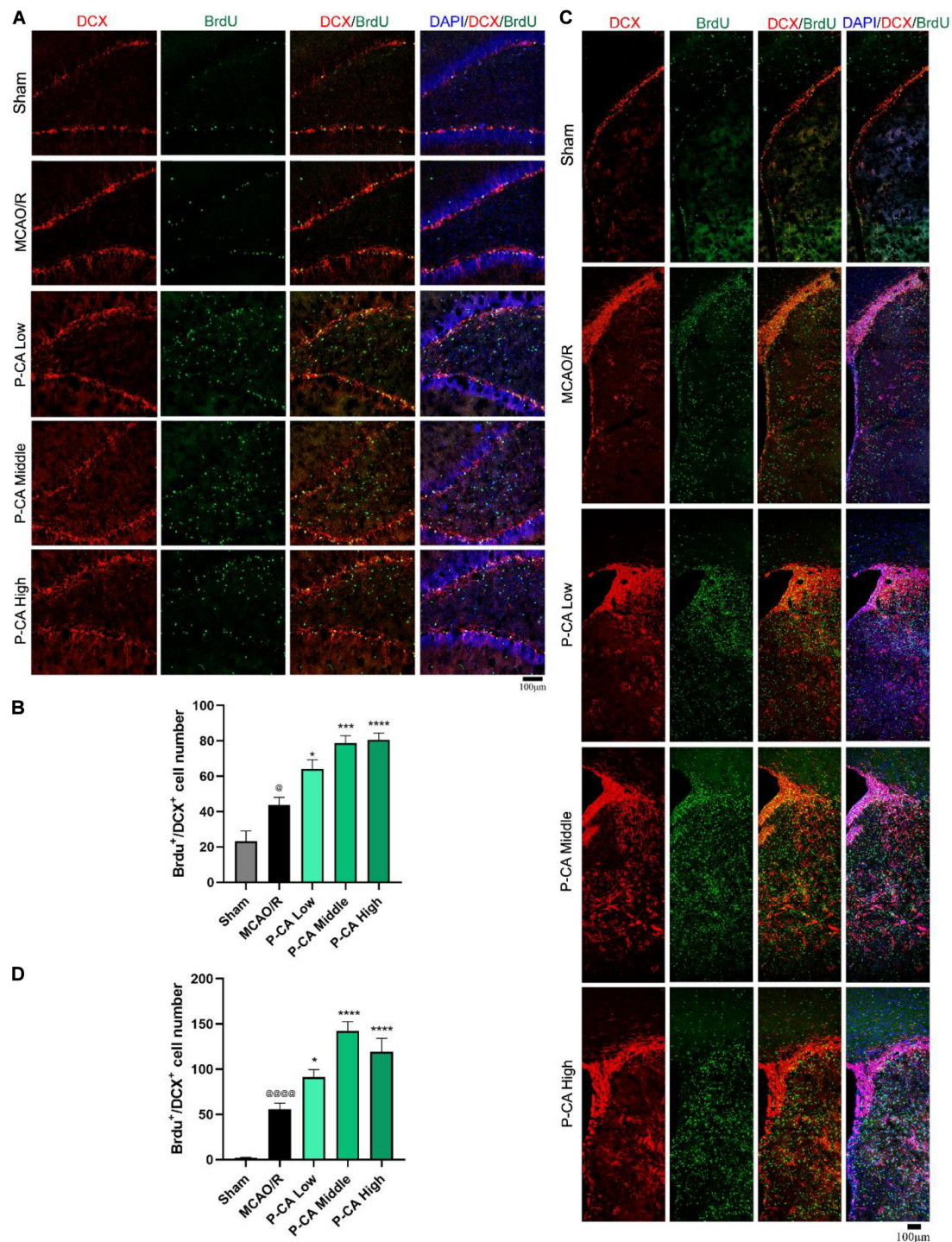


**FIGURE 10 |** P-CA promoted NSC differentiation into immature neurons in hippocampus and striatum of transient MCAO ischemic rats. S.D. rats were divided into sham, MCAO/R and MCAO/R plus P-CA treatment groups (P-CA low 50 mg/kg, P-CA middle 100 mg/kg, P-CA high 200 mg/kg). The rats were subjected to 2 h of MCAO cerebral ischemia plus 14 days of reperfusion. P-CA 50, 100, and 200 mg/kg were intragastrically administered into the rats for following 13 consecutive days, whereas vehicle solution was used in sham-operated group and MCAO vehicle group. **(A)** Representative immunofluorescent imaging for BrdU (green) and DCX (red) positive-staining cells colocalized with nucleus (blue) in hippocampal dentate gyrus (DG). Dual-positive staining of DCX/BrdU refers to the newly differentiated immature neurons. **(B)** Statistical analysis of BrdU<sup>+</sup>/DCX<sup>+</sup> cell number in hippocampus in sham, MCAO/R, and P-CA groups. **(C)** Representative immunofluorescent imaging for BrdU (green) and DCX (red) positive-staining cells colocalized with nucleus (blue) in subventricular zone and striatum. **(D)** Statistical analysis of BrdU<sup>+</sup>/DCX<sup>+</sup> cell number in striatum in sham, MCAO/R, and P-CA groups. Data were presented as mean  $\pm$  SEM ( $n = 3-5$  rats per group, 3-4 tissue sections per brain region used for imaging analysis); vs. sham,  $^{\circ}p < 0.05$ ,  $^{\circ\circ\circ\circ}p < 0.0001$ ; vs. MCAO/R,  $^*p < 0.05$ ,  $^{***}p < 0.001$ ,  $^{****}p < 0.0001$ .



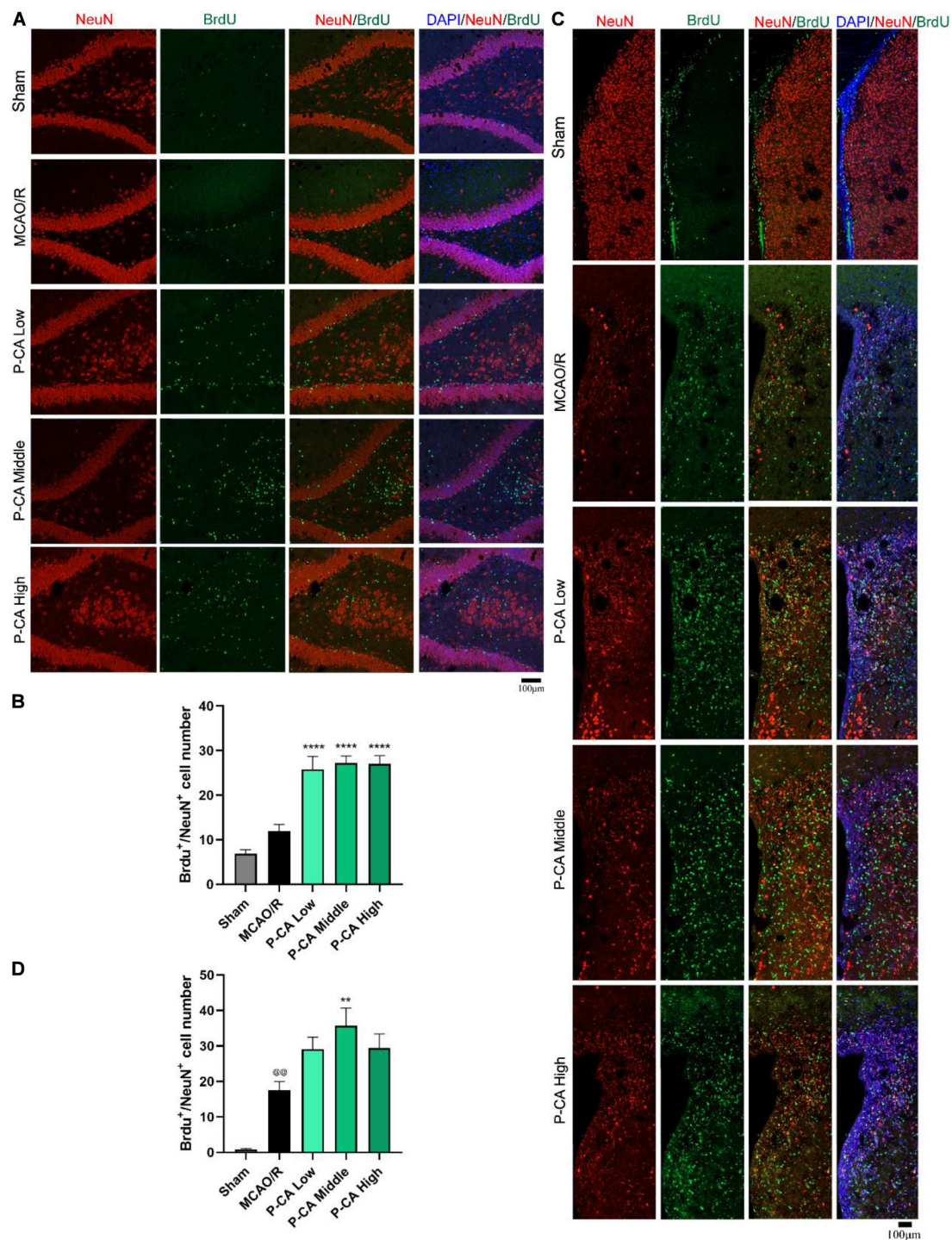


**FIGURE 11 |** P-CA promoted differentiation into mature neurons in hippocampus and striatum of transient MCAO ischemic rats. S.D. rats were divided into sham, MCAO/R and MCAO/R plus P-CA treatment groups (P-CA low 50 mg/kg, P-CA middle 100 mg/kg, P-CA high 200 mg/kg). The rats were subjected to 2 h of MCAO cerebral ischemia plus 14 days of reperfusion. P-CA 50, 100, and 200 mg/kg were intragastrically administered into the rats for following 13 consecutive days, whereas vehicle solution was used in sham-operated group and MCAO vehicle group. **(A)** Representative immunofluorescent imaging for BrdU (green) and NeuN (red) positive-staining cells colocalized with nucleus (blue) in hippocampal dentate gyrus (DG). Dual-positive staining of DCX/BrdU refers to the newly formed mature neurons. **(B)** Statistical analysis of BrdU<sup>+</sup>/NeuN<sup>+</sup> cell number in hippocampus in sham, MCAO/R, and P-CA groups. **(C)** Representative immunofluorescent imaging for BrdU (green) and NeuN (red) positive-staining cells colocalized with nucleus (blue) in subventricular zone and striatum. **(D)** Statistical analysis of BrdU<sup>+</sup>/NeuN<sup>+</sup> cell number in striatum in sham, MCAO/R, and P-CA groups. Data were presented as mean  $\pm$  SEM ( $n = 3-5$  rats per group, three tissue sections per brain region used for imaging analysis). vs. sham control,  $^{@@}p < 0.01$ ; vs. MCAO/R,  $^{**}p < 0.01$ ,  $^{****}p < 0.0001$ .

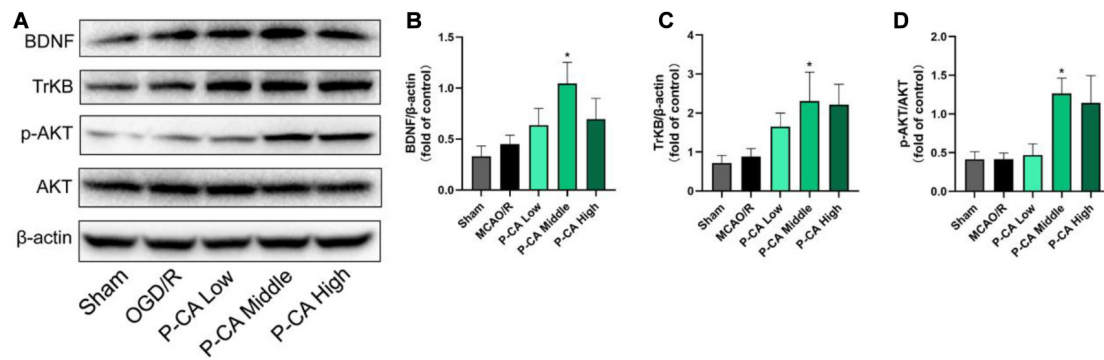


**FIGURE 12 |** P-CA up-regulated expression of TrkB and phosphorylated AKT in the hippocampus of transient MCAO cerebral ischemic rats. S.D. rats were divided into sham control group (Sham), MCAO cerebral ischemia–reperfusion vehicle group (MCAO/R), and MCAO/R plus P-CA treatment groups (P-CA low 50 mg/kg, P-CA middle 100 mg/kg, P-CA high 200 mg/kg). The rats were subjected to 2 h of MCAO cerebral ischemia plus 14 days of reperfusion. P-CA 50, 100, and 200 mg/kg were intragastrically administered into the rats for following 13 consecutive days, whereas vehicle solution was used in sham-operated group and MCAO vehicle group. **(A)** Representative immunoblot results for expression of BDNF, TrkB, and phosphorylated AKT. **(B)** Statistical analysis of relative expression level of BDNF in sham, MCAO/R, and P-CA groups (50, 100, 200 mg/kg). **(C)** Statistical analysis of relative expression level of TrkB in sham, MCAO/R, and P-CA groups (50, 100, 200 mg/kg). **(D)** Statistical analysis of relative expression level of phosphorylated AKT in sham, MCAO/R, and P-CA groups (50, 100, 200 mg/kg). Data were presented as mean  $\pm$  SEM ( $n = 6$ ); vs. MCAO/R, \* $p < 0.05$ .

proliferation-promoting effects of the compounds identified from AOM extract. We counted the BrdU/Ki67 dual-positive populations in the C17.2 cells and found P-CA was the best compound to promote the proliferation of NSCs after the cells were exposed to 4-h OGD plus 20-h reoxygenation. SOX2 is a transcription factor expressed in the NSCs of the developing nervous system. SOX2 characterizes and marks undifferentiated precursor cells including stem cells for the early developmental stages of nerve system (Pevny and Nicolis, 2010). Fluorescent imaging studies revealed that P-CA treatment increased the dual-positive staining of BrdU/Ki67 and BrdU/SOX2 in the C17.2 cells after exposure to OGD. Therefore, P-CA could be a representative compound from AOM to promote the NSC proliferation. Furthermore, P-CA treatment dose-dependently up-regulated the expression of BDNF, TrkB, and p-AKT in the OGD-treated C17.2 cells, whose effects were blocked by ANA12, a BDNF/TrkB specific inhibitor. P-CA also increased the survival rates of the C17.2 cells. We then performed behavioral studies to evaluate the effects of P-CA on neurological deficit scores and spatial learning and memory functions in MCAO ischemic rats. P-CA treatment improved the spatial learning and long-term memory functions in the Morris water maze test, reduced anxiety in the open-field test, and increased short memory in novel objective recognition test. We then sought to determine the underlying mechanisms of P-CA in inducing hippocampal neurogenesis for improving cognitive functions. P-CA treatment significantly increased the dual-positive staining populations to BrdU/DCX and BrdU/NeuN in the DG, SVZ, and striatum of the postischemic brains, indicating the spontaneous neuronal differentiation. P-CA treatment also significantly increased the rates of dual-positive-staining cells to BrdU/Ki67, BrdU/DCX, and BrdU/NeuN in the hippocampal DG, SVZ, and striatum regions. Those data suggest that P-CA has the promoting effects on cell proliferation and neuronal differentiation. The promotion of the neurogenesis contributes to enhance spatial learning,

increase short-term and long-term memory, and reduce anxiety in post-ischemic stroke rats.

P-coumaric acid, also named 4-hydroxycinnamic acid, is a phenolic acid. P-CA and its conjugates exhibit various bioactivities including antioxidant (Nasr et al., 2015), anti-inflammation (Pragasam et al., 2013), and anticancer (Shailasree et al., 2015). Previous studies reported that P-CA attenuated oxidative stress and reduced infarction size and neuronal vulnerability in cerebral ischemia–reperfusion injury (Güven et al., 2015; Sakamula and Thong-Asa, 2018). In the present study, the treatment of P-CA up-regulated the expression of BDNF, TrkB receptor, and p-AKT; promoted hippocampal neurogenesis; enhanced spatial learning; increased short and long-term memory; and attenuated anxiety in ischemic stroke rats. Furthermore, cotreatment of TrkB receptor inhibitor ANA12 blocked the effects of P-CA on proliferation and BDNF/TrkB/AKT signaling pathway in the NSCs. Thus, we conclude that P-CA could be a representative active compound contributing the neurogenesis-promoting effects of AOM through activating BDNF/TrkB/AKT signaling pathway. The enhanced hippocampal neurogenesis subsequently improves cognitive functions and reduces anxiety in the transient MCAO ischemic rats.

Nevertheless, with multiple ingredients in AOM, we should be cautious in interpreting the experimental results. In addition to P-CA, the synergic effects of the different ingredients might also contribute to the neurogenic effects of AOM, which remains to be further explored. Besides, we also performed molecular docking study to evaluate the capacity of P-CA to bind with BDNF. P-CA revealed to directly bind with BDNF (Supplementary Figure 7), suggesting the potential direct interaction between P-CA and BDNF for activating BDNF. However, how the binding regulation of P-CA up-regulates the expression of BDNF and affects the functions of BDNF remains to be further elucidated. Notably, TrkB antagonist, ANA12, abolished the effects of P-CA



on the proliferation of NSCs, indicating that the neurogenic effects of P-CA should be BDNF-TrkB dependent. With complex biochemical and biophysical processes of the molecular dynamics and the intermolecular binding affinity, it is valuable to further explore the underlying mechanisms of P-CA to affect the BDNF protein and the neurogenesis in the postischemic brains.

## CONCLUSION

In conclusion, AOM could be an effective medicinal plant to promote adult hippocampal neurogenesis and improve cognitive impairment in post-ischemic stroke treatment. The underlying mechanisms could be related to inducing BDNF/TrkB/AKT signaling pathway. *p*-Coumaric acid, a representative active compound from AOM, could activate the BDNF/TrkB/AKT signaling pathway and mediate adult hippocampal neurogenesis, subsequently improving cognitive functions, and reducing anxiety.

## DATA AVAILABILITY STATEMENT

The raw data supporting the conclusions of this article will be made available by the authors.

## ETHICS STATEMENT

The animal study was reviewed and approved by the University Committee on the Use of Live Animals in Teaching and Research, University of Hong Kong (CULAR No. 4664-18).

## AUTHOR CONTRIBUTIONS

JS and YH designed the experiments, analyzed the data, and prepared the manuscript. YH and CP identified the compounds

from AOM. YH, SC, and BT performed the cell and animal experiments and Western blot analysis. YH and SQ designed and performed the animal behavior study. ZW and BG performed the molecular docking simulation. JS, SQ, and BG interpreted the experimental data and discussed the experimental designs. CP provided fund for quality identification of AOM extract. JS received fund and organized all experimental activities and manuscript preparation. All authors contributed to the article and approved the submitted version.

## FUNDING

This work was supported by the grant of Areas of Excellence Scheme 2016/17, Research Grants Council, Hong Kong SAR (JS, AoE/P-705/16), General Research Fund (GRF), Research Grants Council, Hong Kong SAR (JS, no.17118717), Seed Fund for Basic Research, University of Hong Kong (JS, no. 201811159037), and State Key Project for Joint Region Innovation Development Scheme, National Natural Science Foundation of China (CP, U19A2010).

## ACKNOWLEDGMENTS

We thank Faculty Core Facility, Li Ka Shing Faculty of Medicine, the University of Hong Kong to supply Carl Zeiss LSM 800 for capturing confocal fluorescent images and GE6500 for high content screening study.

## SUPPLEMENTARY MATERIAL

The Supplementary Material for this article can be found online at: <https://www.frontiersin.org/articles/10.3389/fcell.2020.577790/full#supplementary-material>

## REFERENCES

- Bergami, M., Rimondini, R., Santi, S., Blum, R., Götz, M., and Canossa, M. (2008). Deletion of TrkB in adult progenitors alters newborn neuron integration into hippocampal circuits and increases anxiety-like behavior. *Proc. Natl. Acad. Sci. U.S.A.* 105, 15570–15575. doi: 10.1073/pnas.0803702105
- Bond, A. M., Bhalala, O. G., and Kessler, J. A. (2012). The dynamic role of bone morphogenetic proteins in neural stem cell fate and maturation. *Dev. Neurobiol.* 72, 1068–1084. doi: 10.1002/dneu.22022
- Chang, D.-J., Lee, N., Choi, C., Jeon, I., Oh, S.-H., Shin, D. A., et al. (2013). Therapeutic effect of BDNF-overexpressing human neural stem cells (HB1. F3. BDNF) in a rodent model of middle cerebral artery occlusion. *Cell Transpl.* 22, 1441–1452. doi: 10.3727/096368912x657323
- Chen, J., Sanberg, P. R., Li, Y., Wang, L., Lu, M., Willing, A. E., et al. (2001). Intravenous administration of human umbilical cord blood reduces behavioral deficits after stroke in rats. *Stroke* 32, 2682–2688. doi: 10.1161/hs1101.098367
- Chen, X., Chen, H., He, Y., Fu, S., Liu, H., Wang, Q., et al. (2020). Proteomics-guided study on buyang huanwu decoction for its neuroprotective and neurogenic mechanisms for transient ischemic stroke: involvements of EGFR/PI3K/Akt/Bad/14-3-3 and Jak2/Stat3/Cyclin D1 signaling cascades. *Mol. Neurobiol.* 57, 4305–4321. doi: 10.1007/s12035-020-02016-y
- Choi, S. H., Bylykhashi, E., Chatila, Z. K., Lee, S. W., Pulli, B., Clemenson, G. D., et al. (2018). Combined adult neurogenesis and BDNF mimic exercise effects on cognition in an Alzheimer's mouse model. *Science* 361:eaan8821. doi: 10.1126/science.aan8821
- Deng, W., Aimone, J. B., and Gage, F. H. (2010). New neurons and new memories: how does adult hippocampal neurogenesis affect learning and memory? *Nat. Rev. Neurosci.* 11, 339–350. doi: 10.1038/nrn2822
- Donnan, G., Fisher, M., Macleod, M., and Davis, S. (2008). Stroke. *Lancet* 371, 1612–1623. doi: 10.1016/S0140-6736(08)60694-7
- Egan, M. F., Kojima, M., Callicott, J. H., Goldberg, T. E., Kolachana, B. S., Bertolino, A., et al. (2003). The BDNF val66met polymorphism affects activity-dependent secretion of BDNF and human memory and hippocampal function. *Cell* 112, 257–269. doi: 10.1016/s0092-8674(03)00035-7
- Encinas, J. M., and Enikolopov, G. (2008). Identifying and quantitating neural stem and progenitor cells in the adult brain. *Methods Cell Biol.* 85, 243–272. doi: 10.1016/s0091-679x(08)85011-x
- Eriksson, P. S., Perfilieva, E., Björk-Eriksson, T., Alborn, A.-M., Nordborg, C., Peterson, D. A., et al. (1998). Neurogenesis in the adult human hippocampus. *Nat. Med.* 4, 1313–1317.
- Faigle, R., and Song, H. (2013). Signaling mechanisms regulating adult neural stem cells and neurogenesis. *Biochim. Biophys. Acta (BBA) Gen. Sub.* 1830, 2435–2448. doi: 10.1016/j.bbagen.2012.09.002

- Fraietta, I., and Gasparri, F. (2016). The development of high-content screening (HCS) technology and its importance to drug discovery. *Expert Opin. Drug Discov.* 11, 501–514. doi: 10.1517/17460441.2016.1165203
- Gao, C., Du, Q., Li, W., Deng, R., Wang, Q., Xu, A., et al. (2018). Baicalin modulates APPL2/glucocorticoid receptor signaling cascade, promotes neurogenesis, and attenuates emotional and olfactory dysfunctions in chronic corticosterone-induced depression. *Mol. Neurobiol.* 55, 9334–9348. doi: 10.1007/s12035-018-1042-8
- Goldberg, N. R. S., Caesar, J., Park, A., Sedgh, S., Finogenov, G., Masliah, E., et al. (2015). Neural stem cells rescue cognitive and motor dysfunction in a transgenic model of dementia with lewy bodies through a BDNF-dependent mechanism. *Stem Cell Rep.* 5, 791–804. doi: 10.1016/j.stemcr.2015.09.008
- Grade, S., Weng, Y. C., Snappy, M., Kriz, J., Malva, J. O., and Saghatelian, A. (2013). Brain-derived neurotrophic factor promotes vasculature-associated migration of neuronal precursors toward the ischemic striatum. *PLoS One* 8:e55039. doi: 10.1371/journal.pone.0055039
- Gravanis, I., and Tsirka, S. E. (2008). Tissue-type plasminogen activator as a therapeutic target in stroke. *Exp. Opin. Therap. Targets* 12, 159–170. doi: 10.1517/14728222.12.2.159
- Guven, M., Aras, A. B., Akman, T., Sen, H. M., Ozkan, A., Salis, O., et al. (2015). Neuroprotective effect of p-coumaric acid in rat model of embolic cerebral ischemia. *Iran J. Basic Med. Sci.* 18, 356–363.
- Ho, D. M., Artavanis-Tsakonas, S., and Louvi, A. (2020). The Notch pathway in CNS homeostasis and neurodegeneration. *Wiley Interdiscip. Rev. Dev. Biol.* 9:e358.
- Im, S., Yu, J., Park, E., Lee, J., Kim, H., Park, K. I., et al. (2010). Induction of striatal neurogenesis enhances functional recovery in an adult animal model of neonatal hypoxic-ischemic brain injury. *Neuroscience* 169, 259–268. doi: 10.1016/j.neuroscience.2010.04.038
- Jeong, C. H., Kim, S. M., Lim, J. Y., Ryu, C. H., Jun, J., and Jeun, S.-S. (2014). Mesenchymal stem cells expressing brain-derived neurotrophic factor enhance endogenous neurogenesis in an ischemic stroke model. *BioMed Res. Int.* 2014:129145.
- Johnston, S. C., Easton, J. D., Farrant, M., Barsan, W., Conwit, R. A., Elm, J. J., et al. (2018). Clopidogrel and aspirin in acute ischemic stroke and high-risk TIA. *N. Engl. J. Med.* 379, 215–225. doi: 10.1056/nejmoa1800410
- Kee, N., Sivalingam, S., Boonstra, R., and Wojtowicz, J. (2002). The utility of Ki-67 and BrdU as proliferative markers of adult neurogenesis. *J. Neurosci. Methods* 115, 97–105. doi: 10.1016/S0165-0270(02)00007-9
- Kempermann, G., Song, H., and Gage, F. H. (2015). Neurogenesis in the adult hippocampus. *Cold Spring Harb. Perspectives Biol.* 7:a018812.
- Koo, B.-S., Lee, W.-C., Chang, Y.-C., and Kim, C.-H. (2004). Protective effects of alpineae oxyphyllae fructus (Alpinia oxyphylla MIQ) water-extracts on neurons from ischemic damage and neuronal cell toxicity. *Phytother. Res.* 18, 142–148. doi: 10.1002/ptr.1382
- Lee, H. J., Lim, I. J., Lee, M. C., and Kim, S. U. (2010). Human neural stem cells genetically modified to overexpress brain-derived neurotrophic factor promote functional recovery and neuroprotection in a mouse stroke model. *J. Neurosci. Res.* 88, 3282–3294. doi: 10.1002/jnr.22474
- Lehner, B., Sandner, B., Marschallinger, J., Lehner, C., Furtner, T., Couillard-Despres, S., et al. (2011). The dark side of BrdU in neural stem cell biology: detrimental effects on cell cycle, differentiation and survival. *Cell Tissue Res.* 345:313. doi: 10.1007/s00441-011-1213-7
- Li, C., Che, L. H., Shi, L., and Yu, J. L. (2017). Suppression of basic fibroblast growth factor expression by antisense oligonucleotides inhibits neural stem cell proliferation and differentiation in rat models with focal cerebral infarction. *J. Cell. Biochem.* 118, 3875–3882. doi: 10.1002/jcb.26038
- Li, Y., Luikart, B. W., Birnbaum, S., Chen, J., Kwon, C.-H., Kerner, S. G., et al. (2008). TrkB regulates hippocampal neurogenesis and governs sensitivity to antidepressant treatment. *Neuron* 59, 399–412. doi: 10.1016/j.neuron.2008.06.023
- Liu, L., Zhao, B., Xiong, X., and Xia, Z. (2018). The Neuroprotective roles of sonic hedgehog signaling pathway in ischemic stroke. *Neurochem. Res.* 43, 2199–2211. doi: 10.1007/s11064-018-2645-1
- Lois, C., and Alvarez-Buylla, A. (1994). Long-distance neuronal migration in the adult mammalian brain. *Science* 264, 1145–1148. doi: 10.1126/science.8178174
- Lueptow, L. M. (2017). Novel object recognition test for the investigation of learning and memory in mice. *J. Vis. Exp.* 126:55718.
- Markakis, E. A., and Gage, F. H. (1999). Adult-generated neurons in the dentate gyrus send axonal projections to field CA3 and are surrounded by synaptic vesicles. *J. Compar. Neurol.* 406, 449–460. doi: 10.1002/(sici)1096-9861(19990419)406:4<449::aid-cnc3>3.0.co;2-i
- Mijajlović, M. D., Pavlović, A., Brainin, M., Heiss, W.-D., Quinn, T. J., Ihle-Hansen, H. B., et al. (2017). Post-stroke dementia—a comprehensive review. *BMC Med.* 15:11. doi: 10.1186/s12916-017-0779-7
- Mohammadi, A., Amooeian, V. G., and Rashidi, E. (2018). Dysfunction in Brain-derived neurotrophic factor signaling pathway and susceptibility to schizophrenia, Parkinson's and Alzheimer's Diseases. *Curr. Gene. Ther.* 18, 45–63. doi: 10.2174/1566523218666180302163029
- Nakamura, H., Sasaki, Y., Sasaki, M., Kataoka-Sasaki, Y., Oka, S., Nakazaki, M., et al. (2019). Elevated brain derived neurotrophic factor levels in plasma reflect in vivo functional viability of infused mesenchymal stem cells for stroke in rats. *J. Neurosurg. Sci.* 63, 42–49.
- Nasr, B. N., Kilani, J. S., Kovacic, H., Chekir-Ghedira, L., Ghedira, K., and Luis, J. (2015). The effects of caffeic, coumaric and ferulic acids on proliferation, superoxide production, adhesion and migration of human tumor cells in vitro. *Eur. J. Pharmacol.* 766, 99–105. doi: 10.1016/j.ejphar.2015.09.044
- Pevny, L. H., and Nicolis, S. K. (2010). Sox2 roles in neural stem cells. *Int. J. Biochem. Cell Biol.* 42, 421–424. doi: 10.1016/j.biocel.2009.08.018
- Pragasam, S. J., Venkatesan, V., and Rasool, M. (2013). Immunomodulatory and anti-inflammatory effect of p-coumaric acid, a common dietary polyphenol on experimental inflammation in rats. *Inflammation* 36, 169–176. doi: 10.1007/s10753-012-9532-8
- Rosenblum, S., Smith, T. N., Wang, N., Chua, J. Y., Westbroek, E., Wang, K., et al. (2015). BDNF pretreatment of human embryonic-derived neural stem cells improves cell survival and functional recovery after transplantation in hypoxic-ischemic stroke. *Cell Transplant.* 24, 2449–2461. doi: 10.3727/096368914x679354
- Sakamula, R., and Thong-Asa, W. (2018). Neuroprotective effect of p-coumaric acid in mice with cerebral ischemia reperfusion injuries. *Metab. Brain Dis.* 33, 765–773. doi: 10.1007/s11011-018-0185-7
- Shailasree, S., Venkataramana, M., Niranjana, S. R., and Prakash, H. S. (2015). Cytotoxic effect of p-Coumaric acid on neuroblastoma, N2a cell via generation of reactive oxygen species leading to dysfunction of mitochondria inducing apoptosis and autophagy. *Mol. Neurobiol.* 51, 119–130. doi: 10.1007/s12035-014-8700-2
- Shi, S.-H., Zhao, X., Liu, B., Li, H., Liu, A.-J., Wu, B., et al. (2014). The effects of sesquiterpenes-rich extract of *Alpinia oxyphylla* Miq. on amyloid- $\beta$ -induced cognitive impairment and neuronal abnormalities in the cortex and hippocampus of mice. *Oxid Med. Cell Longev.* 2014:451802.
- Shi, S.-h, Zhao, X., Liu, A.-j, Liu, B., Li, H., Wu, B., et al. (2015). Protective effect of n-butanol extract from *Alpinia oxyphylla* on learning and memory impairments. *Physiol. Behav.* 139, 13–20. doi: 10.1016/j.physbeh.2014.11.016
- Su, H., Li, Z., Fiati, K. S. S., Shi, H., Wang, Y., Song, X., et al. (2017). Joint toxicity of different heavy metal mixtures after a short-term oral repeated-administration in rats. *Int. J. Environ. Res. Public Health* 14:1164. doi: 10.3390/ijerph14101164
- Sun, C., Sun, H., Wu, S., Lee, C. C., Akamatsu, Y., Wang, R. K., et al. (2013). Conditional ablation of neuroprogenitor cells in adult mice impedes recovery of poststroke cognitive function and reduces synaptic connectivity in the perforant pathway. *J. Neurosci.* 33, 17314–17325. doi: 10.1523/jneurosci.2129-13.2013
- Tanaka, R., Tainaka, M., Ota, T., Mizuguchi, N., Kato, H., Urale, S., et al. (2011). Accurate determination of S-phase fraction in proliferative cells by dual fluorescence and peroxidase immunohistochemistry with 5-bromo-2'-deoxyuridine (BrdU) and K167 antibodies. *J. Histochem. Cytochem.* 59, 791–798. doi: 10.1369/0022155411411090
- Wagenaar, N., De Theije, C. G., De Vries, L. S., Groenendaal, F., Benders, M. J., and Nijboer, C. H. (2018). Promoting neuroregeneration after perinatal arterial ischemic stroke: neurotrophic factors and mesenchymal stem cells. *Pediatric Res.* 83, 372–384. doi: 10.1038/pr.2017.243
- Wang, X., Mao, X., Xie, L., Sun, F., Greenberg, D. A., and Jin, K. (2012). Conditional depletion of neurogenesis inhibits long-term recovery after experimental stroke in mice. *PLoS One* 7:e38932. doi: 10.1371/journal.pone.0038932
- Wang, Y., Wang, M., Fan, K., Li, T., Yan, T., and Li, B., et al. (2018). Protective effects of *Alpinia Oxyphylla* Fructus extracts on lipopolysaccharide-induced

- animal model of Alzheimer's disease. *J. Ethnopharmacol.* 217, 98–106. doi: 10.1016/j.jep.2018.02.015
- Wei, P., Liu, Q., Li, D., Zheng, Q., Zhou, J., and Li, J. (2015). Acute nicotine treatment attenuates lipopolysaccharide-induced cognitive dysfunction by increasing BDNF expression and inhibiting neuroinflammation in the rat hippocampus. *Neurosci. Lett.* 604, 161–166. doi: 10.1016/j.neulet.2015.08.008
- Wojtowicz, J. M., and Kee, N. (2006). BrdU assay for neurogenesis in rodents. *Nat. Protoc.* 1:1399. doi: 10.1038/nprot.2006.224
- Xu, D., Hou, K., Li, F., Chen, S., Fang, W., and Li, Y. (2020). Effect of Wnt signaling pathway on neurogenesis after cerebral ischemia and its therapeutic potential. *Brain Res. Bull.* 164, 1–13. doi: 10.1016/j.brainresbull.2020.07.005
- Yan, T., Wu, B., Liao, Z.-Z., Liu, B., Zhao, X., Bi, K.-S., et al. (2016). Brain-derived neurotrophic factor signaling mediates the antidepressant-like effect of the total flavonoids of *alpinia oxyphylla* fructus in chronic unpredictable mild stress mice. *Phytother. Res.* 30, 1493–1502. doi: 10.1002/ptr.5651
- Zhang, Q., Zheng, Y., Hu, X., Hu, X., Lv, W., Lv, D., et al. (2018). Ethnopharmacological uses, phytochemistry, biological activities, and therapeutic applications of *Alpinia oxyphylla* Miquel: a review. *J. Ethnopharmacol.* 224, 149–168. doi: 10.1016/j.jep.2018.05.002
- Zhang, X., Zhou, Y., Li, H., Wang, R., Yang, D., Li, B., et al. (2018). Intravenous administration of DPSCs and BDNF improves neurological performance in rats with focal cerebral ischemia. *Int. J. Mol. Med.* 41, 3185–3194.
- Conflict of Interest:** The authors declare that the research was conducted in the absence of any commercial or financial relationships that could be construed as a potential conflict of interest.

Copyright © 2021 He, Chen, Tsoi, Qi, Gu, Wang, Peng and Shen. This is an open-access article distributed under the terms of the Creative Commons Attribution License (CC BY). The use, distribution or reproduction in other forums is permitted, provided the original author(s) and the copyright owner(s) are credited and that the original publication in this journal is cited, in accordance with accepted academic practice. No use, distribution or reproduction is permitted which does not comply with these terms.



# Microalgae *Aurantiochytrium* Sp. Increases Neurogenesis and Improves Spatial Learning and Memory in Senescence-Accelerated Mouse-Prone 8 Mice

Kazunori Sasaki<sup>1,2,3</sup>, Noelia Geribaldi-Doldán<sup>1,4</sup>, Qingqing Wu<sup>1,4</sup>, Julie Davies<sup>4</sup>, Francis G. Szele<sup>4\*</sup> and Hiroko Isoda<sup>1,2,5\*</sup>

<sup>1</sup> Alliance for Research on the Mediterranean and North Africa (ARENA), University of Tsukuba, Tsukuba, Japan, <sup>2</sup> Open Innovation Laboratory for Food and Medicinal Resource Engineering, National Institute of Advanced Industrial Science and Technology (AIST), University of Tsukuba, Tsukuba, Japan, <sup>3</sup> Faculty of Pure and Applied Sciences, University of Tsukuba, Tsukuba, Japan, <sup>4</sup> Department of Physiology, Anatomy and Genetics, University of Oxford, Oxford, United Kingdom, <sup>5</sup> Faculty of Life and Environmental Sciences, University of Tsukuba, Tsukuba, Japan

## OPEN ACCESS

### Edited by:

Daniele Bottai,  
University of Milan, Italy

### Reviewed by:

Christian Griñán-Ferré,  
University of Barcelona, Spain  
Qi Wang,  
Guangzhou University of Chinese  
Medicine, China  
Ling Chen,  
Hangzhou First People's  
Hospital, China

### \*Correspondence:

Hiroko Isoda  
isoda.hiroko.ga@u.tsukuba.ac.jp  
Francis G. Szele  
francis.szele@dpag.ox.ac.uk

### Specialty section:

This article was submitted to  
Stem Cell Research,  
a section of the journal  
Frontiers in Cell and Developmental  
Biology

**Received:** 30 August 2020

**Accepted:** 23 December 2020

**Published:** 09 February 2021

### Citation:

Sasaki K, Geribaldi-Doldán N, Wu Q, Davies J, Szele FG and Isoda H (2021) Microalgae *Aurantiochytrium* Sp. Increases Neurogenesis and Improves Spatial Learning and Memory in Senescence-Accelerated Mouse-Prone 8 Mice. *Front. Cell Dev. Biol.* 8:600575. doi: 10.3389/fcell.2020.600575

Much attention has recently been focused on nutraceuticals, with minimal adverse effects, developed for preventing or treating neurological diseases such as Alzheimer's disease (AD). The present study was conducted to investigate the potential effect on neural development and function of the microalgae *Aurantiochytrium* sp. as a nutraceutical. To test neuroprotection by the ethanol extract of *Aurantiochytrium* (EEA) and a derivative, the n-Hexane layer of EEA (HEEA), amyloid- $\beta$ -stimulated SH-SY5Y cells, was used as an *in vitro* AD model. We then assessed the potential enhancement of neurogenesis by EEA and HEEA using murine *ex vivo* neurospheres. We also administered EEA or HEEA to senescence-accelerated mouse-prone 8 (SAMP8) mice, a non-transgenic strain with accelerated aging and AD-like memory loss for evaluation of spatial learning and memory using the Morris water maze test. Finally, we performed immunohistochemical analysis for assessment of neurogenesis in mice administered EEA. Pretreatment of SH-SY5Y cells with EEA or the squalene-rich fraction of EEA, HEEA, ameliorated amyloid- $\beta$ -induced cytotoxicity. Interestingly, only EEA-treated cells showed a significant increase in cell metabolism and intracellular adenosine triphosphate production. Moreover, EEA treatment significantly increased the number of neurospheres, whereas HEEA treatment significantly increased the number of  $\beta$ -III-tubulin+ young neurons and GFAP+ astrocytes. SAMP8 mice were given 50 mg/kg EEA or HEEA orally for 30 days. EEA and HEEA decreased escape latency in the Morris water maze in SAMP8 mice, indicating improved memory. To detect stem cells and newborn neurons, we administered BrdU for 9 days and measured BrdU+ cells in the dentate gyrus, a neurogenic stem cell niche of the hippocampus. In SAMP8 mice, EEA rapidly and significantly increased the number of BrdU+GFAP+ stem cells and their progeny, BrdU+NeuN+ mature neurons. In conclusion, our data in aggregate indicate that EEA and its constituents could be developed into a nutraceutical for promoting brain health and function against several age-related diseases, particularly AD.

**Keywords:** *Aurantiochytrium* sp., neuroprotection, adult neurogenesis, neuronal stem cells, SAMP8 mice



## INTRODUCTION

Alzheimer's disease (AD), a growing worldwide health problem, is the most common form of dementia representing ~70% of all dementia cases. Up to now, effective therapy for AD has not been established, and no promising therapies are forthcoming. However, the number of patients with neurodegenerative diseases such as AD has been increasing; therefore, many studies on the treatment and improvement of AD with various approaches have been carried out. Lifestyle components such as exercise, intellectual stimulation activities, and sleep optimization have been reported to reduce the risk of AD and slow its progression (Fratiglioni et al., 2004; Forbes et al., 2013; Xie et al., 2013). In addition, several epidemiological studies have investigated the association between nutritional supplements, such as vitamin C, vitamin E, and omega-3 fatty acids, and the risk of AD and cognitive decline (Mangialasche et al., 2013; Shinto et al., 2014). Also, exposure to environmental enrichment has a protective effect by slowing the progression of AD and reducing AD-like cognitive impairment (Barak et al., 2013). Importantly, there has been growing interest in the potential for natural products such as nutraceuticals to treat or prevent AD.

It is estimated that about 72,500 algal species exist worldwide (Guiry, 2012). Algae produce a variety of bioactive secondary metabolites that include polyphenolic compounds, polysaccharides, steroids, fatty acids, carotenoids, mycosporine-like amino acids, halogenated compounds, polyketides, lectins, peptides, and their derivatives (Sathasivam et al., 2019). There is growing interest in exploring metabolites from algae, and attention has focused on exploring novel bioactive compounds with the potential for future therapeutic use (Blunt et al., 2017). A large number of biological functions have been found for algal natural products. They can have antioxidant, anti-inflammatory, anticancer, immunomodulatory, antidiabetic, antimicrobial, antiviral, and anticoagulant functions, tyrosinase inhibition, and ultraviolet-protective effects (Blunt et al., 2017).

*Aurantiochytrium* is an oleaginous microorganism in the Thraustochytriaceae family that has attracted attention because of its ability to produce high levels of polyunsaturated fatty acids and squalene. A research group at the University of Tsukuba found a high squalene-producing (198 mg/g) strain, 18W-13a, of *Aurantiochytrium* sp. from among 150 strains of thraustochytrids isolated in the Okinawa prefecture of Japan (Kaya et al., 2011). Squalene is a biosynthesized triterpene hydrocarbon and a precursor for all steroids in animals and plants. Squalene is used in the pharmaceutical and medical industries because it increases cellular and non-specific immune functions, decreases serum cholesterol levels, suppresses tumor proliferation, modulates fatty acid metabolism, and shows an adjuvant effect (Kelly, 1999; Aguilera et al., 2005; Kaya et al., 2011; Kumar et al., 2016; Bhilwade et al., 2019). Thus, *Aurantiochytrium* sp. may be useful in the search for new medicines and is considered to have great potential as a renewable source of chemical products, with squalene being of major interest. There have been few reports exploring the physiological effects of *Aurantiochytrium* sp. However, recent studies demonstrated that an ethanol

extract obtained from *Aurantiochytrium* sp. (EEA) had anti-inflammatory effects on RAW264.7 cells (Takahashi et al., 2018). Moreover, EEA also showed an antidepressant-like effect *via* anti-inflammation (Sasaki et al., 2019a). However, the effects of *Aurantiochytrium* sp. on central nervous system (CNS) activity such as learning and memory or adult neurogenesis are unknown.

Senescence-accelerated mouse-prone 8 (SAMP8) mice are a good animal model for age-associated diseases, such as AD (Morley et al., 2012a,b). They exhibit deterioration in memory and learning accompanied by CNS inflammation, vascular impairment, gliosis, increased oxidative stress, amyloid- $\beta$  (A $\beta$ ) accumulation, and tau hyperphosphorylation (Morley et al., 2012a; Cheng et al., 2014). Moreover, Griñán-Ferré et al. (2016) used environmental enrichment in SAMP8 mice and found altered chromatin-modifying gene expression in the hippocampus, increased expression of antioxidant genes, and reduced expression of pro-inflammatory genes. Another interesting study showed that environmental enrichment increased cognition, reduced Tau hyperphosphorylation, and increased synaptic protein expression in the 5XFAD mouse model of AD (Griñán-Ferré et al., 2018). Thus, not only diet but other lifestyle changes could also influence AD symptoms in humans. We previously showed that SAMP8 mice given the polyphenol 3,4,5-tricaffeoylquinic acid exhibited increased neurogenesis (Sasaki et al., 2019b). In physiologic conditions, neurogenesis occurs in the adult brain in two principal regions, the subgranular zone (SGZ) of the hippocampus (Altman and Das, 1965; Kempermann, 2002) and the wall of the lateral ventricles, the subventricular zone (SVZ) (Alvarez-Buylla and Garcia-Verdugo, 2002).

Thus, in the present study, we studied the effects of EEA on cell viability, adenosine triphosphate (ATP) production, and neural differentiation in SH-SY5Y human neuroblastoma cells. We performed complementary *in vitro* murine neurosphere assays to determine the effects of EEA on proliferation and differentiation of neural stem cells and neural precursor cells (NPCs). The SGZ has been implicated in learning and memory, and therefore, we examined learning and memory with the Morris water maze in SAMP8 mice administered EEA. Finally, we studied the effects of EEA on SGZ and SVZ stem cell activation and neurogenesis *in vivo*.

## MATERIALS AND METHODS

### Preparation of Ethanol Extract of *Aurantiochytrium* sp.

Dried powders of *Aurantiochytrium* sp. cells were provided by Professor Makoto Watanabe (Algae Biomass and Energy System R&D Center, University of Tsukuba, Japan). The algae dried powders were stored at  $-80^{\circ}\text{C}$  until extraction for maintenance of the quality. The algae dried powders were extracted using 99.5% ethanol, in the dark, and at room temperature for 2 weeks, with shaking of the mixture occurring at least once a day. At the end of the procedure, the liquid fraction was collected

and filtered through a 0.22- $\mu$ m filter. For both *in vitro* and *in vivo* experiments, the EEA liquid fraction was concentrated using a SpeedVac (Thermo Fisher Scientific, Japan). For *in vitro* experiments, the concentrated EEA was dissolved in serum-free Eagle's minimum essential medium (OPTI-MEM; Gibco, Japan) with sonication, and for *in vivo* experiments, the concentrated 150-mg EEA was dissolved in 10-ml milliQ water with sonication. For both *in vitro* and *in vivo* experiments, EEA was aliquoted and stored at  $-80^{\circ}\text{C}$  for maintenance of quality.

### Preparation of n-Hexane Layer of Ethanol Extract of *Aurantiochytrium* Using Liquid-Liquid Distribution

To obtain the extract, *Aurantiochytrium* sp. 18W-13a strain was extracted as mentioned earlier with 99.5% EtOH for 2 weeks, and the EtOH extract was filtered and evaporated *in vacuo*. The concentrated EEA (200 mg) was dissolved in 100-ml n-Hexane, and 100-ml 90% MeOH was added to the extract. The extract was partitioned between the 90% MeOH layer and the n-Hexane layer due to the difference in their solubility. Partitioning the 90% MeOH layer and n-Hexane layer was repeated twice with 100-ml n-Hexane. Next, the n-Hexane layer containing EEA (HEEA) was concentrated using *vacuo*; 100 mg of this concentrate was dissolved in 1 ml of 99.5% EtOH and used for *in vitro* experiments. After dissolving in 99.5% EtOH, HEEA was aliquoted and stored at  $-80^{\circ}\text{C}$ . For animal dosing for the *in vivo* assay, the HEEA was concentrated, and the dried 150-mg HEEA was dissolved in 10-ml milliQ water with sonication. The HEEA solution, for *in vivo* experiments, was also aliquoted and stored at  $-80^{\circ}\text{C}$  until use for maintenance of quality.

### Preparation of Squalene

Squalene was purchased from Wako Co, Ltd. (Tokyo, Japan). For *in vitro* assays, squalene was dissolved in medium and sonicated before use in the experiment because it was difficult to dissolve in the medium.

### SH-SY5Y Cell Culture

The human neuroblastoma SH-SY5Y cell line was purchased from the American Type Culture Collection. SH-SY5Y cells were cultured in a 1:1 (v/v) mixture of Dulbecco's modified Eagle medium and Ham's F-12 medium (Gibco, Japan) supplemented with 15% heat-inactivated fetal bovine serum (Bio West, U.S.A) and 1% penicillin (5,000  $\mu\text{g/ml}$ )-streptomycin (5,000 IU/ml) (Lonza, Japan) at  $37^{\circ}\text{C}$  in a humidified atmosphere of 5%  $\text{CO}_2$  in the air. SH-SY5Y cells were cultured in 100-mm Petri dishes or 96-well plates. OPTI-MEM was used to culture the cells for the cell viability assay.

### 3-(4,5-Dimethylthiazol-2-yl)-2,5-Diphenyltetrazolium Bromide Assay

Cell viability and mitochondrial activity were determined using a 3-(4,5-dimethylthiazol-2-yl)-2,5-diphenyltetrazolium bromide (MTT) assay to check for effects of EEA (20  $\mu\text{g/ml}$ ), HEEA (20  $\mu\text{g/ml}$ ), squalene (50  $\mu\text{M}$ ), and  $\text{A}\beta$  (15  $\mu\text{M}$ ) on cytotoxicity.

SH-SY5Y cells were seeded at  $2 \times 10^5$  cells/ml in 96-well plates and incubated for 24 h. After 24-h incubation, SH-SY5Y cells were treated with EEA, HEEA, squalene, or  $\text{A}\beta$  for 72 h. To evaluate the neuroprotective effects of EEA, HEEA, and squalene against  $\text{A}\beta$ -induced cytotoxicity, SH-SY5Y cells were pretreated with 20  $\mu\text{g/ml}$  EEA, 20  $\mu\text{g/ml}$  HEEA, and 50- $\mu\text{M}$  squalene for 10 min before 15- $\mu\text{M}$   $\text{A}\beta$  treatment. After sample treatment, a solution of 5 mg/ml MTT dissolved in phosphate-buffer saline (PBS) was added (10  $\mu\text{l/well}$ ) and incubated for another 24 h. The resulting MTT formazan was dissolved in 100  $\mu\text{l}$  of 10% sodium dodecyl sulfate (w/v), and the absorbance was measured using a microtiter plate reader (Dainippon Sumitomo Pharma Co., Ltd., Japan).

### Adenosine Triphosphate Assay

The effect of EEA on ATP production of SH-SY5Y cells was determined using a luciferase luminescence assay kit (ATP reagents for cell: TOYO Ink, Tokyo, Japan). SH-SY5Y cells were seeded at  $2 \times 10^5$  cells/ml and incubated for 24 h. After incubation, SH-SY5Y cells were treated with 20  $\mu\text{g/ml}$  EEA. After 6-, 12-, and 24-h incubation, the ATP assay reagent was added (100  $\mu\text{l/well}$ ) and incubated for 10 min at room temperature while avoiding light exposure. After the incubation, the solution was transferred into a white clear-bottom 96-well-plate (BD Falcon), and the luminescence was detected using a microplate reader (Dainippon Sumitomo Pharma Co., Ltd., Japan).

### Primary Neurosphere Culture

NPCs were obtained from the SVZ of 7-day-old postnatal mice following the procedure described by Torroglosa et al. (2007). Six CD1 mice were used for each independent culture. Neurosphere cultures were maintained in a defined medium composed of Dulbecco's modified Eagle's medium/F12 medium 1:1 (v/v) with 1 mg/L gentamicin (GIBCO) and B27 supplement (Invitrogen, Carlsbad, CA). Epidermal growth factor (EGF) (20 ng/ml, GIBCO) and basic fibroblast growth factor (bFGF) (10 ng/ml, Peprotech, Frankfurt, Germany) were added to cultures to stimulate cell proliferation and culture expansion. All animal procedures were approved by the Animal Study Committee of Tsukuba University and according to the guidelines for the Care and Use of Animals approved by the Council of the Physiological Society of Japan.

To test the effect of EEA (20  $\mu\text{g/ml}$ ) and HEEA (20  $\mu\text{g/ml}$ ) on primary neurospheres, single cells from mechanically disaggregated neurospheres were seeded in anti-adherent 96 well-plates (Corning, NY, USA) at a density of 20,000 cells/ml. EEA (20  $\mu\text{g/ml}$ ) or HEEA (20  $\mu\text{g/ml}$ ), EGF (20 ng/ml), and bFGF (10 ng/ml) were added at the time of seeding. Seventy-two hours after seeding, the number of newly formed neurospheres was counted with phase microscopy. To measure neurosphere size, images of at least 50 neurospheres per well were taken. The size was measured using ImageJ software. Each treatment was performed in triplicate and repeated at least three independent times.

## Immunocytochemistry

Cells in medium without growth factors were added onto poly-L-ornithine coated 8-well-glass slide chambers (Lab-Tek) with EEA. After 72 h, cells were fixed with 4% (w/v) paraformaldehyde. After three washes, cells were incubated with a blocking solution composed of PBS containing 2.5% (w/v) bovine serum albumin for 1 h to avoid non-specific antibody binding. Primary antibody incubations were carried out overnight at 4°C in blocking solution. Then, cells were washed with PBS and incubated with the appropriate secondary antibody for 1 h.

The primary antibodies used were mouse anti- $\beta$ -III-tubulin (Promega, 1:1,000) and rabbit anti-GFAP (DAKO, 1:3,000). The secondary antibodies used were donkey anti-rabbit Alexa Fluor 488 and donkey anti-mouse 594 (Invitrogen, 1:1,000). Nuclei were counterstained with 4',6-diamidino-2-phenylindole using drops of ProLong Gold Antifade Mountant (Thermo SCIENTIFIC, Japan). Fluorescence was detected with a Leica DMI 4000B epifluorescent microscope (Leica, Germany). Quantification was performed in 12 predetermined visual fields/well and 3 wells/condition. Experiments were repeated a minimum of three times, and results were expressed as the mean  $\pm$  SEM.

## Animals

Adult male SAMP8 (4 months old) and senescence-accelerated resistant mouse 1 (SAMR1) (4 months old) (SLC Japan) were used for *in vivo* experiments. After acclimatization to laboratory conditions (7 days), SAMP8 mice were divided into three groups: SAMP8 control group, orally administered only with water ( $n = 10$ ), EEA-treated group ( $n = 10$ ), and HEEA-treated group ( $n = 7$ ). SAMR1 mice ( $n = 10$ ) were used as normal aging controls. Animals were housed under controlled conditions of temperature (21–23°C) and light:dark cycle (12:12 h) with free access to food and water. All animal procedures were approved by the Animal Study Committee of Tsukuba University (No. 16-041) and according to the guidelines for the Care and Use of Animals approved by the Council of the Physiological Society of Japan.

In our previous study, we orally administered 100 mg/kg of EEA for 14 consecutive days to depression model mice to evaluate its antidepressant-like activities (Sasaki et al., 2019a). Considering this previous study, 50 mg/kg was determined as the concentration for oral administration of EEA and HEEA. Oral administration (gavage) of EEA (50 mg/kg) and HEEA (50 mg/kg), dissolved in water, was performed 1  $\times$  per day for 30 days. An equal volume of water was administered to the water-administration group. In addition, BrdU (1 mg/ml), which is incorporated into proliferative cells at the S-phase of the cell cycle, was provided in the drinking water and provided to the SAMR1 control mice, the SAMP8 control group, and the EEA-treated group during nine consecutive days starting with the 14th day of oral administration.

## Morris Water Maze

Spatial learning and memory were analyzed using the Morris water maze (MWM) as previously described (Sasaki et al., 2019b). A circular pool (120 cm in diameter and 45 cm in height) was

filled to a depth of 30 cm with water ( $23 \pm 2^\circ\text{C}$ ) and was divided into four quadrants designated as north, east, west, and south. A platform (10 cm in diameter) was placed in the northeast quadrant and was submerged 1 cm below the water surface so that it was invisible to mice at water level. Each mouse had daily sessions of four trials for seven consecutive days using a single hidden platform in one quadrant, with the start point rotating around the other three quadrants. When the mice succeeded, they were allowed to stay for 15 s on the platform. When mice failed for more than 60 s, the experimenter assisted them in finding the platform. A probe trial was performed 24 h after the last training session of MWM. The platform was removed from the pool in this trial, and mice were allowed to swim freely for 60 s. The number of crossings over the previous position of the platform and the time spent in the target quadrant in which the platform was hidden during the acquisition trials were recorded as measures for spatial memory.

## Tissue Processing and Immunohistochemistry

Mice were killed by cervical dislocation after the MWM test; brains were removed and fixed with 4% paraformaldehyde for 24 h at 4°C. After, brains were cryoprotected in 30% sucrose (w/v) in PBS for 48 h at 4°C. Serial 30- $\mu\text{m}$  coronal brain sections were obtained using a microtome on dry ice. Sections were stored at  $-20^\circ\text{C}$  in cryoprotectant solution (ethylene glycol, glycerol, 0.1-M phosphate buffer, pH 7.4, 1:1:1:2 by volume). Pretreatment of tissue was required for BrdU detection. BrdU antigen retrieval was achieved with 1-M HCl at 38.5°C for 1 h. Sections were blocked with a solution composed of PBS, 0.1% Triton X-100, and 1% bovine serum albumin (Sigma) for 1 h, after washing abundantly with PBS. Primary antibodies were incubated overnight at 4°C. Sections were washed and incubated with fluorochrome-conjugated specific secondary antibodies overnight at 4°C. Primary antibodies used were sheep polyclonal anti-BrdU (1:500, Abcam), rat monoclonal anti-GFAP (1:400, Life Technologies), mouse monoclonal anti-NeuN (1:400, Millipore), and goat polyclonal anti-DCX (1:100, Santa Cruz). The secondary antibodies were conjugated to Alexa-488, -568, or -647 (Invitrogen Paisley, Renfrewshire, UK; 1:500). Sections were mounted with Prolong Antifade Kit (Molecular Probes, Eugene, USA). A Leica DMIRB microscope with a Hamamatsu C4742-95 digital camera or a Leica DMR microscope with a Leica DFC-500 digital camera was used to obtain epifluorescence images. Confocal images were obtained with a Zeiss LSM 710 laser scanning confocal microscope using the Z-stack and tile functions as appropriate.

Double labeling was carefully examined using a 40 $\times$  objective and the digital zoom options of FIJI (ImageJ) software. Stereological methods were used for cell counting and to estimate the number of positive cells for each specific marker using the procedures in Geribaldi-Doldán et al. (2018). Five to six animals were used per condition to analyze SVZ and SGZ neurogenesis. Cells were counted in every fifth 30- $\mu\text{m}$  thick-serial coronal section. In each section, cells were counted in the lateral wall of lateral ventricles in the case of the SVZ and the SGZ in the case of



the dentate gyrus (DG). Sections were analyzed under confocal microscopy at 40× magnification. Confocal images of each section were obtained using a Zeiss LSM 710 microscope using the Z-stack function using 5–7 2-micron increments. Double labeling of individual cells was confirmed with orthogonal views of the cells. The total number of cells was determined within the volume analyzed. Mice were coded depending on the treatment, and quantification was done in a blinded analysis.

## Statistics

All analysis was performed by experimenters blind to the condition on coded slides as previously described (Kandasamy et al., 2015). Data from quantifications were collated into Microsoft Excel, and statistical analyses were performed using GraphPad Prism 6 and SPSS Statistics 22. First, to test for normality, we performed the Shapiro–Wilk test. Homogeneity of variance was confirmed with Levene's test. Accordingly, a normal distribution parametric test was used to compare means. When more than two treatment groups were compared, statistical analyses were performed using one-way ANOVA followed by Bonferroni's *post hoc* test or the Ryan–Einot–Gabriel–Welsch multiple range test. To compare two groups, Student's *t*-tests were performed. If data were not normally distributed or the variances were not homogeneous, non-parametric tests were performed to compare means using Kruskal–Wallis tests and Dunn's *post hoc* analysis. Results are expressed as mean ± SEM. Results were considered statistically significant when  $p < 0.05$  for specific *p*-values.

## RESULTS

### Ethanol Extract of *Aurantiochytrium*, n-Hexane Layer Containing Ethanol Extract of *Aurantiochytrium*, and Squalene Inhibit Amyloid- $\beta$ -Induced Cell Death and Ethanol Extract of *Aurantiochytrium* Increased Adenosine Triphosphate Production

SH-SY5Y cells were treated with EEA (20  $\mu$ g/ml), HEEA (20  $\mu$ g/ml), or squalene (20  $\mu$ g/ml) for 72 h and cell viability measured with the MTT assay. To evaluate the neuroprotective effect of EEA and HEEA, SH-SY5Y cells were pretreated with 20  $\mu$ g/ml EEA or 20  $\mu$ g/ml HEEA for 10 min. Also, A $\beta$  was added (final concentration: 15  $\mu$ M) and co-treated with EEA or HEEA for 72 h. Then, cell viability was measured with the MTT assay. The A $\beta$ -treated group showed a significant reduction in cell viability compared with the non-treated group ( $40.9 \pm 1.4\%$ ,  $P < 0.01$ ). In contrast, pretreatment with 20  $\mu$ g/ml EEA or 20  $\mu$ g/ml HEEA ameliorated A $\beta$ -induced cytotoxicity ( $186.8 \pm 6.9\%$  and  $138.9 \pm 4.2\%$  compared with 100% in A $\beta$ -treated cells, respectively,  $P < 0.01$ ; **Figures 1A,B**). Interestingly, EEA only-treated cells showed a significant increase in cell viability compared with non-treated cells (**Figure 1A**). Moreover, pretreatment with 50- $\mu$ M squalene for 10 min also reversed A $\beta$ -induced cell death, resulting in a significant increase in cell

viability ( $136.0 \pm 4.0\%$  compared with 100% in A $\beta$ -treated cells,  $P < 0.01$ ; **Figure 1C**).

Because EEA increased cell viability in SH-SY5Y cells (**Figure 1A**), we asked if EEA affects intracellular ATP levels. In addition, A $\beta$  is used as an oxidative stress inducer, which can decrease intracellular ATP levels by causing dysfunction in mitochondria. We found that 20  $\mu$ g/ml EEA treatment significantly increased intracellular ATP levels,  $112.8 \pm 3.8$ ,  $121.5 \pm 3.4$ , and  $124.9 \pm 2.5\%$  compared with non-treated cells after 6-, 12-, and 24-h incubation, respectively ( $P < 0.01$ ; **Figure 1D**).

### Ethanol Extract of *Aurantiochytrium* Increased Number of Neurospheres

Based on our results that EEA increased cell viability and ATP production in SH-SY5Y cells, we evaluated the effects of EEA and HEEA on proliferation and differentiation using neurosphere assays. Murine neurospheres were treated for 72 h with 20  $\mu$ g/ml EEA or 20  $\mu$ g/ml HEEA. EEA treatment significantly increased the number of neurospheres ( $P < 0.01$ ) but did not modify neurosphere size (**Figure 2**). In contrast to EEA, HEEA treatment did not modify neurosphere number or neurosphere size (**Figures 2B,C**).

### Ethanol Extract of *Aurantiochytrium* and n-Hexane Layer Containing Ethanol Extract of *Aurantiochytrium* Had Opposite Effects on Neural Differentiation

To study the fate of neurosphere-derived cells treated with EEA and HEEA (**Figure 3A**), we performed immunocytochemistry for the young neuron marker  $\beta$ -III-tubulin and the astrocytic and stem cell marker GFAP. Cells were seeded onto poly-L-ornithine pretreated 8-well-glass slides and cultured in media containing 20  $\mu$ g/ml EEA or 20  $\mu$ g/ml HEEA for 72 h. None of the treatments decreased cell viability (**Figure 3B**). However, EEA significantly ( $P < 0.01$ ) decreased the number of  $\beta$ -III-tubulin+ cells and also the number of GFAP+ cells compared with controls, suggesting that EEA can preserve the undifferentiated state of these cells (**Figures 3C,D**). In contrast, treatment with HEEA increased the number of  $\beta$ -III-tubulin+ and GFAP+ cells compared with control and with EEA, suggesting that the squalene-rich fraction of EEA increased differentiation of these cells (**Figures 3C,D**).

### Ethanol Extract of *Aurantiochytrium* and n-Hexane Layer Containing Ethanol Extract of *Aurantiochytrium* Improved Spatial Learning and Memory in Senescence-Accelerated Mouse-Prone 8 Mice

To evaluate the effect of EEA and HEEA (squalene-rich fraction of EEA) on spatial learning and memory in SAMP8 mice, the MWM test was performed. To assess the effect of EEA and HEEA on spatial learning and memory, we measured the time mice needed to swim to the platform (escape latency). As shown in **Figure 5A**, the escape latency of EEA-treated SAMP8 mice was



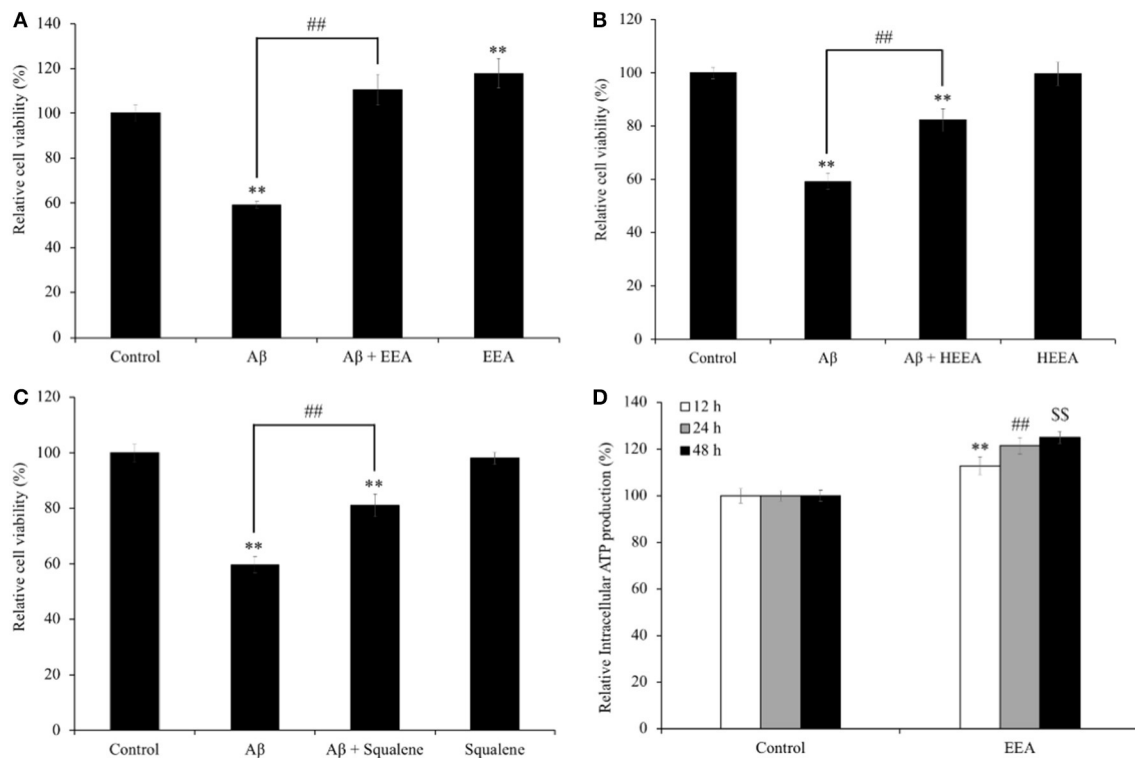


**FIGURE 1 |** Effect of (A) ethanol extract of *Aurantiochytrium* sp. (EEA), (B) hexane layer of EEA (HEEA), and (C) squalene on the cell viability and Amyloid-β (Aβ)-induced changes in SH-SY5Y cells viability. (D) Effects of ethanol extract of EEA on ATP production of SH-SY5Y cells. In MTT assay, cells were pretreated with EEA (20 μg/ml) or HEEA (20 μg/ml) or squalene (50 μM) for 10 min, and then, cells were treated with 15-μM Aβ for 72 h. For ATP assay, cells were treated with EEA (20 μg/ml) for 6, 12, and 24 h. After treatment, intracellular ATP production level was measured. Each bar represents mean ± SEM ( $n = 5$  independent experiments). \*\* $P < 0.01$  vs. control cells, ## $P < 0.01$  vs. Aβ-treated cells.

significantly ( $P < 0.01$ ) decreased compared with water-treated SAMP8 mice from the 6th and 7th day of training. There was no difference in the escape latency between SAMR1 mice and EEA-treated SAMP8 mice. Moreover, HEEA-treated SAMP8 mice also showed a significantly decreased escape latency time compared with water-treated SAMP8 mice at day 7 (Figure 4A).

Figures 4B,C show that the time spent in the target quadrant and the number of times the mouse crossed the platform was significantly higher in the EEA-treated SAMP8 group compared with the water-treated SAMP8 group ( $P < 0.01$ ). However, no significant difference was observed in the number of crossings of the target quadrant between the HEEA-treated SAMP8 group and the water-treated SAMP8 group.

### Ethanol Extract of *Aurantiochytrium* Increases Neural Stem Cells and Neurogenesis in Hippocampus of Senescence-Accelerated Mouse-Prone 8 Mice

To test EEA (50 mg/kg) effects on neurogenic niches, we administered it orally to SAMP8 mice for 30 days, carried out the MWM test, and brains were collected and immunohistochemistry performed. We designated BrdU+ cells

that co-express the NSC and astrocytic marker GFAP as SGZ stem cells. We also co-labeled BrdU+ cells with the mature neuronal marker NeuN and double-positive cells were considered to be neurons that were born during BrdU administration that had matured. We studied the effects of EEA on the anterior DG and the posterior DG separately because the former is associated with spatial memory and the latter more with limbic functions (Motta-Teixeira et al., 2015). The number of BrdU+GFAP+ cells was significantly increased in both the anterior and the posterior DG of EEA-treated SAMP8 mice compared with water-treated SAMP8 mice ( $P < 0.01$ ) (Figures 5B,E). In the anterior DG, EEA also significantly increased the number of newborn neurons that had mature BrdU+NeuN+ cells ( $P < 0.01$ ; Figure 5C). In the posterior DG, there was a trend toward an increased number of newborn neurons in the EEA-treated SAMP8 mice, but this did not reach statistical significance (Figures 5D,F).

We next asked if EEA affects the other major neurogenic niche, the SVZ. We found that the total number of BrdU+ cells was greater in SAMP8 mice compared with SAMR1 control mice, independent of treatment (Figures 6A,B). However, there were no significant differences in the number of BrdU+ cells that co-express the astrocyte and stem cell marker GFAP (Figure 6C). Nevertheless, SAMP8 EEA-treated mice exhibited a significant

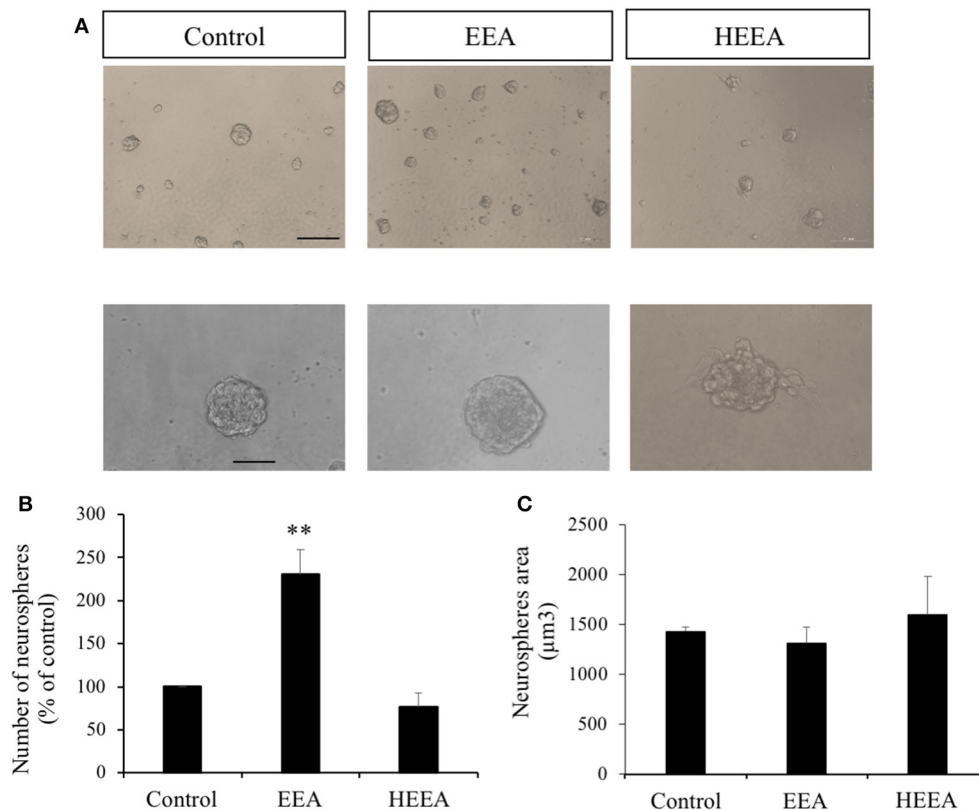


**FIGURE 2 |** Effect of ethanol extract of *Aurantiochytrium* sp. (EEA) and hexane layer of EEA (HEEA) on NPCs proliferation. Proliferation was tested using neurosphere cultures in the presence of EGF (20 ng/ml) and bFGF (10 ng/ml). **(A)** Phase-contrast microscopy images of neurospheres treated with or without EEA (20  $\mu$ g/ml) or HEEA (20  $\mu$ g/ml) during 72 h. Scale bar indicates 100  $\mu$ m. **(B)** Neurosphere number after treatment with grape extract. **(C)** Size of neurospheres after treatment with EEA or HEEA. \*\* $P < 0.01$  compared with control in a one-way ANOVA followed by Ryan–Einot–Gabriel–Welsch multiple range test.

increase in the number of BrdU+ cells that co-express the neuroblast marker DCX in the SVZ compared with SAMP8 + water-treated mice ( $P < 0.01$ ; **Figures 6D,E**). We used DCX instead of NeuN here because NeuN expression only occurs once SVZ neuroblasts have reached the olfactory bulbs, whereas DCX is expressed in newborn neurons in the SVZ (Brown et al., 2003).

We also performed double-labeling immunohistochemistry for BrdU and DCX in the DG. There was no statistically significant difference between groups in the anterior DG; however, we observed a clear tendency indicating an increase in the number of BrdU+DCX+ cells in EEA-treated SAMP8 mice compared with SAMR1 and SAMP8 water-treated mice (data not shown). Similar to the anterior DG, there was no statistically significant difference in the posterior DG among the three groups (data not shown).

## DISCUSSION

Increasing neurogenesis by increasing NSCs is important to investigate as a treatment for AD. In this study, we focused on a microalgae *Aurantiochytrium* as a nutraceutical for the treatment of AD. We evaluated an EEA's neuroprotective effect

on human neural SH-SY5Y cells and stem cell properties in murine neurosphere primary cultures. Moreover, we also evaluated the effect of EEA on spatial learning and memory and *in vivo* neurogenesis in SAMP8 mice, a good model for aging-related brain dysfunction such as AD. In this study, we have shown that the microalgae *Aurantiochytrium* has multiple neuroprotective effects on brain health. It inhibited neuronal death caused by A $\beta$  and increased ATP in SH-SY5Y cells. In SAMP8 mice brains, it augmented hippocampal stem cells and neurogenesis and improved spatial memory loss.

These findings are important, as the development of preventive or therapeutic drugs and functional foods for these diseases is still challenging. Nutraceuticals are at the intersection of pharmaceuticals and nutrition and render health or medical benefits, including the prevention and treatment of disease. Other studies have also demonstrated the neuroprotective effects of nutraceuticals against toxic compounds associated with neurodegenerative diseases *via* mechanisms such as modulation of energy metabolism, oxidative stress, neuroinflammation, and promotion of neurogenesis *via* growth factors and neurotrophins (Dadhania et al., 2016; Pandareesh et al., 2018).

A $\beta$ , a 39–43 amino acid peptide, is a major component of neuritic plaques and a pathological hallmark of AD, along with

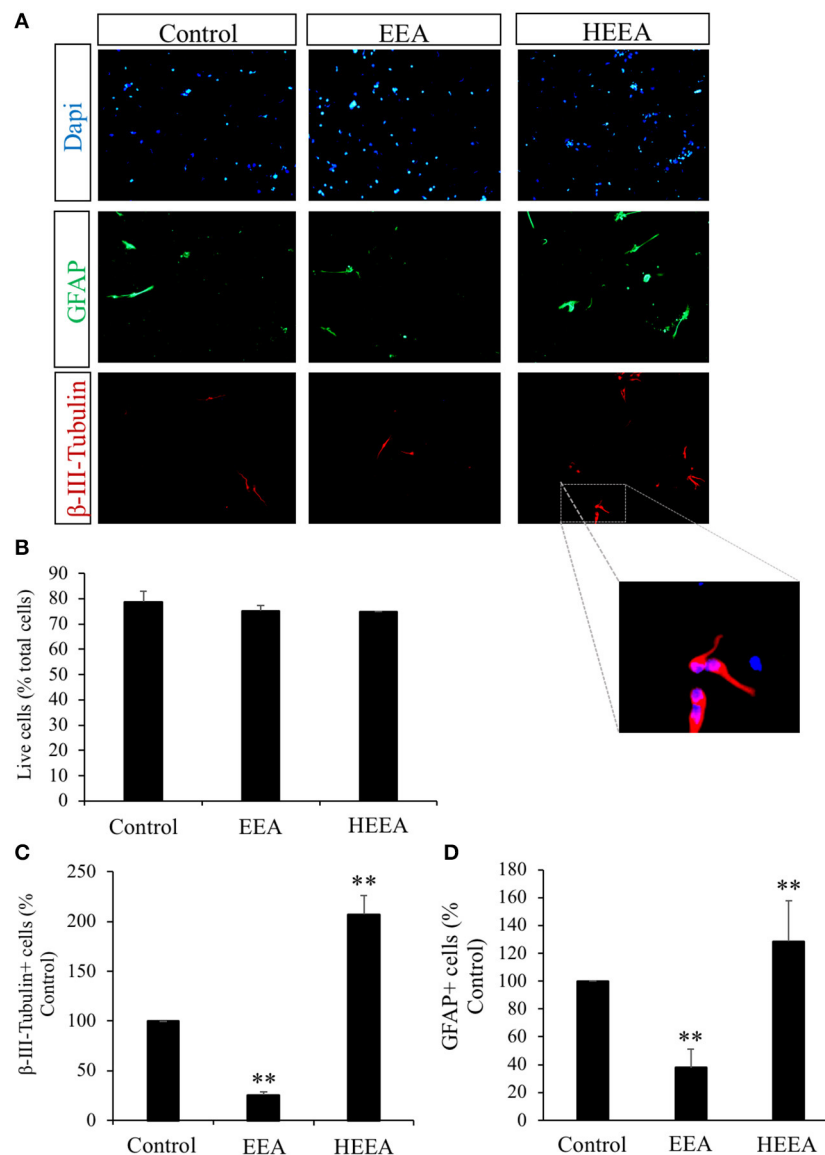
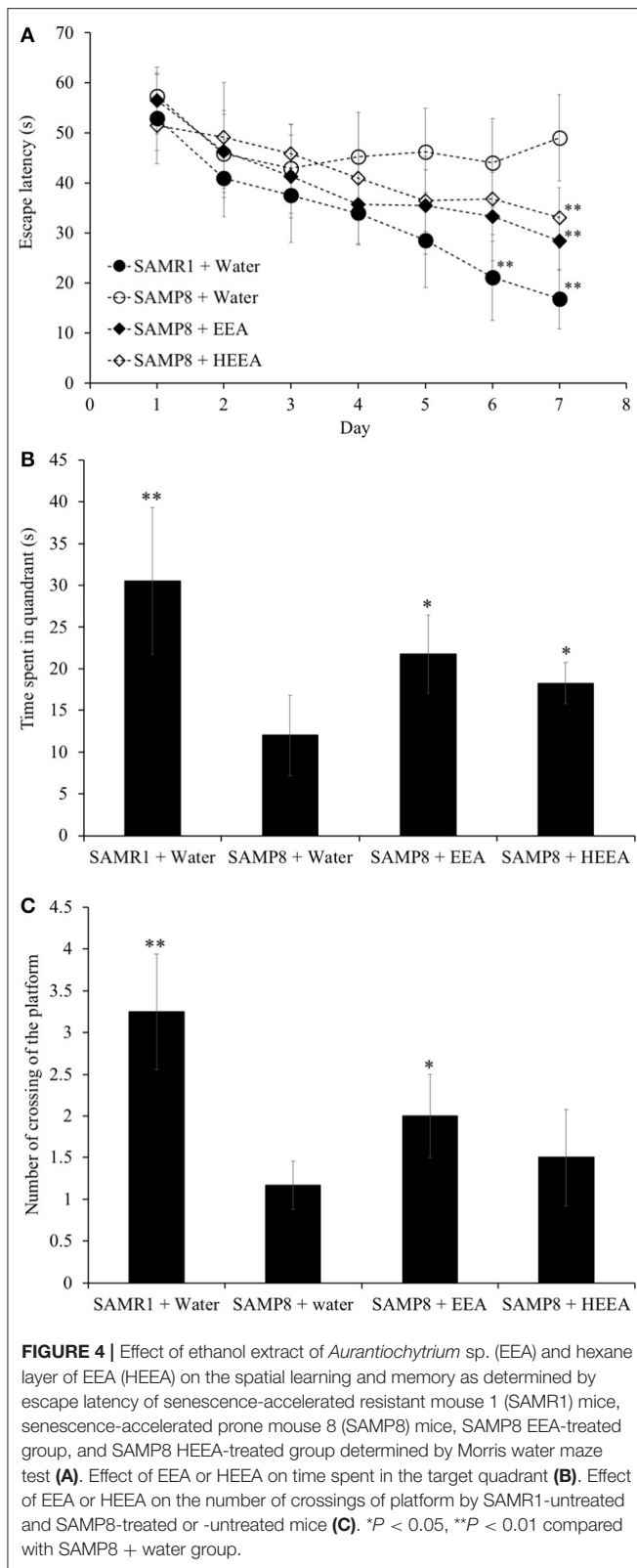


**FIGURE 3 |** Effect of ethanol extract of *Aurantiochytrium* sp. (EEA) and hexane layer of EEA (HEEA) on NPCs proliferation. Two types of differentiation markers ( $\beta$ -III-tubulin for neurons and GFAP for astrocytes) were used. Neurospheres were treated with or without EEA (20  $\mu$ g/ml) or HEEA (20  $\mu$ g/ml) for 72 h. **(A)** Immunofluorescence images demonstrating expression of  $\beta$ -III-tubulin and GFAP. **(B)** Numbers of live cells after EEA or HEEA treatment. **(C)** Numbers of  $\beta$ -III-tubulin+ cells after treatment with EEA or HEEA. **(D)** Numbers of GFAP+ cells after treatment with EEA or HEEA. \*\* $P < 0.01$  vs. control cells.

neurofibrillary tangles. A $\beta$  is formed from amyloid precursor protein upon cleavage by  $\beta$ - and  $\gamma$ -secretase. This process is the amyloidogenic processing pathway that generates A $\beta_{1-40}$  and A $\beta_{1-42}$ , which are neurotoxic. The molecular mechanism that links A $\beta$  to the development of neurotoxicity is poorly understood, but some evidence suggests that it is caused by oxidative stress (Castillo et al., 2019), neuroinflammation (Webers et al., 2020), and dysfunction of mitochondria (Wang et al., 2020). The current study aimed to first evaluate the EEA for its *in vitro* neuroprotective effect on human SH-SY5Y cells treated with A $\beta$ . SH-SY5Y neural cells were selected, as they are

used widely for the evaluation of neurotoxic, neuroprotective, and neuroadaptive properties of various phytoconstituents and other chemical entities (Ramkumar et al., 2017; Marmit et al., 2020). In our present study, EEA (20  $\mu$ g/ml)-treated cells significantly increased cell viability against the decrease of A $\beta$ -induced cytotoxicity. Moreover, the HEEA and squalene, a major constituent of EEA, also showed the neuroprotective effect on A $\beta$ -treated cells. Our study also showed that treatment of EEA increased cell viability as well as intracellular ATP levels. Dysfunction of energy metabolism in the brain occurs during aging but is further exacerbated in neurodegenerative diseases



and is considered to be another hallmark of neurodegeneration (Camandola and Mattson, 2017). Also, the high availability of energy is important for the CNS because neurons require

ATP for many critical functions, including firing action potentials, survival, proliferation, and differentiation in stem cell niches. Therefore, our results suggested that EEA may improve mitochondrial dysfunction induced by A $\beta$  and activated mitochondria. Regulation of the amyloidogenic processing reduces A $\beta$  production and may ameliorate Alzheimer's pathology, which is a potential target for AD. In addition, inhibition of A $\beta$  assembly is another potential means to slow down AD pathogenesis. In the future, therefore, multiple studies on A $\beta$  production, amyloidogenic processing, and A $\beta$  assembly are required for understanding the mechanism underlying the neuroprotective effect of EEA (Li et al., 2020; Patil et al., 2020).

Metabolic states influence stem cell activation and neurogenesis (Llorens-Bobadilla et al., 2015), suggesting EEA could increase these processes according to the result of MTT and ATP assay. Therefore, we first analyzed the effect of EEA and HEEA in neurosphere cultures. Neurospheres are primary cultures of the stem and progenitor cells isolated from neurogenic niches consisting of floating aggregates of cells that can be used to evaluate the effects of molecules on NPCs. The size of neurospheres is indicative of NPC proliferation, whereas neurosphere numbers are indicative of self-renewal and survival. Experiments were performed in the presence of EGF and bFGF to stimulate neurosphere formation. We isolated neural stem cells and NPCs from the brain and grew neurospheres in proliferation conditions using the growth factors EGF and bFGF to promote neurosphere formation. We measured the number and size of neurospheres, where neurosphere number indirectly indicates the number of cells that enter the cell cycle or their self-renewal capacity (Reynolds and Weiss, 1996; Reynolds and Rietze, 2005) and size indicates the rate of proliferation (Torroglosa et al., 2007). We found that EEA significantly increased the number of neurospheres but not their size, suggesting an increase in this stem cell property of self-renewal upon exposure to EEA. Not only NSCs but also transit-amplifying progenitor cells can form new neurospheres, and some data suggest quiescent stem cells are not detected in neurospheres (Pastrana et al., 2011). Thus, EEA may have had an effect on multiple different cells in our cultures. In contrast to EEA, we found that HEEA did not affect neurosphere proliferation or self-renewal. We surmise that there were constituents in EEA that induced these effects but that were absent from the HEEA, hexane-purified EEA.

We subsequently found additional differences in the effects of EEA vs. HEEA. In terms of neurosphere differentiation, EEA decreased the number of  $\beta$ -III-tubulin+ neurons, whereas HEEA increased it. The same occurred with the number of GFAP+ cells. These results suggest that HEEA can induce differentiation of NPC into both neurons or glia, whereas EEA keeps them in an undifferentiated state. Recent studies showed EEA and one of its active components, squalene, have neuroprotective effects, protecting stressed neurons from cell death (Sasaki et al., 2019a). Moreover, several genes related to chemokine signaling pathways are downregulated in EEA-treated mice and may contribute to anti-inflammatory effects (Sasaki et al., 2019a). Squalene, which is concentrated in the HEEA layer, is essential in NSCs and NPC cholesterol biosynthesis. Ablation of squalene synthase promoted apoptosis in newborn neurons and reduced brain size (Saito et al.,



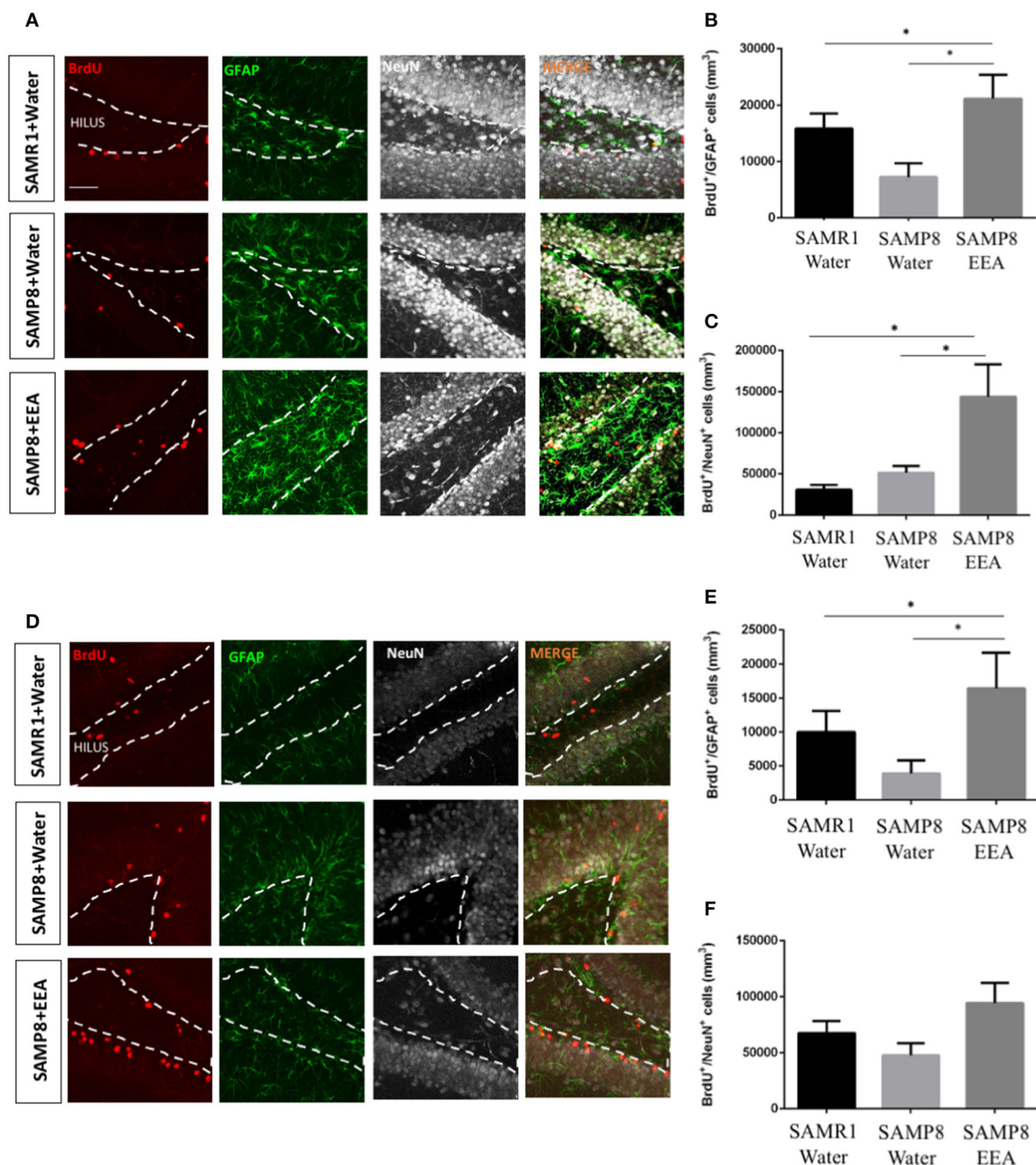


**FIGURE 5 |** Effect of oral administration of ethanol extract of *Aurantiochytrium* sp. (EEA) on anterior and posterior dentate gyrus (DG) stem cell activation and neurogenesis. SAMP8 mice were orally administered with EEA (50 mg/kg) for 30 days. Photomicrographs show coronal sections containing the anterior (A) and posterior (D) DG processed for immunohistochemical detection of BrdU+ cells (red) and stem cell marker GFAP (green). Graphs represent number of BrdU+ cells that co-express stem cell marker GFAP in anterior (B) and posterior (E) DG. Graph representing number of BrdU+ cells that co-express mature neuronal marker NeuN in anterior (C) and posterior (F) DG. Each bar represents mean  $\pm$  SEM. \* $P < 0.05$  SAMP8 + EEA group compared with SAMP8 + water group or SAMR1 + water group (B,C,E).

2009). Also, disruption of cholesterol synthesis affected the radial glia fiber scaffold necessary for the migration of newborn neurons and was related to reduced cell self-renewal (Driver et al., 2016).

In our previous work, we evaluated the neuroprotective effects of several natural compounds on A $\beta$ -treated SH-SY5Y cells as an *in vitro* model of AD (Han et al., 2010; Sasaki et al., 2013).

Interestingly, this AD model showed a strong correlation with the results of our previous behavioral experiments (MWM) using SAMP8 mice (Han et al., 2010; Sasaki et al., 2013). The present study also sought to evaluate the effects of EEA and HEEA treatment in spatial and learning memory in SAMP8, a well-characterized model for studying brain aging and

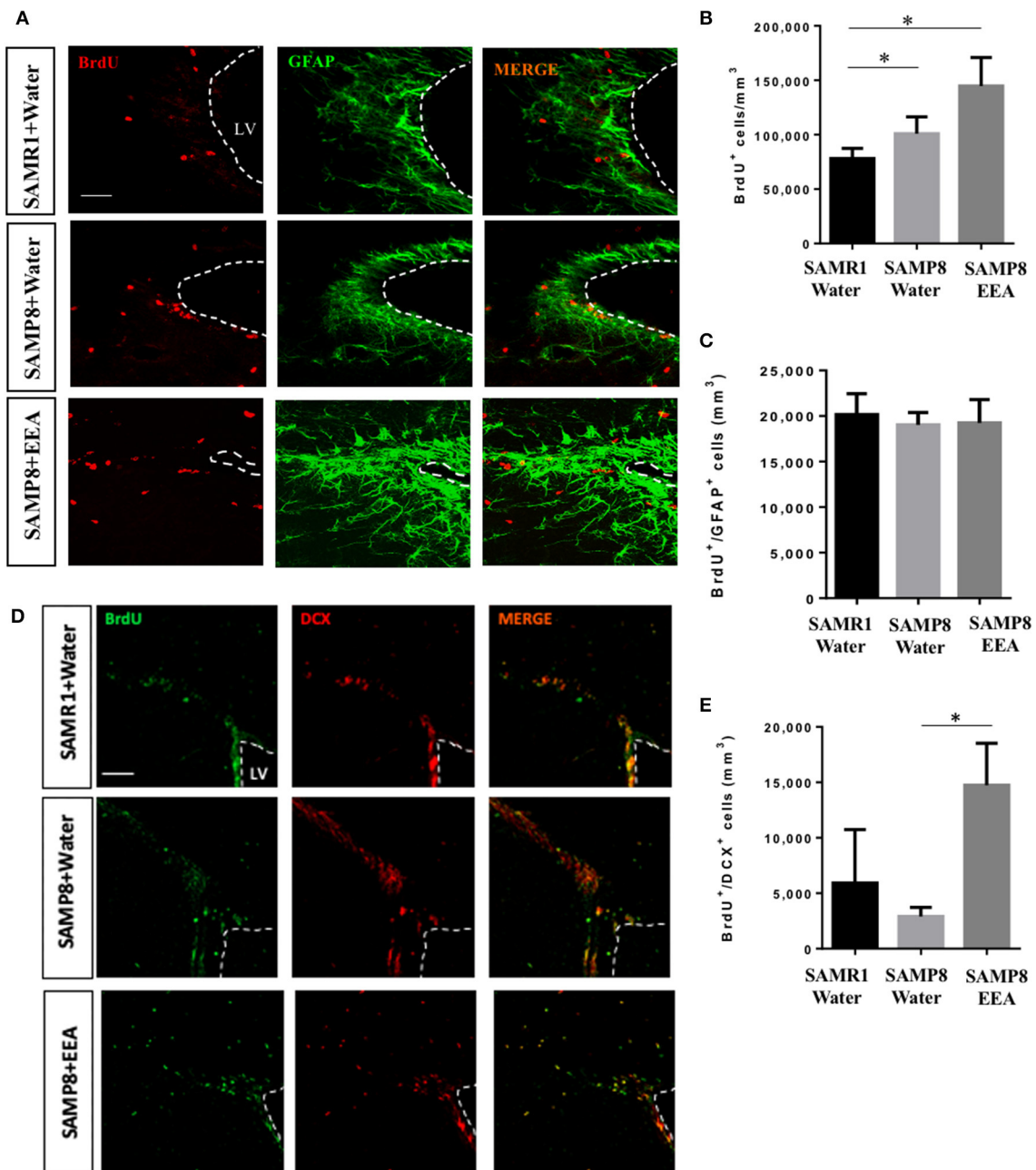


**FIGURE 6 |** Effect of oral administration of ethanol extract of *Aurantiochytrium* sp. (EEA) on subventricular zone (SVZ) proliferation. EEA (50 mg/kg) was orally administered to SAMP8 mice for 30 days. **(A)** Photomicrograph shows SVZ in coronal sections processed for immunohistochemical detection of proliferating BrdU+ cells (red) and astrocyte marker GFAP (green), and **(D)** BrdU+ cells (green) and neuroblast marker doublecortin (DCX, red). **(B)** Graph represents number of BrdU+ cells in SVZ. **(C)** Graph showing number of BrdU cells that co-express stem cell and glial marker GFAP. **(E)** Graph showing number of BrdU cells that co-express DCX. Each bar represents mean  $\pm$  SEM. \* $P < 0.05$  SAMP8 + EEA group or SAMR1 + water group compared with SAMP8 + water group **(B,E)**.

neurodegeneration (Morley et al., 2012a,b) using the MSM test. The MWM is a widely used tool to assess spatial learning and memory in rodents. In the MWM, the animal finds or is placed on a platform concealed under the surface of the water in a pool. The time each mouse takes to subsequently swim to the platform indicates how quickly it can recall the location of the platform.

SAMP8 mice show age-related deterioration in learning and memory ability with comprehensive brain pathological changes, including the deterioration of amyloid pathology by alterations in the amyloid pathway (Porquet et al., 2015) and have been used as a non-transgenic murine model for accelerated senescence and AD (Hong et al., 2020). In our study, we found that SAMP8

mice treated with EEA or HEEA demonstrated increased learning ability in the MWM test. Thus, our results suggested that EEA and HEEA may potentially restore neuronal damage and death induced by A $\beta$ , which may help improve spatial learning and memory in SAMP8 mice.

Using gavage, EEA was administered to SAMP8 and SAMR1 mice to study proliferation *in vivo* in the neurogenic stem cell niches. The hippocampal SGZ has been shown to mediate learning and memory (Anacker and Hen, 2017). In the SGZ, we found significantly more cells that co-express the proliferation marker BrdU and the mature neuronal marker NeuN, indicating that EEA encourages neurogenesis in this region. Additionally, we observed increased numbers of BrdU+ cells co-expressing the glial and stem cell marker GFAP in the anterior SGZ. This increase suggests that quiescent NSCs could be activated by EEA, eventually increasing neuronal production. One potential mechanism is related to fatty acid metabolism. EEA could induce *de novo* lipogenesis, which is key in neurogenesis (Knobloch et al., 2013) and so ameliorate SAMP8 cognitive deficiencies. We also studied the other important neurogenesis niche, the SVZ, and found more BrdU+ cells that co-express the neuroblast marker DCX in the SVZ of SAMP8 mice treated with EEA. In contrast, we found no significant changes in the number of BrdU+ cells that co-express the glial and neural stem cell marker GFAP, suggesting that EEA induced neurogenesis in the SVZ but did not activate NSCs. Moreover, our hippocampal results indicate increased neurogenesis after EEA administration, and this may contribute to their enhanced performance in the MWM spatial memory test. However, it is important to point out that EEA administered mice may have altered strategy use, motivation, or stress resilience, and the MWM results may not be entirely due to increased hippocampal neurogenesis. The relationship between adult neurogenesis and AD has been recently debated (Moreno-Jiménez et al., 2019; Scopa et al., 2020). Previous studies have reported reduced expression of neurogenesis markers in the SVZ and DG regions of postmortem AD brain. Moreover, several studies demonstrated increased neurogenesis in animal models and humanized three-dimensional systems of AD (Bhattarai et al., 2016; Choi et al., 2018; Papadimitriou et al., 2018).

## REFERENCES

- Aguilera, Y., Dorado, M. E., Prada, F. A., Martinez, J. J., Quesada, A., and Ruiz-Gutierrez, V. (2005). The protective role of squalene in alcohol damage in the chick embryo retina. *Exp. Eye Res.* 80, 535–543. doi: 10.1016/j.exer.2004.11.003
- Altman, J., and Das, G. D. (1965). Autoradiographic and histological evidence of postnatal hippocampal neurogenesis in rats. *J. Comp. Neurol.* 124, 319–335. doi: 10.1002/cne.901240303
- Alvarez-Buylla, A., and Garcia-Verdugo, J. M. (2002). Neurogenesis in adult subventricular zone. *J. Neurosci.* 22, 629–634. doi: 10.1523/JNEUROSCI.22-03-00629.2002
- Anacker, C., and Hen, R. (2017). Adult hippocampal neurogenesis and cognitive flexibility - linking memory and mood. *Nat. Rev. Neurosci.* 18, 335–346. doi: 10.1038/nrn.2017.45
- Barak, B., Shvarts-Serebro, I., Modai, S., Gilam, A., Okun, E., Michaelson, D. M., et al. (2013). Opposing actions of environmental enrichment and Alzheimer's disease on the expression of hippocampal microRNAs in mouse models. *Transl. Psychiatry* 3:e304. doi: 10.1038/tp.2013.77

## CONCLUSION

Taken together, our present research suggests that *Aurantiochytrium* improves spatial learning and memory in SAMP8 mice, an animal model of aging. This was accompanied by enhancement of neurogenesis in the hippocampal DG. Our new findings in aggregate suggest that EEA could be used as a new therapeutic agent for the treatment of neurodegenerative diseases or other age-related problems such as AD.

## DATA AVAILABILITY STATEMENT

The raw data supporting the conclusions of this article will be made available by the authors, without undue reservation.

## ETHICS STATEMENT

The animal study was reviewed and approved by the Animal Study Committee of Tsukuba University.

## AUTHOR CONTRIBUTIONS

KS, FS, and HI conceived and designed the experiments. KS, NG-D, and QW performed the experiments. KS and NG-D prepared the figures and tables. KS and NG-D analyzed and interpreted the results and wrote the paper. FS and HI edited and revised the manuscript. All authors contributed to the article and approved the submitted version.

## FUNDING

This work was supported by Japan Science and Technology Agency; Science and Technology Research Partnership for Sustainable Development (Grant No. JPMJSA1506).

## ACKNOWLEDGMENTS

This article has been released as a preprint at Research Square (Sasaki et al., 2020).

- Bhattarai, P., Thomas, A. K., Cosacak, M. I., Papadimitriou, C., Mashkaryan, V., Froc, C., et al. (2016). IL4/STAT6 signaling activates neural stem cell proliferation and neurogenesis upon amyloid- $\beta$ 42 aggregation in adult zebrafish brain. *Cell Rep.* 17, 941–948. doi: 10.1016/j.celrep.2016.09.075
- Bhilwade, H. N., Tatewaki, N., Konishi, T., Nishida, M., Eitsuka, T., Yasui, H., et al. (2019). The adjuvant effect of squalene, an active ingredient of functional foods, on doxorubicin-treated allograft mice. *Nutr. Cancer* 71, 1153–1164. doi: 10.1080/01635581.2019.1597900
- Blunt, J. W., Carroll, A. R., Copp, B. R., Davis, R. A., Keyzers, R. A., and Prinsep, M. R. (2017). Marine natural products. *Nat. Prod. Rep.* 34, 235–294. doi: 10.1039/C6NP00124F
- Brown, J. P., Couillard-Després, S., Cooper-Kuhn, C. M., Winkler, J., Aigner, L., and Kuhn, H. G. (2003). Transient expression of doublecortin during adult neurogenesis. *J. Comp. Neurol.* 467, 1–10. doi: 10.1002/cne.10874
- Camandola, S., and Mattson, M. P. (2017). Brain metabolism in health, aging, and neurodegeneration. *EMBO J.* 36, 1474–1492. doi: 10.15252/embj.201695810
- Castillo, C., Fernández-Méndivil, C., Buendia, I., Saavedra, P., Meza, C., Parra, N. C., et al. (2019). Neuroprotective effects of EpoL against oxidative



- stress induced by soluble oligomers of A $\beta$  peptide. *Redox Biol.* 24:101187. doi: 10.1016/j.redox.2019.101187
- Cheng, X. R., Zhou, W. X., and Zhang, Y. X. (2014). The behavioral, pathological and therapeutic features of the senescence-accelerated mouse prone 8 strain as an Alzheimer's disease animal model. *Ageing Res. Rev.* 13, 13–37. doi: 10.1016/j.arr.2013.10.002
- Choi, S. H., Bylykbashi, E., Chatila, Z. K., Lee, S. W., Pulli, B., Clemenson, G. D., et al. (2018). Combined adult neurogenesis and BDNF mimic exercise effects on cognition in an Alzheimer's mouse model. *Science* 361:eaan8821. doi: 10.1126/science.aan8821
- Dadhania, V. P., Trivedi, P. P., Vikram, A., and Tripathi, D. N. (2016). Nutraceuticals against neurodegeneration: a mechanistic insight. *Curr. Neuropharmacol.* 14, 627–640. doi: 10.2174/1570159X14666160104142223
- Driver, A. M., Kratz, L. E., Kelley, R. I., and Stottmann, R. W. (2016). Altered cholesterol biosynthesis causes precocious neurogenesis in the developing mouse forebrain. *Neurobiol. Dis.* 91, 69–82. doi: 10.1016/j.nbd.2016.02.017
- Forbes, D., Thiessen, E. J., Blake, C. M., Forbes, S. C., and Forbes, S. (2013). Exercise programs for people with dementia. *Cochrane. Database. Syst. Rev.* 4:CD006489. doi: 10.1002/14651858.CD006489.pub3
- Fratiglioni, L., Paillard-Borg, S., and Winblad, B. (2004). An active and socially integrated lifestyle in late life might protect against dementia. *Lancet Neurol.* 3, 343–353. doi: 10.1016/S1474-4422(04)00767-7
- Geribaldi-Doldán, N., Carrasco, M., Murillo-Carretero, M., Domínguez-García, S., García-Cózar, F. J., Muñoz-Miranda, J. P., et al. (2018). Specific inhibition of ADAM17/TACE promotes neurogenesis in the injured motor cortex. *Cell Death Dis.* 9:862. doi: 10.1038/s41419-018-0913-2
- Griñán-Ferré, C., Izquierdo, V., Otero, E., Puigoriol-Illamola, D., Corpas, R., Sanfeliu, C., et al. (2018). Environmental enrichment improves cognitive deficits, AD hallmarks and epigenetic alterations presented in 5xFAD mouse model. *Front. Cell. Neurosci.* 12:224. doi: 10.3389/fncel.2018.00224
- Griñán-Ferré, C., Puigoriol-Illamola, D., Palomera-Avalos, V., Pérez-Cáceres, D., Companys-Aleman, J., Camins, A., et al. (2016). Environmental enrichment modified epigenetic mechanisms in SAMP8 mouse hippocampus by reducing oxidative stress and inflammation and achieving neuroprotection. *Front. Aging Neurosci.* 8:241. doi: 10.3389/fnagi.2016.00241
- Guiry, M. D. (2012). How many species of algae are there? *J. Phycol.* 48, 1057–1063. doi: 10.1111/j.1529-8817.2012.01222.x
- Han, J., Miyamae, Y., Shigemori, H., and Isoda, H. (2010). Neuroprotective effect of 3,5-di-caffeoylquinic acid on SH-SY5Y cells and senescence-accelerated-prone mice 8 through the up-regulation of phosphoglycerate kinase-1. *Neuroscience* 169, 1039–1045. doi: 10.1016/j.neuroscience.2010.05.049
- Hong, H., Mo, Y., Li, D., Xu, Z., Liao, Y., Yin, P., et al. (2020). Aberrant expression profiles of lncRNAs and their associated nearby coding genes in the hippocampus of the SAMP8 mouse model with AD. *Mol. Ther. Nucleic Acids* 20, 140–154. doi: 10.1016/j.omtn.2020.02.008
- Kandasamy, M., Rosskopf, M., Wagner, K., Klein, B., Couillard-Despres, S., Reitsamer, H. A., et al. (2015). Reduction in subventricular zone-derived olfactory bulb neurogenesis in a rat model of Huntington's disease is accompanied by striatal invasion of neuroblasts. *PLoS ONE* 10:e0116069. doi: 10.1371/journal.pone.0116069
- Kaya, K., Nakazawa, A., Matsuura, H., Honda, D., Inouye, I., and Watanabe, M. M. (2011). Thraustochytrid *Aurantiochytrium* sp. 18W-13a accumulates high amounts of squalene. *Biosci. Biotech. Biochem.* 75, 2246–2248. doi: 10.1271/bbb.110430
- Kelly, G. S. (1999). Squalene and its potential clinical uses. *Altern. Med. Rev.* 4, 29–36.
- Kempermann, G. (2002). Why new neurons? Possible functions for adult hippocampal neurogenesis. *J. Neurosci.* 22, 635–638. doi: 10.1523/JNEUROSCI.22-03-00635.2002
- Knobloch, M., Braun, S. M., Zurkirchen, L., von Schoultz, C., Zamboni, N., Arauzo-Bravo, M. J., et al. (2013). Metabolic control of adult neural stem cell activity by Fasn-dependent lipogenesis. *Nature* 493, 226–230. doi: 10.1038/nature11689
- Kumar, S. R., Yamauchi, I., Narayan, B., Katsuki, A., Hosokawa, M., and Miyashita, K. (2016). Squalene modulates fatty acid metabolism: enhanced EPA/DHA in obese/diabetic mice (KK-Ay) model. *Eur. J. Lipid Sci. Technol.* 118, 1935–1941. doi: 10.1002/ejlt.201600006
- Li, Y., Zhanga, J., Wana, J., Liub, A., and Sun, J. (2020). Melatonin regulates A $\beta$  production/clearance balance and A $\beta$  neurotoxicity: a potential therapeutic molecule for Alzheimer's disease. *Biomed. Pharmacother.* 132:110887. doi: 10.1016/j.biopha.2020.110887
- Llorens-Bobadilla, E., Zhao, S., Saiz-Castro, G., Zwadlo, K., and Martin-Villalba, A. (2015). Single-Cell Transcriptomics reveals a population of dormant neural stem cells that become activated upon brain injury. *Cell Stem Cell* 17, 329–340. doi: 10.1016/j.stem.2015.07.002
- Mangialasche, F., Westman, E., Kivipelto, M., Muehlboeck, J. S., Cecchetti, R., Baglioni, M., et al. (2013). Classification and prediction of clinical diagnosis of Alzheimer's disease based on MRI and plasma measures of  $\alpha$ - $\gamma$ -tocotrienols and  $\gamma$ -tocopherol. *J. Intern. Med.* 273, 602–621. doi: 10.1111/joim.12037
- Marmit, D. J., Alves, C., Silva, J., Pinteus, S., Schneider, T., Christ Vianna Santos, R., et al. (2020). Neuroprotective potential of myricaria plinioides D. Legrand extract in an *in vitro* human neuroblastoma model. *Inflammopharmacology* 28, 737–748. doi: 10.1007/s10787-019-00652-y
- Moreno-Jiménez, E. P., Flor-García, M., Terreros-Roncal, J., Rábano, A., Cafini, F., Pallas-Bazarra, N., et al. (2019). Adult hippocampal neurogenesis is abundant in neurologically healthy subjects and drops sharply in patients with Alzheimer's disease. *Nat. Med.* 25, 554–560. doi: 10.1038/s41591-019-0375-9
- Morley, J. E., Armbricht, H. J., Farr, S. A., and Kumar, V. B. (2012a). The senescence accelerated mouse (SAMP8) as a model for oxidative stress and Alzheimer's disease. *Biochim. Biophys. Acta* 1822, 650–656. doi: 10.1016/j.bbdis.2011.11.015
- Morley, J. E., Farr, S. A., Kumar, V. B., and Armbricht, H. J. (2012b). The SAMP8 mouse: a model to develop therapeutic interventions for Alzheimer's disease. *Curr. Pharm. Des.* 18, 1123–1130. doi: 10.2174/138161212799315795
- Motta-Teixeira, L. C., Takada, S. H., Machado-Nils, A. V., Nogueira, M. I., and Xavier, G. F. (2015). Spatial learning and neurogenesis: effects of cessation of wheel running and survival of novel neurons by engagement in cognitive tasks. *Hippocampus* 26, 794–803. doi: 10.1002/hipo.22560
- Pandareesh, M. D., Kandikattu, H. K., Razack, S., Amruta, N., Choudhari, R., Vikram, A., et al. (2018). Nutrition and nutraceuticals in neuroinflammatory and brain metabolic stress: implications for neurodegenerative disorders. *CNS Neurol. Disord. Drug. Targets.* 17, 680–688. doi: 10.2174/1871527317666180625104753
- Papadimitriou, C., Celikkaya, H., Cosacak, M. I., Mashkaryan, V., Bray, L., Bhattarai, P., et al. (2018). 3D culture method for Alzheimer's disease modeling reveals interleukin-4 rescues Abeta42-induced loss of human neural stem cell plasticity. *Dev. Cell* 46, 85–101.e108. doi: 10.1016/j.devcel.2018.06.005
- Pastrana, E., Silva-Vargas, V., and Doetsch, F. (2011). Eyes wide open: a critical review of sphere-formation as an assay for stem cells. *Cell Stem Cell* 8, 486–498. doi: 10.1016/j.stem.2011.04.007
- Patil, G. V., Joshi, R. S., Kazi, R. S., Kulsange, S. E., and Kulkarni, M. J. (2020). A possible role of glycation in the regulation of amyloid  $\beta$  precursor protein processing leading to amyloid  $\beta$  accumulation. *Med. Hypotheses* 142:109799. doi: 10.1016/j.mehy.2020.109799
- Porquet, D., Andrés-Benito, P., Griñán-Ferré, C., Camins, A., Ferrer, I., Canudas, A. M., et al. (2015). Amyloid and tau pathology of familial Alzheimer's disease APP/PS1 mouse model in a senescence phenotype background (SAMP8). *Age* 37:12. doi: 10.1007/s11357-015-9747-3
- Ramkumar, M., Rajasankar, S., Gobi, V. V., Dhanalakshmi, C., Manivasagam, T., Justin, T. A., et al. (2017). Neuroprotective effect of demethoxycurcumin, a natural derivative of curcumin on rotenone induced neurotoxicity in SH-SY5Y Neuroblastoma cells. *BMC Complem. Altern. Med.* 17:217. doi: 10.1186/s12906-017-1720-5
- Reynolds, B. A., and Rietze, R. L. (2005). Neural stem cells and neurospheres—re-evaluating the relationship. *Nat. Methods* 2, 333–336. doi: 10.1038/nmeth758
- Reynolds, B. A., and Weiss, S. (1996). Clonal and population analyses demonstrate that an EGF-responsive mammalian embryonic CNS precursor is a stem cell. *Dev. Biol.* 175, 1–13. doi: 10.1006/dbio.1996.0090
- Saito, K., Dubreuil, V., Arai, Y., Wilsch-Brauninger, M., Schwudke, D., Saher, G., et al. (2009). Ablation of cholesterol biosynthesis in neural stem cells increases their VEGF expression and angiogenesis but causes neuron apoptosis. *Proc. Natl. Acad. Sci. U.S.A.* 106, 8350–8355. doi: 10.1073/pnas.0903541106



- Sasaki, K., Davies, J., Doldán, N. G., Arao, S., Ferdousi, F., Szele, F. G., et al. (2019b). 3,4,5-Tricaffeoylquinic acid induces adult neurogenesis and improves deficit of learning and memory in aging model senescence-accelerated prone 8 mice. *Aging* 11, 401–422. doi: 10.18632/aging.101748
- Sasaki, K., Doldán, N. G., Wu, Q., Davies, J., Szele, F. G., and Isoda, H. (2020). The microalgae *Aurantiochytrium* Sp. increases neurogenesis and improves spatial learning and memory in senescence-accelerated prone 8 mice. *Res Squ. [Pre-print]*. doi: 10.21203/rs.3.rs-51260/v1
- Sasaki, K., Han, J., Shimozone, H., Villareal, M. O., and Isoda, H. (2013). Caffeoylquinic acid-rich purple sweet potato extract, with or without anthocyanin, imparts neuroprotection and contributes to the improvement of spatial learning and memory of SAMP8 mouse. *J. Agric. Food Chem.* 61, 5037–5045. doi: 10.1021/jf3041484
- Sasaki, K., Othman, M. B., Ferdousi, F., Yoshida, M., Watanabe, M., Tominaga, K., et al. (2019a). Modulation of the neurotransmitter systems through the anti-inflammatory and antidepressant-like effects of squalene from *Aurantiochytrium* sp. *PLoS ONE* 14:e0218923. doi: 10.1371/journal.pone.0218923
- Sathasivam, R., Radhakrishnan, R., Hashem, A., and Abd Allah, E. F. (2019). Microalgae metabolites: A rich source for food and medicine. *Saudi J. Biol. Sci.* 26, 709–722. doi: 10.1016/j.sjbs.2017.11.003
- Scopa, C., Marrocco, F., Latina, V., Ruggeri, F., Corvaglia, V., La Regina, F., et al. (2020). Impaired adult neurogenesis is an early event in Alzheimer's disease neurodegeneration, mediated by intracellular A $\beta$  oligomers. *Cell Death Differ.* 27, 934–948. doi: 10.1038/s41418-019-0409-3
- Shinto, L., Quinn, J., Montine, T., Dodge, H. H., Woodward, W., Baldauf-Wagner, S., et al. (2014). A randomized placebo-controlled pilot trial of omega-3 fatty acids and alpha lipoic acid in Alzheimer's disease. *J. Alzheimers. Dis.* 38, 111–120. doi: 10.3233/JAD-130722
- Takahashi, S., Sakamaki, M., Ferdousi, F., Yoshida, M., Demura, M., Watanabe, M. M., et al. (2018). Ethanol extract of *aurantiochytrium mangrovei* 18W-13a strain possesses anti-inflammatory effects on murine macrophage RAW264 cells. *Front. Physiol.* 9:1205. doi: 10.3389/fphys.2018.01205
- Torroglosa, A., Murillo-Carretero, M., Romero-Grimaldi, C., Matarredona, E. R., Campos-Caro, A., and Estrada, C. (2007). Nitric oxide decreases subventricular zone stem cell proliferation by inhibition of epidermal growth factor receptor and phosphoinositide-3-kinase/Akt pathway. *Stem Cells* 25, 88–97. doi: 10.1634/stemcells.2006-0131
- Wang, H., Zhang, T., Ge, X., Chen, J., Zhao, Y., and Fu, J. (2020). Parkin overexpression attenuates A $\beta$ -induced mitochondrial dysfunction in HEK293 cells by restoring impaired mitophagy. *Life Sci.* 244:117322. doi: 10.1016/j.lfs.2020.117322
- Webers, A., Heneka, M. T., and Gleeson, P. A. (2020). The role of innate immune responses and neuroinflammation in amyloid accumulation and progression of Alzheimer's disease. *Immunol. Cell Biol.* 98, 28–41. doi: 10.1111/imcb.12301
- Xie, L., Kang, H., Xu, Q., Chen, M. J., Liao, Y., Thiagarajan, M., et al. (2013). Sleep drives metabolite clearance from the adult brain. *Science* 342, 373–377. doi: 10.1126/science.1241224

**Conflict of Interest:** The authors declare that the research was conducted in the absence of any commercial or financial relationships that could be construed as a potential conflict of interest.

Copyright © 2021 Sasaki, Geribaldi-Doldán, Wu, Davies, Szele and Isoda. This is an open-access article distributed under the terms of the Creative Commons Attribution License (CC BY). The use, distribution or reproduction in other forums is permitted, provided the original author(s) and the copyright owner(s) are credited and that the original publication in this journal is cited, in accordance with accepted academic practice. No use, distribution or reproduction is permitted which does not comply with these terms.



# Fraxinellone Has Anticancer Activity by Inducing Osteosarcoma Cell Apoptosis via Promoting Excessive Autophagy Flux

Bin He<sup>1,2,3,4\*</sup>, Wenkan Zhang<sup>1,2,3</sup> and Jiaming He<sup>1,2,3</sup>

<sup>1</sup>Department of Orthopedic Surgery, The Second Affiliated Hospital, Zhejiang University School of Medicine, Hangzhou, China, <sup>2</sup>The Second Affiliated Hospital, Zhejiang University School of medicine, Hangzhou, China, <sup>3</sup>Key Laboratory of Motor System Disease Research and Precision Therapy of Zhejiang Province, Hangzhou, China, <sup>4</sup>The Fourth Affiliated Hospital, Zhejiang University School of Medicine, Hangzhou, China

## OPEN ACCESS

### Edited by:

Kazunori Sasaki,  
National Institute of Advanced  
Industrial Science and Technology  
(AIST), Japan

### Reviewed by:

Hemlata Sukhija,  
City of Hope National Medical Center,  
United States  
Maen Abdelrahim,  
Houston Methodist Research Institute,  
United States

### \*Correspondence:

Bin He  
2316419@zju.edu.cn

### Specialty section:

This article was submitted to  
Pharmacology of Anti-Cancer Drugs,  
a section of the journal  
Frontiers in Pharmacology

**Received:** 14 January 2021

**Accepted:** 23 March 2021

**Published:** 19 April 2021

### Citation:

He B, Zhang W and He J (2021)  
Fraxinellone Has Anticancer Activity by  
Inducing Osteosarcoma Cell  
Apoptosis via Promoting Excessive  
Autophagy Flux.  
Front. Pharmacol. 12:653212.  
doi: 10.3389/fphar.2021.653212

Osteosarcoma is a malignant bone tumor that is easy to metastasize in the early stage and has a very poor prognosis. Fraxinellone (FRA) is one of the main components isolated from the *D. dasycarpus* plant. Its anti-inflammatory and neuroprotective effects have been confirmed, but the research on the anti-cancer effect of FRA and its potential mechanism is relatively scarce. In this study, we found that FRA inhibited the proliferation and migration of osteosarcoma cells HOS and MG63 in a dose-dependent manner. Immunofluorescence, fluorescence staining and western blotting analysis showed that FRA could simultaneously induce osteosarcoma cell apoptosis and increase autophagy flux. Subsequent turnaround experiments suggested that the pro-apoptotic effect of FRA was achieved through excessive autophagy flux. The results of the xenograft orthotopic model further supported the anti-cancer effects of FRA, indicating that FRA treatment inhibited the growth of osteosarcoma, and the pro-apoptotic and autophagy effects of FRA were also proved *in vivo*. These studies provide new ideas for the future treatment of osteosarcoma and offer theoretical support for the anti-cancer mechanism of FRA.

**Keywords:** fraxinellone, proliferation, cancer therapy, autophagy, apoptosis

## INTRODUCTION

Osteosarcoma is one of the most common primary bone malignancies that occurs in children and adolescents, even though its incidence is very low, about three per million (Ritter and Bielack, 2010; Anderson, 2016). The pathological feature is the presence of malignant mesenchymal cells that produce osteoid and immature bone, and metastasize to a distant place in the early stage of the disease. The most common metastatic organ is the lung (Lin et al., 2017; Tang et al., 2019). The 5-years survival rate of non-metastatic patients is about 60%, while the 5-years survival rate of metastatic patients is only 20–30% (Biazzo and De Paolis, 2016; Harrison et al., 2018). Micrometastasis in the lungs that existed before the surgical resection of the primary tumor is the most important factor for the poor prognosis of those metastatic patients (Moore and Luu, 2014).

**Abbreviations:** ATG, autophagy-related genes; DMEM, dulbecco's modified eagle's medium; FBS, fetal bovine serum; FRA, fraxinellone; HOS, human osteosarcoma cell lines MNNG/HOS; TEM, transmission electron microscopy.

At present, surgical treatment, neoadjuvant chemotherapy and postoperative adjuvant chemotherapy have improved the survival and prognosis of patients, but the survival rate of patients with osteosarcoma has not fundamentally changed, which has prompted us to develop novel treatment strategies (Isakoff et al., 2015).

*Dictamnus dasycarpus* is a traditional herbal medicine used to treat inflammatory diseases and has been used in Eastern countries such as Korea and China for thousands of years (Gu et al., 2011). According to recent studies, fraxinellone (FRA) is a limonin component isolated from *Dictamnus dasycarpus*. Compared with other ingredients, it is the main active ingredient with anti-inflammatory and neuroprotective affects (Jeong et al., 2010; Jung et al., 2018; Kim et al., 2019). In addition, studies have suggested that FRA has vasodilator activity (Kim et al., 2009). It is worth noting that the study found that FRA can down-regulate the STAT3 and HIF-1 $\alpha$  signaling pathways and inhibit the expression of PD-L1, thereby inhibiting cancer cell proliferation and reducing tumor angiogenesis (Xing et al., 2018). However, research on the anti-tumor effect of FRA is very rare. Considering that traditional Chinese medicine has shown good potential in clinical treatment in recent years, we want to explore whether it has anti-tumor activity against osteosarcoma.

A recent study revealed that FRA inhibits senescence via restoring the H<sub>2</sub>O<sub>2</sub>-impaired autophagic flux (Han et al., 2018). Autophagy, also known as type II cell death, is a process in which cells use lysosomes to degrade their damaged organelles and macromolecular substances under the control of autophagy-related genes (ATG) (Ravanan et al., 2017). Simply put, after the cell receives the autophagy-inducing signal, it forms a phagophore, and the phagophore continues to extend to absorb the components in the cytoplasm to form a spherical autophagosome. After the autophagosome is formed, it can fuse with the lysosome to become an autolysosome. After the inner membrane of the autophagosome is degraded by the lysosomal enzyme, the “cargo” in the autophagosome is also degraded, and the available product is transported to the cytoplasm. The residue is either discharged outside the cell or retained in the cytoplasm (Amaravadi et al., 2016; Yan et al., 2019). Autophagy plays an important role in cell metabolism, structural reconstruction, growth and development (Saha et al., 2018). The relationship between autophagy and tumors is very complicated and has not yet been fully elucidated. On the one hand, the enhancement of normal cell autophagy can exhibit the function of inhibiting tumorigenesis; on the other hand, tumor cells can also enhance cell autophagy to resist the stress response induced by hypoxia, metabolites, and therapeutic drugs (Onorati et al., 2018; Russo and Russo, 2018). In our current research, we have explored the regulatory effect of FRA on autophagy.

Cell death is a complex process regulated by the body. Apoptosis, as the first programmed cell death (PCD) program recognized, its role and regulatory network are relatively clear (Kaczanowski, 2016). In some cases, autophagy can inhibit apoptosis and is a survival way for cells to protect themselves. However, autophagy itself can also induce cell death, or it can be used as a backup mechanism to induce cell death in the absence of apoptosis. The two pathways are interrelated and regulate each

other (Mariño et al., 2014). Research and use of these interactions will help to further reveal the occurrence and development of tumors and other diseases.

In this study, we found that FRA inhibited the proliferation and migration of the two cell lines of osteosarcoma HOS and MG63. In addition, it could induce tumor cell apoptosis by promoting autophagy of osteosarcoma cells, thereby inhibiting tumor growth *in vivo* and *in vitro*.

## MATERIALS AND METHODS

### Cell Culture and Reagents

The human osteosarcoma cell lines MNNG/HOS (HOS) (CRL-1547TM, ATCC) and MG63 (CRL-1427TM, ATCC) were purchased from the Cell Bank of the Chinese Academy of Sciences (Shanghai, China). HOS and MG63 cells were cultured in Dulbecco's modified Eagle's medium (DMEM) with penicillin (100 units/ml)-streptomycin (100 units/ml) and 10% fetal bovine serum (FBS). The cells were incubated at 37°C in an environment with 1% O<sub>2</sub>, 94% N<sub>2</sub>, and 5% CO<sub>2</sub> at 37°C. FRA (Cat: 28808-62-0) were purchased from Sigma-Aldrich technology (St. Louis, MO, United States); The purity of FRA was >95% in HPLC analysis.

### Cell Proliferation Assays

The inhibitory effect of FRA on osteosarcoma cells was tested by CCK8 kit (Dojindo Laboratories, Kumamoto, Japan). The cells were seeded into 96-well plates, each with about 4,000 cells. After the cells adhered to the bottom of the well, we changed the medium and cultured osteosarcoma cells with various concentrations of FRA (0–320  $\mu$ M) for different periods of time (0–48 h). In order to verify the potential mechanism of FRA on autophagy, cells were treated with different concentrations of FRA and incubated with 3-MA (3 mM) or rapamycin (100 nM). Then, CCK8 reagent (10  $\mu$ l) was added to each well, and after incubating for 2 h, the absorbance was measured at 450 nm using a MR7000 microplate reader (Dynatech, NV, United States). We evaluated cell proliferation viability through colony formation experiments. The cells in the exponential growth phase were seeded into a 6-well plate and allowed to adhere, and the cell density per well was controlled to 500 cells. The cells were treated with different concentrations of FRA (0, 40, and 80  $\mu$ M) for 15 days. The colony was washed three times with 1x phosphate buffered saline (PBS), then fixed with paraformaldehyde for about 20 min, and stained with 0.1% crystal violet (Beyotime); Next, they were counted under a microscope and photographed. Count the number of colonies (>50 cells/colony).

### Cell Migration Analysis

A wound healing assay was used to detect the migration ability of two human osteosarcoma cell lines. When the cell proliferation in the 6-well plate reaches about 90% confluence, use a 10  $\mu$ l pipette tip to evenly scrape the cell layer to form a scratch. After that, gently wash three times with PBS to remove scraped cell debris. After adding serum-free medium, immediately photograph the

thickness of the scratch under the microscope. Then, culture with different conditions (control group, 40  $\mu$ M FRA group, 80  $\mu$ M FRA group). After 12 h of treatment, pictures of the cell scratches were taken again, and the wound area was analyzed using ImageJ software.

In addition, the classic transwell chamber (membrane with 8  $\mu$ m pore size, Corning Life Sciences, United States) was used to further evaluate the migration ability of tumor cells. Add 600  $\mu$ L treatment medium (control group, 40  $\mu$ M FRA group, 80  $\mu$ M FRA group) containing 10% FBS to the lower chamber.  $10^6$  cells were resuspended in 200  $\mu$ L of serum-free medium and then planted in the upper chamber. After incubating for 12 h, the cells were washed with PBS, then fixed with 4% paraformaldehyde for 30 min, and finally stained with 0.1% crystal violet for 10 min. Then, the cells in the upper layer of the chamber were wiped off with a cotton swab, the cells under the membrane were counted and photographed through an inverted microscope.

## Transmission Electron Microscope

Transmission electron microscopy (TEM) is a commonly used technique to observe the ultrastructure of cells (Harris, 2015). Through TEM, apoptotic bodies, nuclear condensation and autophagosomes can be clearly observed. Simply put, after the treated cells are fixed with 2.5% glutaraldehyde and 1% osmium acid, they are dehydrated with different concentrations of alcohol (30–100%), and then the cells are embedded in Epon to prepare ultrathin sections (70–90 nm) for observation under a transmission electron microscope.

## Cell Apoptosis Assays

Cell apoptosis was detected by flow cytometry and cells were stained using the reagent Annexin V-FITC/PI (Multi-Sciences, Hangzhou, Zhejiang, China). Cells were treated with different concentrations of FRA (0, 40 and 80  $\mu$ M) and 3-MA (3 mM) or rapamycin (100 nM) for 24 h. After washing with 1XPBS two times, cells were resuspended in binding buffer. One hundred microliters of cell suspension were incubated with 5  $\mu$ L annexin V FITC and 10  $\mu$ L PI for 30 min at normal temperature in the dark. Cells were then detected by a flow cytometer (FACSCalibur, BD, San Jose, CA, United States).

## Hoechst 33342 Stain

The morphological changes of apoptotic cells can be observed by Hoechst 33342 staining, such as nuclear shrinkage and nuclear lysis. After washed with PBS, the treated cells were incubated with Hoechst 33342 dye solution in the dark for about 15 min. Then, the morphological changes of apoptotic cells were observed under a wavelength of 365 nm by a fluorescence microscope (Olympus, Tokyo, Japan).

## Western Blotting

Collect all the cells that have undergone different treatments, and then wash them twice with PBS. According to the instructions, the cells were lysed with RIPA buffer (Sigma-Aldrich, St. Louis, Missouri, United States) containing a mixture of protease inhibitors and phosphatase inhibitors. After the protein supernatant is obtained, the protein concentration is measured

by BCA protein assay kit (Beyotime). The same amount of protein samples was electrophoresed by 8–15% SDS-PAGE at 80 V, and then the proteins were transferred to a polyvinylidene fluoride (PVDF) membrane (Millipore, Billerica, MA, United States) in a humid environment. The membrane was blocked with 5% nonfat milk (BSA; Sigma-Aldrich) and incubated with the primary antibody at 4°C overnight. Wash with TBST 3 times, after 10 min each time, then each membrane was incubated with anti-rabbit or anti-mouse IgG sheep antibody (Huabio, Hangzhou, Zhejiang, China) for 1 h at room temperature. Visualize the reactive protein using an enhanced chemiluminescence kit (Millipore). The details for the primary antibodies are as follows: Bcl-2 (1:2000, Cat: ab182858, ABCAM, MA, United States), Cleaved-caspase-3 (1:1000, Cat: 9664S, CST), Cleaved-caspase-7 (1:1000, Cat: 8438S, CST), Autophagy Antibody Sampler Kit (1:1000, Cat: 4445T, CST), Phospho-SQSTM1/p62 (1:1000, Cat: 16177S, CST). The secondary antibodies were as follows: goat anti-rabbit IgG-HRP (1:2000, Cat: 7074S, CST) and goat anti-mouse IgG-HRP (1:2000, Cat: 7076S, CST).

## MDC Staining

The cells with different treatments were collected, and washed twice by wash buffer, then counted and adjusted their concentration to  $10^6$ /ml. An appropriate amount of 90  $\mu$ L of cell suspension and 10  $\mu$ L of MDC stain were move into a new EP tube, and mixed gently, incubated at room temperature for 30 min in the dark. Then washing the cells twice with wash buffer and discarding the supernatant. Add 100  $\mu$ L of collection buffer to resuspend the cells, drop them onto a glass slide and add a cover glass. The cells were observed under a fluorescence microscope (excitation filter wavelength 355 nm, blocking filter wavelength 512 nm), counted and taken pictures.

## Turnaround Experiment

In order to verify that FRA indeed induces an increase in apoptosis by promoting autophagy of tumor cells, we incubated FRA-treated HOS and MG63 cells with autophagy inducer rapamycin (100 nM) or autophagy inhibitor 3-MA (3 mM). After incubating with rapamycin or 3-MA, the total protein is extracted.

The cytotoxicity in the turnover experiment was analyzed by CCK8 assay and flow cytometry. HOS and MG63 cells were seeded in 96-well plates ( $5 \times 10^3$  cells/well) and six-well plates ( $1 \times 10^5$  cells/well), respectively, and treated with the above conditions. Then conduct CCK8 test and flow cytometry to detect the rescue and aggravating effects of autophagy inhibitors or promoters.

## Immunofluorescence

Visually observe the expression intensity of related proteins in cells through immunofluorescence technology. The cells were treated with different concentrations of FRA (0, 80  $\mu$ M) for 24 h. Following the conventional method, the treated cells were fixed with 4% paraformaldehyde, permeabilized with 0.5% Triton X-100, blocked with 5% BSA, and incubated with the primary antibody overnight at 4°C. After the secondary antibody was



incubated for 1 h, the cells were observed and photographed under a fluorescence microscope.

### **In Vivo Xenograft Assay**

All experiments were carried out in accordance with the guidelines of the Ethics Committee of Zhejiang University and approved by the Research Ethics Committee of the Second Affiliated Hospital of Zhejiang University School of Medicine, China. All surgical procedures and applications on animals comply with IACUC guidelines. About  $2 \times 10^6$  stably transfected HOS cells [which have been transfected with luciferase (HOS-Luc) for *in vivo* imaging] were injected into the bone marrow cavity of the right tibia of a four-week-old nude mouse (Shanghai Experimental Animal Center, Chinese Academy of Sciences) (Sampson et al., 2013). After 7 days, those mice with too high or too low fluorescence intensity were eliminated, and then the remaining mice were randomly divided into three groups (three mice in each group). Starting from the seventh day, the FRA low-dose group received 50 mg/kg FRA per day by gavage, while the FRA high-dose group was given 100 mg/kg, and the mice in the control group received 200  $\mu$ L PBS per day. After 21 days of treatment, the luminescence intensity of each mouse was measured and recorded by *in vivo* fluorescence. The mice were anesthetized with chloral hydrate, and all mice were sacrificed by cervical dislocation. Then, the tibial tumor was resected, weighed, and fixed with 4% paraformaldehyde for subsequent histological analysis.

### **In Vivo Bioluminescence Assay**

After intraperitoneal injection of 200  $\mu$ L of fluorescein (100 mg/ml), the tumor-bearing mice were anesthetized with isoflurane inhalation. IVIS 200 imaging system was used for *in vivo* imaging, and Living Image Software (version 3.0.4, Xenogen, Hopkinton, MA, United States) was used to analyze the results.

### **Histology and Immunohistochemistry**

The tissue fixed in 4% formaldehyde was decalcified, embedded in paraffin, and cut into 4  $\mu$ m sections. The tumor tissue and other organ tissue sections were deparaffinized in xylene solution and stained with hematoxylin and eosin. According to the instructions of the IHC kit (Boster Bio, China), the tumor tissue sections were deparaffinized, rehydrated and immunostained. Then, sections were extracted in 0.01 M pH 6.0 citrate buffer using heat-induced epitopes. After the sections were washed with PBS and blocked with BSA, they were incubated with the primary antibody (cleaved-caspase 3, LC3B, P62) at 4°C overnight. Then, the sections were incubated with the secondary antibody (Huabio, China) for 1 h at room temperature, and then stained with the enzyme substrate 3',3'-diaminobenzidinetetrahy-drochloride (DAB, Huabio, China). The staining intensity of each section was scored by Image Pro Plus 6.0. Each part was independently analyzed by two pathologists.

After deparaffinization and hydration, the sections were incubated with proteinase K (20  $\mu$ g/ml) at 37°C for 30 min. Then the sections were blocked with 3% BAS and incubated with the primary antibody for 1 h at room temperature. Finally, the sections were incubated with the TUNEL reaction mixture, and after counterstaining, the sections were dehydrated and sealed, and then observed and photographed under a fluorescence microscope.

### **Statistical Analysis**

The results were expressed as the mean  $\pm$  standard deviation (SD). A comparison of the results was performed with one-way ANOVA and Student's t-test. All statistics were analyzed by IBM SPSS Statistics 20.0 software (IBM, Armonk, NY, United States). Statistically significant differences between groups were defined as  $p < 0.05$ .

## **RESULTS**

### **FRA Inhibits the Proliferation of HOS and MG63 Cells *In Vitro***

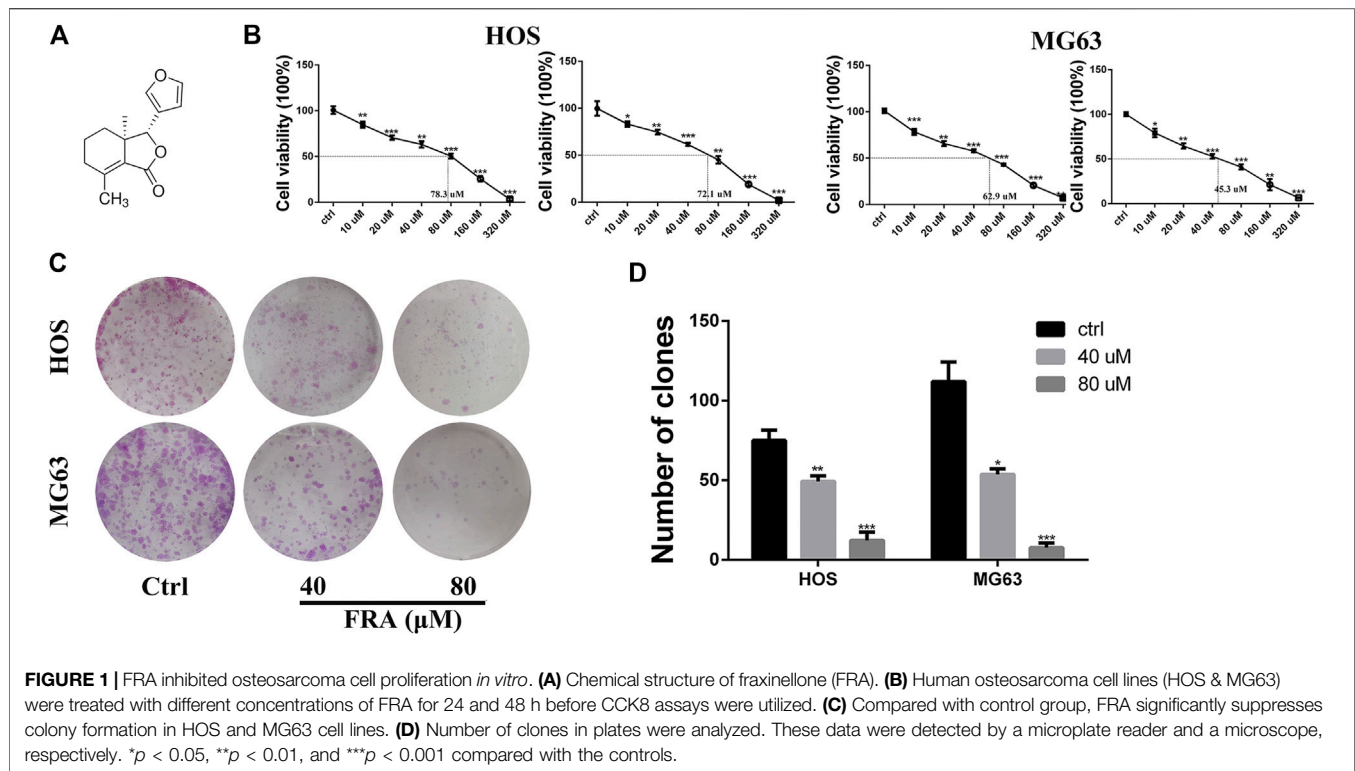
One of the main effects of FRA on human osteosarcoma cells HOS and MG63 is to inhibit cell proliferation. The CCK8 assay and colony formation assay were used to evaluate cell viability (Figure 1). The results (Figure 1B) showed that as the dose of FRA increased, the viability of tumor cells would be more and more significantly inhibited. According to the numerical analysis of absorbance, the IC<sub>50</sub> values of FRA in HOS cells is 78.3  $\mu$ M (24 h) and 72.1  $\mu$ M (48 h); while the IC<sub>50</sub> values in MG63 cells are 62.9  $\mu$ M (24 h) and 45.3  $\mu$ M (48 h). In addition, as shown in Figure 1C, the results of colony formation assay showed that FRA can inhibit the monoclonal proliferation of HOS and MG63 cells to form clumps. After 15 days, there were about  $450 \pm 23$  clonal clumps in the control group,  $279 \pm 12$  in the 40  $\mu$ M FRA group and  $63 \pm 5$  in the 80  $\mu$ M group (Figure 1D). The above results suggest that with the increase of FRA dose, the proliferation activity of the two types of osteosarcoma cells was significantly inhibited.

### **FRA Inhibits the Migration Ability of HOS and MG63 Cells *In Vitro***

Based on the results obtained before, we selected low-dose concentration of 40  $\mu$ M and high-dose concentration of 80  $\mu$ M FRA for follow-up studies, and performed the cell wound healing assay at 12 h. In Figure 2A, compared with the control group, FRA significantly blocked the cell recolonization in the wound area in the HOS and MG63 cell lines. As shown in Figure 2B, the presence of FRA resulted in a significant reduction in the number of cells covered by the scratched area, and the inhibitory effect of the high-dose group was more obvious. In addition, we have also obtained consistent phenomena through the transwell assay. Relatives to the control, FRA could reduce the migration of these two types of osteosarcoma cells to the lower membrane of the chamber (Figures 2C,D). These data indicated that FRA inhibited the migration of human osteosarcoma cells HOS and MG63 in a dose-dependent manner.

### **FRA Regulates Osteosarcoma Cell Autophagy and Apoptosis**

In addition to inhibiting cell migration, high concentrations of FRA can also induce apoptosis and autophagy. According to previous studies on FRA, the induction of apoptosis is its main anti-tumor effect. Therefore, we performed apoptosis-related



assays in two cell lines to evaluate its specific apoptosis effects. In **Figure 3A**, the simple Hoechst 33342 staining results suggested that FRA could promote the generation of apoptotic cells with nuclear shrinkage and highlight. Annexin V-FITC/PI flow cytometry assay further confirmed that FRA induced apoptosis of HOS and MG63 cells. In terms of specific data in **Figure 3B**, the apoptosis rate of FRA treatment group (HOS: 40 μM 21.19%, 80 μM 48.55%; MG63: 40 μM 31.17%, 80 μM 60.01%) was significantly higher than Control group (HOS: NC 5.68%; MG63: NC 8.22%). The expression of apoptosis-related proteins was examined by western blotting to verify the pro-apoptotic effect induced by FRA. As shown in the **Figure 3C**, whether in the HOS or MG63 cell line, after FRA treatment, the protein expression of cleaved-caspase 3 and cleaved-caspase 7 protein were significantly up-regulated, while the Bcl-2 protein expression was down-regulated. Finally, as one of the gold standards for apoptosis detection, we performed TEM observations and photographed those FRA-treated cells. The pictures under the microscope in **Figure 4A** indicated that compared with the control group, the FRA group could clearly see the shrinkage of nuclear chromosomes (red arrows). These results all indicate that FRA induces apoptosis of HOS and MG63 osteosarcoma cell lines *in vitro*.

What is interesting is that we found in the TEM images that there were typical autophagosomes (green arrows) in the cytoplasm of tumor cells after FRA treatment. Considering the complex relationship between autophagy and apoptosis, we subsequently explored the influence of FRA on the autophagy of osteosarcoma cells. MDC is a specific eosinophilic stain commonly used to detect autophagosome formation. In

**Figure 3E**, the results of MDC staining revealed that there were more autophagosomes in the FRA treatment group (green dots in the cytoplasm). In addition, the higher the concentration of FRA, the more dots in the cytoplasm and the higher the fluorescence intensity. Western blot and immunofluorescence were used to evaluate the autophagy regulation of FRA. As shown in **Figure 4D**, relative to the control group, after cells were treated with FRA, the ratio of LC3B-II/LC3B-I bands and the expression of ATG5 and beclin-1 protein increased significantly in a dose-dependent manner. The current study believes that P62 is a substrate involved in the degradation of autophagosomes (Moscat et al., 2016). In our research results, the expression of P62 protein will also increase with the appearance of FRA. Immunofluorescence staining also directly showed that the expression of Beclin-1 and P62 in FRA-treated cells increased. These results suggest that FRA can promote the formation of autophagosomes and accelerate its degradation, thereby increasing the autophagy flux of cells.

## FRA Induces Cell Apoptosis by Promoting Excessive Autophagy Flux

Then we explore the specific relationship between FRA-induced autophagy and apoptosis. Through the intervention of 100 nM rapamycin (autophagy promoter) and 3 mM 3-MA (autophagy inhibitor), we found that FRA promoted the apoptosis process of osteosarcoma cells by inducing autophagy flux. Results of western blot experiment showed that with the addition of rapamycin, FRA could further increase the apoptosis-related proteins, and flow cytometry detected more apoptotic cells. After adding the

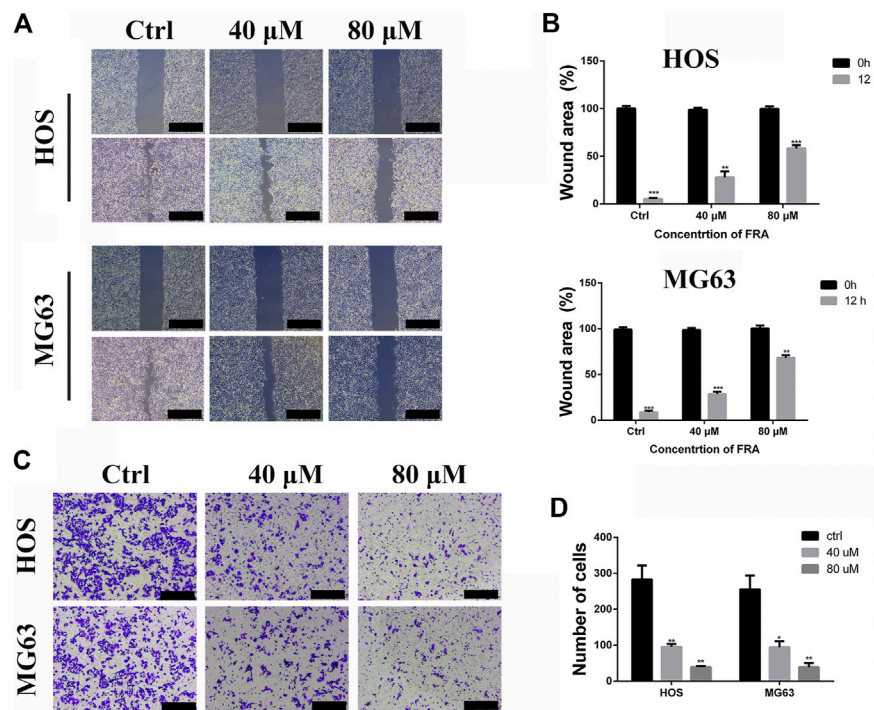


**FIGURE 2 |** FRA inhibits osteosarcoma cell migration *in vitro*. **(A)** The HOS and MG63 osteosarcoma cell lines were incubated with various doses of FRA (0; 40  $\mu$ M; 80  $\mu$ M) for 12 h, and photographs taken at 0 and 12 h were statistically analyzed by Image J software. The results of wound-healing assay showed that FRA significantly blocked the cell recolonization in the wound area in the HOS and MG63 cell lines. **(C)** In the transwell assay under the same conditions, the number of cells in the FRA treatment group was significantly lower than that of the control group, and the number of cells in the high dose was less than that in the low dose. Percentages of wound area **(B)** and number of clones **(D)** in the lower membrane were counted. Error bar = mean  $\pm$  SEM of at least triplicate experiments. Magnification,  $\times 40$  **(A)**,  $\times 100$  **(C)**. Scale bar, 500  $\mu$ m **(A)**, 200  $\mu$ m **(C)**. \* $p < 0.05$ , \*\* $p < 0.01$ , \*\*\* $p < 0.001$ , # $p < 0.0001$ .

autophagy blocker 3-MA, the pro-apoptotic effect of FRA was obviously inhibited (Figures 4B,D). In Figure 4C, the expression of these proteins that shown in figure B were analyzed. The above experimental results verified our hypothesis that FRA caused apoptosis through excessive autophagy flux.

### FRA Hinders Tumor Growth *In Vivo*

The last part of this research was to explore the anti-tumor effect of FRA *in vivo*. We followed the conventional modeling method, that is, injecting the HOS cell, stably transfected with luciferase, into the tibia marrow cavity of nude mice. As shown in Figure 5A, the level of fluorescence intensity meant the size of the tumor in mice. Compared with the control group, the fluorescence intensity of the FRA treatment group was significantly weaker, and the tumor intensity of the high-dose group was lower than that of the low-dose group. The pictures of Figures 5B,C intuitively showed that after 21 days of FRA treatment, there were differences in tumor size and weight between the FRA-treatment group and the control group, as well as the high and low dose groups. These data indicated that FRA exhibited a good anti-tumor ability *in vivo*. The subsequent histopathological examinations include TUNEL, H&E staining and immunohistochemistry. TUNEL and H&E confirmed that there were more dead cells in the tumor sections of the FRA treatment group (Figure 5D). As shown in Figure 5E,

immunohistochemical quantitative analysis showed that the expression levels of cleaved-caspase 3, LC3B, and P62 in the FRA group were higher than those in the control group, which indicated that FRA also induced autophagy and apoptosis of osteosarcoma *in vivo*. In addition, as shown in Figure 5F, the vital organs of mice (including the heart, liver, spleen, lungs and kidneys) did not show significant toxicity throughout the experimental. All in all, FRA inhibits the growth of osteosarcoma *in vivo*, induces autophagy pathway and promotes apoptosis.

### DISCUSSION

Osteosarcoma is one of the most common primary malignant bone tumors in the world, which mainly occurs in children and adolescents (Simpson et al., 2017). Different subtypes or grades of cancer cells lead to different treatment options for patients with osteosarcoma. For patients with low or moderate grade osteosarcoma, extensive resection is the main treatment. However, patients with high-grade osteosarcoma often require multiple treatments, including surgery, radiation therapy or chemotherapy (Bishop et al., 2016). Although surgery and chemotherapy have increased the disease-free survival rate to more than 60%, many patients still suffer from poor clinical

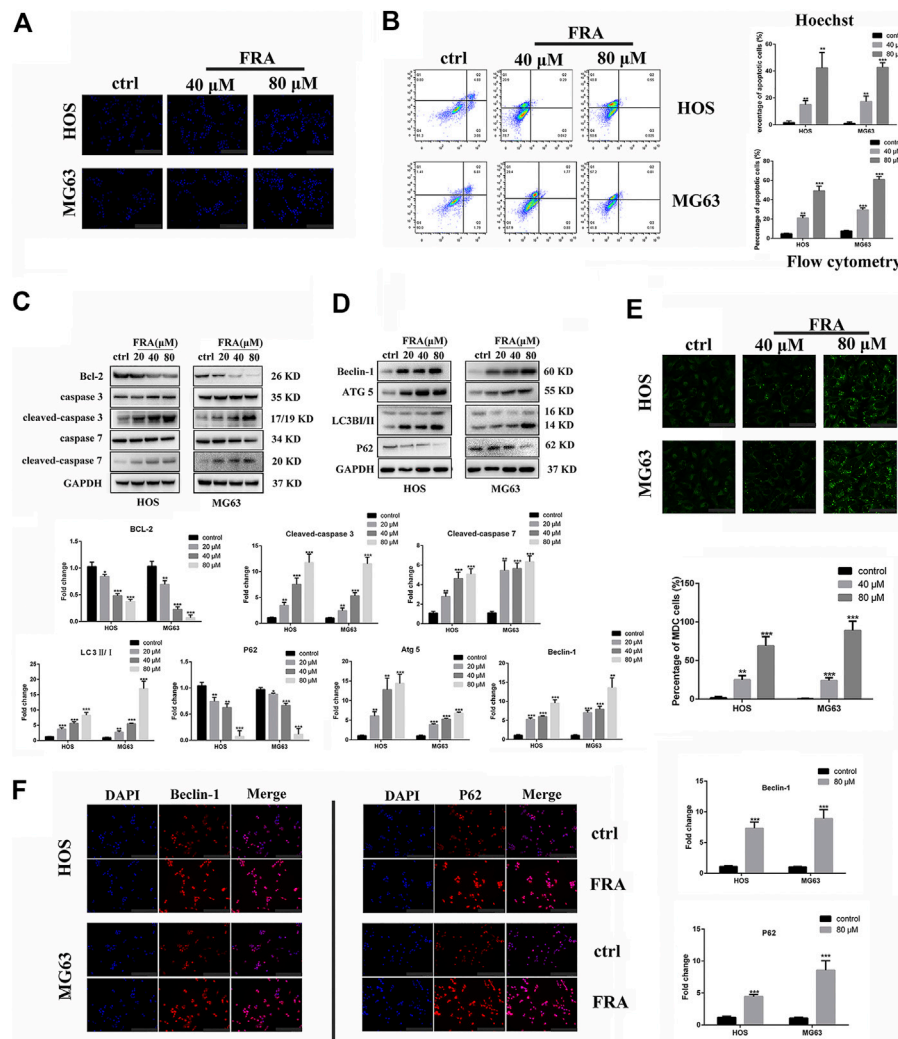


**FIGURE 3 |** FRA induces autophagy and apoptosis of osteosarcoma cells *in vitro*. **(A)** Cells treated with different conditions were stained with Hoechst 33342, and results showed that the percentage of apoptotic cells in the FRA group was higher than in the control group. The highlight dots mean apoptotic cells. **(B)** After staining with an Annexin FITC/PI kit, the treated cells were tested by flow cytometry. The results indicated that the percent of total apoptotic cells significantly increased in the FRA-treated group in a dose manner. **(C)** The expression of the following apoptosis-related proteins was determined by Western blot analysis: Bcl-2, cleaved-caspase 3, caspase-3, cleaved-caspase 7, and caspase 7. **(D)** The expression of those autophagy-related proteins: Beclin-1, ATG5, LC3B and P62. **(E)** Cells treated with different conditions were stained with MDC, and results showed that the number of autophagosome in the FRA group was higher than in the control group. The green dots mean autophagosome. **(F)** The HOS and MG63 osteosarcoma cell lines were incubated with FRA (80  $\mu$ M) or control for 24 h. The expression level of the Beclin-1 and P62 were significantly increased after FRA treatment detected via immunofluorescence assays. Each assay was repeated three times. Magnification,  $\times 200$  **(A)**,  $\times 1000$  **(D)**,  $\times 200$  **(F)**. Scale bar, 100  $\mu$ m **(A)**, 20  $\mu$ m **(E)**, 100  $\mu$ m **(F)**. Error bar = mean  $\pm$  SD of at least triplicate experiments. \* $p < 0.05$ , \*\* $p < 0.01$ , \*\*\* $p < 0.001$  versus control.

outcomes, such as high recurrence rate, low survival rate of patients after cancer metastasis (Meazza and Scanagatta, 2016). Although many large-scale clinical trials have been conducted to adjust the dose of chemotherapy or combined with immunotherapy to improve the prognosis, the survival rate of patients with osteosarcoma metastasis has not been significantly improved (Kansara et al., 2014). Considering that traditional Chinese medicine has demonstrated various anti-tumor effects and mechanisms in the past few thousand years, we explored the anti-osteosarcoma effects of FRA in this study. Our study found

that FRA can inhibit the proliferation and migration of osteosarcoma cell lines HOS and MG63 *in vitro*.

Fraxinellone (FRA) is a degradable limonin isolated from the root bark of the *Dictamnus* plant, which has relatively strong insecticidal activity (Bailly and Vergoten, 2020). In addition, the natural product also has anti-inflammatory and immunomodulatory effects (Lei et al., 2020). Recent studies have shown that it can induce the downregulation of the TGF $\beta$  signal transduction pathway to inactivate cancer-related fibroblasts, and cause a decrease in the number of M2



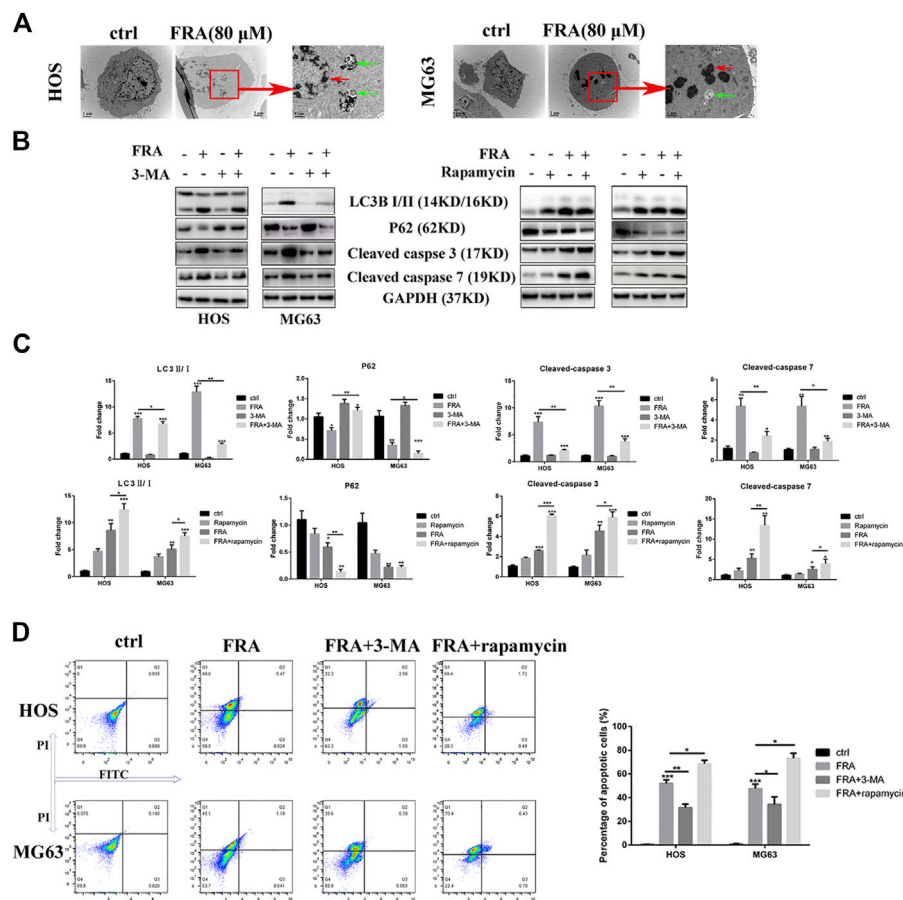


**FIGURE 4 |** FRA induces cell apoptosis by promoting excessive autophagy flux. **(A)** Transmission electron microscopy (TEM) shows the morphological changes in cells induced treated with FRA. The red arrows mean apoptotic bodies and nuclear condensation. The green arrows mean autophagosomes. Magnification,  $\times 10,000$ , Scale bar, 2  $\mu\text{m}$ . HOS and MG63 cells were treated with or without FRA (8  $\mu\text{M}$ ), with or without 3-MA (3 mM), or with or without rapamycin (100 nM) for 24 h. **(B)** The protein expressions of LC3B, p62, cleaved-caspase 3 and cleaved-caspase 7 were measured by Western blotting. **(C)** The corresponding histogram statistics of these proteins. Each assay was repeated three times. **(D)** The cells after different treatments were stained with the Annexin FITC/PI kit, and then the percentage of apoptotic cells was detected by flow cytometry. Error bar = mean  $\pm$  SD. \* $p < 0.05$ , \*\* $p < 0.01$ , \*\*\* $p < 0.001$  versus control.

macrophages *in vivo* and *in vitro*, thereby inducing remodeling of the tumor microenvironment (Hou et al., 2018). In this research, we want to explore whether it has a direct killing effect on tumor cells. Recently, studies on the premature senescence model induced by  $\text{H}_2\text{O}_2$  have explored the effect of FRA on senescence inhibition, and proved that the activation of AMPK signaling pathway and autophagy play a role in this process. And it is proposed that FRA can be considered as a new drug with potential anti-aging drugs (Kim et al., 2009).

Autophagy is an extremely complex biological behavior, and its role in tumors such as osteosarcoma is also contradictory (Ravanan et al., 2017). In the initial stage of tumorigenesis, autophagy is proposed to have anti-tumor effects. The specific mechanism is to inhibit the occurrence of chromosomal mutations, reduce oxidative stress, and induce autophagy cell death to prevent distant metastasis. In the later stages of tumorigenesis, autophagy maintains tumor cell homeostasis by various means to promote cancer progression or tumor metastasis to act as a tumor activator (Shibutani et al., 2015;

Huang et al., 2018). In the current study, we investigated the potential role of FRA in the regulation of autophagy and found that the application of FRA can enhance autophagy in osteosarcoma cells. In addition to autophagy, FRA also significantly promotes the apoptosis of osteosarcoma cells, and this effect is dose-dependent. Further studies have shown that the use of chloroquine to inhibit autophagy activation can promote cell apoptosis. The presence of autophagy inhibitors can weaken the pro-apoptotic effect of FRA. The pro-autophagy effect of FRA we inferred is consistent with previous research conclusions of others (Han et al., 2018). Moreover, excessive autophagy can promote tumor cell apoptosis is also a generally accepted research conclusion, which may be because a single protein that plays an important role in autophagy may have other roles in pro-apoptotic signal transduction (Mariño et al., 2014). At present, the potential of autophagy regulation in the treatment of tumors and other diseases is confusing due to the complex interaction with apoptosis. A comprehensive understanding of the interaction between autophagy and apoptosis and the

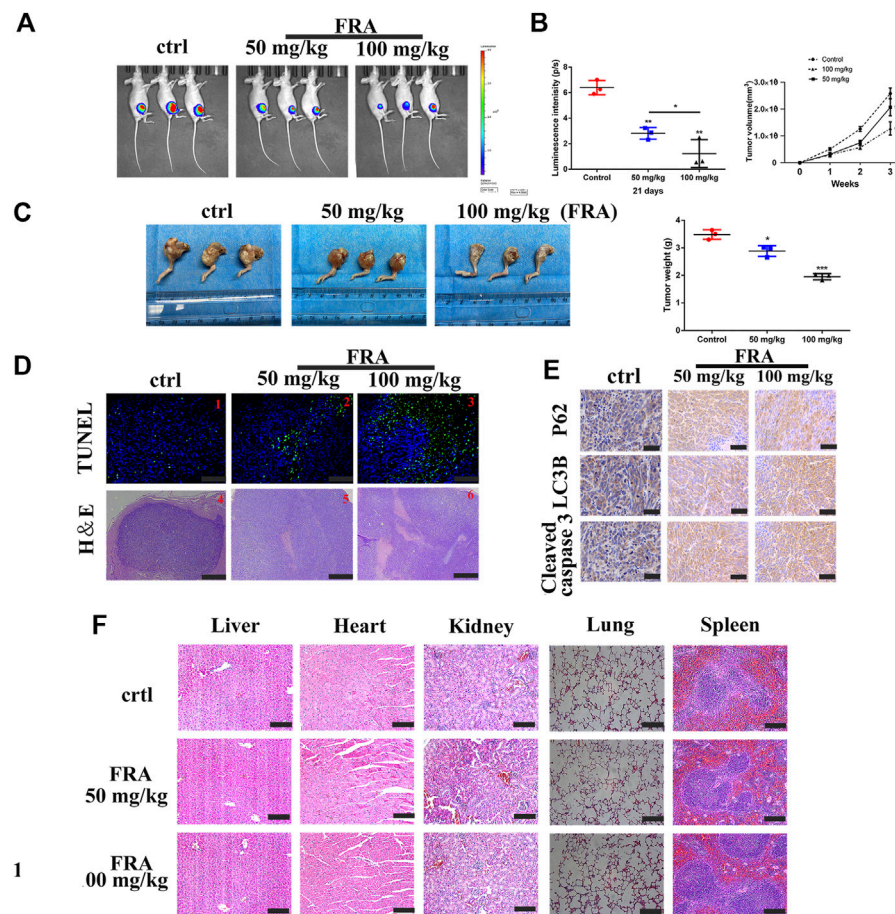


**FIGURE 5 |** FRA hinders osteosarcoma growth *in vivo*. **(A)** After 21 days of FRA treatment, luciferase intensity of tumor was measured and calculated by an *in vivo* imaging system. **(B)** The luciferase intensity of tumor was analyzed. The curves of tumor volume showed a significant difference among the groups after 3 weeks administration of FRA. **(C)** The photographs show that there was a significant difference in tumor weights between the three groups after 21 days. **(D)** TUNEL assays were used to measure the apoptotic status of tumor tissues. FRA promoted extensive tumor cell necrosis was proved by H&E staining. **(E)** The levels of LC3B, P62 and cleaved-caspase 3 were further examined by immunohistochemistry. **(F)** The vital organs of mice (including the heart, liver, spleen, lungs and kidneys) did not show significant toxicity throughout the experimental. Error bar = mean  $\pm$  SEM. Magnification,  $\times 200$  (D1–3),  $\times 40$  (D4–6),  $\times 400$  (E). Scale bar, 100  $\mu$ m (D1–3), 500  $\mu$ m (D4–6), 50  $\mu$ m (E). Error bar = mean  $\pm$  SD. \* $p < 0.05$ , \*\* $p < 0.01$ .

molecular mechanism is the main challenge for current research (Maiuri et al., 2007; Kaminsky and Zhivotovsky, 2014). Unfortunately, in our research, we did not find an important protein target between the two after the application of FRA. Moreover, considering the cost and time cost, we did not explore the important signal pathways between the two, such as P53/DAPK/BH3 only proteins.

Previous reports have confirmed the anti-inflammatory and neuroprotective effects of FRA *in vivo* (Hou et al., 2018; Bailly and Vergoten, 2020; Lei et al., 2020). However, there are few studies on the anti-tumor effects of FRA. We described the autophagy and apoptosis regulation effects of FRA on osteosarcoma cells for the first time, and confirmed that FRA can inhibit tumor growth *in vivo*. Based on the results of previous studies (Xing et al., 2018), we chose 30 mg/kg and 100 mg/kg for *in vivo* research. However, the results suggested that the dose of 30 mg/kg did not exhibit a significant tumor

suppressor effect, so we considered 50 mg/kg as the low dose and 100 mg/kg as the high dose. The tumor size and weight of the FRA treatment group were significantly lower than those of the control group, and the tumors of the high-dose group did not protrude from the muscle layer of the mice. In addition, during our experiment, no side effects of using FRA (loss of appetite, blood in the stool, lethargy, etc.) were observed, and no obvious necrosis was observed in the HE staining of important organ sections, which indicates that FRA is safe. Unfortunately, at the end of the experiment, we did not find any metastases in the lungs of any mouse (referring to osteosarcoma is the most prone to lung metastasis, so we focus on the lungs). We found that the presence of FRA can enhance the sensitivity of mice to the chemotherapy drug cisplatin, thereby enhancing its anti-tumor effect. And this effect may be related to PD-L1 and macrophages. Our research lays the first step for the follow-up anti-tumor

application of FRA, and also provides theoretical support for other research. This result makes it impossible for us to resolve whether FRA It can inhibit the metastasis of osteosarcoma. These results indicate that FRA may be a promising anti-osteosarcoma drug, because FRA can inhibit the growth of osteosarcoma and has biological safety.

In short, FRA can inhibit the proliferation and migration of osteosarcoma, and also promote apoptosis by inducing autophagic flux. In addition, FRA shows good anti-tumor activity and has no obvious side effects. Our results provide a potential direction for traditional Chinese medicine in the treatment of osteosarcoma.

## DATA AVAILABILITY STATEMENT

The original contributions presented in the study are included in the article/Supplementary Material, further inquiries can be directed to the corresponding author.

## REFERENCES

- Amaravadi, R., Kimmelman, A. C., and White, E. (2016). Recent insights into the function of autophagy in cancer. *Genes Dev.* 30, 1913–1930. doi:10.1101/gad.287524.116
- Anderson, M. E. (2016). Update on survival in osteosarcoma. *Orthop. Clin. North America* 47, 283–292. doi:10.1016/j.ocln.2015.08.022
- Bailly, C., and Vergoten, G. (2020). Fraxinellone: from pesticidal control to cancer treatment. *Pestic. Biochem. Physiol.* 168, 104624. doi:10.1016/j.pestbp.2020.104624
- Biazzo, A., and De Paolis, M. (2016). Multidisciplinary approach to osteosarcoma. *Acta Orthop. Belg.* 82, 690–698.
- Bishop, M. W., Janeway, K. A., and Gorlick, R. (2016). Future directions in the treatment of osteosarcoma. *Curr. Opin. Pediatr.* 28, 26–33. doi:10.1097/mop.0000000000000298
- Gu, H.-M., Xu, H., Zhong, Z.-Z., Zhu, H.-L., and Li, Q.-S. (2011). Fraxinellone. *Acta Cryst. E* 67, o1472. doi:10.1107/s1600536811018393
- Han, X., Chen, H., Zhou, J., Tai, H., Gong, H., Wang, X., et al. (2018). The inhibitory effect in Fraxinellone on oxidative stress-induced senescence correlates with AMP-activated protein kinase-dependent autophagy restoration. *J. Cel Physiol* 233, 3945–3954. doi:10.1002/jcp.26169
- Harris, J. R. (2015). Transmission electron microscopy in molecular structural biology: a historical survey. *Arch. Biochem. Biophys.* 581, 3–18. doi:10.1016/j.abb.2014.11.011
- Harrison, D. J., Geller, D. S., Gill, J. D., Lewis, V. O., and Gorlick, R. (2018). Current and future therapeutic approaches for osteosarcoma. *Expert Rev. anticancer Ther.* 18, 39–50. doi:10.1080/14737140.2018.1413939
- Hou, L., Liu, Q., Shen, L., Liu, Y., Zhang, X., Chen, F., et al. (2018). Nano-delivery of fraxinellone remodels tumor microenvironment and facilitates therapeutic vaccination in desmoplastic melanoma. *Theranostics* 8, 3781–3796. doi:10.7150/thno.24821
- Huang, T., Song, X., Yang, Y., Wan, X., Alvarez, A. A., Sastry, N., et al. (2018). Autophagy and hallmarks of cancer. *Crit. Rev. Oncog* 23, 247–267. doi:10.1615/critrevoncog.2018027913
- Isakoff, M. S., Bielack, S. S., Meltzer, P., and Gorlick, R. (2015). Osteosarcoma: current treatment and a collaborative pathway to success. *Jco* 33, 3029–3035. doi:10.1200/jco.2014.59.4895
- Jeong, G.-S., Byun, E., Li, B., Lee, D.-S., An, R.-B., and Kim, Y.-C. (2010). Neuroprotective effects of constituents of the root bark of *Dictamnus dasycarpus* in mouse hippocampal cells. *Arch. Pharm. Res.* 33, 1269–1275. doi:10.1007/s12272-010-0818-9
- Jung, S. M., Lee, J., Baek, S. Y., Lee, J., Jang, S. G., Hong, S.-M., et al. (2018). Fraxinellone attenuates rheumatoid inflammation in mice. *Int. J. Mol. Sci.* 19(3):829. doi:10.3390/ijms19030829
- Kaczanowski, S. (2016). Apoptosis: its origin, history, maintenance and the medical implications for cancer and aging. *Phys. Biol.* 13, 031001. doi:10.1088/1478-3975/13/3/031001
- Kaminsky, V. O., and Zhivotovsky, B. (2014). Free radicals in cross talk between autophagy and apoptosis. *Antioxid. Redox Signaling* 21, 86–102. doi:10.1089/ars.2013.5746
- Kansara, M., Teng, M. W., Smyth, M. J., and Thomas, D. M. (2014). Translational biology of osteosarcoma. *Nat. Rev. Cancer* 14, 722–735. doi:10.1038/nrc3838
- Kim, J.-H., Park, Y.-M., Shin, J.-S., Park, S. J., Choi, J.-H., Jung, H.-J., et al. (2009). Fraxinellone inhibits lipopolysaccharide-induced inducible nitric oxide synthase and cyclooxygenase-2 expression by negatively regulating nuclear factor-kappa B in RAW 264.7 macrophages cells. *Biol. Pharm. Bull.* 32, 1062–1068. doi:10.1248/bpb.32.1062
- Kim, M.-J., Bae, G.-S., Jo, I.-J., Choi, S.-B., Kim, D.-G., Jung, H.-J., et al. (2019). Fraxinellone inhibits inflammatory cell infiltration during acute pancreatitis by suppressing inflammasome activation. *Int. immunopharmacology* 69, 169–177. doi:10.1016/j.intimp.2019.01.043
- Lei, J., Gou, X., Wei, S., Zhou, J., and Li, Z. (2020). Spectroscopy, thermodynamics and molecular docking of fraxinellone with DNA. *Bull. Environ. Contam. Toxicol.* 104, 864–870. doi:10.1007/s00128-020-02860-7
- Lin, Y.-H., Jewell, B. E., Gingold, J., Lu, L., Zhao, R., Wang, L. L., et al. (2017). Osteosarcoma: molecular pathogenesis and iPSC modeling. *Trends Molecular Medicine* 23, 737–755. doi:10.1016/j.molmed.2017.06.004
- Maiuri, M. C., Zalckvar, E., Kimchi, A., and Kroemer, G. (2007). Self-eating and self-killing: crosstalk between autophagy and apoptosis. *Nat. Rev. Mol. Cel Biol* 8, 741–752. doi:10.1038/nrm2239
- Mariño, G., Niso-Santano, M., Baehrecke, E. H., and Kroemer, G. (2014). Self-consumption: the interplay of autophagy and apoptosis. *Nat. Rev. Mol. Cel Biol* 15, 81–94. doi:10.1038/nrm3735
- Meazza, C., and Scanagatta, P. (2016). Metastatic osteosarcoma: a challenging multidisciplinary treatment. *Expert Rev. anticancer Ther.* 16, 543–556. doi:10.1586/14737140.2016.1168697
- Moore, D. D., and Luu, H. H. (2014). Osteosarcoma. *Osteosarcoma. Cancer Treatment Research* 162, 65–92. doi:10.1007/978-3-319-07323-1\_4
- Moscat, J., Karin, M., and Diaz-Meco, M. T. (2016). p62 in cancer: signaling adaptor beyond autophagy. *Cell* 167, 606–609. doi:10.1016/j.cell.2016.09.030
- Onorati, A. V., Dyczynski, M., Ojha, R., and Amaravadi, R. K. (2018). Targeting autophagy in cancer. *Cancer* 124, 3307–3318. doi:10.1002/cncr.31335
- Ravanan, P., Srikumar, I. F., and Talwar, P. (2017). Autophagy: the spotlight for cellular stress responses. *Life Sci.* 188, 53–67. doi:10.1016/j.lfs.2017.08.029
- Ritter, J., and Bielack, S. S. (2010). Osteosarcoma. *Ann. Oncol.* 21 (Suppl. 7), vii320–vii325. doi:10.1093/annonc/mdq276

## ETHICS STATEMENT

All experiments were carried out in accordance with the guidelines of the Ethics Committee of Zhejiang University and approved by the Research Ethics Committee of the Second Affiliated Hospital of Zhejiang University School of Medicine, China.

## AUTHOR CONTRIBUTIONS

All authors listed have made a substantial, direct, and intellectual contribution to the work and approved it for publication.

## FUNDING

This study was supported by grants from the National Natural Science Foundation of China (No. 81872173; No. 82072959).

- Russo, M., and Russo, G. L. (2018). Autophagy inducers in cancer. *Biochem. Pharmacol.* 153, 51–61. doi:10.1016/j.bcp.2018.02.007
- Saha, S., Panigrahi, D. P., Patil, S., and Bhutia, S. K. (2018). Autophagy in health and disease: a comprehensive review. *Biomed. Pharmacother.* 104, 485–495. doi:10.1016/j.biopha.2018.05.007
- Sampson, V. B., Kamara, D. F., and Kolb, E. A. (2013). Xenograft and genetically engineered mouse model systems of osteosarcoma and Ewing's sarcoma: tumor models for cancer drug discovery. *Expert Opin. Drug Discov.* 8, 1181–1189. doi:10.1517/17460441.2013.817988
- Shibutani, S. T., Saitoh, T., Nowag, H., Münz, C., and Yoshimori, T. (2015). Autophagy and autophagy-related proteins in the immune system. *Nat. Immunol.* 16, 1014–1024. doi:10.1038/ni.3273
- Simpson, S., Dunning, M. D., de Brot, S., Grau-Roma, L., Mongan, N. P., and Rutland, C. S. (2017). Comparative review of human and canine osteosarcoma: morphology. *Epidemiol. prognosis. Treat. Genet.* 59, 71. doi:10.1186/s13028-017-0341-9
- Tang, H., Tang, Z., Jiang, Y., Wei, W., and Lu, J. (2019). Pathological and therapeutic aspects of matrix metalloproteinases: implications in osteosarcoma. *Asia Pac. J. Clin. Oncol.* 15, 218–224. doi:10.1111/ajco.13165
- Xing, Y., Mi, C., Wang, Z., Zhang, Z. H., Li, M. Y., Zuo, H. X., et al. (2018). Fraxinellone has anticancer activity *in vivo* by inhibiting programmed cell death-ligand 1 expression by reducing hypoxia-inducible factor-1 $\alpha$  and STAT3. *Pharmacol. Res.* 135, 166–180. doi:10.1016/j.phrs.2018.08.004
- Yan, X., Zhou, R., and Ma, Z. (2019). Autophagy-cell survival and death. *Adv. Exp. Med. Biol.* 1206, 667–696. doi:10.1007/978-981-15-0602-4\_29

**Conflict of Interest:** The authors declare that the research was conducted in the absence of any commercial or financial relationships that could be construed as a potential conflict of interest.

Copyright © 2021 He, Zhang and He. This is an open-access article distributed under the terms of the Creative Commons Attribution License (CC BY). The use, distribution or reproduction in other forums is permitted, provided the original author(s) and the copyright owner(s) are credited and that the original publication in this journal is cited, in accordance with accepted academic practice. No use, distribution or reproduction is permitted which does not comply with these terms.





# Luteolin Modulates Neural Stem Cells Fate Determination: *In vitro* Study on Human Neural Stem Cells, and *in vivo* Study on LPS-Induced Depression Mice Model

Mariem Achour<sup>1,2</sup>, Farhana Ferdousi<sup>2,3,4</sup>, Kazunori Sasaki<sup>2,4</sup> and Hiroko Isoda<sup>2,3,4\*</sup>

<sup>1</sup> Laboratory of Metabolic Biophysics and Applied Pharmacology, Faculty of Medicine of Sousse, University of Sousse, Sousse, Tunisia, <sup>2</sup> Alliance for Research on the Mediterranean and North Africa (ARENA), University of Tsukuba, Tsukuba, Japan, <sup>3</sup> Faculty of Life and Environmental Sciences, University of Tsukuba, Tsukuba, Japan, <sup>4</sup> National Institute of Advanced Industrial Science and Technology (AIST)-University of Tsukuba Open Innovation Laboratory for Food and Medicinal Resource Engineering (FoodMed-OIL), University of Tsukuba, Tsukuba, Japan

## OPEN ACCESS

### Edited by:

Lei Ye,

National Heart Centre Singapore,  
Singapore

### Reviewed by:

Bingli Liu,

Nanjing Medical University, China

Mark Denham,

Aarhus University, Denmark

### \*Correspondence:

Hiroko Isoda

isoda.hiroko.ga@u.tsukuba.ac.jp

### Specialty section:

This article was submitted to  
Stem Cell Research,  
a section of the journal  
*Frontiers in Cell and Developmental  
Biology*

**Received:** 04 August 2021

**Accepted:** 11 October 2021

**Published:** 01 November 2021

### Citation:

Achour M, Ferdousi F, Sasaki K  
and Isoda H (2021) Luteolin  
Modulates Neural Stem Cells Fate  
Determination: *In vitro* Study on  
Human Neural Stem Cells, and *in vivo*  
Study on LPS-Induced Depression  
Mice Model.  
*Front. Cell Dev. Biol.* 9:753279.  
doi: 10.3389/fcell.2021.753279

Luteolin is a natural flavone with neurotrophic effects observed on different neuronal cell lines. In the present study, we aimed to assess the effect of luteolin on hNSCs fate determination and the LPS-induced neuroinflammation in a mouse model of depression with astrocytogenesis defect. hNSCs were cultured in basal cell culture medium (control) or medium supplemented with luteolin or AICAR, a known inducer of astrogenesis. A whole-genome transcriptomic analysis showed that luteolin upregulated the expressions of genes related to neurotrophin, dopaminergic, hippo, and Wnt signaling pathways, and downregulated the genes involved in p53, TNF, FOXO, and Notch signaling pathways. We also found that astrocyte-specific gene GFAP, as well as other genes of the key signaling pathways involved in astrogenesis such as Wnt, BMP, and JAK-STAT pathways were upregulated in luteolin-treated hNSCs. On the other hand, neurogenesis and oligodendrogenesis-related genes, *TUBB3*, *NEUROD 1* and *6*, and *MBP*, were downregulated in luteolin-treated hNSCs. Furthermore, immunostaining showed that percentages of GFAP+ cells were significantly higher in luteolin- and AICAR-treated hNSCs compared to control hNSCs. Additionally, RT-qPCR results showed that luteolin upregulated the expressions of *GFAP*, *BMP2*, and *STAT3*, whereas the expression of *TUBB3* remained unchanged. Next, we evaluated the effects of luteolin in LPS-induced mice model of depression that represents defects in astrocytogenesis. We found that oral administration of luteolin (10 mg/Kg) for eight consecutive days could decrease the immobility time on tail suspension test, a mouse behavioral test measuring depression-like behavior, and attenuate LPS-induced inflammatory responses by significantly decreasing IL-6 production in mice brain-derived astrocytes and serum, and TNF $\alpha$  and corticosterone levels in serum. Luteolin treatment also significantly increased mature BDNF, dopamine, and noradrenaline levels in the hypothalamus of LPS-induced depression mice. Though the behavioral effects of luteolin did not reach statistical significance, global gene expression analyses of mice hippocampus and brain-derived NSCs highlighted the modulatory effects of luteolin on

different signaling pathways involved in the pathophysiology of depression. Altogether, our findings suggest an astrocytogenic potential of luteolin and its possible therapeutic benefits in neuroinflammatory and neurodegenerative diseases. However, further studies are required to identify the specific mechanism of action of luteolin.

**Keywords:** luteolin, human neural stem cells, stem cell differentiation, astrogenesis, AICAR, LPS-induced depression model, NSCs isolation, astrocyte isolation

## INTRODUCTION

Neural stem cells (NSCs) are self-renewal cells that can be differentiated into neurons or glial cells following neurogenesis and gliogenesis processes, respectively (Apple et al., 2017). For most of the 20th century, it was believed that neurogenesis is restricted to a limited period during development and ceased shortly after birth (Cajal, 1930; Ming and Song, 2011; Taverna et al., 2014; Apple et al., 2017). However, Eriksson et al., have shown that neurogenesis is a life-long continuous process in almost all mammals, including humans (Eriksson et al., 1998). Peng et al. have determined that adult neurogenesis occurs in three different regions of human and mouse brain, namely the subventricular zone, the striatum and the hippocampus (Peng and Bonaguidi, 2018). Recent evidence pointed out that the neurogenesis process is both behaviorally and biochemically linked to different psychiatric and neurodegenerative diseases (Apple et al., 2017; Peng and Bonaguidi, 2018), while other evidence highlighted the crucial roles of astrocytes and astrogenesis in the installation of central nervous system (CNS) pathologies, suggesting that the re-establishment or the enhancing of normal astrocytic functions may be of great therapeutic interest (Lee et al., 2015). Astrocytes, the largest and the most prevalent glial cell type in CNS, maintain the homeostasis control of the blood-brain barrier, and dynamically modulate synapse formation, maturation, and plasticity processes (Sahay et al., 2011; Akers et al., 2014). Defects in astrogenesis or early functions of astrocytes are reported to be involved in the development of different psychiatric disorders (Gonzales et al., 2017; Cohen and Torres, 2019; Pajarillo et al., 2019; Valles et al., 2019). Therefore, both neurons and astrocytes should be targeted simultaneously to re-establish the physiological functions in damaged brain. Although NSCs proliferation and differentiation processes are spontaneously stimulated in pathological conditions, they cannot overcome the damage and restore the brain tissue. It is in this context that pharmacological stimulation of NSCs fate determination plays an important role in cell therapy and regenerative medicine in debilitating brain diseases (Zhuang et al., 2012). Numerous studies have shown that small molecules, such as growth factors and retinoic acid, can regulate the biological characteristics of neural stem cells and promote neurogenesis and astrocytogenesis (Jacobs et al., 2006; Leker et al., 2009; Lee et al., 2015). However, the increasing incidences of lack of efficacy and undesirable side effects of existing pharmacological intervention have led to particular attention to several medicinal plants and their bioactive compounds. In this context, different

studies have reported the ability of phytochemicals to target NSCs for inducing brain self-repair through modulating neurogenesis (Matias et al., 2016; Gonzales et al., 2017; Sasaki et al., 2019).

The natural flavone luteolin (3', 4', 5, 7-tetrahydroxyflavone), present in several edible plants, in fruits and tea including rosemary tea (Miean and Mohamed, 2001; Achour et al., 2018; Aziz et al., 2018), has been reported to exert anti-inflammatory, anti-carcinogenic, cardioprotective effects as well as several neurotrophic benefits (Luo et al., 2017; Aziz et al., 2018; Imran et al., 2019). It enhances the cholinergic activity, increases the expressions of neuronal differentiation markers and induces the neurites outgrowth in PC12 cells, a neuronal cell model derived from a pheochromocytoma of rat adrenal medulla and in SH-SY5Y cells, a serotonergic neuronal cell model (Lin et al., 2010; El Omri et al., 2012; Bandaruk et al., 2014). Besides, the neuroprotective effects of luteolin have been reported in Alzheimer's disease models and were explained by its antioxidant and anti-inflammatory properties (Sawmiller et al., 2014; Wang et al., 2016a). Despite all the aforementioned promising beneficial effects of luteolin on neural cells and neurodegenerative disease models, its effects on human neural stem cells (hNSCs) have never been explored.

Recently, neuro-inflammation was shown to be involved in the pathogenesis of different CNS diseases such as depression (Wu et al., 2019). In addition, it was reported that defects occurred in astrocytes and neurons are associated with this neuroinflammatory pathology and that natural compounds may exert an antidepressant effect by rewarding this defect (Lee and Giuliani, 2019; Wu et al., 2019).

The present study aimed to assess the effect of luteolin on hNSCs fate determination and to explore the effect of luteolin on a pathological animal model with astrocytogenesis defect, the LPS-induced depression mice.

## MATERIALS AND METHODS

### Treatment Solutions Preparation

Luteolin, C<sub>15</sub>H<sub>10</sub>O<sub>6</sub> (**Supplementary Figure 1A**) was purchased from Sigma-Aldrich Co., Ltd. (St. Louis, MO, United States). To prepare the stock solution, luteolin was dissolved in Dimethyl sulfoxide (DMSO). For *in vitro* assays, luteolin stock was dissolved in the cell culture medium and for animal experiment it was dissolved in PBS.

AICAR, C<sub>9</sub>H<sub>15</sub>N<sub>4</sub>O<sub>8</sub> (**Supplementary Figure 1B**), is an adenosine analog and extensively used to activate 5' adenosine

monophosphate (AMP)-activated protein kinase (AMPK). This molecule was used in the present study since it is reported to induce the differentiation of rodent neural stem cells into astrocytes (Zang et al., 2008). It was purchased from Sigma-Aldrich Co., Ltd. (St. Louis, MO, United States). To prepare the stock solution, AICAR was dissolved in Dimethyl sulfoxide (DMSO), and then, for *in vitro* assays, AICAR stock was dissolved in the cell culture medium.

The Lipopolysaccharide (LPS), is the major component of the outer membrane of Gram-negative bacteria. It was used in the present study to induce depression in mice. This molecule was purchased from Wako (Japan). To prepare the mice treatment solution, LPS was dissolved in PBS.

## SH-SY5Y Cells Culture

The human neurotypic SH-SY5Y cells were purchased from the American Type Culture Collection (ATCC). The cells were cultured in 100 mm petri dish or 96-well plates depending on the purpose, with a 1:1 (v/v) mixture of Dulbecco's minimum essential medium (Sigma, United States) and Ham's F-12 nutrient mixture (Sigma, United States) supplemented with 15% fetal bovine serum (Sigma, United States), and 1% penicillin (5,000 µg/mL)-streptomycin (5,000 IU/mL) solution (ICN Biomedicals, Japan) and 1% non-essential amino-acid at 37°C in a 95% humidified air-5% CO<sub>2</sub> incubator.

## Experiment on Human Neural Stem Cells

### Human Neural Stem Cells Culture

The hNSCs (StemPro™ Neural Stem Cells) are cryopreserved human fetal brain-derived neural stem cells derived from cortex of a male fetus donor aged 16 weeks that were purchased from Gibco, United States (Cat. no. A15654). It was cultured in T25 flasks (BD Falcon), or in 6-well plates (BD Falcon) with KnockOut™ DMEM/F-12 (Gibco, United States, cat. no. 12660012) supplemented with 2% StemPro™ Neural Supplement (Gibco, Cat. no. A1050801), 20 ng/mL of fibroblast growth factor (FGF) basic recombinant human, 20 ng/mL epidermal growth factor (EGF) recombinant human and 2 mM GlutaMAX™-I Supplement (Cat. no. 35050), 6 U/mL heparin (Sigma, Cat. no. H3149), and 200 µM ascorbic acid (Sigma, Cat. no. A8960). For adhesion, Geltrex® (Gibco, Cat. no. A14133) was used to coat the 6-well plate. The hNSCs were cultured at 37°C in a 95% air/5% CO<sub>2</sub> humidified incubator. The medium was changed every 2 days.

### Determination of Human Neural Stem Cells Viability

Cell viability was determined using a tetrazolium salt reduction assay: the MTT (3-[4,5-dimethylthiazol-2-yl]-2,5-diphenyltetrazolium bromide) assay on the human neurotypic SH-SY5Y cells. Cells were seeded at the density of  $2 \times 10^5$  on 96 well plates and treated with 1–50 µM of luteolin or 0.5–500 µM of AICAR for 48 h. Treatment solutions were made by dilution of luteolin and AICAR solutions in low reduced-serum minimal essential medium (OptiMEM™, Gibco). After treatment, 5 mg/ml of MTT was added, and the cells were

incubated for further 12 h. The MTT formazan was dissolved in 100 µl of 10% SDS (w/v). Absorbance was measured at 570 nm using a microtiter plate reader after overnight incubation (Biotech, United States).

### Human Neural Stem Cells Differentiation Assay

Differentiation of hNSCs was induced following the previously described protocol (Sasaki et al., 2019). Briefly, hNSCs were seeded into 6 wells culture vessels coated with Geltrex® at a density of  $2.5 \times 10^4$  cells/cm<sup>2</sup>. After 48 h, growth medium was replaced by differentiation medium: Knockout DMEM/F12 supplemented with 2% StemPro® neural supplement, 2 mM GlutaMAX-I supplement, 6 units/mL heparin and 200 µM ascorbic acid, supplemented or not with 1 µM of Luteolin or 1 µM of AICAR. Throughout the study, differentiated hNSCs were used at P<sub>0</sub>.

### Immunocytochemistry on Human Neural Stem Cells

For immunocytochemistry, cells were seeded in the Nunc Lab-Tek Chamber Slide System (Thermo Scientific, Japan) coated with Geltrex® at the density of  $2.5 \times 10^4$  cells/cm<sup>2</sup> and were incubated at 37°C, 5% CO<sub>2</sub> for 48 h. After incubation, cells were treated with a differentiation medium supplemented or not 1 µM luteolin or 1 µM AICAR at 37°C for 24 h. After incubation, the cells were washed twice with PBS and fixed using 4% (w/v) cold formaldehyde (Wako, Japan) diluted in cold PBS for 30 min at room temperature. The fixed cells were later washed three times with PBS and permeabilized using 0.2% Triton-X surfactant (Sigma Aldrich, United States) diluted in PBS for 5 min at room temperature. After removing the Triton-X solution, cells were washed twice again using PBS, then blocked for 1 h at room temperature by 5% Fetal Goat Serum (Sigma, Japan) diluted in PBS. After incubation, the blocking buffer was removed and replaced by the diluted primary antibody solution. We used the primary antibodies of the rabbit polyclonal anti-Glial fibrillary acidic protein (GFAP) primary antibody (Cat. no. ab7260), the mouse monoclonal anti-beta III Tubulin (β3-tubulin) primary antibody (Cat. no. ab78078) and the rabbit polyclonal anti-Myelin Basic Protein (MBP) primary antibody (Cat. no. ab124493) to stain astrocytes, neurons, and oligodendrocytes, respectively. The antibodies were purchased from Abcam (Japan) and were diluted in 1% Fetal Goat Serum in PBS before use. After overnight incubation with primary antibodies at 4°C, cells were washed with PBS and incubated with the secondary antibodies solution Goat-anti mouse Alexa Fluor® 594 (ab150116, Abcam, Japan) and Goat-anti-rabbit IgG H&L Alexa Fluor® 488 (ab150077, Abcam, Japan) appropriately diluted in 1% Fetal Goat Serum in PBS for 2 h at room temperature avoiding light exposure. After incubation, cells were washed with PBS, and nuclei were counterstained with DAPI using drops of ProLong Diamond Antifade Mountant (Thermo Scientific, Japan). Fluorescence was detected with the IXplore Pro microscope system (OLYMPUS CORPORATION, Japan) monitored by OLYMPUS CellSens Dimension 1.18 software version XV3.17 (OLYMPUS CORPORATION, Japan, Copyright 2009–2017). Automated multichannel Cell count

and cell imaging were performed by CellSens Dimension 1.18 software at magnification  $\times 10$ .

## Animal Experiments

### Animals, Treatment Protocol and Behavioral Test

Healthy adult male ICR mice (21 weeks old, weighting between 33 and 46 g) were used for animal experiments. All animals were purchased from Charles River Laboratories JAPAN Inc., Kanagawa, Japan and were housed individually at controlled temperature (25°C), with a 12/12 h light/dark cycle, and had access to food and water *ad libitum*. After acclimatization, the mice were randomly assigned into four experimental groups ( $n = 6/\text{group}$ ): Control group (PBS), the depression model group: lipopolysaccharide group (LPS), control group treated with Luteolin (PBS + L) and lipopolysaccharide group treated with Luteolin (LPS + L). All experimental animals were maintained in accordance with the Guide for the Care and Use of Laboratory Animals, and the protocol was approved by the Animal Ethics Committee of the University of Tsukuba, Japan. At day 1 and prior to depression induction by LPS, the behavioral test: Tail Suspension Test (TST) was performed to all mice to screen their initial stress status. The TST methodology used in our study was as described by Steru (Steru et al., 1985). Briefly, the duration of the test was 6 min and the immobility time was measured on the last 4 min of the test. The mouse was considered immobile only when it is hanged passively, showing no resistance to the stress applied by the test. The experiment was recorded using a camera and scored by videos observations. Immediately after performing the TST test, LPS (850  $\mu\text{g}/\text{kg}$ ) was injected via the intraperitoneal route (i.p.) to the LPS and LPS + L groups and PBS was injected by the same route to the PBS and PBS + L groups. Starting from Day 2 and during eight consecutive days, luteolin (10 mg/kg) and PBS were orally administrated to mice once per day. Luteolin (10 mg/kg) was administrated to the LPS + L and PBS + L groups and PBS to both PBS and LPS groups. At day 9, a second TST test was conducted to evaluate the antidepressant effect exerted by luteolin on treated mice.

### Brains Collection

After performing the second TST test on day 9, all mice were sacrificed by cervical dislocation. Two mice brains from each group were used to separate NSCs, two mice brains were used to separate astrocytes and the remaining two brains were washed twice with cold PBS and immersed in liquid nitrogen prior to their storage at  $-80^\circ\text{C}$ .

### Neural Stem Cells and Primary Astrocytes Separation

Prior to NSCs and astrocytes isolation, the whole mice brain tissues were dissociated using the Adult Brain Dissociation Kit (Miltenyi Biotec Inc., CA, United States, order no. 130-107-677) in accordance to the manufacturer's instructions. This kit permitted to obtain single cell suspensions by combining mechanical dissociation with enzymatic degradation of the extracellular matrix. Briefly, the neural tissue was enzymatically digested using the kit components and the gentleMACS™ Dissociators (Miltenyi Biotec Inc., CA, United States) were used for the mechanical dissociation steps. After dissociation,

the Debris Removal Solution was used for the removal of debris followed by a subsequent removal of erythrocytes using the Red Blood Cell Removal Solution. Cells were processed immediately for separation.

Immediately after the brains tissues dissociations, the NSCs were separated using the Anti-Prominin-1 MicroBeads (Miltenyi Biotec Inc., CA, United States, order no. 130-092-333) and the astrocytes were isolated using the Anti-ACSA-2 (astrocyte cell surface antigen-2) MicroBeads kit (Miltenyi Biotec Inc., CA, United States, order no. 130-092-333) according the manufacturer's instructions. Briefly, for the separation of NSCs, first the prominin-1 + cells were magnetically labeled with AntiProminin-1 MicroBeads. Then, the cell suspension was loaded onto a MACS® Column, which was placed in the magnetic field of a MACS Separator. The magnetically labeled prominin-1 + cells were retained within the column. The unlabeled cells run through; this cell fraction is thus depleted of prominin-1 + cells. After removing the column from the magnetic field, the magnetically retained prominin-1 + cells were eluted as the positively selected cell fraction. To separate the astrocytes, first Fc receptors were blocked with the mouse FcR Blocking Reagent. Then, the ACSA-2 + cells were magnetically labeled with Anti-ACSA-2 MicroBeads. The cell suspension was loaded onto a MACS® Column, which was placed in the magnetic field of a MACS Separator. The magnetically labeled ACSA-2 + cells were retained within the column. The unlabeled cells run through; this cell fraction was thus depleted of ACSA-2 + cells. After removing the column from the magnetic field, the magnetically retained ACSA-2 + cells were eluted as the positively selected cell fraction.

### Count and Culture of Isolated Mice Primary Astrocytes

After separation with the Anti-ACSA-2 MicroBeads kit (Miltenyi Biotec Inc., CA, United States, order no. 130-092-333), the negative and positive ACSA-2 cells fractions were collected separately and counted using the Guava ViaCount Software (Version Number – 2.5.2), then the astrocyte fraction was cultured in 30 mm petri dish in DMEM, high glucose cell culture medium supplemented with 10% inactivated fetal bovine serum (Sigma, United States), and 1% penicillin (5,000  $\mu\text{g}/\text{mL}$ )-streptomycin (5,000 IU/mL) solution (ICN Biomedicals, Japan) at  $37^\circ\text{C}$  in a 95% humidified air-5%  $\text{CO}_2$  incubator for 7 days.

### ELISA Analysis

ELISA tests were performed on astrocytes culture media, on mice sera and on mice hypothalamus and frontal cortex tissues to confirm the installation of depression in LPS treated mice, and to confirm the antidepressant effect of luteolin in this mice model.

The pro-inflammatory cytokine IL-6 was quantified in the mice primary astrocyte culture medium at day 1, day 3, and day 7 and in mice sera using the mouse Quantikine® ELISA kit (cat. number. M6000B, R&D Systems, United States). The Tumor Necrosis Factor  $\text{TNF}\alpha$ , and the corticosterone levels were quantified in all mice sera using the Quantikine® ELISA kit cat. number MTA00B purchased from R&D Systems, United States. The Corticosterone ELISA kit (cat. number ADI-900-097)



purchased from Enzo Life Sciences, NY, United States was used to quantify corticosterone levels in mice sera.

The serotonin (Sert), noradrenaline (NA), dopamine, pro- and mature-BDNF levels were quantified in mice hypothalamus and frontal cortex (2 mice from each group were used). First, we homogenized 20 mg of tissue in 1 mL of RIPA buffer. The homogenate was centrifuged for 5 min at  $10,000 \times g$ ,  $4^{\circ}\text{C}$ . The supernatant was collected and stored at  $-80^{\circ}\text{C}$ . The dopamine, Sert and NA were quantified using ELISA kits (Immumol SAS, Talence, France). Pro and mature BDNF were measured by colorimetric sandwich ELISA kit (Proteintech, Rosemont, IL, United States). The experiments were conducted following the manufacturer's instructions. The results of each treatment group were corrected by their respective total protein content determined using Pierce<sup>TM</sup> BCA Protein Assay Kit (Cat. number 23225, Thermo Scientific, Japan).

## RNA Isolation

To extract hNSCs RNA, cells were seeded in 6 well plates at the density of  $2.5 \times 10^4$  cells/cm<sup>2</sup> and were incubated at  $37^{\circ}\text{C}$  for 48 h. After that, they were treated with differentiation medium with or without 1  $\mu\text{M}$  of luteolin or 1  $\mu\text{M}$  of AICAR and were incubated at  $37^{\circ}\text{C}$  for 8 and 24 h. After the treatment, cells were washed twice with ice-cold PBS (–). To extract RNA from mice hippocampus, two mice brains of each animal group were dissected and hippocampus tissues were used. The isolated NSCs from two mice brains were immediately used to extract total RNA.

The ISOGEN kit (Nippon Gene Co., Ltd., Japan) was used for all total RNA extraction experiments following the manufacturer's instructions, as reported previously by Sasaki et al. (2019). Total RNA was purified using chloroform and Isopropanol (Wako, Japan) and quantified and assessed for quality with a NanoDrop 2000 spectrophotometer (Thermo Scientific, Wilmington, DE, United States).

## DNA Microarray Analysis

To elucidate the molecular mechanism underlying the effect of luteolin treatment on hNSCs fate determination, we compared the global gene expression of untreated and luteolin-treated hNSCs and to elucidate the molecular mechanism underlying the effect of luteolin treatment on LPS-induced depression model NSCs and hippocampus, we performed three global gene expression comparison studies. First, we compared the global gene expression of LPS group and control group (LPS vs. PBS), then we compared the global gene expression of control group treated with luteolin and untreated control group (PBS + L vs. PBS) and finally we compared the LPS group treated with luteolin and LPS group (LPS + L vs. LPS).

These genomic analyses were made by performing microarray analysis using Affymetrix GeneChip 3' IVT PLUS reagent kit (Affymetrix Inc., Santa Clara, CA, United States) according to the kit user's guide. Data normalization and transformation was done by Expression Console software. Subsequent analysis of the differentially expressed genes was performed using Transcriptome Analysis Console (version 4) and DAVID online tool (Huang et al., 2009; Sherman and Lempicki, 2009). Heatmap

was generated using a freely available web tool Heatmapper (Babicki et al., 2016).

## Real-Time Polymerase Chain Reaction Analysis on Human Neural Stem Cells

RNA extracts obtained from hNSCs treated or not with 1  $\mu\text{M}$  luteolin for 8 and 24 h were used to validate the microarray data. Reverse transcription was performed using the Superscript IV reverse transcriptase kit (Invitrogen, United States) following the manufacturer's guidelines. A mixture of RNA samples (30 ng/ $\mu\text{l}$ ) and Oligo d (T)<sub>20</sub>/dNTP were incubated for 5 min at  $5^{\circ}\text{C}$ , then placed in ice for 1 min. The Superscript<sup>®</sup> IV reverse transcriptase solution was added. The mixture was vortexed and centrifuged, then TaqMan probes specific to, Glial Fibrillary Acidic Protein (GFAP) (Hs 00909233\_m1), Bone Morphogenetic Protein 2 (BMP2) (Hs00154192\_m1), Signal Transducer and Activator of Transcription (STAT3) (Hs00374280\_m1), Tubulin, beta 3 class III (TUBB3) (Hs00801390\_s1), NOTCH 1 (Hs01062014\_m1), NOTCH 3 (Hs00166432\_m1), Myelin Basic Protein (MBP) (Hs 00921945\_m1) genes and master mix TaqMan were added to 100 ng/9  $\mu\text{L}$  of obtained cDNA, and the mixture was introduced to 7500 Fast Real-time PCR (Applied Biosystems, United States) and the following conditions were applied:  $50^{\circ}\text{C}$  for 2 min, followed by  $95^{\circ}\text{C}$  for 10 min, and 40 cycles of  $95^{\circ}\text{C}$  for 15 s followed by  $60^{\circ}\text{C}$  for 1 min. Glyceraldehyde-3-Phosphate Dehydrogenase (GAPDH) gene (Hs02786624\_g1 GAPDH) was used as an endogenous control. All primers were purchased from (Applied Biosystems, CA, United States), and all reactions were run in triplicates.

## Statistical Analysis

Statistical analysis was performed using SPSS software (Version 24; IBM, Armonk, NY, United States). A Student's *t*-test was used when two groups were compared in MTT assay, astrocytes quantification and all ELISA tests. Statistical analysis of the results obtained in the immunocytochemistry and the real-time polymerase chain reaction (RT-qPCR) validation results were carried out using one-way analysis of variance (ANOVA) followed by Dunnett's *post hoc* test. The difference in signal intensities between control and luteolin-treated hNSCs was tested using student's *t*-test. Statistical analysis of TST results were carried out using paired *t*-test to compare the same groups results obtained between Day 1 and Day 8, and using One-way ANOVA test to compare different groups results at Day 1 and at day 8. Results are expressed as mean  $\pm$  standard deviation unless otherwise indicated. The criterion of statistical significance was  $p < 0.05$ .

## RESULTS

### Results Obtained From the *in vitro* Study Cell Viability

Results from MTT assay indicate that 1  $\mu\text{M}$  luteolin slightly increased cell viability of SH-SY5Y cells after 24 h and 48 h treatment ( $p < 0.001$ ), concentrations ranged from 5 to 10  $\mu\text{M}$

did not affect cell viability while higher concentrations induced cell toxicity in a dose dependent-manner after 24 and 48 h treatment (**Supplementary Figure 2**). Treatment with 0.5  $\mu\text{M}$  of AICAR for 24 h could slightly increase SH-SY5Y cell viability ( $104.1\% \pm 1.9$ ,  $p < 0.01$ ). Concentrations ranged between 0.5 and 5  $\mu\text{M}$  did not affect cell viability, while higher concentration significantly reduced the viable SH-SY5Y cell number to 70% (Data not shown).

### Luteolin Affected Global Gene Expression During Human Neural Stem Cells Differentiation

We evaluated the effect of luteolin on the transcriptomic changes in hNSCs during differentiation at 24 h using DNA microarray. We found that treatment with 1  $\mu\text{M}$  luteolin could significantly regulate the expressions of 5870 genes in hNSCs ( $-1.3 < \text{Fold change} < 1.3$ ;  $p < 0.05$ ), with upregulation of 2638 genes and downregulation of 3232 genes. Top 10 significantly up and downregulated genes and their functions are presented in **Supplementary Tables 1, 2**, respectively.

Top 10 significantly enriched biological processes between 1  $\mu\text{M}$  luteolin treated hNSCs and untreated control hNSCs are shown in **Figure 1A**. Fifty-five regulated genes were related to cell differentiation (GO:0030154), 24 to neurogenesis (GO:022008), 23 to generation of neurons (GO:0048699), 17 to neuron development (GO:0048666), 14 to neuron projection development (GO:0031175), 13 to cell morphogenesis involved in differentiation (GO:000904), 12 to regulation of cell differentiation (GO:0045595), 12 to brain development (GO:0007420), 10 to neuron differentiation (GO:0030182), 6 to regulation of neurogenesis (GO:0050767).

(GO:0048667), 12 to regulation of cell differentiation (GO:0045595), 12 to brain development (GO:0007420), 10 to neuron differentiation, and 6 regulated genes to regulation of neurogenesis (GO:0050767). Besides, the essential gene expressions related to astrocyte differentiation biological process (GO:0048708), negative regulation of astrocyte differentiation (GO:0048712), and positive regulation of astrocyte differentiation (GO:0048712) were also regulated in luteolin treated hNSCs compared to untreated control cells (**Figure 1B** and **Supplementary Tables 3–5**).

Significantly regulated top KEGG signaling pathways by 1  $\mu\text{M}$  luteolin treatment for 24 h are shown in **Figure 1C**. Luteolin treatment upregulated 26 genes in Hippo signaling ( $p = 0.052$ ), 23 genes involved in Wnt signaling pathway ( $p = 0.091$ ), 23 genes in the dopaminergic synapse ( $p = 0.025$ ) and 23 genes involved in the Neurotrophin pathway ( $p = 0.024$ ). Also, luteolin treatment downregulated 30 genes in FOXO signaling ( $p = 0.026$ ), 29 genes in dopaminergic synapse ( $p = 0.046$ ), 26 genes in TNF signaling ( $p = 0.015$ ), 19 genes involved in p53 signaling pathway ( $p = 0.009$ ), and 13 genes in notch signaling ( $p = 0.049$ ) (**Figure 1C** and **Table 1**).

We further evaluated the effect of 24 h treatment with 1  $\mu\text{M}$  luteolin on 37 selected genes that were reported to be involved in neural stem cells (NSCs) differentiation process (Yao and Jin, 2014; Hsieh and Zhao, 2016; **Figure 1D**). We found that luteolin treatment upregulated the expressions of 17 genes and downregulated the expressions of 20 genes ( $-1.3 < \text{Fold}$

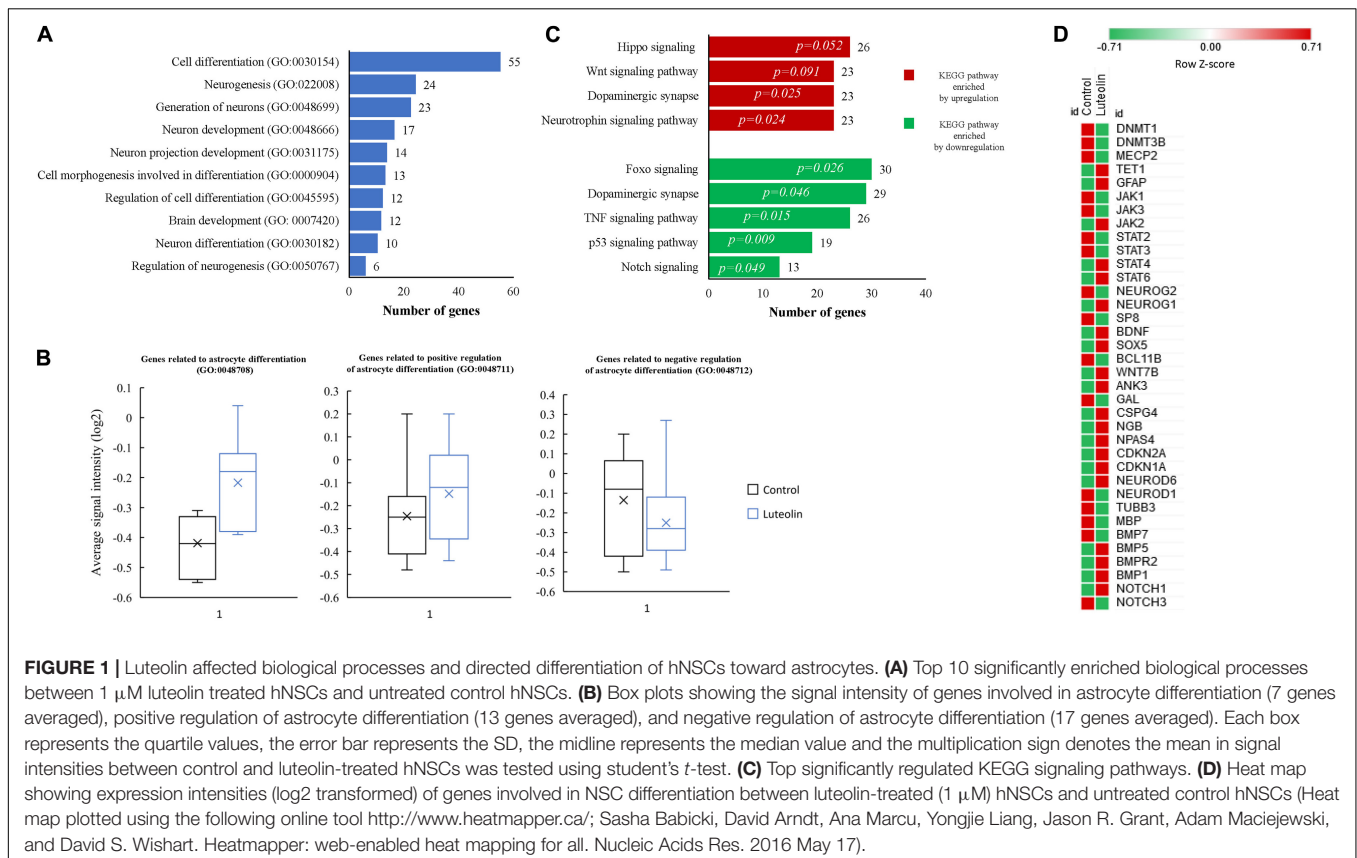


**TABLE 1** | Top significantly enriched KEGG signaling pathways in NSCs of LPS-induced depression mice (LPS) compared to untreated mice (PBS).

Regulation	KEGG signaling	Genes
Downregulation	<b>Estrogen signaling pathway (mmu04915)</b>	FBJ osteosarcoma oncogene ( <b>Fos</b> )
		GNAS (guanine nucleotide binding protein, alpha stimulating) complex locus ( <b>Gnas</b> )
		cAMP responsive element binding protein 3 ( <b>Creb3</b> )
		guanine nucleotide binding protein (G protein), alpha inhibiting 2 ( <b>Gnai2</b> )
		heat shock protein 1B ( <b>Hspa1b</b> )
		heat shock protein 8 ( <b>Hspa8</b> )
		heat shock protein 90 alpha (cytosolic), class B member 1 ( <b>Hsp90ab1</b> )
	<b>Thyroid hormone synthesis (mmu04918)</b>	heat shock protein 90, alpha (cytosolic), class A member 1 ( <b>Hsp90aa1</b> )
		heat shock protein 90, beta (Grp94), member 1 ( <b>Hsp90b1</b> )
		phosphatidylinositol 3-kinase catalytic delta polypeptide ( <b>Pik3cd</b> )
		ATPase, Na <sup>+</sup> /K <sup>+</sup> transporting, alpha 2 polypeptide ( <b>Atp1a2</b> )
		ATPase, Na <sup>+</sup> /K <sup>+</sup> transporting, beta 2 polypeptide ( <b>Atp1b2</b> )
		GNAS (guanine nucleotide binding protein, alpha stimulating) complex locus ( <b>Gnas</b> )
		cAMP responsive element binding protein 3 ( <b>Creb3</b> )
	<b>Adherens junction (mmu04520)</b>	heat shock protein 90, beta (Grp94), member 1 ( <b>Hsp90b1</b> )
		WAS protein family, member 2 ( <b>Wasf2</b> )
		actin, beta ( <b>Actb</b> )
		actin, gamma, cytoplasmic 1 ( <b>Actg1</b> )
		catenin (cadherin associated protein), beta 1 ( <b>Ctnnb1</b> )
		protein tyrosine phosphatase, receptor type, B ( <b>Ptprb</b> )
	<b>cAMP signaling pathway (mmu04024)</b>	protein tyrosine phosphatase, receptor type, B ( <b>Ptprb</b> )
		ATPase, Na <sup>+</sup> /K <sup>+</sup> transporting, alpha 2 polypeptide ( <b>Atp1a2</b> )
		ATPase, Na <sup>+</sup> /K <sup>+</sup> transporting, beta 2 polypeptide ( <b>Atp1b2</b> )
		FBJ osteosarcoma oncogene ( <b>Fos</b> )
		GNAS (guanine nucleotide binding protein, alpha stimulating) complex locus ( <b>Gnas</b> )
		cAMP responsive element binding protein 3 ( <b>Creb3</b> )
		calcium/calmodulin-dependent protein kinase II alpha ( <b>Camk2a</b> )
	<b>Glutamatergic synapse (mmu04724)</b>	guanine nucleotide binding protein (G protein), alpha inhibiting 2 ( <b>Gnai2</b> )
		nuclear factor of kappa light polypeptide gene enhancer in B cells inhibitor, alpha ( <b>Nfkb1a</b> )
		phosphatidylinositol 3-kinase catalytic delta polypeptide ( <b>Pik3cd</b> )
		GNAS (guanine nucleotide binding protein, alpha stimulating) complex locus ( <b>Gnas</b> )
		glutamate-ammonia ligase (glutamine synthetase) ( <b>Glu1</b> )
		guanine nucleotide binding protein (G protein), alpha inhibiting 2 ( <b>Gnai2</b> )
		guanine nucleotide binding protein (G protein), beta 1 ( <b>Gnb1</b> )
	<b>Cholinergic synapse (mmu04725)</b>	predicted gene 15776 ( <b>Gm15776</b> )
		solute carrier family 1 (glial high affinity glutamate transporter), member 2 ( <b>Slc1a2</b> )
		solute carrier family 1 (glial high affinity glutamate transporter), member 3 ( <b>Slc1a3</b> )
		FBJ osteosarcoma oncogene ( <b>Fos</b> )
		cAMP responsive element binding protein 3 ( <b>Creb3</b> )
		calcium/calmodulin-dependent protein kinase II alpha ( <b>Camk2a</b> )
		guanine nucleotide binding protein (G protein), alpha inhibiting 2 ( <b>Gnai2</b> )
	<b>Dopaminergic synapse (mmu04728)</b>	guanine nucleotide binding protein (G protein), beta 1 ( <b>Gnb1</b> )
		phosphatidylinositol 3-kinase catalytic delta polypeptide ( <b>Pik3cd</b> )
		predicted gene 15776 ( <b>Gm15776</b> )
		FBJ osteosarcoma oncogene ( <b>Fos</b> )
		GNAS (guanine nucleotide binding protein, alpha stimulating) complex locus ( <b>Gnas</b> )
		cAMP responsive element binding protein 3 ( <b>Creb3</b> )
		calcium/calmodulin-dependent protein kinase II alpha ( <b>Camk2a</b> )
	<b>Dopaminergic synapse (mmu04728)</b>	guanine nucleotide binding protein (G protein), alpha inhibiting 2 ( <b>Gnai2</b> )
		guanine nucleotide binding protein (G protein), beta 1 ( <b>Gnb1</b> )
		guanine nucleotide binding protein (G protein), beta 1 ( <b>Gnb1</b> )
		guanine nucleotide binding protein (G protein), beta 1 ( <b>Gnb1</b> )
		guanine nucleotide binding protein (G protein), beta 1 ( <b>Gnb1</b> )
		guanine nucleotide binding protein (G protein), beta 1 ( <b>Gnb1</b> )
		guanine nucleotide binding protein (G protein), beta 1 ( <b>Gnb1</b> )

(Continued)

TABLE 1 | (Continued)

Regulation	KEGG signaling	Genes
		<p>predicted gene 15776 (<b>Gm15776</b>)</p> <p>protein phosphatase 2, regulatory subunit B, alpha (<b>Ppp2r2a</b>)</p>
	<b>PI3K-Akt signaling pathway (mmu04151)</b>	<p>FMS-like tyrosine kinase 1 (<b>Flt1</b>)</p> <p>Von Willebrand factor (<b>Vwf</b>)</p> <p>cAMP responsive element binding protein 3 (<b>Creb3</b>)</p> <p>eukaryotic translation initiation factor 4E member 2 (<b>Eif4e2</b>)</p> <p>fibronectin 1 (<b b="" fn1<="">)</b></p> <p>guanine nucleotide binding protein (G protein), beta 1 (<b>Gnb1</b>)</p> <p>heat shock protein 90 alpha (cytosolic), class B member 1 (<b>Hsp90ab1</b>)</p> <p>heat shock protein 90, alpha (cytosolic), class A member 1 (<b>Hsp90aa1</b>)</p> <p>heat shock protein 90, beta (Grp94), member 1 (<b>Hsp90b1</b>)</p> <p>phosphatidylinositol 3-kinase catalytic delta polypeptide (<b>Pik3cd</b>)</p> <p>predicted gene 15776 (<b>Gm15776</b>)</p> <p>protein phosphatase 2, regulatory subunit B, alpha (<b>Ppp2r2a</b>)</p> <p>ribosomal protein S6 (<b>Rps6</b>)</p> <p>tyrosine 3-monooxygenase/tryptophan 5-monooxygenase activation protein, epsilon polypeptide (<b>Ywhae</b>)</p> <p>tyrosine 3-monooxygenase/tryptophan 5-monooxygenase activation protein, theta polypeptide (<b>Ywhaq</b>)</p>
Downregulation	<b>Thyroid hormone signaling pathway (mmu04919)</b>	<p>ATPase, Na<sup>+</sup>/K<sup>+</sup> transporting, alpha 2 polypeptide (<b>Atp1a2</b>)</p> <p>ATPase, Na<sup>+</sup>/K<sup>+</sup> transporting, beta 2 polypeptide (<b>Atp1b2</b>)</p> <p>actin, beta (<b>Actb</b>)</p> <p>actin, gamma, cytoplasmic 1 (<b>Actg1</b>)</p> <p>catenin (cadherin associated protein), beta 1 (<b>Ctnnb1</b>)</p> <p>phosphatidylinositol 3-kinase catalytic delta polypeptide (<b>Pik3cd</b>)</p> <p>solute carrier family 2 (facilitated glucose transporter), member 1 (<b>Slc2a1</b>)</p> <p>solute carrier organic anion transporter family, member 1c1 (<b>Slco1c1</b>)</p>
	<b>Gap junction (mmu04540)</b>	<p>GNAS (guanine nucleotide binding protein, alpha stimulating) complex locus (<b>Gnas</b>)</p> <p>Gap junction protein, alpha 1 (<b>Gja1</b>)</p> <p>Gap junction protein, delta 2 (<b>Gjd2</b>)</p> <p>guanine nucleotide binding protein (G protein), alpha inhibiting 2 (<b>Gnai2</b>)</p> <p>tubulin, alpha 1A (<b>Tuba1a</b>)</p> <p>tubulin, alpha 1B (<b>Tuba1b</b>)</p>
	<b>Insulin secretion (mmu04911)</b>	<p>ATPase, Na<sup>+</sup>/K<sup>+</sup> transporting, alpha 2 polypeptide (<b>Atp1a2</b>)</p> <p>ATPase, Na<sup>+</sup>/K<sup>+</sup> transporting, beta 2 polypeptide (<b>Atp1b2</b>)</p> <p>GNAS (guanine nucleotide binding protein, alpha stimulating) complex locus (<b>Gnas</b>)</p> <p>RAB3A, member RAS oncogene family (<b>Rab3a</b>)</p> <p>cAMP responsive element binding protein 3 (<b>Creb3</b>)</p> <p>calcium/calmodulin-dependent protein kinase II alpha (<b>Camk2a</b>)</p> <p>solute carrier family 2 (facilitated glucose transporter), member 1 (<b>Slc2a1</b>)</p>
Upregulation	<b>Salivary secretion (mmu04970)</b>	<p>cathelicidin antimicrobial peptide (<b>Camp</b>)</p> <p>lysozyme 1 (<b>Lyz1</b>)</p> <p>lysozyme 2 (<b>Lyz2</b>)</p>
	<b>Systemic lupus erythematosus (mmu05322)</b>	<p>H2A histone family, member Z (<b>H2afz</b>)</p> <p>cathepsin G (<b>Ctsg</b>)</p> <p>histone cluster 1, H2ac (<b>Hist1h2ac</b>)</p>

Gene abbreviations are indicated in bold.

change  $< 1.3$ ;  $p < 0.05$ ; **Figure 1D** and **Table 2**). It downregulated the expressions of neurogenin 2 (**NEUROG2**), DNA (cytosine-5-)-methyl transferase 1 (**DNMT1**), DNA (cytosine-5-)-methyl

transferase 3 beta (**DNMT3B**), neuronal differentiation 1 (**NEUROD1**), neuronal differentiation 6 (**NEUROD6**), **NOTCH3**, bone morphogenic protein (**BMP7**), and **TUBB3** that are known



**TABLE 2 |** Top significantly enriched KEGG signaling pathways in NSCs of LPS-induced depression mice treated with luteolin (LPS + L) compared to untreated mice LPS-induced depression mice (LPS).

Regulation	KEGG signaling	Genes
Upregulation	<b>Parkinson's disease (mmu05012)</b>	<p>ATP synthase, H+ transporting, mitochondrial F0 complex, subunit C3 (subunit 9) (<b>Atp5g3</b>)</p> <p>ATP synthase, H+ transporting, mitochondrial F0 complex, subunit D (<b>Atp5h</b>)</p> <p>ATP synthase, H+ transporting, mitochondrial F1 complex, O subunit (<b>Atp5o</b>)</p> <p>ATP synthase, H+ transporting, mitochondrial F1 complex, epsilon subunit (<b>Atp5e</b>)</p> <p>ATP synthase, H+ transporting, mitochondrial F1 complex, gamma polypeptide 1 (<b>Atp5c1</b>)</p> <p>NADH dehydrogenase (ubiquinone) 1 alpha subcomplex, 13 (<b>Ndufa13</b>)</p> <p>NADH dehydrogenase (ubiquinone) 1 alpha subcomplex, 3 (<b>Ndufa3</b>)</p> <p>NADH dehydrogenase (ubiquinone) 1 alpha subcomplex, 9 (<b>Ndufa9</b>)</p> <p>NADH dehydrogenase (ubiquinone) 1 beta subcomplex, 11 (<b>Ndufb11</b>)</p> <p>NADH dehydrogenase (ubiquinone) 1 beta subcomplex, 5 (<b>Ndufb5</b>)</p> <p>NADH dehydrogenase (ubiquinone) flavoprotein 3 (<b>Ndufv3</b>)</p> <p>NADH dehydrogenase [ubiquinone] 1 subunit C2 (<b>LOC102641347</b>)</p> <p>NADH dehydrogenase subunit 5 (<b>ND5</b>)</p> <p>cytochrome c oxidase subunit IV isoform 1 (<b>Cox4i1</b>)</p> <p>cytochrome c oxidase subunit VIIa 2 (<b>Cox7a2</b>)</p> <p>cytochrome c oxidase subunit VIIa polypeptide 2-like (<b>Cox7a2l</b>)</p> <p>cytochrome c oxidase subunit VIa polypeptide 1 (<b>Cox6a1</b>)</p> <p>cytochrome c oxidase subunit Va (<b>Cox5a</b>)</p> <p>cytochrome c oxidase subunit Vb (<b>Cox5b</b>)</p> <p>cytochrome c oxidase, subunit VIb polypeptide 1 (<b>Cox6b1</b>)</p> <p>guanine nucleotide binding protein (G protein), alpha inhibiting 2 (<b>Gnai2</b>)</p> <p>solute carrier family 25 (mitochondrial carrier, adenine nucleotide translocator), member 4 (<b>Slc25a4</b>)</p> <p>solute carrier family 25 (mitochondrial carrier, adenine nucleotide translocator), member 5 (<b>Slc25a5</b>)</p> <p>ubiquinol-cytochrome c reductase binding protein (<b>Uqcrb</b>)</p>
	<b>Alzheimer's disease (mmu05010)</b>	<p>ATP synthase, H+ transporting, mitochondrial F0 complex, subunit D (<b>Atp5h</b>)</p> <p>ATP synthase, H+ transporting, mitochondrial F1 complex, O subunit (<b>Atp5o</b>)</p> <p>ATP synthase, H+ transporting, mitochondrial F1 complex, epsilon subunit (<b>Atp5e</b>)</p> <p>ATP synthase, H+ transporting, mitochondrial F1 complex, gamma polypeptide 1 (<b>Atp5c1</b>)</p> <p>ATPase, Ca++ transporting, cardiac muscle, slow twitch 2 (<b>Atp2a2</b>)</p> <p>ATP synthase, H+ transporting, mitochondrial F0 complex, subunit D (<b>Atp5h</b>)</p> <p>ATP synthase, H+ transporting, mitochondrial F1 complex, O subunit (<b>Atp5o</b>)</p> <p>NADH dehydrogenase (ubiquinone) 1 alpha subcomplex, 13 (<b>Ndufa13</b>)</p> <p>NADH dehydrogenase (ubiquinone) 1 alpha subcomplex, 3 (<b>Ndufa3</b>)</p> <p>NADH dehydrogenase (ubiquinone) 1 alpha subcomplex, 9 (<b>Ndufa9</b>)</p> <p>NADH dehydrogenase (ubiquinone) 1 beta subcomplex, 11 (<b>Ndufb11</b>)</p> <p>NADH dehydrogenase (ubiquinone) 1 beta subcomplex, 5 (<b>Ndufb5</b>)</p> <p>NADH dehydrogenase (ubiquinone) flavoprotein 3 (<b>Ndufv3</b>)</p> <p>NADH dehydrogenase [ubiquinone] 1 subunit C2 (<b>LOC102641347</b>)</p> <p>amyloid beta (A4) precursor protein (<b>Apo</b>)</p> <p>apolipoprotein E (<b>ApoE</b>)</p> <p>calmodulin 1 (<b>Calm1</b>)</p> <p>cytochrome c oxidase subunit IV isoform 1 (<b>Cox4i1</b>)</p> <p>cytochrome c oxidase subunit VIIa 2 (<b>Cox7a2</b>)</p> <p>cytochrome c oxidase subunit VIIa polypeptide 2-like (<b>Cox7a2l</b>)</p> <p>cytochrome c oxidase subunit VIa polypeptide 1 (<b>Cox6a1</b>)</p> <p>cytochrome c oxidase subunit Va (<b>Cox5a</b>)</p> <p>cytochrome c oxidase subunit Vb (<b>Cox5b</b>)</p>

(Continued)

TABLE 2 | (Continued)

Regulation	KEGG signaling	Genes
		cytochrome c oxidase, subunit VIb polypeptide 1 ( <b>Cox6b1</b> ) glyceraldehyde-3-phosphate dehydrogenase, pseudogene 15 ( <b>Gapdh-ps15</b> ) presenilin enhancer gamma secretase subunit ( <b>Psenen</b> ) ubiquinol-cytochrome c reductase binding protein ( <b>Uqcrb</b> )
	Huntington's disease (mmu05016)	ATP synthase, H+ transporting, mitochondrial F0 complex, subunit C3 (subunit 9) ( <b>Atp5g3</b> ) ATP synthase, H+ transporting, mitochondrial F0 complex, subunit D ( <b>Atp5h</b> ) ATP synthase, H+ transporting, mitochondrial F1 complex, O subunit ( <b>Atp5o</b> ) ATP synthase, H+ transporting, mitochondrial F1 complex, epsilon subunit ( <b>Atp5e</b> ) ATP synthase, H+ transporting, mitochondrial F1 complex, gamma polypeptide 1 ( <b>Atp5c1</b> ) NADH dehydrogenase (ubiquinone) 1 alpha subcomplex, 13 ( <b>Ndufa13</b> ) NADH dehydrogenase (ubiquinone) 1 alpha subcomplex, 3 ( <b>Ndufa3</b> ) NADH dehydrogenase (ubiquinone) 1 alpha subcomplex, 9 ( <b>Ndufa9</b> ) NADH dehydrogenase (ubiquinone) 1 beta subcomplex, 11 ( <b>Ndufb11</b> ) NADH dehydrogenase (ubiquinone) 1 beta subcomplex, 5 ( <b>Ndufb5</b> ) NADH dehydrogenase (ubiquinone) flavoprotein 3 ( <b>Ndufv3</b> ) NADH dehydrogenase [ubiquinone] 1 subunit C2 ( <b>LOC102641347</b> ) cAMP responsive element binding protein 3 ( <b>Creb3</b> ) clathrin, light polypeptide (Lca) ( <b>Cltla</b> ) cytochrome c oxidase subunit IV isoform 1 ( <b>Cox4i1</b> ) cytochrome c oxidase subunit VIIa 2 ( <b>Cox7a2</b> ) cytochrome c oxidase subunit VIIa polypeptide 2-like ( <b>Cox7a2l</b> ) cytochrome c oxidase subunit VIa polypeptide 1 ( <b>Cox6a1</b> ) cytochrome c oxidase subunit Va ( <b>Cox5a</b> ) cytochrome c oxidase subunit Vb ( <b>Cox5b</b> ) cytochrome c oxidase, subunit VIb polypeptide 1 ( <b>Cox6b1</b> ) dynactin 1 ( <b>Dctn1</b> ) solute carrier family 25 (mitochondrial carrier, adenine nucleotide translocator), member 4 ( <b>Slc25a4</b> ) solute carrier family 25 (mitochondrial carrier, adenine nucleotide translocator), member 5 ( <b>Slc25a5</b> ) superoxide dismutase 1, soluble ( <b>Sod1</b> ) ubiquinol-cytochrome c reductase binding protein ( <b>Uqcrb</b> )
Upregulation	Estrogen signaling pathway (mmu04915)	GNAS (guanine nucleotide binding protein, alpha stimulating) complex locus ( <b>Gnas</b> ) cAMP responsive element binding protein 3 ( <b>Creb3</b> ) calmodulin 1 ( <b>Calm1</b> ) guanine nucleotide binding protein (G protein), alpha inhibiting 2 ( <b>Gnai2</b> ) heat shock protein 1B ( <b>Hspa1b</b> ) heat shock protein 8 ( <b>Hspa8</b> ) heat shock protein 90 alpha (cytosolic), class B member 1 ( <b>Hsp90ab1</b> ) heat shock protein 90, alpha (cytosolic), class A member 1 ( <b>Hsp90aa1</b> ) heat shock protein 90, beta (Grp94), member 1 ( <b>Hsp90b1</b> ) phosphatidylinositol 3-kinase catalytic delta polypeptide ( <b>Pik3cd</b> )
	Thyroid hormone signaling pathway (mmu4919)	ATPase, Na+/K+ transporting, alpha 2 polypeptide ( <b>Atp1a2</b> ) ATPase, Na+/K+ transporting, beta 2 polypeptide ( <b>Atp1b2</b> ) actin, beta ( <b>Actb</b> ) actin, gamma, cytoplasmic 1 ( <b>Actg1</b> ) catenin (cadherin associated protein), beta 1 ( <b>Ctnnb1</b> )

(Continued)

TABLE 2 | (Continued)

Regulation	KEGG signaling	Genes
		phosphatidylinositol 3-kinase catalytic delta polypeptide ( <b>Pik3cd</b> ) phospholipase C, gamma 1 ( <b>Plcg1</b> ) solute carrier family 16 (monocarboxylic acid transporters), member 2 ( <b>Slc16a2</b> ) solute carrier family 2 (facilitated glucose transporter), member 1 ( <b>Slc2a1</b> ) solute carrier organic anion transporter family, member 1c1 ( <b>Slco1c1</b> )
	<b>HIF-1 signaling pathway (04066)</b>	FMS-like tyrosine kinase 1 ( <b>Flt1</b> ) Enolase 1, alpha non-neuron ( <b>Eno1</b> ) Glyceraldehyde-3-phosphate dehydrogenase, pseudogene 15 ( <b>Gapdh-ps15</b> ) phosphatidylinositol 3-kinase catalytic delta polypeptide ( <b>Pik3cd</b> ) phospholipase C, gamma 1 ( <b>Plcg1</b> ) predicted gene 9840 ( <b>Gm9840</b> ) ribosomal protein S6 ( <b>Rps6</b> ) solute carrier family 2 (facilitated glucose transporter), member 1 ( <b>Slc2a1</b> ) transferrin receptor ( <b>Tfrc</b> )
	<b>Glycolysis/Gluconeogenesis (mmu00010)</b>	aldo-keto reductase family 1, member A1 (aldehyde reductase) ( <b>Akr1a1</b> ) aldolase A, fructose-bisphosphate ( <b>Aldoa</b> ) aldolase C, fructose-bisphosphate ( <b>Aldoc</b> ) enolase 1, alpha non-neuron ( <b>Eno1</b> ) glucose phosphate isomerase 1 ( <b>Gpi1</b> ) glyceraldehyde-3-phosphate dehydrogenase, pseudogene 15 ( <b>Gapdh-ps15</b> ) lactate dehydrogenase B ( <b>Ldhb</b> )
	<b>Adherens junction (mmu04520)</b>	actin, beta ( <b>Actb</b> ) actin, gamma, cytoplasmic 1 ( <b>Actg1</b> ) catenin (cadherin associated protein), alpha 1 ( <b>Ctnna1</b> ) catenin (cadherin associated protein), beta 1 ( <b>Ctnnb1</b> ) cell division cycle 42 ( <b>Cdc42</b> ) protein tyrosine phosphatase, receptor type, B ( <b>Ptpnb1</b> ) sorbin and SH3 domain containing 1 ( <b>Sorbs1</b> )
Downregulation	<b>Systemic lupus erythematosus (mmu05322)</b>	H2A histone family, member Z ( <b>H2afz</b> ) cathepsin G ( <b>CtsG</b> ) histone cluster 1, H2ac ( <b>Hist1h2ac</b> )

Gene abbreviations are indicated in bold.

to regulate neuron differentiation. The expression of methyl-CpG binding protein 2 (*MECP2*) that is known to regulate neuron maturation, was also downregulated (**Figure 1D** and **Table 2**). Besides, luteolin treatment regulated several genes related to astrocyte development, astrocyte differentiation, and signaling pathways that direct astrocytogenesis. Luteolin upregulated Wnt family member 7B (*WNT7B*), *GFAP*, and Janus kinase (*JAK*) 2 expression (**Figure 1D** and **Table 2**), whereas downregulated the most important oligodendrocyte genesis gene, *MBP*.

Taken together, results from microarray analysis showed that 1  $\mu$ M luteolin treatment for 24 h induced differentiation of hNSCs and directed its fate toward astrocytes. Besides, these results also suggest that luteolin modulated the differentiation of hNSCs toward astrocytes via upregulation of astrogenic genes such as *GFAP*, *WNT*, and *JAK*, while it suppressed the neuronal and oligodendrocytes differentiation by downregulation of *NEUROG2*, *DNMT1*, *DNMT3B*, *NEUROD1*, *NEUROD6*, *NOTCH3*, *BMP7* and *TUBB3*, and *MBP*.

## Luteolin Increased the Number of GFAP+ Cells After 24 h Incubation

We performed immunostaining to quantify neuronal and glial cell populations after 24 h of differentiation induction in the presence or absence of luteolin and AICAR. It was previously reported that hNSCs fate is determined within 24 h of differentiation induction (Sasaki et al., 2019). The immunostaining of hNSCs showed that untreated control, and both AICAR- and luteolin-treated cells were exclusively differentiated into neurons and astrocytes. Only TUBB3<sup>+</sup> and GFAP<sup>+</sup> cells were detected after 24 h of incubation (**Figure 2A**). MBP<sup>+</sup> cells were not detected within 24 h of differentiation induction with both control and treatment solutions (Data not shown). When treated with differentiation medium, 59.97% of hNSCs were differentiated into neurons (TUBB3<sup>+</sup> cells) and 40.03% cells were differentiated into astrocytes (GFAP<sup>+</sup> cells); however, 1  $\mu$ M AICAR and 1  $\mu$ M Luteolin treatments significantly decreased the percentages of TUBB3<sup>+</sup> cells to

respectively 36.66 and 33.2% ( $p < 0.05$ ) and increased the percentages of astrocytes (GFAP<sup>+</sup> cells) to 64.44 and 67.8%, respectively ( $p < 0.05$ ). These data indicate that as AICAR treatment, luteolin treatment enhanced the differentiation of hNSCs into astrocytes (Figure 2B).

### Luteolin Regulated Astroglial Gene Expressions in Human Neural Stem Cells

We validated the expressions of astroglial genes using RT-qPCR. As shown in Figure 2C, *GFAP* was not expressed in any treatment condition after 8 h even in repeated RT-qPCR experiments. However, after 24 h, *GFAP* was significantly overexpressed in AICAR-treated (relative *GFAP* mRNA expression = 1.8,  $p = 0.001$ ) and luteolin treated (relative *GFAP* mRNA expression = 1.69,  $p = 0.003$ ) cells compared to differentiation medium-treated control cells. This finding confirms that luteolin stimulated the differentiation of hNSCs into astrocytes.

Different signaling pathways, including BMP, JAK-STAT, Wnt, Notch, TGF- $\beta$ , and FGF signaling, are known to regulate the expression *GFAP* gene, which, in turn, induces astrocytogenesis (Wen et al., 2009; Lee et al., 2015). Therefore, we evaluated the expressions of the *BMP2* as a representative gene of BMP signaling, and *NOTCH1* and *NOTCH3* as representative genes of Notch signaling. We also evaluated the expression of the transcription factor *STAT3*, which binds to the promoter of *GFAP* to induce its expression.

*BMP2* gene was not expressed after 8 h treatment in both controls and treated cells, while it was significantly overexpressed after 24 h treatment with 1  $\mu$ M luteolin (Relative *BMP2* mRNA expression = 3.26,  $p = 0.003$ ) and with the positive astrogenic inducer AICAR (Relative *BMP2* mRNA expression = 3.36,  $p = 0.002$ ) (Figure 2C). *STAT3* was significantly overexpressed after 8 h in luteolin-treated hNSCs (Relative *STAT3* mRNA expression = 1.25,  $p = 0.059$ ) and it was significantly decreased after 24 h treatment (Relative *STAT3* mRNA expression = 0.41,  $p = 0.0001$ ) (Figure 2C). On the other hand, the AICAR treatment significantly decreased the *STAT3* expression after 8 h treatment (Relative *STAT3* mRNA expression = 0.55,  $p = 0.005$ ), and it increased after 24 h treatment (Relative *STAT3* mRNA expression = 1.15,  $p = 0.03$ ) (Figure 2C).

*NOTCH1* and *NOTCH3* were not expressed in any treatment condition after 8 h (Figure 2C). When treated for 24 h with 1  $\mu$ M luteolin, the expressions of *NOTCH1* and *NOTCH3* were significantly decreased to 0.39 and 0.48, respectively ( $p = 0.001$  and  $0.0001$  respectively). When treated with 1  $\mu$ M AICAR for the same duration (24 h), the expression of *NOTCH1* gene was unchanged and that of *NOTCH3* significantly increased to 1.48 ( $p = 0.001$ ). This result shows that unlike AICAR, luteolin inhibited Notch signaling and therefore inhibited the self-renewal of hNSC (Figure 2C).

### Luteolin Treatment Did Not Affect Neurogenic Gene Expression in Human Neural Stem Cells

The validation of *TUBB3* gene expression using RT-qPCR showed that luteolin treatment for 8 and 24 h did not affect the expression of *TUBB3* in hNSCs (Relative *TUBB3* mRNA

expression = 1.02,  $p = 0.92$  and 1.03,  $p = 0.949$  respectively for 8 and 24 h treatment) (Figure 2C). On the other hand, when treated with AICAR, the expressions of *TUBB3* in hNSCs were increased to 1.39 and 2.09, respectively, following 8 and 24 h of incubation ( $p = 0.21$  and  $p = 0.0001$  respectively) (Figure 2C) suggesting, thus, that AICAR is not a specific astrocytogenesis inducer.

### Luteolin Treatment Inhibited Oligogenic Gene Myelin Basic Protein Expression in Human Neural Stem Cells

Our immunostaining results using the oligodendrocytes marker anti-MBP protein antibody showed that 1  $\mu$ M luteolin treated hNSCs did not differentiate into oligodendrocytes within 24 h of differentiation induction (data not shown). In its turn, the global gene expression analysis shows that this treatment downregulates the MBP gene (FC = -1.37,  $p < 0.05$ ). The validation analysis of this gene expression using RT-qPCR also showed that hNSCs did not express the MBP gene after 24 h of luteolin treatment (Data not shown), confirming, therefore, that luteolin did not induce oligodendrocyte genesis of hNSCs.

## Results Obtained From the Animal Experiments

Figure 3A shows the animal experiment design.

### Effect of Luteolin Treatment on the Immobility Time in Lipopolysaccharide-Induced Depression Mice

Results from TST test indicate that the daily oral administration of luteolin (10 mg/kg body weight) slightly decreased the immobility time of LPS-induced depression mice on the 8th day of TST to  $77.5 \pm 52.5$  s compared to the initial test performed on the 1st day with a value of  $107.17 \pm 41.1$  s. It also decreased the immobility time of mice treated with PBS + L to  $77.17 \pm 35.5$  s compared to the initial test at day 1 ( $86.83 \pm 55.4$  s). These decreases were statistically non-significant (Figure 3B).

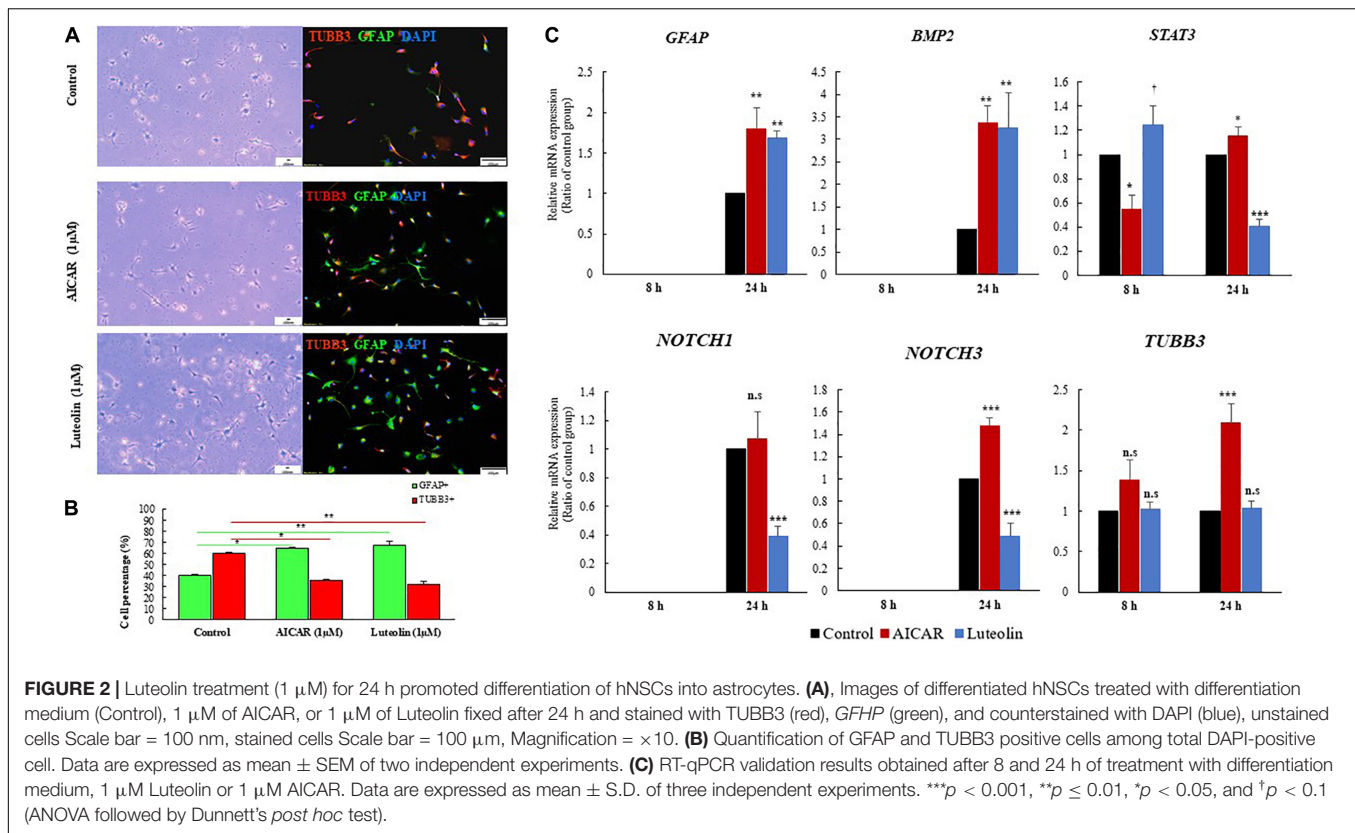
### Effect of Luteolin Treatment on Lipopolysaccharide Induced Depression Mice Astrocytes' Number

In the present study, the number of isolated astrocytes from whole brain of the LPS-induced depression mice was compared to that of LPS-induced depression mice treated with luteolin and control mice. Results show that LPS significantly reduced the number of astrocytes ( $p = 0.008$ ), however, luteolin treatment didn't restore the loss of astrocytes number (Figure 3C).

### Effect of Luteolin Treatment on IL-6 Secretion by Lipopolysaccharide Induced Depression Mice Astrocytes'

The quantification of the pro-inflammatory cytokine IL-6 in the cell culture media of primary isolated astrocytes after 1, 3, and 7 days post *in vitro* isolation show that luteolin treatment didn't affect the IL-6 level in PBS mice (PBS + L vs. PBS group), while LPS treatment significantly increase the production of IL-6 by astrocytes (LPS vs. PBS group), and luteolin treatment significantly decreased this pro-inflammatory cytokine secretion by astrocytes in LPS-induced depression mice (LPS + L vs. LPS group) (Figure 3D).





## Luteolin Treatment Changed Depression's Biomarkers Levels

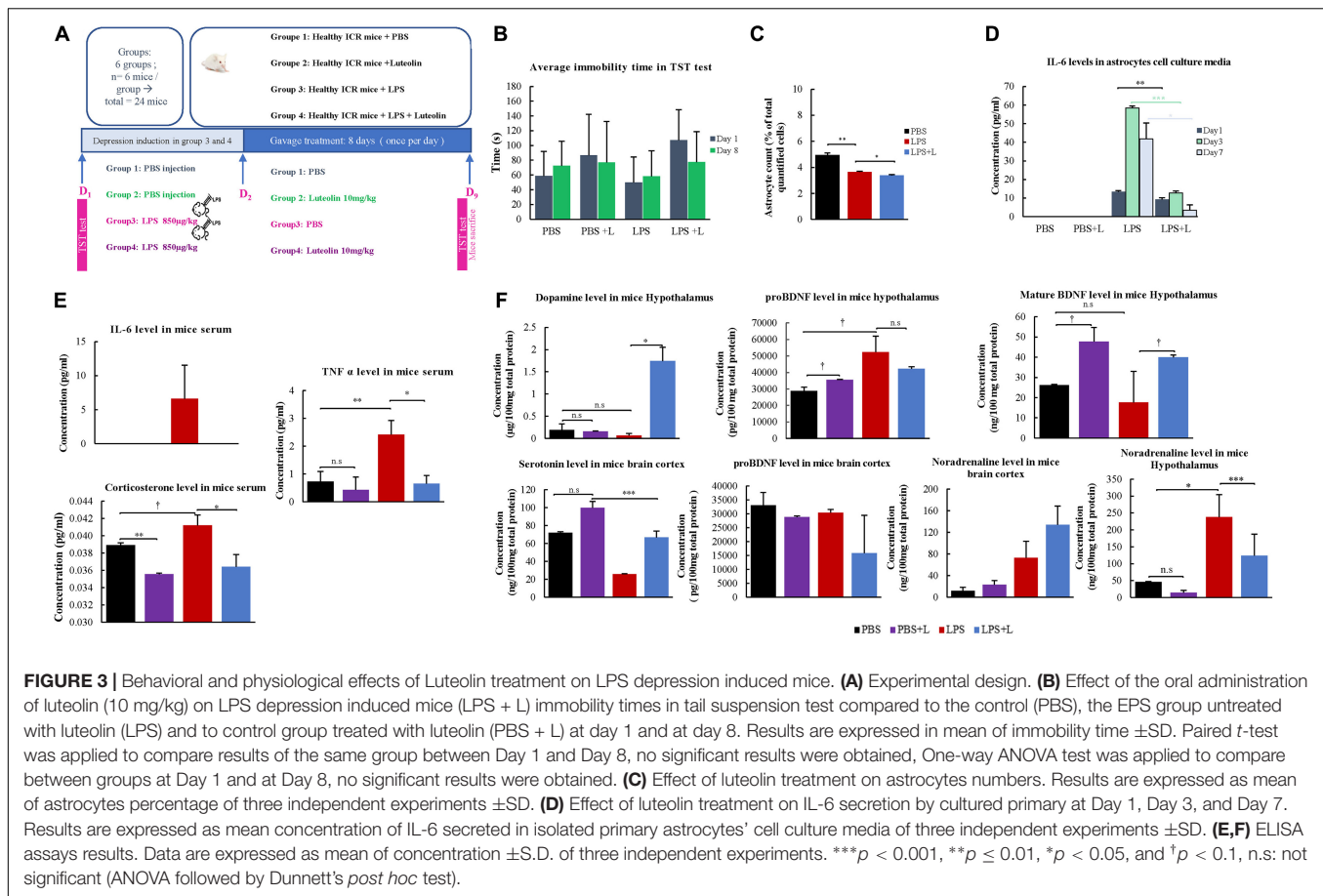
We evaluated the level of serum and central nervous system depression's biological markers in mice. **Figure 3E** shows that the oral administration of luteolin (10 mg/kg) changed the levels of the proinflammatory cytokines IL-6 and TNF $\alpha$ , and that of corticosterone in mice sera. IL-6 level was increased in LPS treated mice group compared to control group (PBS group), and luteolin treatment normalized this increase in LPS-induced depression mice (LPS + L group). Although statistically not significant ( $p$  > 0.05), the TNF- $\alpha$  level showed a decrease of 41.1% in control mice treated with luteolin (PBS + L) compared to untreated mice (PBS). LPS treatment significantly increased this pro-inflammatory cytokine level of 2.31% in mice sera compared to control mice ( $p$  = 0.01), and a statistically significant decrease of this cytokine level (73.15%) was observed when LPS-induced depression mice were treated with luteolin ( $p$  = 0.04) (**Figure 3E**). The corticosterone level showed a decrease of 8.49% in control mice treated with luteolin (PBS + L) compared to untreated mice (PBS) ( $p$  = 0.007). LPS treatment significantly increased this stress hormone level of 0.06% compared to control mice ( $p$  = 0.1), and luteolin treatment significantly decreased its level in LPS-induced depression mice (a decrease of 73.15% compared to untreated LPS-induced depression mice,  $p$  = 0.05).

The oral administration of luteolin (10 mg/kg) also significantly changed the levels of the mature BDNF, the noradrenaline and the dopamine in the hypothalamus of LPS-induced depression mice, and it didn't significantly affect the

level of pro-BDNF. Likewise, it didn't change ( $p$  > 0.05) the levels of pro-BDNF, serotonin and noradrenaline in the cerebral cortex of LPS-induced depression mice model (**Figure 3F**).

## Luteolin Treatment Affected Global Gene Expression in Neural Stem Cells of Lipopolysaccharide-Induced Depression Model

We evaluated the effect of LPS treatment on global genes expression in the NSCs of the chosen depression animal model (LPS-induced depression mice) by evaluating the transcriptomic changes in NSCs. Results show that LPS injection (850  $\mu$ g/kg) significantly regulated 382 genes ( $-1.3$  < Fold change < 1.3;  $p$  < 0.05). It downregulated 325 genes and upregulated 57 genes compared to untreated mice (PBS group) (data not shown). Five neuronal biological processes, namely neuron migration (GO:001764), negative regulation of neurogenesis (GO:0050768), generation of neurons (GO:0048699), regulation of neuron projection development (GO:0010975), and neurogenesis (GO:0022008); two glial biological processes particularly the gliogenesis (GO:0042063) and glial cell proliferation (GO:0014009); and four development biological processes related to brain development (GO:0007420), central nervous system development (GO:0007417), cell differentiation (GO:0030154) and nervous system development (GO:0007399), were enriched by downregulation (**Figure 4A**). The 33 downregulated genes related to neurogenesis are *Ddx6*, *Rab3a*, *Actb*, *Apcdd*, *Apoe*, *B2m*, *Camk2a*, *Cttnb1*, *Clu*, *Dbi*, *Dynl1f*, *Eef1a1*, *Fn1*, *Gja1*, *Gstp1*, *Gpm6a*, *Hspb1*, *Hsp90aa1*, *H2-D1*, *H2-K1*, *Id3*, *Itm2c*,



*Ppia*, *Pcnt*, *Plpp3*, *Ptn*, *Prom1*, *Rpl4*, *Serpine2*, *Slc1a3*, *Sod1*, *Ywhae*, and *Vim*, and the 11 genes related to gliogenesis include the *Apcdd1*, *Ctnnb1*, *Clu*, *Dbi*, *Fn1*, *Gstp1*, *Plpp3*, *Ptn*, *Serpine2*, *Sod1*, and *Vim*. Besides, two biological processes related to angiogenesis (GO:0001525) and to response to polysaccharide (GO:0032496) were enriched by upregulation (Figure 4A). The LPS injection significantly regulated genes related to different KEGG signaling pathways (Figure 4B). The estrogen signaling pathway (mmu04915), with ten genes being regulated, was the most significantly KEGG signaling pathway enriched by downregulation ( $p = 9.87E-05$ ). The downregulated genes include the *Fos*, *Gnas*, *Creb3*, *Gnai2*, *Hspa1b*, the *Hspa8*, *Hsp90ab1*, *Hsp90aa1*, *Hsp90b1* and the *Pik3cd* (Figure 4B and Table 1). The KEGG signaling pathways, Thyroid hormone synthesis (mmu04918), Adherens junction (mmu04520), cAMP signaling pathway (mmu04024), glutamatergic and dopaminergic synapses (mmu04724, mmu04728), PI3K-AKT signaling pathway (mmu04151), the thyroid hormone signaling pathway (mmu04919), gap junction (mmu04540) and insulin secretion (mmu04911) were also enriched by downregulation (Figure 4B). Details about regulated genes are mentioned in Table 1.

We also evaluated the effect of oral administration of luteolin (10 mg/kg body weight) on the transcriptomic changes in NSCs of LPS-induced depression mice. The obtained results show that

treatment with luteolin could significantly regulate the expression of 687 genes in NSCs of this animal model ( $-1.3 < \text{Fold change} < 1.3$ ;  $p < 0.05$ ) compared to untreated depression model mice (LPS + L group vs. LPS group), with upregulation of 642 genes and downregulation of 45 genes (data not shown). Top 10 significantly up and downregulated genes and their functions are presented in Supplementary Tables 6, 7, respectively. The upregulated genes significantly enriched biological processes related to nervous system development, glial and neuronal processes as well as signaling biological processes (Figure 4C). Interestingly, in these induced depression mice neural stem cells, the luteolin treatment upregulated 53 and 18 genes related to the neurogenesis and gliogenesis biological processes respectively. The genes related to neurogenesis biological process are: the *Arf1*, *Ddx6*, *Ndr1*, *Rab3a*, *Actb*, *Apcdd1*, *App*, *Apoe*, *B2m*, *Ctnna1*, *Ctnnb1*, *Cav1*, *Cdc42*, *Clu*, *Dbi*, *Dynl1f*, *Eef1a1*, *Eef2*, *Eif4g2*, *Fn1*, *Gja1*, *Gstp1*, *Gpm6a*, *Hey1*, *Hspb1*, *Hsp90aa1*, *Hexa*, *H2-D1*, *H2-K1*, *Id3*, *Id4*, *Itm2c*, *Il2*, *Mif*, *Mt2*, *Mt3*, *Mgll*, *Ntrk2*, *Ppia*, *Pcnt*, *Pmp22*, *Plpp3*, *Ptn*, *Prom1*, *Plp1*, *Rpl4*, *Serpine2*, *Slc1a3*, *Slc9a3r1*, *Snx3*, *Sod1*, *Ywhae*, and *Vim*, while those modulating the gliogenesis biological process are: *Ndr1*, *Apcdd1*, *Ctnnb1*, *Clu*, *Dbi*, *Eef2*, *Fn1*, *Gstp1*, *Id4*, *Mt2*, *Mt3*, *Ntrk2*, *Plpp3*, *Ptn*, *Plp1*, *Serpine2*, *Sod1*, *Vim*. The regulated genes also significantly modulated different KEGG signaling pathways (Figure 4D). The KEGG signaling pathway Parkinson's disease

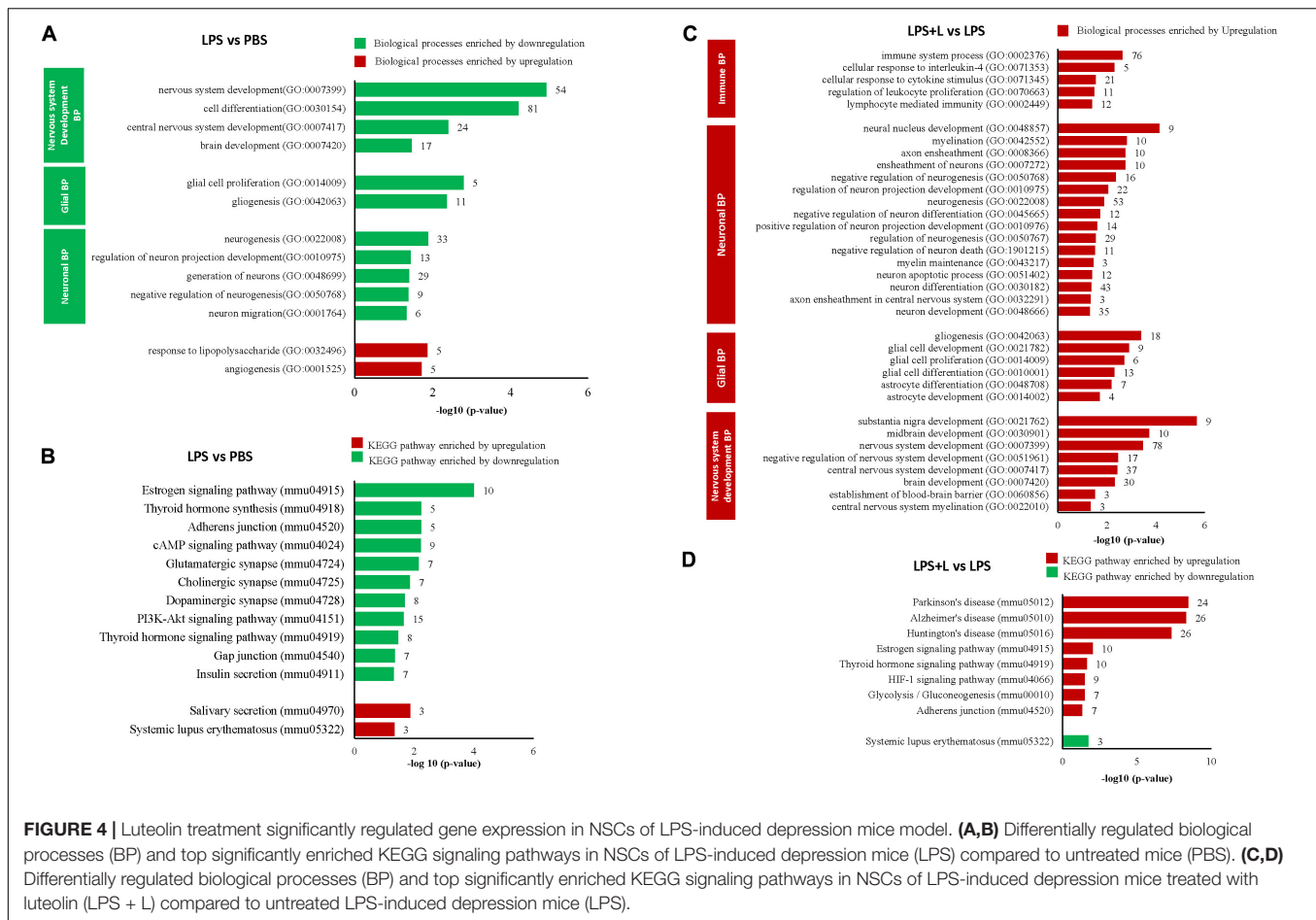


**FIGURE 4 |** Luteolin treatment significantly regulated gene expression in NSCs of LPS-induced depression mice model. **(A,B)** Differentially regulated biological processes (BP) and top significantly enriched KEGG signaling pathways in NSCs of LPS-induced depression mice (LPS) compared to untreated mice (PBS). **(C,D)** Differentially regulated biological processes (BP) and top significantly enriched KEGG signaling pathways in NSCs of LPS-induced depression mice treated with luteolin (LPS + L) compared to untreated LPS-induced depression mice (LPS).

(mmu05012) was the most significantly enriched signaling pathway by upregulation ( $p = 3.53E-09$ ). Twenty-four genes of this signaling pathway were enriched by upregulation. It includes 5 genes modulating the ATP synthase, H<sup>+</sup> transporting mitochondrial complexes (*Atp5g3*, *Atp5h*, *Atp5o*, *Atp5e*, *Atp5c1*), 8 genes of NADH dehydrogenase (*Ndufa13*, *Ndufa3*, *Ndufa9*, *Ndufb11*, *Ndufb5*, *Ndufv3*, *LOC102641347*, *ND5*), 6 genes of cytochrome c oxidase subunits (*Cox4i1*, *Cox7a2*, *Cox7a2l*, *Cox6a1*, *Cox5a*, *Cox5b*, *Cox6b*), as well as guanine *Gnai2*, *Slc25a4*, *Slc25a5*, and *Uqcrrb*. Also, twenty-six genes in Alzheimer's disease KEGG signaling pathway (mmu05010,  $p = 4.76E-09$ ), 26 genes in Huntington's disease KEGG signaling pathway (mmu05016,  $p = 4.77E-08$ ), 17 genes in Non-alcoholic fatty liver disease (NAFLD) KEGG signaling pathway (mmu04932,  $p = 0.0001$ ), 10 in Estrogen signaling pathway (mmu04915,  $p = 0.0093$ ) KEGG signaling pathway, 10 genes in thyroid hormone signaling pathway (mmu04919;  $p = 0.02$ ), 9 genes in HIF-1 signaling pathway (mmu04066,  $p = 0.03$ ), 7 genes glycolysis/gluconeogenesis (mmu00010,  $p = 0.03$ ), and 7 genes in adherens junction (mmu04520,  $p = 0.04$ ) were also enriched by upregulation. Systemic lupus erythematosus (mmu05322,  $p = 0.017$ ), was the only KEGG signaling pathway enriched by downregulation. Details about regulated genes are mentioned in Table 2.

Ultimately, we evaluated the effect of oral luteolin treatment (10 mg/kg body weight) on the transcriptomic changes in NSCs of normal mice (PBS + L group vs. PBS group, **Supplementary Figure 4**). The obtained results point out the modulation of gene expression by luteolin treatment in NSCs of normal mice ( $-1.3 < \text{Fold change} < 1.3$ ;  $p < 0.05$ ) compared to untreated normal mice, with upregulation of 314 genes and downregulation of 428 genes (data not shown). Moreover, we found that luteolin treatment significantly downregulated 4 glial biological processes, namely the glial cell migration (GO:008347), negative regulation of gliogenesis (GO:0014014), glial cell differentiation (GO:0010001), and negative regulation of oligodendrocyte differentiation (GO:0048715) in NSCs of normal mice (PBS + L group), while it downregulated 8 neuronal biological processes, up regulated 9 others (**Supplementary Figure 4A**). In this mice group NSCs, the effect of luteolin treatment on glial biological processes was more pronounced than that of the neurogenic effect and it was revealed by the downregulation of three genes related to the negative regulation of oligodendrocytes differentiation (*Cttnb1*, *Notch1*, and *Sirt2*), the downregulation of 9 genes involved in the glial cell differentiation (*Ndr1*, *Cttnb1*, *Clu*, *Notch1*, *Plpp3*, *Serpine2*, *Sirt2*, *Sod1*, *Vim*), the downregulation of 4 genes related to the negative regulation of gliogenesis (*Cttnb1*,



*Notch1*, *Ptn*, *Sirt2*) and the downregulation of the 4 genes involved in the glial cell migration (*Apcdd1*, *Ctnnb1*, *Fn1*, *Vim*). The luteolin treatment also enriched 8 KEGG signaling pathway by downregulation and only one KEGG signaling by upregulation (Supplementary Figure 4B). The enriched KEGG signaling by upregulation was the Wnt KEEG signaling pathways (mmu04310,  $p = 0.04$ ) with 6 genes being upregulated (*Apc2*, *Camk2a*, *Ccnd2*, *Prickle2*, *Tcf7l1*, *Wnt11*). The KEGG signaling pathways enriched by downregulation were Hippo signaling pathway (mmu04390,  $p = 3.24E-02$ , 9 genes), tight junction (mmu04530,  $p = 2.31E-02$ , 7 genes), thyroid hormone signaling pathway (mmu04919,  $p = 0.022$ , 8 genes), gap junction (mmu04540,  $p = 0.019$ , 7 genes), HIF-1 signaling (mmu04066,  $p = 0.012$ , 8 genes), dopaminergic synapse (mmu04728,  $p = 0.005$ , 10 genes), Alzheimer's disease (mmu05010,  $p = 0.0004$ , 14 genes), and Parkinson's disease (mmu05012,  $p = 0.0003$ , 13 genes) (Supplementary Figure 4B). Details about regulated genes are mentioned in Supplementary Table 8.

### Luteolin Treatment Affected Global Gene Expression in Hippocampus of Lipopolysaccharide-Induced Depression Model

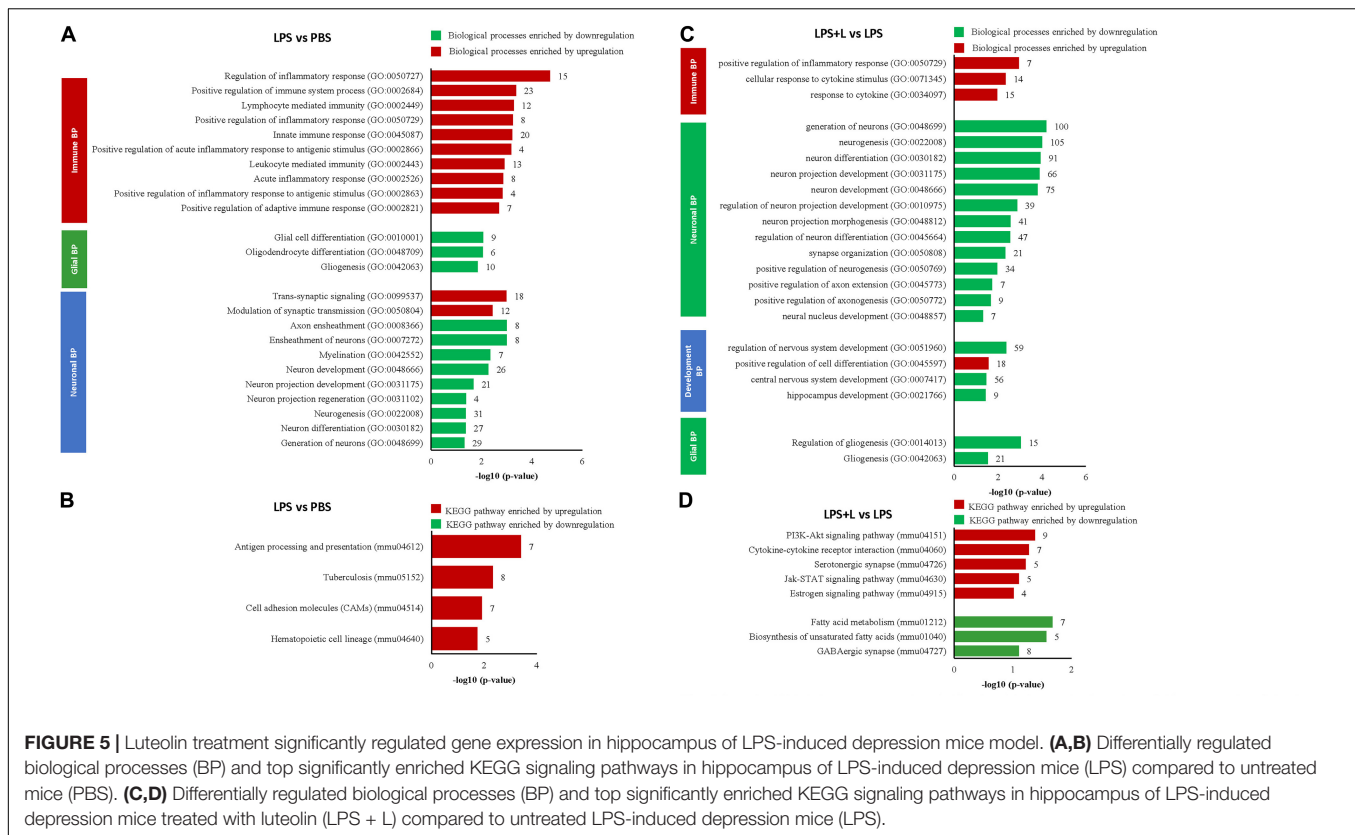
We used DNA microarray to study the transcriptomic changes in the hippocampus of the depression mice model. Results show that LPS injection (850  $\mu\text{g/kg}$ ) significantly regulated 665 genes ( $-1.3 < \text{Fold change} < 1.3$ ;  $p < 0.05$ ). It downregulated 348 genes and upregulated 317 genes in this animal model of depression (LPS group mice) compared to untreated mice (PBS group) (data not shown). Nine neuronal biological processes including neuron differentiation (GO:0030182), neurogenesis (GO:0022008) were significantly downregulated. Ten genes related to gliogenesis (GO:0042063), 6 genes related to oligodendrocyte differentiation (GO:0048709), and 9 genes related to glial cell differentiation (GO:0010001) were also significantly downregulated. However, ten immune biological processes were significantly upregulated (Figure 5A). Thirty-one genes related to the neurogenesis biological process were downregulated. It includes the *Atp7a*, *Bcl11a*, *C1qtnf5*, *Cd9*, *Ndr1*, *Rufy3*, *Abi2*, *Aspa*, *Camk2a*, *Ctnna1*, *Col25a1*, *Cdkn1c*, *Ddr1*, *Enpp2*, *Folr1*, *Hspa5*, *Lpar1*, *Micall1*, *Mapk8*, *Miat*, *Myo7a*, *Ntn4*, *Otx2*, *Prex2*, *Plp1*, *Rtn4*, *Robo3*, *Six3*, *Slc11a2*, *Stx3* and the *Tspo*. Equally, in these mice hippocampus, the LPS injection downregulated 10 genes related to gliogenesis (*Cd9*, *Ndr1*, *Aspa*, *Enpp2*, *Lpar1*, *Miat*, *Otx2*, *Plp1*, *Rtn4* and *Tspo*). LPS injection also significantly enriched KEEG signaling pathways by upregulation (Figure 5B). It includes the hematopoietic cell lineage (mmu04640,  $p = 0.018$ , 5 genes), cell adhesion molecules (CAMs) (mmu04514,  $p = 0.012$ , 7 genes), tuberculosis (mmu05152,  $p = 0.004$ , 8 genes), and antigen processing and presentation (mmu04612,  $p = 3.95E-04$ , 7 genes). Details about regulated genes are presented in Table 3.

We further used DNA microarray to study the transcriptomic changes in the hippocampus of the depression mice model after oral administration of luteolin (10 mg/kg body weight). Results show that treatment with luteolin significantly regulated the expression of 1371 genes in hippocampus of this animal model ( $-1.3 < \text{Fold change} < 1.3$ ;  $p < 0.05$ ) compared to untreated depression model mice (LPS + L group vs. LPS group), with

upregulation of 324 genes and downregulation of 1047 genes (Data not shown). Top 10 significantly up and downregulated genes and their functions are presented in Supplementary Tables 9, 10, respectively. The upregulated genes significantly enriched biological processes related to different immune responses namely; response to cytokine (GO:0034097), cellular response to cytokine stimulus (GO:0071345) and positive regulation of inflammatory response (GO:0050729) as well as to the development biological process positive regulation of cell differentiation (GO:0045597) (Figure 5C). The downregulated genes significantly enriched 13 neuronal biological processes; mainly generation of neurons (GO:0048699, 100 genes), neurogenesis (GO:0022008, 105 genes), neuron differentiation (GO:0030182, 91 genes), 3 development processes including regulation of nervous system development (GO:0051960, 59 genes), central nervous system development (GO:0007417, 56 genes) and hippocampus development (GO:0021766), and 2 glial processes namely regulation of gliogenesis (GO:0014013, 15 genes) and gliogenesis (GO:0042063, 21 genes) (Figure 5C). The regulated genes also significantly enriched different KEEG signaling pathways (Figure 5D and Table 4). Luteolin treatment upregulated 9 genes involved in PI3K-Akt signaling (mmu04151,  $p = 0.04$ ) namely the *Col2a1*, *Egfr*, *Egfr*, *Fgf18*, *Il4ra*, *Lama5*, *Pik3cg*, *Prlr*, *Rxra*, and the *Rps6*; 7 genes in cytokine-cytokine receptor interaction (mmu04060,  $p = 0.05$ ) including the *Relt*, *Ccr2*, *Eda*, *Inhbb*, *Il17ra*, *Il4ra*, and the *Prlr*; 5 genes in serotonergic synapse (mmu04726,  $p = 0.05$ ) namely the *Htr5b*, *Gnas*, *Alox12*, *Alox15*, *Alox8*; 5 genes in Jak-STAT signaling (mmu04630,  $p = 0.07$ ) including the *Crebbp*, *Il4ra*, *Pik3cg*, *Prlr*, and the *Stat5b*; and 4 genes in Estrogen signaling pathway (mmu04915,  $p = 0.096$ ) including the *Elovl5*, *Acaa1a*, *Acaa2*, *Acs13*, *Acadl*, *Elovl2*, and the *Fads2*. Besides, luteolin treatment downregulated 7 genes in fatty acid metabolism KEEG signaling (mmu012,  $p = 0.02$ ) particularly the *Elovl5*, *Acaa1a*, *Acaa2*, *Acs13*, *Acadl*, *Elovl2*, *Fads2*; 5 genes in biosynthesis of unsaturated fatty acids (mmu01040,  $p = 0.02$ ) including the *Elovl5*, *Acaa1a*, *Acot1*, *Elovl2*, *Fads2*, and 8 genes in GABAergic synapse (mmu04727,  $p = 0.07$ ) namely the *Gabrb3*, *Gphn*, *Gad1*, *Glul*, *Gnai3*, *Gnb1*, *Gng2*, and the *Prkacb* (Figure 5D and Table 4).

Ultimately, we evaluated the effect of oral luteolin treatment (10 mg/kg body weight) on the transcriptomic changes in hippocampus of normal mice (PBS + L group vs. PBS group) using DNA microarray (Supplementary Figures 4C,D). The obtained results point out the modulation of gene expression by luteolin treatment in hippocampus of normal mice ( $-1.3 < \text{Fold change} < 1.3$ ;  $p < 0.05$ ) compared to untreated normal mice, with upregulation of 381 genes and downregulation of 978 genes (Data not shown). Luteolin treatment significantly downregulated 5 immune biological processes, including inflammatory response (GO:0006954, 18 genes), 6 glial processes including gliogenesis (GO:0042063, 13 genes), glial cell differentiation (GO:0010001), oligodendrocyte differentiation (GO:0048709), and 4 neuronal processes namely neuron projection development (GO:0031175, 21 genes), neuron differentiation (GO:0030182, 29 genes), neurogenesis (GO:0022008, 38 genes) and myelination (GO:0042552, 8 genes) (Supplementary Figure 4C). Besides, luteolin treatment significantly upregulated the expression of





18 genes related to gliogenesis (GO:0042063) including the *Phgdh*, *Kras*, *Adgrg1*, *Atxn1*, *Ctnnb1*, *Dcx*, *Egr2*, *Fgfr3*, *Gfap*, *Mecp2*, *Nf2*, *Ntrk2*, *Ntrk3*, *Pten*, *Pdgfb*, *Synj1*, *Tenm4*, *Vtn*, while it downregulated 13 others (*Ndr1*, *Apcdd1*, *Ctnnb1*, *Clu*, *Dbi*, *Fn1*, *Notch1*, *Plpp3*, *Ptn*, *Serpine2*, *Sirt2*, *Sod1*, and *Vim*), as well as different neuronal processes, particularly, neurogenesis (GO:0022008, 118 genes), neuron differentiation (GO:0030182, 101 genes), positive regulation of neurogenesis (GO:0050769, 40 genes), and positive regulation of neuron differentiation (GO:0045666) (**Supplementary Figure 4C**).

Along with other KEGG signaling pathways presented in **Supplementary Figure 4D**, dopaminergic synapse (mmu04728,  $p = 0.08$ , 9 genes), GABAergic synapse (mmu04727,  $p = 0.07$ , 7 genes), neurotrophin signaling pathway (mmu04722,  $p = 0.05$ , 9 genes), hippo signaling pathway (mmu04390,  $p = 0.013$ , 12 genes), PI3K Akt signaling pathway (mmu04151,  $p = 0.008$ , 22 genes) and signaling pathways regulating pluripotency of stem cells (mmu04550,  $p = 0.007$ , 12 genes), were significantly upregulated (**Supplementary Figure 4D**). Details about regulated genes are mentioned in **Supplementary Table 11**.

## DISCUSSION

The present study is the first to report the effects of the natural flavonoid luteolin on hNSCs fate determination highlighting; therefore, its potential beneficial use, especially as an astroglialgenesis promoting compound. We have evaluated

the effect of luteolin on the fate choice of hNSCs isolated from the fetal cortex. In terms of the therapeutic potential of NSCs in neurodegenerative diseases and neural injury, both fetal and adult brain-derived hNSCs have shown promising effects (Casarosa et al., 2014). However, fetal brain-derived NSCs grown as neurospheres can better mimic the brain developmental processes, including trilineage differentiation, proliferation, apoptosis, and migration (Schmuck et al., 2017). We found that luteolin could regulate the expression of the astrogenic gene *GFAP*, along with genes involved in WNT- $\beta$ -catenin-BMP2-STAT3 pathways, which have been implicated in astrogliogenesis. In addition, an increased number of GFAP+ cells observed in immunostaining confirms the astrogliogenesis-inducing effects of luteolin on hNSCs. Besides, we compared our findings with a well-known positive astrogenic inducer AICAR, which further signifies the astrocyte-specific differentiation-inducing effects of luteolin.

The present study is also the first study to evaluate whether luteolin may exert an antidepressant effect by directing the fate choice of mice NSCs into astroglial and neuronal cells, restoring, therefore, the brain cells loss in the neuroinflammatory model of depression (LPS-induced depression mice). Numerous studies reported that a modification of astrocytes in the frontolimbic regions like the hippocampus, amygdala and ventral striatum is associated with depression. Likewise, most major depressed patients' post-mortem brain analyses reported a decreased number of astrocytes in frontolimbic structures (Altshuler et al., 2010; Rajkowska and Stockmeier, 2013; Peng et al., 2015;

**TABLE 3 |** Top significantly enriched KEGG signaling pathways in Hippocampus of LPS-induced depression mice (LPS) compared to untreated normal mice (PBS).

Regulation	KEGG signaling	Genes
Upregulation	<b>Hematopoietic cell lineage (mmu04640)</b>	CD44 antigen ( <b>Cd44</b> )
		Fc receptor, IgG, high affinity I ( <b>Fcgr1</b> )
		colony stimulating factor 1 receptor ( <b>Csf1r</b> )
		histocompatibility 2, class II antigen E beta ( <b>H2-Eb1</b> )
		sialic acid binding Ig-like lectin H ( <b>Siglech</b> )
	<b>Cell adhesion molecules (CAMs) (mmu04514)</b>	H-2 class I histocompatibility antigen, K-D alpha chain ( <b>LOC101056305</b> )
		cadherin 15 ( <b>Cdh15</b> )
		contactin 2 ( <b>Cntn2</b> )
		golgi apparatus protein 1 ( <b>Glg1</b> )
		histocompatibility 2, K1, K region ( <b>H2-K1</b> )
		histocompatibility 2, Q region locus 6 ( <b>H2-Q6</b> )
		histocompatibility 2, class II antigen E beta ( <b>H2-Eb1</b> )
	<b>Tuberculosis (mmu05152)</b>	CD74 antigen (invariant polypeptide of major histocompatibility complex, class II antigen-associated) ( <b>Cd74</b> )
		Fc receptor, IgE, high affinity I, gamma polypeptide ( <b>Fcer1g</b> )
		Fc receptor, IgG, high affinity I ( <b>Fcgr1</b> )
		Fc receptor, IgG, low affinity III ( <b>Fcgr3</b> )
		apoptotic peptidase activating factor 1 ( <b>Apaf1</b> )
		calcium/calmodulin-dependent protein kinase II, delta ( <b>Camk2d</b> )
		cathepsin S ( <b>Ctss</b> )
	<b>Antigen processing and presentation (mmu04612)</b>	CD74 antigen (invariant polypeptide of major histocompatibility complex, class II antigen-associated) ( <b>Cd74</b> )
		H-2 class I histocompatibility antigen, K-D alpha chain ( <b>LOC101056305</b> )
		beta-2 microglobulin ( <b>B2m</b> )
		cathepsin S ( <b>Ctss</b> )
		histocompatibility 2, K1, K region ( <b>H2-K1</b> )
		histocompatibility 2, Q region locus 6 ( <b>H2-Q6</b> )
		histocompatibility 2, class II antigen E beta ( <b>H2-Eb1</b> )

Gene abbreviations are indicated in bold.

Rial et al., 2016). The causality between astrocytic dysfunction and depression was also provided by animal studies showing that the selective destruction of frontocortical astrocytes is sufficient to induce depressive behavior (Banasr and Duman, 2008). Moreover, several studies evidence the reduced neurogenesis in animal models of depression and postmortem studies of depressed patients (Huffman and Taylor, 2020). Our results point out that luteolin treatment may exert an antidepressant effect in LPS mice by decreasing IL-6 production by astrocytes, decreasing the levels of IL-6, TNF alpha, and corticosterone in serum, and by increasing mature BDNF, dopamine and noradrenaline levels in the hypothalamus. Moreover, we found that luteolin treatment significantly regulated global genes expression, biological processes, and KEGG signaling in the isolated NSC and the hippocampi of the LPS induced depression mice model. It regulated gliogenesis and neurogenesis processes in the isolated mice' NSCs and the hippocampi with a clearer gliogenesis upregulation observed in NSCs, highlighting then the potential use of luteolin as a neuro-glial enhancer to overcome depression.

Gene ontology enrichment analysis of differentially expressed genes between luteolin-treated and untreated control hNSCs showed that the most significantly enriched biological process

was cell differentiation, followed by, but not limited to, neurogenesis, neuron development, neuron projection development, brain development, and regulation of astrocyte differentiation. When we averaged the signal intensities of genes related to astrogenesis-specific biological processes, we found that astrocyte differentiation- and positive regulation of astrocyte differentiation-related genes had higher signal intensity in luteolin-treated hNSCs compared to control cells, whereas negative regulation of astrocyte differentiation-related genes had lower signal intensity. Several KEGG signaling pathways, namely NOTCH, FOXO, TNF, p53, Hippo, dopaminergic synapse, and neurotrophin pathways, were also significantly regulated.

Considering previously published studies on genes involved in neural stem cell differentiation, we evaluated the effect of luteolin on 37 selected genes. We found similar expression patterns of these genes in luteolin-treated hNSCs (Hsieh et al., 2004; Cahoy et al., 2008; Yao and Jin, 2014; Hsieh and Zhao, 2016; Bejoy et al., 2019). Our results were marked by the downregulation of the stemness genes *NOTCH1* and *NOTCH3* (Venkatesh et al., 2017), neurogenic genes *DNMT1*, *DNMT3B*, *NEUROG2*, *BCL11B*, *NEUROD1*, *NEUROD1*, *NEUROD6*, *NOTCH1*, *NOTCH3*, and *TUBB3* (Yao and Jin, 2014), and oligodendrocyte genesis gene *MBP*. Besides, our findings were also marked by the upregulation

of the astrogenic gene *GFAP* as well as other genes of the key signaling pathways involved in astrogenesis such as Wnt, BMP, and JAK-STAT pathways (Takouda et al., 2017). It is worth noting

that DNA methylation, one of the core epigenetic modifications, has been implicated in several extrinsic pathways during neurogenesis both in physiologic and in diseased conditions

**TABLE 4 |** Top significantly enriched KEGG signaling pathways in Hippocampus of LPS-induced depression mice treated with luteolin (LPS + L) compared to untreated LPS-induced depression mice (LPS).

Regulation	KEGG signaling	Genes
Upregulation	<b>PI3K-Akt signaling pathway (mmu04151)</b>	collagen, type II, alpha 1 ( <i>Col2a1</i> ) epidermal growth factor receptor ( <i>Egfr</i> ) fibroblast growth factor 18 ( <i>Fgf18</i> ) interleukin 4 receptor, alpha ( <i>Il4ra</i> ) laminin, alpha 5 ( <i>Lama5</i> ) phosphoinositide-3-kinase, catalytic, gamma polypeptide ( <i>Pik3cg</i> ) prolactin receptor ( <i>Prlr</i> ) retinoid X receptor alpha ( <i>Rxra</i> ) ribosomal protein S6 ( <i>Rps6</i> )
	<b>Cytokine-cytokine receptor interaction (mmu04060)</b>	RELt tumor necrosis factor receptor ( <i>Relt</i> ) chemokine (C-C motif) receptor 2 ( <i>Ccr2</i> ) ectodysplasin-A ( <i>Eda</i> ) inhibin beta-B ( <i>Inhbb</i> ) Interleukin 17 receptor A ( <i>Il17ra</i> ) Interleukin 4 receptor, alpha ( <i>Il4ra</i> ) prolactin receptor ( <i>Prlr</i> )
	<b>Serotonergic synapse (mmu04726)</b>	5-hydroxytryptamine (serotonin) receptor 5B ( <i>Htr5b</i> ) GNAS (guanine nucleotide binding protein, alpha stimulating) complex locus ( <i>Gnas</i> ) arachidonate 12-lipoxygenase ( <i>Alox12</i> ) arachidonate 15-lipoxygenase ( <i>Alox15</i> ) arachidonate 8-lipoxygenase ( <i>Alox8</i> )
	<b>Jak-STAT signaling pathway (mmu04630)</b>	CREB binding protein ( <i>Crebbp</i> ) interleukin 4 receptor, alpha ( <i>Il4ra</i> ) phosphoinositide-3-kinase, catalytic, gamma polypeptide ( <i>Pik3cg</i> ) prolactin receptor ( <i>Prlr</i> ) signal transducer and activator of transcription 5B ( <i>Stat5b</i> )
	<b>Estrogen signaling pathway (mmu04915)</b>	FK506 binding protein 4 ( <i>Fkbp4</i> ) GNAS (guanine nucleotide binding protein, alpha stimulating) complex locus ( <i>Gnas</i> ) epidermal growth factor receptor ( <i>Egfr</i> ) phosphoinositide-3-kinase, catalytic, gamma polypeptide ( <i>Pik3cg</i> )
Downregulation	<b>Fatty acid metabolism (mmu01212)</b>	ELOVL family member 5, elongation of long chain fatty acids (yeast) ( <i>Elovl5</i> ) acetyl-Coenzyme A acyltransferase 1A ( <i>Acaa1a</i> ) acetyl-Coenzyme A acyltransferase 2 (mitochondrial 3-oxoacyl-Coenzyme A thiolase) ( <i>Acaa2</i> ) acyl-CoA synthetase long-chain family member 3 ( <i>Acsf3</i> ) acyl-Coenzyme A dehydrogenase, long-chain ( <i>Acadl</i> ) elongation of very long chain fatty acids (FEN1/Elo2, SUR4/Elo3, yeast)-like 2 ( <i>Elovl2</i> ) fatty acid desaturase 2 ( <i>Fads2</i> )
	<b>Biosynthesis of unsaturated fatty acids (mmu01040)</b>	ELOVL family member 5, elongation of long chain fatty acids (yeast) ( <i>Elovl5</i> ) acetyl-Coenzyme A acyltransferase 1A ( <i>Acaa1a</i> ) acyl-CoA thioesterase 1 ( <i>Acot1</i> ) elongation of very long chain fatty acids (FEN1/Elo2, SUR4/Elo3, yeast)-like 2 ( <i>Elovl2</i> ) fatty acid desaturase 2 ( <i>Fads2</i> )

(Continued)

TABLE 4 | (Continued)

Regulation	KEGG signaling	Genes
	<b>GABAergic synapse (mmu04727)</b>	<p>gamma-aminobutyric acid (GABA) A receptor, subunit beta 3 (<b>Gabrb3</b>)</p> <p>gephyrin (<b>Gphn</b>)</p> <p>glutamate decarboxylase 1 (<b>Gad1</b>)</p> <p>glutamate-ammonia ligase (glutamine synthetase) (<b>Glu1</b>)</p> <p>guanine nucleotide binding protein (G protein), alpha inhibiting 3 (<b>Gnai3</b>)</p> <p>guanine nucleotide binding protein (G protein), beta 1 (<b>Gnb1</b>)</p> <p>guanine nucleotide binding protein (G protein), gamma 2 (<b>Gng2</b>)</p> <p>protein kinase, cAMP dependent, catalytic, beta (<b>Prkacb</b>)</p>

Gene abbreviations are indicated in bold.

(Wang et al., 2016b). *DNMT1* and *MECP2* are the key regulators of DNA methylation that control the timing and magnitude of astroglial differentiation. Conditional deletion of *DNMT1* in neural progenitor cells increases the expressions of astrocyte marker genes and activates the gliogenic JAK-STAT pathway (Fan et al., 2005). *MECP2* binds to the highly methylated regions of astrocyte-specific genes, such as *GFAP*, and suppresses their expression (Fan et al., 2005), inhibits astrocyte differentiation, and promotes neuronal differentiation (Kohyama et al., 2008; Tsujimura et al., 2009); whereas, loss of *MECP2* elevates the expression of glial markers and accelerates astrogenesis (Okabe et al., 2012; Forbes-Lorman et al., 2014). On the other hand, *TET*, an enzyme responsible for DNA demethylation, has been shown to negatively regulate neuronal differentiation in neuroblastoma cell line independent of its enzymatic activity (Gao et al., 2016). TETs also downregulate the expressions of *DNMT1* and *de novo* methyltransferases *DNMT3A* and *DNMT3B* and increase expression of the neurotrophic factor *BDNF* (Santiago et al., 2014). In this present study, we found that 24 h treatment with luteolin in hNSCs suppressed the expressions of *DNMT1*, *DNMT3B*, *MECP2*, while increased the expressions of Tet methylcytosine dioxygenase 1 (*TET1*), *JAK2*, *STAT4*, *STAT6*, and Brain-derived neurotrophic factor (*BDNF*). Besides, we also found that luteolin treatment could upregulate the expression of *NEUROG1*, whereas downregulate the expression of *NEUROG2*. *NEUROGs* are the proneural genes, which encode basic-helix-loop-helix (bHLH) transcription factors. Although both *NEUROG1* and *NEUROG2* individually promote neurogenesis, *NEUROG1* exerts a non-canonical role through inhibiting the proneural activity of *NEUROG2*, thus, in turn, induces the expression of negative regulators of neurogenesis, and represses the expression of positive regulators of neurogenesis, such as *NEURODs* (Han et al., 2018). Ectopic expression of *NEUROD1*, another important bHLH transcription factor that mediates neuronal fate specification, has been reported to be sufficient to initiate a neurogenic program that closely recapitulates neuronal development *in vivo* (Pataskar et al., 2016). In our study, luteolin treatment repressed the expression of *NEUROD1* as well as *NEUROD 6*. In addition, luteolin treatment downregulated the expression of B-cell CLL/lymphoma 11 B (*BCL11b*), an important zinc finger protein transcription factor implicated in neurogenesis and in a pathological pathway of negative regulation of *BDNF* (Tang et al., 2011; Lennon et al., 2017). Thus, altogether our DNA microarray results suggest

that luteolin treatment could provide an efficient platform for astrocyte differentiation from hNSCs, while negatively regulating the hNSCs self-renewal, neurodifferentiation, and oligodendrocytes genesis.

To validate the astrogenic effect of luteolin on hNSCs, immunocytochemistry was performed on 24 h luteolin-treated hNSCs. Results were compared to that of the positive astrogenic inducer AICAR-treated hNSCs and the untreated control hNSCs. After 24 h of differentiation induction, hNSCs were exclusively differentiated toward *Tubb3+* and *GFAP+* cells corresponding to neurons and astrocytes, respectively. We found that *GFAP+* cells were increased in luteolin-treated hNSCs compared to untreated control hNSCs. This increase in the number of *GFAP+* cells was even slightly higher in luteolin-treated cells than that observed in AICAR-treated cells. Conversely, the number of *TUBB3+* cells was slightly lower in luteolin-treated cells compared to AICAR-treated cells. This finding suggests that luteolin would have a more powerful astrogenic effect on hNSCs than AICAR. Besides, *MBP+* cells were not detected within 24 h of differentiation induction with both control and treatment solutions. As Grinspan et al., reported that glial differentiation takes place after neuronal differentiation and that astrocytes arise earlier than oligodendrocytes, our findings suggest that 24 h treatment was not enough to evaluate the effect of luteolin and AICAR on the oligodendrocytes differentiation process (Grinspan, 2002).

Previous studies reported that six signaling pathways, namely Wnt, BMP, Stat3, Notch, Shh, PDGF/EGF, ERK1/2, and JAK/STAT3 are involved in stem cell fate-determining signaling (Wen et al., 2009; Lee et al., 2015; Sasaki et al., 2019). To validate the findings of DNA microarray analysis and immunostaining, we further opted for quantitative genetic analysis using the RT-qPCR method. The expression profiles of seven genes, namely the neuron-specific *TUBB3*, the astrocyte-specific *GFAP*, the oligodendrocyte-specific *MBP* genes as well as the *BMP2*, *STAT3*, *NOTCH1*, and *NOTCH3* were analyzed to elucidate the molecular mechanism followed by luteolin to suppress the self-renewal properties of hNSCs, to attenuate the neurogenesis and to enhance the astrocytic differentiation in hNSCs. Additionally, the effects of AICAR on the expression of the aforementioned genes were also evaluated to compare the molecular mechanism followed by both molecules. The RT-qPCR results of 24 h post-treatment showed that both luteolin and AICAR significantly increased the expressions



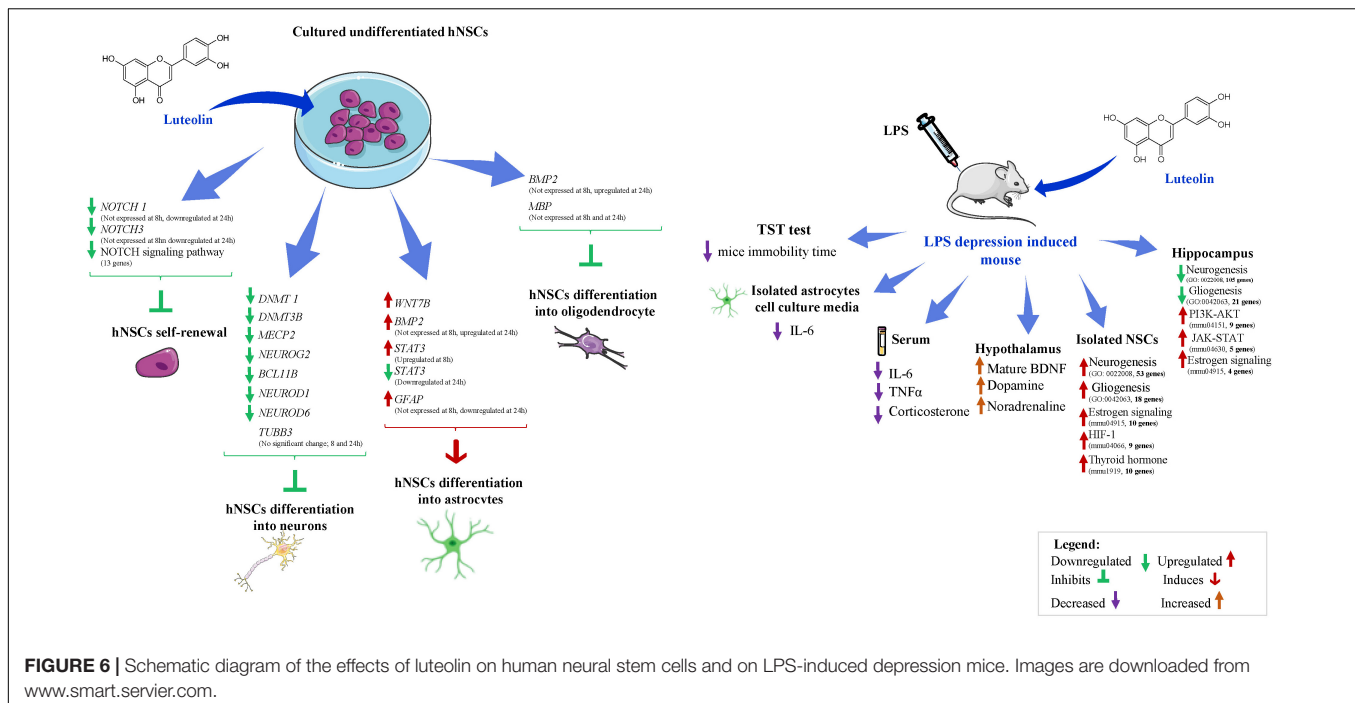
of *GFAP* and *BMP2* and repressed the expression of *MBP*; also, luteolin did not affect *TUBB3* expression, while AICAR increased its expression. And finally, while AICAR treatment increased the expressions of *STAT3*, *NOTCH1*, and *NOTCH3*, luteolin significantly decreased the expressions of these genes. Taken together, the repression of *MBP* expression and the increase of *BMP2* expression by luteolin and AICAR treatment suggest that both molecules induced the astrocytogenesis and repressed the oligodendrocytogenesis possibly *via* the Wnt- $\beta$  catenin signaling pathway. The Wnt signaling, especially the canonical signaling (Wnt- $\beta$  catenin), is crucial for NSC self-renewal and neurogenesis (Kasai et al., 2005; Wen et al., 2009); however, it also promotes astrocyte differentiation and suppresses oligodendroglial differentiation in a phase-dependent manner through BMP signal modulation (Kasai et al., 2005). Besides, the BMP signaling, in its turn, is reported to induce astrocytogenesis and repress oligodendrocyte genesis (Takouda et al., 2017). Among BMP family proteins, *BMP2* signaling is reported to stimulate the astrocytic differentiation of NSCs *via* the initiation of the transcription of the astrogenic gene *GFAP* (Nakashima et al., 1999; Sloan and Barres, 2014; Takouda et al., 2017). Other studies reported that to stabilize the astrocyte phenotype, once *GFAP* is expressed, its transcription factor *STAT3*, together with the activated BMP signaling, triggers an auto-regulatory loop that reinforces itself and permits consolidation of the astrocyte phenotype (Wen et al., 2009). Upregulation of *BMP2* and *GFAP* observed in luteolin-treated hNSCs after 24 h of differentiation induction suggests that luteolin may have induced astrogenesis *via* the *BMP2* signaling pathway. However, these results were contradictory with the significant decrease of the expression of the *STAT3* (at 24 h), the transcription factor of *GFAP*. Therefore, we opted to evaluate the expression of *STAT3*, its upstream regulator *BMP2*, and *GFAP* after 8 h of hNSCs differentiation induction by luteolin treatment. There was an increased expression of the *STAT3* in luteolin-treated hNSCs after 8 h, while *BMP2* and *GFAP* were not expressed. Since it was reported that *GFAP* expression depends on both *BMP2* signals and *STAT3* expression (Lee et al., 2015; Takouda et al., 2017), the non-expression of *GFAP* at 8 h in the present study would be attributed to the absence of *BMP2*. On the other hand, the increase of *BMP2* expression after 24 h of luteolin treatment may be, in part, permitting the activation of *STAT3*, which in turn permitted the expression of *GFAP* and, therefore, induced the differentiation of hNSCs into astrocytes. Moreover, the decrease of *STAT3* expression level after 24 h of luteolin treatment may highlight the activation of the autoregulatory loop that consolidates and stabilizes the astrocyte phenotype. Conjointly, the decreased expression of *NOTCH* receptors in our study (*NOTCH1* and *NOTCH3*) may highlight the inhibitory effect of luteolin treatment on hNSCs self-renewal process (Louvi and Artavanis-Tsakonas, 2006; Wen et al., 2009; Venkatesh et al., 2017). On the other hand, AICAR treatment decreased the expression of *STAT3* after 8 h of treatment; however, it increased the expression of *GFAP* at 24 h, suggesting that AICAR did not enhance the astrogenesis process exclusively *via* *STAT3* signaling. Besides, in contrast to luteolin treatment, AICAR treatment significantly

increased the expression of *NOTCH3* at 24 h of treatment as well as increased the expression of *NOTCH1*, highlighting that AICAR probably induced the astrogenesis *via* Notch signaling. Moreover, the upregulation of *NOTCH1* and *NOTCH3* expressions may witness that AICAR treatment maintains the self-renewal properties of hNSCs (Nagao et al., 2007). Finally, the unchanged expression of *TUBB3* in luteolin-treated hNSCs, and the significant upregulation of this gene expression in AICAR-treated cells after 24 h treatment may highlight that contrary to AICAR, which show neurogenic potential, luteolin has a specific astrogenic effect on hNSCs.

In summary, a comparison of the main molecular changes observed in both luteolin and AICAR-treated hNSCs allows us to conclude that the luteolin is a specific astrogenic enhancer molecule, while AICAR is an astrogenic and neurogenic enhancer as well as self-renewal maintainer of hNSCs. Moreover, these molecular changes may suggest that the astrogenic effect of luteolin on hNSCs was exclusively through the Wnt- $\beta$ -catenin-BMP2-*STAT3* pathway. In contrast, AICAR enhanced both astrogenic and neurogenic differentiation, as well as maintained self-renewal through both Notch and Wnt- $\beta$ -catenin-BMP2-*STAT3* signaling. **Figure 6** summarizes the observed molecular effects of luteolin on hNSCs fate determination.

During recent years, an increasing amount of evidence has suggested the vast potential of NSCs in the area of translational medicine in debilitating neurodegenerative diseases. In this context, the use of natural compounds, such as polyphenols, are also being extensively studied for their potential stimulatory and synergistic effects on stem cells against neurodegenerative diseases (Tandon et al., 2018). There has been an emerging concept of astrocytes as mediators of polyphenol action in the CNS (Matias et al., 2016). Astrocytes are the most abundant type of cells in the brain and play an important role in nervous system integrity. Recent studies highlighted the putative roles of astrocytogenesis in both psychiatric including depression and in neurodegenerative disorders (Altshuler et al., 2010; Rajkowska and Stockmeier, 2013; Lee et al., 2015; Peng et al., 2015; Rial et al., 2016; Apple et al., 2017; Gonzales et al., 2017; Peng and Bonaguidi, 2018). It has been reported that under a loss of cerebral parenchymal integrity, astrocytes maintain homeostatic functions by removing excess glutamate in the synaptic cleft, promoting synaptogenesis, releasing neurotrophic factors, and regulating the blood flow during neuronal activity (Becerra-Calixto and Cardona-Gómez, 2017). It has also been reported that astrocyte homeostasis is tightly influenced by both the acute and chronic use of psychotropic drugs (Hertz et al., 2014). Thus, targeting the modulation of astrocytogenesis along with neurogenesis and/or oligodendrocytogenesis to re-establish the physiological CNS functions in the damaged brain, has been of great interest to treat the aforementioned pathologies. Therefore, our study offers a promising perspective on the beneficial use of luteolin in neuronal diseases.

To validate the modulatory effect of luteolin on astrocytogenesis observed *in vitro*, and to investigate its effect on neurogenesis and/or oligodendrocytogenesis to re-establish the physiological CNS functions in the damaged brain, we evaluated the effect of this flavone *in vivo* in mice animal model.



Although statistically non-significant, our results from the TST test, a test of antidepressant activity in mice where antidepressants decrease the time spent immobile without increasing general locomotor activity (Carr and Lucki, 2010), indicated that luteolin treatment slightly decreased the mice immobility time.

Findings from the quantification of astrocytes cells isolated from whole brains showed that LPS injection significantly reduced the number of astrocytes compared to that of LPS-induced depression mice treated with luteolin and control mice ( $p = 0.008$ ), however, luteolin treatment didn't restore this cell loss. On the other hand, results from isolated mice astrocytes showed that secretion of IL-6 by astrocytes isolated from both the control group (PBS group mice) and the control group treated with luteolin (PBS group + L mice) was unchanged. Besides, this cytokine level was significantly increased in the cell culture media of astrocytes isolated from LPS treated mice, and it was significantly decreased in the cell culture media of astrocytes isolated from luteolin treated LPS-induced depression mice. These results highlighted the installation of the neuroinflammatory process in LPS treated mice that was neutralized by the luteolin treatment. In this context different studies, reported the secretion of IL-6 by astrocytes in different pathological conditions including major depression disease (Erta et al., 2012). Taken together the findings on these isolated cells highlight that luteolin treatment attenuated LPS-induced inflammatory responses in mice brain-derived astrocytes rather than increasing the number of astrocytes in mice brains.

Recently, it was shown that inflammation is involved in the pathogenesis of depression (Lee and Giuliani, 2019), and that some phytochemicals exert their anti-depressant effects through their anti-inflammatory effect (Wu et al., 2019). In the present study, the levels of IL-6, TNFα, and corticosterone were quantified

in the sera of LPS induced depression mice. Results showed that LPS injection significantly increased the IL-6, TNFα, and corticosterone levels in mice sera, suggesting the establishment of the inflammatory stress. The oral administration of luteolin significantly reduced this increase depicting therefore the anti-inflammatory effect of luteolin.

Sabti et al. reported that antidepressants targeting the expression of serotonin and noradrenaline only present limitations and that accordingly antidepressant drugs targeting the dopaminergic system have been developed, whereas the antidepressants acting on serotonergic mechanisms lead to enhancement of BDNF levels in rodents (Sabti et al., 2019). Hence, we assessed the mature BDNF levels, noradrenaline and dopamine levels in mice hypothalamus and serotonin level in mice cortex. The results showed that: mature BDNF levels were significantly increased in the hypothalamus of PBS and LPS group when they are treated with Luteolin, noradrenaline levels were significantly increased in the hypothalamus of LPS group mice and it was significantly decreased when treated with luteolin, and dopamine levels were significantly decreased in the hypothalamus of LPS group mice and significantly increased when treated with luteolin.

Taken together, our results show that luteolin treatment may exert an antidepressant effect in the LPS induced depression mice by decreasing the IL-6 production by astrocytes, decreasing the serum IL-6, TNFα, and corticosterone and by increasing the levels of mature BDNF, dopamine, and noradrenaline levels in the hypothalamus.

The evaluation of the transcriptome in the isolated mice NSCs and mice hippocampi showed that LPS injection significantly downregulated several neuronal and glial biological processes including the neurogenesis (GO: 0022008) and gliogenesis (GO:0042063) that were mostly upregulated with luteolin

treatment in mice NSCs and not in hippocampi. In NSCs, except the *Camk2a* gene, all the downregulated genes by LPS injection were upregulated after luteolin treatment pointing out the restoring effect exerted by luteolin treatment on mice NSCs to overcome the damage related to neurogenesis and astrogenesis processes caused by LPS injection. *Camk2a* gene encodes the subunit alpha of CaMKII protein. This protein isoform is known to be mainly expressed in the brain neurons and it is well established that its abnormal functioning is linked to the pathophysiology of depression. So far most studies associated the decrease in CaMKII alpha levels to the depressive like phenotype in animal models and highlighted the role of antidepressants to increase this protein expression (Sałaciak et al., 2021). In their review paper Sałaciak and colleagues discussed the effect of CaMKII in antidepressant-like effect installation mentioning that this activity requires the activation of both CaMKII $\alpha$  and CaMKIV together with the inactivation of CaMKII $\beta$ . Ahmed and colleagues associated the inhibition of CaMKII $\alpha$  expression to an anxiolytic effect (Ahmed et al., 2017).

Our *in vivo* transcriptomic study showed also that LPS injection enriched different KEGG signaling pathways by downregulation in mice NSCs with the estrogen signaling (mmu04915) being the most enriched signaling pathway ( $p = 9.87E-05$ ). Luteolin treatment enriched by upregulation, the estrogen signaling (mmu04915,  $p = 0.0093$ ), the HIF-1 (mmu04066) and the thyroid hormone (mmu1919). In the NSCs of normal mice group, it enriched the Wnt signaling by upregulation.

Recently, the role of estrogen signaling has been highlighted with studies reporting its neuroprotective effects on the brain by sheltering it from inflammation and stress (Azcoitia et al., 2019; Hwang et al., 2021), and investigations in animal models of psychiatric disorders and in patients, revealed that this signaling is disturbed and associated with cognitive deficits and also with the manifestations of symptoms that could be reversed with treatments targeting estrogen-signaling pathways (Hwang et al., 2021). To add more Li et al. showed that hypoxia-inducible factor-1 (HIF-1) pathway is a promising target for the treatment of depression (Li et al., 2020). Indeed, they reported that HIF-1 may produce beneficial effects on depression, as it targets genes that have been shown to elicit antidepressant effects in animal models (erythropoietin (EPO) and vascular endothelial growth factor (VEGF) genes (Li et al., 2020).

On the other hand, thyroid hormone signaling, a key modulator of neuropsychiatric disorders including depression, is known as a regulator of the developmental program in the brain. The thyroid hormone action targets diverse cellular processes such as progenitor turnover, cell survival and differentiation, cellular homeostasis, and metabolic regulation. In mice embryonic neural stem cells, it promotes neuronal differentiation by inhibiting STAT3 signaling through the thyroid receptor  $\alpha 1$ , and inhibits astrocytic differentiation, in rodents Thyroid Hormone signaling activates mitochondrial metabolism during NSC commitment to neuronal precursor cells, and in humans, it regulates hippocampal neurogenesis dependent behaviors such as mood-related behaviors (Ming and Song, 2011;

Chen et al., 2012; Kapoor et al., 2015; Miller and Hen, 2015; Gothié et al., 2020).

As previously mentioned, the Wnt signaling plays a crucial role for NSC self-renewal and neurogenesis (Kasai et al., 2005; Wen et al., 2009); and it promotes astrocyte differentiation and suppresses oligodendroglial differentiation in a phase-dependent manner through BMP signal modulation (Kasai et al., 2005).

Considering these findings, our results point out an antidepressant effect of luteolin treatment exerted especially *via* the modulation of the estrogen, HIF-1 and thyroid hormone signaling pathways in the NSCs of mice. Equally these findings highlight the modulatory effect exerted by luteolin on signaling pathways involved in NSCs fate determination namely the Wnt signaling.

In the hippocampus of LPS induced depression model mice, the luteolin treatment enriched the GABAergic synapse by downregulation, and the PI3K-AKT (mmu04151), the JAK-STAT (mmu04630), and the estrogen signaling (mmu04915) by upregulation.

Recently, PI3K/Akt/GSK-3 $\beta$ /mTOR signaling pathway has been associated to neurobiology of depression and seems to be modulated by some pharmacological antidepressant strategies. Ludka et al. (2016) have shown a behavioral anti-depressant effect of Atorvastatin that was supported by neurochemical observations revealed by an increase of the immunocontent of the phosphorylated isoforms of Akt, GSK-3 $\beta$  and mTOR in the hippocampus of mice (Ludka et al., 2016).

In addition to its aforementioned role in the modulation of GFAP gene expression, JAK/STAT pathway is involved in mediating several functions of the central nervous system, including neurogenesis, synaptic plasticity, gliogenesis, and microglial activation, and all of which have been implicated in the pathophysiology of mood disorders. Moreover, there is also direct evidence from studies in populations with depressive disorders, suggesting that JAK/STAT pathways may be involved in the pathophysiology of depression and the antidepressant actions of current treatments have been shown to be mediated by JAK/STAT-dependent mechanisms (Wen et al., 2009; Lee et al., 2015; Shariq et al., 2019). **Figure 6** summarizes the observed molecular effects of luteolin LPS-induced depression mice.

Thus, along with the results obtained in our *in vitro* study using hNSCs, the *in vivo* study confirms the potential astrogenic effect of luteolin in the defected astrogenesis model and highlights its modulatory effect on WNT-JAK-STAT signaling. This *in vivo* study highlighted also the modulatory effect of luteolin on different signaling pathways involved in the pathophysiology of depression. So far, the anti-depressant effect of luteolin treatment *via* Suppressing Endoplasmic Reticulum Stress was reported (Ishisaka et al., 2011), however to the best of our knowledge, this is the first study to show: that luteolin treatment might alter some signaling pathways associated with depression *via* the modulation of NSCs fate determination and that this flavone had a restoring effect on NSCs signaling to overcome the damage caused by LPS injection.

Given the non-static nature of NSCs, the effects of its source and its derivation method that may significantly affect its differentiation potential into specific cell types, the disrupt

of commercialization of the hNSCs used in our study (StemPro<sup>TM</sup> neural stem cells, Cat. no. A15654) limited the study of the protein expression of genes evaluated by RT-qPCR as well as the study of the composition of the NSC population including the percentage of SOX2 and PAX6 expression that would be informative and the percentage of mature neurons and TUBB3 percentage within the NSC population. The results from this *in vitro* study, therefore, require a future replication with other type of hNSCs.

## CONCLUSION

In summary, our *in vitro* study in hNSCs showed that luteolin significantly increased the expression of *GFAP* and the number of GFAP+ cells as well as altered the WNT-BMP2-STAT3 pathways suggesting its potential for astrocytogenesis. Our *in vivo* findings showed luteolin significantly attenuated LPS-induced neuroinflammation by decreasing the IL-6 production in mice brain-derived astrocytes, reducing the serum IL-6, TNF $\alpha$  and corticosterone levels, and increasing the mature BDNF, dopamine, and noradrenaline levels in the hypothalamus. Whole-genome transcriptome analysis suggests that luteolin treatment may restore LPS-induced alterations in biological functions related to neurogenesis and astrocytogenesis in mice hypothalamus and brain-derived NSCs. Although the antidepressant behavioral effects of luteolin did not reach statistical significance, a number of signaling pathways involved in the pathophysiology of depression were modulated by luteolin treatment. Our study is the first to report astrocytogenic potential of luteolin and thus highlighting its possible therapeutic benefits in neuroinflammatory and neurodegenerative diseases. However, future studies are required to confirm its molecular mechanism of action.

## DATA AVAILABILITY STATEMENT

All data generated or analyzed during this study are included in this published article and its supplementary information

## REFERENCES

- Achour, M., Mateos, R., Ben Fredj, M., Mtraoui, A., Bravo, L., and Saguem, S. (2018). A comprehensive characterisation of rosemary tea obtained from *Rosmarinus officinalis* L. collected in a sub-humid area of Tunisia. *Phytochem. Anal.* 29, 87–100. doi: 10.1002/pca.2717
- Ahmed, M. E., Dong, Y., Lu, Y., Tucker, D., Wang, R., and Zhang, Q. (2017). Beneficial effects of a CaMKII $\alpha$  inhibitor TatCN21 peptide in global cerebral ischemia. *J. Mol. Neurosci.* 61, 42–51. doi: 10.1007/s12031-016-0830-8
- Akers, K. G., Martinez-Canabal, A., Restivo, L., Yiu, A. P., De Cristofaro, A., Hsiang, H.-L. L., et al. (2014). Hippocampal neurogenesis regulates forgetting during adulthood and infancy. *Science* 344, 598–602. doi: 10.1126/science.1248903
- Altshuler, L. L., Abulseoud, O. A., Foland-Ross, L., Bartzokis, G., Chang, S., Mintz, J., et al. (2010). Amygdala astrocyte reduction in subjects with major depressive disorder but not bipolar disorder. *Bipolar Disord.* 12, 541–549. doi: 10.1111/j.1399-5618.2010.00838.x

files. Microarray data are deposited in the Gene Expression Omnibus (GEO) under Accession Numbers: GSE148160 (<https://www.ncbi.nlm.nih.gov/geo/query/acc.cgi?acc=GSE148160>), GSE181285 (<https://www.ncbi.nlm.nih.gov/geo/query/acc.cgi?acc=GSE181285>), and GSE181522 (<https://www.ncbi.nlm.nih.gov/geo/query/acc.cgi?acc=GSE181522>).

## ETHICS STATEMENT

The animal study was reviewed and approved by the Animal Ethics Committee of the University of Tsukuba, Japan.

## AUTHOR CONTRIBUTIONS

MA contributed to conceptualization, methodology, investigation, formal analysis, visualization, software, and writing – original draft. FF contributed to formal analysis, visualization, software, validation, and writing – review and editing. KS contributed to methodology, investigation, and supervision. HI contributed to conceptualization, resources, supervision, project administration, and funding acquisition. All authors read and approved the final manuscript.

## FUNDING

The authors acknowledge the financial support from Japan Science and Technology Agency (JST), Science and Technology Research Partnership for Sustainable Development (SATREPS, Grant No. JPMJSA1506), and the Japan International Cooperation Agency (JICA).

## SUPPLEMENTARY MATERIAL

The Supplementary Material for this article can be found online at: <https://www.frontiersin.org/articles/10.3389/fcell.2021.753279/full#supplementary-material>

- Apple, D. M., Fonseca, R. S., and Kokovay, E. (2017). The role of adult neurogenesis in psychiatric and cognitive disorders. *Brain Res.* 1655, 270–276. doi: 10.1016/j.brainres.2016.01.023
- Azcoitia, I., Barreto, G. E., and Garcia-Segura, L. M. (2019). Molecular mechanisms and cellular events involved in the neuroprotective actions of estradiol. analysis of sex differences. *Front. Neuroendocrinol.* 55:100787. doi: 10.1016/j.yfrne.2019.100787
- Aziz, N., Kim, M.-Y., and Cho, J. Y. (2018). Anti-inflammatory effects of luteolin: a review of *in vitro*, *in vivo*, and *in silico* studies. *J. Ethnopharmacol.* 225, 342–358. doi: 10.1016/j.jep.2018.05.019
- Babicki, S., Arndt, D., Marcu, A., Liang, Y., Grant, J. R., Maciejewski, A., et al. (2016). Heatmapper: web-enabled heat mapping for all. *Nucleic Acids Res.* 44, W147–W153. doi: 10.1093/nar/gkw419
- Banasar, M., and Duman, R. S. (2008). Glial loss in the prefrontal cortex is sufficient to induce depressive-like behaviors. *Biol. Psychiatry* 64, 863–870. doi: 10.1016/j.biopsych.2008.06.008



- Bandaruk, Y., Mukai, R., and Terao, J. (2014). Cellular uptake of quercetin and luteolin and their effects on monoamine oxidase-A in human neuroblastoma SH-SY5Y cells. *Toxicol. Rep.* 1, 639–649. doi: 10.1016/j.toxrep.2014.08.016
- Becerra-Calixto, A., and Cardona-Gómez, G. P. (2017). The role of astrocytes in neuroprotection after brain stroke: potential in cell therapy. *Front. Mol. Neurosci.* 10:88. doi: 10.3389/fnmol.2017.00088
- Bejoy, J., Bijonowski, B., Marzano, M., Jeske, R., Ma, T., and Li, Y. (2019). Wnt-Notch signaling interactions during neural and astroglial patterning of human stem cells. *Tissue Eng. Part A* 26, 419–431. doi: 10.1089/ten.tea.2019.0202
- Cahoy, J. D., Emery, B., Kaushal, A., Foo, L. C., Zamanian, J. L., Christopherson, K. S., et al. (2008). A transcriptome database for astrocytes, neurons, and oligodendrocytes: a new resource for understanding brain development and function. *J. Neurosci.* 28, 264–278. doi: 10.1523/JNEUROSCI.4178-07.2008
- Cajal, R. Y. (1930). Degeneration and regeneration of the nervous system. *Nature* 125, 230–231. doi: 10.1038/125230a0
- Carr, G. V., and Lucki, I. (2010). The role of serotonin in depression. *Handb. Behav. Neurosci.* 21, 493–505. doi: 10.1016/S1569-7339(10)70098-9
- Casasosa, S., Bozzi, Y., and Conti, L. (2014). Neural stem cells: ready for therapeutic applications? *Mol. Cell. Therapies* 2, 31–31. doi: 10.1186/2052-8426-2-31
- Chen, C., Zhou, Z., Zhong, M., Zhang, Y., Li, M., Zhang, L., et al. (2012). Thyroid hormone promotes neuronal differentiation of embryonic neural stem cells by inhibiting STAT3 signaling through TR $\alpha$ 1. *Stem Cells Dev.* 21, 2667–2681. doi: 10.1089/scd.2012.0023
- Cohen, J., and Torres, C. (2019). Astrocyte senescence: evidence and significance. *Aging Cell* 18, e12937. doi: 10.1111/accel.12937
- El Omri, A., Han, J., Kawada, K., Abdabbah, M. B., and Isoda, H. (2012). Luteolin enhances cholinergic activities in PC12 cells through ERK1/2 and PI3K/Akt pathways. *Brain Res.* 1437, 16–25. doi: 10.1016/j.brainres.2011.12.019
- Eriksson, P. S., Perfilieva, E., Björk-Eriksson, T., Alborn, A.-M., Nordborg, C., Peterson, D. A., et al. (1998). Neurogenesis in the adult human hippocampus. *Nat. Med.* 4, 1313–1317. doi: 10.1038/3305
- Erta, M., Quintana, A., and Hidalgo, J. (2012). Interleukin-6, a major cytokine in the central nervous system. *Int. J. Biol. Sci.* 8:1254. doi: 10.7150/ijbs.4679
- Fan, G., Martinowich, K., Chin, M. H., He, F., Fouse, S. D., Hutnick, L., et al. (2005). DNA methylation controls the timing of astroglial differentiation through regulation of JAK-STAT signaling. *Development* 132, 3345–3356. doi: 10.1242/dev.01912
- Forbes-Lorman, R. M., Kurian, J. R., and Auger, A. P. (2014). MeCP2 regulates GFAP expression within the developing brain. *Brain Res.* 1543, 151–158. doi: 10.1016/j.brainres.2013.11.011
- Gao, J., Ma, Y., Fu, H.-L., Luo, Q., Wang, Z., Xiao, Y.-H., et al. (2016). Non-catalytic roles for TET1 protein negatively regulating neuronal differentiation through srGAP3 in neuroblastoma cells. *Protein Cell* 7, 351–361. doi: 10.1007/s13238-016-0267-4
- Gonzales, M. M., Insel, P. S., Nelson, C., Tosun, D., Mattsson, N., Mueller, S. G., et al. (2017). Cortical atrophy is associated with accelerated cognitive decline in mild cognitive impairment with subsyndromal depression. *Am. J. Geriatr. Psychiatry* 25, 980–991. doi: 10.1016/j.jagp.2017.04.011
- Gothie, J.-D., Vancamp, P., Demeneix, B., and Remaud, S. (2020). Thyroid hormone regulation of neural stem cell fate: from development to ageing. *Acta Physiol.* 228:e13316. doi: 10.1111/apha.13316
- Grinspan, J. (2002). Cells and signaling in oligodendrocyte development. *J. Neuropathol. Exp. Neurol.* 61, 297–306. doi: 10.1093/jnen/61.4.297
- Han, S., Dennis, D. J., Balakrishnan, A., Dixit, R., Britz, O., Zinyk, D., et al. (2018). A non-canonical role for the proneural gene Neurog1 as a negative regulator of neocortical neurogenesis. *Development* 145:dev157719. doi: 10.1242/dev.157719
- Hertz, L., Song, D., Li, B., Du, T., Xu, J., Gu, L., et al. (2014). Signal transduction in astrocytes during chronic or acute treatment with drugs (SSRIs, antidepressants, GABA-ergic drugs, and benzodiazepines) ameliorating mood disorders. *J. Signal Transduction* 2014:593934. doi: 10.1155/2014/593934
- Hsieh, J., Nakashima, K., Kuwabara, T., Mejia, E., and Gage, F. H. (2004). Histone deacetylase inhibition-mediated neuronal differentiation of multipotent adult neural progenitor cells. *Proc. Natl. Acad. Sci. U S A* 101, 16659–16664. doi: 10.1073/pnas.0407643101
- Hsieh, J., and Zhao, X. (2016). Genetics and epigenetics in adult neurogenesis. *Cold Spring Harb. Perspect. Biol.* 8:a018911. doi: 10.1101/cshperspect.a018911
- Huang, D. W., Sherman, B. T., and Lempicki, R. A. (2009). Bioinformatics enrichment tools: paths toward the comprehensive functional analysis of large gene lists. *Nucleic Acids Res.* 37, 1–13. doi: 10.1093/nar/gkn923
- Huffman, J., and Taylor, G. T. (2020). *Stress, Neurogenesis, and Mood*. New York, NY: Wiley.
- Hwang, W. J., Lee, T. Y., Kim, N. S., and Kwon, J. S. (2021). The role of estrogen receptors and their signaling across psychiatric disorders. *Int. J. Mol. Sci.* 22:373.
- Imran, M., Rauf, A., Abu-Izneid, T., Nadeem, M., Shariati, M. A., Khan, I. A., et al. (2019). Luteolin, a flavonoid, as an anticancer agent: a review. *Biomed. Pharmacotherapy* 112:108612. doi: 10.1016/j.biopha.2019.108612
- Ishisaka, M., Kakefuda, K., Yamauchi, M., Tsuruma, K., Shimazawa, M., Tsuruta, A., et al. (2011). Luteolin shows an antidepressant-like effect via suppressing endoplasmic reticulum stress. *Biol. Pharm. Bull.* 34, 1481–1486. doi: 10.1248/bpb.34.1481
- Jacobs, S., Lie, D. C., Decicco, K. L., Shi, Y., Deluca, L. M., Gage, F. H., et al. (2006). Retinoic acid is required early during adult neurogenesis in the dentate gyrus. *Proc. Natl. Acad. Sci. U S A* 103, 3902–3907. doi: 10.1073/pnas.0511294103
- Kapoor, R., Fanibunda, S. E., Desouza, L. A., Guha, S. K., and Vaidya, V. A. (2015). Perspectives on thyroid hormone action in adult neurogenesis. *J. Neurochem.* 133, 599–616. doi: 10.1111/jnc.13093
- Kasai, M., Satoh, K., and Akiyama, T. (2005). Wnt signaling regulates the sequential onset of neurogenesis and gliogenesis via induction of BMPs. *Genes Cells* 10, 777–783. doi: 10.1111/j.1365-2443.2005.00876.x
- Kohyama, J., Kojima, T., Takatsuka, E., Yamashita, T., Namiki, J., Hsieh, J., et al. (2008). Epigenetic regulation of neural cell differentiation plasticity in the adult mammalian brain. *Proc. Natl. Acad. Sci. U S A* 105, 18012–18017. doi: 10.1073/pnas.0808417105
- Lee, C.-H., and Giuliani, F. (2019). The role of inflammation in depression and fatigue. *Front. Immunol.* 10:1696. doi: 10.3389/fimmu.2019.01696
- Lee, H.-R., Lee, J., Jajoo, R., Kong, S.-Y., Shin, J.-Y., Kim, J.-O., et al. (2015). Discovery of a small molecule that enhances astrocytogenesis by activation of stat3, smad1/5/8, and erk1/2 via induction of cytokines in neural stem cells. *ACS Chem. Neurosci.* 7, 90–99. doi: 10.1021/acscchemneuro.5b00243
- Leker, R. R., Lasri, V., and Chernoguz, D. (2009). Growth factors improve neurogenesis and outcome after focal cerebral ischemia. *J. Neural. Transm.* 116, 1397–1402. doi: 10.1007/s00702-009-0329-3
- Lennon, M. J., Jones, S. P., Lovelace, M. D., Guillemain, G. J., and Brew, B. J. (2017). Bcl11b—A critical neurodevelopmental transcription factor—roles in health and disease. *Front. Cell. Neurosci.* 11:89. doi: 10.3389/fncel.2017.00089
- Li, G., Zhao, M., Cheng, X., Zhao, T., Feng, Z., Zhao, Y., et al. (2020). FG-4592 improves depressive-like behaviors through HIF-1-Mediated neurogenesis and synapse plasticity in rats. *Neurotherapeutics* 17, 664–675. doi: 10.1007/s13311-019-00807-3
- Lin, C.-W., Wu, M.-J., Liu, I. Y. C., Su, J.-D., and Yen, J.-H. (2010). Neurotrophic and cytoprotective action of luteolin in PC12 cells through ERK-dependent induction of Nrf2-driven HO-1 expression. *J. Agric. Food Chem.* 58, 4477–4486. doi: 10.1021/jf904061x
- Louvi, A., and Artavanis-Tsakonas, S. (2006). Notch signalling in vertebrate neural development. *Nat. Rev. Neurosci.* 7, 93–102. doi: 10.1038/nrn1847
- Ludka, F. K., Constantino, L. C., Dal-Cim, T., Binder, L. B., Zomkowski, A., Rodrigues, A. L. S., et al. (2016). Involvement of PI3K/Akt/GSK-3 $\beta$  and mTOR in the antidepressant-like effect of atorvastatin in mice. *J. Psychiatr. Res.* 82, 50–57. doi: 10.1016/j.jpsychires.2016.07.004
- Luo, Y., Shang, P., and Li, D. (2017). Luteolin: a flavonoid that has multiple cardioprotective effects and its molecular mechanisms. *Front. Pharmacol.* 8:692. doi: 10.3389/fphar.2017.00692
- Matias, I., Buosi, A. S., and Gomes, F. C. A. (2016). Functions of flavonoids in the central nervous system: astrocytes as targets for natural compounds. *Neurochem. Int.* 95, 85–91. doi: 10.1016/j.neuint.2016.01.009
- Miean, K. H., and Mohamed, S. (2001). Flavonoid (myricetin, quercetin, kaempferol, luteolin, and apigenin) content of edible tropical plants. *J. Agric. Food Chem.* 49, 3106–3112. doi: 10.1021/jf000892m
- Miller, B. R., and Hen, R. (2015). The current state of the neurogenic theory of depression and anxiety. *Curr. Opin. Neurobiol.* 30, 51–58. doi: 10.1016/j.conb.2014.08.012

- Ming, G.-L., and Song, H. (2011). Adult neurogenesis in the mammalian brain: significant answers and significant questions. *Neuron* 70, 687–702. doi: 10.1016/j.neuron.2011.05.001
- Nagao, M., Sugimori, M., and Nakafuku, M. (2007). Cross talk between notch and growth factor/cytokine signaling pathways in neural stem cells. *Mol. Cell. Biol.* 27, 3982–3994. doi: 10.1128/MCB.00170-07
- Nakashima, K., Yanagisawa, M., Arakawa, H., Kimura, N., Hisatsune, T., Kawabata, M., et al. (1999). Synergistic signaling in fetal brain by STAT3-Smad1 complex bridged by p300. *Science* 284, 479–482. doi: 10.1126/science.284.5413.479
- Okabe, Y., Takahashi, T., Mitsumasa, C., Kosai, K.-I., Tanaka, E., and Matsuishi, T. (2012). Alterations of gene expression and glutamate clearance in astrocytes derived from an MeCP2-null mouse model of Rett syndrome. *PLoS One* 7:e35354. doi: 10.1371/journal.pone.0035354
- Pajarillo, E., Rizor, A., Lee, J., Aschner, M., and Lee, E. (2019). The role of astrocytic glutamate transporters GLT-1 and GLAST in neurological disorders: potential targets for neurotherapeutics. *Neuropharmacology* 161:107559. doi: 10.1016/j.neuropharm.2019.03.002
- Pataskar, A., Jung, J., Smialowski, P., Noack, F., Calejari, F., Straub, T., et al. (2016). NeuroD1 reprograms chromatin and transcription factor landscapes to induce the neuronal program. *EMBO J.* 35, 24–45. doi: 10.15252/embj.201591206
- Peng, L., and Bonaguidi, M. A. (2018). Function and dysfunction of adult hippocampal neurogenesis in regeneration and disease. *Am. J. Pathol.* 188, 23–28. doi: 10.1016/j.ajpath.2017.09.004
- Peng, L., Verkhatsky, A., Gu, L., and Li, B. (2015). Targeting astrocytes in major depression. *Expert Rev. Neurotherapeutics* 15, 1299–1306. doi: 10.1586/14737175.2015.1095094
- Rajkowska, G., and Stockmeier, C. A. (2013). Astrocyte pathology in major depressive disorder: insights from human postmortem brain tissue. *Curr. Drug Targets* 14, 1225–1236. doi: 10.2174/13894501113149990156
- Rial, D., Lemos, C., Pinheiro, H., Duarte, J. M., Gonçalves, F. Q., Real, J. I., et al. (2016). Depression as a glial-based synaptic dysfunction. *Front. Cell. Neurosci.* 9:521. doi: 10.3389/fncel.2015.00521
- Sabti, M., Sasaki, K., Gadhi, C., and Isoda, H. (2019). Elucidation of the molecular mechanism underlying *Lippia citriodora* (Lim.)-induced relaxation and anti-depression. *Int. J. Mol. Sci.* 20:3556. doi: 10.3390/ijms20143556
- Sahay, A., Scobie, K. N., Hill, A. S., O'carroll, C. M., Kheirbek, M. A., Burghardt, N. S., et al. (2011). Increasing adult hippocampal neurogenesis is sufficient to improve pattern separation. *Nature* 472:466. doi: 10.1038/nature09817
- Salaciak, K., Koszalka, A., Żmudzka, E., and Pytko, K. (2021). The Calcium/Calmodulin-Dependent kinases II and IV as therapeutic targets in neurodegenerative and neuropsychiatric disorders. *Int. J. Mol. Sci.* 22:4307. doi: 10.3390/ijms22094307
- Santiago, M., Antunes, C., Guedes, M., Sousa, N., and Marques, C. J. (2014). TET enzymes and DNA hydroxymethylation in neural development and function — how critical are they? *Genomics* 104, 334–340.
- Sasaki, K., Davies, J., Doldán, N. G., Arao, S., Ferdousi, F., Szele, F. G., et al. (2019). 3, 4, 5-Tricaffeoylquinic acid induces adult neurogenesis and improves deficit of learning and memory in aging model senescence-accelerated prone 8 mice. *Aging (Albany NY)* 11:401. doi: 10.18632/aging.101748
- Sawmiller, D., Li, S., Shahaduzzaman, M., Smith, A. J., Obregon, D., Giunta, B., et al. (2014). Luteolin reduces Alzheimer's disease pathologies induced by traumatic brain injury. *Int. J. Mol. Sci.* 15, 895–904. doi: 10.3390/ijms15010895
- Schmuck, M. R., Temme, T., Dach, K., De Boer, D., Barenys, M., Bendt, F., et al. (2017). Omnisphero: a high-content image analysis (HCA) approach for phenotypic developmental neurotoxicity (DNT) screenings of organoid neurosphere cultures in vitro. *Arch. Toxicol.* 91, 2017–2028. doi: 10.1007/s00204-016-1852-2
- Shariq, A. S., Brietzke, E., Rosenblat, J. D., Pan, Z., Rong, C., Ragguett, R.-M., et al. (2019). Therapeutic potential of JAK/STAT pathway modulation in mood disorders. *Rev. Neurosci.* 30, 1–7. doi: 10.1515/revneuro-2018-0027
- Sherman, B. T., and Lempicki, R. A. (2009). Systematic and integrative analysis of large gene lists using DAVID bioinformatics resources. *Nat. Protocols* 4, 44–57. doi: 10.1038/nprot.2008.211
- Sloan, S. A., and Barres, B. A. (2014). Mechanisms of astrocyte development and their contributions to neurodevelopmental disorders. *Curr. Opin. Neurobiol.* 27, 75–81. doi: 10.1016/j.conb.2014.03.005
- Steru, L., Chermat, R., Thierry, B., and Simon, P. (1985). The tail suspension test: a new method for screening antidepressants in mice. *Psychopharmacology (Berl)* 85, 367–370. doi: 10.1007/BF00428203
- Takouda, J., Katada, S., and Nakashima, K. (2017). Emerging mechanisms underlying astrogenesis in the developing mammalian brain. *Proc. Japan Acad. Series B* 93, 386–398. doi: 10.2183/pjab.93.024
- Tandon, A., Singh, S. J., and Chaturvedi, R. K. (2018). Stem cells as potential targets of polyphenols in multiple sclerosis and Alzheimer's disease. *BioMed. Res. Int.* 2018, 1–30. doi: 10.1155/2018/1483791
- Tang, B., Di Lena, P., Schaffer, L., Head, S. R., Baldi, P., and Thomas, E. A. (2011). Genome-wide identification of Bcl11b gene targets reveals role in brain-derived neurotrophic factor signaling. *PLoS One* 6:e23691. doi: 10.1371/journal.pone.0023691
- Taverna, E., Götz, M., and Huttner, W. B. (2014). The cell biology of neurogenesis: toward an understanding of the development and evolution of the neocortex. *Annu. Rev. Cell Dev. Biol.* 30, 465–502. doi: 10.1146/annurev-cellbio-101011-155801
- Tsujimura, K., Abematsu, M., Kohyama, J., Namihira, M., and Nakashima, K. (2009). Neuronal differentiation of neural precursor cells is promoted by the methyl-CpG-binding protein MeCP2. *Exp. Neurol.* 219, 104–111. doi: 10.1016/j.expneurol.2009.05.001
- Valles, S. L., Iradi, A., Aldasoro, M., Vila, J. M., Aldasoro, C., De La Torre, J., et al. (2019). Function of glia in aging and the brain diseases. *Int. J. Med. Sci.* 16:1473. doi: 10.7150/ijms.37769
- Venkatesh, K., Reddy, L. V. K., Abbas, S., Mullick, M., Moghal, E. T. B., Balakrishna, J. P., et al. (2017). NOTCH signaling is essential for maturation, self-renewal, and tri-differentiation of in vitro derived human neural stem cells. *Cell. Reprogramm.* 19, 372–383. doi: 10.1089/cell.2017.0009
- Wang, H., Wang, H., Cheng, H., and Che, Z. (2016a). Ameliorating effect of luteolin on memory impairment in an Alzheimer's disease model. *Mol. Med. Rep.* 13, 4215–4220. doi: 10.3892/mmr.2016.5052
- Wang, Z., Tang, B., He, Y., and Jin, P. (2016b). DNA methylation dynamics in neurogenesis. *Epigenomics* 8, 401–414.
- Wen, S., Li, H., and Liu, J. (2009). Dynamic signaling for neural stem cell fate determination. *Cell Adhesion Migration* 3, 107–117. doi: 10.4161/cam.3.1.7602
- Wu, Y., Qiu, A., Yang, Z., Wu, J., Li, X., Bao, K., et al. (2019). Malva sylvestris extract alleviates the astrogliosis and inflammatory stress in LPS-induced depression mice. *J. Neuroimmunol.* 336:577029. doi: 10.1016/j.jneuroim.2019.577029
- Yao, B., and Jin, P. (2014). Unlocking epigenetic codes in neurogenesis. *Genes Dev.* 28, 1253–1271. doi: 10.1101/gad.241547.114
- Zang, Y., Yu, L.-F., Pang, T., Fang, L.-P., Feng, X., Wen, T.-Q., et al. (2008). AICAR induces astroglial differentiation of neural stem cells via activating the JAK/STAT3 pathway independently of AMP-activated protein kinase. *J. Biol. Chem.* 283, 6201–6208. doi: 10.1074/jbc.M708619200
- Zhuang, P., Zhang, Y., Cui, G., Bian, Y., Zhang, M., Zhang, J., et al. (2012). Direct stimulation of adult neural stem/progenitor cells in vitro and neurogenesis in vivo by salvianolic acid B. *PLoS One* 7:e35636. doi: 10.1371/journal.pone.0035636

**Conflict of Interest:** The authors declare that the research was conducted in the absence of any commercial or financial relationships that could be construed as a potential conflict of interest.

**Publisher's Note:** All claims expressed in this article are solely those of the authors and do not necessarily represent those of their affiliated organizations, or those of the publisher, the editors and the reviewers. Any product that may be evaluated in this article, or claim that may be made by its manufacturer, is not guaranteed or endorsed by the publisher.

Copyright © 2021 Achour, Ferdousi, Sasaki and Isoda. This is an open-access article distributed under the terms of the Creative Commons Attribution License (CC BY). The use, distribution or reproduction in other forums is permitted, provided the original author(s) and the copyright owner(s) are credited and that the original publication in this journal is cited, in accordance with accepted academic practice. No use, distribution or reproduction is permitted which does not comply with these terms.

# Frontiers in Cell and Developmental Biology

Explores the fundamental biological processes of life, covering intracellular and extracellular dynamics.

The world's most cited developmental biology journal, advancing our understanding of the fundamental processes of life. It explores a wide spectrum of cell and developmental biology, covering intracellular and extracellular dynamics.

## Discover the latest Research Topics

[See more →](#)

### Frontiers

Avenue du Tribunal-Fédéral 34  
1005 Lausanne, Switzerland  
[frontiersin.org](https://frontiersin.org)

### Contact us

+41 (0)21 510 17 00  
[frontiersin.org/about/contact](https://frontiersin.org/about/contact)

